State University of New York Report

DNS, LES and Stochastic Modeling of Turbulent Reacting Flows

by

Peyman Givi
Department of Mechanical and Aerospace Engineering
State University of New York at Buffalo
Buffalo, New York 14260-4400

Final Report for June 1, 1990 through April 30, 1994
Grant N00014-90-J-4013

May 1994

Prepared for
OFFICE OF NAVAL RESEARCH
Mechanics Division, Code 33B
800 North Quincy Street
Arlington, Virginia 22217-5000

State University of New York Report

DNS, LES and Stochastic Modeling of Turbulent Reacting Flows

by

Peyman Givi
Department of Mechanical and Aerospace Engineering
State University of New York at Buffalo
Buffalo, New York 14260-4400

Final Report for June 1, 1990 throu h April 30, 1994
Grant N00014-90-J-4013

May 1994

Prepared for
OFFICE OF NAVAL RESEARCH
Mechanics Division, Code 33B
800 North Quincy Street
Arlington, Virginia 22217-5000

Contents

DNS, LES and Stochastic Modeling of Turbulent Reacting Flows

Peyman Givi
Department of Mechanical and Aerospace Engineering
State University of New York at Buffalo
Buffalo, New York 14260-4400

Abstract

This is a Final Report providing a summary of accomplishments in our research sponsored by the Office of Naval Research (ONR), Grant N00014-90-J-4013 (Young Investigator Program - FY 1990) under the management of Dr. Gabriel D. Roy, Mechanics Division, Code 1132P. The contributions made in each part of this investigation are described, followed by a highlight of our important findings. A few of the technical papers written in conjunction with this work are attached as appendices for those who are interested in reviewing our work in a greater detail.

1 Introduction

The field of computational turbulent combustion has been an area of active research in the U.S. and abroad within the past thirty years. A review of the contributions made within this period indicates that presently there are three primary methodologies by which turbulent flows are treated by computational simulations [1]: (1) Direct Numerical Simulation (DNS), (2) Large Eddy Simulation (LES), and (3) Reynolds Averaged Navier-Stokes Simulation (RANS). The procedures in following these approaches are different and each methodology portrays some advantages and (needless to say) some drawbacks. In the past decade, the first two approaches have been somewhat more visible. This is

to a large extent due to dazzling rate of progress made in the supercomputer technology and the availability of these computers to a larger number of users. However, now it can be stated that all of these approaches are equally competent (at least in the opinion of this PI), and an objective research effort devoted to computational turbulence should consider all of them.

In this research, we initiated a systematic study towards extending the capabilities of each of the three methodologies indicated above. For this purpose we concentrated our research on both *deterministic* and *probabilistic* description of turbulent reacting flows. The first descriptor is for DNS, the second one is for RANS and the combination of the two is used for LES. Due to the nature of the program, several different modeling approaches were followed and various flow configurations simulated by several different numerical schemes were utilized. Because of the rather diverse scope of this research, it is somewhat impossible to provide a review of all our accomplishments in a single report. Therefore, we have selected to include some of the research papers resulting from this work as the primary means of reporting our results (Appendix 1 - through Appendix 10). In the sections to follow, a guideline is provided of the content of these papers. Each section provides a summary of our important findings in each of the programs considered.

2 Mathematical Modeling of the Reactant Conversion in Homogeneous Turbulent Reacting Flows

In this work, closed form analytical expressions are obtained for predicting the limiting rate of mean reactant conversion in homogeneous turbulent flows under the influence of a binary reaction of the type $F + rO \rightarrow (1 + r)$ Product. These relations are obtained by means of a "single-point" Probability Density Function (PDF) method based on the *Amplitude Mapping Closure* (AMC) [2–4]. It is demonstrated that with this model, the maximum rate of the mean reactants' decay can be conveniently expressed in terms of definite integrals of the Parabolic Cylinder Functions [5]. For the cases with complete initial segregation, it is shown that the results agree very closely with those predicted by employing a Beta density of the first kind for an appropriately defined Shvab-Zeldovich

scalar variable. With this assumption, the final results can also be expressed in terms of closed form analytical expressions which are based on the Incomplete Beta Functions. With both models, the dependence of the results on the stoichiometric coefficient and the equivalence ratio can be expressed in an explicit manner. For a stoichiometric mixture, the analytical results simplify significantly. With the AMC, these results are expressed in terms of simple trigonometric functions. For the Beta density model, they are in the form of Gamma Functions. In all the cases considered, the results are shown to agree well with data generated by DNS. Due to the simplicity of these expressions and because of nice mathematical features of the Parabolic Cylinder and the Incomplete Beta Functions, these models are recommended for estimating the limiting rate of mean reactant conversion in homogeneous reacting flows [6–9]. These results also provide a valuable tool in assessing the extent of validity of turbulence closures for modeling of nonpremixed reacting flows. Some discussions are provided on the extension of the models for treating more complicated reacting systems including realistic kinetics schemes and multi-scalar mixing with finite rate chemical reactions in more complex configurations.

Key Findings

For a complete review of our findings in this part of our work, we refer to Refs. [10–13] (please see Appendix 1 and Appendix 2). These findings are highlighted below:

• Based on the AMC a closed form expression is obtained for the limiting rate of mean reactant conversion in homogeneous reacting turbulent flows. Our results are better than all the other alternatives available in the literature for the past thirty years.

• Our model is valid for both stoichiometric and non-stoichiometric mixtures. This is very encouraging since most previous closures are valid *only* for stoichiometric mixtures. Even for such mixtures our results compare with DNS data better than all the other closures.

3 Johnson-Edgeworth Translation for Probability Modeling of Scalar Mixing in Turbulent Flows

In this work, a family of PDF's generated by *Johnson-Edgeworth* Translation (JET) [14, 15] is proposed for statistical modeling of the mixing of an initially binary scalar in homogeneous turbulence. The frequencies obtained by this translation are shown to satisfy some of the characteristics of the PDF's generated by the AMC. In fact, the solution obtained by one of the members of this family is shown to be identical to that developed by the AMC [4]. Due to this similarity and due to the demonstrated capabilities of the AMC, a justification is provided for the use of other members of JET frequencies for the modeling of the binary mixing problem. This similarity also furnishes the reasoning for the applicability of the *Pearson Family* (PF) [16] of frequencies for modeling of the same phenomena. The mathematical requirements associated with the applications of JET in the modeling of the binary mixing problem are provided, and all the results are compared with data generated by DNS. These comparisons indicate that the *Logit-Normal* frequency [17] portrays some subtle features of the mixing problem better than the other closures. However, none of the models considered (JET, AMC, and PF) are capable of predicting the evolution of the conditional expected dissipation and/or the conditional expected diffusion of the scalar field in accordance with DNS. It is demonstrated that this is due to the incapability of the models to account for the variations of the scalar bounds as the mixing proceeds. A remedy is suggested for overcoming this problem which can be useful in probability modeling of turbulent mixing, especially when accompanied by chemical reactions. While in the context of a single-point description the evolution of the scalar bounds cannot be predicted, the qualitative analytical-computational results portray a physically plausible behavior.

Key Findings

For a complete review of our findings in this part of our work, we refer to Refs. [18] (please see Appendix 3). These findings are highlighted below:

• For the first time, it is proven mathematically that AMC can be viewed as a particular case of the Johnson-Edgeworth Translation (JET).

• For the first time, appropriate models are suggested for the conditional statistics of scalars (the conditional expected dissipation and the conditional expected diffusion) in homogeneous turbulent flows. These mathematical results have proven extremely useful in assessing the physics of turbulent mixing and also in aiding the modeling of non-premixed reacting flow systems.

• In view of the similarity of JET and AMC, other simple PDF families such as those belonging to the PF can be used for modeling of practical reacting systems.

• For the first time it is shown that none of the new mixing models are capable of capturing the phenomenon of boundary encroachment in the scalar composition domain as as mixing proceeds.

4 Description of Binary and Trinary Scalar Mixing by the AMC

In this work, the AMC is used for statistical description of the mixing process by Fickian diffusion of a stochastically distributed scalar variable. This closure is invoked in the context of an evolution equation for the single-point PDF of the scalar from initially symmetric binary and trinary states. In the binary case, a simple recipe is provided for the time scaling relation which is very useful in model implementation. In the trinary case, it is shown that after a fixed elapsed time, the PDF relaxes to a distribution similar to that of the binary mixing. The magnitude of this time is independent of the initial extent of departure from a binary state; however, the rate of evolution towards an asymptotic Gaussian state depends on the level of the departure. In both cases, the closure predictions for the scalar flatness factor and the correlation of the mean square scalar-scalar gradients agree well with those obtained by DNS. However, some features of the results are different from those of earlier DNS of mixing in stationary turbulence. These differences are likely attributed to inadequacy of the AMC at the single-point level in accounting for the effects

of turbulence stretching.

Key Findings

For a complete review of our findings in this part of our work, we refer to Ref. [19] (please see Appendix 4). These findings are highlighted below:

• Many details of binary and trinary scalar mixing in the context of both univariate and multivariate statistical analyses are studied by PDF methods. With this study some of the shortcomings of AMC in predicting the asymptotic stages of mixing are captured.

• For the first time a closed form mathematical expression is obtained for describing the decay of the scalar variance for the binary mixing problem as described by AMC. In a previous work on this topic [4] only the *asymptotic* asymptotic rate of this decay could be predicted. Please note that for a closure at the "single-point" the description of the variance is very important.

5 Modeling of Isotropic Reacting Turbulence by a Hybrid Mapping-EDQNM Closure

In this work, a hybrid model is developed and implemented for predicting the limiting bound of the reactant conversion rate in an isotropic turbulent flow under the influence of a reaction of the type $F + O \rightarrow$ Product. This model is based on the AMC for the molecular mixing of a stochastically distributed scalar, and the Eddy-Damped Quasi-Normal Markovian (EDQNM) spectral closure [20,21] for the two-point scalar covariance. The results predicted by this model compare well with available experimental data in both gaseous and aqueous plug flow reactors [7,22,23] but point to the need for more detail measurements in future experimental studies. With the implementation of the AMC a simple analytical expression is obtained for the decay rate of the unmixedness. This expression is very convenient and is recommended for practical applications in the modeling and design of plug flow reactors.

Key Findings

For a complete review of our findings in this part of our work, we refer to Ref. [24, 13] (please see Appendix 5). These findings are highlighted below:

• For the first time the Eddy Damped Quasi-Normal Markovian (EDQNM) closure is used for modeling of turbulent reacting systems. Its combination with AMC provides the best agreement with laboratory data.

• The complexity of this research convinced us that we are *not* yet capable of using "two-point" statistical closures for modeling of :practical" flow systems.

6 Structure of a Turbulent Reacting Mixing Layer

In this work, a monotone Flux Corrected Transport [25,26] algorithm is employed for DNS of a three-dimensional (3D) temporally developing forced mixing layer. A chemical reaction of the type $F + rO \rightarrow (1 + r)$ Product is considered. The objective of this study is to examine the following specific issues pertaining to the structure of turbulent mixing layers and flames: (1) the effects of transition on mixing characteristics of the layer, (2) the existence and manifestation of eddy shocklets in 3D, (3) validity assessment of the steady laminar diffusion flamelet model in depicting the compositional structure of turbulent flames, and (4) evaluation of the basic assumptions of the approach based on the conditional moment method for statistical description of turbulent flames. Simulation of high Reynolds number flow allows the capturing of the cause and effects of transition on the mixing process.

The results indicate that the pairing of large scale vortices causes the interaction of "cup" structures which aid in the initialization of transition. Single point PDF's of the mixture fraction, extracted from DNS data, reveal features in accord with laboratory data. In addition to reproducing many of the qualitative and quantitative results observed in previous experiments, new insights are made as to the nature of the transition process. It is shown that during the transition, both pure unmixed fluids and fully mixed fluids are found

with high probability throughout the entire layer. The effect of chemical heat release is to delay the onset of pairing and the subsequent transition. In constant rate kinetics, reduced mixing results in decreased product formation. However, in an Arrhenius reaction case, chemical heat release causes higher local reaction rates which overcome mixing reduction and results in a relative increase in product formation.

At sufficiently high convective Mach numbers, (larger than 1.25) eddy shocklets are found in 3D mixing layers. Comparison of the shocklets observed in 3D simulations with those in two-dimensional (2D) at the same Reynolds and Convective Mach numbers indicates that the shocklets are stronger in the 2D case.

DNS results for different Damköhler numbers, stoichiometric coefficients, and heat release parameters are compared with prediction results based on a 1D laminar opposed jet system. For all the flames considered, it is concluded that the performance of the steady laminar diffusion flamelet model (SLDFM) [27–31] improves as the magnitude of either the local or global Damköhler number is increased. This is understandable considering the flamelet concept is deemed valid at high but finite reaction rates. Also, as the value of r is increased the agreement between the DNS data and the model is improved. This is promising in view of the fact that the flame surface in typical hydrocarbon flames is at low stoichiometric mixture fraction values. The results for both constant and Arrhenius rate reactions with heat release show an improved agreement with the model in comparison to those of a non-heat releasing layer. This is attributed to the effect of thermal expansion in reducing the instantaneous scalar dissipation rate and thus increasing the magnitudes of the local Damköhler number.

DNS generated results of reacting mixing layers are also used to examine the basic assumption of the Conditional Moment Method CMM) [32–34]. It is shown that the neglect of the conditional unmixedness term is acceptable. Also, the cross-stream variations of the first order conditional moments (conditional averages) of the reacting variables can be assumed negligible. However, higher order conditional moments of these variables show substantial y dependence. This may lead to problems in mathematical modeling of these higher order conditional moments for predictive assessments.

Key Findings

For a complete review of our findings in this part of our work, we refer to Ref. [35–37] (please see Appendix 6). These findings are highlighted below:

• The SLDFM does not perform well in predicting the rate of mean reactant conversion in turbulent flows under the influence of finite-rate chemical reaction.

• The CMM provides a better means (in comparison with SLDFM) of predicting the compositional structure of non-equilibrium turbulent flames, but is more complicated to use.

• The CMM is effective in predicting the first order moments, but its use for capturing the role of higher order moments is very complicated. Some progress has been recently made in this regard [38], but the suggested models awaits future DNS validation.

• Neither CMM nor SLDFM are effective in dealing with non-equilibrium phenomena such as ignition and extinction. Both models can be further extended for this purpose, but we feel that higher order methods such as single-point PDF schemes perform better.

• Exothermicity may actually enhance the rate of reactant conversion in turbulent flames, even though the results of linear stability analysis indicates that mixing is reduced at elevated exothermicity levels.

7 Compressibility and Exothermicity in a Reacting Mixing Layer

In this work, results are provided of DNS of a 2D temporally developing high speed mixing layer under the influence of a second-order non-equilibrium chemical reaction of the type $A + B \rightarrow Products + Heat$. Simulations are performed with different magnitudes of the convective Mach number and with different chemical kinetics parameters for the purpose of examining the isolated effects of the compressibility and the heat released by the chemical reaction on the structure of the layer. A full compressible code is developed

and utilized, so that the coupling between mixing and chemical reaction is captured in a realistic manner. The results of numerical experiments indicate that at the initial stages of the layer's growth, the heat release results in a slight enhanced mixing, whereas at the intermediate and the final stages, it has a reverse influence. The effect of compressibility is the same in all stages of the development; increased compressibility results in a suppressed mixing and, thus, in a reduced reaction conversion rate. Mixing augmentation by heat release is due to expansion of the layer caused by the exothermicity, and mixing abation is caused by suppression of the growth of the instability modes due to increased heat release and/or compressibility. Calculations are performed with a constant rate kinetics model and an Arrhenius prototype, and the results are shown to be sensitive to the choice of the chemistry model. In the Arrhenius kinetics calculations, the increase of the temperature due to chemical reaction is substantially higher than that of the constant rate kinetics simulations. This results in a more pronounced response of the layer in all stages of the growth, *i.e.*, an increased thickening of the layer at the initial phase of growth, followed by subdued thickening at later stages.

For a complete review of our findings in this part of our work, we refer to Refs. [39,40] (please see Appendix 7).

8 DNS of Non-Circular Jets

In this work, detailed numerical experiments are conducted to study mixing and entrainment properties of the flowfield produced by non-circular turbulent jets. Simulations are conducted of jet flows originating from elliptic, rectangular, and triangular nozzles with aspect-ratios of 1:1 and 2:1. The results are compared with those of a circular jet of the same equivalent diameter to determine the relative efficiency of non-circular nozzles in mixing enhancement. Flow visualization results show that for both cornered and non-cornered jets, large scale coherent structures are formed. The shape and dynamics of these structures depend on the azimuthal variation of the curvature of the profiles at the jet exit. The triangular jets exhibit characteristics markedly different from the other jets. Coherent large scale structures in these jets are quickly masked by the small scale structures formed

at the corners. In the elliptic and the rectangular jets, the orientations of the cross-sections are modified by the axes-switching. The rectangular jet switches its axes at a stream-wise distance approximately twice that of the elliptic jet. This can be attributed to the effect of the corners. Although the square jet does not show axes-switching, it is shown that a 45° rotation of its initial profile entrains considerable free-stream fluid. The triangular jets switch their axes twice. In the isosceles triangular jet, the first axis cross-over occurs approximately twice as far downstream as that in the equilateral triangle. This is attributed to the larger aspect-ratio of the isosceles triangular jet.

The entrainment and mixing in the near field of these jets are characterized by the aspect ratio of the nozzle, the initial shape and dynamics of large scale vortical structures, and the induced mean secondary flow field of the stream-wise vortices. The isosceles triangular jet is shown to be the most efficient mixer. Analysis shows that this jet contains large scale structures, superimposed by small scale structures produced at the corners and a complicated pattern of stream-wise vortices. Non-unity aspect-ratio, sharp corners, and long flat surfaces combine to make an efficient mixing configuration. In the case of the rectangular jet, although it contains many of these features, its axes switch too far downstream to cause significant near-field mixing. Although a non-unity aspect-ratio is important for mixing enhancement, it is not sufficient for large entrainment in the near-field. The square jet ranks as the second most efficient mixer. This jet produces the most intricate network of stream-wise vortices which results in enhanced mixing. A comparison of the flow fields produced by the two triangular jets reveals that the formation of small scale structures at the corners does not have a significant influence in entraining free-stream fluid. The aspect-ratio is the primary difference between these two jets. The effect of the larger aspect-ratio of the isosceles triangular jet is to alter the vorticity dynamics in this jet as compared to the equilateral triangular jet. This results in a different stream-wise vorticity pattern which enhances the free-stream fluid entrainment in this jet.

The limiting rate of the reactant conversion in reacting jets in which the fuel is discharged to ambient oxidizer is evaluated by considering the transport of a Shvab-Zeldovich scalar variable. It is shown that the isosceles triangular jet yields the highest amount of chemical products, whereas the circular jet yields the lowest. However, the magnitudes of the cross-stream product density approaches a plateau in all the jets. The magnitudes at

this plateau are approximately the same in all the jets. With the transport of the Shvab-Zeldovich variable, a scalar core is also defined. It is shown that the 2:1 aspect-ratio triangular jet has the shortest and the rectangular jet has the longest core.

Key Findings

For a complete review of our findings in this part of our work, we refer to Ref. [41](please see Appendix 8). These findings are highlighted below:

• DNS of elliptic, rectangular and triangular jets are conducted. The axis-switching phenomenon is captured in all non-unity aspect-ratio jets and also in the equilateral triangular jet. The square jet does not show axis-switching; however, the rotation of its axes by 45° is shown to play a significant role in its entrainment characteristics. All the non-circular configurations are shown to provide more efficient mixers than does the circular jet; the isosceles triangular jet is the most efficient one. The trends observed in DNS generated results are shown to be in accord with those in laboratory data [42,43].

9 LES of Turbulent Reacting Flows by Assumed PDF Methods

In this work, *a priori* and *a posteriori* analyses are conducted for validity assessments of assumed PDF methods as potential subgrid scale (SGS) closures for LES of turbulent reacting flows. Simple non-premixed reacting systems involving an isothermal reaction of the type $F + O \rightarrow$ Product under both chemical equilibrium and non-equilibrium conditions are considered. *A priori* analyses are conducted of a homogeneous box flow, and a spatially developing planar mixing layer to investigate the performance of the *Pearson Family* of PDF's as SGS models. *A posteriori* analyses are conducted of the mixing layer using a hybrid one-equation Smagorinsky/PDF SGS closure. The Smagorinsky closure augmented by the solution of the subgrid turbulent kinetic energy equation is employed to account for hydrodynamic fluctuations, and the PDF is employed for modeling the

effects of scalar fluctuations. The implementation of the model requires the knowledge of the local values of the first two SGS moments. These are provided by additional modeled transport equations. In both *a priori* and *a posteriori* analyses, the predicted results are appraised by comparison with subgrid averaged results generated by DNS.

Key Findings

For a complete review of our findings in this part of our work, we refer to Refs. [44,45,13] (please see Appendix 9). These findings are highlighted below:

• Several different PDF methods are used for the purpose of providing subgrid closures in LES of turbulent reacting flows. Our conclusion at this point is that conventional Smagorinsky-based closures are not suitable for LES of reacting flows and we need higher closure levels for this purpose.

• Prediction of subgrid mean quantities in LES are "relatively" easy based on current technology. However, the prediction of the second order moments is not at a satisfactory level.

• The use of AMC and JET for multi-scalar mixing is difficult [4,18,46,47]. Therefore, at this point, PF [48] provides the only PDF scheme for LES of reacting turbulent flows.

10 The Inter-Layer Diffusion Model of Mixing

A mechanistic model termed the *Inter-Layer Diffusion Model* (ILDM) is developed and is implemented for the probabilistic description of scalar mixing in homogeneous turbulent flows. The essential element of the model is based on the lamellar theory of mixing in the context developed by Kerstein [49], and proposes that there are two distinct but coupled mechanisms by which the mixing process is described. These mechanisms are due to: (1) local events and (2) integrated global events. The mathematical formalities by which the closure is invoked are described and it is shown that the conditional expected diffusion of the scalar field depicted by the model depends more directly on local events. With

the manipulation of each of these two mechanisms, several families of scalar probability density functions (PDF's) are generated. These families include some of the distributions generated by other mixing closures. The ILDM provides a physical format by which these other closures can be viewed. The similarity of local events imply the similarity of the conditional expected diffusion as generated via these models. The global events manifest themselves by the evolution of the conditional expected dissipation, and also the boundedness of the composition domain. While the PDF's generated in this way are very different, their applications for modeling of mixing limited reactions do not significantly different results.

Key Findings

For a complete review of our findings in this part of our work, we refer to Refs. [50,51] (please see Appendix 10). These findings are highlighted below:

• A unique closure termed "The Inter-Layer Diffusion Model" (ILDM) is developed. This model provides a unifying theorem of *all* available turbulent mixing closures. The model also suggests that some of the conditions under which the comparisons made with DNS in previous contributions are *meaningless*. The model suggests that several mixing scenarios are possible. Thus, models such as AMC are not fully appropriate for general applications.

11 Visibility

In order to demonstrate our visibility in our previous ONR-supported research, here we shall list the awards and the noticeable achievements of the personnel involved in this program.

Research Personnel Involved

Students Graduated:

Steven H. Frankel, Ph.D. Degree in Aerospace Engineering, SUNY-Buffalo, Dissertation:

Probabilistic and Deterministic Description of Turbulent Flows with Nonpremixed Reactants, June 1993. Current position: Assistant Professor of School of Mechanical Engineering, Purdue University, West Lafayette, Indiana.

Richard S. Miller, M.S. Degree in Aerospace Engineering, SUNY-Buffalo, June 1993. Thesis: Structure of a Reacting Turbulent Mixing Layer. Current position: Ph.D. candidate at SUNY-Buffalo.

Senior Personnel Contributed:

Dr. Cyrus K. Madnia (Post Doctoral Fellow, October 1989 - August 1992). Ph.D. in Aerospace Engineering from the University of Michigan in August 1989. Dr. Madnia is currently a Research Assistant Professor at SUNY-Buffalo.

Dr. Tail-Lun Jiang (Post Doctoral Fellow, September 1990 - September 1991). Ph.D. in Mechanical Engineering from SUNY at Stony Brook in August 1990.

Current Students Involved in ONR Research:

(1) Mr. Virgil Adumitroaie, Ph.D. candidate, Teaching Assistant, (2) Mr. Farhad A. Jaberi, Ph.D. candidate, Research Assistant, (3) Mr. Richard S. Miller, Ph.D. candidate, Research Assistant, (4) Mr. George Sabini, M.S. candidate, Teaching Assistant, (5) Mr. Scott W. Foster, Undergraduate.

Awards and Honors

Promotions of the PI:

Promoted to Professor, Department of Mechanical and Aerospace Engineering, State University of New York at Buffalo, Buffalo, New York, September 1993.

Promoted to Associate Professor, Department of Mechanical and Aerospace Engineering, SUNY at Buffalo, September 1991.

Appointed to Director, Computational Fluid Dynamics Laboratory, School of Engineering and Applied Sciences, SUNY at Buffalo, September 1991.

b.2. Awards to the PI:

Presidential Faculty Fellowship, Awarded by President George Bush, The White House (1992-1995).

Research profile, interests and achievements published in several newspapers and magazines in U.S., Canada, Europe and Asia. Also interviewed in several radio broadcasts.

Biographical data recorded in *American Men and Women of Science*, 18th edition (1992-1993).

Awards to Students:

Mr. Richard S. Miller, First Prize winner at the Graduate Technical Paper Competition of AIAA Northeast Regional Student Conference. Title of paper: "The Manifestation of Eddy Shocklets and Laminar Diffusion Flamelets in a Shear Layer," April 1992.

Mr. Steven H. Frankel, Second Prize winner at the Graduate Technical Paper Competition of AIAA Northeast Regional Student Conference. Title of paper: "Probabilistic and Deterministic Description of Turbulent Flows with Nonpremixed Reactants," April 1992.

Mr. Richard S. Miller, winner of *Abe M. Zarem Award for Distinguished Achievement in Aeronautics*. This award is in relation to Mr. Miller's AIAA paper entitled: "The Manifestation of Eddy Shocklets and Laminar Diffusion Flamelets in a Shear Layer," 1993.

References

[1] Libby, P. A. and Williams, F. A., editors, *Turbulent Reacting Flows*, Academic Press, London, UK, 1994, in press.

[2] Kraichnan, R. H., Closures for Probability Distributions, *Bull. Amer. Phys. Soc.*, 34:2298 (1989).

[3] Chen, H., Chen, S., and Kraichnan, R. H., Probability Distribution of a Stochastically Advected Scalar Field, *Phys. Rev. Lett.*, 63(24):2657–2660 (1989).

[4] Pope, S. B., Mapping Closures for Turbulent Mixing and Reaction, *Theoret. Comput. Fluid Dynamics*, 2:255–270 (1991).

[5] Abramowitz, M. and Stegun, I. A., *Handbook of Mathematical Functions and Formulas, Graphs, and Mathematical Tables*, Government Printing Office, Washington, D.C., 1972.

[6] Toor, H. L., Mass Transfer in Dilute Turbulent and Nonturbulent Systems with Rapid Irreversible Reactions and Equal Diffusivities, *AIChE J.*, 8:70–78 (1962).

[7] Toor, H. L., The Non-Premixed Reaction: $A + B \rightarrow Products$, in Brodkey, R. S., editor, *Turbulence in Mixing Operations*, pp. 123–166, Academic Press, New York, NY, 1975.

[8] Hill, J. C., Homogeneous Turbulent Mixing with Chemical Reaction, *Ann. Rev. Fluid Mech.*, 8:135–161 (1976).

[9] Dutta, A. and Tarbell, J. M., Closure Models for Turbulent Reacting Flows, *AIChE J.*, 35(12):2013–2027 (1989).

[10] Frankel, S. H., Madnia, C. K., and Givi, P., Comparative Assessment of Closures for Turbulent Reacting Flows, *AIChE J.*, 39(5):899–903 (1993).

[11] Madnia, C. K., Frankel, S. H., and Givi, P., Reactant Conversion in Homogeneous Turbulence: Mathematical Modeling, Computational Validations and Practical Applications, *Theoret. Comput. Fluid Dynamics*, 4:79–93 (1992).

[12] Madnia, C. K., Frankel, S. H., and Givi, P., Direct Numerical Simulations of the Unmixedness in Homogeneous Reacting Turbulence, *Chem. Eng. Comm.*, 109:19–29 (1991).

[13] Frankel, S. H., Probabilistic and Deterministic Description of Turbulent Flows with Nonpremixed Reactants, Ph.D. Thesis, Department of Mechanical and Aerospace Engineering, State University of New York at Buffalo, Buffalo, NY, 1993.

[14] Johnson, N. L., Systems of Frequency Curves Generated by Methods of Translation, *Biometrika*, 36:149–176 (1949).

[15] Edgeworth, F. Y., On the Representation of Statistical Frequency by a Series, *Journal of the Royal Statistical Society, Series A.*, 70:102–106 (1907).

[16] Pearson, K., Contributions to the Mathematical Theory of Evolution: II. Skew Variations in Homogeneous Material, *Philos. Trans. of the Royal Soc. of London, Series A.*, 186:343–414 (1895).

[17] Johnson, N. L. and Kotz, S., *Distributions in Statistics: Continious Multivariate Distributions*, John Wiley and Sons, New York, NY, 1972.

[18] Miller, R. S., Frankel, S. H., Madnia, C. K., and Givi, P., Johnson-Edgeworth Translation for Probability Modeling of Binary Mixing in Turbulent Flows, *Combust. Sci. and Tech.*, 91(1-3):21–52 (1993).

[19] Jiang, T.-L., Gao, F., and Givi, P., Binary and Trinary Scalar Mixing by Fickian Diffusion-Some Mapping Closure Results, *Phys. Fluids A*, 4(5):1028–1035 (1992).

[20] Orszag, S. A., Lectures on the Statistical Theory of Turbulence, in *Fluid Dynamics*, pp. 237–374, Gordon and Breach Sciene Publishers, 1977.

[21] Lesieur, M., *Turbulence in Fluids*, Kluwer Academic Publishers, Boston, MA, 1990, Second Revised Edition.

[22] Ajmera, P. V., Singh, M., and Toor, H. L., Reactive Mixing in Turbulent Gases, *Chem. Eng. Comm.*, 2:115 (1976).

[23] Brodkey, R. S., Fundamental of Turbulent Motion, *Chem. Eng. Comm.*, 8:1–23 (1981).

[24] Frankel, S. H., Jiang, T.-L., and Givi, P., Modeling of Isotropic Reacting Turbulence by a Hybrid Mapping-EDQNM Closure, *AIChE J.*, 38(4):535–543 (1992).

[25] Boris, J. P. and Book, D. L., Solution of the Continuity Equations by the Method of Flux Corrected Transport, in *Methods in Computational Physics*, pp. 85–129, Academic Press, New York, NY, 1976.

[26] Oran, E. S. and Boris, J. P., *Numerical Simulations of Reactive Flows*, Elsevier Publishing Company, Washington, D.C., 1987.

[27] Williams, F. A., Recent Advances in Theoretical Description of Turbulent Diffusion Flames, in Brodkey, R. S., editor, *Turbulence in Mixing Operations*, pp. 189–209, Academic Press, New York, NY, 1975.

[28] Peters, N., Laminar Diffusion Flamelet Models In Non-Premixed Turbulent Combustion, *Prog. Energy Combust. Sci.*, 10:319–339 (1984).

[29] Peters, N., Laminar Flamelet Concepts in Turbulent Combustion, in *Proceedings of 21st Symp. (Int.) on Combustion*, pp. 1231–1250, The Combustion Institute, Pittsburgh, PA, 1986.

[30] Peters, N. and Williams, F. A., Liftoff Characteristics of Turbulent Jet Diffusion Flames, *AIAA J.*, 21:423–429 (1983).

[31] Williams, F. A., Structure of Flamelets in Turbulent Reacting Flows and Influences of Combustion on Turbulence Fields, in Borghi, R. and Murthy, S. N. B., editors, *Turbulent Reactive Flows, Lecture Notes in Engineering*, Vol. 40, pp. 195–212, Springer-Verlag, New York, NY, 1989.

[32] Bilger, R. W., Conditional Moment Closure for Turbulent Reacting Flow, *Phys. Fluids A.*, 5(2):436–444 (1993).

[33] Smith, N. S., Bilger, R. W., and Chen, J.-Y., Modeling of Non-Premixed Hydrogen Jet Flames Using a Conditional Moment Closure Method, in *Proceedings of 24th Symp. (Int.) on Combustion*, pp. 271–278, The Combustion Institute, Pittsburgh, PA, 1992.

[34] Klimenko, A. Y., Multicomponent Diffusion of Various Mixtures in Turbulent Flow, *Fluid Dynamics*, 25:327–334 (1990).

[35] Miller, R. S., Madnia, C. K., and Givi, P., Structure of a Turbulent Reacting Mixing Layer, *Combust. Sci. and Tech.*, (1993), in press.

[36] Miller, R. S., The Manifestation of Eddy Shocklets and Laminar Diffusion Flamelets in a Shear Layer, AIAA Paper 93-0011, 1993.

[37] Miller, R. S., Structure of a Turbulent Reacting Mixing Layer, M.S. Thesis, Department of Mechanical and Aerospace Engineering, State University of New York at Buffalo, Buffalo, NY, 1993.

[38] Lin, J. D. and Bilger, R. W., Measurement and Prediction of the Conditional Variance in a Turbulent Reactive-Scalar Mixing Layer, *Phys. Fluids A.*, 5(12):3255–3264 (1993).

[39] Givi, P., Madnia, C. K., Steinberger, C. J., Carpenter, M. H., and Drummond, J. P., Effects of Compressibility and Heat Release in a High Speed Reacting Mixing Layer, *Combust. Sci. and Tech.*, 78:33–68 (1991).

[40] Drummond, J. P. and Givi, P., Suppression and Enhancement of Mixing in High-Speed Reacting Flow Fields, in Hussaini, M. Y., Buckmaster, J. D., Jackson, T. L., and Kumar, A., editors, *Combustion in High-Speed Flows*, Kluwer Academic Publishers, The Netherlands, 1994, in press.

[41] Miller, R. S., Madnia, C. K., and Givi, P., Near Field Entrainment and Mixing in Non-Circular Jets, *Bull. Amer. Phys. Soc.*, 38(12):2281 (1993), Submitted to *Computers & Fluids*.

[42] Gutmark, E., Schadow, K. C., Parr, D. M., Harris, C. K., and Wilson, K. J., The Mean and Turbulent Structure of Non-Circular Jets, AIAA Paper 85-0543, 1985.

[43] Gutmark, E., Schadow, K. C., Parr, T. P., Hanson-Parr, M., D., and Wilson, K. J., Noncircular Jets in Combustion Systems, *Experiments in Fluids*, 7:248–258 (1989).

[44] Madnia, C. K. and Givi, P., Direct Numerical Simulation and Large Edddy Simulation of Reacting Homogeneous Turbulence, in Galperin, B. and Orszag, S. A., editors, *Large Eddy Simulations of Complex Engineering and Geophysical Flows*, chapter 15, pp. 315–346, Cambridge University Press, Cambridge, U.K., 1993.

[45] Frankel, S. H., Adumitroaie, V., Madnia, C. K., and Givi, P., Large Eddy Simulations of Turbulent Reacting Flows by Assumed PDF Methods, in Ragab, S. A. and Piomelli, U., editors, *Engineering Applications of Large Eddy Simulations, FED-Vol. 162*, pp. 81–101, ASME, 1993.

[46] Gao, F. and O'Brien, E. E., A Mapping Closure for Multispecies Fickian Diffusion, *Phys. Fluids A*, 3(5):956–959 (1991).

[47] Johnson, N. L., Bivariate Distributions Based on Simple Translation Systems, *Biometrika*, 36:297–304 (1949).

[48] Johnson, M. E., *Multivariate Statistical Simulation*, John Wiley and Sons, New York, NY, 1987.

[49] Kerstein, A. R., Flapping Model of Scalar Mixing in Turbulence, *Phys. Fluids A*, 27(12):2819–2827 (1991).

[50] Jaberi, F. A. and Givi, P., Inter-Layer Diffusion Model of Scalar Mixing in Homogeneous turbulence, *Bull. Amer. Phys. Soc.*, 38(12):2229 (1993), Submitted to *Phys. Fluids A*.

[51] Jaberi, F. A. and Givi, P., On the Lamellar Description of Mixing in Turbulent Flows, in Hussaini, M. Y., , Jackson, T. L., and Kumar, A., editors, *Proceedings of ICASE Workshop on Transition, Turbulence and Combustion*, Kluwer Academic Publishers, The Netherlands, 1994, in press.

APPENDIX 1

Comparative Assessment of Closures for Turbulent Reacting Flows

Reprinted from AICHE JOURNAL, MAY 1993

Comparative Assessment of Closures for Turbulent Reacting Flows

S. H. Frankel, C. K. Madnia, and P. Givi
Dept. of Mechanical and Aerospace Engineering, State University of New York, Buffalo, NY 14260

In a recent article, Dutta and Tarbell (1989) made a comparative study of several turbulence closures for predicting the mean rate of reactant conversion in a chemical reaction of the type $A+B\rightarrow$ products in homogeneous turbulent flows. In this work, we use recent developments in the approach based on the probability density function (PDF) method for treating the problem considered by Dutta and Tarbell (1989). With this method, we propose a simple algebraic relation for predicting the limiting rate of mean reactant conversion. The PDF model is based on the amplitude mapping closure (AMC) of Kraichnan (Kraichnan, 1989; Chen et al., 1989), whose superiority has been demonstrated in a number of validation studies (Pope, 1991; Gao, 1991; Frankel et al., 1992, Chen et al., 1989; Madnia et al., 1991b; Madnia et al., 1992). In accordance with the problem discussed by Dutta and Tarbell (1989), we consider a stoichiometric mixture with initially segregated reactants. This is convenient for expressing the final results in a simple algebraic form. However, it is understood that the AMC can be employed for modeling of nonequilibrium chemically reacting flows under arbitrary initial conditions (Pope, 1991).

For comparison, in addition to the closure of Toor (1962) and the three-environment (3E) model of Dutta and Tarbell (1989), several other closures are also considered. These are the PDF methods based on the generalized coalescence/dispersion (C/D) models and those based on "assumed" frequencies. For the C/D models, the closures of Curl (1963), and Janicka et al. (1979) are examined. The assumed distributions are based on the beta density of the first kind (Pearson, 1895) and the Logit-normal density (Johnson, 1949a). The applicability of these assumed densities for the problem under consideration has been ascertained by Madnia et al. (1991a) and Miller et al. (1993). Finally, to assess the performance of the models, the results predicted by all the closures are compared with those generated by direct numerical simulations (DNS). These simulations have proven very effective in validation studies of turbulent reacting flows (Eswaran and Pope, 1988; Givi and McMurtry, 1988; Givi, 1989; Leonard and Hill, 1991) and provide a useful tool in model assessments of the type pursued here.

Formulations and Model Presentation

With the assumption of an infinitely fast chemistry, all the pertinent statistics of the reacting field are related to those of an appropriate conserved scalar variable, hereby denoted by $\mathcal{Z}$ (Hawthorne et al., 1949; Bilger, 1980). Under this assumption, in a stoichiometric mixture, the single-point PDF of the reacting scalar is related to that of the conserved scalar by (Bilger, 1980; Kosaly and Givi, 1987):

$$\mathcal{P}_A(\psi,t)=\frac{1}{2}\mathcal{P}_{\mathcal{Z}}\left(\frac{\psi+1}{2},t\right)+\frac{1}{2}\delta(\psi),\quad 1>\psi>0. \tag{1}$$

Here, δ denotes the delta function. Therefore, based on Eq. 1, if the PDF of the conserved scalar is known, all the statistical information regarding the reacting scalars A and B is available.

C/D Closures

The C/D models consist of PDF transport equations, in which the effects of molecular mixing are modeled in terms of a particle-pair interaction process. The most general form of the model can be expressed by the evolution equation (Pope, 1982; Kosaly and Givi, 1987; Dutta and Tarbell, 1989):

$$\frac{\partial\mathcal{P}(\psi,t)}{\partial t}=-2\beta\omega\mathcal{P}(\psi,t)+2\beta\omega\int_{-\infty}^{\infty}\int_{-\infty}^{\infty}d\psi'\,d\psi''\,\mathcal{P}(\psi',t)\mathcal{P}(\psi'',t)\times\int_{-\infty}^{\infty}d\alpha\mathcal{G}(\alpha)\delta\left[\psi-(1-\alpha)\psi'-\frac{1}{2}\alpha(\psi'+\psi'')\right]. \tag{2}$$

In this equation, the random variable $\alpha\in[0,1]$ and the kernel $\mathcal{G}(\alpha)$ controls the extent of mixing. The parameter β is the controlling factor which yields the same variance for all members of the C/D family and ω is the mixing frequency (Pope, 1982). Different C/D closures are obtained by different choices for the function $\mathcal{G}(\alpha)$. This function is nonzero, nonnegative and normalized to unity within $\alpha\in[0,1]$. Some of the more widely utilized members of the C/D family are the models of

Curl (1963) and Janicka et al. (1979), and the LMSE closure of O'Brien (1980). These closures imply, respectively, $\mathcal{Q}(\alpha)=\delta(\alpha-1)$, $\mathcal{Q}(\alpha)=1$, and $\mathcal{Q}(\alpha)=\mathrm{Lim}_{\epsilon\to 0}\delta(\alpha-\epsilon)$. For the problem under consideration, the results obtained from the LMSE model are identical to those based on Toor's hypothesis (Kosaly and Givi, 1987).

With a combination of Eqs. 1 and 2, the mean reactant conversion rate is determined from the knowledge of $\mathcal{P}_A(\psi)$ [or $\mathcal{P}_B(\psi)$]. The numerical solution of the C/D transport equation (Eq. 2) can be obtained by Monte-Carlo methods (Pope, 1981).

Mapping Closure

The amplitude mapping closure (AMC) involves the mapping of the scalar field of interest to a Gaussian reference field. The knowledge of this mapping allows determination of the scalar PDF (Chen et al., 1989; Pope, 1991). For the binary problem under consideration here, the solution for the mapping function has been obtained by Pope (1991) and the resulting PDF is of the form:

$$\mathcal{P}(\psi)=\frac{\gamma}{\sqrt{2}}\exp\left\{-\left[\frac{\gamma^2}{2}-1\right][\mathrm{erf}^{-1}(2\psi-1)]^2\right\}, \tag{3}$$

where the parameter γ depends on the missing two-point information and is not known *a priori* in the context of a single-point description. It is convenient to relate this parameter to the variance of the conserved scalar. This relation has been established by Jiang et al. (1992):

$$I_s=\frac{\sigma^2(t)}{\sigma^2(0)}=\frac{2}{\pi}\arctan\left(\frac{2}{\gamma\sqrt{\gamma^2+4}}\right), \tag{4}$$

where I_s is known as the "intensity of segregation" (Brodkey, 1975). The parameter γ can also be related to the ensemble-mean value of the reacting scalar. This relation is obtained by substituting Eq. 3 into Eq. 1. After significant algebraic operations, the final results yield (Frankel, 1993):

$$\frac{\langle A\rangle(t)}{\langle A\rangle(0)}=1-\frac{2\arctan\left(\frac{\gamma}{\sqrt{2}}\right)}{\pi} \tag{5}$$

Now, with the establishment of Eqs. 4-5, the mean fractional conversion can be expressed in terms of I_s:

$$\mathcal{F}=1-\frac{\langle A\rangle(t)}{\langle A\rangle(0)}=1-\frac{2}{\pi}\arcsin\left(\sqrt{\sin\left[\frac{\pi I_s}{2}\right]}\right) \tag{6}$$

Assumed Frequencies

Miller et al. (1993) have recently shown that for the binary mixing problem considered here, the AMC can be viewed as a member of the general family of distributions generated by the Johnson-Edgeworth transformation (JET) (Johnson, 1949a; Edgeworth, 1907). With this transformation, alternative frequencies can be developed for the modeling of turbulent mixing. One such frequency that has proven effective is the "Logit-normal" distribution (Miller et al., 1993):

$$\mathcal{P}(\psi)=\frac{\Delta}{\sqrt{2\pi}\psi(1-\psi)}\exp\left\{-\left[\frac{\Delta^2}{2}\log^2\left(\frac{\psi}{1-\psi}\right)\right]\right\}, \tag{7}$$

where Δ, analogous to γ in the AMC, is not known *a priori*. For this PDF, neither the variance nor the reactant decay can be determined analytically, and their evaluation is possible solely by numerical means (Johnson, 1949a).

The similarity between the Logit-normal distribution and the family of Pearson (1895) frequencies suggests the use of the beta density of the first kind as a potential assumed PDF for the modeling of the mixing phenomena. For a random scalar variable within [0,1], this density is parameterized by its first two moments (Casella and Berger, 1990):

$$\mathcal{P}(\psi)=\psi^{\beta_1-1}(1-\psi)^{\beta_2-1}\frac{\Gamma(\beta_1+\beta_2)}{\Gamma(\beta_1)\Gamma(\beta_2)}, \tag{8}$$

where Γ is the Gamma function (Abramowitz and Stegun, 1972), and β_1 and β_2 are determined from the first two moments of the random variable. With a combination of this equation and Eq. 1, the mean fractional conversion can be obtained analytically. Following the same procedure as that for the AMC, the final result after some manipulations can be expressed as:

$$\mathcal{F}=1-\frac{\Gamma\left(\frac{1}{2I_s}\right)}{\sqrt{\pi}\Gamma\left(\frac{1}{2I_s}+\frac{1}{2}\right)} \tag{9}$$

Comparisons

The relations for the mean fractional conversion obtained by the models described above are compared with those obtained by employing the 3E model of Dutta and Tarbell (1989) and Tarbell (1992):

$$\mathcal{F}=\frac{1-I_s}{1+I_s}, \tag{10}$$

and that based on Toor's hypothesis (Toor, 1962, 1975):

$$\mathcal{F}=1-\sqrt{I_s}. \tag{11}$$

To examine the performance of the models, the predicted results via all the closures are compared against DNS data. The DNS procedure is similar to that of previous simulations of this type (Givi and McMurtry, 1988; Madnia and Givi, 1993). The subject of the present DNS is the three-dimensional periodic homogeneous box flow under the influence of a binary reaction of the type described above. The initial species field is assumed to be composed of out-of-phase square waves for the two reactants A and B. The computational package is based on the modification of a spectral-collocation procedure using Fourier basis functions developed by Erlebacher et al. (1987, 1990a, 1990b). The hydrodynamic field is assumed isotropic and is initialized in a similar manner to that of Erlebacher et al. (1990a). The turbulent field is of a decaying nature in that

there is no artificial forcing mechanism to feed energy to low wave numbers. The code is capable of simulating flows with different levels of compressibility (Erlebacher et al., 1990b; Hussaini et al., 1990). Here, only the results obtained for a low compressible case are discussed, since most previous analyses of plug-flow reactors have dealt primarily with incompressible flows (Toor, 1975; Hill, 1976; Brodkey, 1981; Leonard and Hill, 1991). The resolution consists of 96 collocation points in each direction. Therefore, at each time step 96^3 is the sample size for statistical analyses. This resolution allows simulations with a Reynolds number (based on the Taylor microscale) of $Re_\lambda \approx 41$. The value of the molecular Schmidt number is set equal to unity.

The PDFs generated by the AMC, JET, and the beta density are somewhat similar. For the binary mixing problem, all these models are capable of predicting the PDF evolution from an initially double delta state (segregated reactants) to an asymptotic Gaussian-like distribution near the mean at small variances. This behavior cannot be predicted by any of the other closures considered here.

Figure 1 shows the temporal variation of the fractional conversion for these three models along with the DNS data. All these closures yield almost identical results and exhibit good agreement with the DNS data during all stages of the mixing process. In light of this, to compare with the other closures, only the AMC is considered, as shown in Figure 2. At large times, the profiles are bounded above and below by the 3E model and the Toor closure, respectively. Initially, the results via the 3E closure are very close to those obtained by AMC. At all times, the results generated by the numerical integration of the C/D models of Curl (1963) and Janicka et al. (1979) overpredict the DNS data more than the simple expression generated by the AMC. Finally, as indicated before, the results obtained by LMSE are identical to those based on Toor's hypothesis. These comparisons indicate that the AMC, the beta density, and the Logit-Normal distribution yield the best overall behavior in predicting the rate of reactant conversion in accordance with the DNS data. This agreement follows from the compatibility of the model PDFs with those of the DNS, at least for the case of binary mixing considered here. Furthermore, a nice feature of these models is the explicit form of the final equations expressing these statistical quantities. It is noted that explicit analytical relations can be obtained only for the AMC and the beta density. Therefore, in the absence of better alternatives Eqs. 6 and 9 are recommended for effective and practical modeling of unpremixed plug-flow reactors.

Despite the favorable features of our simple mathematical expressions, the ramifications of the assumptions made in deriving these expressions must be emphasized. First, due to the assumption of infinitely fast chemistry, only the limiting rate of reactant conversion is obtained. The extensions to finite rate chemistry, reversible reactions, and multistep kinetics systems require numerical integration of the PDF. For these cases, the implementation of AMC for the binary case is straightforward, since it provides a closure for the joint PDFs of the scalar quantities (Pope, 1991). However, the validity of a multivariate beta (usually known as the "Dirichlet" (Johnson and Kotz, 1972; Wilks, 1962)) distribution and multivariate forms of the JET generated frequencies (Johnson, 1949b) cannot be guaranteed for general applications. Secondly, the simple formulas presented here are valid only for initially segregated reactants in stoichiometric proportion. This condition is compatible with the majority of previous works on nonpremixed plug-flow reactors (Toor, 1975; Brodkey, 1981; Leonard and Hill, 1988; Kosaly and Givi, 1987; Givi and McMurtry, 1988; Givi, 1989). The AMC and the beta density can be used for modeling nonstoichiometric mixtures, but the final results can be evaluated only by numerical means. For more complicated initial conditions, the use of beta and JET generated frequencies cannot be justified, while the AMC can be utilized in conjunction with appropriate numerical algorithms (Pope, 1991; Valiño et al., 1991). Finally, in the context of a single-point PDF formulation, there is no information pertaining to the evolution of the relevant turbulent length scales. Therefore, the final expressions can be only presented in terms of I, or other related physical parameters (such as, σ^2, γ, and Δ). In this context, these parameters must be provided by external means, including experimental data and turbulence models (Frankel et al., 1992). Also, in nonequilibrium reacting systems, the segregation parameter should be defined to include

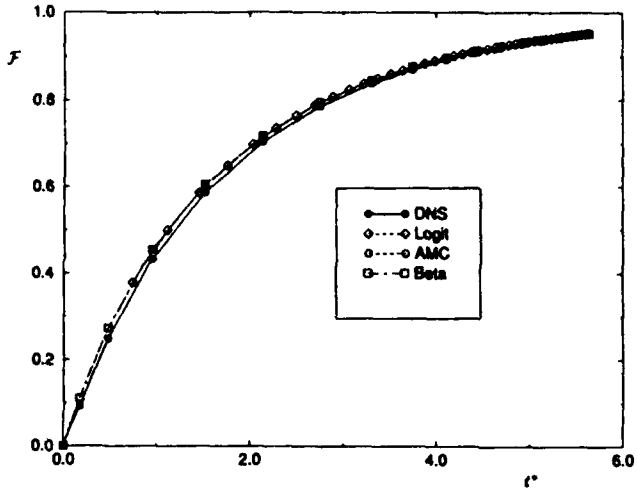

Figure 1. Fractional conversion vs. normalized time.

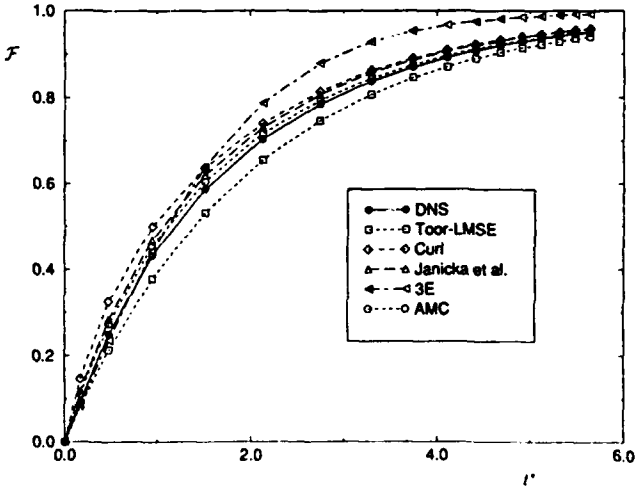

Figure 2. Fractional conversion vs. normalized time.

the information pertaining to the length-scale evolution of the reacting scalar.

In spite of these assumptions, it is very encouraging to have physically plausible algebraic relations for direct and accurate estimate of the reactant conversion rate in plug-flow reactors. Because of the simplicity of our final results, these expressions are recommended for routine and economical engineering predictions in nonpremixed binary reacting systems such as those in batch mixers.

Acknowledgment

The authors are indebted to John Tarbell for pointing out the appropriate form of the 3E closure considered in this study. The authors are also grateful to Richard Miller for many useful discussions. This work is part of a research effort sponsored by the Office of Naval Research under grant N00014-90-J-4013. Acknowledgment is also made to the Donors of the Petroleum Research Funds administrated by the American Chemical Society for partial support of this work under grant ACS-PRF#25129-AC7E, 6. The computational support is provided by the NCSA facilities at the University of Illinois.

Notation

A, B = reactant concentration
$\mathcal{G}$ = kernel of the C/D closure
I_s = intensity of segregation
$\mathfrak{I}$ = conserved scalar variable
$\mathfrak{F}$ = fractional conversion
t = time
t^* = normalized time $= -\ln[\sigma^2(t)/\sigma^2(0)]$

Greek letters

δ = Delta function
Δ = parameter of Logit-normal distribution
γ = parameter of the AMC closure
Γ = gamma function
σ^2 = variance of the conserved scalar variable
ω = frequency of mixing

Subscripts

0 = time zero (inlet of plug-flow reactor)

Other symbol

$\langle\ \rangle$ = ensemble average

Literature Cited

Abramowitz, M., and I. A. Stegun, *Handbook of Mathematical Functions and Formulas, Graphs, and Mathematical Tables*, Government Printing Office, Washington, DC (1972).

Bilger, R. W., "Turbulent Flows with Nonpremixed Reactants," *Turbulent Reacting Flows*, P. A. Libby and F. A. Williams, eds., Chap. 3, p. 65, Springer-Verlag, Heidelberg (1980).

Brodkey, R. S., ed., *Turbulence in Mixing Operation*, Academic Press, New York (1975).

Brodkey, R. S., "Fundamental of Turbulent Motion," *Chem. Eng. Comm.*, **8**, 1 (1981).

Casella, G., and R. L. Berger, *Statistical Inference*, Brooks/Cole Publishing Co., Belmont, CA (1990).

Chen, H., S. Chen, and R. H. Kraichnan, "Probability Distribution of a Stochastically Advected Scalar Field," *Phys. Rev. Lett.*, **63**, 2657 (1989).

Curl, R. L., "Dispersed Phase Mixing: I. Theory and Effects in Simple Reactors," *AIChE J.*, **9**, 175 (1963).

Dutta, A., and J. M. Tarbell, "Closure Models for Turbulent Reacting Flows," *AIChE J.*, **35**, 2013 (1989).

Edgeworth, F. Y., "On the Representation of Statistical Frequency by a Series," *J. of the Roy. Stat. Soc.*, Ser. A, **70**, 102 (1907).

Erlebacher, G., M. Y. Hussaini, C. G. Speziale, and T. A. Zang, "Toward the Large Eddy Simulation of Compressible Turbulent Flows," ICASE Report 87-20, NASA Langley Research Center, Hampton, VA, also available as NASA CR 178273 (1987).

Erlebacher, G., M. Y. Hussaini, C. G. Speziale, and T. A. Zang, "Toward the Large Eddy Simulation of Compressible Turbulent Flows," ICASE Report 90-76, NASA Langley Research Center, Hampton, VA, also available as NASA CR 187460 (1990).

Erlebacher, G., M. Y. Hussaini, H. O. Kreiss, and S. Sarkar, "The Analysis and Simulation of Compressible Turbulence," *Theoret. Comput. Fluid Dynamics*, **2**, 73 (1990).

Eswaran, V., and S. B. Pope, "Direct Numerical Simulations of the Turbulent Mixing of a Passive Scalar," *Phys. Fluids*, **31**, 506 (1988).

Frankel, S. H., T.-L. Jiang, and P. Givi, "Modeling of Isotropic Reacting Turbulence by a Hybrid Mapping-EDQNM Closure," *AIChE J.*, **38**, 535 (1992).

Frankel, S. H., "Probabilistic and Deterministic Description of Turbulent Flows with Nonpremixed Reactants," PhD Thesis, Dept. of Mechanical and Aerospace Engineering, State University of New York at Buffalo (1993).

Gao, F., "An Analytical Solution for the Scalar Probability Density Function in Homogeneous Turbulence," *Phys. Fluids A*, **3**, 511 (1991).

Givi, P., and P. A. McMurtry, "Nonpremixed Reaction in Homogeneous Turbulence: Direct Numerical Simulations," *AIChE J.*, **34**, 1039 (1988).

Givi, P., "Model Free Simulations of Turbulent Reactive Flows," *Prog. Energy Combust. Sci.*, **15**, 1 (1989).

Hawthorne, W. R., D. S. Wedell, and H. C. Hottel, "Mixing and Combustion in Turbulent Gas Jets," *Symp. on Combustion, Flames and Explosion Phenomena*, p. 266, The Combustion Institute, Pittsburgh (1949).

Hill, J. C., "Homogeneous Turbulent Mixing with Chemical Reaction," *Ann. Rev. Fluid Mech.*, **8**, 135 (1976).

Hussaini, M. Y., C. G. Speziale, and T. A. Zang, "The Potential and Limitations of Direct and Large Eddy Simulations," *Whither Turbulence? Turbulence at the Crossroads*, J. L. Lumley, ed., *Lecture Notes in Physics*, Vol. 357, p. 354, Springer (1990).

Janicka, J., W. Kolbe, and W. Kollmann, "Closure of the Transport Equation for the Probability Density Function of Turbulent Scalar Field," *J. Nonequil. Thermodyn.*, **4**, 47 (1979).

Jiang, T.-L., P. Givi, and F. Gao, "Binary and Trinary Scalar Mixing by Fickian Diffusion-Some Mapping Closure Results," *Phys. Fluids A*, **4**, 1028 (1992).

Johnson, N. L., and S. Kotz, *Distributions in Statistics: Continuous Multivariate Distributions*, Wiley, New York (1972).

Johnson, N. L., "Systems of Frequency Curves Generated by Methods of Translation," *Biometrika*, **36**, 149 (1949a).

Johnson, N. L., "Bivariate Distributions Based on Simple Translation Systems," *Biometrika*, **36**, 297 (1949b).

Kosaly, G., and P. Givi, "Modeling of Turbulent Molecular Mixing," *Combust. Flame*, **70**, 101 (1987).

Kraichnan, R. H., "Closures for Probability Distributions," *Bull. Amer. Phys. Soc.*, **34**, 2298 (1989).

Leonard, A. D., and J. C. Hill, "Direct Numerical Simulation of Turbulent Flows with Chemical Reaction," *J. of Scientific Comput.*, **3**, 25 (1988).

Leonard, A. D., and J. C. Hill, "Scalar Dissipation and Mixing in Turbulent Reacting Flows," *Phys. Fluids A.*, **3**, 1286 (1991).

Madnia, C. K., and P. Givi, "On DNS and LES of Homogeneous Reacting Turbulence," *Large Eddy Simulations of Complex Engineering and Geophysical Flows*, B. Galperin and S. A. Orszag, eds., Cambridge University Press, Cambridge, U.K., in press (1993).

Madnia, C. K., S. H. Frankel, and P. Givi, "Direct Numerical Simulations of the Unmixedness in Homogeneous Reacting Turbulence," *Chem. Eng. Comm.*, **109**, 19 (1991a).

Madnia, C. K., S. H. Frankel, and P. Givi, "Mathematical Modeling of the Reactant Conversion Rate by Single-Point PDF Methods," *Proc. Technical Meeting of the Combustion Institute*, Ithaca, NY (1991b).

Madnia, C. K., S. H. Frankel, and P. Givi, "Reactant Conversion in Homogeneous Turbulence: Mathematical Modeling, Computa-

tional Validations and Practical Applications," *Theoret. Comput. Fluid Dynamics*, **4**, 79 (1992).
Miller, R. S., S. H. Frankel, C. K. Madnia, and P. Givi, "Johnson-Edgeworth Translation for Probability Modeling of Binary Scalar Mixing in Turbulent Flows," *Combust. Sci. and Tech.*, **91**, 21 (1993).
O'Brien, E. E., "The Probability Density Function (PDF) Approach to Reacting Turbulent Flows," *Turbulent Reacting Flows*, P. A. Libby and F. A. Williams, eds., Chap. 5, p. 185, Springer-Verlag, Heidelberg (1980).
Pearson, K., "Contributions to the Mathematical Theory of Evolution: II. Skew Variations in Homogeneous Material," *Philos. Trans. of the Royal Soc. of London*, Ser. A, **186**, 343 (1895).
Pope, S. B., "A Monte Carlo Method for the pdf Equations of Turbulent Reactive Flow," *Combust. Sci. and Tech.*, **25**, 159 (1981).
Pope, S. B., "An Improved Turbulent Mixing Model," *Combust. Sci. and Tech.*, **28**, 131 (1982).
Pope, S. B., "Mapping Closures for Turbulent Mixing and Reaction," *Theoret. Comput. Fluid Dynamics*, **2**, 255 (1991).
Tarbell, J. M., private communication (1992).
Toor, H. L., "Mass Transfer in Dilute Turbulent and Nonturbulent Systems with Rapid Irreversible Reactions and Equal Diffusivities," *AIChE J.*, **8**, 70 (1962).
Toor, H. L., "The Non-premixed Reaction: $A + B \rightarrow Products$," *Turbulence in Mixing Operations*, R. S. Brodkey, ed., p. 123, Academic Press, New York (1975).
Valiño, L., J. Ros, and C. Dopazo, "Monte Carlo Implementation and Analytic Solution of an Inert-Scalar Turbulent-Mixing Test Problem Using a Mapping Closure," *Phys. Fluids A*, **3**, 2191 (1991).
Wilks, S. S., *Mathematical Statistics*, 2nd ed., Wiley, New York (1962).

Manuscript received June 22, 1992, and revision received Oct. 13, 1992.

APPENDIX 2

Reactant Conversion in Homogeneous Turbulence

Theoret. Comput. Fluid Dynamics (1992) 4: 79-93

Theoretical and Computational Fluid Dynamics

Reactant Conversion in Homogeneous Turbulence: Mathematical Modeling, Computational Validations, and Practical Applications[1]

C.K. Madnia, S.H. Frankel, and P. Givi

Department of Mechanical and Aerospace Engineering, State University of New York, Buffalo, NY 14260, U.S.A.

Communicated by M.Y. Hussaini

Received 24 March 1992 and accepted 27 July 1992

Abstract. Closed form analytical expressions are obtained for predicting the limiting rate of mean reactant conversion in homogeneous turbulent flows under the influence of a binary reaction of the type $F + rO \rightarrow (1 + r)$ *Product*. These relations are obtained by means of a single-point Probability Density Function (PDF) method based on the *Amplitude Mapping Closure* (Kraichnan, 1989; Chen *et al.*, 1989; Pope, 1991). It is demonstrated that with this model, the maximum rate of the mean reactants' decay can be conveniently expressed in terms of definite integrals of the parabolic cylinder functions. For the cases with complete initial segregation, it is shown that the results agree very closely with those predicted by employing a beta density of the first kind for an appropriately defined Shvab–Zeldovich scalar variable. With this assumption, the final results can also be expressed in terms of closed form analytical expressions which are based on the incomplete beta functions. With both models, the dependence of the results on the stoichiometric coefficient and the equivalence ratio can be expressed in an explicit manner. For a stoichiometric mixture the analytical results simplify significantly. In the mapping closure these results are expressed in terms of simple trigonometric functions. For the beta density model they are in the form of gamma functions. In all the cases considered, the results are shown to agree well with data generated by Direct Numerical Simulations (DNS). Due to the simplicity of these expressions and because of nice mathematical features of the parabolic cylinder and the incomplete beta functions, these models are recommended for estimating the limiting rate of mean reactant conversion in homogeneous reacting flows. These results also provide a valuable tool in assessing the extent of validity of turbulence closures for the modeling of unpremixed reacting flows. Some discussions are provided on the extension of the models for treating more complicated reacting systems, including realistic kinetics schemes and multiscalar mixing with finite rate chemical reactions in more complex configurations.

Nomenclature

a, b, c: some constant.
B: the beta function.
$\mathscr{D}$: the parabolic cylinder function.
Da: the Damköhler number.
F: fuel.
$\mathscr{G}$: the parameter in the mapping closure.

[1] This work was sponsored by the NASA Langley Research Center under Grant NAG-1-1122, and by the Office of Naval Research under Grant N00014-90-J-4013. Computational resources were provided by NCSA at the University of Illinois.

g: half the inverse of the normalized variance of the Shvab–Zeldovich variable.
H: the Heaviside function.
$\mathcal{I}$: the incomplete beta function.
$\mathcal{J}$: the Shvab–Zeldovich variable.
O: the oxidizer.
$\mathcal{P}$: the PDF.
r: the stoichiometric coefficient.
t: the physical time.
W: the area weight of the reactant.
y: the dummy variable of integration.
$\mathcal{Y}$: the unmixedness ratio.

Greek Letters

$\beta_1, \beta_2, \ldots$: parameters of the beta density.
γ: the equivalence ratio.
Γ: the gamma function.
δ: the delta function.
ξ: the composition space for the PDF.
φ_0: the composition space for a Gaussian reference field.
τ: the normalized time.
χ: the mapping function.

Subscripts

0: time zero (inlet of plug flow reactor).
G: Gaussian.
st: stoichiometric.

Other symbols

$\langle\ \rangle$: the probability average.
$'$: the fluctuation for the ensemble mean.

1. Introduction

For the past 40 years, since the early work of Hawthorne *et al.* (1949), estimation of the mean reactant conversion rate has been the subject of wide investigations in mathematical modeling of turbulent reacting flows. In unpremixed reacting systems, including diffusion flames, there are two factors by which this rate is influenced: (1) the speed at which the reactants are brought into the reaction zone, and (2) the rate at which they are converted to products through chemical reactions. The relative importance of the two mechanisms is characterized by magnitude of the Damköhler number (Da), which is the ratio of the characteristic frequency of the chemical reaction to that of the hydrodynamics. The role of the Damköhler number in the characterization of reacting flows is very important (Williams, 1985). In the limit of $Da \to \infty$, the rate of reactant consumption is governed by the hydrodynamics, i.e., the reaction is "mixing controlled" and is determined by the speed at which the reactants are brought into an infinitely thin reaction zone (Bilger, 1980). Obviously, with the assumption of an infinitely fast chemistry, it is not possible to account for many interesting issues associated with nonequilibrium effects in unpremixed flames (Libby and Williams, 1980). However, as indicated in the original pioneering work of Toor (1962), and later by O'Brien (1971) and Bilger (1980), it is very important to have a prior estimate of the "limiting" rate of mean reactant conversion in practical modeling of combustion systems. In this limit the problem reduces to the simpler problem of "mixing," in which its analysis is much simpler (Toor, 1962, 1975).

Development of an appropriate turbulence model which can predict the mean rate of reactant conversion has been the subject of extensive investigations (for reviews see Toor, 1975; Brodkey, 1981; Libby and Williams, 1980; Williams, 1985). Amongst the theoretical tools developed, it is now firmly accepted that the approach based on the single-point Probability Density Function (PDF) of the scalar quantities is particularly useful, and this approach has been very popular for modeling the reactant conversion in a variety of turbulent reacting flow systems (Kollmann, 1990; Pope, 1985, 1990, 1991). The advantage of PDF methods is due to their inherent capability to include all the single-

point statistical information pertaining to the scalar field. Therefore, once the PDF (or the joint PDF) of the scalar variables is determined, all the relevant one-point statistics of the field are available without need for additional closures.

The most logical and systematic means of determining the PDF involves the solution of an appropriate transport equation governing its evolution. In this equation, due to the nature of the formulation, the effects of chemical reaction appear in a closed form (Pope, 1976), regardless of its degree of complexity. However, the influences of molecular action cannot be fully described, and can be treated only by means of employing an appropriate closure. As noted by Pope (1991), in most previous applications this problem has been circumvented through the use of the Coalescence/ Dispersion (C/D) models. Examples of such models are the early C/D prototype of Curl (1963), the Linear Mean Square Estimation (LMSE) theory (O'Brien, 1980), the closure of Janicka *et al.* (1979), among others (Pope, 1982, 1985; Kosaly and Givi, 1987; Givi, 1989; Dutta and Tarbell, 1989). Despite their advantageous characteristics, the shortcomings associated with the C/D closures in the probabilistic description of scalar transport are well recognized. Namely, none of the aforementioned models predict an asymptotic Gaussian distribution for the PDF of a conserved scalar variable in homogeneous turbulence (Pope, 1982, 1991; Kosaly and Givi, 1987); and those which are capable of doing so (e.g., Pope, 1982), do not predict the initial stages of mixing correctly (Kosaly, 1986; Kosaly and Givi, 1987).

Recent development of the Amplitude Mapping Closure by Kraichnan and coworkers (Kraichnan, 1989; Chen *et al.*, 1989) (see also Pope, 1991) has provided a promising way of alleviating some of the problems associated with the C/D closures. This closure, in essence, provides a means of accounting for the transport of the PDF in composition space, and its validity and physical applicability have been evidenced in a number of comparisons against data generated by means of both direct numerical simulations (Pope, 1990, 1991; Gao, 1991a, b, Madnia *et al.*, 1991b; Jiang *et al.*, 1992) and laboratory experiments (Frankel *et al.*, 1992a). These results suggest that, at least in the setting of an isotropic turbulent flow, this closure has some superior features over all the previous C/D-type models.

Based on this demonstrated superiority, our objective here is to examine further the properties of this closure and to assess its capabilities for applications in modeling of unpremixed turbulent reacting flow systems. In particular, it is intended to provide a reasonably simple recipe that can be used in conjunction with this closure for predicting the limiting rate of mean reactant conversion. However, since this is the first study of this type, and due to mathematical complexities (that soon become apparent), we have made some simplifying assumptions which are indicated here. Firstly, we consider an idealized irreversible binary reaction of the type $F + rO \rightarrow (1 + r)$ *Product* with initially segregated reactants (F and O). In accordance with the discussions above, only the maximum rate of mean reactant conversion is considered. Secondly, the turbulence field is assumed statistically homogeneous. Thirdly, all the chemical species are assumed to have identical and constant thermodynamic properties. Finally, the flow field is assumed isothermal in which the dynamic role of the chemical reaction on the hydrodynamic field is ignored.

With all these assumptions, the reacting system considered is obviously an idealized prototype of conventional combustion systems. However, it does provide a good model for dilute reacting systems in typical mixing controlled plug flow reactors (Toor, 1962, 1975; Bilger, 1980; Hill, 1976; Brodkey, 1981). Moreover, because of the mathematical complexities, even in this simple case, it is deemed necessary to analyze this simplified system before considering more complex scenarios. Nevertheless, the model is capable of accounting for arbitrary values of the stoichiometric coefficients and for any equivalence ratio. This allows the capture of many interesting features, as will be demonstrated.

For the idealized case of initially segregated reactants, the initial marginal PDFs of their concentrations are composed of "delta functions." Therefore, it is speculated that the approach based on an *assumed* probability distribution may also provide a reasonably good closure. Therefore, in addition to the mapping closure, a member of the family of *Pearson* frequencies is also considered. The results obtained by this frequency are compared with those of the mapping closure, and are also assessed against data generated by means of DNS.

In the next section the problem under consideration is outlined along with the mathematical basis by which the single-point PDF methods are used. In Section 2.1 the salient features of the mapping

closure at the single-point level are analyzed including a discussion on the formalities of the closure for our purpose. With this closure, a closed form analytical expression is provided for the limiting bound of the mean reactant conversion. This limiting rate is also predicted by means of the beta density model in Section 2.2. In both these subsections the simplifications for the case of a stoichiometric mixture are made, motivating the use of our final "simple" analytical expressions in practical modeling of stoichiometric plug flow reactors. In Section 3.1 the results predicted by both models are compared against those generated by DNS of a three-dimensional homogeneous turbulent flow. In Section 3.2 some discussions are presented highlighting the implications of these results in turbulence modeling. This paper is drawn to a close in Section 4 with some discussions for possible future extension of the two models for the statistical description of more complicated chemically reacting turbulent flows.

2. Formulation

With the assumptions described in the introduction, the statistical behavior of the reacting field in the reaction $F + rO \rightarrow (1 + r)$ *Product* can be related to the statistics of an appropriate conserved Shvab–Zeldovich mixture fraction, $\mathcal{J}$ (Bilger, 1980). This mixture fraction can be normalized in such a way to yield values of unity in the fuel F stream and zero in the oxidizer O stream. For the purpose of statistical treatment, we define $\mathcal{P}_F(\xi, t)$, $\mathcal{P}_O(\xi, t)$, and $\mathcal{P}_\mathcal{J}(\xi, t)$, respectively, as the marginal PDFs of the concentration of F, the concentration of O, and the Shvab–Zeldovich variable $\mathcal{J}$. For initially segregated reactants with no fuel in the oxidizer stream (and vice versa), the initial conditions for the marginal PDFs of the concentrations of the two reactants are given by

$$\begin{aligned} \mathcal{P}_F(\xi, 0) &= W_F\delta(\xi - F_i) + W_O\delta(\xi), \\ \mathcal{P}_O(\xi, 0) &= W_O\delta(\xi - O_i) + W_F\delta(\xi), \qquad 0 \le \xi \le 1. \end{aligned} \tag{1}$$

Here, F_i and O_i denote the initial concentrations of the two species in the two feeds, and W_F and W_O represent the relative weights of the reactants at the initial time (i.e., the area ratios at the inlet of a plug flow reactor). With the normalized value of the concentrations equal to unity at the feeds, i.e., $F_i = O_i = 1$, the stoichiometric value of the Shvab–Zeldovich variable, $\mathcal{J}_{st}$, is determined from the parameter r. With the assumption of an infinitely fast chemistry, the marginal PDFs of the reactants' concentrations are related to the frequency of the Shvab–Zeldovich variable (Bilger, 1980; Kosaly and Givi, 1987):

$$\begin{aligned} \mathcal{P}_F(\xi, t) &= (1 - \mathcal{J}_{st})\mathcal{P}_\mathcal{J}(\mathcal{J}_{st} + \xi(1 - \mathcal{J}_{st}), t) + \vartheta_F(t)\delta(\xi), \\ \mathcal{P}_O(\xi, t) &= \mathcal{J}_{st}\mathcal{P}_\mathcal{J}(\mathcal{J}_{st}(1 - \xi), t) + \vartheta_O(t)\delta(\xi). \end{aligned} \tag{2}$$

Here, $\xi \ge 0$ and

$$\begin{aligned} \vartheta_F(t) &= \int_{-\infty}^{\mathcal{J}_u} \mathcal{P}_\mathcal{J}(\xi, t)\, d\xi, \\ \vartheta_O(t) &= \int_{\mathcal{J}_u}^{\infty} \mathcal{P}_\mathcal{J}(\xi, t)\, d\xi = 1 - \vartheta_F(t). \end{aligned} \tag{3}$$

The initial condition for the PDF of the Shvab–Zeldovich variable is given by

$$\mathcal{P}_\mathcal{J}(\xi, 0) = W_F\delta(\xi - 1) + W_0\delta(\xi). \tag{4}$$

Equation (4) implies that $\langle\mathcal{J}\rangle(t = 0) = W_F$. Since $\mathcal{J}$ is a conserved variable, its mean value remains constant, i.e., $\langle\mathcal{J}\rangle(t) = \langle\mathcal{J}\rangle(0) = W_F$. The integration of (2) yields the temporal variation of the statistics of the species field at all times, if the PDFs of $\mathcal{J}$ are known. As indicated above, in the setting of a mixing controlled reaction this PDF provides all the desired statistical properties of the reacting field.

2.1. Amplitude Mapping Closure

The implementation of the amplitude mapping closure involves a mapping of the random field of interest ξ to a stationary Gaussian reference field φ_0, via a transformation $\xi = \chi(\varphi_0, t)$. Once this

relation is established, the PDF of the random variable ξ, $\mathscr{P}(\xi)$, is related to that of a Gaussian distribution. In homogeneous turbulence, the transport equation for this function satisfies (Chen *et al.*, 1989; Pope, 1991)

$$\frac{\partial \chi}{\partial \tau} = -\varphi_0 \frac{\partial \chi}{\partial \varphi_0} + \frac{\partial^2 \chi}{\partial \varphi_0^2}. \tag{5}$$

In this equation, τ is a normalized time within which the scalar length scale information is embedded. The relations between this time and the physical time, i.e., $\tau(t)$, cannot be determined in the context of single-point PDF description and must be provided by external means (Pope, 1990; Jiang *et al.*, 1992). For the case considered here, with the initial PDF of the variable $\mathscr{J}$ given by (4), the corresponding form of the initial mapping is

$$\chi(\varphi_0, 0) = H(\varphi_0 - \varphi^*), \qquad -\infty \le \varphi_0 \le \infty, \tag{6}$$

where H is the Heaviside function and φ^* is a measure of the initial asymmetry of the initial PDF around the ensemble mean of the variable $\mathscr{J}$:

$$\varphi^* = \sqrt{2}\,\mathrm{erf}^{-1}(1 - 2\langle \mathscr{J} \rangle), \tag{7}$$

where "erf" denotes the error function. The mapping function is obtained by solving (5) subject to initial condition (6). The general solution of this equation has the form (Gao, 1991a)

$$\chi(\varphi_0, \tau) = \frac{\sqrt{\mathscr{G}^2 + 1}}{\sqrt{2\pi}\mathscr{G}} \int_{-\infty}^{\infty} \chi(y, 0) \exp\left[-\frac{(\varphi_0 e^{-\tau} - y)^2 (1 + \mathscr{G}^2)}{2\mathscr{G}^2} \right] dy, \tag{8}$$

where $\mathscr{G}(\tau) = \sqrt{\exp(2\tau) - 1}$. Inserting (6) for $\chi(\varphi_0, 0)$ in (8), we have

$$\chi(\varphi_0, \tau) = \tfrac{1}{2}[1 + \mathrm{erf}(a\varphi_0 + b)], \tag{9}$$

where

$$a(\tau) = \frac{1}{\sqrt{2}\mathscr{G}}, \qquad b(\tau) = \frac{-\varphi^* \sqrt{1 + \mathscr{G}^2}}{\sqrt{2}\mathscr{G}}. \tag{10}$$

Finally, the solution for the PDF of $\mathscr{J}$ is determined directly from the mapping relation between the physical field ξ and the Gaussian reference field φ_0:

$$\mathscr{P}_{\mathscr{J}}(\chi(\varphi_0, \tau), \tau) = \mathscr{P}_G(\varphi_0) \left(\frac{\partial \chi}{\partial \varphi_0} \right)^{-1}. \tag{11}$$

Here, $\mathscr{P}_G$ denotes the PDF of a standardized Gaussian distribution, i.e., $\mathscr{P}_G(\varphi_0) = (1/\sqrt{2\pi}) \exp(-\varphi_0^2/2)$. A combination of (11) and (9) yields the final result for the PDF of the Shvab–Zeldovich variable:

$$\mathscr{P}_{\mathscr{J}}(\chi(\varphi_0, \tau), \tau) = \mathscr{G} \exp\left[\frac{(\varphi_0 e^{-\tau} - \varphi^*)^2}{2(1 - e^{-2\tau})} - \frac{\varphi_0^2}{2} \right]. \tag{12}$$

With a combination of (12) and (2), all the pertinent single-point statistics of the reacting field are determined. The most important of these statistics are the ensemble mean values of the reactants' concentrations. These mean values are obtained directly by integrating their respective PDFs. The intermediate steps in deriving these relations are not presented but are provided by Frankel (1992). Here, only the essential steps are presented. For the mean fuel concentration, $\langle F \rangle$, the first part of (2) reads

$$\langle F \rangle(\tau) = \int_{\mathscr{J}_{st}}^{1} F(\xi) \mathscr{P}_{\mathscr{J}}(\xi, \tau)\, d\xi = \int_{\varphi_0(\chi = \mathscr{J}_{st})}^{\infty} F(\chi(\varphi_0, \tau), \tau) \mathscr{P}_G(\varphi_0)\, d\varphi_0, \tag{13}$$

where the lower limit of the last integral corresponds to the value of φ_0 at which χ is equal to the stoichiometric value of the Shvab–Zeldovich variable. Evaluating this limit from (9), equation (13) can be analytically integrated. This is possible by representing the error function in the form of its definition, and performing the resulting definite, double exponential integral. The results after extensive algebraic manipulations yield

$$\langle F \rangle(\tau) = \frac{(1 - 2\mathscr{J}_{st})}{4(1 - \mathscr{J}_{st})} \left[1 + \mathrm{erf}\left(\frac{b/a + c}{\sqrt{2}} \right) \right] + \frac{1}{\pi \sqrt{2} a (1 - \mathscr{J}_{st})} \exp\left(-\frac{b^2}{2a^2} - \frac{c^2}{2} - \frac{bc}{a} \right) \Theta_+. \tag{14}$$

Similar expressions can be obtained for the mean oxidizer concentration:

$$\langle O\rangle(\tau) = \frac{1}{2}\left(1 - \frac{1}{2\mathcal{J}_{st}}\right)\left[1 - \operatorname{erf}\left(\frac{b/a + c}{\sqrt{2}}\right)\right] - \frac{1}{\pi\sqrt{2}a\mathcal{J}_{st}} \exp\left(-\frac{b^2}{2a^2} - \frac{c^2}{2} - \frac{bc}{a}\right)\Theta_{-}. \tag{15}$$

In these equations, c is related to the stoichiometric coefficient,

$$c = \frac{-1}{a}\operatorname{erf}^{-1}(2\mathcal{J}_{st} - 1), \tag{16}$$

and

$$\Theta_{\pm} = \int_0^1 dy \exp\left(-a^2c^2y^2 + \frac{y_{\pm}^2}{8y_2}\right)\left[\frac{1}{2y_2}\mathcal{D}_{-2}\left(\frac{y_{\pm}}{\sqrt{2y_2}}\right) - \frac{ac}{\sqrt{2y_2}}\mathcal{D}_{-1}\left(\frac{y_{\pm}}{\sqrt{2y_2}}\right)\right],$$

$$y_2 = y^2 + \frac{1}{2a^2}, \tag{17}$$

$$y_{\pm} = \mp 2acy^2 - \frac{b}{a^2} - \frac{c}{a}.$$

Here, $\mathcal{D}_{-2}$ and $\mathcal{D}_{-1}$ are, respectively, the parabolic cylinder functions of order -2 and -1, belonging to the family of degenerate hypergeometric functions (Abramowitz and Stegun, 1972).

Due to nice properties of the degenerate hypergeometric functions, many of the interesting features of (14) and (15) can be depicted. First, simple manipulation of this equation shows that for a stoichiometric mixture, $\langle\mathcal{J}\rangle = \mathcal{J}_{st}$, both reactants decay at the same rate, i.e.,

$$\frac{\langle F\rangle(t)}{\langle F\rangle(0) = W_F} = \frac{\langle O\rangle(t)}{\langle O\rangle(0) = W_O},$$

and for a nonstoichiometric initial condition, the limits of the concentration values as $\tau, \mathcal{G} \to \infty$, asymptote to

$$\lim_{\tau,\mathcal{G}\to\infty} \langle F\rangle(\tau) = \begin{cases} 0, & \mathcal{J}_{st} \geq \langle\mathcal{J}\rangle, \\ \dfrac{\langle\mathcal{J}\rangle - \mathcal{J}_{st}}{1 - \mathcal{J}_{st}}, & \mathcal{J}_{st} \leq \langle\mathcal{J}\rangle, \end{cases}$$

$$\lim_{\tau,\mathcal{G}\to\infty} \langle O\rangle(\tau) = \begin{cases} 0, & \mathcal{J}_{st} \leq \langle\mathcal{J}\rangle, \\ 1 - \dfrac{\langle\mathcal{J}\rangle}{\mathcal{J}_{st}}, & \mathcal{J}_{st} \geq \langle\mathcal{J}\rangle, \end{cases} \tag{18}$$

These limits are obtained by employing the Taylor series expansion of the relevant functions as $\mathcal{G} \to \infty$, and indicate the limiting bound of the concentrations of the unconsumed reactants in both fuel-rich and fuel-lean mixtures. While these limiting behaviors are rather trivial from a physical standpoint, in a computational procedure it must be made sure that they are satisfied. Because of the mathematical properties of the parabolic cylinder functions, these limiting cases can be realized in our computational procedure in a relatively easy manner. It would be very difficult to obtain these limiting behaviors numerically in an integration procedure within the original unbounded domain.

At first glance, (14) and (15) may appear somewhat complicated. However, due to nice mathematical properties of the parabolic cylinder functions (Abramowitz and Stegun, 1972), these equations can be integrated rather easily within the finite domain ($0 \leq y \leq 1$). For fuel-lean or fuel-rich mixtures, the integration can only be done by means of employing numerical methods. However, for a stoichiometric mixture, the results simplify further as demonstrated below.

Stoichiometric Mixture. For practical applications in stoichiometric plug flow reactors, the equations simplify considerably. For a stoichiometric mixture, and an initially symmetric PDF around the mean value (i.e., $\langle\mathcal{J}\rangle = \mathcal{J}_{st} = \frac{1}{2}$), both parameters b and c are zero. Under this condition, the first terms on the right-hand sides of (14) and (15) drop. Knowing $\mathcal{D}_{-2}(0) = \mathcal{D}_{-1}(0) = 1$, the remaining terms yield

$$\frac{\langle F\rangle(\tau)}{\langle F\rangle(0)} = \frac{\langle O\rangle(\tau)}{\langle O\rangle(0)} = \frac{1}{\pi\sqrt{2}a}\int_0^1 \frac{dy}{2y^2 + 1/a^2} = 1 - \frac{2\arctan\mathcal{G}(\tau)}{\pi}. \tag{19}$$

The simplicity of this equation is noteworthy and very pleasing. Because of this simplicity, (19) is strongly recommended for engineering predictions of the mean reactant conversion rate in stoichiometric homogeneous flows, such as the plug flow reactors considered in numerous previous investigations (Toor, 1962, 1975; Brodkey, 1981; Hill, 1976; O'Brien, 1971; Kosaly and Givi, 1987).

2.2. The Beta Density Model

For initially segregated reactants, the initial PDF of the Shvab–Zeldovich variable is composed of two delta functions at the extreme limits of the variable. Therefore, it is proposed that the family of Pearson (1895) frequencies may provide a reasonable means of estimating this distribution at all times (Frankel *et al.*, 1991; Girimaji, 1991a). The appropriate form of the Pearson distribution is in this case the beta density of the first kind. This density has been employed in the statistical description of turbulent reacting flows by Rhodes (1975), Jones and Priddin (1978), Lockwood and Moneib (1980), Peters (1984), and Janicka and Peters (1982) amongst others (for recent reviews, see Givi, 1989; Priddin, 1991). For an initially nonsymmetric PDF, the beta density corresponds to Pearson Type I and for the symmetric case to Pearson Type II. The relevance of the latter in modeling of molecular mixing from an initial symmetric binary state has been described by Madnia *et al.* (1991a) and Girimaji (1991a). In both cases the PDF of the Shvab–Zeldovich variable is represented by (Abramowitz and Stegun, 1972)

$$\mathscr{P}_{\mathscr{J}}(\xi) = \frac{1}{B(\beta_1, \beta_2)} \xi^{\beta_1 - 1}(1 - \xi)^{\beta_2 - 1}, \qquad 0 \le \xi \le 1, \tag{20}$$

where $B(\beta_1, \beta_2)$ denotes the beta function, and the parameters β_1 and β_2 are dependent on the mean and the variance of the random variable $\mathscr{J}$. In applications to the mixing controlled reaction considered here, we assume that the PDF of the Shvab–Zeldovich variable always retains a beta distribution. Thus all the statistics of the reacting scalar are subsequently determined. The ensemble mean values are determined by a combination of (20) and (2). Following the same procedure as that described in the section on the mapping closure, after some manipulations the final results can be expressed as (Frankel, 1992)

$$\langle F \rangle(t) = \frac{\mathscr{J}_{st}^{\beta_1}(1 - \mathscr{J}_{st})^{\beta_2 - 1}}{(\beta_1 + \beta_2)B(\beta_1, \beta_2)} + \frac{1}{1 - \mathscr{J}_{st}}\left(\frac{\beta_1}{\beta_1 + \beta_2} - \mathscr{J}_{st}\right)(1 - \mathscr{J}_{\mathscr{J}_{st}}(\beta_1, \beta_2)), \tag{21}$$

$$\langle O \rangle(t) = \frac{\mathscr{J}_{st}^{\beta_1 - 1}(1 - \mathscr{J}_{st})^{\beta_2}}{(\beta_1 + \beta_2)B(\beta_1, \beta_2)} + \left(1 - \frac{\beta_1}{(\beta_1 + \beta_2)\mathscr{J}_{st}}\right)\mathscr{J}_{\mathscr{J}_{st}}(\beta_1, \beta_2), \tag{22}$$

where $\mathscr{J}$ denotes the incomplete beta function (Abramowitz and Stegun, 1972).

Due to nice mathematical properties of the beta function, the final results are cast in terms of its integral. In this case, however, the integral can be expressed in terms of the incomplete beta function. The mathematical properties of this special function are well known, and the expressions above are conveniently amenable to numerical integration (Frankel, 1992). Again, the physical limiting conditions discussed before are realized by (21) and (22). That is, in a stoichiometric mixture, both reactants decay at the same rate; and in lean or rich mixtures, the same limiting conditions as those in (18) are realized.

Stoichiometric Mixture. Again, in the case of an initially symmetric PDF under stoichiometric conditions, the final expressions become simpler. Under this condition, $\beta_1 = \beta_2$, and knowing $\mathscr{J}_{1/2}(x, x) = \frac{1}{2}$, (21) and (22) reduce to

$$\frac{\langle F \rangle(t)}{\langle F \rangle(0)} = \frac{\langle O \rangle(t)}{\langle O \rangle(0)} = \frac{1}{\sqrt{\pi}} \frac{\Gamma(g)}{\Gamma(g + \frac{1}{2})}, \tag{23}$$

where g is half the inverse of the normalized variance of the Shvab–Zeldovich variable, and Γ denotes the gamma function.

3. Results

The final forms of (14), (15), (19), (21), (22), and (23) are gratifying since they provide a relatively simple and effective means of estimating the maximum rate of mean reactant conversion in homogen-

eous reacting flows. As indicated before, the mathematical operations leading to these equations are somewhat involved, but the final results can be conveniently expressed in terms of known special functions. However, since both models are based on single-point PDF descriptions, these equations are not in a complete closed form and are dependent on the parameters g and/or $\mathcal{G}$. In this context this parameter cannot be determined by the model and must therefore be specified by external means (Pope, 1991; Jiang *et al.*, 1992; Frankel *et al.*, 1992a). This deficiency is not particular to the two models considered here, and exists in any single-point statistical description, including all of those based on the C/D models.

The extent of validity of these simple relations can be demonstrated by a comparison between the model predictions and the data obtained by means of DNS. The comparison is made here for several values of $\langle \mathcal{J} \rangle$ and $\mathcal{J}_{st}$ for the purpose of demonstration. In this comparison the magnitudes of the normalized variance of the Shvab–Zeldovich variable are matched with those of DNS. This implies that, for given values of $\langle \mathcal{J} \rangle$ and $\mathcal{J}_{st}$, the parameters g, $\mathcal{G}$, β_1, and β_2 are provided externally from the DNS data. With this provision, the model prediction results can be directly assessed against DNS data.

The DNS procedure is similar to that of previous simulations of this type. For a detailed description we refer the reader to Madnia and Givi (1992). The subject of the present DNS is a three-dimensional periodic homogeneous box flow under the influence of a binary reaction of the type described above. The initial species field is composed of out-of-phase square waves for the two reactants F and O. The computational package is based on the modification of a spectral-collocation procedure using Fourier basis functions developed by Erlebacher *et al.* (1990a) (see also Erlebacher *et al.*, 1987, 1990b). The hydrodynamic field is assumed isotropic, and is initialized in a similar manner to that of Erlebacher *et al.* (1990a) and Passot and Pouquet (1987). The turbulent field is of a decaying nature in that there is no artificial forcing mechanism to feed energy to low wave numbers. The code is capable of simulating flows with different levels of compressibility (Hussaini *et al.*, 1990). Here, only the results obtained for a low compressible case are discussed, since most previous analyses of plug flow reactors have dealt primarily with incompressible flows (Toor, 1975; Hill, 1976; Brodkey, 1981; Leonard and Hill, 1988a, b, 1991). The resolution consists of 96 collocation points in each direction. Therefore, at each time step 96^3 is the sample size for statistical analyses. With this resolution, simulations with a Reynolds number (based on the Taylor microscale) of $Re_\lambda \approx 41$ are attainable. The value of the molecular Schmidt number is set equal to unity.

3.1. Validations

The statistical behavior of the scalar field is depicted by examining the evolution of the PDFs of the Shvab–Zeldovich variable $\mathcal{J}$. These are shown in Figures 1 and 2 at times close to the initial ($t1$) and

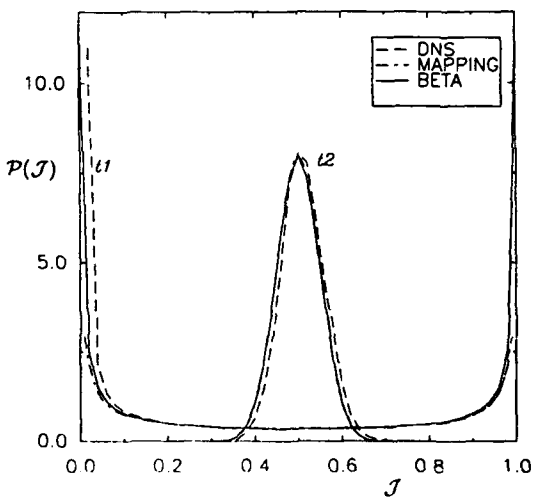

Figure 1. PDF of the Shvab–Zeldovich variable at two times ($t2 > t1$) for the symmetric case ($\langle \mathcal{J} \rangle = \frac{1}{2}$).

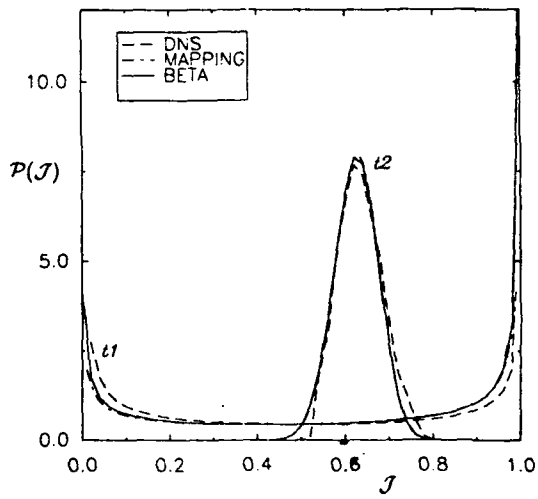

Figure 2. PDF of the Shvab–Zeldovich variable at two times ($t2 > t1$) for the nonsymmetric case ($\langle \mathcal{J} \rangle = 0.625$).

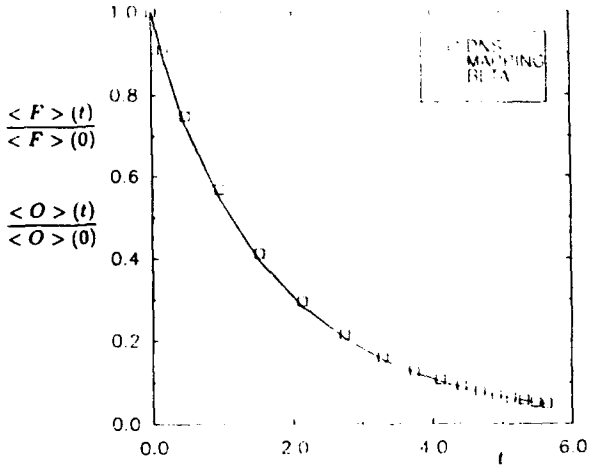

Figure 3. Normalized mean concentration of fuel and the oxidizer for the symmetric case, and $\mathcal{J}_{st} = 0.5$.

the final ($t2$) states. These figures correspond, respectively, to the cases of an initially symmetric ($\langle \mathcal{J} \rangle = \frac{1}{2}$) and nonsymmetric ($\langle \mathcal{J} \rangle = 0.625$) PDFs. At the initial time, the PDF is approximately composed of two delta functions at $\mathcal{J} = 0, 1$ indicative of the two initially segregated reactants, F and O. At later times, the PDF evolves through an inverse-like diffusion in composition space. The heights of the delta functions decrease, and the PDF is redistributed at other $\mathcal{J}$ values in the range [0, 1], and subsequently becomes centralized around the mean value. Proceeding further in time results in a sharper peak at this mean value, and in both cases the PDF can be approximated by a Gaussian distribution near the mean scalar value. The trend for the symmetric case is the same as that presented in earlier DNS studies (Eswaran and Pope, 1988; Givi and McMurtry, 1988). For the nonsymmetric case there are no DNS data in the literature, but the present results verify that the asymptotic PDF can still be approximated by a Gaussian distribution near its mean value.

The PDFs obtained by the mapping closure and those by an assumed beta density are also presented in Figures 1 and 2. In these figures the model PDFs are parametrized with the same first two moments obtained from DNS. In this parametrization only the normalized magnitude of the variance of the models are forced equal to that of the DNS and no attempt was made to account for the departure from the "exact" initial double delta distribution in DNS. With this matching, nevertheless, the results clearly indicate that the model predictions compare very well with the DNS results. Also, both models yield an asymptotic Gaussian-like PDF.

The temporal variation of the ensemble mean of the reactants' concentration by the two models are compared against those of DNS in Figures 3 and 4. These figures correspond to the two cases of

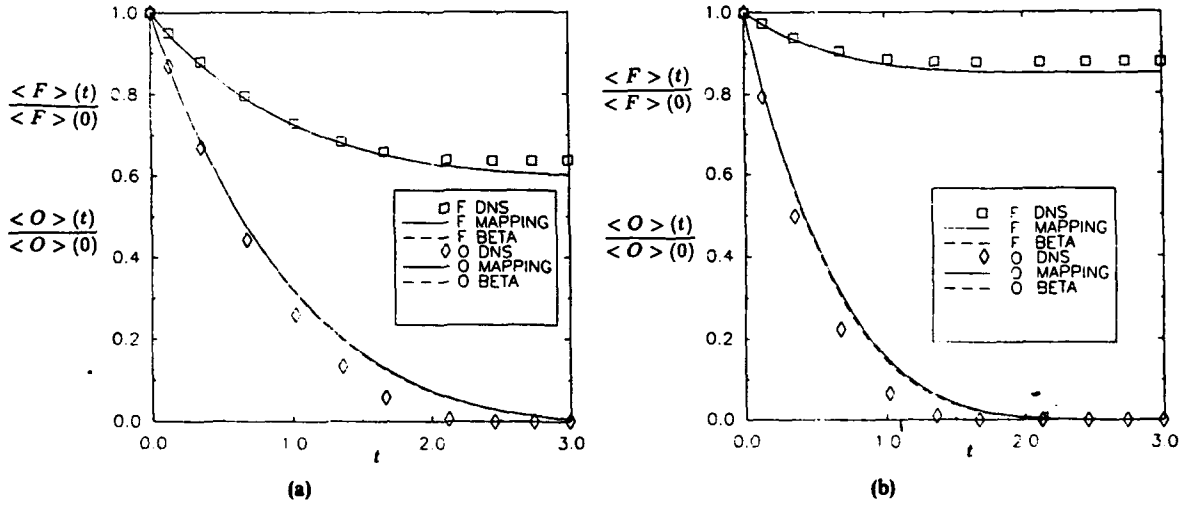

Figure 4. Normalized mean concentration of fuel and the oxidizer for the nonsymmetric case. (a) $\mathcal{J}_{st} = 0.4$, (b) $\mathcal{J}_{st} = 0.2$.

symmetric and nonsymmetric initial PDFs, respectively. In the symmetric case, under stoichiometric conditions, the results are simply obtained from the analytical expressions in (19) and (23). In the nonsymmetric case, numerical integration of (14) and (15) and evaluation of the incomplete beta function in (21) and (22) are necessary. In both cases the agreement of the models with the DNS data is noteworthy. Also, a comparison between parts (a) and (b) of Figure 4 shows that as the magnitude of $\mathcal{J}_{st}$ decreases, the rate of consumption of the oxidizer increases.

The agreements noted above follow from the compatibility of the model PDFs and those of DNS, at least for the case of binary mixing considered here. This finding is not new and has been well documented in previous works, at least those considering an initially symmetric PDF (Pope, 1990, 1991; Madnia and Givi, 1992; Madnia *et al.*, 1991a; Girimaji, 1991a). However, a nice feature of the models is the explicit form of the final equations expressing these statistical quantities. Supported by this quantitative agreement, it is proposed that, in the absence of a better alternative, the relations obtained above be used as an explicit simple means for predicting the maximum rate of mean reactant conversion in homogeneous reacting systems.

Despite the simplicity of these equations and their ease of application, it must be mentioned that these equations predict the rate of mean decay of the reactants' concentration far better than all the previous turbulence closures based on the C/D models (see Givi, 1989). This is particularly advantageous in that this evaluation can be made by a simple algebraic relation, whereas the C/D implementations usually require more expensive numerical simulations (Kosaly and Givi, 1987; McMurtry and Givi, 1989). Even for nonunity equivalence ratios, the numerical integration required by the two models above is considerably less computationally demanding than those of the C/D models. The only input in these models, similar to those in C/D closures, is the variance of the Shvab–Zeldovich variable. This is provided here by means of DNS. In an actual implementation, this variance can be obtained from experimental data or by means of an appropriate turbulence model (Frankel *et al.*, 1992a). The provision of such data is not very difficult since they can be obtained in the setting of a nonreacting flow.

3.2. Applications

The relations obtained here can be used in determining the extent of validity of other conventional closures for predicting the limiting rate of mean reactant conversion in turbulent flows. As an example, here we consider the model based on the famous hypothesis of Toor (1962, 1975), which has received considerable attention in practical modeling of unpremixed homogeneous reacting systems (Bilger, 1980; Brodkey, 1981; Leonard and Hill, 1987, 1988a, b; Kosaly and Givi, 1987; Kosaly, 1987; Givi and McMurtry, 1988; McMurtry and Givi, 1989; Givi, 1989). According to this hypothesis, in an isothermal homogeneous reacting turbulent flow, the decay of the unmixedness, denoted by $\Psi = \langle F'O' \rangle(t)/\langle F'O' \rangle(0)$, where the prime quantities indicate fluctuation from the ensemble mean value, is independent of the magnitude of the Damköhler number. This implies that the normalized unmixedness parameter, defined by

$$\mathcal{Y} = \frac{\Psi(t)|_{Da}}{\Psi(t)|_{Da=0}}, \tag{24}$$

is the same under both reacting and nonreacting conditions, i.e., $\mathcal{Y}(t) = \text{constant} = 1$ for all values of Da. In previous DNS assessments of this hypothesis, it has been shown that for the case of initially segregated reactants this model cannot be employed, and the normalized unmixedness ratio depends on the nature of mixing and the magnitude of the Damköher number (Givi and McMurtry, 1988; McMurtry and Givi, 1989). In particular, it has been demonstrated that even for $Da \to \infty$, while the normalized unmixedness is equal to unity at the initial time, its limiting lower bound depends on the asymptotic frequency of the Shvab–Zeldovich variable. That is, $\mathcal{Y}(t = 0) = 1 > \mathcal{Y}(t) > \mathcal{Y}(t \to \infty) = C$, where C is the lower limiting bound. For an asymptotic Gaussian distribution, it can be easily shown that, for a mixture under stoichiometric conditions, the lower bound limits asymptotes to the constant value $C = 2/\pi$ (Kosaly, 1987; Givi and McMurtry, 1988).

This deviation from unity can be realized by the two models considered. With the mapping closure, under symmetric stoichiometric conditions, from (2), (14), and (15), following the same integration

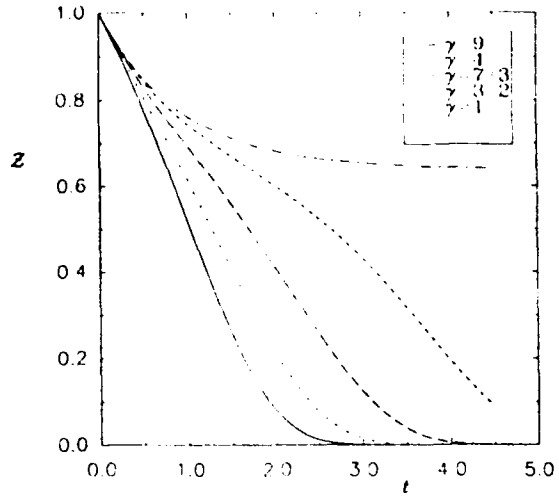

Figure 5. The unmixedness ratio at several values of the equivalence ratio.

procedure as before, it is shown that

$$\mathscr{Z}_{\mathrm{m}} = \frac{\langle F'O' \rangle (Da \to \infty)}{\langle F'O' \rangle (Da = 0)} = \frac{2(\arctan(1/\mathscr{G}))^2}{\pi \arctan(1/\mathscr{G}\sqrt{\mathscr{G}^2 + 2})}. \tag{25}$$

For the beta density model, the corresponding form of the unmixedness ratio for $\beta_1 = \beta_2$ is given by

$$\mathscr{Z}_{\beta} = \frac{2g}{\pi}\left(\frac{\Gamma(g)}{\Gamma(g + \frac{1}{2})}\right)^2. \tag{26}$$

In (25) and (26), the subscripts m and β are added to denote the mapping and the beta density model. It is easy to show that these equations satisfy the correct limiting conditions for a stoichiometric mixture. This is for both the initial time, i.e., the inlet of the reactor,

$$\lim_{[\mathscr{G} \to 0]} \mathscr{Z}_{\mathrm{m}} = \lim_{[g \to 1/2]} \mathscr{Z}_{\beta} = 1, \tag{27}$$

and at large distances from it:

$$\lim_{[\mathscr{G} \to \infty]} \mathscr{Z}_{\mathrm{m}} = \lim_{[g \to \infty]} \mathscr{Z}_{\beta} = C = \frac{2}{\pi}. \tag{28}$$

The latter limiting condition cannot be realized in any of the previously used C/D models, or by means of Toor's models (McMurtry and Givi, 1989; Givi, 1989).

The results based on the applications of Toor's model become less accurate for nonstoichiometric mixtures. For equivalence ratios other than unity, with the depletion of one of the reactants, the unmixedness parameter approaches zero faster. This is demonstrated by the solution of the mapping closure shown in Figure 5 for several values of the equivalence ratio (γ). Note that as the magnitude of this ratio increases above one, the unmixedness ratio goes to zero more rapidly. For an unity equivalence ratio, the correct asymptotic value of $2/\pi$ is realized.

4. Extensions for Modeling of More Complex Reacting Turbulent Flows

Despite the pleasing features of our simple mathematical expressions, there are several restricting assumptions which were necessarily imposed in deriving these equations. Here, we would like to address the ramifications associated with these assumptions, and to provide the means of overcoming them in future extensions of these models.

Firstly, due to the assumption of infinitely fast chemistry, only the *maximum rate* of the mean reactant conversion is obtained. While this rate is very useful in describing unpremixed flames, from both a theoretical standpoint and for practical applications (Givi, 1989; McMurtry and Givi, 1989; Kosaly and Givi, 1987; Toor, 1962, 1975; O'Brien, 1971; Bilger, 1980; Williams, 1985; Dutta and

Tarbell, 1989), the model is not capable of describing some of the important features of the turbulent flames, especially those associated with nonequilibrium effects. The extensions to finite rate chemistry, reversible reactions, nonequilibrium flames, and multistep kinetics systems require numerical integration of the PDF transport equation. For these cases the problem cannot be mathematically reduced to that of keeping track of a single scalar variable (like $\mathcal{J}$), and requires the use of *multivariate* statistical descriptions. For this, the implementation of mapping closure is relatively straightforward since it provides a transport equation for the joint PDFs of the scalar variable in a multivariable sense (Pope, 1991; Gao and O'Brien, 1991). However, it is not presently clear how to devise an efficient computational procedure, typically based on Monte Carlo methods (Pope, 1981), for the numerical treatment of these equations. Some work in this regard is currently under way (Valiño and Gao, 1991; Valiño *et al.*, 1991).

The extension of assumed distributions based on the beta density for treating multiscalars is more straightforward but less trivial to justify. The most obvious means is to implement the multivariate form of the Pearson distributions. The direct analogue of the beta density is the *Dirichlet* frequency (Johnson, 1987; Johnson and Kotz, 1972; Wilks, 1962; Narumi, 1923). For a mixture composed of $N+1$ species, the joint PDF of N concentrations $(\psi_1, \psi_2, \ldots, \psi_N)$ is described in terms of an N-variate density of the form

$$\mathscr{P}(\psi_1, \psi_2, \ldots, \psi_N) = \frac{\Gamma(\beta_1 + \beta_2 + \cdots + \beta_{N+1})}{\Gamma(\beta_1)\Gamma(\beta_2), \ldots, \Gamma(\beta_{N+1})} \psi_1^{\beta_1 - 1} \psi_2^{\beta_2 - 1} \cdots \psi_N^{\beta_N - 1} (1 - \psi_1 - \psi_2 - \cdots - \psi_N)^{\beta_{N+1} - 1} \quad (29)$$

subject to the physical constraint

$$\sum_{i=1}^{N+1} \psi_i = 1. \quad (30)$$

The application of this density in modeling of multispecies reactions has been nicely discussed by Girimaji (1991a). Due to the mathematical properties of the gamma function, this density is pleasing from a mathematical viewpoint and most statistical cross correlations of the random variables $(\psi_1, \psi_2, \ldots)$ can be conveniently obtained by means of simple analytical relations (Frankel, 1992). Some points in this regard have been made by Girimaji (1991b). However, the use of the Dirichlet frequency cannot be justified for modeling of unpremixed reacting flow in a general sense (Frankel, 1992). In fact, there is no way of implementing this density directly for modeling of nonequilibrium flames, involving strong temperature variations. This is simply due to the additivity constraints of this density requiring the unity sum of the normalized random variables (30).

Secondly, the mathematical derivations presented here are only valid for initially segregated reactants. In both models the complete segregation facilitates significant simplifications of the final equations. This assumption is compatible with that made in the majority of previous works on unpremixed reacting flows (Toor, 1975; Brodkey, 1981; Bilger, 1980). For other initial conditions, e.g., partial premixing of the reactants, or non-delta-like distributions, numerical integration of the PDF transport equation is required. Again, an appropriately devised numerical procedure can accommodate such conditions. However, the use of a beta density (or any other assumed distributions) cannot be justified for other complex initial conditions.

Thirdly, the final mathematical expressions are only valid in the setting of a homogeneous flow. Extension to inhomogeneous flow predictions is also straightforward, but requires numerical integration of the modeled equations. Both models can be directly implemented into appropriately devised numerical procedures. The mapping closure can be invoked in the *mixing* step of a fractional stepping procedure, similar to that of typical Monte Carlo procedures (Pope, 1981). The beta density requires modeled transport equations for the low-order statistics of the reacting field. These equations include the required information pertaining to the spatial inhomogeneity of the flow through the parameters $\beta_1, \beta_2, \ldots$. With this information, all the higher-order statistics of the reacting field can be provided by simple analytical means (Girimaji, 1991b; Frankel *et al.*, 1992b).

Finally, in the context of the single-point PDF formulation presented, there is no information pertaining to the evolution of the relevant turbulent length scales. The final expressions can only be presented in terms of other physical parameters (here, through the variance of the Shvab–Zeldovich variable). In the context considered, this parameter has been provided by the DNS data. In a practical

application, this must be provided by external means (turbulence models, experimental data, etc.). Jiang *et al.* (1992) and Frankel *et al.* (1992a) provide further discussions related to this issue.

5. Concluding Remarks

It is demonstrated that the mapping closure of Kraichnan (Chen *et al.*, 1989; Pope, 1991) yields closed-form analytical expressions for predicting the limiting bound of the mean reactant conversion rate in simple chemistry of the type $F + rO \rightarrow (1 + r)$ *Product* in homogeneous, isothermal turbulent flows. It is also shown that, for the case of complete initial segregation, the scalar PDFs generated by this closure can be well approximated by a beta density. This density also provides closed-form analytical expressions for the limiting rate of mean reactant conversion. A nice feature of the mathematical results generated by the two models is their capability of revealing the influence of the stoichiometric coefficient and the equivalence ratio. In both cases the mathematical expressions simplify significantly for a stoichiometric mixture. The prediction results via both models compare favorably with data generated by DNS. This agreement follows from the compatibility of the models' PDFs with those of DNS. The simple final results generated here are superior to those of previous closures based on typical C/D models, and those based on Toor's hypothesis.

These closed-form relations are furnished with the imposition of several restrictive assumptions. The ramifications associated with these assumptions are discussed, and some suggestions for future extensions are provided. Despite these assumptions, it is very encouraging to have physically plausible algebraic relations for the direct estimate of the mean reactant conversion rate in homogeneous turbulent flows, typical of those in plug flow reactors.

Acknowledgments

The original version of the DNS computer code was provided by Dr. Gordon Erlebacher (ICASE, NASA LaRC). The authors are grateful to Dr. Erlebacher for his invaluable assistance in modifying this code. The authors are also indebeted to Dr. J. Philip Drummond (NASA LaRC) and to Mr. Richard S. Miller (SUNY—Buffalo) for their suggestions and many helpful discussions in regard to this work.

References

Abramowitz, M., and Stegun, I.A. (1972). *Handbook of Mathematical Functions and Formulas, Graphs, and Mathematical Tables.* Government Printing Office, Washington, DC.

Bilger, R.W. (1980). Turbulent flows with nonpremixed reactants. In Libby, P.A., and Williams, F.A., editors, *Turbulent Reacting Flows*, pp. 65–113. Springer-Verlag, Heidelberg.

Brodkey, R.S. (1981). Fundamentals of turbulent motion. *Chem. Engrg. Comm.* **8**, 1–23.

Chen, H., Chen, S., and Kraichnan, R.H. (1989). Probability distribution of a stochastically advected scalar field. *Phys. Rev. Lett.* **63**, 2657–2660.

Curl, R.L. (1963). Dispersed phase mixing: I. Theory and effects in simple reactors. *AIChE J.* **9**, 175–181.

Dutta, A., and Tarbell, J.M. (1989). Closure models for turbulent reacting flows. *AIChE J.* **35**, 2013–2027.

Erlebacher, G., Hussaini, M.Y., Speziale, C.G., and Zang, T.A. (1987). Toward the large eddy simulation of compressible turbulent flows. ICASE Report 87-20, NASA Langley Research Center, Hampton, VA. Also available as NASA CR 178273.

Erlebacher, G., Hussaini, M.Y., Speziale, C.G., and Zang, T.A. (1990a). On the large-eddy simulation of compressible isotropic turbulence. In *Proc. 12th Internat. Conf. on Numerical Methods in Fluid Dynamics.*

Erlebacher, G., Hussaini, M.Y., Kreiss, H.O., and Sarkar, S. (1990b). The analysis and simulation of compressible turbulence. *Theoret. Comput. Fluid Dynamics* **2**, 73–95.

Eswaran, V., and Pope, S.B. (1988). Direct numerical simulations of the turbulent mixing of a passive scalar. *Phys. Fluids* **31**, 506–520.

Frankel, S.H. (1992). Ph.D. Thesis, Department of Mechanical and Aerospace Engineering, State University of New York at Buffalo, Buffalo, NY, in preparation.

Frankel, S.H., Madnia, C.K., and Givi, P. (1991). On the modeling of the unmixedness in homogeneous reacting turbulence. *Chem. Engrg. Comm.* **104**, 117–125.

Frankel, S.H., Jiang, T.J., and Givi, P. (1992a). Modeling of isotropic reacting turbulence by a hybrid mapping-EDQNM closure. *AIChE J.* **38**, 535-543.

Frankel, S.H., Madnia, C.K., and Givi, P. (1992b). Modeling of the reactant conversion rate in a turbulent shear flow. *Chem. Engrg. Comm.* **113**, 197-209.

Gao, F. (1991a). An analytical solution for the scalar probability density function in homogeneous turbulence. *Phys. Fluids A* **3**, 511-513.

Gao, F. (1991b). Mapping closure and non-Gaussianity of the scalar probability density functions in isotropic turbulence. *Phys. Fluids A* **3**, 2438-2444.

Gao, F., and O'Brien, E.E. (1991). A mapping closure for multispecies Fickian diffusion. *Phys. Fluids A* **3**, 956-959.

Girimaji, S.S. (1991a). Assumed β-pdf model for turbulent mixing: validation and extension to multiple scalar mixing. *Combust. Sci. Technol.* **78**, 177-196.

Girimaji, S.S. (1991b). A simple recipe for modeling reaction-rates in flows with turbulent-combustion. AIAA paper AIAA-91-1792.

Givi, P. (1989). Model free simulations of turbulent reactive flows. *Progr. Energy Combust. Sci.* **15**, 1-107.

Givi, P., and McMurtry, P.A. (1988). Non-premixed reaction in homogeneous turbulence: direct numerical simulations. *AIChE J.* **34**, 1039-1042.

Hawthorne, W.R., Wedell, D.S., and Hottel, H.C. (1949). Mixing and combustion in turbulent gas jets. In *Proc. 3rd Symp. on Combustion, Flames and Explosion Phenomena*, pp. 266-288. The Combustion Institute, Pittsburgh, PA.

Hill, J.C. (1976). Homogeneous turbulent mixing with chemical reaction. *Ann. Rev. Fluid Mech.* **8**, 135-161.

Hussaini, M.Y., Speziale, C.G., and Zang, T.A. (1990). The potential and limitations of direct and large eddy simulations. In Lumley, J.L., editor, *Whither Turbulence? Turbulence at the Crossroads*, pp. 354-368. Lecture Notes in Physics, vol. 357. Springer-Verlag, Berlin.

Janicka, J., and Peters, N. (1982). Prediction of turbulent jet diffusion flame lift-off using a pdf transport equation. In *Proc. 19th Internat. Symp. on Combustion*, pp. 367-374. The Combustion Institute, Pittsburgh, PA.

Janicka, J., Kolbe, W., and Kollmann, W. (1979). Closure of the transport equation for the probability density function of turbulent scalar field. *J. Nonequil. Thermodyn.* **4**, 47-66.

Jiang, T.-L., Givi, P., and Gao, F. (1992). Binary and trinary scalar mixing by Fickian diffusion-some mapping closure results. *Phys. Fluids A* **4**, 1028-1035.

Johnson, M.E. (1987). *Multivariate Statistical Simulation.* Wiley, New York.

Johnson, N.L., and Kotz, S. (1972). *Distributions in Statistics: Continuous Multivariate Distributions.* Wiley, New York.

Jones, W.P., and Priddin, C.H. (1978). Predictions of the flowfield and local gas composition in gas turbine combustors. In *Proc. 17th Internat. Symp. on Combustion*, pp. 399-409. The Combustion Institute, Pittsburgh, PA.

Kollmann, W. (1990). The pdf approach to turbulent flow. *Theoret. Comput. Fluid Dynamics* **1**, 249-285.

Kosaly, G. (1986). Theoretical remarks on a phenomenological model of turbulent mixing. *Combust. Sci. Technol.* **49**, 227-234.

Kosaly, G. (1987). Non-premixed simple reaction in homogeneous turbulence. *AIChE J.* **33**, 1998-2002.

Kosaly, G., and Givi, P. (1987). Modeling of turbulent molecular mixing. *Combust. Flame* **70**, 101-118.

Kraichnan, R.H. (1989). Closures for probability distributions. *Bull. Amer. Phys. Soc.* **34**, 2298.

Leonard, A.D., and Hill, J.C. (1987). A simple chemical reaction in numerically simulated homogeneous turbulence. AIAA paper AIAA-87-0134.

Leonard, A.D., and Hill, J.C. (1988a). Direct numerical simulation of a homogeneous turbulent reacting flow. AIAA paper AIAA-88-3624.

Leonard, A.D., and Hill, J.C. (1988b). Direct numerical simulation of turbulent flows with chemical reaction. *J. Sci. Comput.* **3**, 25-43.

Leonard, A.D., and Hill, J.C. (1991). Scalar dissipation and mixing in turbulent reacting flows. *Phys. Fluids A.* **3**, 1286-1299.

Libby, P.A., and Williams, F.A., editors (1980). *Turbulent Reacting Flows.* Topics in Applied Physics, vol. 44. Springer-Verlag, Heidelberg.

Lockwood, F.C., and Moneib, H.A. (1980). Fluctuating temperature measurement in a heated round free jet. *Combust. Sci. Technol.* **22**, 63-81.

Madnia, C.K., and Givi, P. (1992). On DNS and LES of homogeneous reacting turbulence. In Galperin, B., and Orszag, S.A., editors, *Large Eddy Simulations of Complex Engineering and Geophysical Flows.* Cambridge University Press, Cambridge, in press.

Madnia, C.K., Frankel, S.H., and Givi, P. (1991a). Direct numerical simulations of the unmixedness in homogeneous reacting turbulence. *Chem. Engrg. Comm.* **109**, 19-29.

Madnia, C.K., Frankel, S.H., and Givi, P. (1991b). Mathematical modeling of the reactant conversion rate by single-point pdf methods. In *Proc. Fall Technical Meeting of the Combustion Institute, Eastern Section*, Ithaca, NY.

McMurtry, P.A., and Givi, P. (1989). Direct numerical simulations of mixing and reaction in a nonpremixed homogeneous turbulent flow. *Combust. Flame* **77**, 171-185.

Narumi, S. (1923). On the general form of bivariate frequency distributions which are mathematically possible when regression and variation are subjected to limiting conditions, I. *Biometrika* **15**, 77-88.

O'Brien, E.E. (1971). Turbulent mixing of two rapidly reacting chemical species. *Phys. Fluids* **14**, 1326.

O'Brien, E.E. (1980). The probability density function (PDF) approach to reacting turbulent flows. In Libby, P.A., and Williams, F.A., editors, *Turbulent Reacting Flows*, pp. 185-218. Springer-Verlag, Heidelberg.

Passot, T., and Pouquet, A. (1987). Numerical simulation of compressible homogeneous flows in the turbulent regime. *J. Fluid Mech.* **181**, 441-466.

Pearson, K. (1895). Contributions to the mathematical theory of evolution: II. Skew variations in homogeneous material. *Philos. Trans. Roy. Soc. London Ser. A.* **186**, 343–414.

Peters, N. (1984). Laminar diffusion flamelet models in non-premixed turbulent combustion. *Progr. Energy Combust. Sci.* **10**, 319–339.

Pope, S.B. (1976). The probability approach to modelling of turbulent reacting flows. *Combust. Flame* **27**, 299–312.

Pope, S.B. (1981). A Monte Carlo method for the pdf equations of turbulent reactive flow. *Combust. Sci. Techol.* **25**, 159–174.

Pope, S.B. (1982). An improved turbulent mixing model. *Combust. Sci. Technol.* **28**, 131–145.

Pope, S.B. (1985). PDF methods for turbulent reacting flows. *Progr. Energy Combust. Sci.* **11**, 119–192.

Pope, S.B. (1990). Computations of turbulent combustion: progress and challenges. In *Proc. 23rd Internat. Symp. on Combustion*, pp. 591–612. The Combustion Institute, Pittsburgh, PA.

Pope, S.B. (1991). Mapping closures for turbulent mixing and reaction. *Theoret. Comput. Fluid Dynamics* **2**, 255–270.

Priddin, C.H. (1991). Turbulent combustion modelling—a review. In Johansson, A.V., and Alfredsson, P.H., editors, *Advances in Turbulence 3*, pp. 279–299. Springer-Verlag, Berlin.

Rhodes, P.R. (1975). A probability distribution function for turbulent flows. In Murthy, S.N.B., editor, *Turbulent Mixing in Non-Reactive and Reactive Mixing*, pp. 235–241. Plenum, New York.

Toor, H.L. (1962). Mass transfer in dilute turbulent and nonturbulent systems with rapid irreversible reactions and equal diffusivities. *AIChE J.* **8**, 70–78.

Toor, H.L. (1975). The non-premixed reaction: $A + B \rightarrow Products$. In Brodkey, R.S., editor, *Turbulence in Mixing Operations*, pp. 123–166. Academic Press, New York.

Valiño, L., and Gao, F. (1991). Monte Carlo implementation of the mapping closure for turbulent reacting flows. In *Fluid Dynamics Division Meeting of the American Physical Society*, Phoenix, AZ.

Valiño, L., Ros, J., and Dopazo, C. (1991). Monte Carlo implementation and analytic solution of an inert-scalar turbulent-mixing test problem using a mapping closure. *Phys. Fluids A* **3**, 2191–2198.

Wilks, S.S. (1962). *Mathematical Statistics*, 2nd edn. Wiley, New York.

Williams, F.A. (1985). *Combustion Theory*, 2nd edn. Benjamin/Cummings, Menlo Part, CA.

APPENDIX 3

Johnson-Edgeworth Translation for Probability Modeling of Turbulent Mixing

Combust. Sci. and Tech., 1993, Vol. 91, pp. 21-52
Photocopying permitted by license only

Johnson-Edgeworth Translation for Probability Modeling of Binary Scalar Mixing in Turbulent Flows

R. S. MILLER, S. H. FRANKEL, C. K. MADNIA, and P. GIVI *Department of Mechanical and Aerospace Engineering, State University of New York, Buffalo, NY 14260*

(Received August 14, 1992; in final form November 2, 1992)

Abstract—A family of Probability Density Functions (PDF's) generated by *Johnson-Edgeworth* Translation (JET) is used for statistical modeling of the mixing of an initially binary scalar in isotropic turbulence. The frequencies obtained by this translation are shown to satisfy some of the characteristics of the PDF's generated by the *Amplitude Mapping* Closure (AMC) (Kraichnan, 1989; Chen *et al.*, 1989). In fact, the solution obtained by one of the members of this family is shown to be identical to that developed by the AMC (Pope, 1991). Due to this similarity and due to the demonstrated capabilities of the AMC, a justification is provided for the use of other members of JET frequencies for the modeling of the binary mixing problem. This similarity also furnishes the reasoning for the applicability of the *Pearson Family* (PF) of frequencies for modeling of the same phenomena. The mathematical requirements associated with the applications of JET in the modeling of the binary mixing problem are provided, and all the results are compared with data generated by Direct Numerical Simulations (DNS). These comparisons indicate that the *Logit-Normal* frequency portrays some subtle features of the mixing problem better than the other closures. However, none of the models considered (JET, AMC, and PF) are capable of predicting the evolution of the conditional expected dissipation and/or the conditional expected diffusion of the scalar field in accordance with DNS. It is demonstrated that this is due to the incapability of the models to account for the variations of the scalar bounds as the mixing proceeds. A remedy is suggested for overcoming this problem which can be useful in probability modeling of turbulent mixing, especially when accompanied by chemical reactions. While in the context of a single-point description the evolution of the scalar bounds cannot be predicted, the qualitative analytical-computational results portray a physically plausible behavior.

1 INTRODUCTION

The problem of binary mixing in turbulent flows has been the subject of widespread investigations over the past two decades (Dopazo, 1973; Pope, 1979; Pope, 1985; Pope, 1990; Givi, 1989; Kollmann, 1990). This problem has been particularly useful in assessing the extent of validity of the closures developed within this period for modeling of turbulent mixing by Probability Density Function (PDF) methods (Dopazo, 1973; Pope, 1976; Pope, 1979; Janicka *et al.*, 1979; Pope, 1982; Kosaly and Givi, 1987; Norris and Pope, 1991). Usually the problem is considered in the setting of a spatially homogeneous turbulent flow in which the temporal evolution of the PDF is considered. In this setting, development of a closure which can accurately predict the evolution of the PDF has been the main objective of these investigations (for recent reviews see Pope (1990); Kollmann (1990); Givi (1989)).

Computational experiments based on Direct Numerical Simulations (DNS) have proven very useful in evaluating the performance of new closures (Givi, 1989; Pope, 1990). The binary mixing problem is well-suited for DNS investigation, and current computational capabilities allow consideration of flows at sufficiently large Reynolds numbers in which the behavior of the models can be assessed (Eswaran and Pope, 1988; Givi and McMurtry, 1988; McMurtry and Givi, 1989; Madnia and Givi, 1992). The results of all the previous work on DNS of the binary mixing problem portray a clear picture of the PDF evolution, at least at the single-point level. A successful closure is one which can predict all the stages of mixing, as depicted by DNS, from an initially binary state (total segregated) to a final mixed condition.

Amongst the models developed in the literature, the recent Amplitude Mapping Closure (AMC) (Kraichnan, 1989; Chen *et al.*, 1989; Pope, 1991) has proven effective in producing a physically correct PDF evolution. In the application of this model to the problem of binary mixing it has been demonstrated that the closure is capable of approximating a reasonably correct evolution at all stages of mixing (Pope, 1991). Namely, the evolution from an initial double delta PDF to an asymptotic Gaussian distribution. This is a trend which has been observed in DNS (Eswaran and Pope, 1988; Givi and McMurtry, 1988; McMurtry and Givi, 1989; Madnia and Givi, 1992) and also corroborated by experimental investigations (Miyawaki *et al.*, 1974). However, it is shown by Gao (1991); O'Brien and Jiang (1991) that the PDF adopts an asymptotic Gaussian-like distribution only near the mean scalar value, and the conditional expected dissipation does not correspond to that of a Gaussian field everywhere within the composition domain.

Our first objective in this work is to present another means by which the AMC can be viewed. It is demonstrated that in the binary mixing problem, this closure can be considered as a member of the family of frequencies generated by the method of Johnson-Edgeworth Translation (JET). In fact, it is shown that the result produced by the AMC is identical to that generated by one of the members of this translation. With this observation, a justification for employing other simpler "assumed" frequencies is provided. Our second objective is to make a detailed examination of the conditional expected dissipation and the conditional expected diffusion of the scalar variable as predicted by the closures. This examination provides an effective means of demonstrating the deficiencies of these models in reproducing the correct physical behavior as depicted by DNS results. With the development of analytical relations for some of these closures, a remedy is suggested for overcoming the model deficiencies.

1.1 Outline

In the next section, the problem of binary mixing and its solution via the AMC is briefly reviewed. In Section 3, the Johnson-Edgeworth Translation is introduced with a highlight on the mathematical constraints associated with its application for the modeling of the mixing problem. Due to the previously established similarity of the JET frequencies with those based on the Pearson Family (PF), the Beta density of the first kind is also presented in this section. The PDF's generated by these three models (AMC, JET and PF) are compared against each other and also with data generated by Direct Numerical Simulations (DNS) in Section 4. The results for the conditional expected scalar dissipation, and the conditional expected scalar diffusion for all the closures are discussed, respectively, in Section 5 and in Section 6. In Section 7, some theoretical remarks pertaining to the evolution of the scalar in an isotropic field are presented. With this presentation, the problems associated with all three closures become more clear. In Sections 2-7, the discussions are limited to those associated with the transport of a passive scalar from an initially symmetric binary state in isotopic turbulence. Therefore, in Section 8 some discussions are presented of the applications of the models for treating more general problems. This paper is drawn to a conclusion in Section 9.

2 BINARY MIXING PROBLEM

We consider the mixing of a scalar variable $\phi = \phi(\mathbf{x}, t)$ ($\mathbf{x}$ is the position vector, and t denotes time) from an initially symmetric binary state within the bounds $\phi_\ell \leq \phi \leq \phi_u$. In this section, we assume that the lower and the upper bounds of the scalar range remain fixed (*i.e.* ϕ_u, ϕ_ℓ are constant). Within this domain, the single-point PDF of the variable ϕ at initial time is given by

$$P_1(\phi, t = 0) = \frac{1}{2}[\delta(\phi - \phi_\ell) + \delta(\phi - \phi_u)], \tag{1}$$

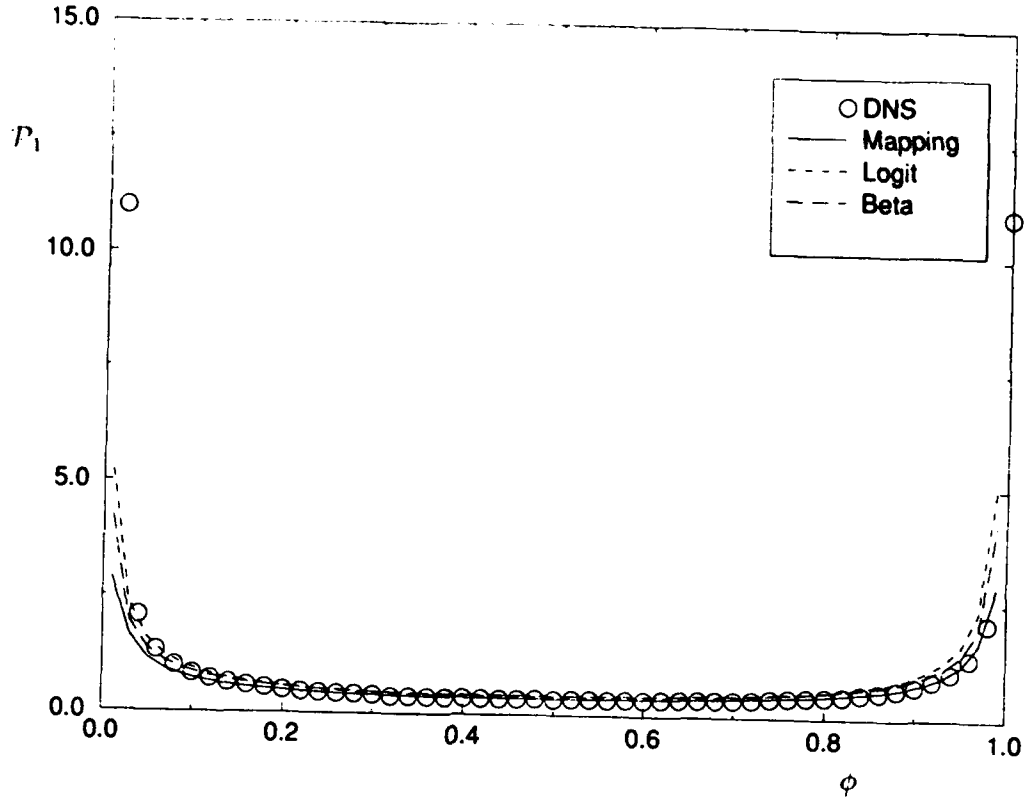

FIGURE 1a The comparison of the PDF's as predicted by the models with DNS data. (a) $\sigma^2 = 0.173$.

which obviously infers the following relations for the mean and the variance

$$< \phi >= (\phi_u + \phi_l)/2, < \phi'^2 >= \sigma^2 = \frac{1}{4}(\phi_u - \phi_l)^2. \tag{2}$$

Here, <> indicates the probability mean, σ^2 denotes the variance, and the prime represents the instantaneous deviation from the mean. In isotropic incompressible turbulence, the evolution of the PDF is governed by the transport equation

$$\frac{\partial P_1}{\partial t} + \frac{\partial^2(\epsilon P_1)}{\partial \phi^2} = 0, \qquad \phi_l \le \phi \le \phi_u \tag{3}$$

where ϵ represents the expected value of the scalar dissipation with diffusion coefficient Γ, $\xi(= \Gamma \nabla\phi \cdot \nabla\phi)$, conditioned on the value of the scalar $\phi(\mathbf{x}, t)$,

$$\epsilon = \epsilon(\phi, t) =< \xi | \phi(\mathbf{x}, t) > . \tag{4}$$

Equation (3) can alternatively be expressed by

$$\frac{\partial P_1}{\partial t} + \frac{\partial(DP_1)}{\partial \phi} = 0, \qquad \phi_l \le \phi \le \phi_u, \tag{5}$$

where D denotes the conditional expected value of the scalar diffusion

$$D = D(\phi, t) =< \Gamma \nabla^2 \phi | \phi(\mathbf{x}, t) > . \tag{6}$$

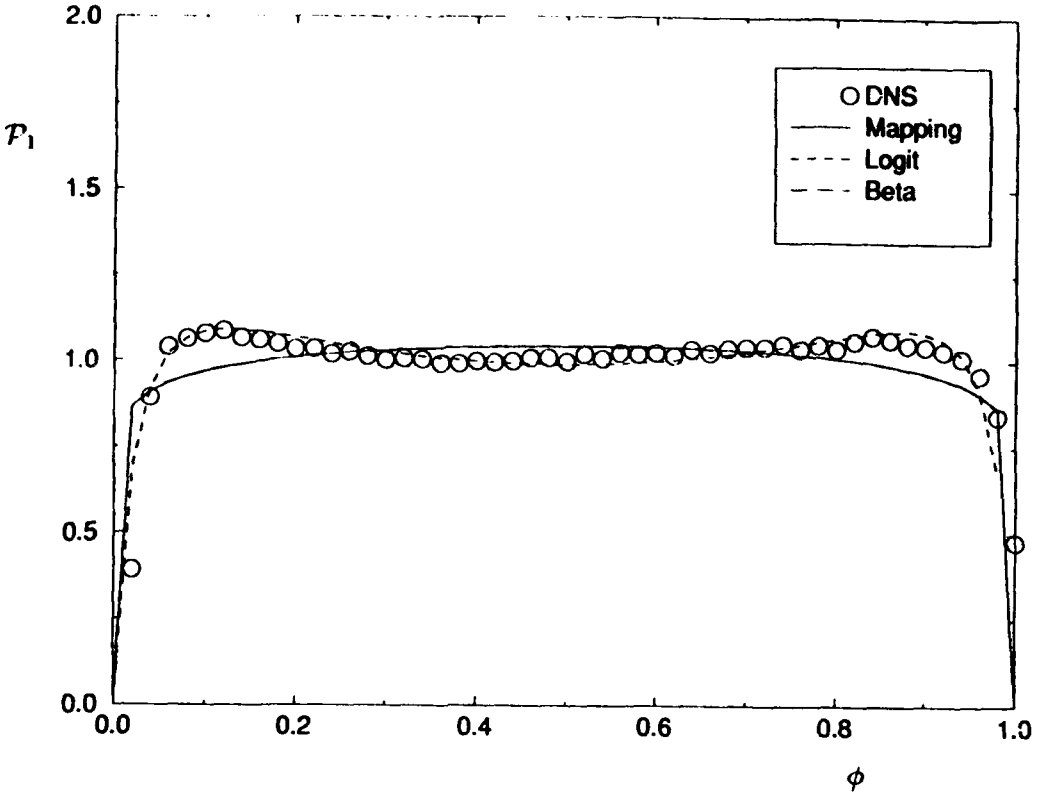

FIGURE 1b The comparison of the PDF's as predicted by the models with DNS data. (b) $\sigma^2 = 0.079$.

The closure problem in determining the PDF, P_1, is associated with the unknown conditional expected dissipation, ϵ, and/or the conditional expected diffusion, D. These two are related through Eqs. (1)-(6),

$$D(\phi, t) = \frac{1}{P_1(\phi, t)} \frac{\partial(\epsilon P_1)}{\partial \phi}. \tag{7}$$

At the single-point level neither the conditional mean dissipation nor the conditional mean diffusion are known (neither are their unconditional mean values). Their specifications require external information.

With the application of the AMC, this external information is obtained in an implicit manner. As explained in detail by Pope (1991), the AMC involves a *mapping* of the random field of interest ϕ to a stationary Gaussian reference field ϕ_0, via a transformation $\phi = \chi(\phi_0, t)$. Once this relation is established, the PDF of the random variable ϕ, $P_1(\phi)$, is related to that of a Gaussian distribution. In a domain with fixed upper and lower bounds, *i.e.* fixed ϕ_ℓ, ϕ_u, the corresponding form of the mapping function is obtained by Pope (1991). The solution for a symmetric field with zero mean, $< \phi >= 0, \phi_u = -\phi_\ell$, is represented in terms of an unknown time τ

$$\chi(\phi_0, \tau) = \phi_u \quad \text{erf}\left(\frac{\phi_0}{\sqrt{2}G}\right), G(\tau) = \sqrt{\exp(2\tau) - 1}. \tag{8}$$

With this transformation, the PDF is determined from the physical requirement

$$P_1(\chi(\phi_0, \tau), \tau) d\chi = P_G(\phi_0) d\phi_0, \tag{9}$$

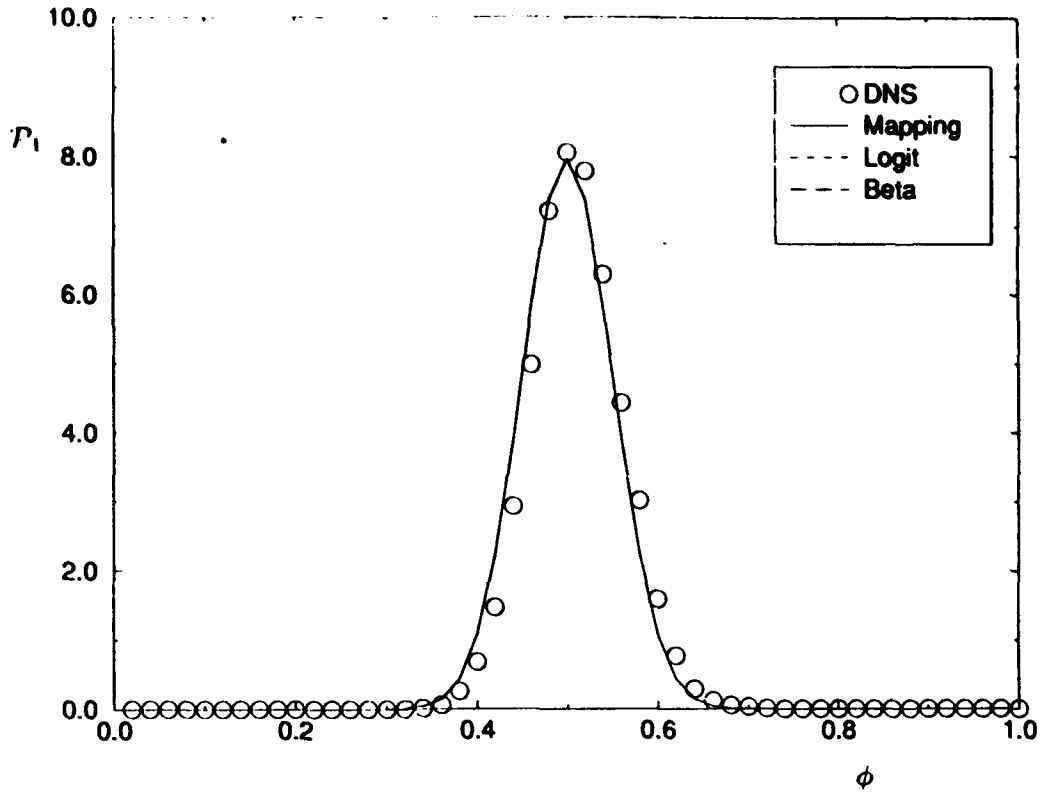

FIGURE 1c The comparison of the PDF's as predicted by the models with DNS data. (c) $\sigma^2 = 0.00247$.

where P_G denotes the PDF of a standardized Gaussian distribution, *i.e.* $P_G(\phi_0) = \frac{1}{\sqrt{2\pi}} \exp(-\phi_0^2/2)$. A combination of Eq. (8) and Eq. (9) yields

$$P_1(\phi,\tau) = \frac{G}{2\phi_u} \exp\left\{-(G^2-1)\left[\mathrm{erf}^{-1}(\frac{\phi}{\phi_u})\right]^2\right\}. \tag{10}$$

In these equations, the relation between τ and the physical time t is unknown in the context of a single-point description. This relation can be obtained only through knowledge of the higher order statistical properties of the scalar field. For example, it is shown by Madnia *et al.* (1992); Frankel *et al.* (1992a) that the mapping closure yields the algebraic relation for the normalized variance,

$$\frac{<\sigma^2>(\tau)}{<\sigma^2>(0)} = \frac{2}{\pi} \arctan\left(\frac{1}{G\sqrt{G^2+2}}\right), \tag{11}$$

in which the variance is related to the unknown mean dissipation $\epsilon(t)$ by integrating Eq. (3),

$$\sigma \frac{d\sigma}{dt} = -\epsilon(t), \tag{12}$$

where,

$$\epsilon(t) = \int_{\phi_l}^{\phi_u} P_1(\phi,t)\epsilon(\phi,t)d\phi = -\int_{\phi_l}^{\phi_u} \phi P_1(\phi,t)D(\phi,t)d\phi. \tag{13}$$

3 JOHNSON-EDGEWORTH TRANSLATION

The AMC captures some of the basic features of the binary mixing problem as described by Pope (1991). Namely, the inverse diffusion of the PDF in the composition domain from a double delta distribution to an asymptotic Gaussian distribution centered around $< \phi >$, as $\sigma^2 \rightarrow 0$ (or $G \rightarrow \infty$). This asymptotic Gaussian distribution near the mean scalar value cannot be realized in any of the previous mixing models based on the so called Coalescence/Dispersion (C/D) closures (Curl, 1963; Janicka *et al.*, 1979; Pope, 1982; Kosaly and Givi, 1987). And those modified C/D models which do yield such an asymptotic state, *e.g.* Pope (1982), do not predict the initial stages of mixing correctly (Kosaly, 1986). This deficiency of the C/D models in yielding asymptotic Gaussianity has been a motivating factor for recent investigations resulting in the development of the AMC (Pope, 1991).

In the spirit of "mapping" to a specified reference field, it is speculated that there are perhaps other means of "driving" the PDF toward Gaussianity in a physically acceptable manner. In fact, this subject has been of major interest to statisticians and biometricians within the last century since the early work of Edgeworth (1907). The scheme was referred to by Edgeworth as the Method of Translation, and was later detailed by Johnson (1949a). In today's literature of statistics and biometrics, the scheme is known as Johnson-Edgeworth frequency generation, and has many applications in statistical analysis.

The essential element of Johnson-Edgeworth Translation (JET) is similar to that of the AMC. Namely, it involves the transformation of the random physical field, here, ϕ, to a fixed standard Gaussian reference field by means of a translation (or mapping) of the form

$$\phi = Z\left[\frac{\phi_0}{\gamma(t)}\right],$$

$$\gamma(t=0) = 0 \leq \gamma(t) \leq \gamma(t \rightarrow \infty) \rightarrow \infty. \tag{14}$$

In this equation, the function $\gamma(t)$ plays a role similar to that of G in the AMC. With an appropriate form for the function Z, the scalar PDF is determined from Eq. (9). For application in the problem of mixing from an initially symmetric binary state of zero mean within a fixed domain $\phi_l = -\phi_u \leq \phi \leq \phi_u$, the appropriate JET must satisfy the following physical constraints:

$$(i)\mathrm{Lim}_{(\gamma \rightarrow 0)} Z\left(\frac{\phi_0}{\gamma}\right) \approx H(\phi_0)$$

$$(ii)\mathrm{Lim}_{(\gamma \rightarrow \infty)} Z\left(\frac{\phi_0}{\gamma}\right) \approx C\phi_0 + O(\phi_0^3) + \ldots$$

(iii) $Z(\frac{\phi_0}{\gamma})$ is an odd function with respect to the scalar mean for any value of σ^2.

(iv) $Z(\frac{\phi_0}{\gamma})$ is bounded and is a non-decreasing function of ϕ_0, and $-\phi_u \leq Z \leq \phi_u$ at all times.

(15)

In these relations, H denotes the Heaviside function, and C is constant. Constraint (i) implies an initially symmetric and segregated binary state. The second constraint ensures an asymptotic Gaussian distribution for $P_1(\phi)$ near the mean scalar value. Condition (iii) preserves the symmetry of the PDF around the mean value at all times, and constraint (iv) implies the boundedness of the scalar field, *i.e.* $-\phi_u \leq \phi \leq \phi_u$. A function Z

which satisfies all the above constraints, is therefore expected to provide an acceptable means of approximating the PDF. An example is the *Logit*-Normal (or $\tanh^{-1}$-Normal) distribution, as originally proposed by Johnson (1949a). For the symmetric problem within a fixed domain, this distribution is produced by a mapping of the form[1]

$$Z = \phi_u \tanh\left(\frac{\phi_0}{\gamma}\right). \tag{16}$$

With this mapping, together with Eq. (9), the PDF of the scalar adopts the form,

$$P_1(\phi, t) = \frac{\gamma}{\sqrt{2\pi}\left(1 - (\frac{\phi}{\phi_u})^2\right)} \exp\left\{-\frac{\gamma^2}{2}\left[\tanh^{-1}(\frac{\phi}{\phi_u})\right]^2\right\}. \tag{17}$$

It is easily verified that this frequency satisfies the physical constraints of the symmetric binary mixing problem (Eq. (15)). At $t = 0$, the PDF is approximately composed of two delta functions at $\phi = \pm\phi_u$, and as $t \to \infty$ the PDF adopts an approximate Gaussian-like distribution centered around the zero mean. These features are similar to those portrayed by the PDF generated by the AMC (Eq. (10)).

This example demonstrates that with the satisfaction of the above indicated constraints, several other frequencies can be generated for effective modeling of the binary mixing problem. In fact, it is easy to show that the solution generated by the AMC can also be viewed as a member of the JET family. This is demonstrated by considering a translation of the form

$$Z = \phi_u \operatorname{erf}\left(\frac{\phi_0}{\gamma}\right), \tag{18}$$

From Eq. (9), this translation yields the PDF

$$P_1(\phi, t) = \frac{\gamma}{2\sqrt{2}\phi_u} \exp\left\{-(\frac{\gamma^2}{2} - 1)\left[\operatorname{erf}^{-1}\left(\frac{\phi}{\phi_u}\right)\right]^2\right\}. \tag{19}$$

This frequency can be termed the erf^{-1}-Normal distribution and is identical to the form presented by Eq. (10). The difference is due to the terms containing G and γ. But this is unimportant since in the context of single-point statistics neither of the two parameters can be determined by the PDF. Therefore, with $G \equiv \frac{\gamma}{\sqrt{2}}$, both expressions are equivalent. With this equivalence, the closed form relation for the variance of the erf^{-1}-Normal distribution has the same algebraic form given by Eq. (11). It is easy to show that many other distributions can be generated to display similar characteristics. In the discussions to follow, we only consider the Logit-Normal and the erf^{-1}-Normal distributions, the latter being identical to the distribution generated by AMC.

Pearson Family

The similarity of the AMC and JET in generating equivalent PDF's is also useful in explaining the applicability of the frequencies generated by the Pearson family (Pearson, 1895). For a "bimodal" distribution, a physically acceptable frequency is the Pearson

[1] In recent literature, the Logit-Normal is usually expressed by the mapping $Z = \phi_u \left\{2[1 + \exp(\phi_0/\gamma)]^{-1} - 1\right\}$.

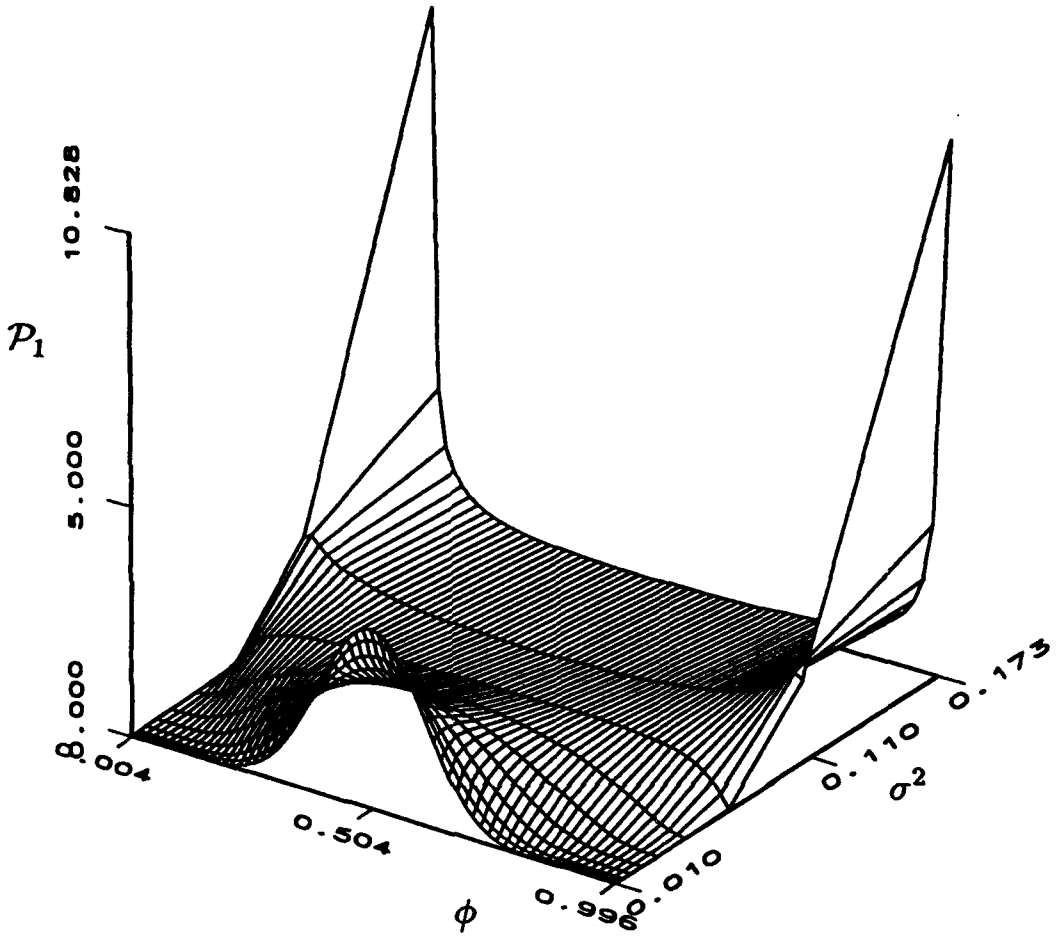

FIGURE 2 Temporal evolution of the Logit-Normal PDF.

Type I, known as the general form of the "Beta density of the first kind". This density is typically expressed in a fixed domain within the range $0 \leq \phi \leq 1$,

$$P_1(\phi) = \frac{1}{B(\beta_1, \beta_2)} \phi^{\beta_1 - 1}(1 - \phi)^{\beta_2 - 1}, 0 \leq \phi \leq 1. \tag{20}$$

Here B denotes the Beta function, and the parameters β_1 and β_2 are determined from the knowledge of the mean and the variance of the random variable. In a symmetric field within [0,1], $< \phi >= \frac{1}{2}$, $\beta_1 = \beta_2 = \beta$, and thus the PDF is characterized by the variance alone.

The similarity of the Pearson distributions and the JET frequencies is well recognized in the statistics literature (see Johnson (1949a)). Therefore, with the equivalence of the AMC and the JET as demonstrated above, it is not surprising that the Beta density and the AMC are also similar. This similarity, without a mathematical proof, has been recognized in previous works (Madnia *et al.*, 1991; Madnia and Givi, 1992).

4 COMPARATIVE ASSESSMENTS

The probability distributions obtained from the three frequency generation methods described above are all capable of providing a reasonable stochastic approximation of

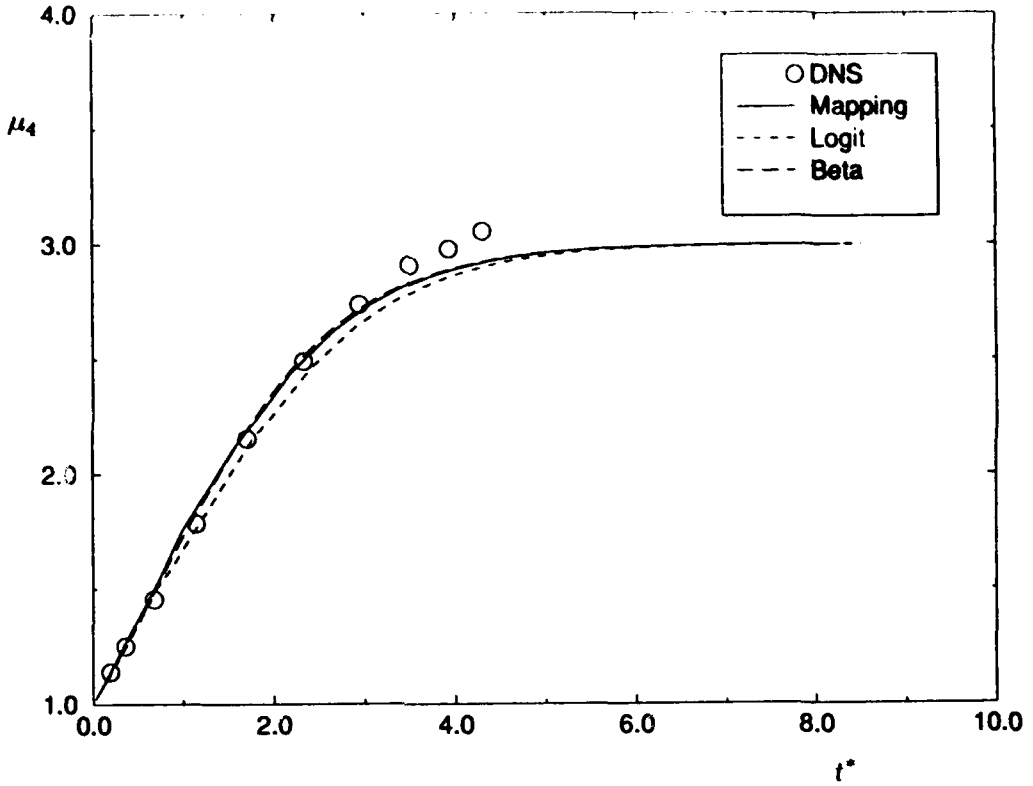

FIGURE 3a Temporal evolution of the centralized moments of the scalar variable as predicted by the models and the comparison with DNS data. (a) μ_4 vs. t^*.

the mixing problem from an initially binary state. Namely, an approximate double delta distribution at $t = 0$, and an approximate Gaussian-like distribution as $t \to \infty$. The former can be realized in the limit of unity normalized variance $\sigma^2(t)/\sigma^2(0) = 1$. In a fixed composition domain, this corresponds to $G = 0$ for AMC ($\gamma = 0$ in JET), and to $\beta = 0$ for the Beta density. The latter is realized in the limit $G, \gamma, \beta \to \infty$. The limiting Gaussian distribution for the AMC has been asserted by Pope (1991). For the JET, the criterion (ii) in Eq. (15) guarantees this condition. For the Beta density, the assertion of an asymptotic Gaussian distribution in the limit of zero variance is established in elementary texts on statistics (*e.g.* Casella and Berger (1990)). At the intermediate stages, however, the PDF's are not identical. It is easily verified by Eqs. (10), (20) that the AMC and the Beta distributions become constant ($P_1(\phi) = \text{constant} = \frac{1}{2}\phi_u$) for $G = \beta = 1$. However, the Logit-Normal PDF does not yield a uniform distribution at any stage of its evolution. Also, as indicated by Johnson (1949a) it is not possible to provide a closed form algebraic expression similar to Eq. (11) for the variance of the Logit-Normal distribution.

In order to make comparative assessments of the models, the frequencies generated by the three methods (AMC, JET, and PF) are compared with each other, and also with PDF's generated by Direct Numerical Simulations (DNS). The DNS procedure is similar to that of previous simulations of this type. Since these simulations are not the major focus of this paper, only a brief outline of the procedure is described; for a detailed discussion we refer the reader to Madnia and Givi (1992). The subject of the DNS is a three-dimensional periodic homogeneous box flow carrying a passive scalar variable. The initial scalar field is composed of square waves with maximum and minimum values of 1 and 0, respectively. These limiting values are arbitrary, and can be translated to

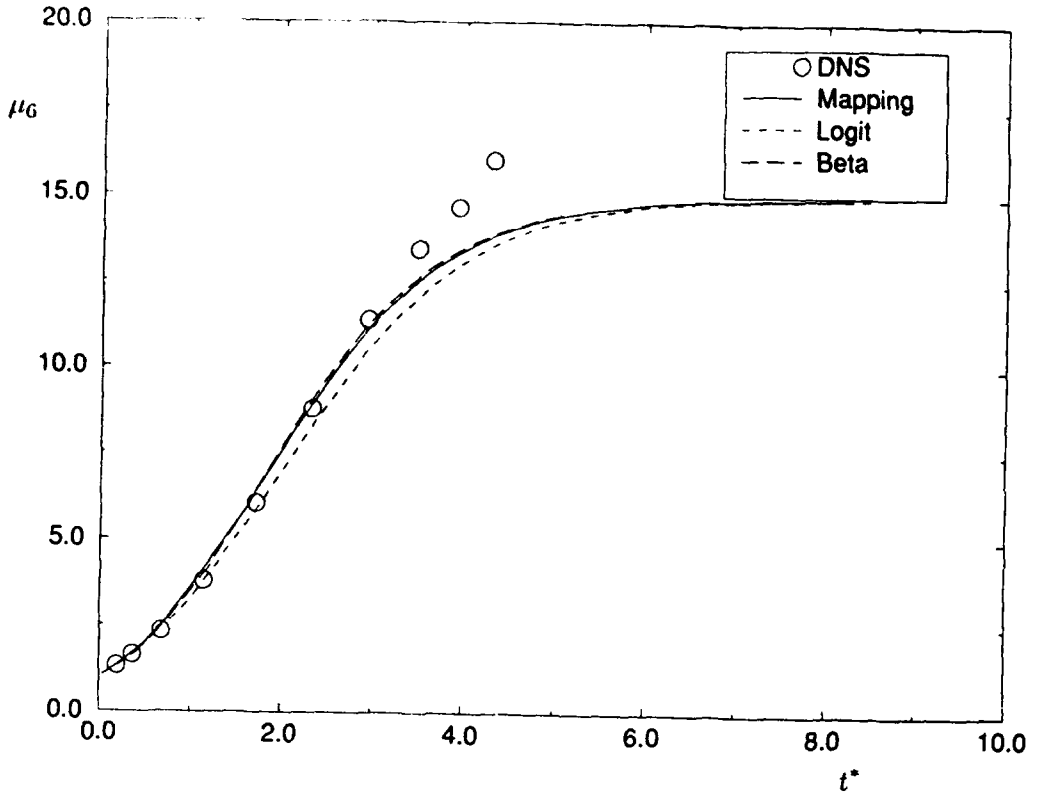

FIGURE 3b Temporal evolution of the centralized moments of the scalar variable as predicted by the models and the comparison with DNS data. (b) μ_6 vs. t^*.

appropriate ϕ_u, ϕ_ℓ for comparison to each of the models. At time zero, in most regions of the flow, the scalar adopts these limiting values (with equal probability), and the spatial regions between the initial maxima and minima are smoothed by a polynomial fit. The degree of this smoothing is minimized, but limited by the computational resolution, to ensure an approximate initial double delta distribution. The computational scheme is based on a spectral-collocation procedure using Fourier basis functions developed by Erlebacher *et al.* (1990a); Erlebacher *et al.* (1987); Erlebacher *et al.* (1990b). The hydrodynamic field is assumed isotropic and is initialized in a similar manner to that by Erlebacher *et al.* (1990a); Passot and Pouquet (1987). The code is capable of simulating flows with different levels of compressibility (Hussaini *et al.*, 1990). Here, only the results obtained for a low compressible case are discussed. The resolution consists of 96 collocation points in each direction. Therefore, at each time step 96^3 is the sample size for statistical analysis. With this resolution, simulations with a Reynolds number (based on the Taylor microscale) of $Re_\lambda \approx 41$ are attainable. The value of the molecular Schmidt number is set equal to unity.

As indicated in Section 1, in order to compare the model predictions with DNS results a matching is required of the higher order statistics of the field as generated by each method. Here, this matching is done through the variance of the conserved scalar. These results are presented in Fig. 1. This figure indicates that at initial times, $\frac{\sigma^2(t)}{\sigma^2(0)} \approx 1$, all the PDF's are approximately composed of two delta functions at $\phi = 0,1$ indicating the initial binary state. At longer times, the PDF's evolve through an inverse-like diffusion in the composition space. The heights of the delta functions decrease and the PDF's are redistributed at other ϕ values within the range [0,1]. At very long times, the PDF's

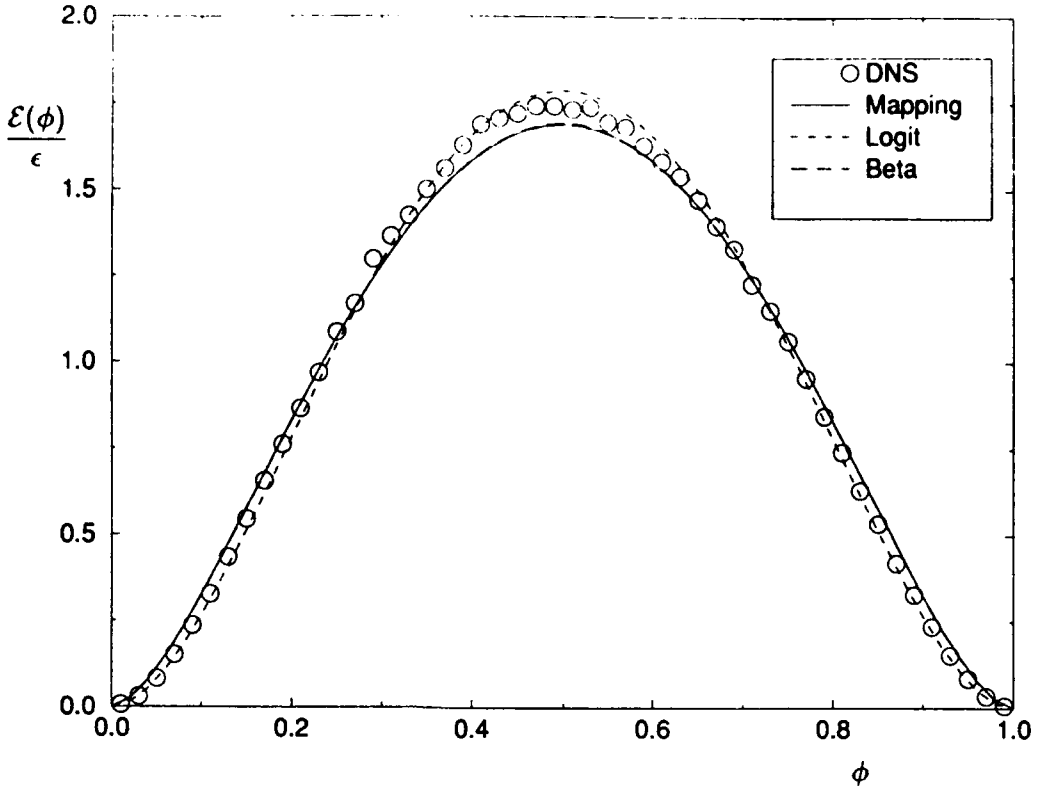

FIGURE 4a Comparisons of the normalized conditional dissipation as predicted by the three models with the DNS data. (a) $\sigma^2 = 0.079$.

become asymptotically concentrated around the mean value in a manner that can be approximated by a Gaussian distribution.

An interesting feature captured in Fig. 1(b), is the capability of the Logit-Normal distribution in depicting a subtle behavior in the frequency distribution. This feature is the double "hump" characteristic of the DNS data at intermediate times and cannot be realized by the AMC or the PF generated frequencies. All the previous DNS results including those of Eswaran and Pope (1988); Givi and McMurtry (1988); Pope (1991) portray this feature. The PDF's generated by the AMC, and the Beta distributions adopt a constant value (of 1/2) when $\sigma^2 = \frac{1}{12}$ (for $0 \leq \phi \leq 1$). This corresponds to $G = 1, \gamma = \sqrt{2}, \beta = 1$. This uniform distribution is not exactly realized in any previous or present DNS results. Therefore, it can be speculated that in the absence of a better alternative, the Logit-Normal distribution may provide the simplest means of providing an *assumed* distribution for the statistical modeling of the symmetric binary mixing problem. The complete evolution of the Logit-Normal PDF is shown in Fig. 2.

Further quantification of the agreements noted above are made by comparing the higher moments of the scalar field. This comparison is made in Fig. 3. In this figure, results are presented for the temporal variations of the kurtosis (μ_4) and the superskewness (μ_6) of the scalar variable ϕ. For the Beta density, the higher order moments are obtained analytically based on the knowledge of the variance. For the AMC, the analytical-numerical results by Jiang *et al.* (1992) are used, while for the Logit-Normal PDF the moments are calculated strictly by numerical means. This figure shows that initially, all these moments are close to unity, and monotonically increase as mixing proceeds. For all the models, the magnitude of the moments asymptotically approach the limiting values of 3 and 15, respectively, corresponding to those of a Gaussian distribution. The DNS

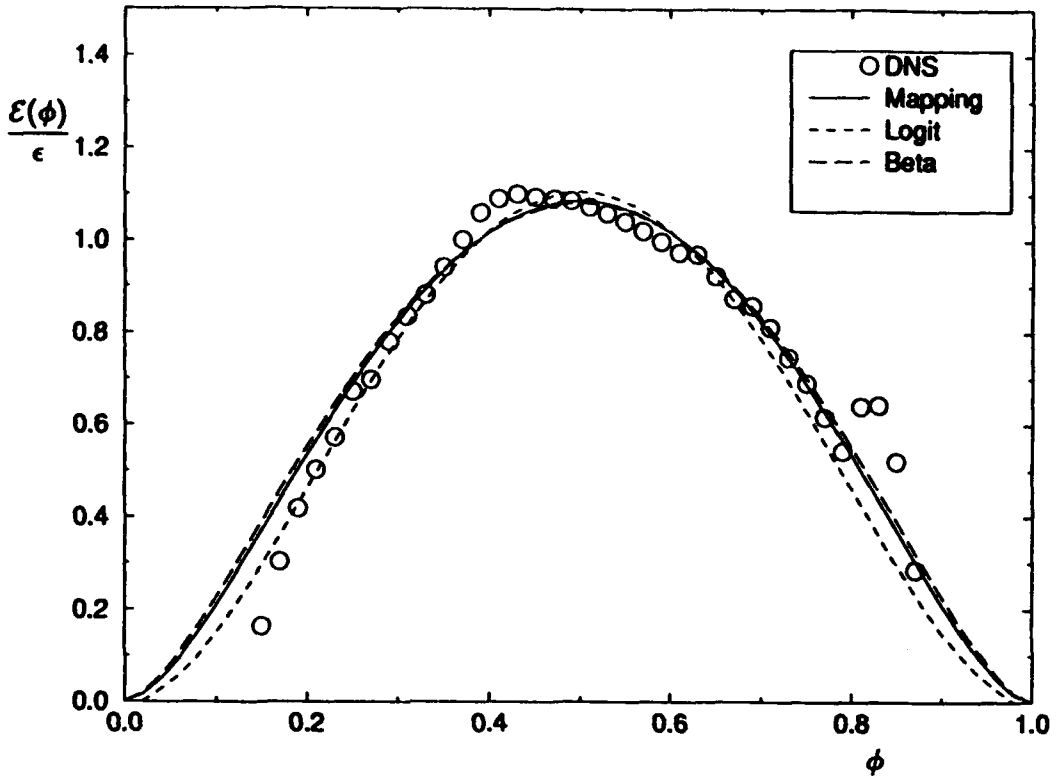

FIGURE 4b Comparisons of the normalized conditional dissipation as predicted by the three models with the DNS data. (b) $\sigma^2 = 0.013$.

results are in good agreement with the model predictions at all times. However, due to obvious numerical difficulties, the simulations could not be continued until the variance approaches zero identically.

5 SCALAR DISSIPATION

The results presented above indicate a good agreement between the model predicted single-point statistics (PDF's and high-order moments) and the DNS data at all the stages of mixing. These results also suggest an approximate asymptotic Gaussian state for all the closure PDF's and those of the DNS. Here, it will be demonstrated that the agreement between the DNS and the model predictions is very good at the initial and the intermediate stages of mixing. However, the agreement worsens at the final stages. Also it will be shown that none of the closures yield "exact" Gaussian distributions at the final stages of mixing. In doing so, it is useful to note that a Gaussian PDF is defined, and is only valid, for an unbounded domain. The frequencies generated here, are all defined within a *fixed and finite* domain. For AMC, it has been established (Gao, 1991; O'Brien and Jiang, 1991) that the finite boundary size at the initial time "maintains" its influence at *all* the subsequent stages of mixing. In other words, the PDF adopts a Gaussian distribution in the limit of zero variance only near the mean value of the scalar. In order to show the departure from Gaussianity at scalar values away from the mean, the conditional expected dissipation of the scalar field is considered.

Given the PDF, as is the case here, Eq. (3) can be used to determine the expected conditional dissipation. It has been shown by Girimaji (1992) (and will be discussed in

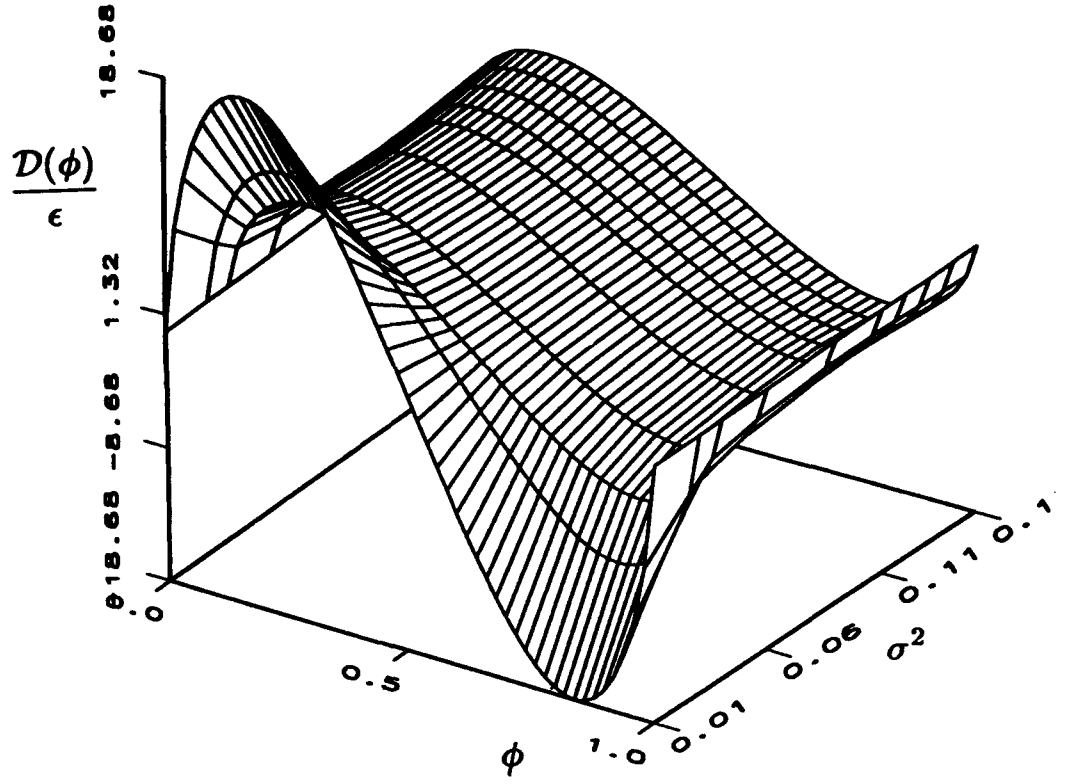

FIGURE 5a Temporal evolution of the conditional expected diffusion normalized with the total dissipation. (a) erf^{-1}-Normal.

detail in Section 7) that for a valid PDF within a defined range, $-\phi_u \leq \phi \leq \phi_u$, the expected conditional scalar dissipation is given by

$$\epsilon(\phi,t) = -\frac{1}{P_1(\phi,t)}\frac{\partial}{\partial t}\left(\int_{-\phi_u}^{\phi} F(\psi,t)d\psi\right), \tag{21}$$

where F denotes the cumulative distribution function (CDF)

$$F(\phi,t) = \int_{-\phi u}^{\phi} P_1(\psi,t)d\psi. \tag{22}$$

With Eq. (21), the expected conditional dissipation can be evaluated for a given PDF. For example, for a Gaussian distribution of zero mean, $P_G(\phi,\sigma^2) = \frac{1}{\sqrt{2\pi}\sigma}\exp(-\frac{\phi^2}{2\sigma^2})$, $-\infty = -\phi_u \leq \phi \leq \phi_u = \infty$, with a non-stationary variance, $\sigma^2 = \sigma^2(t)$, it is easily shown that,

$$\epsilon(\phi,t) = \left[\frac{1}{P_G(\phi,\sigma^2)}\right]\frac{\partial}{\partial t}\left(\frac{\phi}{2} + \frac{\phi}{2}\text{erf}(\frac{\phi}{\sqrt{2}\sigma}) + \frac{\sigma}{\sqrt{2\pi}}\exp(-\frac{\phi^2}{2\sigma^2})\right), -\infty \leq \phi \leq \infty \tag{23}$$

Noting that ϕ is an independent variable (of t), and evaluating the derivatives on the RHS of Eq. (23) yields, after some simple manipulations,

$$\epsilon(\phi,t) = \text{constant} = -\sigma\frac{d\sigma}{dt}, \tag{24}$$

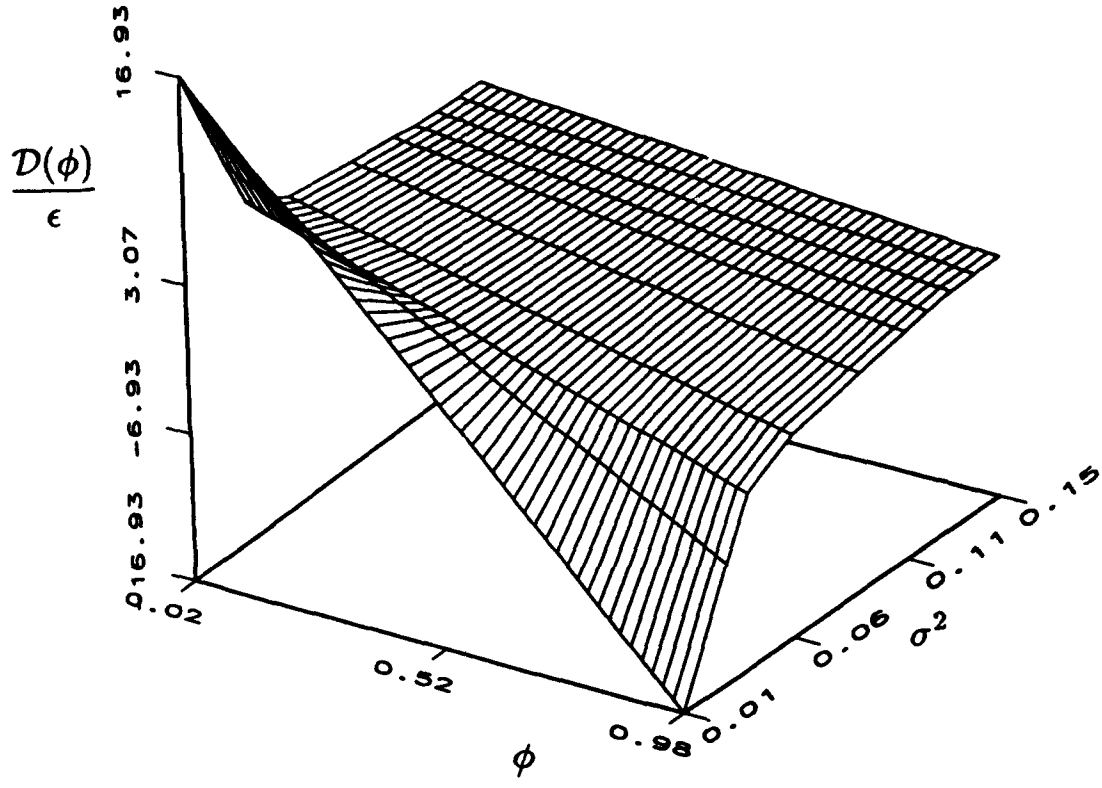

FIGURE 5b Temporal evolution of the conditional expected diffusion normalized with the total dissipation. (b) LMSE.

with the implications (derived from Eqs. (12)-(13)),

$$\frac{\epsilon(\phi,t)}{\epsilon(t)} = \text{constant} = 1, \tag{25}$$

at all times for *all* ϕ values in the range $-\infty$ to $+\infty$. Equations (24-25) indicate the independence of the conditional scalar dissipation and the composition domain for a Gaussian field. These results have also been obtained by Gao (1991); O'Brien and Jiang (1991) by following a different mathematical procedure.

The conditional expected dissipation predicted by the models can be obtained by following a similar course. For the AMC and the PF distribution, the conditional dissipation fields have been obtained by Gao (1991); O'Brien and Jiang (1991) and by Girimaji (1992), respectively. For the purpose of the discussions to follow, these results are presented here in a different form for all three closures. For the erf^{-1}-Normal distribution, the instantaneous CDF is given by

$$F(\phi,t) = \frac{1}{2}\left(1 + \text{erf}\left[\frac{\gamma}{\sqrt{2}}\text{erf}^{-1}\left(\frac{\phi}{\phi_u}\right)\right]\right). \tag{26}$$

Therefore, with Eq. (21), the conditional dissipation can be expressed in terms of the corresponding PDF,

$$\epsilon(\phi,t) = -\frac{1}{P_1(\phi,t)}\frac{\partial}{\partial t}\left\{\frac{1}{2}\int_{-\phi_u}^{\phi}\text{erf}\left[\frac{\gamma}{\sqrt{2}}\text{erf}^{-1}\left(\frac{\phi}{\phi_u}\right)\right]d\phi + \frac{1}{2}(\phi+\phi_u)\right\}. \tag{27}$$

Again, with an independence of ϕ and t this equation reduces to,

$$\varepsilon(\phi,t) = -\frac{1}{P_1(\phi,t)}\frac{\partial H}{\partial t}, \tag{28}$$

where,

$$H = \frac{\phi_u}{\sqrt{\pi}}\int_{-\phi_u}^{\mathrm{erf}^{-1}(\frac{\phi}{\phi_u})} \mathrm{erf}(\frac{\gamma}{\sqrt{2}}z)\exp(-z^2)dz. \tag{29}$$

For a PDF within a fixed domain, the integration procedure becomes simplified by evaluating the time derivatives inside the integral. In this way, the results can be expressed analytically. After some manipulations,

$$\frac{dH}{dt} = \frac{-\sqrt{2}\phi_u\frac{d\gamma}{dt}}{\pi(2+\gamma^2)}\exp\left\{-(1+\frac{\gamma^2}{2})\left[\mathrm{erf}^{-1}(\frac{\phi}{\phi_u})\right]^2\right\}, \tag{30}$$

and, therefore

$$\varepsilon(\phi,t) = \frac{4\phi_u^2\frac{d\gamma}{dt}}{\pi\gamma(2+\gamma^2)}\exp\left\{-2\left[\mathrm{erf}^{-1}(\frac{\phi}{\phi_u})\right]^2\right\}. \tag{31}$$

From this equation, the total dissipation is obtained by direct integration of the conditional mean dissipation field. The results, after significant algebraic manipulations yield

$$\epsilon(t) = \frac{4\phi_u^2\frac{d\gamma}{dt}}{\pi(2+\gamma^2)\sqrt{4+\gamma^2}}, \tag{32}$$

$$\frac{\varepsilon(\phi,t)}{\epsilon(t)} = \left(\sqrt{\frac{1+\sin\left[\frac{\pi\sigma^2(t)}{2\sigma^2(0)}\right]}{1-\sin\left[\frac{\pi\sigma^2(t)}{2\sigma^2(0)}\right]}}\right)\exp\left\{-2\left[\mathrm{erf}^{-1}(\frac{\phi}{\phi_u})\right]^2\right\}. \tag{33}$$

In the form presented above, Eqs. (31)-(33) portray several insightful features of the solution. First, Eq. (33) indicates that the conditional dissipation is always dependent on the magnitude of the scalar, and it maintains the same self-similar functional form of dependence $\exp\left\{-2\left[\mathrm{erf}^{-1}(\frac{\phi}{\phi_u})\right]^2\right\}$. This has been previously indicated by Gao (1991); O'Brien and Jiang (1991). Here, the amplitude $\varepsilon(\phi=0,t)$ can be conveniently expressed in terms of the variance decay, which is very useful for further manipulations. Second, it is interesting to note the similarity of Eqs. (31) and (33) with the results obtained for the instantaneous dissipation of Fickian mixing of a conserved scalar in laminar non-homogeneous flows (such as the typical shear flows (Spalding, 1961; Liñan, 1974; Peters, 1984)). This similarity further asserts the "permanent" influence of the boundaries since in non-homogeneous mixing, the scalar bounds are "fixed" due to the physical constraints. Finally, Eq. (32) suggests an infinitely large dissipation at time zero, *i.e.* when $\sigma^2(t)/\sigma^2(0) \doteq 1$, and the asymptotic behavior

$$\mathrm{Lim}_{(\sigma^2\to 0)}\frac{\varepsilon(\phi)}{\epsilon}\Big|_{\phi=0} = 1. \tag{34}$$

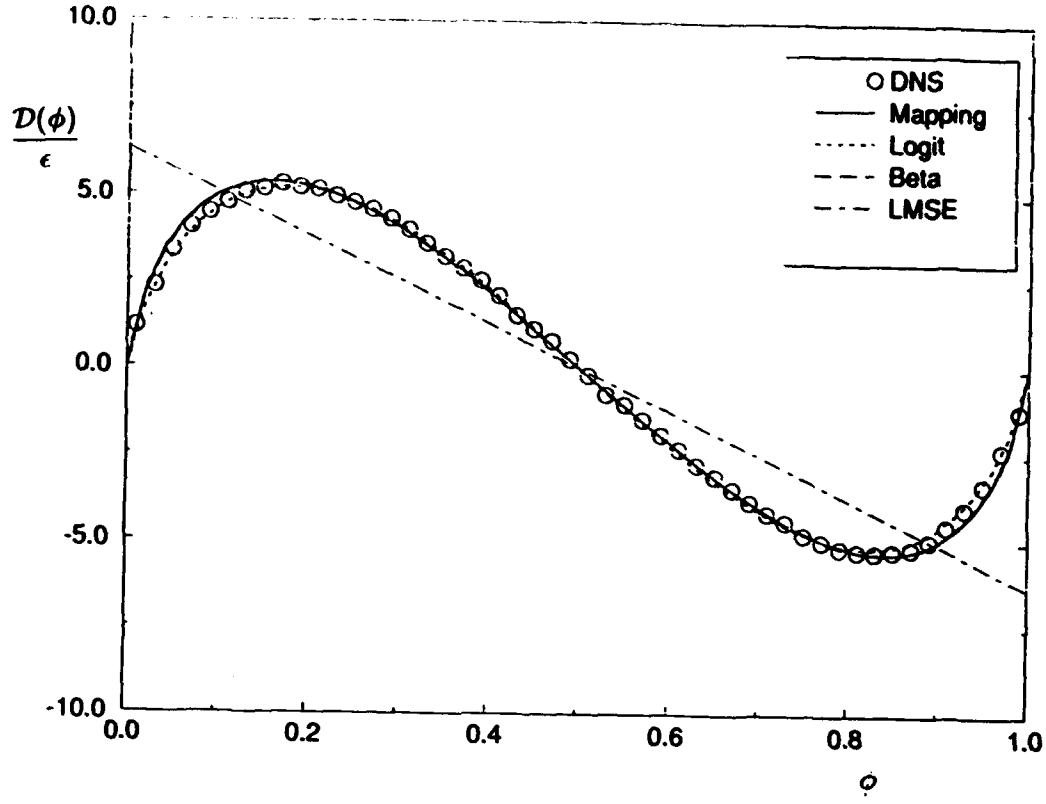

FIGURE 6a Comparisons of the normalized conditional diffusion as predicted by the three models and the LMSE closure, with the DNS data. (a) $\sigma^2 = 0.079$.

This limiting behavior near zero indicates the Gaussianity of the PDF only at the mean value of the scalar.

Following a similar procedure, the conditional expected dissipation can be obtained for the other closures. For the Beta density in the range $0 \leq \phi \leq 1$, the final results can be expressed as

$$\epsilon(\phi,t) = -\frac{1}{P_1(\phi,t)}\frac{\partial}{\partial t}\left(\int_0^{\phi} I_{\phi}(\beta,\beta)d\phi\right), \tag{35}$$

where, I denotes the Incomplete Beta Function (Abramowitz and Stegun, 1972). For the Logit-Normal distribution, the corresponding form is

$$\epsilon(\phi,t) = -\frac{1}{P_1(\phi,t)}\frac{\partial}{\partial t}\left\{\frac{1}{2}\int_{-\phi_u}^{\phi} \mathrm{erf}\left[\frac{\gamma}{\sqrt{2}}\ln\left(\frac{1+\frac{\phi}{\phi_u}}{1-\frac{\phi}{\phi_u}}\right)\right]d\phi\right\}. \tag{36}$$

Neither of the equations (35-36) can be simplified further. Therefore, in order to evaluate the conditional expected dissipation (and the total dissipation), these equations must be evaluated numerically.

In Fig. 4, the evolution of the conditional expected dissipation (normalized by the total dissipation) is presented for the models and the DNS data. This figure shows the similarity of the conditional expected dissipation for all of the models. The bell shape distribution is evident in all the figures with a maximum amplitude near the mean value. Also, as the variance decreases and the PDF becomes concentrated near the mean, the

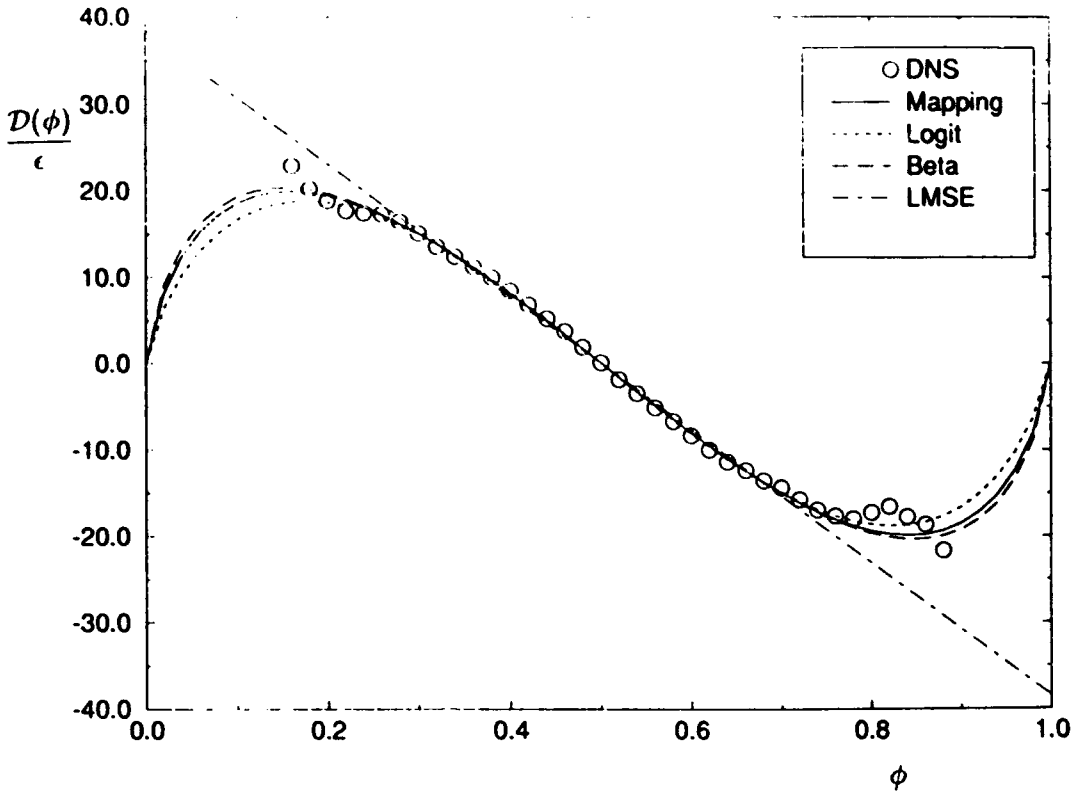

FIGURE 6b Comparisons of the normalized conditional diffusion as predicted by the three models and the LMSE closure, with the DNS data. (b) $\sigma^2 = 0.013$.

amplitude tends to unity. This shape is typical of that observed in previous DNS results of Eswaran and Pope (1988); Nomura and Elgobashi (1992).

The results in Fig. 4 show the ϕ dependency of the results at *all* the stages of mixing. That is, the PDF asymptotically adopts an apparent Gaussian-like distribution only near the mean value of the scalar, and the conditional dissipation does not become independent of the scalar everywhere. For the AMC, this has been discussed by Gao (1991); O'Brien and Jiang (1991). Considering the similarity of the three models, it is therefore concluded that all three models yield the same characteristics. These results also suggest a poor agreement between the model predicted conditional expected dissipations and the DNS data. Note that at the initial stages of mixing, the predicted results compare well with DNS data. However, with mixing progression, at smaller variance values, the agreement is only good near the mean scalar value and worsens near the bounds of the composition domain. This, as described above, is due to the permanent influence of the scalar boundaries at all the stages of mixing.

6 SCALAR DIFFUSION

Albeit directly related to the conditional expected dissipation (Eq. 7), it is useful to examine the behavior of the conditional expected diffusion in light of the discussions above. Given the PDF, again within the fixed range $-\phi_u \leq \phi \leq \phi_u$, the conditional expected diffusion can be determined from

$$D(\phi, t) = -\frac{1}{P_1(\phi, t)} \frac{\partial F}{\partial t}. \tag{37}$$

This equation is very useful in illustrating the properties of the PDF. For example, for a Gaussian distribution within an infinite domain

$$\frac{\partial F}{\partial t} = -\frac{\phi}{\sqrt{2\pi\sigma^2}} \frac{d\sigma^2}{dt} \exp(-\frac{\phi^2}{2\sigma^2}), \tag{38}$$

and consequently

$$\frac{D(\phi,t)}{\epsilon(t)} = \frac{-\phi}{\sigma^2(t)}. \tag{39}$$

It is noted that Eq. (39) is in accord with the Linear Mean Square Estimation (LMSE) closure (O'Brien, 1980).

The mean conditional diffusion can be determined for the three models considered. For the erf^{-1}-Normal PDF with zero mean

$$\frac{\partial F}{\partial t} = \frac{1}{\sqrt{2\pi}} \frac{d\gamma}{dt} \exp\left\{-\frac{\gamma^2}{2}\left[\text{erf}^{-1}(\frac{\phi}{\phi_u})\right]^2\right\} \text{erf}^{-1}(\frac{\phi}{\phi_u}) \tag{40}$$

Again with explicit equations for the total dissipation and the variance, it is possible to obtain an algebraic expression for the conditional expected diffusion. The results after substantial algebraic manipulations yield

$$\frac{D(\phi,t)}{\epsilon(t)} = \left(\frac{-\sqrt{\pi}}{\sin\left[\frac{\pi\sigma^2(:)}{2\sigma^2(0)}\right]} \sqrt{\frac{1+\sin\left[\frac{\pi\sigma^2(t)}{2\sigma^2(0)}\right]}{1-\sin\left[\frac{\pi\sigma^2(t)}{2\sigma^2(0)}\right]}}\right) \exp\left\{-\left[\text{erf}^{-1}(\frac{\phi}{\phi_u})\right]^2\right\} \text{erf}^{-1}(\frac{\phi}{\phi_u}). \tag{41}$$

In this form Eq. (41) is very pleasing since it does reveal the (t,ϕ) separability, and thus the self-similarity, of the diffusion field. The terms inside the parenthesis on the RHS are time dependent, whereas the remaining terms depend explicitly on ϕ only. As indicated by O'Brien and Jiang (1991), this separability cannot be easily deduced from Eq. (5), but is possible with the analytical procedure followed above. The temporal evolution of the conditional expected diffusion for the erf^{-1}-Normal distribution, and its comparison with that of the LMSE closure is presented in Fig. 5.

By following the procedure above, analogous expressions are obtained for the other two closures. Namely,

$$\frac{D(\phi,t)}{\epsilon(t)} = \frac{2\phi_u}{\gamma} \frac{d\gamma}{d\sigma^2} \left[1 - \left(\frac{\phi}{\phi_u}\right)^2\right] \tanh^{-1}(\frac{\phi}{\phi_u}), \tag{42}$$

for the Logit-Normal distribution of zero mean, and

$$\frac{D(\phi,t)}{\epsilon(t)} = \frac{2}{P_1(\phi,t)} \frac{\partial I_\phi(\beta,\beta)}{\partial\sigma^2} \tag{43}$$

for the symmetric Beta density within [0,1]. Equations (42)-(43) cannot be simplified further due to the lack of an explicit analytical relation for the variance of the Logit-Normal distribution (Johnson, 1949a), and the unknown analytical form of the derivatives of the Incomplete Beta Function.

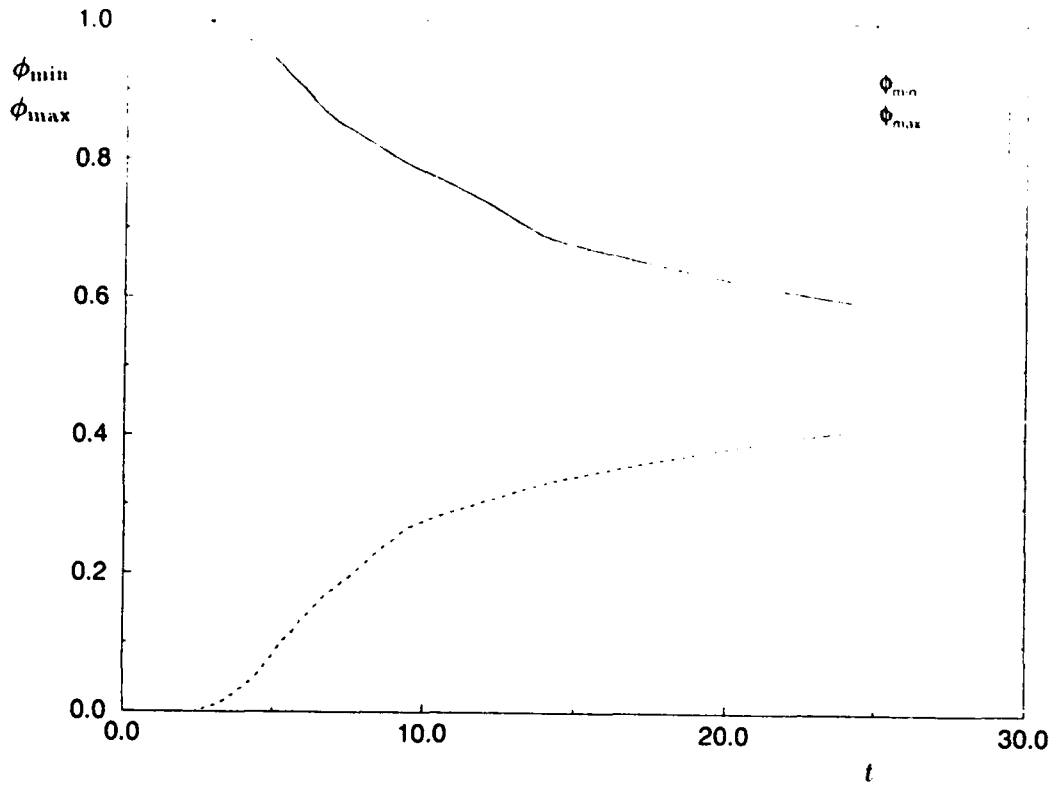

FIGURE 7 The temporal variations of ϕ_{max} and ϕ_{min} generated by DNS.

In Fig. 6, results are presented of the conditional expected diffusion as predicted by the three models, and also that of the LMSE closure. In these figures, the DNS data are also provided at several variance values. The similarity of the modelled results are once again revealed in these figures, which is expected in view of the PDF similarities. At all times, the conditional diffusion field has an odd distribution near the mean scalar value. On the right half of the composition domain, all three closures yield a monotonic decrease of D to an instantaneous minimum, and then a monotonic increase to zero at the upper bound of the scalar. The location and the magnitude of the instantaneous maxima and minima is not the same for the three closures. Also, as Eqs. (41)-(43) indicate, the zeroes of D can only be realized at $\phi = 0, \pm\phi_u$. At the initial times, *i.e.* large variances, all three closures agree reasonably well with the DNS data. This agreement is better for the three models than for the LMSE closure. However, as the variance becomes smaller, the agreement between the model predictions and the DNS data worsens. It is noted that as the variance becomes small, all the closures yield a Gaussian-like PDF near the mean value of the scalar. This is shown in the figures near $\phi =< \phi >$ ($= \frac{1}{2}$ for DNS), where the predicted results are in accord with the LMSE closure, *i.e.* linear profiles of similar slopes. In this region, the results are also in accord with DNS data for all the closures including the LMSE. However, again, the predicted results deviate from the DNS data away from the mean value. It is clearly noted that the DNS generated D values do not go to zero at the scalar bounds.

7 EVOLUTION OF THE SCALAR FIELD

The problems described at the conclusion of the previous two sections stem from a lack of capability of all of the models in accounting for the variations of the scalar

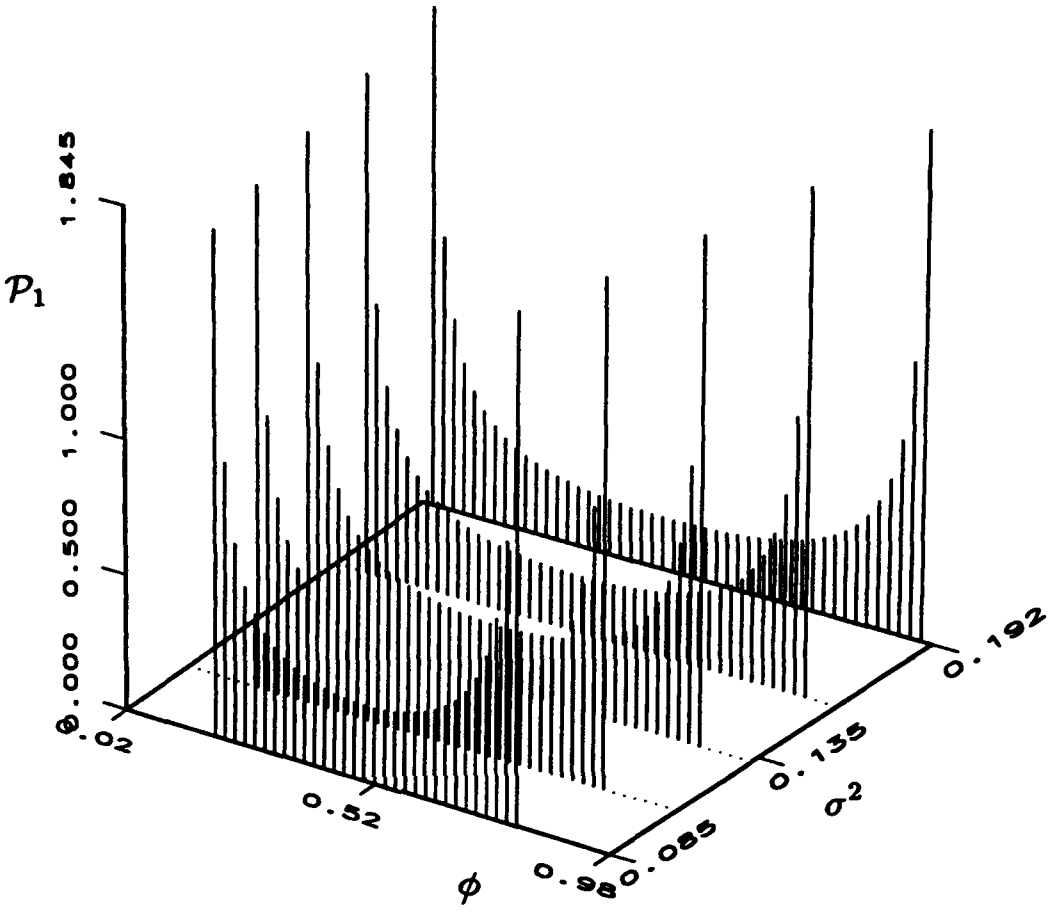

FIGURE 8 The Beta density (Pearson Type II) for a domain with moving boundaries, and $\beta = 0.1$.

bounds as the mixing proceeds. For all three models, the PDF is always *defined* within a fixed range through its course of evolution. It is easy to show that both the conditional expected dissipation and the conditional expected diffusion are correctly predicted by all the models near the mean scalar value. For the erf^{-1}-Normal distribution, this is evident from Eqs. (33) and (41) and can be also shown by analyzing the behavior of Eq. (31) near the region $\phi \approx 0$, as the variance becomes small. Noting that

$$\text{Lim}_{(\phi \approx 0)} \quad \text{erf}\left(\frac{\phi}{\phi_u}\right) \approx \frac{\sqrt{\pi}}{2}\frac{\phi}{\phi_u} \tag{44}$$

and, from Eq. (11)

$$\text{Lim}_{(\sigma^2 \to 0)} \quad \frac{d\gamma}{dt} = \frac{-2\phi_u}{\sqrt{\pi\sigma^2}}\frac{d\sigma}{dt}, \tag{45}$$

it is easily concluded that

$$\text{Lim}_{(t \to \infty)} \quad \varepsilon(\phi \approx 0, t) = -\sigma\frac{d\sigma}{dt}. \tag{46}$$

Following the same procedure, it is derived

$$\mathrm{Lim}_{(t\to\infty)} \quad D(\phi \approx 0, t) = -\frac{\epsilon}{\sigma^2}\phi. \tag{47}$$

Due to the similarity of the three closures, it is reasonable to expect similar behaviors for the other models as well. Equations (46)-(47) indicate a Gaussian-like distribution near the mean $\phi \approx 0$ (Eqs. (24,39)). This is in accord with the DNS data. However, at distances away from the mean value the predicted results do not correspond to that of a Gaussian field. Neither do these results agree well with DNS data. The deficiency of the models in predicting the DNS results is made clear by considering the bounds of the scalar field as the mixing proceeds. This is demonstrated in Fig. 7, showing the temporal decay/growth of the scalar maxima/minima obtained by DNS. This trend is consistent with physical intuition, but is not incorporated into any of the three models. In the AMC and the JET generated frequencies, due to the nature of the translation $Z(\phi_0, t)$ and the constraints imposed by Eq. (15), the scalar is always bounded within the same range. This problem is also encountered in the PF, in that Type I and II distribution families are always defined within the same fixed domain regardless of the magnitude of the variance.

With the examination of the PDF transport equation, it is shown that the physics of the problem requires the migration of the scalar bounds toward the mean value as the mixing proceeds. That is, the instantaneous values of the scalar minima and maxima change with mixing progression. To demonstrate this, again consider a symmetric field with a PDF, $P_1(\phi, t)$, defined within the *time-dependent* domain of zero mean, $\phi\epsilon[\phi_{min}(t) = -\phi_{max}(t), \phi_{max}(t)]$. At all the stages of the evolution, the PDF must satisfy the physical requirements

$$\begin{aligned}
&\int_{\phi_{\min}(t)}^{\phi_{\max}(t)} P_1(\phi, t)d\phi = 1,\\
&<\phi>= \int_{\phi_{\min}(t)}^{\phi_{\max}(t)} \phi P_1(\phi, t)d\phi = 0,\\
&\sigma^2(t) = \int_{\phi_{\min}(t)}^{\phi_{\max}(t)} \phi^2 P_1(\phi, t)d\phi,\\
&\qquad\vdots
\end{aligned} \tag{48}$$

The first of Eq. (48) requires

$$\frac{d}{dt}\int_{\phi_{\min}(t)}^{\phi_{\max}(t)} P_1(\phi, t)d\phi = 0 \tag{49}$$

Evaluating this integral via Leibnitz's rule, and making use of Eqs. (3)-(7), it is shown that

$$P_1(\phi_{\max}(t), t)\frac{d\phi_{\max}}{dt} = -P_1(\phi_{\min}(t), t)\frac{d\phi_{\min}}{dt} = \left\{\frac{\partial}{\partial\phi}[\varepsilon(\phi, t)P_1(\phi, t)]\right\}_{\phi=\phi_u}$$

$$P_1(\phi_{\max}(t), t)\left[\frac{d\phi_{\max}}{dt} - D(\phi_{\max}(t), t)\right] = P_1(\phi_{\min}(t), t)\left[\frac{d\phi_{\min}}{dt} - D(\phi_{\min}(t), t)\right] = 0,$$

$$\phi_{\max}(0) = \phi_u, \quad \phi_{\min}(0) = \phi_\ell = -\phi_u. \tag{50}$$

Following the same procedure for the second of Eq. (48), yields the obvious requirement

$$\int_{\phi_{\min}(t)}^{\phi_{\max}(t)} D(\phi, t) P_1(\phi, t) d\phi = 0. \tag{51}$$

The third part of Eq. (48) yields Eq. (12), and

$$P_1(\phi_{\max}(t), t)\varepsilon(\phi_{\max}(t), t) = P_1(\phi_{\min}(t), t)\varepsilon(\phi_{\min}(t), t) = 0,$$

$$P_1(\phi_{\max}(t), t)\left[\frac{d\phi_{\max}}{dt} - D(\phi_{\max}(t), t)\right] =$$

$$-P_1(\phi_{\min}(t), t)\left[\frac{d\phi_{\min}}{dt} - D(\phi_{\min}(t), t)\right] = 0. \tag{52}$$

The remaining parts of Eq. (48) yield higher order statistical information pertaining to the inner integrated evolution of the conditional expected dissipation and diffusion, and their relation with the higher central moments. With an additional assumption of a nonzero PDF within the region of its definition, that is by defining $\phi_{\max}(t)$ and $\phi_{\min}(t)$ as the extreme locations with nonzero PDF, a combination of Eqs. (50) and (52) yields

$$\varepsilon(\phi_{\max}(t), t) = \varepsilon(\phi_{\min}(t), t) = 0,$$

$$\frac{d\phi_{\max}}{dt} = \frac{\partial \varepsilon}{\partial \phi}|\phi_{\max} = D(\phi_{\max}(t), t),$$

$$\frac{d\phi_{\min}}{dt} = \frac{\partial \varepsilon}{\partial \phi}|\phi_{\min} = D(\phi_{\min}(t), t),$$

$$\phi_{\max}(0) = \phi_u, \phi_{\min}(0) = \phi_\ell. \tag{53}$$

Equation (53) indicates that with fixed boundaries, the conditional dissipation would adopt a zero slope at the boundaries and the conditional diffusion would also be zero there. However, Fig. 7 indicates that in a physical situation the boundaries are not fixed and move inwards as the mixing proceeds. It is interesting to note that this problem is not observed in the numerical results obtained by the C/D type closures. That is, while the C/D closures are not capable of predicting the PDF evolution in accord with DNS data, they do have the mechanism for shrinking the bounds of the composition space. Obviously, in the context of single-point description without the knowledge of the dissipation field, it is not possible to determine *a priori* the temporal bounds of the scalar field. Therefore, the closures can be modified only by making further assumptions in describing this transport. For a general case, the JET frequencies can be generated by the original form proposed by Johnson (1949a)

$$\phi(\phi_0, t) = \lambda(t) z\left(\frac{\phi_0}{\gamma(t)}\right) + \varrho(t), \tag{54}$$

where the additional parameters $\lambda(t)$ and $\varrho(t)$ provide the extra degrees of freedom in order to account for the variations of the instantaneous boundaries of the composition domain. For the PF, the problem can be overcome, for example, by considering a "four-parameter Beta distribution"

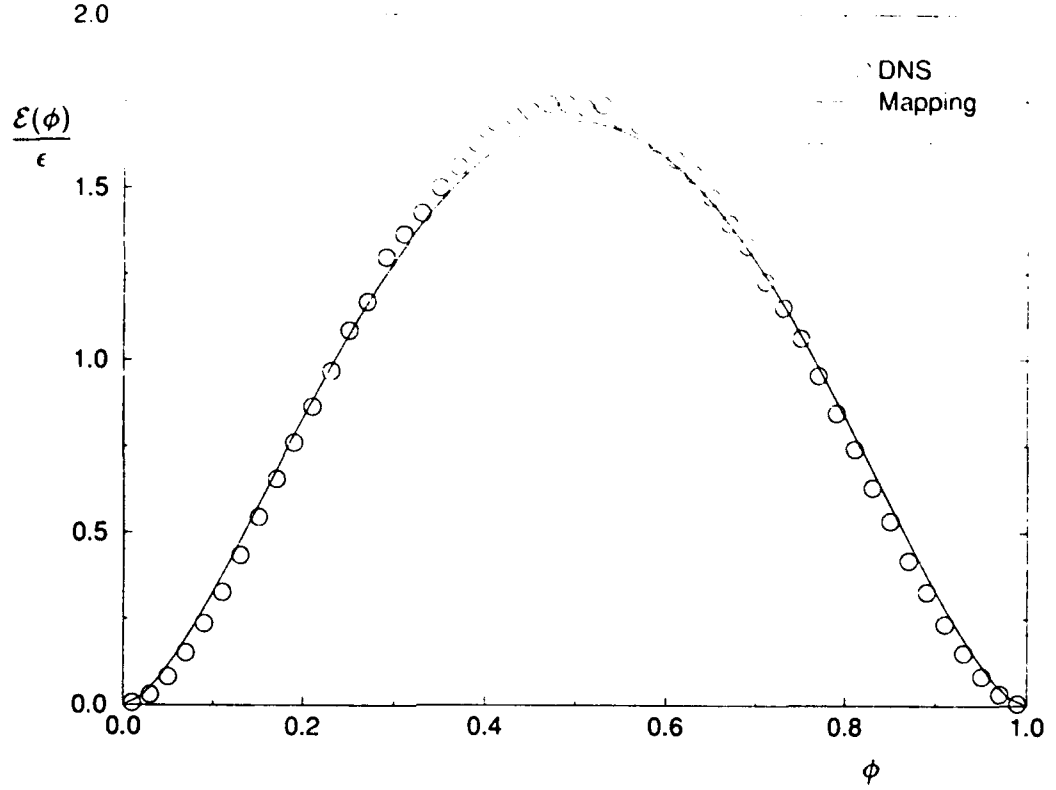

FIGURE 9a The comparison of the conditional expected scalar dissipation normalized with the total dissipation with DNS data as predicted by the AMC with the scalar bounds determined from the DNS results. (a) $\sigma^2 = 0.079$.

$$P_1(\phi,t) = \frac{1}{[\phi_{\max}(t) - \phi_{\min}(t)]B(\beta_1,\beta_2)} \left(\frac{\phi - \phi_{\min}(t)}{\phi_{\max}(t) - \phi_{\min}(t)}\right)^{\beta_1 - 1} \left(1 - \frac{\phi - \phi_{\min}(t)}{\phi_{\max}(t) - \phi_{\min}(t)}\right)^{\beta_2 - 1}, \quad \phi_{\min}(t) \le \phi \le \phi_{\max}(t), \tag{55}$$

with the extra two parameters being $\phi_{\min}(t)$ and $\phi_{\max}(t)$. For a symmetric PDF in the range $[0,1] \equiv [\phi_{\min}(t=0) = \phi_\ell, \phi_{\max}(t=0) = \phi_u]$; therefore, the variance decay can be influenced by increasing β, and/or by decreasing the scalar range $\Delta\phi(t) = \phi_{\max}(t) - \phi_{\min}(t)$. The former recovers the well-known two-parameter Beta distribution (Pearson Type II), while the latter is approximately equivalent to the LMSE closure (O'Brien, 1980). This latter case is presented in Fig. 8 showing a symmetric Beta density with $\beta(t) =$ fixed $= 0.1$. Note that as the mixing proceeds, the variance decays but the PDF preserves its initial approximate double delta shape. In a physical problem, the situation is somewhere between these two limiting cases. The exact situation depends on the characteristics of a particular mixing problem.

The discussions above suggest that in order to predict the final stage of mixing correctly, the effects of mixing on the shrinkage of the domain must be taken into account. To demonstrate this point, the results shown in Fig. 7 can be incorporated into the mixing models to determine the evolution of the conditional expected dissipation and diffusion. This is done here only for the erf^{-1}-Normal, and the results of the conditional expected dissipation are shown in Fig. 9. In the calculations resulting in this figure, analytical

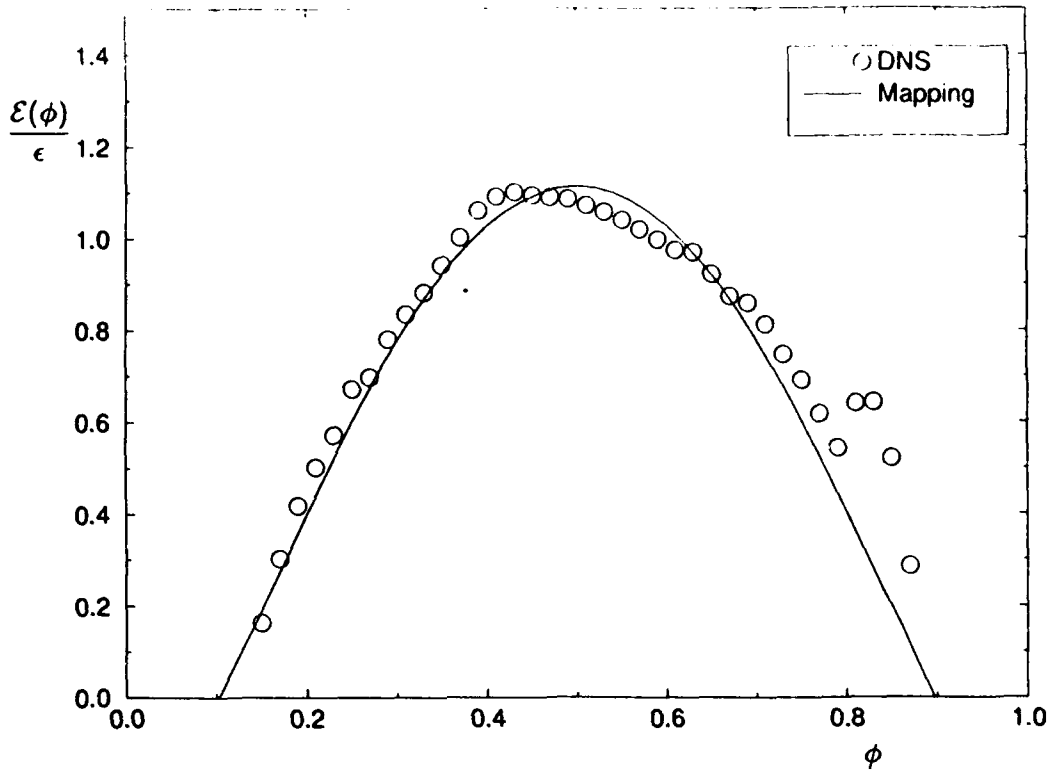

FIGURE 9b The comparison of the conditional expected scalar dissipation normalized with the total dissipation with DNS data as predicted by the AMC with the scalar bounds determined from the DNS results. (b) $\sigma^2 = 0.013$.

solutions are not possible for the moving boundary case. This is demonstrated by the equivalent form of Eq. (29)

$$H(t) = \frac{-\phi_{\max}(t)\gamma}{\sqrt{2}\pi} \int_0^1 \frac{\exp\left\{-\left[\mathrm{erf}^{-1}\left(\frac{\phi}{\phi_{\max}(t)}\right)\right]^2 \left(1+\frac{z^2\gamma^2}{2}\right)\right\}}{1+\frac{z^2\gamma^2}{2}} dz + \frac{1}{2}(\phi+\phi_{\max}(t)). \quad (56)$$

With this equation, therefore, the effect of the temporal variation of the PDF on the conditional dissipation is through the $\partial H/\partial t$ term in Eq. (28). This term has the form

$$\frac{dH}{dt} = \frac{-\sqrt{2}\phi_{\max}(t)\frac{d\gamma}{dt}}{\pi(2+\gamma^2)} \exp\left\{-\left(1+\frac{\gamma^2}{2}\right)\left[\mathrm{erf}^{-1}\left(\frac{\phi}{\phi_{\max}(t)}\right)\right]^2\right\} + \frac{1}{2}\frac{d\phi_{\max}}{dt}$$

$$\left(1 - \frac{\phi}{\phi_{\max}(t)} \exp\left\{\left[\mathrm{erf}^{-1}\left(\frac{\phi}{\phi_{\max}(t)}\right)\right]^2\right\} + \right.$$

$$\left. \frac{2}{\sqrt{\pi}} \int_{-\infty}^{\mathrm{erf}^{-1}\left(\frac{\phi}{\phi_{\max}(t)}\right)} \mathrm{erf}\left(\frac{\gamma z}{\sqrt{2}}\right) \exp(-z^2) dz \right). \quad (57)$$

The first term on RHS of Eq. (57) is the same as that in Eq. (30), and the effects of moving boundaries manifest themselves through the second term. This term cannot be evaluated

analytically. However, Eqs. (56)-(57) show that due to the direct dependence on $\frac{d\phi_{max}}{dt}$, the conditional dissipation does not retain its original functional dependence, suggested by Eq. (33). Also, Fig. 9 shows that the effect of the moving boundaries is to force the conditional expected dissipation to zero at the current scalar maxima/minima. Therefore, the predicted results compare much better with DNS data than those presented in Fig. 4. Due to the similarity of the PDF's, it is expected that the other two closures would also behave in the similar fashion.

The influence of boundary encroachment is also sensed in the conditional expected diffusion field. For the erf^{-1}-Normal scalar PDF, the equivalent form of Eq. (41) is

$$D(\phi,t) = -\frac{2\phi_{max}(t)}{\gamma\sqrt{\pi}}\frac{d\gamma}{dt}\exp\left\{-\left[\text{erf}^{-1}\left(\frac{\phi}{\phi_{max}(t)}\right)\right]^2\right\}$$

$$\text{erf}^{-1}\left(\frac{\phi}{\phi_{max}(t)}\right) + \left(\frac{\phi}{\phi_{max}(t)}\right)\frac{d\phi_{max}}{dt}, \tag{58}$$

with an average dissipation of

$$\epsilon(t) = \frac{4\phi_{max}^2(t)}{\pi(\gamma^2+2)\sqrt{\gamma^2+4}}\frac{d\gamma}{dt} - \frac{2\phi_{max}(t)}{\pi}\arctan\left(\frac{2}{\gamma\sqrt{\gamma^2+4}}\right)\frac{d\phi_{max}}{dt}. \tag{59}$$

Equations (58)-(59) show the influence of the boundary movement through the last term on the RHS of both these equations. With these additional terms, the normalized form similar to Eq. (41) is not very useful, and Eqs. (58)-(59) are evaluated numerically.

The equivalent of Eq. (58) for the Logit-Normal and the Beta density are, respectively,

$$D(\phi,t) = \frac{(\phi_{max}^2-\phi^2)}{\phi_{max}\gamma}\frac{d\gamma}{dt}\tanh^{-1}\left(\frac{\phi}{\phi_{max}(t)}\right) + \left(\frac{\phi}{\phi_{max}(t)}\right)\frac{d\phi_{max}}{dt}, \tag{60}$$

$$D(\phi,t) = -\frac{1}{P_1(\phi,t)}\frac{\partial}{\partial t}\left(I_{\left\{\frac{\phi-\phi_{min}}{\phi_{max}-\phi_{max}}\right\}}(\beta,\beta)\right) \tag{61}$$

An interesting characteristic displayed by Eqs. (58) and (60) is the influence of the terms containing the temporal derivative of $\phi_{max}(t)$. Note that at the boundaries, *i.e.* $\phi = \phi_{max}(t)$, the first term on the RHS of these equations vanishes, but the last term prohibits the conditional expected diffusion from going to zero. This is in accordance with the DNS data as shown in Fig. 6. In order to demonstrate this more clearly, results are presented in Fig. 10 of the conditional expected diffusion predicted by the erf^{-1}-Normal, with the input of the variance and the scalar bounds from DNS. A comparison between this figure and Fig. 6 show the influence of the boundary movement, and a better agreement between the model predictions and the DNS data. This agreement is more pronounced at scalar values away from the mean. Near the mean value, the influence of the boundary migration is slight, as also indicated by Eqs. (58) and (59).

8 DISCUSSIONS AND APPLICATIONS

In previous sections, a rather detailed discussion was presented of the problem of scalar mixing from an initially symmetric binary state. These discussions were primarily intended to provide a means of assessing the differences between the currently available tools in probability modeling of the scalar mixing problem. This problem is of significant interest,

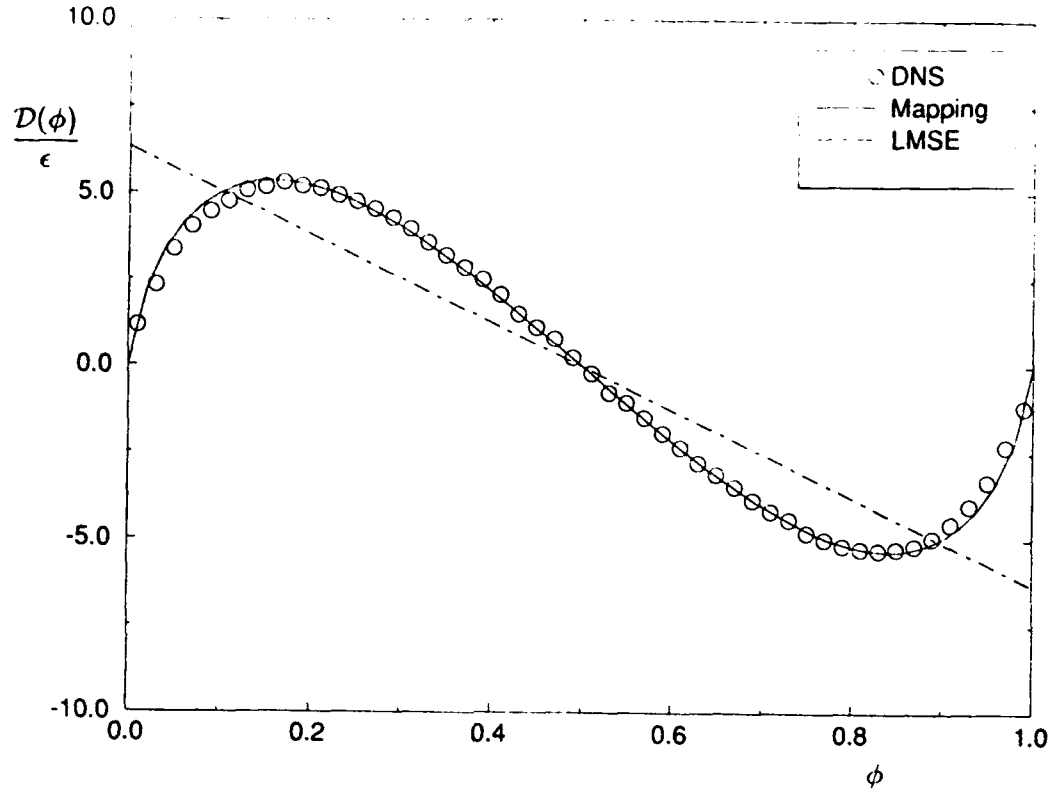

FIGURE 10a The comparison of the conditional expected scalar diffusion normalized with the total dissipation with DNS data as predicted by the AMC and the LMSE closures with the scalar bounds determined from the DNS results. (a) $\sigma^2 = 0.079$.

considering the extent of previous works focused on its analysis (Pope, 1976; Pope, 1979; Pope, 1982; O'Brien, 1980; Dopazo, 1973; Kosaly and Givi, 1987; Pope, 1991; Gao, 1991; O'Brien and Jiang, 1991; Nomura and Elgobashi, 1992). The results obtained here are particularly useful in highlighting some of the deficiencies of these closures, and in suggesting future research towards overcoming these drawbacks. There are, however, many other physical problems that are not subject to the restricting conditions imposed in these analyses. In this section, therefore, some discussions are presented as to the practical implications of these models, together with some speculations on their extensions for future applications.

Perhaps one of the most important practical applications of the closures considered here is the treatment of reactive flow phenomena. In fact, the most important advantage of scalar PDF methods is due to their applicability in the modeling of turbulent combustion (Pope, 1979; Pope, 1985; Pope, 1990; Kollmann, 1990; O'Brien, 1980). The results generated here can be used directly in the modeling of *mixing controlled* homogeneous chemically reacting systems. Namely, in examining the compositional structure of a reacting system under chemical equilibrium, or in determining the limiting rate of reactant conversion in a simple chemistry of the prototype Fuel + Air $\rightarrow$ Products. The determination of this rate has been the subject of extensive investigations over the past forty years (see Hawthorne *et al.* (1949); Toor (1962); Williams (1985)). It is now well-established that in a mixing controlled binary irreversible reaction of this type, the statistics of the reacting fields can be related to those of an appropriately defined conserved scalar (such $\equiv \phi$) (Bilger, 1980; Toor, 1975; Williams, 1985). Therefore, the frequencies generated herein can be utilized for estimating the statistics of the reacting

field with an infinitely fast chemistry model in a homogeneous flow with initially segregated reactants under stoichiometric conditions. Albeit very restricting, this problem is of great practical importance for modeling and design of batch mixers and plug flow reactors in which these conditions prevail (Toor, 1975; Brodkey, 1981; Dutta and Tarbell, 1989). Madnia *et al.* (1991); Madnia *et al.* (1992) have shown that with the erf^{-1}-Normal (AMC) and the Beta density models, this rate can be predicted by simple analytical means. For the Logit-Normal density, a complete analytical solution cannot be obtained and determination of the statistics requires numerical integration of the PDF. The results generated by these closures agree with DNS data better than those obtained by means of the C/D closures (McMurtry and Givi, 1989), or other models previously available in the chemical engineering literature (Dutta and Tarbell, 1989) (see Givi (1989) for a review). Also, the results provided by the AMC (Frankel *et al.*, 1992a) are shown to compare well with experimental data on plug flow reactors if the additional information pertaining to the evolution of the scalar length scale is accurately provided.

The most obvious issues in regard to the applications of these models are associated with their extension for the treatment of (1) non-symmetric binary scalar mixing, (2) non-binary scalar mixing, (3) multiple scalar mixing, and (4) non-homogeneous mixing. The first problem constitutes a more general form of the binary mixing problem and is also important for the analysis of non-stoichiometric reacting systems. The second problem is appropriate for the analysis of other mixing systems in which the initial conditions are not of a two-feed configuration. The third problem is of interest in reacting systems in which the transport of a passive scalar (like ϕ) is not sufficient for a complete analysis. For example, any reacting system under non-equilibrium conditions. Finally, the importance of the fourth problem is obvious in view of the fact that the flow within most practical mixing devices cannot be assumed homogeneous.

In regard to the first issue, all of the three closures considered here can be used for the probability modeling of scalar mixing within a *fixed* scalar domain. The use of the AMC is straightforward, but the mathematical procedure is somewhat complex (Madnia *et al.*, 1992). The Pearson frequencies can be generated easily for non-symmetric problems. In this case, the Pearson Type I provides a reasonably accurate representation of the scalar field regardless of the degree of asymmetry of the PDF (Frankel *et al.*, 1992b; Madnia *et al.*, 1992). The use of the JET in this regard is most difficult, since closed form analytical expressions are not available for the variance of the scalar by which the PDF can be characterized (Johnson, 1949a). In treating these problems, therefore, the first two models can be more readily employed and subsequently used for the treatment of mixing controlled reacting systems under non-stoichiometric conditions. In fact, as demonstrated by Madnia *et al.* (1992) the solution of the non-symmetric form of the AMC and the Beta density provide a very good means of predicting the limiting rate of reactant conversion in homogeneous reacting flows. However, it should be indicated that with both models the problem associated with the scalar bounds still exists and must be dealt with as discussed in Section 7.

In addressing the second issue, it is obvious that the AMC is more appropriate than the other closures for simulating the mixing problem from an initially "arbitrary" state. The extension of JET and PF for treating multi- (higher than bi-) modal distributions have been reported in statistics literature. However, as the degree of modality of the PDF increases the procedure becomes more complex and not suitable for practical applications. Fortunately, in most mixing problems in simple flows, *i.e.* homogeneous turbulence and turbulent shear flows, the PDF exhibits strong bimodal features (Madnia *et al.*, 1992; Frankel *et al.*, 1992b). In those cases, the use of the Beta density can be justified. In fact, in non-homogeneous flows it is easier to use this density, at least until further development of the AMC for practical applications (see Frankel *et al.* (1992b); Gaffney *et al.* (1992)).

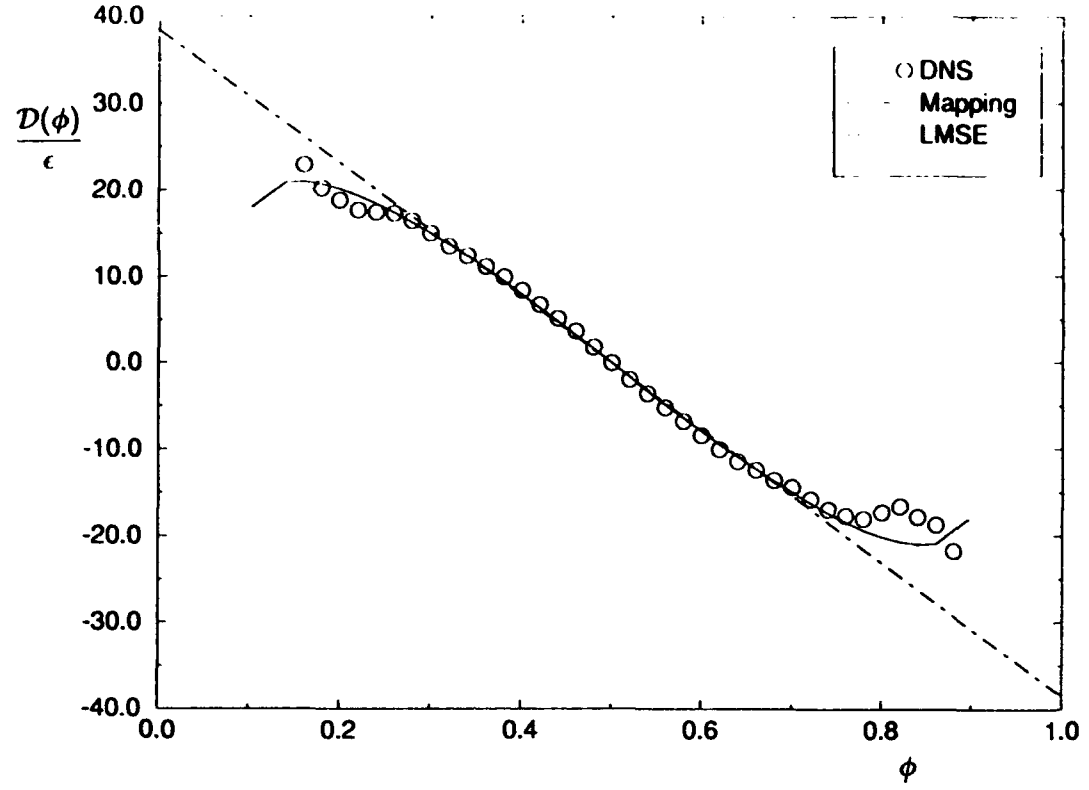

FIGURE 10b The comparison of the conditional expected scalar diffusion normalized with the total dissipation with DNS data as predicted by the AMC and the LMSE closures with the scalar bounds determined from the DNS results. (b) $\sigma^2 = 0.013$.

The extension of all of the three models in describing multi-scalar mixing is possible. The problem naturally falls within the realm of the *multivariate* statistical analyses. In these analyses, the implementation of the AMC is relatively straightforward since it provides a transport equation for the joint PDF's of the scalar variable in a multivariable sense (Pope, 1991). However, it is not presently clear how to devise an efficient computational procedure, typically based on Monte Carlo methods (Pope, 1981), for the numerical treatment of these equations. Some work in this regard is currently under way (Valiño and Gao, 1991). The extension of assumed distributions based on the Beta density for treating multi-scalars is more straightforward but less trivial to justify. The most obvious means is to implement the multivariate form of the PF. The direct analog of the Beta density is the *Dirichlet* frequency (Johnson, 1987; Narumi, 1923; Johnson and Kotz, 1972). The application of this density in modeling of multiple species reactions has been discussed by Girimaji (1991a); Girimaji (1991b); Gaffney *et al.* (1992). However, the use of the Dirichlet frequency cannot be justified for modeling of reacting flows in a general sense (Frankel, 1992). Finally the extension of the JET in generating multivariate frequencies has been reported in statistics literature since the subsequent work of Johnson (1949b). As one may suspect, the procedure is more complex, and the same reservations as those associated with the Dirichlet distributions apply.

All of the models considered here can be extended for the analysis of non-homogeneous mixing (and reacting) systems. Obviously, in most cases, the problem requires numerical integration of the appropriate conservation equations. For instance, the AMC can be invoked in the *mixing* step of a fractional stepping procedure, similar to that of typical Monte Carlo procedures (Pope, 1981). The PF densities (*e.g.* Beta or Dirichlet) and JET

generated frequencies require modelled transport equations for the first two moments and cross moments of the scalar field. These equations, "hopefully", include the essential information pertaining to the spatial inhomogeneity of the flow. Naturally, the PDF is not generally symmetric, and must be determined from the knowledge of the parameters $\beta_1, \beta_2, \gamma, \lambda, \varrho$, and the local $\phi_{max}(t), \phi_{min}(t)$ values. With this information, all the higher order statistics of the scalar field can be determined. In regard to this last issue, it must be indicated that the Beta density has been extensively used for the modeling of non-homogeneous reacting systems (*e.g.* Rhodes (1975); Jones and Priddin (1978); Lockwood and Moneib (1980); Janicka and Peters (1982); Peters (1984); Frankel *et al.* (1992b); Gaffney *et al.* (1992); for recent reviews, see Givi (1989); Priddin (1991)). Due to their special mathematical properties, the Beta and/or the Dirichlet frequencies yield relatively simple analytical solutions for the higher order statistics of the reacting fields. From this point of view, the use of the PF is more practical than the AMC since the solution procedure does not require the numerical treatment of the PDF transport equation. This point has been discussed in detail by Girimaji (1991b). However, as indicated above, the use of the Dirichlet frequency cannot be justified for modeling of unpremixed reacting flow in a general sense. Also, there is no way of implementing this density directly for modeling of non-equilibrium flames, involving strong correlation of the temperature and the species mass fractions. Even with the assumption of statistical independence of the reacting species and the temperature, the question of the local scalar range imposes a severe restriction on the validity of this approximation. For example, it is demonstrated by Gaffney *et al.* (1992) that in the modeling of a reacting turbulent shear flow, depending on the *a priori* choice of the magnitudes of the local scalar bounds the predicted results can be altered significantly. Obviously, this problem is not eliminated with the usage of JET frequencies in either a univariate or multivariate sense.

9 CONCLUDING REMARKS

It is shown that the family of frequencies generated by the Johnson-Edgeworth Translation (JET) provides a reasonable means for statistical modeling of binary symmetric scalar mixing in homogeneous turbulence. It is also shown that the results predicted by one of the members of this family is identical to the solution generated by the Amplitude Mapping Closure (AMC) of Kraichnan. This similarity is useful in two regards: (1) establishing a mathematical reasoning for the similarity of the probability frequency of the Pearson Family (PF) and that of the AMC for the description of the problem, and (2) suggesting the possible use of other members of the JET frequencies in approaches in which the Probability Density Function (PDF) is assumed *a priori*. The PDF's generated by all these models are shown to compare well with each other and also with the results obtained by Direct Numerical Simulations (DNS). However, none of the models are capable of accurately predicting the conditional expected dissipation and the conditional expected diffusion of the scalar field. This problem is associated with the incapability of the models to account for the migration of the scalar bounds as mixing proceeds.

ACKNOWLEDGEMENTS

We are indebted to Dr. Gordon Erlebacher for the use of his computer codes. We also appreciate the efforts of Ms. Debbie Young for assisting us with the literature search. This work is sponsored by the Office of Naval Research under Grant N00014-90-J-1403, by NASA Langley Research Center under Grant NAG-1-1122, and by the National Science Foundation under Grant CTS-9253488. The computational resources are provided by NSF through NCSA at the University of Illinois, and by the program at NASA Ames Research Center.

REFERENCES

Abramowitz, M. and Stegun, I. A. (1972). *Handbook of Mathematical Functions and Formulas, Graphs, and Mathematical Tables.* Government Printing Office, Washington, D.C.

Bilger, R. W. (1980). Turbulent flows with nonpremixed reactants. In Libby, P. A. and Williams, F. A., editors, *Turbulent Reacting Flows*, chapter 3, pages 65-113. Springer-Verlag, Heidelberg.

Brodkey, R. S. (1981). Fundamental of turbulent motion. *Chem. Eng. Comm.* **8**, 1-23.

Casella, G. and Berger, R. L. (1990). *Statistical Inference.* Brooks/Cole Publishing Company, Belmont, CA.

Chen, H., Chen, S., and Kraichnan, R. H. (1989). Probability distribution of a stochastically advected scalar field. *Phys. Rev. Lett.* **63**, 2657-2660.

Curl, R. L. (1963). Dispersed phase mixing: I. Theory and effects in simple reactors. *AIChE J.* **9**, 175-181.

Dopazo, C. (1973), *Non-Isothermal Turbulent Reactive Flows: Stochastic Approaches.* Ph.D. Thesis, Department of Mechanical Engineering, State University of New York at Stony Brook, Stony Brook, NY.

Dutta, A. and Tarbell, J. M. (1989). Closure models for turbulent reacting flows. *AIChE J.* **35**, 2013-2027.

Edgeworth, F. Y. (1907). On the representation of statistical frequency by a series. *Journal of the Royal Statistical Society, Series A.* **70**, 102-106.

Erlebacher, G., Hussaini, M. Y., Speziale, C. G., and Zang, T. A. (1987). Toward the large eddy simulation of compressible turbulent flows. ICASE Report 87-20, NASA Langley Research Center, Hampton, VA. Also available as *NASA CR 178273.*

Erlebacher, G., Hussaini, M. Y., Speziale, C. G., and Zang, T. A. (1990a). Toward the large eddy simulation of compressible turbulent flows. ICASE Report 90-76, NASA Langley Research Center, Hampton, VA. Also available as *NASA CR 187460.*

Erlebacher, G., Hussaini, M.Y., Kreiss, H. O., and Sarkar, S. (1990b). The analysis and simulation of compressible turbulence. *Theoret. Comput. Fluid Dynamics* **2**, 73-95.

Eswaran, V. and Pope, S. B. (1988). Direct numerical simulations of the turbulent mixing of a passive scalar. *Phys. Fluids* **31**, 506-520.

Frankel, S. H., Jiang, T.-L., and Givi, P. (1992a). Modeling of isotropic reacting turbulence by a hybrid mapping-EDQNM closure. *AIChE J.* **38**, 535-543.

Frankel, S. H., Madnia, C. K., and Givi, P. (1992b). Modeling of the reactant conversion rate in a turbulent shear flow. *Chem. Eng. Comm.* **113**, 197-209.

Frankel, S. H. (1992). Ph.D. Thesis, Department of Mechanical and Aerospace Engineering, State University of New York at Buffalo, Buffalo, NY. in preparation.

Gaffney, R. L., White, J. A., Girimaji, S. S., and Drummond, J. P. (1992). Modeling of turbulent/chemistry interactions using assumed pdf methods. AIAA paper AIAA-92-3638.

Gao, F. (1991). Mapping closure and non-Gaussianity of the scalar probability density functions in isotropic turbulence. *Phys. Fluids A* **3**, 2438-2444.

Girimaji, S. S. (1991a). Assumed β-pdf model for turbulent mixing: Validation and extension to multiple scalar mixing. *Combust. Sci. and Tech.* **78**, 177-196.

Girimaji, S. S. (1991b). A simple recipe for modeling reaction-rates in flows with turbulent-combustion. AIAA paper AIAA-91-1792.

Girimaji, S. S. (1992). Towards understand[illegible]rbulent scalar mixing. NASA CR 4446.

Givi, P. and McMurtry, P. A. (1988). No[illegible]ed reaction in homogeneous turbulence: Direct numerical simulations. *AIChE J.* **34**, 1039-1042

Givi, P. (1989). Model free simulations of turbulent reactive flows. *Prog. Energy Combust. Sci.* **15**, 1-107.

Hawthorne, W. R., Wedell, D. S., and Hottel, H. C. (1949). Mixing and combustion in turbulent gas jets. In *3rd Symp. on Combustion, Flames and Explosion Phenomena*, pages 266-288. The Combustion Institute, Pittsburgh, PA.

Hussaini, M. Y., Speziale, C. G., and Zang, T. A. (1990). The potential and limitations of direct and large eddy simulations. In Lumley, J. L., editor, *Whither Turbulence? Turbulence at the Crossroads*, volume 357 of *Lecture Notes in Physics*, pages 354-368. Springer.

Janicka, J. and Peters, N. (1982). Prediction of turbulent jet diffusion flame lift-off using a pdf transport equation. In *Proceedings of 19th Symp. (Int.) on Combustion* pages 367-374. The Combustion Institute, Pittsburgh, PA.

Janicka, J., Kolbe, W., and Kollmann, W. (1979). Closure of the transport equation for the probability density function of turbulent scalar field. *J. Nonequil. Thermodyn.* **4**, 47-66.

Jiang, T.-L., Givi, P., and Gao, F. (1992). Binary and trinary scalar mixing by Fickian diffusion-some mapping closure results. *Phys. Fluids A* **4**, 1028-1035.

Johnson, N. L. and Kotz, S. (1972). *Distributions in Statistics: Continuous Multivariate Distributions.* John Wiley and Sons, New York, NY.

Johnson, N. L. (1949a). Systems of frequency curves generated by methods of translation. *Biometrika* **36**, 149-176.

Johnson, N. L. (1949b). Bivariate distributions based on simple translation systems. *Biometrika* **36**, 297-304.

Johnson, M. E. (1987). *Multivariate Statistical Simulation.* John Wiley and Sons, New York, NY.

Jones, W. P. and Priddin, C. H. (1978). Predictions of the flowfield and local gas composition in gas turbine combustors. In *17th Symp. (Int.) on Combustion*, pages 399-409. The Combustion Institute, Pittsburgh, PA.

Kollmann, W. (1990). The pdf approach to turbulent flow. *Theoret. Comput. Fluid Dynamics* **1**, 249-285.

Kosaly, G. and Givi, P. (1987). Modeling of turbulent molecular mixing. *Combust. Flame* **70**, 101-118.

Kosaly, G. (1986). Theoretical remarks on a phenomenological model of turbulent mixing. *Combust. Sci. and Tech.* **49**, 227-234.

Kraichnan, R. H. (1989). Closures for probability distributions. *Bull. Amer. Phys. Soc.* **34**, 2298.

Liñan, A. (1974). The asymptotic structure of counterflow diffusion flames for large activation energies. *Acta Astronautica* **1**, 1007-1039.

Lockwood, F. C. and Moneib, H. A. (1980). Fluctuating temperature measurement in a heated round free jet. *Combust. Sci. and Tech.* **22**, 63-81.

Madnia, C. K. and Givi, P. (1992). On DNS and LES of homogeneous reacting turbulence. In Galperin, B. and Orszag, S. A., editors, *Large Eddy Simulations of Complex Engineering and Geophysical Flows*. Cambridge University Press, Cambridge, U.K. in press.

Madnia, C. K., Frankel, S. H., and Givi, P. (1991). Mathematical modeling of the reactant conversion rate by single-point pdf methods. In *Proc. Fall Technical Meeting of the Combustion Institute, Eastern Section*, Ithaca, NY.

Madnia, C. K., Frankel, S. H., and Givi, P. (1992). Reactant conversion in homogeneous turbulence: Mathematical modeling, computational validations and practical applications. *Theoret. Comput. Fluid Dynamics*, **4**, 79-93.

McMurtry, P. A. and Givi, P. (1989). Direct numerical simulations of mixing and reaction in a nonpremixed homogeneous turbulent flow. *Combust. Flame* **77**, 171-185.

Miyawaki, O., Tsujikawa, H., and Uraguchi, Y. (1974). Turbulent mixing in multi-nozzle injector tubular mixers. *J. Chem. Eng. Japan* **7**, 52-74.

Narumi, S. (1923). On the general form of bivariate frequency distributions which are mathematically possible when regression and variation are subjected to limiting conditions, I. *Biometrika* **15**, 77-88.

Nomura, K. K. and Elgobashi, S. E. (1992). Mixing characteristics of an inhomogeneous scalar in isotropic and homogeneous sheared turbulence. *Phys. Fluids A* **4**, 606-625.

Norris, A. T. and Pope, S. B. (1991). Turbulent mixing model based on ordered pairing. *Combust. Flame* **83**, 27.

O'Brien, E. E. and Jiang, T.-L. (1991). The conditional dissipation rate of an initially binary scalar in homogeneous turbulence. *Phys. Fluids A* **3**, 3121-3123.

O'Brien, E. E. (1980). The probability density function (PDF) approach to reacting turbulent flows. In Libby, P. A. and Williams, F. A., editors, *Turbulent Reacting Flows*, chapter 5, pages 185-218. Springer-Verlag, Heidelberg.

Passot, T. and Pouquet, A. (1987). Numerical simulation of compressible homogeneous flows in the turbulent regime. *J. Fluid Mech.* **181**, 441-466.

Pearson, K. (1895). Contributions to the mathematical theory of evolution: II. skew variations in homogeneous material. *Philos. Trans. of the Royal Soc. of London, Series A.* **186**, 343-414.

Peters, N. (1984). Laminar diffusion flamelet models in non-premixed turbulent combustion. *Prog. Energy Combust. Sci.* **10**, 319-339.

Pope, S. B. (1976). The probability approach to modelling of turbulent reacting flows. *Combust. Flame* **27**, 299-312.

Pope, S. B. (1979). The statistical theory of turbulent flames. *Phil. Trans. Royal Soc. London* **291**, 529-568.

Pope, S. B. (1981). A Monte Carlo method for the pdf equations of turbulent reactive flow. *Combust. Sci. and Tech.* **25**, 159-174.

Pope, S. B. (1982). An improved turbulent mixing model. *Combust. Sci. and Tech.* **28**, 131-145.

Pope, S. B. (1985). PDF methods for turbulent reacting flows. *Prog. Energy Combust. Sci.* **11**, 119-192.

Pope, S. B. (1990). Computations of turbulent combustion: Progress and challenges. In *Proceedings of 23rd Symp. (Int.) on Combustion*, pages 591-612. The Combustion Institute, Pittsburgh, PA.

Pope, S. B. (1991). Mapping closures for turbulent mixing and reaction. *Theoret. Comput. Fluid Dynamics* **2**, 255-270.

Priddin, C. H. (1991). Turbulent combustion modelling-A review. In Johansson, A. V. and Alfredsson, P. H., editors, *Advances in Turbulence 3*, pages 279-299. Springer-Verlag, Berlin.

Rhodes, P. R. (1975). A probability distribution function for turbulent flows. In Murthy, S. N. B., editor, *Turbulent Mixing in Non-Reactive and Reactive Mixing*, pages 235-241. Plenum Press, New York, NY.

Spalding, S. B. (1961). Theory of mixing and chemical reaction in the opposed-jet diffusion flame. *Journal of the American Rocket Society* **31**, 763-771.

Toor, H. L. (1962). Mass transfer in dilute turbulent and nonturbulent systems with rapid irreversible reactions and equal diffusivities. *AIChE J.* **8**, 70-78.

Toor, H. L. (1975). The non-premixed reaction: $A + B \rightarrow$ *Products*. In Brodkey, R. S., editor, *Turbulence in Mixing Operations*, pages 123-166. Academic Press, New York, NY.

Valiño, L. and Gao, F. (1991). Monte Carlo implementation of the mapping closure for turbulent reacting flows. In *Fluid Dynamics Division Meeting of the American Physical Society*, Phoenix, Arizona.

Williams, F. A. (1985). *Combustion Theory*. The Benjamin/Cummings Publishing Company, Menlo Park, CA, 2nd edition.

APPENDIX 4

AMC Description of Binary and Trinary Scalar Mixing by Fickian Diffusion

Binary and trinary scalar mixing by Fickian diffusion—Some mapping closure results

Tai-Lun Jiang and Peyman Givi
Department of Mechanical and Aerospace Engineering, State University of New York, Buffalo, New York 14260

Feng Gao
Center for Turbulence Research, Stanford University, Stanford, California 94305

(Received 16 September 1991; accepted 4 December 1991)

The amplitude mapping closure of Kraichnan [Bull. Am. Phys. Soc. 34, 2298 (1989); Phys. Rev. Lett. 63, 2657 (1989)] is used for statistical description of the mixing process by Fickian diffusion of a stochastically distributed scalar variable. This closure is invoked in the context of an evolution equation for the single-point probability density function (pdf) of the scalar from initially symmetric binary and trinary states. In the binary case, a simple recipe is provided for the time scaling relation which is very useful in model implementation. In the trinary case, it is shown that after a fixed elapsed time, the pdf relaxes to a distribution similar to that of the binary mixing. The magnitude of this time is independent of the initial extent of departure from a binary state; however, the rate of evolution toward an asymptotic Gaussian state depends on the level of the departure. In both cases, the closure predictions for the scalar flatness factor and the correlation of the mean square scalar–scalar gradients agree well with those obtained by direct numerical simulations (DNS). However, some features of the results are different from those of earlier DNS of mixing in stationary turbulence. These differences are likely attributed to inadequacy of the amplitude mapping closure at the single-point level in accounting for the effects of turbulence stretching.

I. INTRODUCTION

Development of the amplitude mapping closure by Kraichnan and co-workers[1,2] has had a significant impact on statistical modeling of turbulent reacting flows. This closure has proven its capability in probability density function (pdf) modeling of scalar variables in turbulent flows, and has demonstrated its physical plausibility in a number of validation studies by means of comparative assessments against direct numerical simulation (DNS) data.[2-5] Because of its demonstrated relative strength and its sound mathematical-physical basis, it is anticipated that this closure will be extensively utilized in statistical treatment of turbulence, and will gradually replace the closures currently in use in probability modeling of turbulent combustion phenomena.[6-8]

In this work, our objective is to further examine the properties of this closure and to gain a better understanding of the statistical results generated by means of its implementation. It is also intended to provide a reasonably simple recipe that can be used in conjunction with this closure for practical implementations. For these purposes, three distinct but related problems are considered.

The first problem is associated with the time scaling of the mapping closure. The consideration of this problem has been motivated due to the "single-point" statistical nature of the closure. Because of this nature, there is no information pertaining to the evolution of the appropriate length and/or time scale associated with the underlying physical processes. This problem manifests itself by a need for further "external" information for predicting the evolution of these scales. With availability of such information (by whatever means), the problem reduces to that of establishing a time scaling relation by which the mapping closure can be enacted. The mechanism of utilizing this relation is demonstrated here by two simple examples. The examples chosen are those for which the desired information can be furnished by simple analytical procedures. However, an outline is provided of the implementation of this mechanism for more complex conditions.

The second problem is the provision of some analytical results for higher-order statistics generated by the mapping closure. This problem is suitable for addressing the relaxation property of the predicted pdf, including the temporal evolution of the scalar variance, the scalar flatness, and the correlation of the mean square of the scalar and its gradient. The purpose of this study is twofold: (1) to present an algebraic expression for quantitative evolution of the model-generated pdf and its instantaneous deviation from Gaussianity, and (2) to motivate the investigation of the effects of turbulence straining, which is believed to play an important role in physical characteristics of the mapping closure.[2,9]

In both these problems our attention is focused on a basic test problem which has been considered in a number of previous contributions.[6-8] Namely, the probability evolution of a stochastically distributed scalar from an initially binary state in a homogeneous setting. The analytical results presented here are mostly emanated from the general solution already available in a previous work.[10] Also, an extensive DNS data bank is available by which the extent of validity of

 0899-8213/92/051028-08$04.00

the analytical results can be assessed. In a third problem, nevertheless, an extension is made for the modeling of homogeneous mixing from an initially trinary state. This problem is considered since it portrays some salient features of the mapping closure and is believed to provide a more rigorous means of evaluating its performance. In this problem, the results predicted by the mapping closure are discussed in view of their relevance for implementing other simpler probability frequencies. These results are also compared with DNS data for a quantitative assessment.

In comparison against DNS data, only the Fickian diffusion process is the subject of main consideration. This is to remove the complications associated with the effects of turbulent stretching. After establishing a better understanding of the nature of the closure, its extension to problems involving turbulent transport can be more adequately addressed. Also, while the mapping closure (and the general pdf method) is promoted for statistical description of reacting turbulent flows, this study is concentrated only on nonreacting transport, i.e., mixing only. However, all the cases considered are relevant for modeling of turbulent reacting phenomena. The binary mixing problem is pertinent to the study of unpremixed turbulent reacting flows,[8] and the trinary mixing problem is appropriate in modeling of parallel-consecutive chemical reactions in plug flow reactors.[11]

II. MAPPING CLOSURE

We consider the following advection–diffusion equation for a statistically homogeneous scalar field, $\phi(\mathbf{x},t)$ in three-dimensional homogeneous turbulence,

$$\frac{\partial \phi}{\partial t} + \mathbf{u}\cdot\nabla\phi = D\nabla^2\phi, \tag{1}$$

where $\mathbf{x}$ is the position vector, t is time, $\mathbf{u}$ is the incompressible turbulent velocity, and D is the scalar diffusivity and is assumed constant. To invoke the mapping closure for ϕ satisfying Eq. (1), let

$$\phi(\mathbf{x},t) = X(\phi_0(\mathbf{x}),t), \tag{2}$$

where $X(\phi_0,t)$ is the mapping function. This function is shown to evolve according to[2,3,10]

$$\frac{\partial X}{\partial t} = D\langle \xi_0^2\rangle\left(-\phi_0\frac{\partial X}{\partial \phi_0} + \frac{\partial^2 X}{\partial \phi_0^2}\right). \tag{3}$$

The reference scalar field ϕ_0 in Eq. (2) is a time-independent standardized Gaussian variable with mean square gradient $\langle \xi_0^2\rangle$ which, in general, is time-dependent. Here the probability mean is denoted by angle brackets. The scalar pdf $P(\phi,t)$ is determined from the one-to-one mapping function $X(\phi_0,t)$ as

$$P(\phi,t) = \frac{P_G(\phi_0)}{(\partial X/\partial \phi_0)}, \tag{4}$$

where $P_G(\phi_0)$ is the pdf of the Gaussian reference variable ϕ_0. Equations (3) and (4) demonstrate that the incompressible velocity field has no direct influence on the single-point scalar pdf evolution, its only role is through the external time-dependent parameter $\langle \xi_0^2\rangle$. This parameter is related to the scalar mean square gradient $\langle \xi^2\rangle$ by[2]

$$\langle \xi^2\rangle = \left\langle\left(\frac{\partial X}{\partial \phi_0}\right)^2\right\rangle\langle \xi_0^2\rangle. \tag{5}$$

In deriving Eq. (5) use has been made of the fact that ϕ_0 is independent of its gradient ξ_0. Equations (3)–(5) provide the basic framework by which our analytical results are established. The scalar pdf evolution derived from Eq. (1) satisfies[12]

$$\frac{\partial P}{\partial t} + D\frac{\partial^2(E\{\xi^2|\phi\}P)}{\partial \phi^2} = 0, \tag{6}$$

where $E\{\xi^2|\phi\}$ is the expected value of the scalar mean square gradient conditioned on the given value of $\phi(\mathbf{x},t)$. As indicated before, only the Fickian diffusion of the scalar field is considered, even though at the single-point level the scalar pdf obeys the same evolution equation [Eq. (6)] regardless of the structure of the velocity field.

III. BINARY MIXING OF SCALAR

In studying the binary mixing of the scalar ϕ, the initial single-point pdf of ϕ is chosen to be symmetrical about $\phi = 0$ with unit variance,

$$P(\phi,t=0) = \tfrac{1}{2}[\delta(\phi-1) + \delta(\phi+1)]. \tag{7}$$

The initial mapping function, therefore, can be determined by[10]

$$X(\phi_0,0) = 2H(\phi_0) - 1, \tag{8}$$

where H is the Heaviside function. The analytical solution for the mapping function X subject to initial condition, Eq. (8), is given by[10]

$$X(\phi_0,\tau) = \mathrm{erf}(A\phi_0), \tag{9}$$

where "erf" denotes the error function,

$$A^2(\tau) = e^{-2\tau}/2(1-e^{-2\tau}), \tag{10}$$

and the dimensionless time τ is defined by the differential relation

$$d\tau = D\langle \xi_0^2\rangle dt. \tag{11}$$

This equation indicates that τ is a monotonically increasing function of time t. Having Eq. (9), the pdf of ϕ is directly determined by Eq. (4).

A. Time scaling

To overcome the remaining closure problem at the single-point level, a scaling between the dimensionless time τ and the physical time t, i.e., $\tau = \tau(t)$, is required. This relation can be determined from Eqs. (5) and (9) as

$$\left\langle\left(\frac{\partial X}{\partial \phi_0}\right)^2\right\rangle = \frac{2}{\pi}\frac{e^{-2\tau}}{\sqrt{1-e^{-4\tau}}} \equiv S(\tau). \tag{12}$$

An analytical result can be derived for the decay of the scalar variance from Eq. (9),

$$\langle \phi^2\rangle = (2/\pi)\sin^{-1}(e^{-2\tau}) \equiv V(\tau). \tag{13}$$

This equation is very convenient in furnishing the time scaling relation. From Eqs. (5) and (11)–(13) this relation, after some algebraic manipulations, becomes

$$[D/\lambda_0^2(t)]dt = [S(\tau)/V(\tau)]d\tau, \tag{14}$$

where the scalar microlength scale λ_ϕ is defined by

$$1/\lambda_\phi^2 = \langle \xi^2 \rangle / \langle \phi^2 \rangle. \tag{15}$$

From Eq. (1), the decay of the scalar variance is determined by

$$\frac{d\langle \phi^2 \rangle}{dt} = -2D\langle \xi^2 \rangle. \tag{16}$$

Therefore, from Eq. (15) the time scaling relation becomes

$$V(\tau) = \exp\left(-2D \int_0^t \frac{ds}{\lambda_\phi^2(s)} \right) \tag{17}$$

as would have been obtained from Eq. (14).

In determining this scaling relation for the mapping closure at the single-point level, the effects of turbulent stretching on the scalar field as well as other physical processes such as chemical reactions, molecular diffusion, etc., have to be included through the scalar microlength scale. For the present problem of pure diffusion, the required length scale is determined by the scalar energy spectrum $E_\phi(k,t)$ according to

$$\frac{6}{\lambda_\phi^2} = \frac{\int_0^\infty k^2 E_\phi(k,t)dk}{\int_0^\infty E_\phi(k,t)dk}, \tag{18}$$

where the scalar energy spectrum $E_\phi(k,t)$ at wave number k evolves, from Eq. (1), as

$$E_\phi(k,t) = E_\phi(k,0)\exp(-2Dk^2 t) \tag{19}$$

and

$$\langle \phi^2 \rangle = \int_0^\infty E_\phi(k,t)dk. \tag{20}$$

The solution, Eq. (19), follows from the linearity of Eq. (1) with $\mathbf{u} = 0$ and is obtained for a three-dimensional isotropic scalar field.

The following two examples make the procedure for determining this time scaling relation clear. The first is concerned with the self-similar decay of the scalar energy spectrum $E_\phi(k,t)$ from its initial shape,

$$E_\phi(k,0) = \sqrt{\frac{2}{\pi}} \left(\frac{k^2}{k_0^3} \right) \exp\left(-\frac{k^2}{2k_0^2} \right).$$

With this spectrum, Eqs. (14), (18), and (19) provide the desired relation,

$$\exp(-2\tau) = \sin[(\pi/2)(1+4Dk_0^2 t)^{-3/2}]. \tag{21}$$

In the second example it is assumed that the scalar variance decays according to a power-law description, $\langle \phi^2 \rangle = (1+B_0 t)^{-n}$. Equation (16) then yields $\lambda_\phi^2(t) = \lambda_\phi^2(0)(1+B_0 t)$. With this relation, the corresponding time scaling relation is easily determined by equating Eq. (13) to the power-law relation for the scalar variance. Note that the first example also yields a power-law decay for the scalar variance with a decay exponent $n = 1.5$.

These examples demonstrate the procedures of establishing the time scaling relations under simplified conditions. For more complex scenarios, the scalar variance can be used, when justified, to provide the appropriate relations. For example, in a quantitative assessment of the closure against DNS data, the DNS-generated variance and Eq. (13) would directly provide the scaling. In the absence of DNS data, the variance can be determined by means of an appropriate turbulence closure. An example of this is a recent attempt[13] in which the single-point amplitude mapping closure is employed in conjunction with a two-point spectral closure.[14] The results of this combined procedure has shown to yield a reasonable agreement with experimental data in homogeneous reacting flows.

B. Some results

A quantitative measure of the statistical properties of the mapping closure is the magnitude of the higher-order moments and other statistical correlations generated by the model. It has been shown that although the scalar pdf evolving from an initial binary state has an asymptotic leading term of a Gaussian form, the boundedness constraints on the scalar range prevent it from being exactly so at any finite time.[4,5] A partial measure of the instantaneous deviation from Gaussianity is provided by the flatness factor F_4,

$$F_4 = \langle \phi^4 \rangle / \langle \phi^2 \rangle^2. \tag{22}$$

The temporal evolution of F_4 is governed by

$$\frac{dF_4}{dt} = D\frac{\langle \xi^2 \rangle}{\langle \phi^2 \rangle}(4F_4 - 12\rho_2), \tag{23}$$

which corresponds to $n = 2$ of the following general form of the evolution of even-order standardized moments:[15]

$$\frac{\partial \langle x^{2n} \rangle}{\partial t} = D\frac{\langle \xi^2 \rangle}{\langle \phi^2 \rangle} \times [2n\langle x^{2n} \rangle - 2n(2n-1)\langle x^{2n-2} y^2 \rangle]. \tag{24}$$

Here x and y are the standardized scalar fluctuation $\phi/\langle \phi^2 \rangle^{1/2}$ and the standardized scalar square gradient $\xi^2/\langle \xi^2 \rangle$, respectively. The function ρ_2 in Eq. (23) is the correlation function $\langle x^2 y \rangle$ which differs from that in Ref. 16 by unity. An interesting property of Eq. (24) is that all moments of the variable x are entirely determined by the correlations of x^{2n} with the variable y. Another feature of this equation is its validity regardless of the presence or absence of a homogeneous, incompressible turbulent velocity field. Using the time scaling relation, Eq. (14), the evolution equation for $F_4(\tau)$ becomes

$$\frac{dF_4}{d\tau} = \frac{S(\tau)}{V(\tau)}(4F_4 - 12\rho_2), \tag{25}$$

where the correlation function ρ_2 is given by

$$\rho_2 = \langle x^2 y \rangle = \frac{\sin^{-1}\{\exp(-2\tau)/[1+2\exp(-2\tau)]\}}{\sin^{-1}[\exp(-2\tau)]}. \tag{26}$$

In deriving Eq. (26) the following expression is employed for the normalized conditional scalar mean square gradient:[5]

$$E\{\xi^2|\phi\} = E\{\xi^2|0\}\exp\{-2[\operatorname{erf}^{-1}(\phi)]^2\}. \tag{27}$$

Equation (25) indicates that the correlation function ρ_2 acts like a sink term in the transport equation for F_4. This equation has the solution

$$F_4(\tau) = V^3 - \int_0^\tau \exp[3(s-s')]Q(s')ds', \tag{28}$$

with

$$Q(s) = \exp(-s)\sin^{-1}\left(\frac{\sin[\exp(s)]}{1+2\sin[\exp(s)]}\right). \quad (29)$$

Unlike that of variance, the analytical expression for F_4 does not portray a simple algebraic form and its evaluation requires numerical integration. Here this integration is performed with respect to the primitive Gaussian reference variable, ϕ_0. The results depicting the evolutions of F_4 and ρ_2 are presented in Fig. 1. In this figure, the abscissa is the scalar variance conversion, $1-\langle\phi^2\rangle_\tau/\langle\phi_0^2\rangle$, which is a monotonically increasing function of time. From this figure, both F_4 and ρ_2 predicted by the mapping closure are shown to exhibit a monotonic increase in time and approach their respective asymptotic Gaussian values, 3 and 1. The leading term in the asymptotic expansion of F_4 is of the form $F_4 \sim 3 - 4e^{-2\tau} + \mathcal{O}(e^{-4\tau})$ as $\tau \to \infty$, and indeed Eq. (25) yields a stationary solution for a Gaussian state, i.e., $F_4 = 3$ and $\rho = 1$. This realization of an asymptotic Gaussian state has been discussed in Refs. 3, 4, and 9 and is also corroborated in previous DNS studies.[16,17]

The statistical results predicted by the closure are also compared with those of DNS of scalar Fickian diffusion. The DNS data are generated by means of spectral-collocation simulation of an isotropic three-dimensional diffusion. The resolution in DNS consists of 64 Fourier nodes in each of the three directions, which is sufficient for this simulation. The scalar energy spectrum used to generate the initial scalar field has the form $E_\phi(k) = (k^2/k_0^2)\exp(-k^2/k_0^2)$ with $k_0 = 1.5$. With this spectrum, the scalar field is generated randomly in the spectral domain. This field is then transformed into the physical domain for statistical analysis. The temporal evolution of DNS-generated pdf's from this initial condition is presented in Fig. 2. This evolution displays a qualitatively similar behavior to that of previous stationary turbulence simulations[3,16] and is therefore consistent with the mapping closure predictions.[3] A noted feature for the scalar evolution is that it adopts a transient uniform state[3] in $[-1,1]$ at $\tau = \ln 2/2$ at which $\langle\phi^2\rangle = 1/3$ and $F_4 = 9/5$. Such an approximately uniform state has also been realized in DNS as evidenced in Fig. 2 for the scalar pdf at $t = t_2$.

The comparison between the mapping closure results and those generated by DNS is reasonably good for the flatness factor as demonstrated in Fig. 1. Despite this agreement, there is a difference between the model predictions and the DNS data for the parameter ρ_2 at early times. The reason for this discrepancy is due to the deviation in matching the initial state of the scalar field in DNS. This deviation, however, does not seem to have a substantial impact at later times.

IV. TRINARY MIXING OF SCALAR

For trinary mixing, the initial single-point scalar pdf is described by

$$P(\phi,t=0) = c_{-1}\delta(\phi_0+1) + c_0\delta(\phi_0) + c_1\delta(\phi_0-1), \quad (30)$$

and the initial mapping is expressed by

$$Z(\phi,0) = \begin{cases} 1, & \phi_0 > \alpha, \\ 0, & \alpha \geq \phi_0 \geq \beta, \\ -1, & \beta \geq \phi_0, \end{cases}$$

where

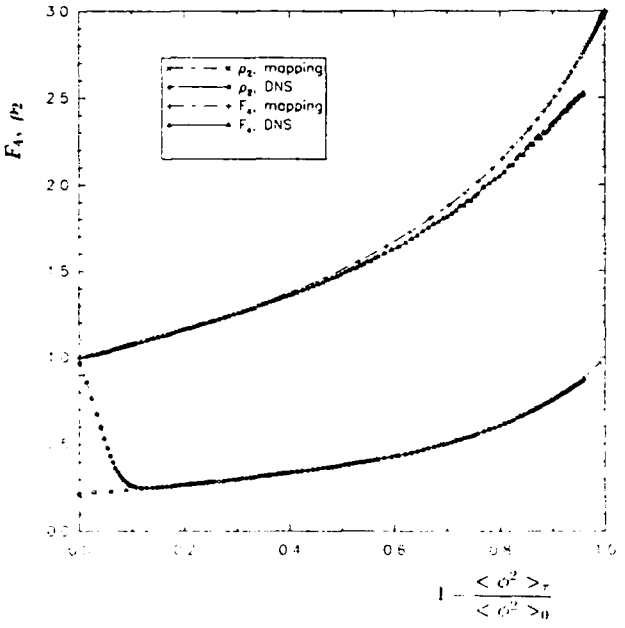

FIG. 1. The scalar flatness factor, F_4, and the correlation of the mean square scalar-scalar gradient, ρ_2, versus the scalar variance conversion, $1-\langle\phi^2\rangle_\tau/\langle\phi^2\rangle_0$.

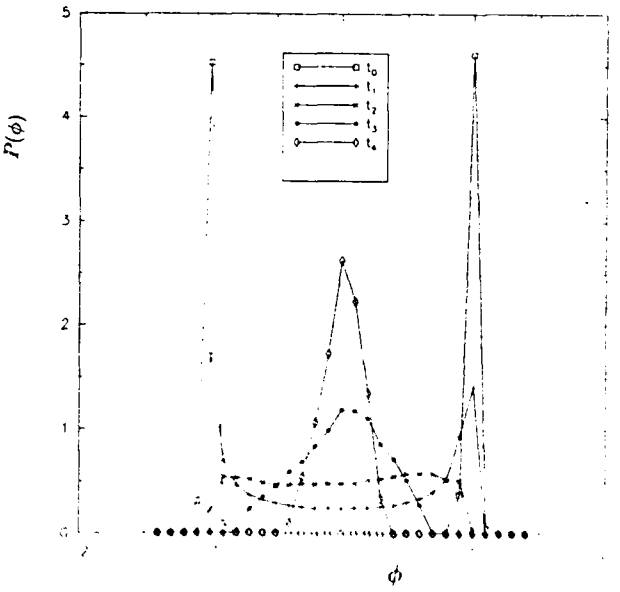

FIG. 2. DNS results for the evolution of the scalar pdf from an initial (t_0) binary state and at four subsequent times, $t_1 < t_2 < t_3 < t_4$.

$$c_{-1} = \frac{1}{\sqrt{2\pi}} \int_{-\infty}^{\beta} \exp\left(-\frac{\phi_0^2}{2}\right) d\phi_0,$$

$$c_1 = \frac{1}{\sqrt{2\pi}} \int_{\alpha}^{\infty} \exp\left(-\frac{\phi_0^2}{2}\right) d\phi_0, \tag{31}$$

$$c_0 = 1 - c_{-1} - c_1.$$

For simplicity, only symmetrical distributions are considered, i.e., $\alpha = -\beta$. For this, the corresponding mapping takes the form[7]

$$\phi = Z(\phi_0,\tau) = \tfrac{1}{2}[\,\mathrm{erf}(A\phi_0 + B) + \mathrm{erf}(A\phi_0 - B)\,], \tag{32}$$

where $B = \alpha/\sqrt{2}a$ and $a = \sqrt{1 - \exp(-2\tau)}$. From Eq. (4), the pdf of ϕ when expressed in terms of ϕ_0 becomes

$$P(\phi,\tau) = \frac{\sqrt{\exp(2\tau) - 1}\,\exp(\alpha^2/2a^2)\,\exp((-\phi_0^2/2)\{1 - [\exp(-2\tau)/a^2]\})}{2\cosh[\alpha\phi_0 \exp(-\tau)/a^2]}. \tag{33}$$

For $\alpha = 0$ the solution for the double-delta case is recovered. For $\alpha \neq 0$ the pdf adopts two distinct distributions depending on τ being greater or smaller than $\tau_f = \ln 2/2$. This corresponds to the instant at which the pdf is uniform in the binary mixing case. The behavior of the pdf at $\phi = 0$ and $\phi = 1$ is of our immediate concern with regard to its relaxation. The corresponding mapping to these two points is from $\phi_0 = 0$ and $\phi_0 = \infty$, respectively. Equation (33) shows that at $\tau > 0$,

$$P(\phi = 0,\tau) = \exp(\alpha^2/2a^2)\sqrt{\exp(2\tau) - 1}. \tag{34}$$

Therefore, it can be shown that $P(0,\tau)$ portrays a decreasing–increasing behavior in τ, and reaches its minimum value at $\tau = \ln(1 + \alpha^2)/2$. The scalar pdf at $\phi = 1$ is infinity when $\tau \leqslant \tau_f$ and is zero otherwise. The exponential nature of the pdf as $\phi \to 1$ is different, however, between $\tau = \tau_f$ and $\tau < \tau_f$, as can be deduced from Eq. (33). The probability distribution for $\alpha = \sqrt{2}\,\mathrm{erf}(1/3)$ (i.e., $c_{-1} = c_0 = c_1 = 1/3$) is shown in Fig. 3 for $\tau < \tau_f$ and in Fig. 4 for $\tau > \tau_f$.

The pdf's extracted from the DNS data are shown in Fig. 5. This figure suggests that at large times the pdf asymptotes to a bell-shaped distribution. However, a transient uniform state similar to that in the binary mixing case is not attained with Eq. (33). Asymptotically, the pdf can be reasonably approximated by simple known frequencies such as the Beta density.[18] To verify the asymptotic Gaussianity of this distribution, the Taylor series expansion of Eq. (32) for $Z(\phi_0,\tau)$ is considered. The following asymptotic expression is obtained in the limit $A \to 0$ as $\tau \to \infty$:

$$Z(\phi_0,\tau) = (2/\sqrt{\pi})\exp(-\alpha^2/2a^2)A\phi_0 + \mathcal{O}[(1 - \alpha^2)A^3\phi_0^3]. \tag{35}$$

This expression indicates that the mapping function has an asymptotic linear form in the Gaussian reference variable ϕ_0, and thus is itself a Gaussian variable. However, the leading exponential term indicates that the rate of evolution depends on magnitude of the parameter α, i.e., the extent of the initial departure from the binary case.

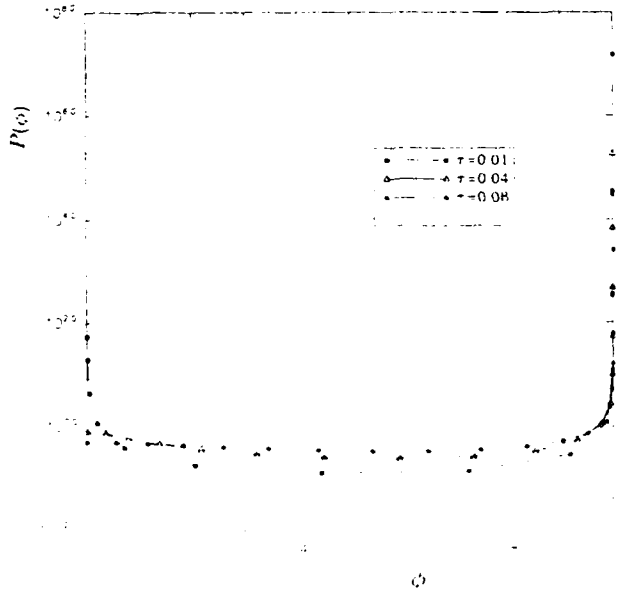

FIG. 3. Evolution of the scalar pdf predicted by the mapping closure for the binary mixing case at small τ values.

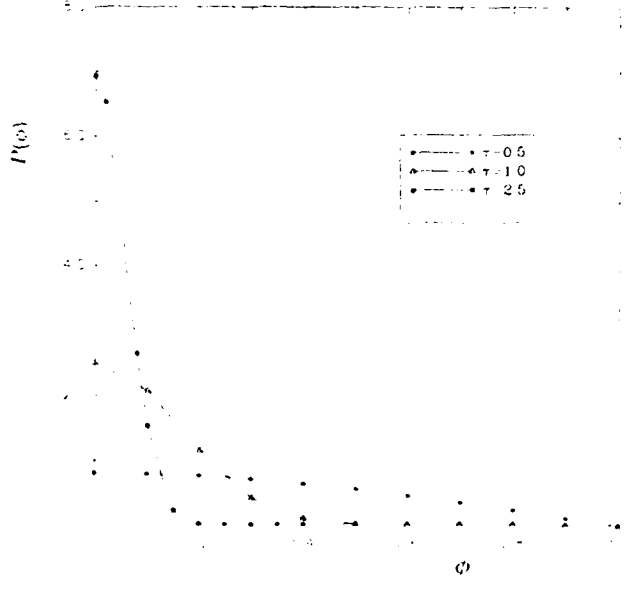

FIG. 4. Evolution of the scalar pdf predicted by the mapping closure for the binary mixing case at large τ values.

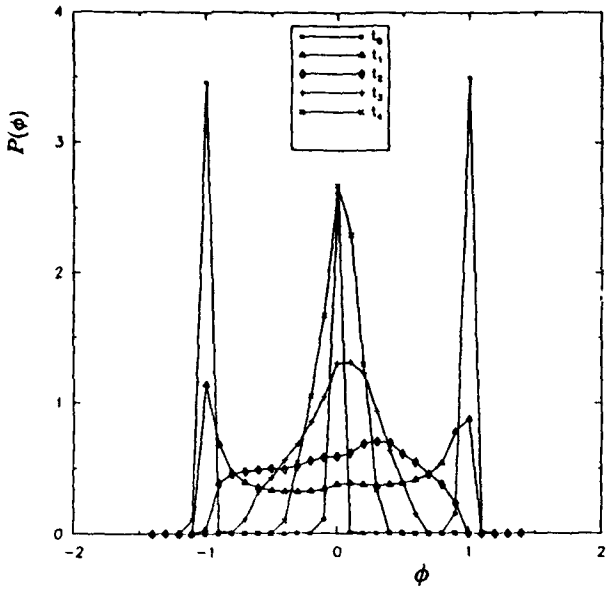

FIG. 5. DNS results for the evolution of the scalar pdf from an initial (t_0) trinary state and at four subsequent times, $t_4 > t_3 > t_2 > t_1 > t_0$.

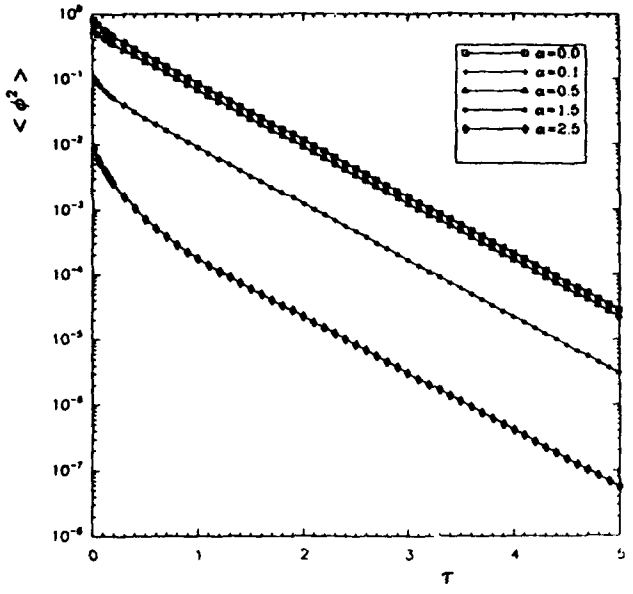

FIG. 6. Scalar variance $\langle \phi^2 \rangle$ vs τ from the mapping closure.

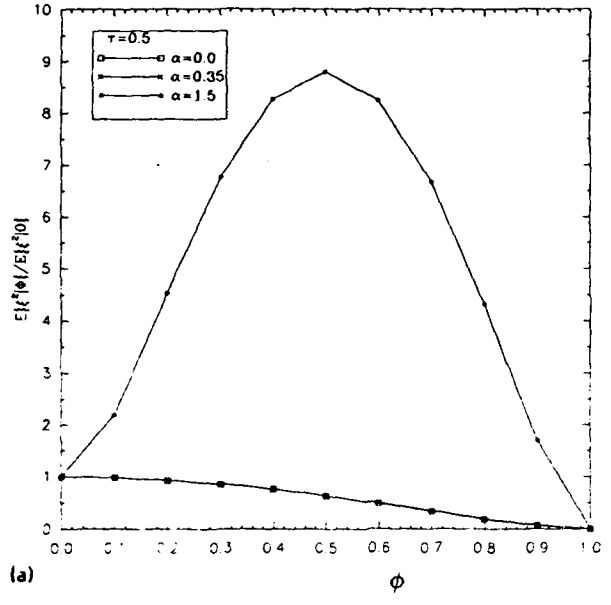

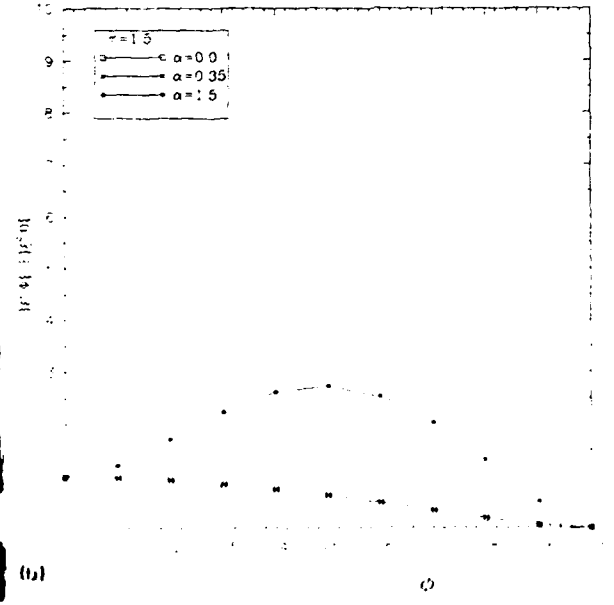

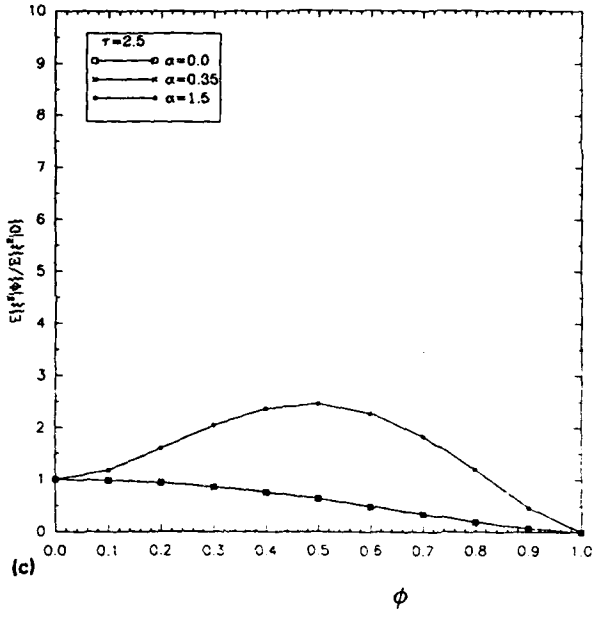

FIG. 7. The evolution of the normalized conditional mean square scalar gradient from the mapping closure. (a) $\tau = 0.5$, (b) $\tau = 1.5$, (c) $\tau = 2.5$.

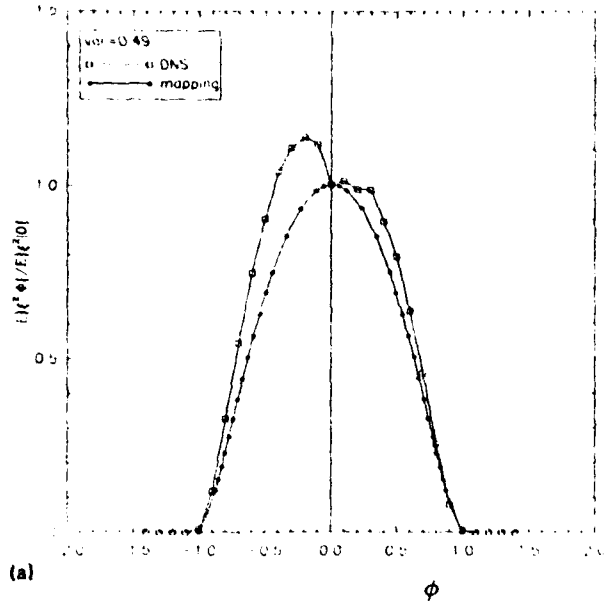

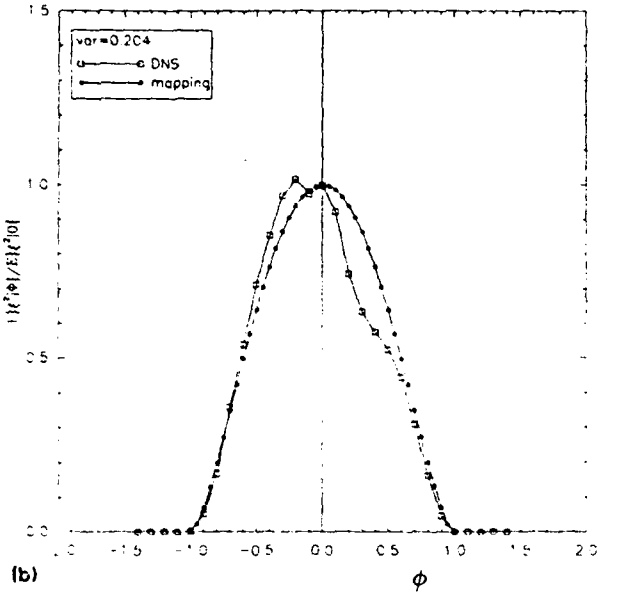

FIG. 8. Comparative results of mapping closure and DNS for the normalized, conditional mean square scalar gradient. (a) $\langle \phi^2 \rangle = 0.49$, (b) $\langle \phi^2 \rangle = 0.204$.

Unlike the binary mixing case, the expression for the scalar variance for the trinary mixing case does not display a simple algebraic form and its evaluation requires numerical integration. Similarly, other higher-order moments, such as F_4 and ρ_2, can be only expressed by integral expressions. As before, the numerical evaluations of these integrals are performed with respect to the Gaussian reference variable.

In Fig. 6 results are presented of the scalar variance for several values of the parameter α. This figure indicates that after an initial transitional period, all the curves adopt an exponential decay in τ with approximately the same rate of exponential decay. This figure also suggests that as the magnitude of the parameter α increases, the initial transitional period becomes somewhat longer. The corresponding form

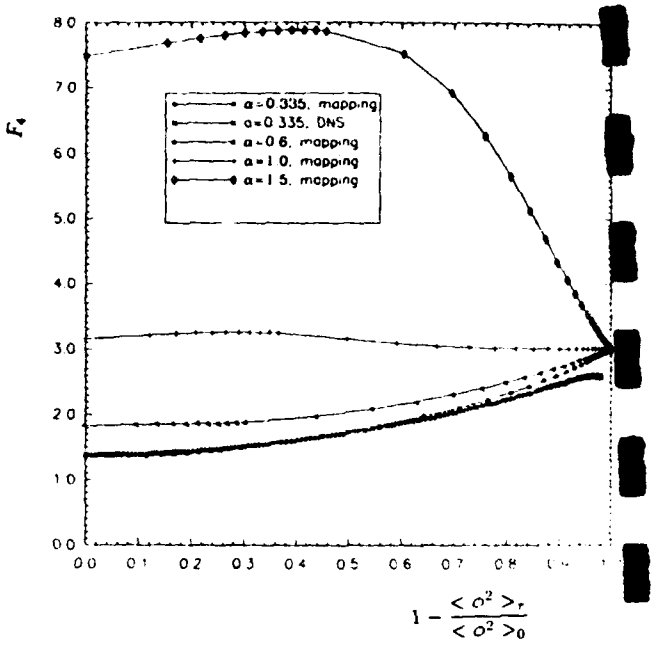

FIG. 9. The evolution of the scalar flatness factor, F_4, versus the normali scalar variance conversion, $1 - \langle \phi^2 \rangle \tau / \langle \phi^2 \rangle_0$.

of the conditional scalar mean square gradient is obtained in terms of the reference Gaussian scalar variable ϕ_0 as

$$E\{\xi^2|\phi\} = E\{\xi^2|0\} \exp(-2A^2\phi_0^2) \cosh(2AB\phi_0), \tag{36}$$

and the mean square scalar gradient "correlation" ρ_2 is give by

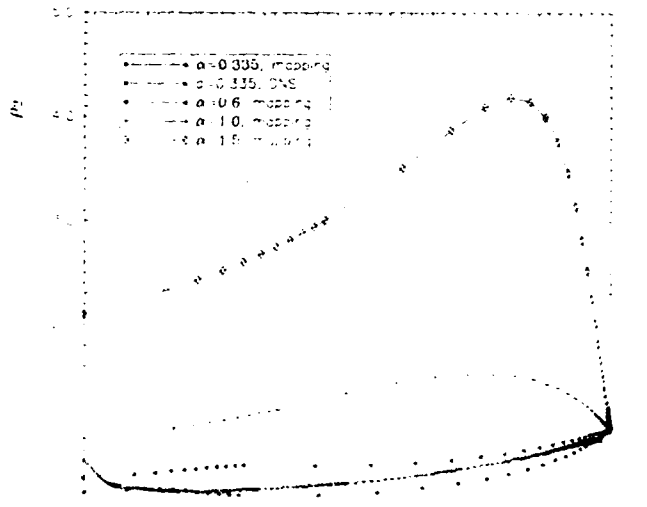

FIG. 10. The evolution of the correlation of the mean square scalar-scalar gradient, ρ_2, versus the normalized scalar variance conversion $1 - \langle \phi^2 \rangle \tau / \langle \phi^2 \rangle_0$.

$$\rho_2 = \frac{\langle Z^2 \exp(-2A^2\phi_0^2)\cosh(2AB\phi_0)\rangle}{\langle Z^2\rangle\langle \exp(-2A^2\phi_0^2)\cosh(2AB\phi_0)\rangle}. \quad (37)$$

Numerical results of the normalized scalar mean square gradient for several values of α are shown in Fig. 7 at different times. This figure suggests that the results are independent of τ when α is small, i.e., the binary case.[5] This clearly reveals the profound influence of this parameter on the evolution of the normalized mean square gradient at small τ values. The comparison of this quantity predicted by the mapping closure at $\alpha = 0.335$ with DNS results, by virtue of matching the scalar variance, is shown in Fig. 8. The general quantitative comparison is quite satisfactory and the results display a qualitatively similar behavior. The temporal evolution of F_4 and ρ_2 are presented, respectively, in Figs. 9 and 10 for several values of α. The comparison with DNS at $\alpha = 0.335$ exhibits an excellent agreement for F_4 and a reasonably good agreement for ρ_2. Again the results indicate the influence of the parameter α on the evolution of both these quantities. A noteworthy behavior of the predicted results is that during the course of evolution both F_4 and ρ_2 reach a relative maximum before monotonically decreasing to their respective asymptotic Gaussian values of 3 and 1 when α is "sufficiently" large. A somewhat similar behavior has been previously observed in DNS of an approximate binary mixing by stationary turbulence.[16] As mentioned before, the binary mixing corresponds to $\alpha = 0$ with F_4 and ρ_2 evolutions as shown in Fig. 1. This figure exhibits a monotonic increase in the magnitudes of these quantities, which is not in accord with the above-mentioned DNS results. This difference may be due to (i) deviation of the initial binary states in DNS and/or (ii) inadequate level (single-point) of the mapping closure. In relation to (i), it should be mentioned that in Ref. 2 an excellent agreement has been observed of the model predictions and DNS results for the case of an initially Gaussian diffusive-reactive scalar. The idealized initial delta-like distributions imposed in the present study provide the advantage of simplifying the analytical procedures, but cannot be realized exactly in numerical implementation. It is not easy to elucidate the consequences of the deviation from such initial conditions, at least at small times. In regard to (ii), in view of the discussions above, it seems that this issue is important in the presence of a turbulent field. A means of dealing with the closure problem at this level requires the escalation of the level of the mapping, e.g., to the scalar and its gradient.[2,9]

The general agreement between the mapping closure predictions and the DNS data is noteworthy. However, this agreement has been demonstrated here only for the two cases of binary and trinary initial states. Therefore, further validation assessments including a wider variety of initial conditions are recommended. Also, as indicated earlier, the effects of turbulence stretching are not included in our analysis. The influence of this stretching and the effects of random advection in homogeneous turbulence are the subject of current investigation.[9]

ACKNOWLEDGMENTS

The work at SUNY–Buffalo is sponsored by the Office of Naval Research under Grant No. N00014-90-J-4013. Computational resources are provided by the National Science Foundation through National Center for Supercomputing Applications at the University of Illinois.

[1]R. H. Kraichnan, "Closures for probability distributions," Bull. Am. Phys. Soc. **34**, 2298 (1989).
[2]H. Chen, S. Chen, and R. H. Kraichnan, "Probability distribution of a stochastically advected scalar field," Phys. Rev. Lett. **63**, 2657 (1989).
[3]S. B. Pope, "Mapping closures for turbulent mixing and reaction," Theor. Comput. Fluid Dyn. **2**, 255 (1991).
[4]F. Gao, "Mapping closure and non-Gaussianity of the scalar probability density functions in isotropic turbulence," Phys. Fluids A **3**, 2438 (1991).
[5]E. E. O'Brien and T.-L. Jiang, "The conditional dissipation rate of an initially binary scalar in homogeneous turbulence," Phys. Fluids A **3**, 3121 (1991).
[6]C. Dopazo, "Relaxation of initial probability density functions in the turbulent convection of scalar fields," Phys. Fluids **22**, 20 (1979).
[7]S. B. Pope, "An improved Turbulent mixing model," Combust. Sci. Technol. **28**, 131 (1982).
[8]G. Kosaly and P. Givi, "Modeling of turbulent molecular mixing," Combust. Flame **70**, 101 (1987).
[9]F. Gao, Y. Kimura, and R. H. Kraichnan, manuscript in preparation (1992).
[10]F. Gao, "An analytical solution for the scalar probability density function in homogeneous turbulence," Phys. Fluids A **3**, 511 (1991).
[11]F. Gao, "Theoretical and numerical investigation of scalar fields in isotropic turbulence," Ph.D. dissertation, SUNY at Stony Brook, New York, 1990.
[12]S. B. Pope, "The probability approach to modelling of turbulent reacting flows," Combust. Flame **27**, 299 (1976).
[13]S. H. Frankel, T.-L. Jiang, and P. Givi, manuscript in preparation (1992).
[14]M. Larrcheveque and M. Lesieur, "The application of eddy-damped Markovian closures to the problem of dispersion of particle pairs," J. Mec. **20**, 113 (1981).
[15]Ya. G. Sinai and V. Yakhot, "Limiting probability distributions of a passive scalar in a random velocity field," Phys. Rev. Lett. **63**, 1962 (1989).
[16]V. Eswaran and S. B. Pope, "Direct numerical simulations of the turbulent mixing of a passive scalar," Phys. Fluids A **1**, 537 (1988).
[17]P. Givi and P. A. McMurtry, "Non-premixed reaction in homogeneous turbulence: Direct numerical simulations," AIChE J. **34**, 1039 (1988).
[18]S. H. Frankel, C. K. Madnia, and P. Givi, "On the modeling of the unmixedness in homogeneous reacting turbulence," Chem. Eng. Comm. **104**, 117 (1991).

APPENDIX 5

A Hybrid Mapping-EDQNM Closure

Modeling of Isotropic Reacting Turbulence by a Hybrid Mapping-EDQNM Closure

Steven H. Frankel, Tai-Lun Jiang, and Peyman Givi
Dept. of Mechanical and Aerospace Engineering, State University of New York at Buffalo, Buffalo, NY 14260

A hybrid model is developed and implemented for predicting the limiting bound of the reactant conversion rate in an isotropic turbulent flow under the influence of a reaction of the type $A+B \rightarrow$ Products. This model is based on the amplitude mapping closure of Kraichnan for the molecular mixing of a stochastically distributed scalar, and the eddy-damped quasi-normal Markovian (EDQNM) spectral closure for the two-point scalar covariance. The results predicted by this model compare well with available experimental data in both gaseous and aqueous plug-flow reactors, but point to the need for more detailed measurements in future experimental studies. With the implementation of the mapping closure, a simple analytical expression is obtained for the decay rate of the unmixedness. This expression is very convenient and is recommended for direct practical applications in the modeling and design of plug-flow reactors.

Introduction

Statistical modeling of the reactant conversion rate in homogeneous reacting turbulence has been the subject of wide investigations since the early pioneering work of Toor (1962). Among the class of statistical methods in use, it is now accepted that the approach based on the probability density function (PDF) of the scalar quantities is most appropriate (Hawthorne et al., 1949; Toor, 1975; Pope, 1979, 1985; Kollmann, 1990). The principal advantage of this method is based on the fundamental property of the PDF, which includes all the statistical information regarding the reacting field. For this reason, PDF methods have been very attractive and popular as evidenced by their wide use in various forms for the statistical treatment of reacting turbulence phenomena (for recent reviews, see Givi, 1989; Kollmann, 1990; Pope, 1990).

The most systematic means of determining the PDF involves the solution of an appropriate transport equation governing the PDF's evolution. In this equation, due to the nature of the formulation, the effects of chemical reaction appear in a closed form. However, the influences of molecular action cannot be fully described and can be treated only by means of employing an appropriate turbulence closure. In many previous applications, this problem has been addressed through the use of coalescence/dispersion (C/D) models. Examples of such models are the early C/D prototype of Curl (1962) (which was not constructed for turbulence applications, but has been widely utilized for PDF modeling of reacting turbulence), the linear mean square estimation (LMSE) theory of O'Brien (1980), and the closure of Janicka et al. (1979), among others. While not all of these closures were originally presented in a C/D form, it is now established that the majority of those in current use (including the three aforementioned) can be cast in a generalized C/D mold (Pope, 1982; Kosaly and Givi, 1987).

Despite their wide utilization in modeling the transport of scalar variables in turbulence, none of the C/D closures currently in use are physically plausible (Pope, 1982; Kosaly and Givi, 1987; McMurtry and Givi, 1989). In all of these models, the C/D-generated PDFs are not entirely consistent with those either measured experimentally or generated by means of direct numerical simulations (DNS). Specifically, none of these closures are capable of producing an asymptotic Gaussian distribution for the PDF of a conserved scalar from an initially non-Gaussian state in homogeneous turbulence. This trend has been observed in DNS (Eswaran and Pope, 1988; Givi and McMurtry, 1988) and has been corroborated by experimental measurements (Miyawaki et al., 1974; Tavoularis and Corrsin, 1981). This deficiency associated with the C/D closure has been long recognized, and within the past decade significant efforts have been devoted toward developing closures that can

Correspondence concerning this article should be addressed to S. H. Frankel.

overcome this nonphysical behavior (for example, Pope, 1982; Norris and Pope, 1991).

For the past few years, Kraichnan and coworkers (Chen et al., 1989) have made rather significant progress in devising a "mapping closure" that can effectively deal with the aforementioned problem. This model, in essence, provides a means of accounting for the transport of the PDF in composition space, and its validity and physical applicability have been convincingly evidenced in a number of comparisons against DNS data (Pope, 1991; Gao, 1991a; Madnia et al., 1991; Jiang et al., 1992). The results of these investigations indicate that, at least for isotropic turbulent transport, this closure is superior to all the previous C/D-type models in depicting a physically plausible PDF evolution.

Based on this demonstrated superiority, we have chosen to utilize the mapping closure for the statistical description of reacting turbulence. For this purpose, we have selected a reacting system under idealized conditions compatible with those considered in many previous works in the chemical engineering community. Namely, the reaction $A + B \rightarrow Products$ in a constant density, isotropic turbulent flow. In this flow, the limiting bound of the reactant conversion rate is predicted by assuming an infinitely fast reaction and ignoring all the nonequilibrium effects associated with the chemical kinetics. In this setting, the only unclosed term requiring a model is the evolution of the appropriate turbulent length scale. This particular closure is not exclusive to the mapping model *per se* and is required in any approach based on a "single-point" statistical description. For this, we have chosen the eddy-damped quasi-normal Markovian (EDQNM) spectral closure. This closure is superior to the commonly used k-ϵ models (Launder and Spalding, 1972), since it includes information regarding the transport of "two-point" statistical quantities. However, its feasibility is currently limited to predictions of flows without spatial inhomogeneities. This does not produce a severe limitation here, since most of the available data on plug-flow reactors display homogeneous characteristics.

In the next section, the problem under consideration is outlined along with the specific assumptions made in developing the hybrid mapping-EDQNM closure. Salient features of the mapping closure at the single-point level are discussed. With this closure, a simple algebraic form is obtained for predicting the limiting bound of reactant conversion. While this algebraic relation is very convenient for practical applications, it is not in a closed form and requires knowledge of the turbulent length scale evolution. The EDQNM closure is capable of providing the required length scale information. In the subsequent section, the formalities of the hybrid closure are discussed, highlighting its relative ease of implementation for practical modeling of plug-flow reactors. And then we compare the results predicted by this combined model with laboratory data for two purposes: (1) to validate the model and (2) to identify some of the relevant parameters in future experiments for such validations. These comparisons are validated by results from a study showing the influence of some factors affecting the rate of reactant conversion. In Section 4, our findings are summarized and some suggestions are made for future work.

Description and Formulation of the Problem

The subject under investigation is a binary reaction of the type $A + B \rightarrow Products$ in an isotropic, isothermal turbulent flow (Toor, 1975; Brodkey, 1975, 1981). The two species A and B are initially segregated and are supplied under stoichiometric conditions. The flow field is assumed constant density, and the influences of the chemical reaction on the dynamics of the turbulence are ignored. The turbulent velocity field is assumed stationary to avoid the complications associated with a varying (decaying) turbulence. This field is parameterized by means of a temporally invariant energy spectrum for the velocity. In this setting, the maximum rate of the reactant conversion is obtained from our hybrid model by implementing the assumption of an infinitely fast chemistry. All the species involved in the reaction are assumed to have identical diffusion coefficients and the same thermodynamical properties. Under these conditions, the statistical behavior of the reacting scalars A, B is related to that of a conserved Shvab-Zeldovich variable, $\mathcal{J}$. This variable is arbitrarily normalized in such a way as to yield $-1 \le \mathcal{J} \le 1$. In the framework of the single-point description, the PDFs of the reactants A and B, denoted by $\mathcal{P}_A(\psi, t)$ and $\mathcal{P}_B(\psi, t)$, respectively, are the same for an equivalence ratio of unity. These PDFs are related to that of the Shvab-Zeldovich variable $\mathcal{P}_{\mathcal{J}}(\psi, t)$ by the relation (Toor, 1962; Bilger, 1980):

$$\mathcal{P}_A(\psi,t) = \mathcal{P}_B(\psi,t) = \mathcal{P}_{\mathcal{J}}(\psi,t) + \frac{1}{2}\,\delta(\psi), \tag{1}$$

where δ is the delta function. Equation 1 demonstrates that all the information pertaining to the statistical behavior of the reacting field is available at all times if the PDF evolution for the conserved scalar field is known. For this, we have employed the mapping closure.

Mapping closure

The implementation of this closure involves a mapping of the random field of interest ψ to a stationary Gaussian reference field η, via a transformation $\psi = \chi(\eta, t)$. Once this relation is established, the PDF of the random variable ψ, $\mathcal{P}(\psi)$, is related to that of a Gaussian distribution $P_G(\eta)$ via (Chen et al., 1989; Pope, 1991):

$$\mathcal{P}(\psi,t) = P_G(\eta)\left(\frac{\partial \chi}{\partial \eta}\right)^{-1}, \quad -\infty \le \eta \le +\infty. \tag{2}$$

In light of this transformation, it is clear that since the random field changes with time, so must the mapping function. Therefore, the probability distribution of the scalar is determined from the knowledge of this mapping function. The transport equation for this function has been developed by Chen et al. (1989). Here, we present only the final results:

$$\frac{\partial \chi}{\partial \tilde{t}} = -\eta\,\frac{\partial \chi}{\partial \eta} + \frac{\partial^2 \chi}{\partial \eta^2}. \tag{3}$$

In this equation, $\tilde{t}$ is a normalized time within which the scalar length scale information is imbedded. The general solution of this equation has the form (Gao, 1991a; Pope, 1991):

$$\chi(\eta,\tilde{t}) = \frac{\sqrt{\Sigma(\tilde{t})^2+1}}{\sqrt{2\pi}\Sigma(\tilde{t})} \int_{-\infty}^{\infty} \chi(\zeta,0) \exp\left\{-\frac{[\eta\exp(-\tilde{t})-\zeta]^2[1+\Sigma(\tilde{t})^2]}{2\Sigma(\tilde{t})^2}\right\} d\zeta, \quad (4)$$

where Σ is related to the normalized time by:

$$\Sigma(\tilde{t})^2 = \exp(2\tilde{t}-1). \quad (5)$$

For the case of initially segregated reactants, the corresponding forms of the initial PDF and the mapping function are:

$$\mathcal{P}_g(\psi,0) = \frac{1}{2}\delta(\psi-1) + \frac{1}{2}\delta(\psi+1), \quad (6)$$

$$\chi(\eta,0) = 2H(\eta) - 1, \quad (7)$$

where H is the Heaviside function. Thus, the solution is obtained by substituting Eq. 7 in Eq. 4 to yield:

$$\chi(\eta,\tilde{t}) = \mathrm{erf}\left(\frac{\eta}{\sqrt{2}\Sigma(\tilde{t})}\right), \quad (8)$$

and consequently, from Eq. 2:

$$\mathcal{P}_g[\chi(\eta,\tilde{t}),\tilde{t}] = \frac{\Sigma(\tilde{t})}{2}\exp\left\{-\frac{\eta^2}{2}[1-\Sigma(\tilde{t})^{-2}]\right\}. \quad (9)$$

With a combination of Eqs. 1 and 9, all the single-point statistical information regarding the reacting scalar field is determined. A parameter that provides a good measure of the reactant conversion and has been the subject of numerous experimental measurements is the "unmixedness," Ψ^2. This parameter is defined as the normalized fluctuation correlation of the two species (Toor, 1975):

$$\Psi^2 = \frac{\langle ab\rangle}{\langle ab\rangle_0}, \quad (10)$$

where $\langle\ \rangle$ denote the ensemble average, and a,b are the concentration fluctuations of the two reactants. The subscript 0 indicates the initial time, that is, at the inlet of the reactor. The temporal evolution of the unmixedness is provided by a combination of Eqs. 1, 9 and 10. After some algebraic manipulations, the final result is in the form (Madhia et al., 1991):

$$\Psi^2(\tilde{t}) = \left\{1 - \frac{2\arctan[\Sigma(\tilde{t})]}{\pi}\right\}^2. \quad (11)$$

Having such a simple algebraic form for the unmixedness parameter is certainly very pleasing. In the manner presented, however, this equation cannot be compared directly with experimental data. This is due to the form of the final result. The decay of the unmixedness is presented in terms of the normalized time $\tilde{t}$ (which as indicated before contains the length scale information), *not* the physical time t. Note that it is the physical time t that can be translated to the physical axis of the reactor, x, for comparison against actual measurements. In the context of single-point analysis, the relation between this time and the normalized time $\tilde{t}$ cannot be described. This demonstrates the need for some external means by which the knowledge of two-point statistics can be brought into the analysis. To provide this information, we have used the EDQNM spectral closure.

EDQNM closure

The formulation presented in the previous section would be in a closed form with the knowledge of the parameter Σ. Making the assumption that the evolution of the length scales is the same under reacting and nonreacting conditions, the knowledge of the variance of the Shvab-Zeldovich variable, $\mathcal{J}$, would be sufficient to cast Eq. 11 in a closed form. To account for this length scale, the model employed in this work is based on a two-point closure, namely the EDQNM model. This model is a "single-time" (but still two-point) closure, and compared with other satisfactory stationary spectral closures, its computational treatment is relatively less demanding (see Herring et al., 1982, for a review of all spectral closures currently in use). Because of this property, the EDQNM has proven very powerful in turbulence modeling and has been widely utilized in many investigations (see Orszag, 1977; Herring et al., 1982; Lesieur, 1990, for review).

The form of the EDQNM closure in use here is similar to those of Larcheveque and Lesieur (1981) and Eswaran and O'Brien (1989). This is in the form of a physical-space diffusion equation for the two-point scalar covariance in spherical coordinates with an effective diffusivity, that is, laminar plus turbulent. This form is relatively simple in appearance, but still contains most of the essential physics of the Navier-Stokes equations. For the readers who are not familiar with the model, we describe the derivation of the final physical space transport equation for the single-time, two-point scalar covariance. The mathematical derivation for this equation is detailed by Larcheveque and Lesieur (1981) and Lesieur (1991). The derivation of the model begins with the equation for the two-point covariance in the spectral domain as well as the evolution equation for the third-order correlation. The quasi-normal (QN) approximation is based on Millionshtchikov's (1941) hypothesis and is invoked to facilitate solution of the third-order correlation in terms of the two-point covariance, thereby closing the hierarchy of moment equations. The eddy-damping feature provides a model for the effects of the discarded fourth-order cumulants, and the Markovianization allows for a relaxation toward quasi-equilibrium by nonlinear transfers. The resulting integrodifferential equation is in the spectral (wave number) domain and is computationally intensive due to the triadic interactions that arise from the nonlinearities in the transport equations. By making assumptions on the form of the characteristic relaxation time, Larcheveque and Lesieur (1981) were able to transform the covariance equation back into physical space and obtain a version more suitable for computation. This physical space equation in the form utilized is:

$$\frac{\partial}{\partial t}\rho(r,t) = \frac{1}{r^2}\frac{\partial}{\partial r}\left\{[\mathcal{K}(r,t)+2\mathcal{D}]r^2\frac{\partial}{\partial r}\rho(r,t)\right\}, \quad (12)$$

where the scalar covariance $\rho(r,\ t)$ is spherically symmetric, $\rho(r,\ t)=\rho(|r|,t)=\rho(\underline{r},t)$, and is defined as:

$$\rho(\underline{r},t)=\langle \mathcal{G}(\underline{x},t)\mathcal{G}(\underline{x}+\underline{r},t)\rangle. \quad (13)$$

In Eq. 12, the molecular diffusivity is $\mathcal{D}$, and the turbulent eddy diffusivity, denoted by $\mathcal{K}$, is defined by:

$$\mathcal{K}(r,t)=\sqrt{\pi}\int_0^\infty \Theta_\kappa(t)E(\kappa,t)\left[\frac{4}{3\sqrt{\pi}}-\left(\frac{2}{\kappa r}\right)^{\frac{3}{2}}J_{3/2}(\kappa r)\right]d\kappa, \quad (14)$$

where $J_{3/2}$ is the Bessel function of order 3/2, and κ denotes the wave number in the spectral domain.

The eddy diffusivity is determined by the turbulent kinetic energy spectrum function $E(\kappa, t)$. An appropriate EDQNM transport equation can also be constructed for this spectrum by a similar procedure as outlined above. In this work, however, it is assumed that the turbulence field is stationary; therefore, this spectrum is temporally invariant, $E=E(\kappa)$. Finally, the quantity $\Theta_\kappa(t)$, which provides a measure of the characteristic time for triad interactions, is modeled as:

$$\Theta_\kappa(t)=\frac{1-\exp(-[\mu''(\kappa)+\nu\kappa^2]t)}{\mu''(\kappa)+\nu\kappa^2}. \quad (15)$$

Here, ν is the kinematic viscosity, and the term $\mu''(\kappa)$ is the eddy relaxation frequency which is a measure of the straining effect of scales larger than κ^{-1} on mode $\underline{\kappa}$. This term is modeled as (Larcheveque and Lesieur, 1981):

$$\mu''(\kappa)=\lambda''\left[\int_0^\kappa p^2E(p)dp\right]^{\frac{1}{2}}, \quad (16)$$

where λ'' is a constant taken as 1.3 (Herring et al., 1982).

Model Implementation and Comparison with Laboratory Data

With a combination of these two models, the closure for the statistical variations of the scalar field is completed. The mapping closure provides an analytic expression for the decay rate of the unmixedness, and the EDQNM complements this relation with an estimate of the real-time evolution for the variance of the Shvab-Zeldovich variable. It is assumed that the evolution of the length scales of the Shvab-Zeldovich variable is not affected by the presence of the chemical reaction. This is a reasonable assumption in view of the recent findings of Jiang (1990) and Gao (1990). With this model, the evaluation of the statistical quantities, at least up to second-order statistics (including the unmixedness), is straightforward. However, the implementation of the EDQNM requires numerical integration. Here, the solution of Eq. 12 is obtained by the Crank-Nicolson finite difference scheme, and the numerical integration for the relaxation time and the eddy damping rate (the righthand side of Eqs. 14 and 16) is accomplished using the Clenshaw-Curtis numerical quadrature (Engels, 1980).

In comparing the results generated by this hybrid model to those of laboratory measurements, the information regarding the parameters describing the turbulent field is necessary. The values of these parameters depend on the particular turbulent flow under consideration and must be specified *a priori*. This requirement presents a difficulty when making detailed quantitative comparisons with experimental data, simply because of an apparent lack of extensive measurements in reacting turbulent flows. Therefore, it is necessary in our comparisons with the available data to make some assumptions with regard to some of these unknown parameters.

At the level of the formulation considered here, specific parameters that characterize the turbulence structure are: the kinetic energy spectrum of the turbulence, $E(\kappa)$; the initial shape of the scalar covariance, $\rho(r,0)$; the jet Reynolds number, Re_D; the molecular Schmidt number, Sc; the relative turbulence intensity, I; the integral length scales of both the velocity field, L; the scalar field, L_g; and the ratio of the Taylor microscale of the scalar field, λ_g, to that of the hydrodynamic field, λ. The magnitude of the hydrodynamic integral scale is coupled with the energy spectrum, and the initial size of the scalar integral scale is determined through the specification of the initial distribution of the scalar covariance. The value of the molecular Schmidt number depends on the reacting system under study, and magnitudes of the Taylor microscales are determined by means of isotropic turbulence scaling relations (Tennekes and Lumley, 1972; Brodkey, 1975). Along with these relations, all the other parameters must be specified *a priori*. The assumption of stationary flow precludes any time evolution of the energy spectrum of turbulence, but its spectral distribution must be prescribed. Here, the spectrum is assumed to have the form:

$$E(\kappa)=\begin{cases} C_1\kappa^4\exp\left[-2\left(\frac{\kappa}{\kappa_1}\right)^2\right] & \text{for } 0\le\kappa\le\kappa_1 \\ C_2\kappa^{-\gamma} & \text{for } \kappa_1\le\kappa\le\kappa_2 \\ 0 & \text{otherwise.}\end{cases} \quad (17)$$

The unknowns C_1, C_2, γ, κ_1, κ_2 are determined from the consistency conditions as described by Jiang (1990). The initial profile of the scalar covariance is assumed to have the distribution:

$$\rho(r,0)=\exp\left[-\left(\frac{r^2}{\lambda_g^2|_0}+C_3\frac{r^4}{\lambda_g^4|_0}\right)\right], \quad (18)$$

where $\lambda_g|_0$ is the initial scalar microscale and C_3 is a constant chosen to be 1.6.

The remaining parameters are specified with the aid of data provided by laboratory measurements. The data considered here are those of Ajmera et al. (1976) and reviewed by Toor (1975). These data are selected since they include information for both gaseous and aqueous reacting systems. Moreover, the reacting fields considered in these experiments are compatible with the assumptions made in our model: very fast reaction involving initially unpremixed, dilute stoichiometric reactants in a constant density, isothermal homogeneous turbulent flow. The plug reactor used in these experiments consisted of a mixing device followed by a reaction tube. The mixing device is a concentric tube in which the reactants are introduced separately in the inner and outer streams. The reacting fields considered are the gaseous nitric oxide and ozone ($Sc=0.73$), and the aqueous hydrochloric acid and sodium hydroxide ($Sc=700$). In both of these systems, reactant conversion data are available for cases with jet Reynolds numbers of 3,500, 6,700 and 12,000. There is no information provided on any

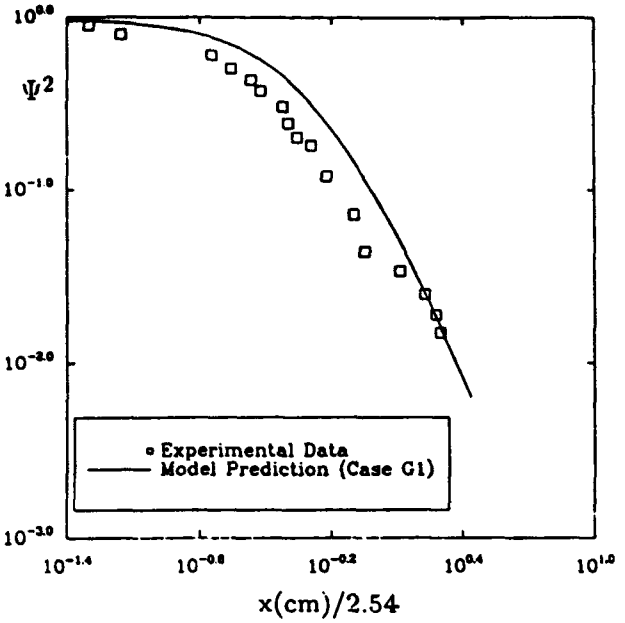

Figure 1. Reactant conversion distance in gaseous system for $Re = 3,500$.

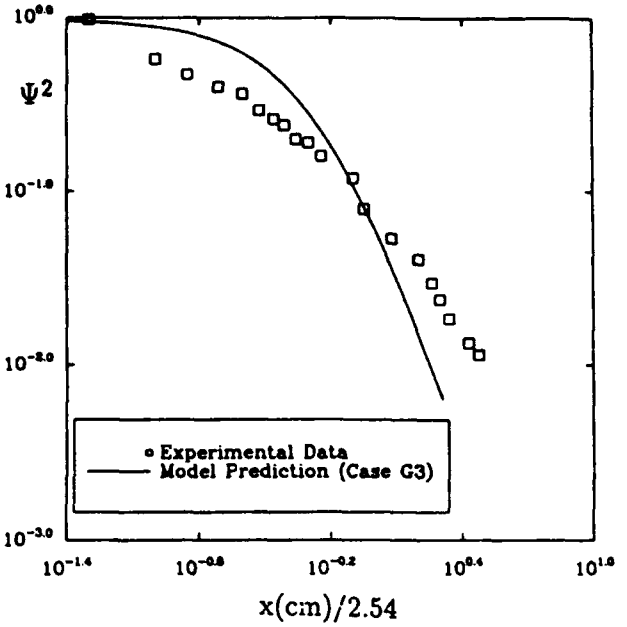

Figure 3. Reactant conversion distance in gaseous system for $Re = 12,000$.

turbulent length scales or the turbulent intensities in these experiments. For comparison, we assume that the reactor tube diameter, D, is representative of the integral scale of turbulence, L, considering a value for the turbulence intensity, I. (The ramifications of these assumptions will be examined later.)

The final results of our predictions are compared with experimental data in Figures 1-6. In these figures, the reactant conversion (Ψ^2)-distance curves for both gaseous and aqueous reactions are presented for all three Reynolds numbers. The relative turbulence intensity in these comparisons was selected as $I = 5\%$, since this value provided the best overall match with the data. This intensity level is perhaps somewhat lower than that of typical fully-developed, homogeneous turbulent flows. In most laboratory flows, however, the turbulence field is usually of decaying nature. Therefore, while at the initial stages of development the laboratory flow may have a higher turbulence intensity, the magnitude of this intensity decreases further downstream. In our stationary turbulence simulations, a constant turbulence level is a compromise and, in essence, represents an average of the corresponding data in laboratory

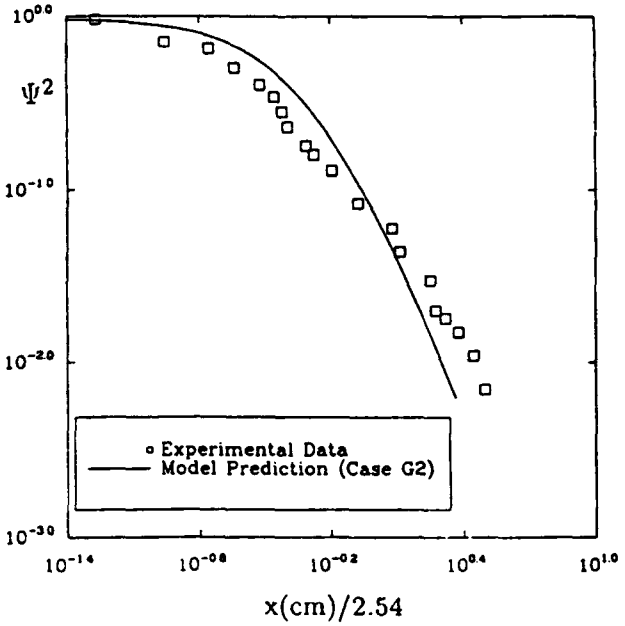

Figure 2. Reactant conversion distance in gaseous system for $Re = 6,700$.

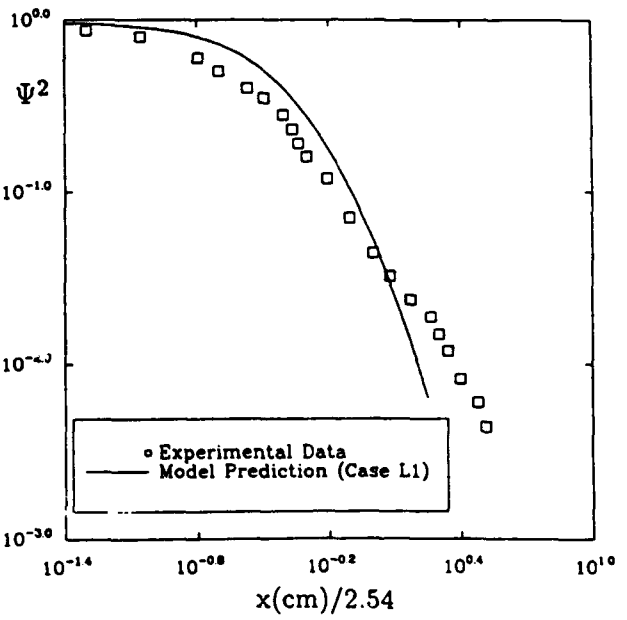

Figure 4. Reactant conversion distance in aqueous system for $Re = 3,500$.

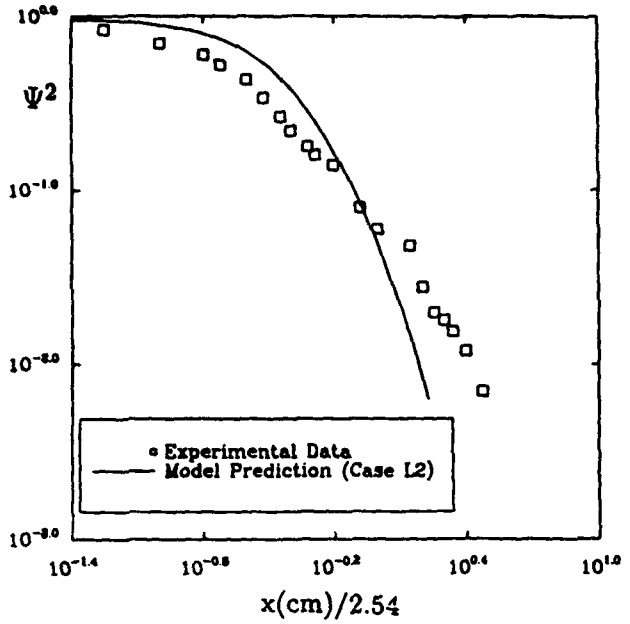

Figure 5. Reactant conversion distance in aqueous system for $Re = 6{,}700$.

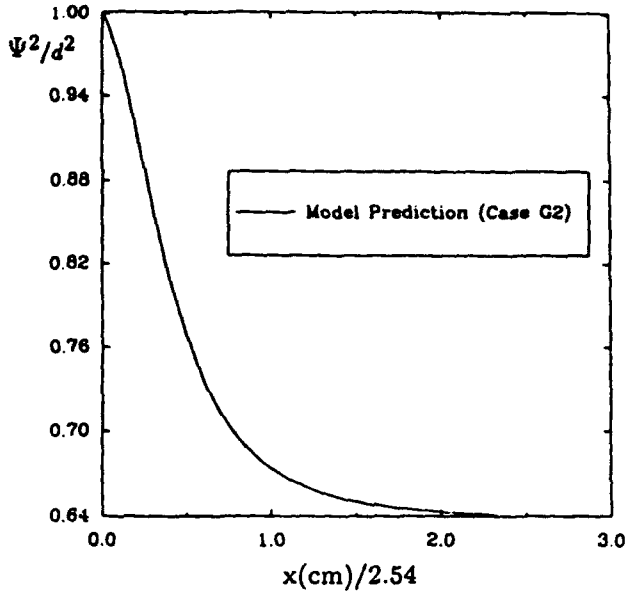

Figure 7. Ratio of reacting to nonreacting unmixedness in gaseous system for $Re = 6{,}700$.

experiments. The conditions in these figures are identified by the symbols $G1$, $G2$, $G3$, $L1$, $L2$, and $L3$, where the letters indicate the type of experiment (gas or liquid), and the numbers 1, 2 and 3 denote the corresponding Reynolds number (3,500, 6,700, and 12,000, respectively).

The trends observed in these figures generally exhibit good agreement between the model predictions and the experimental data for all the cases. In particular, our results indicate that as the magnitude of the Reynolds number and the Schmidt number increases, the decay of reactant conversion rate is slightly faster. These trends are consistent with the results of measurements by Toor (1975). In making these comparisons, however, two points should be made. First, the discrepancies at high Reynolds number may be attributed to experimental error as mentioned by Ajmera et al. (1976). Second, in all the experiments it is implied that the decay of the unmixedness is independent of the chemistry and thus is the same under both nonreacting and reacting conditions. Our results do not show this feature. To demonstrate this point, the unmixedness profile normalized by its value in the limit of no chemistry (mixing only), $[\Psi^2(Da \to \infty)]/[\Psi^2(Da = 0)]$, is presented for the case $G2$ in Figure 7. Note that the asymptotic value of this normalized variable approaches the constant value of $2/\pi$. This value is due to an asymptotic Gaussian distribution for the PDF of the random variable $\mathcal{J}$ and is consistent with that obtained in previous DNS results of Givi and McMurtry (1988) and discussed by Kosaly (1987). This limiting value is valid only if the reactants are completely segregated at the inlet of the reactor.

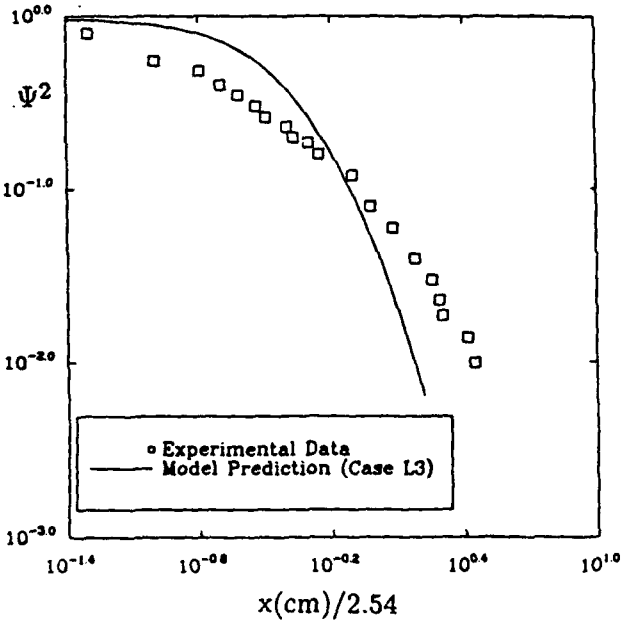

Figure 6. Reactant conversion distance in aqueous system for $Re = 12{,}000$.

Despite the good overall agreement between the model predictions and the experimental data, our simulations point to the need for more detailed laboratory measurements of the turbulence parameters. Since the initial turbulent integral length scale and the intensity were chosen to best reproduce the experimental data, it was deemed necessary to investigate the effects of these parameters. Therefore, a study was undertaken to determine the influences of the turbulent scale and the relative turbulent intensity on the conversion rate. For this study, the gaseous experiment with the jet Reynolds number of 6,700 was chosen.

The results of our model predictions indicate that both the integral length scale of turbulence and the turbulence intensity have a significant influence on the extent of reactant conversion. Figure 8 shows the effect of varying the turbulent integral scale (L). Three cases are considered: $L = D$, $L = D/2$, and $L = D/4$. These cases are identified by symbols $G2$, $G4$, and $G5$, respectively. The results show that generally, as the mag-

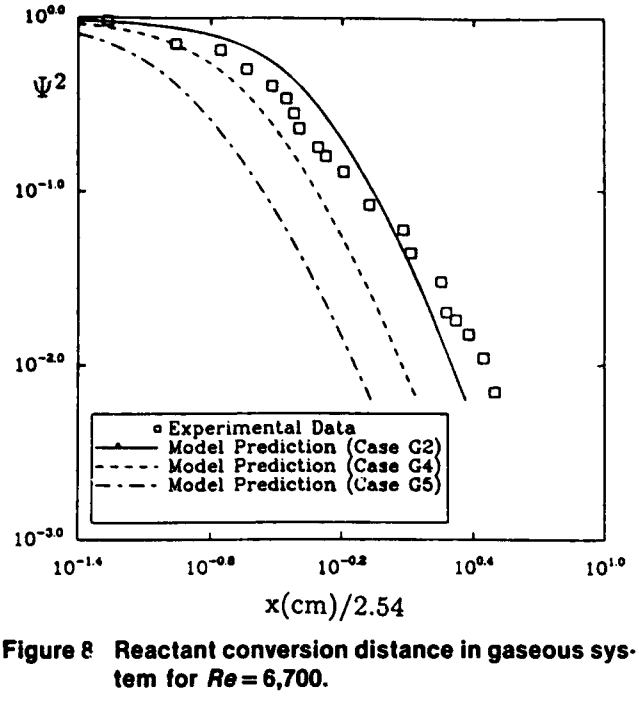

Figure 8 Reactant conversion distance in gaseous system for $Re = 6{,}700$.

nitude of the integral scale decreases, the reactant conversion occurs at a faster pace. The integral scale represents the characteristic length of the large-scale turbulent motion. For smaller L we expect smaller eddies on average and thus a faster eddy motion which in turn leads to enhanced diffusion and reaction. A somewhat analogous physical scenario is observed in the results generated by varying the magnitude of the relative turbulence intensity. This is shown in Figure 9, in which the model predictions are presented, along with the experimental data, for turbulence levels of $I = 5\%$, 10%, 15%, and 20%, identified respectively by symbols $G2$, $G6$, $G7$, and $G8$. This figure indicates that in general, the higher the level of turbulent fluctuations, the faster the decay of the unmixedness. This is also justified physically. Turbulence fluctuations serve to transport fluid blobs of one species into contact with fluid blobs of another species through eddy motion. Hence, by increasing the intensity of these fluctuations, the stirring mechanism generated by turbulence becomes more pronounced. This higher mixing results in a higher reaction, at least in an equilibrium flow, thereby resulting in a more rapid conversion rate.

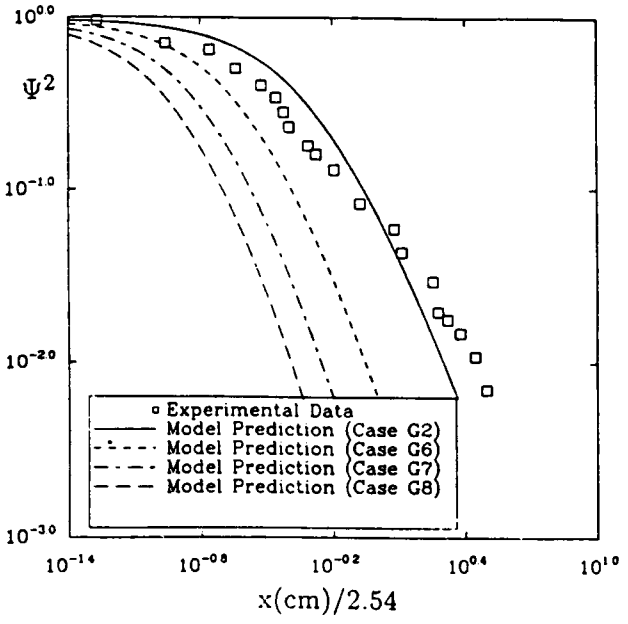

Figure 9. Reactant conversion distance in gaseous system for $Re = 6{,}700$.

The quantitative behavior presented in these figures indicates the dependence of the results on the turbulence parameters. In future experiments, it is recommended to provide a more quantitative measure of these or other relevant parameters that can be used in model validations.

Concluding Remarks

Development of the mapping closure for molecular mixing has had a significant impact on the statistical description of scalar quantities by PDF methods. In this work, we have employed this closure for predicting the limiting bound of the reactant conversion rate in a stationary isotropic turbulent flow. This has been realized for a simple chemistry of the type $A + B \rightarrow Products$ in an isothermal and constant density turbulent field. With the use of the mapping closure, the limiting bound of the conversion rate can be predicted by a simple analytic expression. This expression is very convenient due to its simplicity of utilization for modeling of plug-flow reactors (for excellent reviews on this issue, see Brodkey, 1975, 1981; Toor, 1975; and Hill, 1976). However, in the context of a single-point statistical description, the information pertaining to the evolution of the turbulent scales cannot be recovered by this expression and must be furnished by external means. To provide this information, we have implemented the EDQNM spectral closure for the physical evolution of the covariance of the relevant Shvab-Zeldovich variable characterizing the compositional structure of the reacting field.

The results predicted by the hybridized Mapping-EDQNM closure portray qualitative features similar to those of laboratory experiments and show trends in agreement with the results of previous DNS. However, in the absence of detailed experimental data, quantitative features can be matched only with laboratory data by making certain assumptions with respect to the initialization of the turbulence scales. The results of a parametric study reveal the importance of these scales for practical and realistic applications of the model.

The good overall agreement with experimental data is encouraging. This agreement is particularly noteworthy since the model employed to generate the data is rather simple and is very easy to implement computationally. Most of the computational efforts are those associated with the numerical solution of the EDQNM closure. In a laboratory experiment, these calculations can simply be replaced with the measurements of the decay of the covariance of a conserved scalar. With such measurements, our closed form algebraic relation can then be used for an efficient and reasonably effective estimate of the limiting bound of the conversion rate.

There are many ways by which the model can be improved. It would be desired to extend the hybrid methodology for less restrictive and more physically complex reacting flow systems;

for example, nonequilibrium, exothermic chemistry in variable density, decaying turbulent fields. In such circumstances, the extension of the mapping closure is straightforward since this closure is based on the PDF of the scalar quantities and can account for the effects of complex chemistry. However, the results may not be presentable by simple analytical relations as derived here and would require numerical solution of the mapping function (Valiño and Gao, 1991). Also, the development of EDQNM for compressible turbulence is somewhat more involved, but has been recently initiated (Marion et al., 1989). These new developments can be utilized in capturing the effects of compressibility in reacting turbulence phenomenon.

In future application, the assumption of spatial isotropy may be relaxed. The EDQNM model can be used in homogeneous (but nonisotropic) flows. Also it is possible to implement the model for a decaying turbulence field. In fact, this model was originally developed for the hydrodynamic closure before its application for transport of scalar quantities (Lesieur, 1991). Therefore, the assumption of stationary turbulence imposed in these simulations can be relaxed. In the present work, this was not deemed necessary due to the accuracy range of the experimental data. Finally, the extension of the mapping closure to account directly for the length scale information can be accomplished by an appropriate mapping procedure for the joint PDF of the scalar(s) and its (their) gradient(s). However, such a mapping is very complicated and still requires certain external information for a complete closure (Chen et al., 1989; Pope, 1991). Some issues regarding the shortcomings of the single-point mapping closure in predicting the statistics of the gradient field are discussed by Gao (1991b) and Jiang et al. (1992).

In comparison with currently available alternatives, our model seems very attractive, even with the imposition of several restricting assumptions. This is primarily due to a firm mathematical-physical basis of the model and the simplicity of the final results. As such, the procedure is plausible in both basic research on the physics of reacting turbulent transport and practical applications in the modeling and design of plug-flow reactors. Current work by Kraichnan on further extension of the mapping closure and identification of its capabilities and drawbacks would be very useful in the future work in this direction.

Acknowledgment

This work is supported by the National Science Foundation under Grant CTS-9012832, and by the Office of Naval Research under Grant N00014-90-J-4013. Acknowledgment is also made to the Donors of the Petroleum Research Funds administrated by the American Chemical Society for partial support of the authors under Grant ACS-PRF#25129-AC7E,6. Computational support is provided by NCSA at the University of Illinois.

Notation

A,B = reactants concentration
a,b = fluctuating components of reactant concentrations
C_1,C_2,C_λ = constants
D = reactor tube diameter
$\mathcal{D}$ = molecular diffusivity of species
Da = Damkohler number
E = turbulent energy spectrum function
H = Heaviside function
I = relative turbulence intensity
$\mathcal{J}$ = Shvab-Zeldovich conserved scalar variable
$J_{3/2}$ = Bessel function of 3/2 order
$\mathcal{K}$ = turbulent eddy diffusivity
L = hydrodynamic integral scale
$L_\mathcal{J}$ = scalar integral scale
$\mathcal{P}$ = PDF
Re = Reynolds number
r = physical radial coordinate
Sc = molecular Schmidt number
t = physical time
x = spatial coordinate (downstream distance from the reactor inlet)

Greek letters

γ = constant in EDQNM closure
δ = delta function
η = composition space for a Gaussian reference field
Θ = triad interaction time
κ = wave number in spectral domain
λ = Taylor microscale for the hydrodynamic field
$\lambda_\mathcal{J}$ = Taylor microscale for the Shvab-Zeldovich variable
λ^* = constant in EDQNM closure
μ^* = eddy relaxation frequency
ν = kinematic viscosity
ρ = scalar covariance
Σ = parameter in mapping closure
χ = mapping function
Ψ^2 = unmixedness parameter
ψ = composition domain

Subscripts

0 = time zero (inlet of plug-flow reactor)
G = Gaussian

Other symbols

$\langle\ \rangle$ = ensemble average
$\tilde{\ }$ = normalized value

Literature Cited

Ajmera, P. V., M. Singh, and H. L. Toor, "Reactive Mixing in Turbulent Gases," *Chem. Eng. Commun.*, **2**, 115 (1976).

Bilger, R. W., "Turbulent Flows with Nonpremixed Reactants," *Turbulent Reacting Flows*, P. A. Libby and F. A. Williams, eds., Chap. 3, Vol. 44, Topics in Applied Physics, Springer-Verlag Berlin, Heidelberg (1980).

Brodkey, R. S., ed., "Mixing in Turbulent Fields," *Turbulence in Mixing Operations*, Academic Press, New York (1975).

Brodkey, R. S., "Fundamentals of Turbulent Motion, Mixing and Kinetics," *Chem. Eng. Commun.*, **8**, 1 (1981).

Chen, H., S. Chen, and R. H. Kraichnan, "Probability Distribution of a Stochastically Advected Scalar Field," *Phys. Rev. Lett.*, **53**, 2657 (1989).

Engels, H., *Numerical Quadrature and Cubature*, Academic Press, New York (1980).

Eswaran, V., and E. E. O'Brien, "Simulations of Scalar Mixing in Grid Turbulence Using an Eddy-Damped Closure Model," *Phys. Fluids A*, **1**(3), 537 (1989).

Eswaran, V., and S. B. Pope, "Direct Numerical Simulations of the Turbulent Mixing of a Passive Scalar," *Phys. Fluids A*, **31**, 506 (1988).

Gao, F., "Theoretical and Numerical Investigations of Scalar Fields in Isotropic Turbulence," PhD Thesis, State University of New York at Stony Brook (1990).

Gao, F., "An Analytical Solution for the Scalar Probability Density Function in Homogeneous Turbulence," *Phys. Fluids A*, **3**(4), 511 (1991a).

Gao, F., "Mapping Closure and Non-Gaussianity of the Scalar Prob-

ability Density Functions in Isotropic Turbulence," *Phys. Fluids A*, 3(10) (1991b).
Givi, P., "Model Free Simulations of Turbulent Reactive Flows," *Prog. Energy Combust. Sci.*, 15(1), 1 (1989).
Givi, P., and McMurtry, P. A., "Nonpremixed Reaction in Homogeneous Turbulence: Direct Numerical Simulations," *AIChE J.*, 34(6), 1039 (1988).
Hawthorne, W. R., D. S. Wedell, and H. C. Hottel, "Mixing and Combustion in Turbulent Gas Jets," *Symp. on Combustion, Flames and Explosion Phenomena*, p. 266, Combustion Inst., Pittsburgh (1949).
Herring, J. R., D. Schertzer, M. Lesieur, G. R. Newman, J. P. Chollet, and M. Larcheveque, "A Comparative Assessment of Spectral Closures as Applied to Passive Scalar Diffusion," *J. Fluid Mech.*, **124**, 411 (1982).
Hill, J. C., "Homogeneous Turbulent Mixing with Chemical Reaction," *Ann. Rev. Fluid Mech.*, **8**, 135 (1976).
Janicka J., W. Kolbe, and W. Kollmann, "Closure of the Transport Equation for the Probability Density Function of Turbulent Scalar Fields," *J. Non-Equilib. Thermodyn.*, **4**, 47 (1979).
Jiang, T.-L., "Turbulent Mixing in Nonreacting and Reacting Flows: a PDF Approach at the Two-Point Level," PhD Thesis, State University of New York at Stony Brook (1990).
Jiang, T.-L., F. Gao, and P. Givi, "Binary and Trinary Scalar Mixing by Fickian Diffusion—Some Mapping Closure Results," *Phys. Fluids A.*, in press (1992).
Kollmann, W., "The PDF Approach to Turbulent Flow," *Theoret. Comput. Fluid Dynamics*, **1**, 249 (1990).
Kosaly, G., "Nonpremixed Simple Reaction in Homogeneous Turbulence," *AIChE J.*, 33(12), 1998 (1987).
Kosaly, G., and P. Givi, "Modeling of Turbulent Molecular Mixing," *Combust. Flame*, **70**, 101 (1987).
Larcheveque, M., and M. Lesieur, "The Application of Eddy-Damped Markovian Closures to the Problem of Dispersion of Particle Pairs," *J. Mech.*, **20**, 113 (1981).
Launder, B. E., and D. B. Spalding, *Lectures in Mathematical Models of Turbulence*, Academic Press, New York (1972).
Lesieur, M., *Turbulence in Fluids*, Nijhoff, Dordrecht (1990).
McMurtry, P. A., and P. Givi, "Direct Numerical Simulations of Mixing and Reaction in a Nonpremixed Homogeneous Turbulent Flow," *Combust. Flame*, **77**, 171 (1989).
Madnia, C. K., S. H. Frankel, and P. Givi, "Mathematical Modeling of the Reactant Conversion Rate by Single-Point PDF Methods," *Proc. of Combustion Inst.*, Ithaca, NY (1991).
Marion, J. D., J. P. Bertoglio, and J. Mathieu, "An Eddy Damped Quasi Normal Markovian Approach to Compressible Isotropic and Homogeneous Turbulence," *Advances in Turbulence 2*, H. H. Fernholz and H. E. Fielder, eds., Springer-Verlag Berlin, Heidelberg (1989).
Millionshtchikov, M., "On the Theory of Homogeneous Isotropic Turbulence," *C. R. Acad. Sci. U.R.S.S.*, **32**, 615 (1941).
Miyawaki, O., H. Tsujikawa, and Y. Uraguchi, "Turbulent Mixing in Multi-Nozzle Injector Tubular Mixer," *J. Chem. Eng. Japan*, **7**, 52 (1974).
Norris, A. T., and S. B. Pope, "Turbulent Mixing Model Based on Ordered Pairing," *Combust. Flame*, **27**, 83 (1991).
O'Brien, E. E., "Turbulent Reacting Flows," *Topics in Applied Physics*, P. A. Libby and F. A. Williams, eds., Chap. 5, Vol. 44, Springer-Verlag Berlin, Heidelberg (1980).
Orszag, S. A., "Statistical Theory of Turbulence," *Fluid Dynamics*, R. Balian and J. L. Peabe, eds., Gordon and Breach, New York (1977).
Pope, S. B., "The Statistical Theory of Turbulent Flames," *Phil. Trans. R Soc. Lond.*, **291**, 529 (1979).
Pope, S. B., "PDF Methods for Turbulent Reacting Flows," *Prog. Energy Combust. Sci.*, **11**, 119 (1985).
Pope, S. B, "An Improved Turbulent Mixing Model," *Combust. Sci. Tech.*, **28**, 131 (1982).
Pope, S. B., "Computations of Turbulent Combustion: Progress and Challenges," *Proc. of Int. Symp. on Combustion*, The Combustion Institute, Pittsburgh, p. 591 (1990).
Pope, S. B., "Mapping Closures for Turbulent Mixing and Reaction," *Theoret. Comput. Fluid Dynamics*, **2**, 255 (1991).
Tavoularis, S., and S. Corrsin, "Experiments in Nearly Homogeneous Turbulent Shear Flow With a Uniform Mean Temperature Gradient," *J. Fluid Mech.*, **104**, 311 (1981).
Tennekes, H., and J. L. Lumley, *A First Course in Turbulence*, MIT Press, Cambridge, MA (1972).
Toor, H. L., "Mass Transfer in Dilute Turbulent and Nonturbulent Systems with Rapid Irreversible Reactions and Equal Diffusivities," *AIChE J.*, **8**(1), 70 (1962).
Toor, H. L., "The Nonpremixed Reaction: $A + B \rightarrow$ *Products*," *Turbulence in Mixing Operations*, R. S. Brodkey, ed., Academic Press, New York (1975).
Valiño, L., and F. Gao, "Monte Carlo Implementation of the Mapping Closure for Turbulent Reacting Flows," Amer. Phys. Soc., Phoenix, AZ (Nov. 1991).

Manuscript received Aug. 26, 1991, and revision received Feb. 7, 1992.

APPENDIX 6

Structure of a Turbulent Reacting Mixing Layer

Revised manuscript submitted for publication in *Combustion Science and Technology.*

Structure of a Turbulent Reacting Mixing Layer

by

R.S. Miller, C.K. Madnia, and P. Givi
Department of Mechanical and Aerospace Engineering
State University of New York at Buffalo
Buffalo, NY 14260-4400

(October 1993)

All the correspondence should be addressed to Peyman Givi, Tel: 716-645-2433, Fax: 716-645-3875, E-mail: givi@eng.buffalo.edu.

Structure of a Turbulent Reacting Mixing Layer

R.S. Miller, C.K. Madnia, and P. Givi
Department of Mechanical and Aerospace Engineering
State University of New York at Buffalo
Buffalo, NY 14260-4400

Abstract

Results are presented of direct numerical simulations (DNS) of an unsteady, three-dimensional, temporally developing, compressible mixing layer under both non-reacting and reacting non-premixed conditions. In the reacting case, a simple chemistry model of the type $A + rB \rightarrow (1 + r)$Products is considered. Based on simulated results, it is shown that at sufficiently large Reynolds numbers the global and statistical features of mixing transition are similar to those observed experimentally. At sufficiently large Mach numbers, it is shown that eddy shocklets do indeed exist in three-dimensional (3D) flow. However, the strength of these shocks is less than that in two-dimensional (2D) layers of the same compressibility level. Aided by the analysis of the DNS data, the extent of validity of the "Steady Laminar Diffusion Flamelet Model" (SLDFM) and the "Conditional Moment Method" (CMM) are assessed. In the evaluation of the SLDFM, DNS results for different stoichiometric coefficients and reaction types are analyzed. It is shown that DNS results compare well with model predictions as the magnitude of the Damköhler number is increased. The agreement is improved as the value of r is increased and also as the effects of exothermicity become more pronounced. In the assessment of the CMM, it is shown that the conditional reaction rate can be reasonably approximated in terms of the conditional averages of the scalar variables. Also, the cross-stream variation of the conditional scalar mean values is negligible. However, this is not the case for the variation of higher order moments of the scalar variables.

1 Introduction

In a recent article Givi *et al.* (1991) reported the results of Direct Numerical Simulations (DNS) of a two-dimensional (2D) temporally developing, compressible reacting mixing layer. The main purpose of these simulations was to assess the effects of compressibility and chemical heat release on the extent of mixing and chemical reaction and to understand their influence on statistical characteristics of the reacting layer. The main conclusions drawn from

this work are: (1) both compressibility and exothermicity result in reduced mixing within the layer, and (2) at sufficiently large Mach numbers, the layer is dominated with "eddy shocklets". The results of this work and those of previous investigations (see Givi and Riley (1992); Drummond and Givi (1993) for reviews) are useful in view of current needs for understanding the fundamentals of compressible turbulent reacting flows (Libby and Williams, 1993). In fact, within the past decade, DNS have proven very valuable in providing a means of investigating the intricate physics of such flows. Some recent examples are the contributions by McMurtry *et al.* (1986); McMurtry *et al.* (1989); Sekar and Mukunda (1990); Grinstein and Kailasanath (1991); Grinstein and Kailasanath (1992); Steinberger (1992). Most of these efforts have been primarily focused on the analysis of 2D and/or weakly 3D flows. This is understandably due to severe computational requirements associated with complex 3D simulations (Givi, 1989; Reynolds, 1990). However, with larger availability of supercomputer resources it is now possible to consider more realistic flows with the hope of gaining new insights into the fundamentals of turbulent combustion.

Our intention in this work is to make further progress in extracting physical information from DNS results to portray the structure of turbulent reacting mixing layers. These simulations are primarily intended for the purpose of understanding the complex nature of 3D turbulent combustion. Our particular interest is to focus on the following specific issues: (1) mixing characteristics in pre- and post- transitional regions of the layer, (2) manifestation of eddy shocklets, and (3) flame structure under non-equilibrium conditions in a turbulent environment. In regard to the first issue, DNS of transitional mixing layers have been recently reported by Moser and Rogers (1991); Moser and Rogers (1992). Therefore, it is proposed to make use of the findings in this work for investigating the phenomena of mixing in 3D layers. Pertaining to the second issue, previous DNS results of 2D compressible shear flows have indicated the formation of eddy shocklets (Givi *et al.*, 1991; Menon and Fernando, 1990; Sekar and Mukunda, 1990; Lele, 1989). However, such shocklets have not been captured in any previous 3D simulations of parallel mixing layers. Finally, in regard to the third issue, assessments of closures based on both the steady laminar diffusion flamelet model (SLDFM) (Peters, 1984; Peters, 1986) and the conditional moment methods (CMM) (Bilger, 1993), have not been made in the setting of 3D reacting mixing layers.

Due to the nature of the problems considered, most of the simulations presented here are necessarily of 3D flows. However, some 2D simulations are also performed for the purpose of comparison. External forcing is imposed to expedite the formation of large scale structures.

However, due to obvious limitations of DNS (Givi, 1989; Reynolds, 1990; Oran and Boris, 1991), several simplifying assumptions are imposed. The nature of these assumptions is indicated in the discussions which follow.

2 Description of the Problem

The flow configuration considered is that of a 3D, temporally developing mixing layer similar to that of previous temporal simulations (Riley *et al.*, 1986; McMurtry *et al.*, 1989) (Fig. 1). The geometry is defined by the cartesian coordinates x (streamwise), y (cross-stream), and z (spanwise). The flow field is initialized with a mean hyperbolic tangent velocity distribution with a specified initial vorticity thickness $(\delta_\omega|_0)$[1]. The free stream velocity of the top stream is denoted by U_∞, and of the bottom stream by $-U_\infty$. For simulations involving chemical reaction, an irreversible second-order reaction of the type $A + rB \rightarrow (1 + r)$Products is considered. Reactant A is introduced in the top stream and reactant B in the bottom stream. Both finite rate (non-equilibrium) and infinitely fast (equilibrium) chemical reactions are considered. In the former, the mass fractions of the species denoted by Y_i, $i = A, B, P$ are the primary chemical parameters. In the latter, the normalized mixture fraction J is of fundamental importance (Williams, 1985). This mixture fraction is defined in such a way as to yield the limiting values of 0 and 1 in the streams carrying species B and A, respectively.

The compressible form of the Navier-Stokes equations, the energy conservation and the species conservation equations are considered with Fourier heat conduction and Fickian diffusion assumptions. No turbulence or subgrid models are employed. All of the species are assumed to have identical thermodynamic properties and are assumed to be calorically perfect. The fluid viscosity, the thermal conductivity, and the mass diffusion coefficients are assumed constant along with the assumption of unity Prandtl and Schmidt numbers. The ramifications of these assumptions are not considered - being postponed for future investigations. The assumption of a temporally developing flow does not modify any of the conclusions to be drawn in regard to the issues considered.

The DNS procedure is based on an explicit time marching procedure by means of a monotone Flux Corrected Transport (FCT) algorithm (Boris and Book, 1976; Oran and Boris, 1987). This scheme is second order accurate in time, fourth order phase accurate in space and has

[1] All variables are listed in the nomenclature

been shown to be reliable for capturing steep gradients (Oran and Boris, 1987). The size of the computational domain and the magnitudes of the physical parameters that can be simulated reliably are dictated by computational resources. In order to accommodate the full growth and development of the Kelvin Helmholtz instability, the size of the domain is prescribed as $L_x = L_y \approx 7n\delta_\omega|_0$, where n is the number of large scale vortices to be formed in the initial rollup. The length of the domain in the spanwise direction is $L_z \approx 0.6L_x$. The original version of the computer code use here was developed by Miller (1993).

The mass fractions of the two reactants are set equal to unity in their respective origins. This implies an initially non-premixed, two-feed configuration. The initial temperature, density, and pressure fields are uniform across the layer. The initial temperature is set at $300K$ and the density is set equal to $1kg/m^3$. The chemical reaction between the two species is taken to be second order, irreversible with the kinetics mechanisms modeled either as (1) constant rate or (2) Arrhenius. In the former, the reaction rate parameter K_F is constant. In the latter, K_F is a temperature dependent function of the form: $K_F = A_F \exp(-\frac{ZeT_\infty}{T})$. In this case, the free stream temperature is used for evaluating the magnitude of the Damköhler number (Da). With this convention, the reaction rate for the concentration is expressed by $\omega_i = K_F MW_i C_A C_B$. Combustion exothermicity is measured by the energy liberated per unit mass by the chemical reaction, $-\Delta H^0$. The magnitude of this energy release is parameterized by a non-dimensional heat release parameter Ce.

External forcing is imposed at the most unstable mode and the first sub-harmonic of the hyperbolic tangent velocity profile. These modes are calculated from the linear temporal inviscid stability analysis of a non-reacting incompressible flow (Michalke, 1964). These perturbations are imposed to expedite the formation of vortical structures and the subsequent interactions amongst the vortices. This is acceptable in view of the fact that stability characteristics of the reacting layer (Jackson, 1992) are not the subject of this investigation. Rather, it is the subsequent development of the flow which is of interest. The disturbance amplitude is $\approx$ 10% of the mean flow. In order to simulate three dimensionality, the 2D disturbances are multiplied by a function of the form $f(z)cos(\pi z/\lambda_z)$. A choice of $f(z) = 1 - \frac{2|z|}{\pi}$ is found to provide sufficient 3D effects within a normalized spanwise coordinate $-\pi/2 \leq z \leq \pi/2$. The forcing wavelength of the spanwise disturbance is $\lambda_z \approx 0.6\lambda_x$ (Moser and Rogers, 1992; Pierrehumbert and Widnall, 1982).

3 Presentation of Results

The resolution in each simulation depends on the magnitudes of the physical parameters and on the size of the computational domain. In 3D simulations, as many as $150 \times 150 \times 90$ grid points are employed. All 2D simulations are performed in a domain with 256×256 grids. In all cases, the grids are compressed by a factor approximately equal to 3 in the vicinity of the $x - z$ centerplane. This produces a finer resolution at the center of the layer where the majority of mixing and chemical reaction occur.

3.1 Flow Structure and Mixing Transition

An important feature of laboratory mixing layers is the phenomenon of mixing transition. In previous experimental investigations it has been observed that at sufficiently large Reynolds numbers the onset of transition results in a marked influence on mixing characteristics (Koochesfahani and Dimotakis, 1986; Masutani and Bowman, 1986; Dimotakis, 1991). Namely, mixing and chemical reactions are significantly enhanced in the post-transitional region. In most previous DNS studies of spatially developing flows, this feature could not be captured due to resolution constraints (Givi, 1989). That is, while many features of 3D transport are elucidated, the effects of mixing transition similar to those of laboratory layers could not be reproduced. In order to capture the transition process, the procedure suggested by Moser and Rogers (1992) is followed. The Reynolds number is set to $Re = 250$, and the streamwise size of the box (L_x) is selected in such a way that both single- and double-pairings of large scale vortical structures are accommodated. These simulations are of a reacting layer, both with and without the influence of chemical heat release. Consistent with laboratory experiments, only low compressibility mixing layers are considered. The convective Mach number in these simulations is kept fixed at $M_c = 0.2$.

For the purpose of flow visualization, in Fig. 2 results are presented of surfaces of constant vorticity magnitude in a single pairing simulation. The foreground cross section cut shows contours of vorticity magnitude. This figure shows the pairing of two neighboring large scale vortical structures and provides a qualitative description of the internal activity of the pairing vortices. The observance of new small scale structures within the layer is one indication that the mixing transition process has been initiated. These small scales have vorticity of both the same and opposite signs as their parent structures. In a reacting layer,

the effect of small scales is to stretch and distort the flame surface within the roller. Figure 3 shows a plot of the mixture fraction contours during the pairing process in both a spanwise and a streamwise plane. In the limit of infinitely fast chemistry, the surface of the flame is identified by the contour ($J = 0.5$). This line is cross hatched for clarity. The warping of the flame surface by the small scales provides a graphical indication of the initiation of mixing transition. However, in this flow with just one single pairing the layer becomes saturated with the completion of the pairing and the transition process is not completed.

Simulations with a larger effective box size accommodate multiple pairing of vortical structures. Multiple pairing allows for the continued growth of the layer and for the culmination of the mixing transition process. Figure 4 shows contours of the vorticity magnitude along a spanwise plane of the layer during the second pairing. The layer is now in a state that can be justifiably labeled as "turbulent". The small scale eddies cover an almost uniformly thick layer across the domain, and large scale structures lie embedded within the turbulence and are increasingly difficult to distinguish. The qualitative features shown in this figure are similar to those observed experimentally in the post-transitional region of laboratory mixing layers (Koochesfahani and Dimotakis, 1986). The spanwise distribution of the mixture fraction located in the braid planes (Fig. 5) is also in accord with experimental observations (Bernal and Roshko, 1986) and previous DNS results (Metcalfe *et al.*, 1987). It is noted that turbulence and background fluctuations destroy the initial symmetry of the layer.

In order to provide a quantitative means of illustrating mixing transition, the statistical behavior of the mixture fraction is considered. Similar to the procedure followed by Koochesfahani and Dimotakis (1986); Masutani and Bowman (1986), the Probability Density Function (PDF) of the mixture fraction at several stages of the layer's development is considered. These PDF's are shown in Fig. 6 illustrating the cross stream variations of the PDF in the pre-, mid-, and post-transitional regions. The pre-transitional PDF (Fig. 6(a)) is characterized by two prominent approximate delta functions located at $J = 0, 1$, *i.e.* unmixed fluids. On the other end of the spectrum in Figure 6(c), the PDF's indicate significantly enhanced mixing. This is manifested by a large peak of the PDF at the mixed fluid concentration (*i.e.* $J = 0.5$). The probability of finding pure reactants in the center of the layer is approximately zero. In accord with experimental measurements (*e.g.* Koochesfahani and Dimotakis (1986); Masutani and Bowman (1986)), the shape of the PDF is approximately similar across the layer. The PDF's during the mixing transition (Fig. 6(b)) show somewhat different characteristics than those in either the pre- or post-transitional regions. In this case, there is a

relatively large probability of finding both unmixed and mixed fluids throughout the layer. This is due to rapid engulfment of the free stream fluids by the pairing of vortical structures. However, the highest probability at the center of the layer corresponds to that of pure mixed fluid. In Fig. 7 the three regions of transition are portrayed in terms of the cross-stream variation of the probability of finding either pure unmixed fluids ($J = 0, 1$), or completely mixed fluid ($J = 0.5$). In the pre-transition regime (Fig. 7(a)) the flow field is characterized by a very low probability of finding fully mixed fluid. Once the transition has commenced (Fig. 7(b)) a greater amount of mixed fluid is formed and unmixed fluids are found throughout the entire layer. Finally, in the post transition region (Fig. 7(c)) the mixed fluid is dominant and fairly evenly dispersed throughout the shear zone. Pure unmixed reactants can only be found on their respective sides of the layer and the probability curves adopt a concave upward shape.

Another perspective by which the effects of mixing transition can be viewed is through the evolution of pertinent statistical properties. Presented in Fig. 8 is the time evolution of the product thickness, the vorticity thickness, and the ratio of the two. The product thickness is calculated from the normalized total mass of product in the limit of infinitely fast chemistry, and the ratio is referred to as the cross-stream product density (CSPD). The vorticity thickness shows a sharp increase at the onset of the first pairing ($t^* \approx 0.5$), and also at the onset of the second pairing ($t^* \approx 1.5$). As transition proceeds, the effects of large vortical structures become increasingly masked by those of the small scales. This manifests itself in both the vorticity thickness and the product thickness becoming increasingly linear in time. The slope of the CSPD is initially non-zero due to the external forcing. A relatively sharp rise during the first pairing ($t^* \approx 0.8$) indicates the onset of mixing transition. By the time the second pairing occurs the CSPD has reached a plateau and does not change as the growth of both product and vorticity thicknesses remain linear. This plateau indicates the culmination of mixing transition. This feature is further quantified by examining the time development of the amount of pure mixed fluid within the central shear zone of the layer. This is depicted in Fig. 9, presenting the probability of finding pure mixed fluid, conditioned on $-1 \leq y^* \leq 1$. This figure exhibits the same type of plateau as that in Fig. 8. Based on these two figures, it can then be concluded that mixing transition is initiated at $t^* \approx 0.8$ and is completed by $t^* \approx 1.4$.

In Fig. 10 turbulence intensities are compared for pre- and post-transitional flow fields. Figure 10(a) presents the root mean square (rms) values for the streamwise velocity. The

post-transitional field displays larger rms values than does the pre-transitional region. An opposite trend is observed for the mixture fraction rms values (Fig. 10(b)). Increased mixing due to turbulence results in a reduction in the magnitude of the scalar fluctuations. Note that the post-transition profile is characterized by two maxima, in agreement with incompressible flow studies (Fiedler, 1974). This is in contrast to the pre-transition profile which has its maxima located at the center of the layer.

Chemical exothermicity typically delays the transition process. This feature has been well recognized from linear stability analysis of heat releasing parallel mixing layers (*e.g.* Jackson and Grosch (1989); Jackson and Grosch (1990); Shin and Ferziger (1992); Colucci (1993), see Jackson (1992) for an excellent recent review), and is also verified in the present simulations. Presented in Fig. 11 is the temporal variation of the vorticity thickness of a single pairing layer for two different heat release rates, $Ce = 0$ and $Ce = 0.2$. This figure shows that the major influence of exothermicity is to decrease the growth of the layer and to delay the pairing process. There is an exception for early times at which thermal expansion caused by heat release results in a slight thickening of the layer. This feature is also corroborated by the results of Fig. 12 indicating a reduction in kinetic energy of turbulence at elevated heat release. It has become generally accepted that the effect of heat release is to decrease the amount of product formation in reacting shear flows (Hermanson and Dimotakis, 1989; McMurtry *et al.*, 1989; Givi *et al.*, 1991; Givi and Riley, 1992; Riley and McMurtry, 1989; Steinberger, 1992). However, this has been established for constant rate kinetics chemistry and is not necessarily the case for temperature dependent kinetics. To illustrate this point, Fig. 13 is presented showing the temporal evolution of the product thickness. In Fig. 13(a), the temporal evolution of δ_p is shown for the case of constant rate kinetics. Clearly, the effect of heat release is to reduce the mass of product formed. This is consistent with previous findings of McMurtry *et al.* (1989); Givi *et al.* (1991). Figure 13(b) presents results for an Arrhenius kinetics model. The trends observed in this figure are opposite to those in constant rate simulations. This comparison suggests that the effect of reduced layer growth is overcome by the increase in reaction rate due to temperature increase in Arrhenius simulations.

3.2 Eddy Shocklets

Previous simulations of 2D shear flows have demonstrated the influence of compressibility on mixing characteristics of shear flows (*e.g.* Givi *et al.* (1991); Menon and Fernando (1990); Sekar and Mukunda (1990); Lele (1989); Sandham and Reynolds (1989); Mukunda *et al.* (1992)). These simulations indicate that increased compressibility results in a reduced growth of the layer and also results in the formation of "eddy shocklets." However, in no previous simulations of 3D mixing layers have these eddy shocklets been observed (Menon and Fernando, 1990; Sandham and Reynolds, 1989). Our present results suggest that the lack of shocklet formation in previous simulations is perhaps due to the range of low compressibility levels considered. This may possibly be attributed to the numerical difficulties involved with high convective Mach number 3D simulations. To demonstrate this, 2D and 3D simulations are conducted with $Re = 350$ and with the convective Mach number in the range $0.7 \leq M_c \leq 2.5$. In order to meet the resolution requirements, only simulations with an initialization appropriate for a single rollup are conducted. In 2D simulations, eddy shocklets are formed for $M_c \geq 0.8$ consistent with previous simulations (Givi *et al.*, 1991). In 3D, simulation results indicate, for the first time, that eddy shocklets do indeed form. However, they are formed at a higher convective Mach number as compared to those in a 2D flow. Here, shocklets are observed for $M_c \approx 1.25$ and larger. As is the case for 2D, shocklets form in the regions above and below the central region of the layer and penetrate into the free streams on each side. To demonstrate this, shown in Fig. 14 are plots of the Mach number contour obtained by 3D simulation at $M_c = 2.5$. The contour plots correspond to the center plane in the spanwise direction. The shocklets are marked by the regions of sharp gradients. Examination of the contours of the streamwise component of vorticity shows strong vorticity braids, indicating the 3D nature of the flow. Figure 15 helps to assess the compressive nature of the shocklets through examination of the divergence of the velocity field. The strong compression regions of the shocklets do not penetrate very far into the actual mixing layer. The strongest compression occurs outside of the layer. For a detailed discussion on the reasoning for the formation of shocklets at this region, we refer to Givi *et al.* (1991).

To establish whether the regions of steep gradient in these simulations do indeed constitute a shock, the pressure, density, and temperature ratios across the region are compared with the values in gas dynamics tables. These values correspond to a perfect gas with $\gamma = 1.4$. The maximum normal component of the Mach number corresponding to the flow upstream of the region of high gradient was determined to be $M_{1n} \approx 1.33$ at the location with the most

negative value of the velocity divergence at the center spanwise plane. From gas dynamics tables for this Mach number, $\frac{p_2}{p_1} = 1.897$, $\frac{\rho_2}{\rho_1} = 1.568$, and $\frac{T_2}{T_1} = 1.21$. The pressure jump ratio across the sharp gradient zones of Fig. 14 in the positive U_∞ region is 1.902. Also, the density and temperature ratios across this region are $\frac{\rho_2}{\rho_1} = 1.582$ and $\frac{T_2}{T_1} = 1.201$.

It should be mentioned here that 3D simulation results show weaker shocks than those found in 2D. A plausible explanation for this is that in 3D, the flow has another dimension along which it can change direction in order to avoid the high pressure regions created by the presence of vortical structures. In other words, the three dimensionality of the flow allows a relaxation of the high compressibility regions and thus results in the formation of a less severe shock.

3.3 Structure of the Reacting Mixing Layer

With the aid of the DNS generated data, the extent of applicability of two recently proposed models for portraying the structure of non-premixed diffusion flames are examined. These models are based on the "Steady Laminar Diffusion Flamelet Model (SLDFM) (Williams, 1975; Peters, 1984; Peters, 1986), and a statistical closure based on the "Conditional Moment Method" (CMM) (Bilger, 1993). Both of these closures provide a means of predicting the compositional structure of non-equilibrium turbulent flames in such a way as to decouple the effects of turbulence from those of chemistry.

In the flamelet concept, a turbulent flame is assumed to be an ensemble of laminar diffusion flamelets (Williams, 1975). At sufficiently large but finite Damköhler numbers, the flamelets are assumed 1D and quasi-steady (Peters, 1984; Peters, 1986). In this way, it is speculated that the flame portrays the same structure as that of an equivalent flame in a laminar flow configuration. Peters (1986) proposes the flame produced by a steady laminar opposed jet (Tsuji, 1982) as a simple and effective model for the 1D laminar flow. In this way, it is straightforward (Liñan, 1974; Spalding, 1961) to show that the evolution of a scalar variable, say ψ is uniquely determined from the local values of the mixture fraction, J and its dissipation, χ. This implies that $\psi = \psi(J, \chi)$. A comparison of this relation with that of equilibrium flames, *i.e.* $\psi = \psi(J)$ indicates that under non-equilibrium conditions the dissipation rate provides the additional parameter by which the structure of the flame is to be described. Furthermore, with the flamelet concept the effects of chemistry with (J, χ) dependence is determined from the flamelet library generated by the solution of the transport

equation for the 1D laminar system.

A more direct means of accounting for the J dependence of the reacting variables has been proposed by the CMM of Bilger (1993) (also see Klimenko (1990); Smith *et al.* (1992)). This approach is based on conventional moment methods; however, the statistics are defined "conditionally" on a given value of the mixture fraction. That is, the dependence on the mixture fraction is through the ensemble average of the data but the averages are made only at given (conditional) values of the mixture fraction (Klimenko, 1990). This implies $< \psi|J >=< \psi|J > (x,t,J)$, where $< |J >$ denotes averaging conditioned on mixture fraction. This procedure, in comparison with traditional moment methods, has the obvious disadvantage of introducing the extra dimensionality of the conditioning parameter. However, Bilger (1993) suggests that in typical flames such as those in shear layers, this problem is offset by cross-stream "independence" of statistical quantities. Also, it is proposed that in the transport equations governing the evolution of conditional averages, the effects of conditional fluctuations are negligible in contrast to those in typical Reynolds averaging. This means that in the evaluation of the conditionally averaged reaction rate, the approximation $< \omega(\psi)|J > \approx \omega(< \psi|J >)$ is assumed valid.

In order to study the validity of the two models considered here, DNS results of 3D reacting layers are analyzed for both constant and temperature dependent chemistry models for several values of the Damköhler number and the heat release parameter. Table 1 provides a listing of the chemistry parameters for the simulations conducted in this study. Due to computational expenses, only single rollup simulations are conducted. The Reynolds number is set at $Re = 70$ for all cases. Also, in order to minimize the compressibility effects all simulations are performed with $M_c = 0.2$. In order to assess the performance of the models, it is desired to have the flow as three dimensional as possible. Therefore, simulations are continued until a time at which the effects of secondary instabilities are most significant.

3.4 Steady Laminar Diffusion Flamelet Model

The configuration of a quasi-1D opposed jet system (Spalding, 1961; Liñan, 1974) is considered in order to construct a flamelet library. This counterflow configuration has been studied in many previous investigations (*e.g.* Pandya and Weinberg (1964); Hahn *et al.* (1981); Kim and Williams (1990) amongst others). With the assumption of quasi-steady, incompressible 1D planar flow, the mass fraction of a reacting scalar, ψ is related to the mixture

fraction through the diffusion equation obtained by Crocco transformation (Liñan, 1974; Williams, 1989):

$$\frac{d^2\psi}{dJ^2} = -\frac{2}{\chi}\omega_\psi \tag{1}$$

In this configuration the dissipation is expressed as:

$$\chi = \chi_s \exp\left[-2\left(\mathrm{erfc}^{-1}(2J)\right)^2\right] \tag{2}$$

where the parameter χ_s denotes the magnitude of the dissipation at the stagnation plane of the opposed jet. In order to compare the DNS to model predictions, at each grid point a corresponding value of χ_s is calculated from Eq. (2). The chemistry parameters (K_F and Ce) have the same values as those employed in DNS. Therefore, at fixed Ce the flamelet library yields $\psi(J)$ curves which are functions of the non-dimensional parameter K_F/χ_s. This parameter is termed the local Damköhler number. The solution of the system equation is obtained numerically. For constant rate kinetics at large local Damköhler numbers, this solution was found to be in agreement with the analytical results derived by Fendell (1965) via the method of matched asymptotic expansions. A typical DNS scatter plot of the product mass fraction (Y_P) vs. the mixture fraction is given in Fig. 16. In this figure, 1D opposed jet predictions are represented by solid curves. The DNS results in the figure correspond to simulation Run 1 (Table 1). This figure indicates that both DNS scatter and the flamelet model predictions are strong functions of the local Damköhler number At a constant value of the mixture fraction, an increase in K_F/χ_s corresponds to an increase in product mass fraction. The agreement between the model and the DNS improves as the local Damköhler number is increased. Also, as the mixture fraction approaches its limiting values of 0 and 1, the scatter tends to group together and its deviation from the model becomes minimal. Therefore, the most restrictive testing of the model should be made at the region near the stoichiometric surface J_s, where the scatter is most severe.

Figure 17 shows product mass fraction scatter plots for the data of Run 1 and Run 2. A comparison between the two parts of this figure indicates that the effect of increasing the Damköhler number is to have the scatter closer to the equilibrium curve. Figure 18 presents product mass fraction at the stoichiometric surface $Y_P(J = J_s)$ vs. K_F/χ_s for the data of Fig. 17. In addition to clarity, this representation has the advantage that the model curves

of parts (a) and (b) are identical. This figure illustrates the strong dissipation (or K_F) dependence of the flame. As expected, the deviation from the DNS data is less for the higher Damköhler number flame (Run 2).

The results pertaining to stoichiometric coefficient of $r = 3$ (Run 3) are presented in Fig. 19. This figure indicates that the effect of increasing r is to skew the scatter towards the stoichiometric surface $J_s = 1/4$. This kinetics mechanism represents a better approximation to hydrocarbon flames which are typically characterized by low values of J_s. The migration of the scatter near the stoichiometric surface suggests that the performance of SLDFM improves as the magnitude of r is increased.

The stoichiometric product mass fraction scatter plot is compared with SLDFM predictions in Fig. 20 for Run 4 corresponding to a heat releasing flame. A comparison of this figure with Fig. 18(b) indicates that the model's performance is improved over all ranges of the local Damköhler number. This improvement is due to the influence of thermal expansion, even though a constant density flamelet library model is used for comparison. The effect of expansion is to smooth the steep gradients of the scalar field. This smoothing effect is illustrated in Fig. 21 by means of the PDF's of the scalar dissipation for Run 2 and Run 4. Of particular note in this figure is the "double hump" feature of the PDF's. Flow visualization shows that these two humps at low and high dissipation rates correspond roughly to the data sampled at the roller core and braids, respectively. The PDF's for Run 4 are shifted towards lower values of the dissipation rate, consistent with earlier findings of McMurtry *et al.* (1989). This shifting results in larger values of the local Damköhler number and, as noted earlier, improves the validity of the SLDFM. The results for simulations with an Arrhenius kinetics model (Run 5) portray a similar behavior.

3.5 Conditional Moment Method

Simulation results with the chemistry parameters listed in Table I are also used to examine the modeling assumptions imposed for implementing the CMM for statistical description of the compositional flame structure. The first assessment of the model is associated with the influence of the conditional correlation of a scalar on the conditionally averaged reaction rate. In order to examine this effect, in Fig. 22(a) results are presented for both $< \omega(\psi)|J >$ and $\omega(< \psi|J >)$ in the composition domain. The data correspond to the simulations in Run 1. The figure suggests that the approximation is reasonably justified. This comparison

should be compared with that corresponding to the case in which the averages are defined unconditionally. For this simulation, the comparison between traditional averages $< \omega(\psi) >$ and $\omega(< \psi >)$ is presented in Fig. 22(b). This figure indicates that the two averages differ substantially. Therefore, the approximation $< \omega(\psi) >= \omega(< \psi >)$ cannot be justified. For temperature dependent kinetics, the reaction rate is also dependent on the conditionally averaged temperature, *i.e.* $< T|J >$. The assessment of the CMM approximation for the data of Run 5 is made in Fig. 23. Similar to that of Fig. 22(a), the agreement is good.

Independence of the conditionally averaged values from the cross-stream direction is important from the viewpoint of practicality of CMM (Bilger, 1993). This is tested in Fig. 24 for Run 1, and in Fig. 25 for Run 5. In both cases, the conditionally averaged mass fractions of species A and product are presented vs. the mixture fraction. For the temperature dependent kinetics, the conditionally averaged temperature is also presented in Fig. 25(c). The results for the conditionally averaged species mass fractions show small deviations near the stoichiometric surface. The y independence appears to be approximately valid for these average quantities. The extent of independence is less for the higher order moments. In Fig. 26, the conditional variances of the mass fraction of species A vs. y are presented for Run 1 and Run 5. It is clear from this figure that higher order moments have a strong y dependence.

In regard to applicability of CMM, two final points are addressed: (1) Its implementation for describing flames far from equilibrium conditions, and (2) its practical applications for making actual predictions. In regard to (1), an important consideration is for describing the compositional structure of flames near ignition or extinction. In these cases, in addition to mixture fraction another progress variable must be used in defining the conditional averages. None of the flames considered in the simulations here display extinction. Therefore, conditioning on the mixture fraction alone is sufficient for constructing averages. For flames with severe departure from equilibrium, the use of the model may not be practical since the analysis requires the modeling of higher order conditional moments. Since these moments do not seem to be independent of cross-stream direction, the extra dimensionality in the problem formulation makes the analysis somewhat difficult from a practical standpoint. In regard to (2), the actual implementation of the CMM for cases which temperature dependence is not significant, the most important extra closure is the expected value of the dissipation of the mixture fraction conditioned on the value of the mixture fraction (Bilger, 1993). In a recent article, Miller *et al.* (1993) provide several suggestions for modeling of

this conditional dissipation. The use of this closure in a transport equation which governs the conditional mean value of the reacting species mass fractions is very effective in assessing the mean compositional structure.

4 Conclusions

A monotone Flux Corrected Transport algorithm is employed for direct numerical simulations of a 3D temporally developing forced mixing layer. The objective of this study is to examine the following specific issues pertaining to the structure of turbulent mixing layers and flames: (1) the effects of transition on mixing characteristics of the layer, (2) the existence and manifestation of eddy shocklets in 3D, (3) validity assessment of the steady laminar diffusion flamelet model in depicting the compositional structure of turbulent flames, and (4) evaluation of the basic assumptions of the approach based on the conditional moment method for statistical description of turbulent flames.

Simulation of moderately high Reynolds number flow allows capturing of the cause and effects of transition on the mixing process. Single point PDF's of the mixture fraction, extracted from DNS data, reveal features in accord with laboratory data. In addition to reproducing many of the qualitative and quantitative results observed in previous experiments, new insights are gained as to the nature of the transition process. It is shown that during the transition, both pure unmixed fluids and fully mixed fluids are found with high probability throughout the entire layer. The effect of chemical heat release is to delay the onset of pairing and the subsequent transition. In constant rate kinetics, reduced mixing results in decreased product formation. However, in an Arrhenius reaction case, chemical heat release causes higher local reaction rates which overcome mixing reduction and results in a relative increase in product formation.

At sufficiently high convective Mach numbers, (larger than ≈ 1.25) eddy shocklets are found in 3D mixing layers. Comparison of the shocklets observed in 3D simulations with those in 2D at the same Reynolds and convective Mach numbers indicates that the shocklets are stronger in the 2D case.

DNS results for different Damköhler numbers, stoichiometric coefficients, and heat release parameters are compared with predictions based on a 1D steady laminar opposed jet flame. For all the flames considered, it is concluded that the performance of the flamelet model

improves as the magnitude of either the local or the global Damköhler number is increased. This is understandable considering the flamelet concept is deemed valid at high but finite reaction rates. Also, as the value of r is increased the agreement between the DNS data and the model is improved. This is promising in view of the fact that the flame surface in typical hydrocarbon flames is at low values of the stoichiometric mixture fraction. The results for both constant and Arrhenius rate reactions with heat release show an improved agreement with the model in comparison to those of a non-heat releasing layer. This is attributed to thermal expansion, reducing the instantaneous scalar dissipation rate and thus increasing the magnitudes of the local Damköhler numbers.

DNS generated results for reacting mixing layers are also used to examine the basic assumptions of the conditional moment method. It is shown that the neglect of the conditional unmixedness term is acceptable. Also, the cross-stream variations of the first conditional moments (that is, the conditional averages) of the reacting variables can be assumed negligible. However, higher conditional moments of these variables show cross-stream dependence. This may be problematic in mathematical modeling of these higher moments.

Nomenclature

A. Chemical species A.

B. Chemical species B.

C_i. Concentration of species i

C_P. Specific heat of the mixture at constant pressure.

C_V. Specific heat of the mixture at constant volume.

E. Activation energy for the Arrhenius chemical reaction.

J. The mixture fraction.

$J_s = \frac{1}{1+r}$. Stoichiometric value of mixture fraction.

K_F. Pre-exponential factor of the reaction rate.

(L_x, L_y, L_z). The size of the computational domain.

$M_c = \frac{U_\infty}{\sqrt{\gamma R T_\infty}}$. The convective Mach number.

MW_i. Molecular weight of species i.

P. Chemical product.

P. Probability.

PDF. Single-Point Probability Density Function.

Pr. The Prandtl number.

$q^2/2$. Turbulence kinetic energy.

$\mathcal{R}$. Universal gas constant.

r. Stoichiometric coefficient.

Sc. The Schmidt number.

T. Temperature.

U. Streamwise velocity.

x, y, z Streamwise, cross-stream and spanwise directions.

Y_i. Mass fraction of species i.

$< >$. Ensemble average.

$< |J >$. Ensemble average conditioned on the mixture fraction.

$-\Delta H°$. Enthalpy of combustion.

Greek Symbols and Subscripts

μ. Molecular viscosity.

γ. The ratio of the specific heats. $= C_P/C_V$.

Γ. Species diffusivity.

ρ. Density.

σ^2. Conditional variance.

ω. Reaction rate.

ω_ψ. Appropriate reaction rate for the scalar variable ψ.

χ. The scalar dissipation.

χ_s. Magnitude of the scalar dissipation at the stagnation plane of the counterflow diffusion flame.

∞. Free stream.

Normalized parameters

$Ce = \frac{-\Delta H^0}{C_P T_\infty}$. Heat release parameter.

$Da = \frac{K_P \delta_\omega|_0}{U_\infty}$. The Damköhler number. With this definition, $\rho_\infty Da/MW$ is a non-dimensionalized parameter.

$Re = \frac{\rho_\infty U_\infty \delta_\omega|_0}{\mu}$. The Reynolds Number.

$t^* = \frac{tU_\infty}{L_x}$.

$y^* = \frac{y}{\delta_\omega|_{t^*}}$.

$y_L = \frac{y}{L_y}$.

$Ze = \frac{E}{RT_\infty}$. The Zeldovich number.

$\delta_p|_{t^*} = \int_{-\infty}^{+\infty} \rho Y_P \, dx \, dy \, dz$. Total instantaneous product.

$\delta_p = \delta_p|_{t^*}/\delta_p|_{t^*=0} - 1$. Normalized total product.

$\delta_\omega|_{t^*} = \frac{2U_\infty}{\frac{\partial \langle U \rangle}{\partial y}|_{max}}$. Vorticity thickness.

$\delta_\omega = \delta_\omega|_{t^*}/\delta_\omega|_0$. Normalized vorticity thickness.

$\delta_\omega|_0 = \delta_\omega|_{t^*=0}$.

Acknowledgments

We are indebted to Professor Forman A. Williams for helpful discussions. This work is sponsored by the Office of Naval Research under Grant N00014-90-J-1403, and by the National Science Foundation under Grant CTS-9012832. Computational resources are provided by NSF through NCSA at the University of Illinois and by the NAS program at NASA Ames Research Center.

References

Bernal, L. P. and Roshko, A. (1986). Streamwise vortex structures in plane mixing layers. *J. Fluid Mech.* **170**, 499–525.

Bilger, R. W. (1993). Conditional moment closure for turbulent reacting flow. *Phys. Fluids A.* **5**, 436–444.

Boris, J. P. and Book, D. L. (1976). Solution of the continuity equations by the method of flux corrected transport. In *Methods in Computational Physics*, volume 16, pages 85–129. Academic Press, New York, NY.

Colucci, P. (1993), Linear stability analysis of density stratified parallel shear flows. M.S. Thesis, Department of Mechanical and Aerospace Engineering, State University of New York at Buffalo, Buffalo, NY.

Dimotakis, P. E. (1991). Turbulent free shear layer mixing and combustion. In Murthy, S. N. B. and Curran, E. T., editors, *High Speed Flight Propulsion Systems*, volume 137 of *Progress in Astronautics and Aeronautics*, chapter 5, pages 265–340. AIAA Publishing Co., Washington, D.C.

Drummond, J. P. and Givi, P. (1993). Suppression and enhancement of mixing in high-speed reacting flow fields. In Buckmaster, J. D., Jackson, T. L., and Kumar, A., editors, *Combustion in High-Speed Flows.* in press.

Fendell, F. E. (1965). Ignition and extinction in combustion of initially unmixed reactants. *J. Fluid Mech.* **21**, 281–303.

Fiedler, H. (1974). Transport of heat across a plane turbulent mixing layer. In Landsburg, H. E. and Mieghem, J. V., editors, *Advances in Geophysics*, pages 93–109. Academic Press, New York, NY. Vol 18A.

Givi, P. and Riley, J. J. (1992). Some current issues in the analysis of reacting shear layers: Computational challenges. In Hussaini, M. Y., Kumar, A., and Voigt, R. G., editors, *Major Research Topics in Combustion*, pages 588–650. Springer-Verlag.

Givi, P., Madnia, C. K., Steinberger, C. J., Carpenter, M. H., and Drummond, J. P. (1991). Effects of compressibility and heat release in a high speed reacting mixing layer. *Combust. Sci. and Tech.* **78**, 33–68.

Givi, P. (1989). Model free simulations of turbulent reactive flows. *Prog. Energy Combust. Sci.* **15**, 1–107.

Grinstein, F. F. and Kailasanath, K. (1991). Chemical energy release, spanwise excitation, and dynamics of transitional, reactive, free shear flows. AIAA Paper 91-0247.

Grinstein, F. F. and Kailasanath, K. (1992). Chemical energy release and dynamics of transitional, reactive shear flows. *Phys. Fluids A.* **4**, 2207–2221.

Hahn, V. A., Wendt, J. O. L., and Tyson, J. (1981). Analysis of the flat laminar opposed jet diffusion flame with finite rate detailed chemical kinetics. *Combust. Sci. and Tech.* **27**, 1–17.

Hermanson, J. C. and Dimotakis, P. E. (1989). Effects of heat release in a turbulent, reacting shear layer. *J. Fluid. Mech.* **199**, 333–375.

Jackson, T. L. and Grosch, C. E. (1989). Effects of heat release and equivalence ratio on the inviscid spatial stability of a supersonic reacting mixing layer. In Dervieux, A. and Larroutuiou, B., editors, *Numerical Combustion*, pages 362–372. Springer-Verlag.

Jackson, T. L. and Grosch, C. E. (1990). Inviscid spatial stability of a compressible mixing layer. Part 2. The flame sheet model. *J. Fluid Mech.* **217**, 391–420.

Jackson, T. L. (1992). A review of spatial stability analysis of compressible reacting mixing layers. In Hussaini, M. Y., Kumar, A., and Voigt, R. G., editors, *Major Research Topics in Combustion*, pages 131–161. Springer-Verlag.

Kim, J. S. and Williams, F. A. (1990). Theory of counterflow mixing of fuel with hot reaction products. *Combust. Sci. and Tech.* **73**, 575–588.

Klimenko, A. Y. (1990). Multicomponent diffusion of various mixtures in turbulent flow. *Fluid Dynamics* **25**, 327–334.

Koochesfahani, M. M. and Dimotakis, P. E. (1986). Mixing and chemical reactions in a turbulent liquid mixing layer. *J. Fluid. Mech.* **170**, 83–112.

Lele, S. K. (1989). Direct numerical simulation of compressible free shear flows. AIAA Paper 89-0374.

Liñan, A. (1974). The asymptotic structure of counterflow diffusion flames for large activation energies. *Acta Astronautica* **1**, 1007–1039.

Libby, P. A. and Williams, F. A., editors. (1993). *Turbulent Reacting Flows.* Academic Press, London, UK. in press.

Masutani, S. M. and Bowman, C. T. (1986). The structure of a chemically reacting plane mixing layer. *J. Fluid Mech.* **72**, 93–126.

McMurtry, P. A., Jou, W.-H., Riley, J. J., and Metcalfe, R. W. (1986). Direct numerical simulations of a reacting mixing layer with chemical heat release. *AIAA J.* **24**, 962–970.

McMurtry, P. A., Riley, J. J., and Metcalfe, R. W. (1989). Effects of heat release on the large scale structures in a turbulent reacting mixing layer. *J. Fluid Mech.* **199**, 297–332.

Menon, S. and Fernando, E. (1990). A numerical study of mixing and chemical heat release in supersonic mixing layers. AIAA Paper 90-0152.

Metcalfe, R. W., Orszag, S. A., Brachet, M. E., Menon, S., and Riley, J. J. (1987). Secondary instabilities of a temporally growing mixing layer. *J. Fluid Mech.* **184**, 207–243.

Michalke, A. (1964). On the inviscid instability of the hyperbolic tangent velocity profile. *J. Fluid Mech.* **19**, 543–556.

Miller, R. S., Frankel, S. H., Madnia, C. K., and Givi, P. (1993). Johnson-Edgeworth translation for probability modeling of binary mixing in turbulent flows. *Combust. Sci. and Tech.* **91**, 21–52.

Miller, R. S. (1993). The manifestation of eddy shocklets and laminar diffusion flamelets in a shear layer. AIAA Paper 93-0011.

Moser, R. D. and Rogers, M. M. (1991). Mixing transition and the cascade of small scales in a plane mixing layer. *Phys. Fluids A* **3**, 1128–1134.

Moser, R. D. and Rogers, M. M. (1992). The three dimensional evolution of a plane mixing layer: Pairing and transition to turbulence. *J. Fluid Mech.* . Submitted for publications.

Mukunda, H. S., Sekar, B., Carpenter, M. H., Drummond, J. P., and Kumar, A. (1992). Direct simulation of high-speed mixing layers. NASA TP 3186.

Oran, E. S. and Boris, J. P. (1987). *Numerical Simulations of Reactive Flows.* Elsevier Publishing Company, Washington, D.C.

Oran, E. S. and Boris, J. P., editors. (1991). *Numerical Approaches to Combustion Modeling*, volume 135 of *Progress in Astronautics and Aeronautics.* AIAA Publishing Co., New York, NY.

Pandya, T. P. and Weinberg, F. J. (1964). The structure of flat, counter-flow diffusion flames. *Proc. of the Royal Soc. London A* **279**, 544–561.

Peters, N. (1984). Laminar diffusion flamelet models in non-premixed turbulent combustion. *Prog. Energy Combust. Sci.* **10**, 319–339.

Peters, N. (1986). Laminar flamelet concepts in turbulent combustion. In *Proceedings of 21st Symp. (Int.) on Combustion*, pages 1231–1250. The Combustion Institute, Pittsburgh, PA.

Pierrehumbert, R. T. and Widnall, S. E. (1982). The two and three dimensional instabilities of a spatially periodic shear layer. *J. Fluid Mech.* **114**, 59–82.

Reynolds, W. C. (1990). The potential and limitations of direct and large eddy simulations. In Lumley, J. L., editor, *Whither Turbulence? Turbulence at the Crossroads*, volume 357 of *Lecture Notes in Physics*, pages 313–343. Springer-Verlag.

Riley, J. J. and McMurtry, P. A. (1989). The use of direct numerical simulation in the study of turbulent chemically reacting flows. In Borghi, R. and Murthy, S. N. B., editors, *Turbulent Reactive Flows*, Lecture Notes in Engineering, pages 486–514. Springer-Verlag.

Riley, J. J., Metcalfe, R. W., and Orszag, S. A. (1986). Direct numerical simulations of chemically reacting mixing layers. *Phys. Fluids* **29**, 406–422.

Sandham, N. D. and Reynolds, W. C. (1989). A numerical investigation of the compressible mixing layer. Report No. TF-45, Stanford University, Department of Mechanical Engineering, Thermosciences Division, Stanford, CA.

Sekar, B. and Mukunda, H. S. (1990). A computational study of direct numerical simulation of high speed mixing layers without and with chemical heat release. In *Proceedings of 23rd Symp. (Int.) on Combustion*, pages 707–713. The Combustion Institute, Pittsburgh, PA.

Shin, D. S. and Ferziger, J. H. (1992). Stability of the compressible reacting mixing layer. Report No. TF-53, Stanford University, Department of Mechanical Engineering, Thermosciences Division, Stanford, CA.

Smith, N. S., Bilger, R. W., and Chen, J.-Y. (1992). Modeling of non-premixed hydrogen jet flames using a conditional moment closure method. In *Proceedings of 24th Symp. (Int.) on Combustion*, pages 271–278. The Combustion Institute, Pittsburgh, PA.

Spalding, S. B. (1961). Theory of mixing and chemical reaction in the opposed-jet diffusion flame. *Journal of the American Rocket Society* **31**, 763–771.

Steinberger, C. J. (1992). Model free simulations of a high speed reacting mixing layer. AIAA Paper 92-0257.

Tsuji, H. (1982). Counterflow diffusion flames. *Prog. Energy Combust. Sci.* **8**, 93.

Williams, F. A. (1975). Recent advances in theoretical description of turbulent diffusion flames. In Brodkey, R. S., editor, *Turbulence in Mixing Operations*, pages 189–209. Academic Press, New York, NY.

Williams, F. A. (1985). *Combustion Theory*. The Benjamin/Cummings Publishing Company, Menlo Park, CA, 2nd edition.

Williams, F. A. (1989). Structure of flamelets in turbulent reacting flows and influences of combustion on turbulence fields. In Borghi, R. and Murthy, S. N. B., editors, *Turbulent Reactive Flows*, Lecture Notes in Engineering, pages 195–212. Springer-Verlag.

Figure Captions

Figure 1. Schematic diagram of temporally developing mixing layer.

Figure 2. Pairing vortical structures as depicted by the plots of vorticity magnitude contours at $t^* = 1.2$.

Figure 3. Plot of the mixture fraction contours. The isolevel of $J = 0.5$, corresponding to flame sheet is cross hatched. (a) a spanwise plane, (b) a streamwise plane.

Figure 4. Post-transitional flow field as depicted by the plot of vorticity contours at $t^* = 2.0$.

Figure 5. Plot of streamwise mixture fraction contours in the braid plane at $t^* = 1.2$.

Figure 6. Probability density functions of mixture fraction vs. y^*. (a) $t^* = 0.5$, (b) $t^* = 0.95$, (c) $t^* = 1.85$.

Figure 7. Probability of finding pure species within the mixing layer. (a) $t^* = 0.5$, (b) $t^* = 0.95$, (c) $t^* = 1.85$.

Figure 8. Temporal evolution of the product thickness, the vorticity thickness and their ratio.

Figure 9. Probability of finding pure mixed fluid within the mixing layer.

Figure 10. Cross-stream variation of turbulence intensities: (a) streamwise velocity rms, (b) mixture fraction rms.

Figure 11. Temporal variation of the vorticity thickness.

Figure 12. Cross-stream variation of turbulence kinetic energy.

Figure 13. Temporal variation of product thickness for several values of the heat release parameter. (a) constant rate kinetics, (b) Arrhenius rate kinetics.

Figure 14. Plot of Mach number contours, $M_c = 2.5$.

Figure 15. Plot of velocity divergence contours, $M_c = 2.5$.

Figure 16. Local Damköhler (K_F/χ_s) dependence of both DNS (Run 1) and SLDFM data.

Figure 17. Scatter plot of product mass fraction obtained from DNS. (a) Run 1, (b) Run 2.

Figure 18. Stoichiometric product mass fraction vs. the local Damköhler number. (a) Run 1, (b) Run 2. The solid line indicates SLDFM prediction.

Figure 19. Scatter plot of product mass fraction obtained from DNS for Run 3.

Figure 20. Stoichiometric product mass fraction vs. the local Damköhler number for Run 4. The solid line indicates SLDFM prediction.

Figure 21. Probability density functions for scalar dissipation.

Figure 22. (a) Conditionally averaged reaction rates for data of Run 1. (b) Reynolds-averaged reaction rates for data of Run 1.

Figure 23. Conditionally averaged reaction rates for data of Run 5.

Figure 24. Cross-stream variation of conditional averages for data of Run 1. (a) reactant mass fraction, (b) product mass fraction.

Figure 25. Cross-stream variation of conditional averages for data of Run 5. (a) reactant mass fraction, (b) product mass fraction, (c) temperature.

Figure 26. Cross-stream variation of reactant mass fraction variance. (a) Run 1, (b) Run 5.

Run	r	Da	Ce	Kinetic model
1	1	1	0	constant rate
2	1	5	0	constant rate
3	3	1	0	constant rate
4	1	5	0.2	constant rate
5	1	2.2	0.2	Arrhenius rate

Table 1

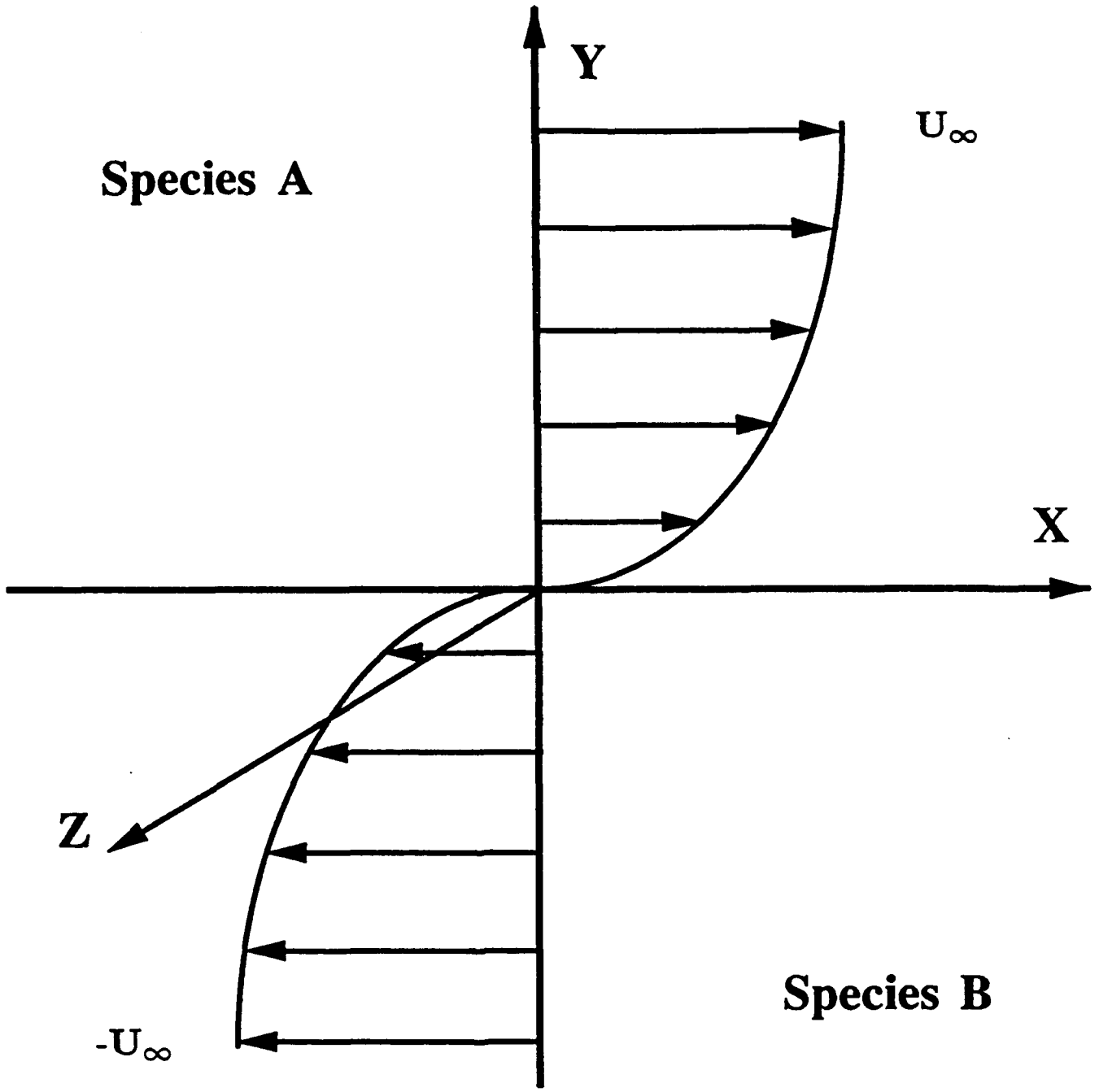

Figure 1

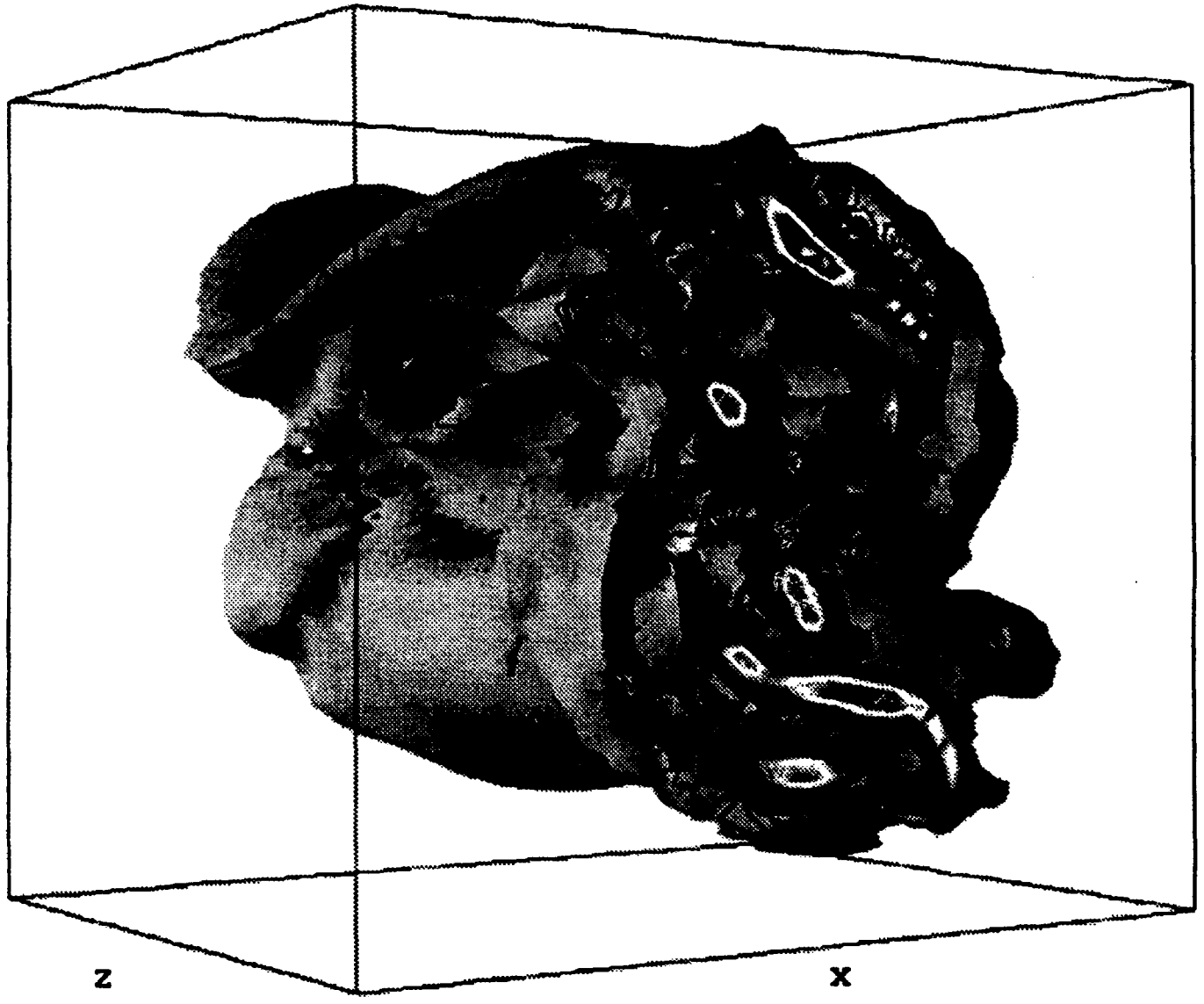

Figure 2

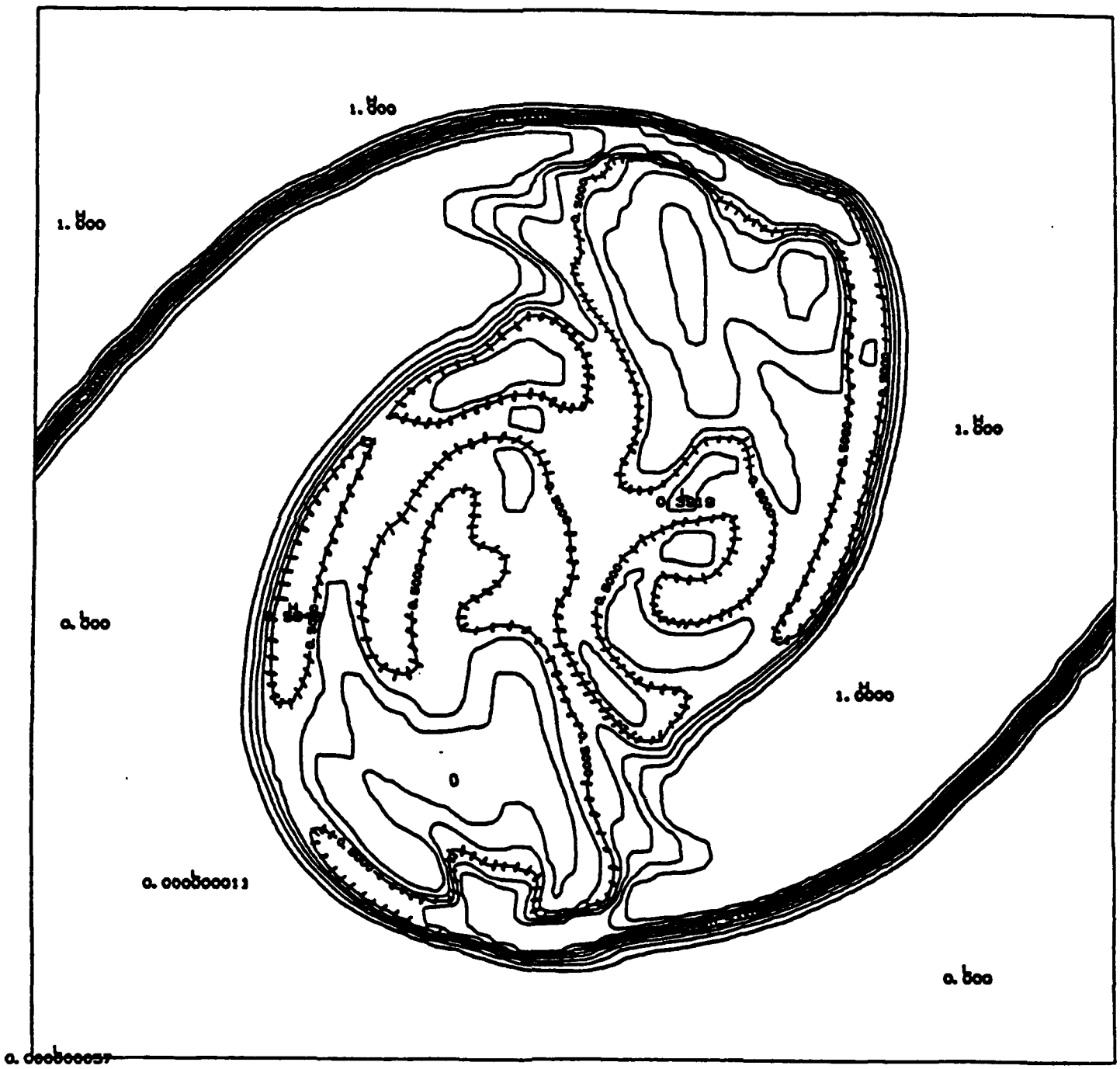

Figure 3(a)

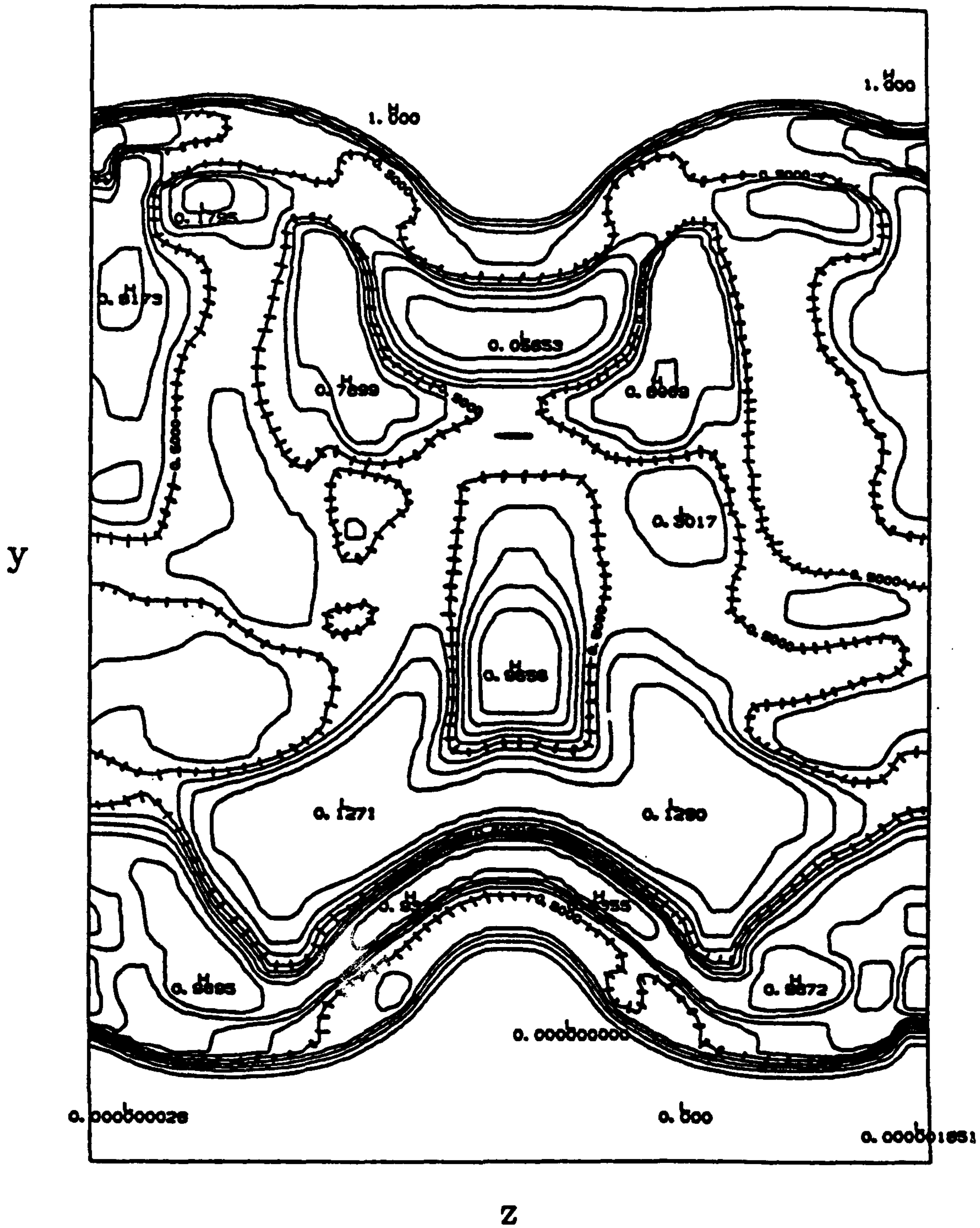
1.000
1.000
0.1755
0.8173
0.06853
0.7899
0.8069
0.3017
0.8686
0.1271
0.1280
0.8885
0.8872
0.000000000
0.00000028
0.500
0.00001851
y
z

Figure 3(b)

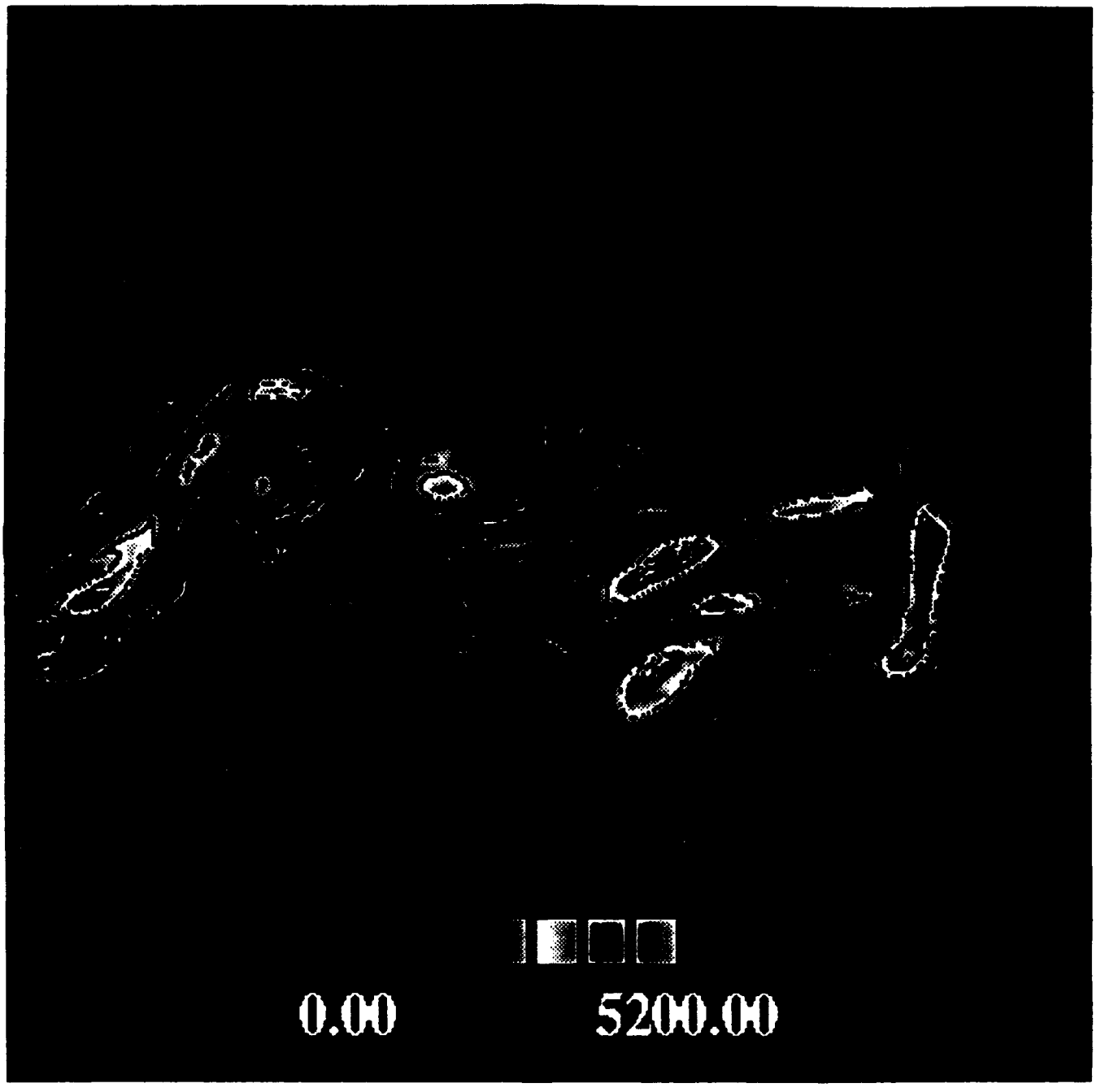

Figure 4

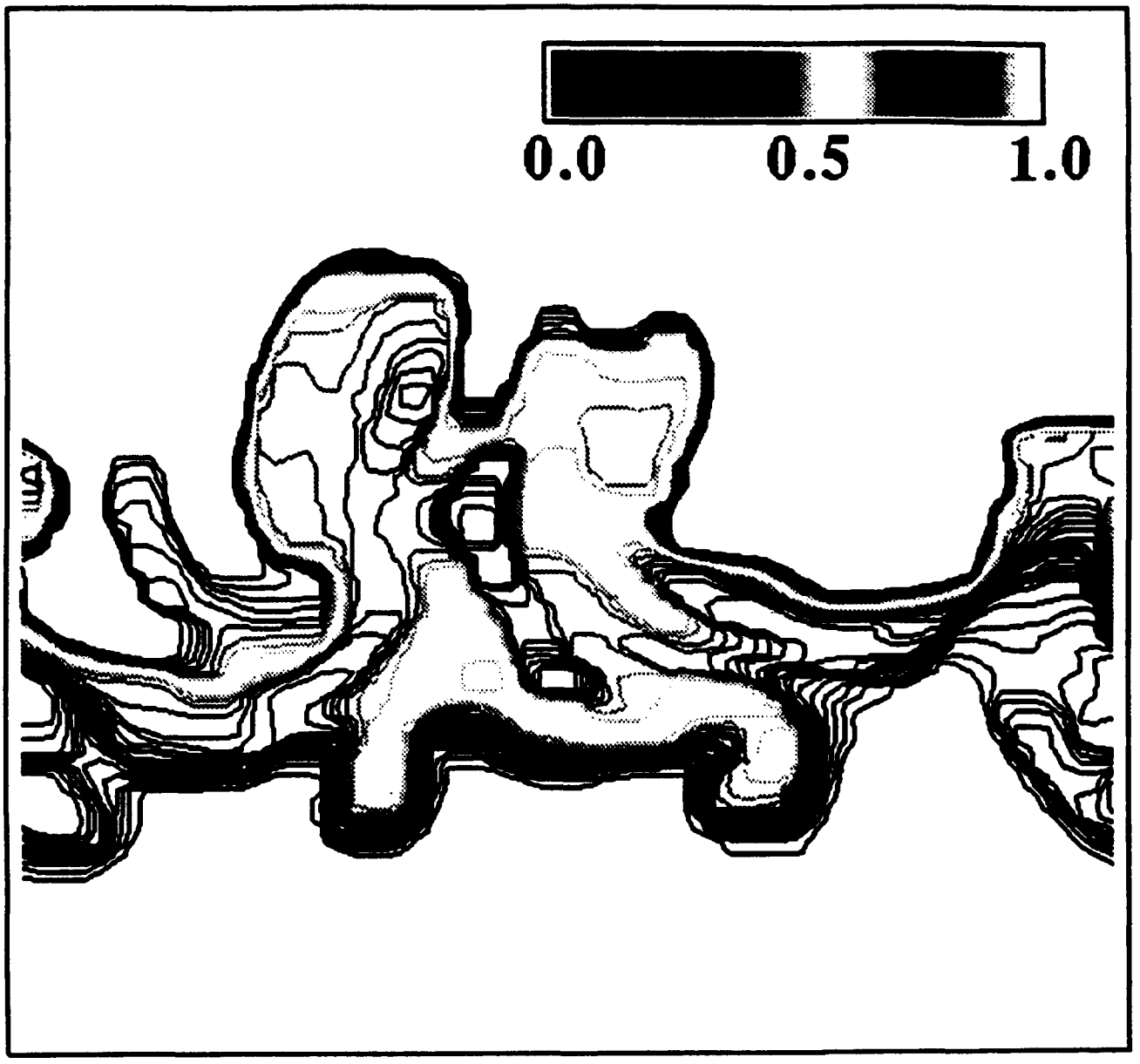

Figure 5

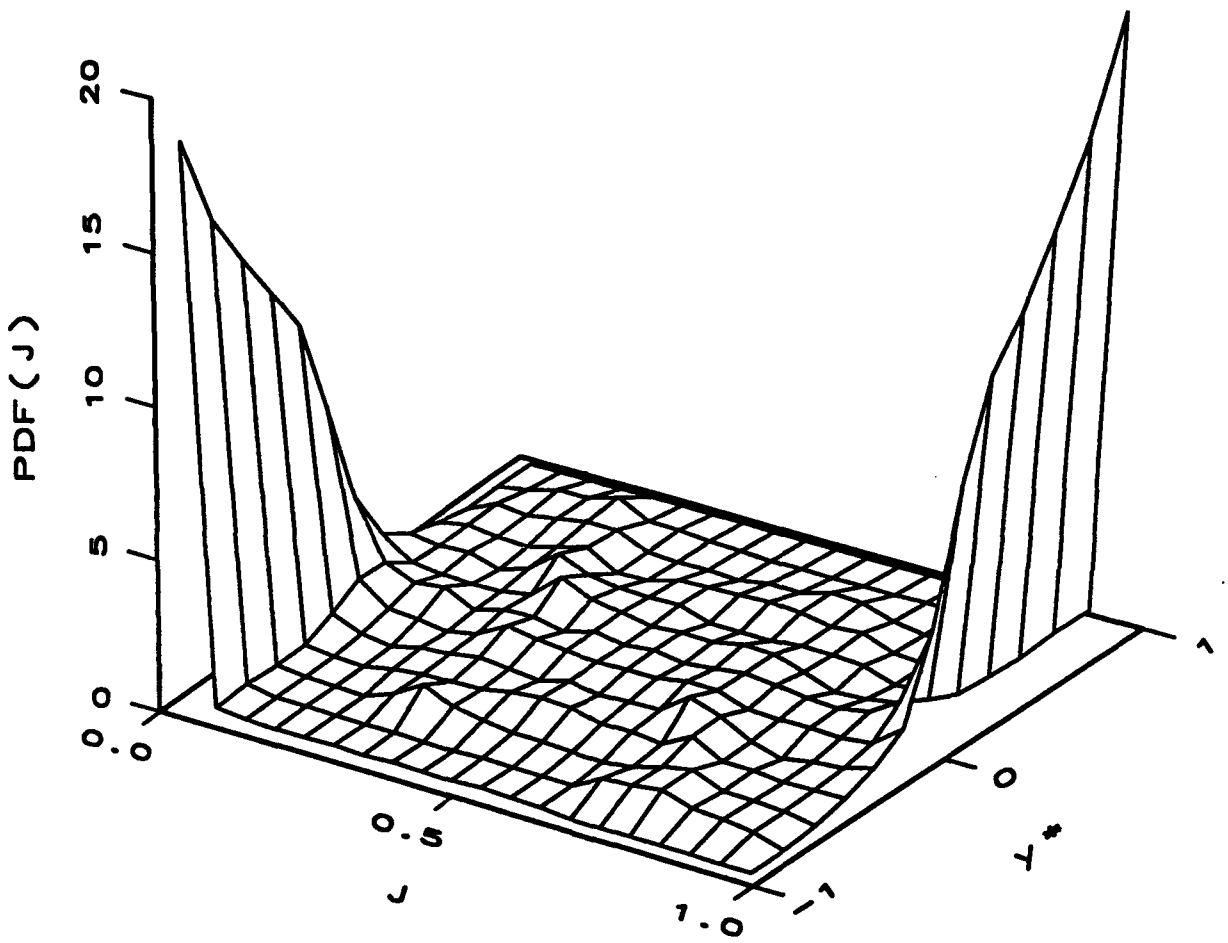

Figure 6(a)

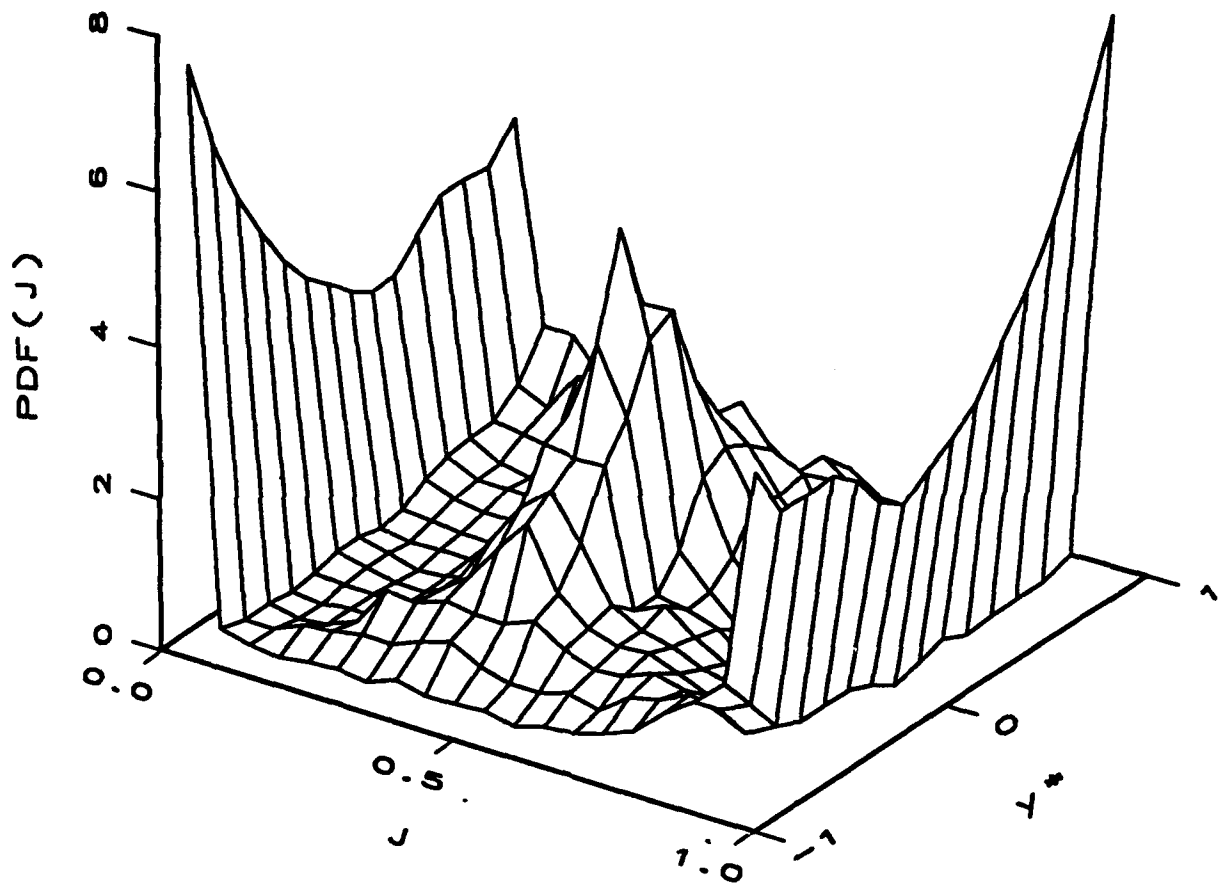

Figure 6(b)

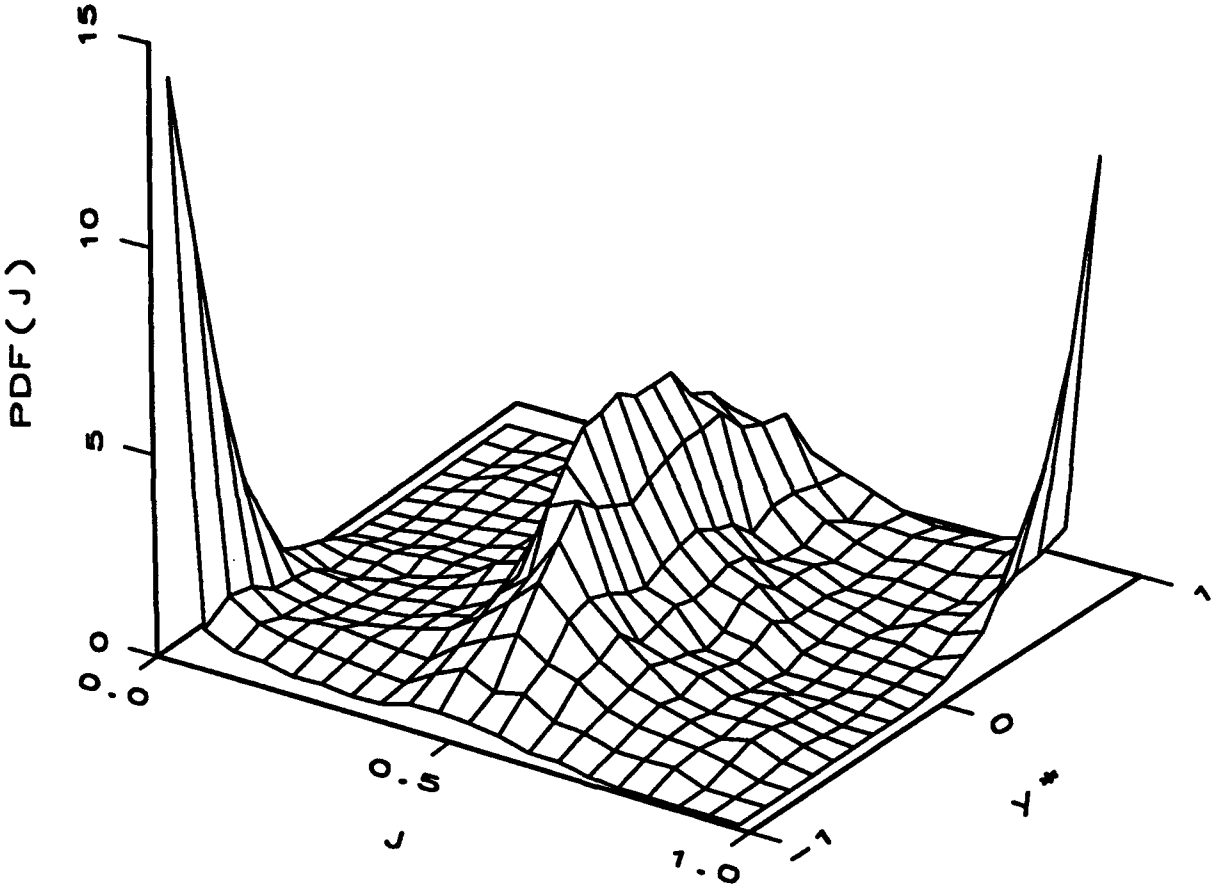

Figure 6(C)

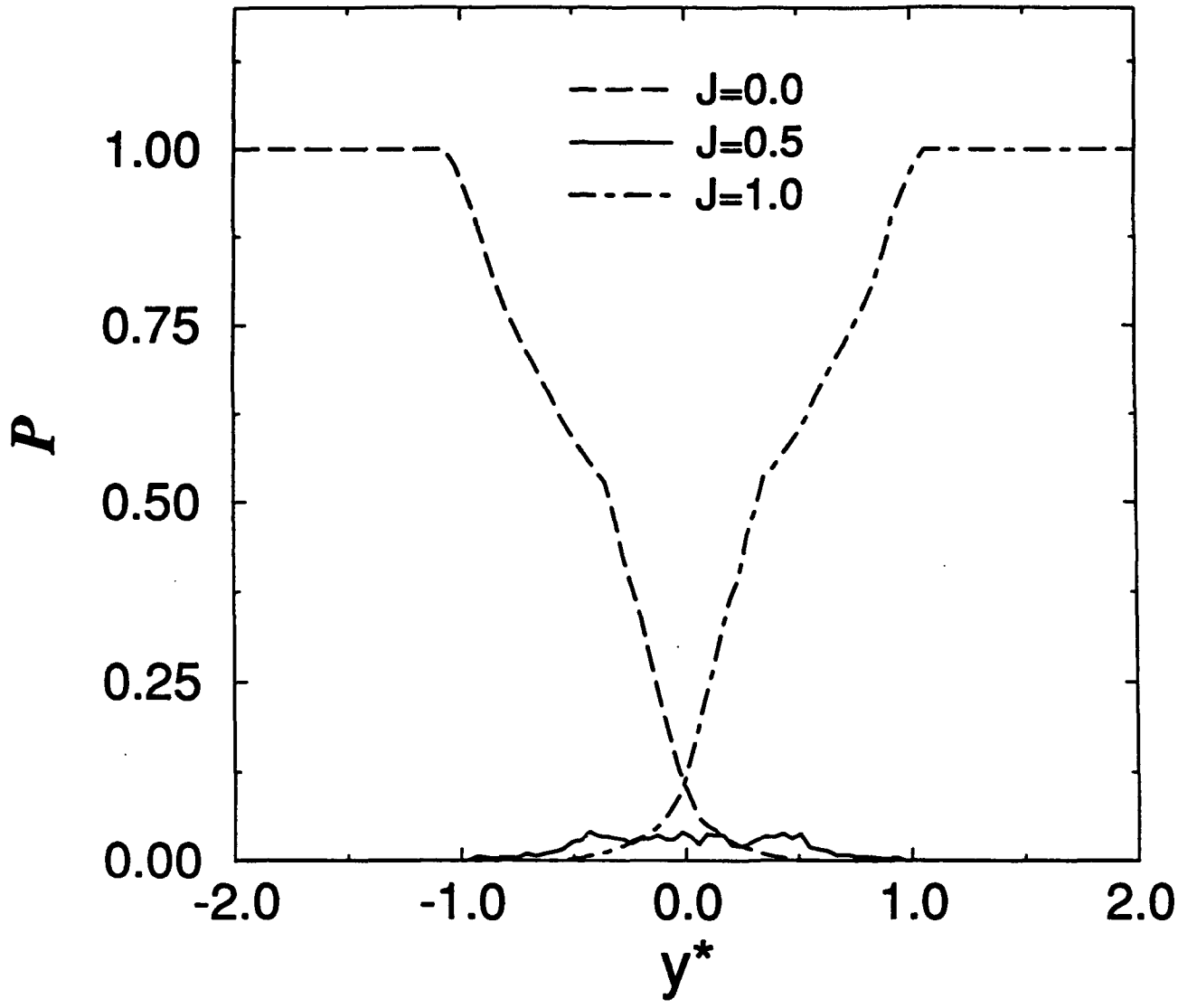

Figure 7 (a)

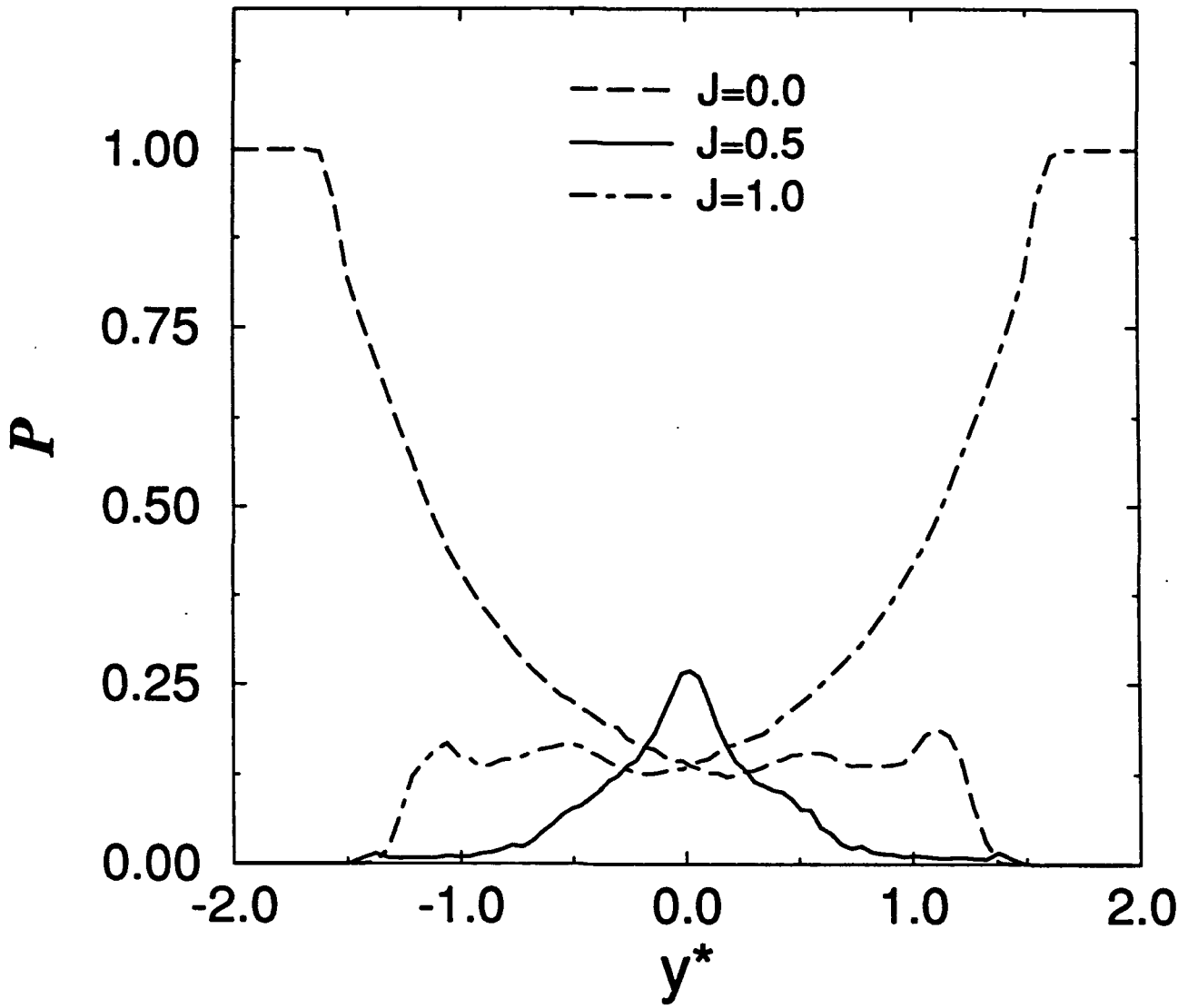

Figure 7(b)

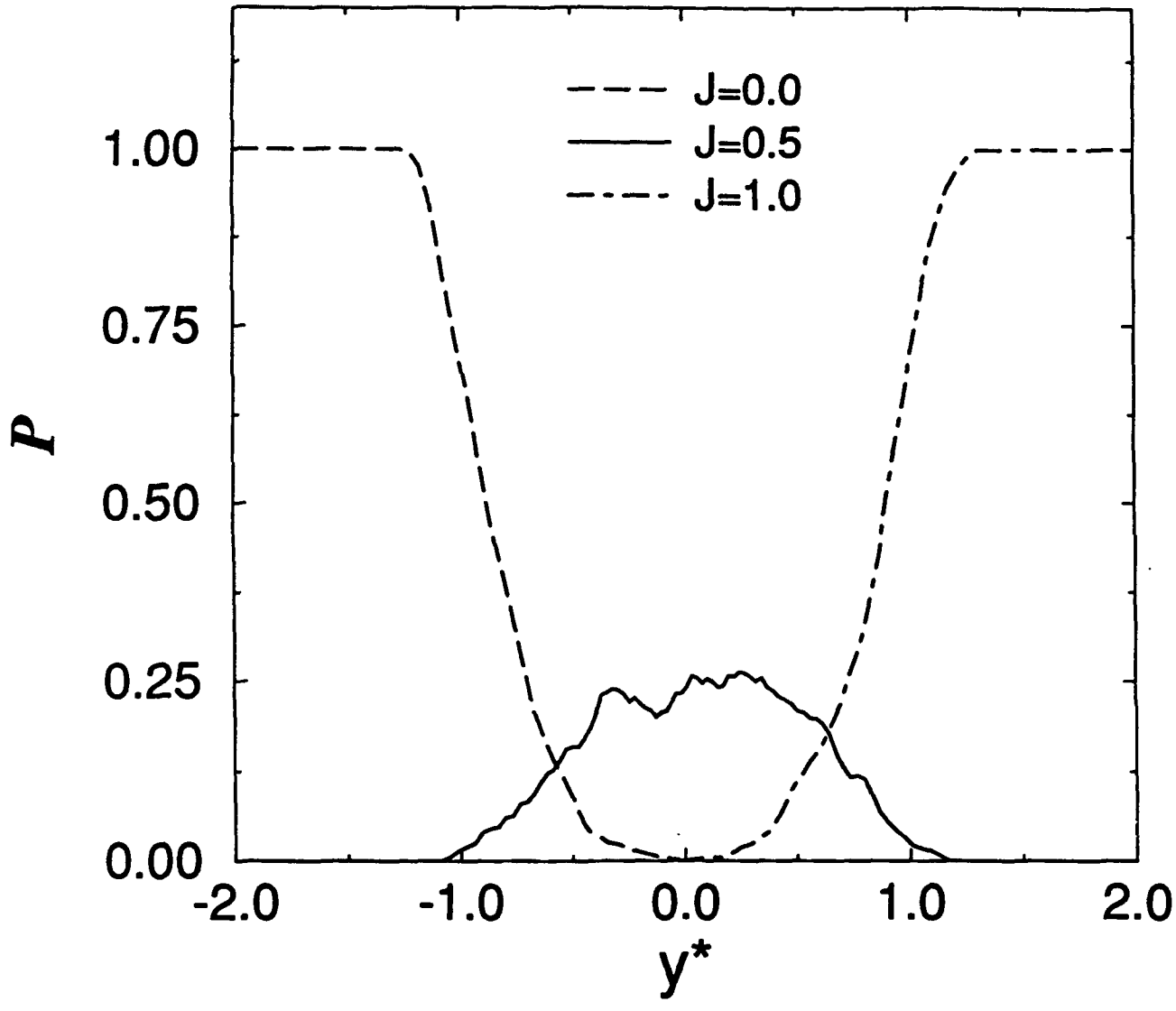

Figure 7(c)

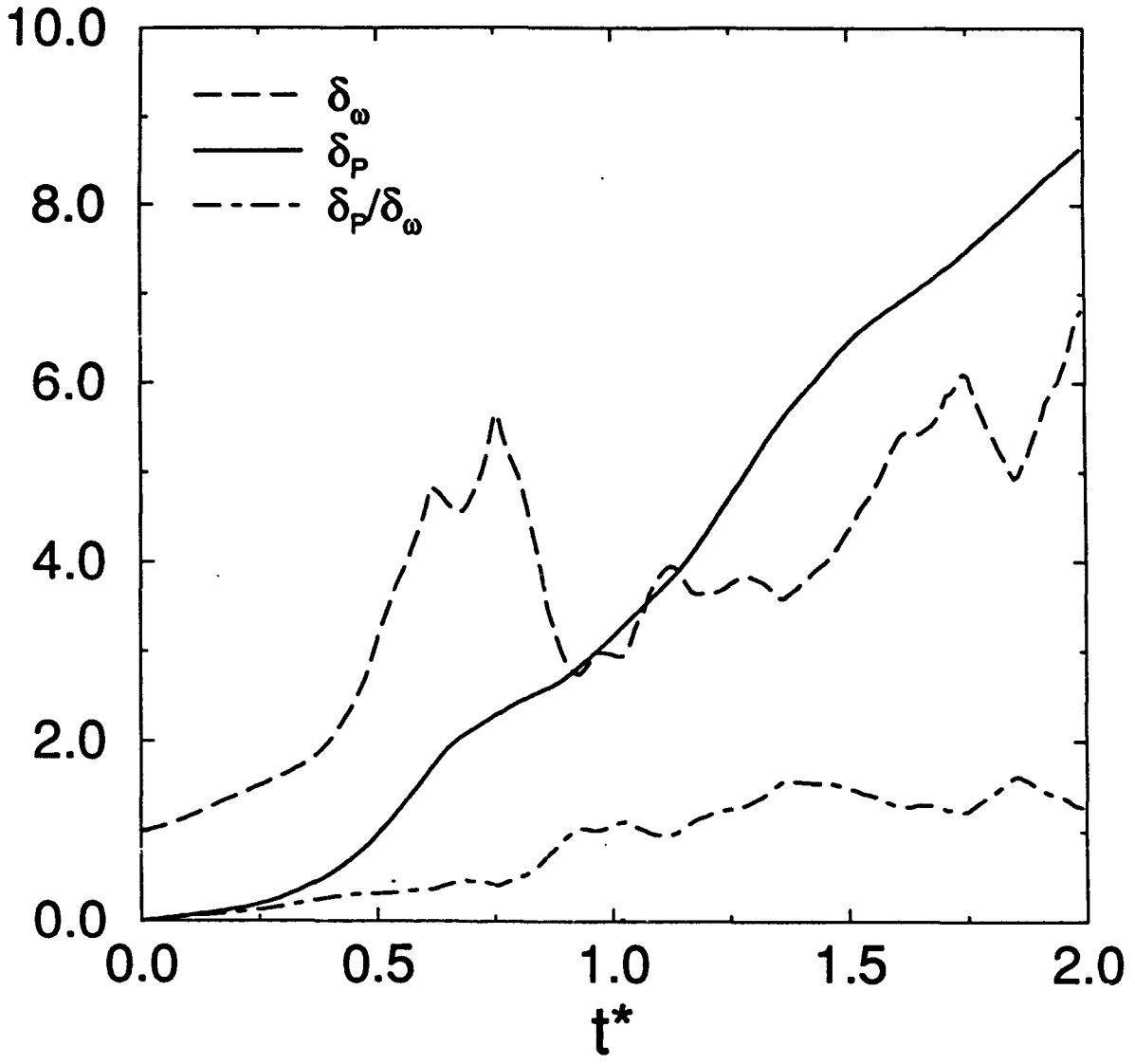
10.0
8.0
6.0
4.0
2.0
0.0
0.0
0.5
1.0
1.5
2.0
t*
δ_ω
δ_P
δ_P/δ_ω

Figure 8

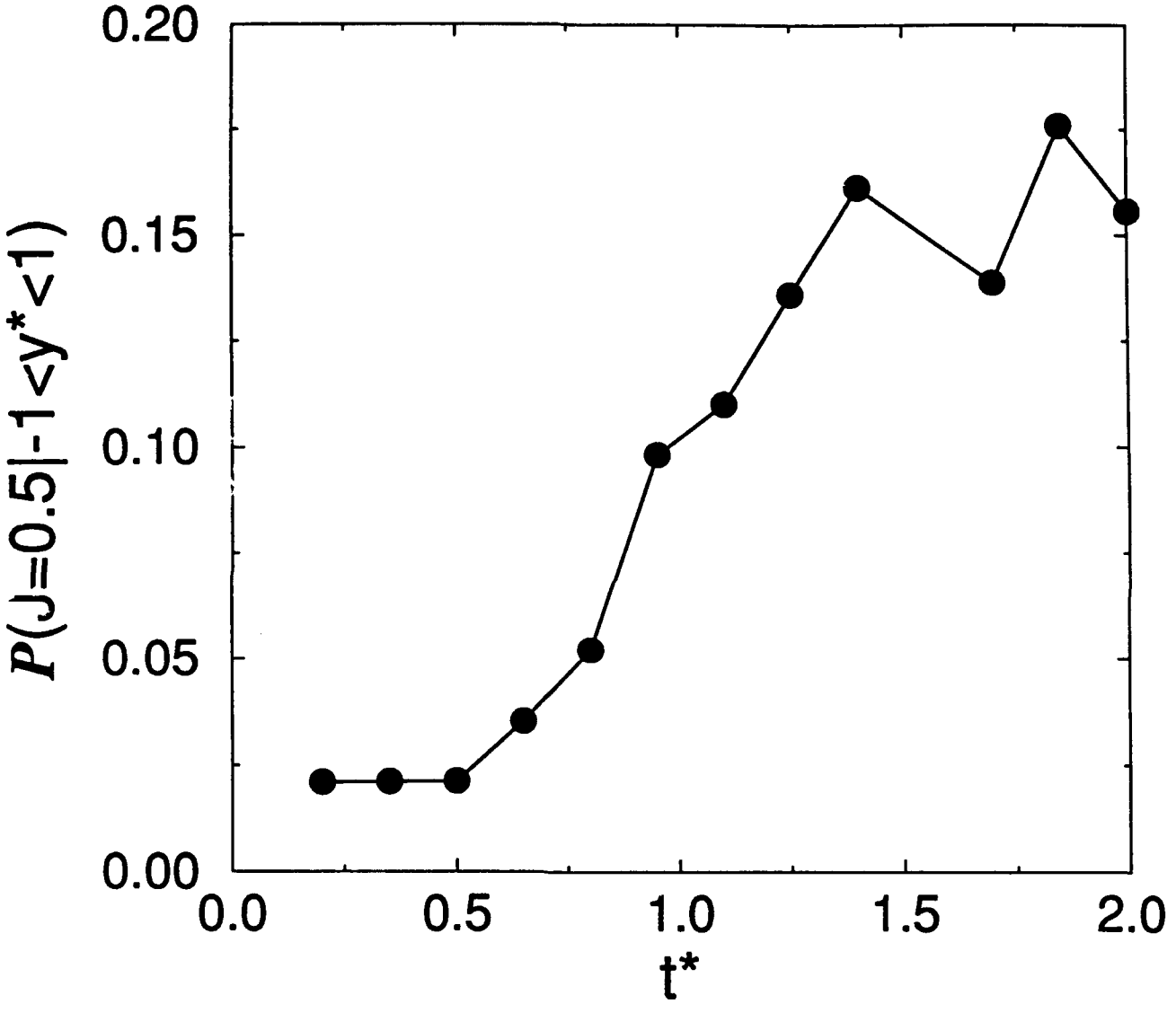

Figure 9

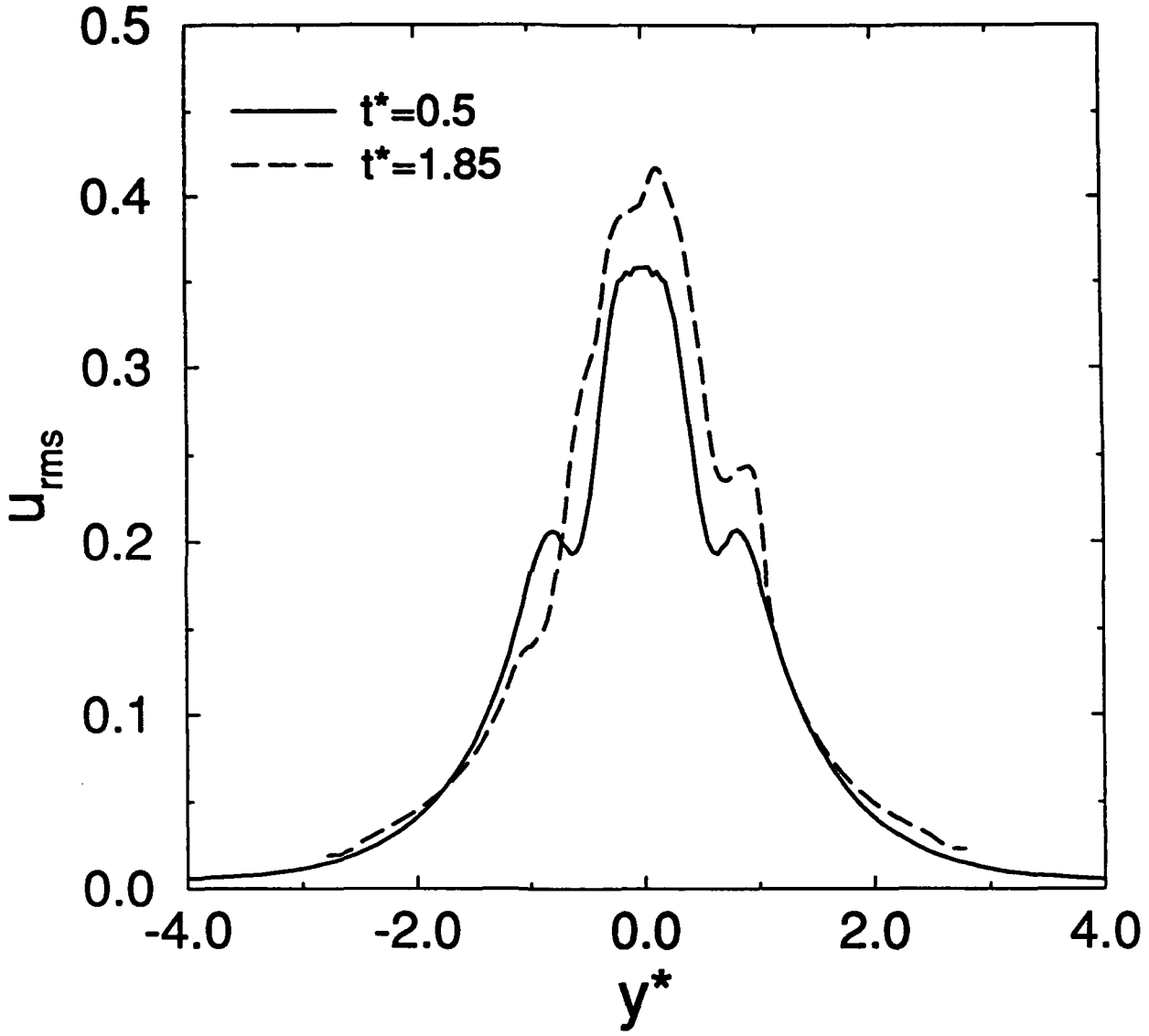

Figure 10(a)

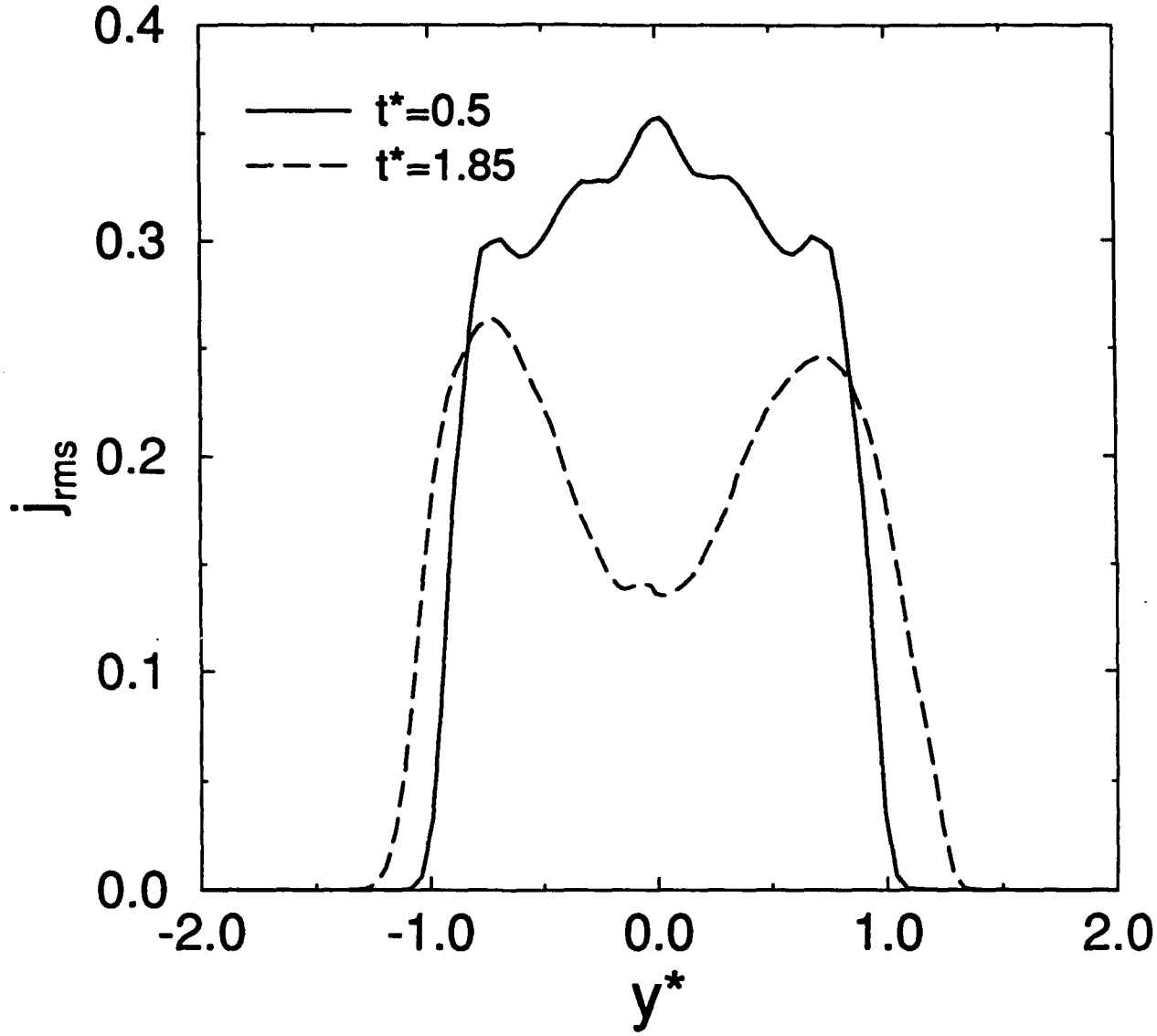

Figure 10(b)

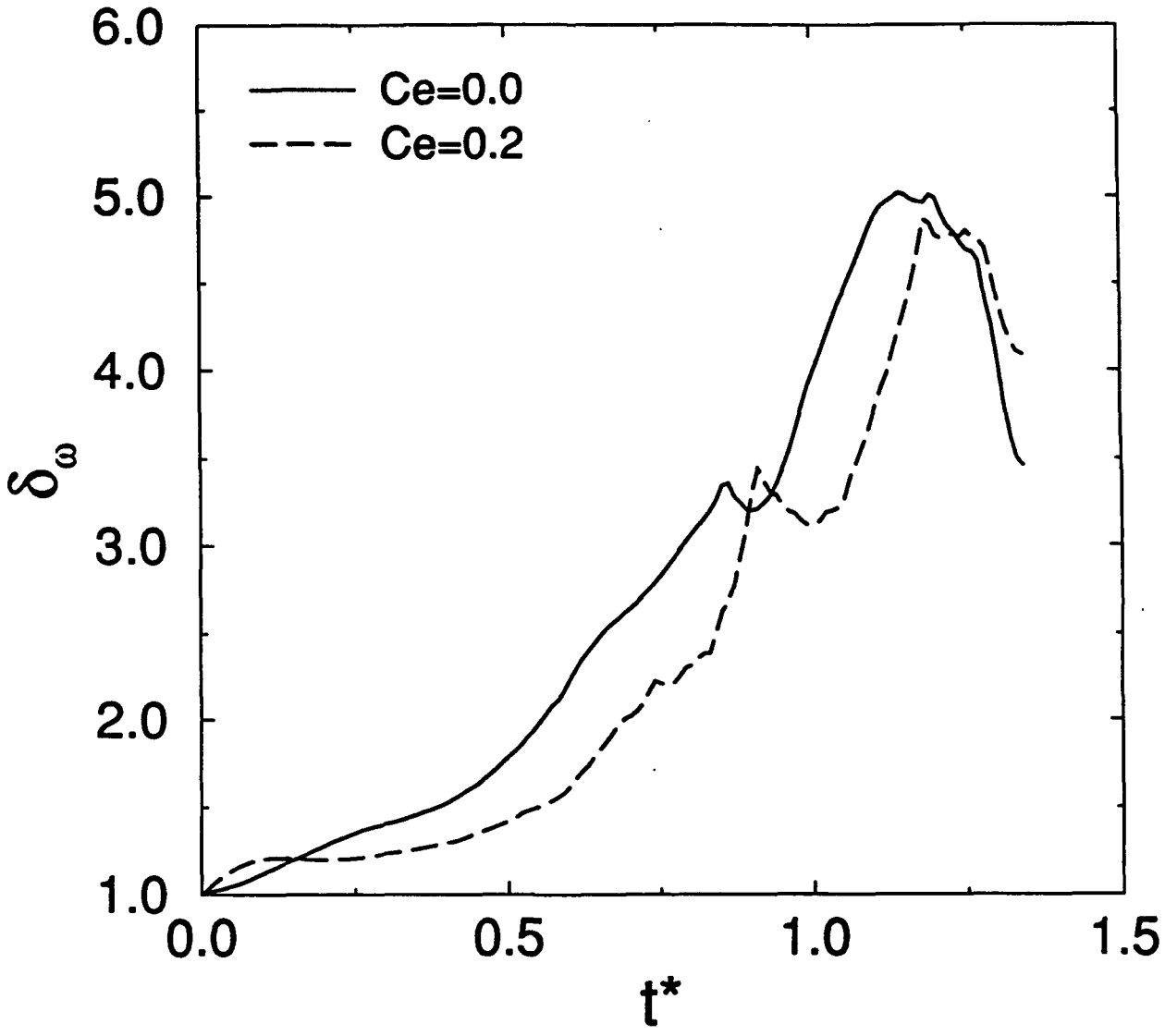

Figure 11

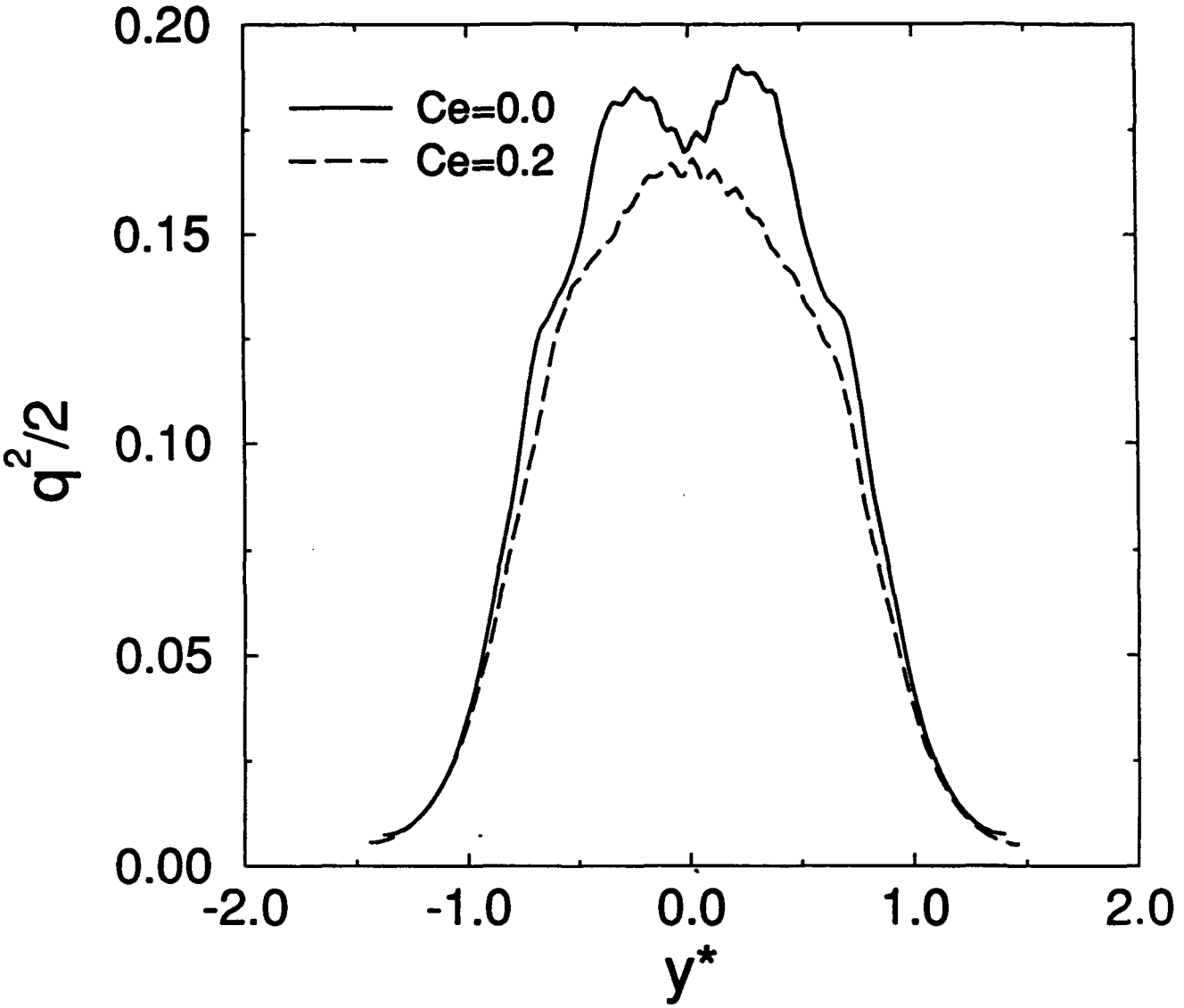

Figure 12

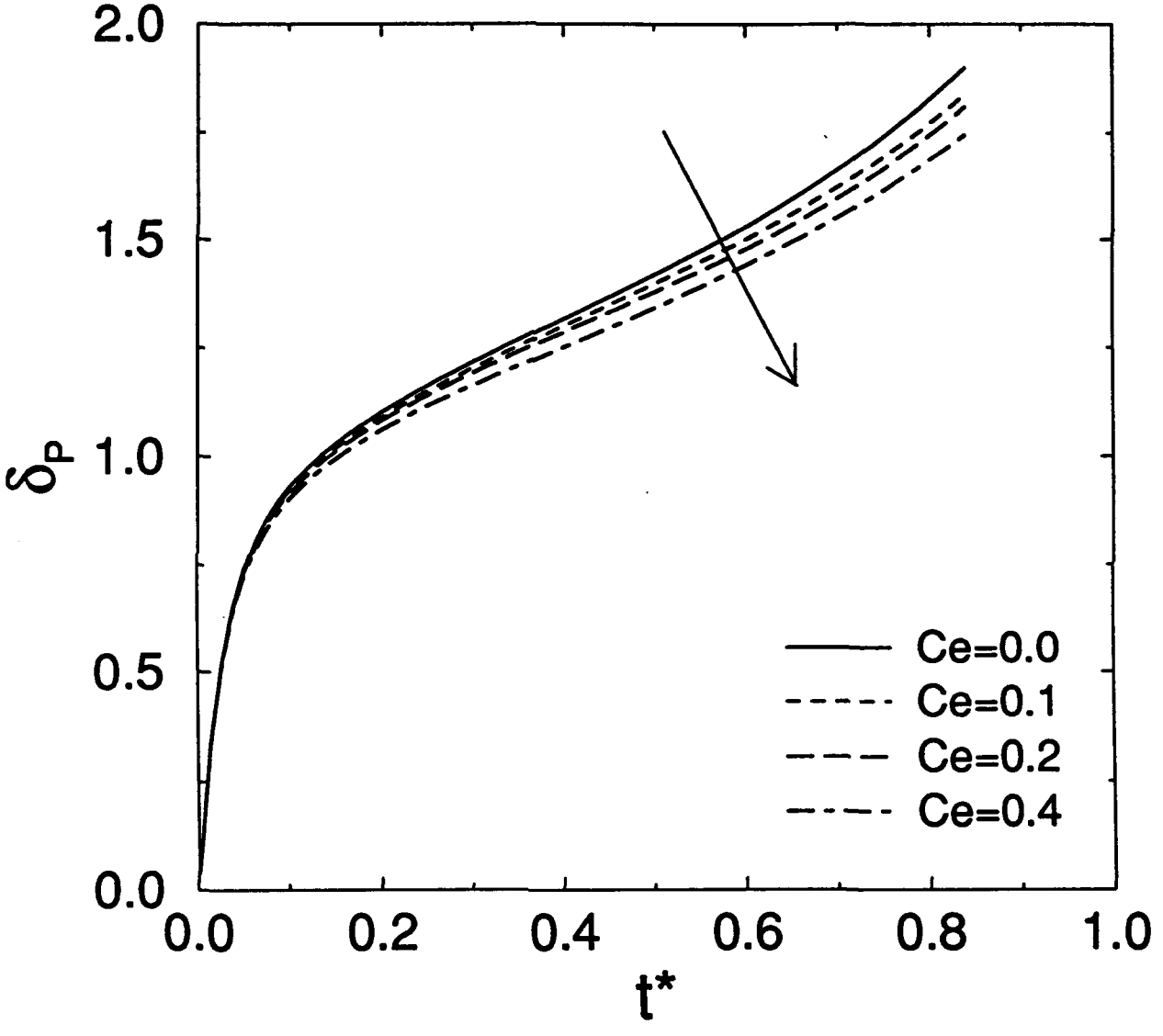

Figure 13 (a)

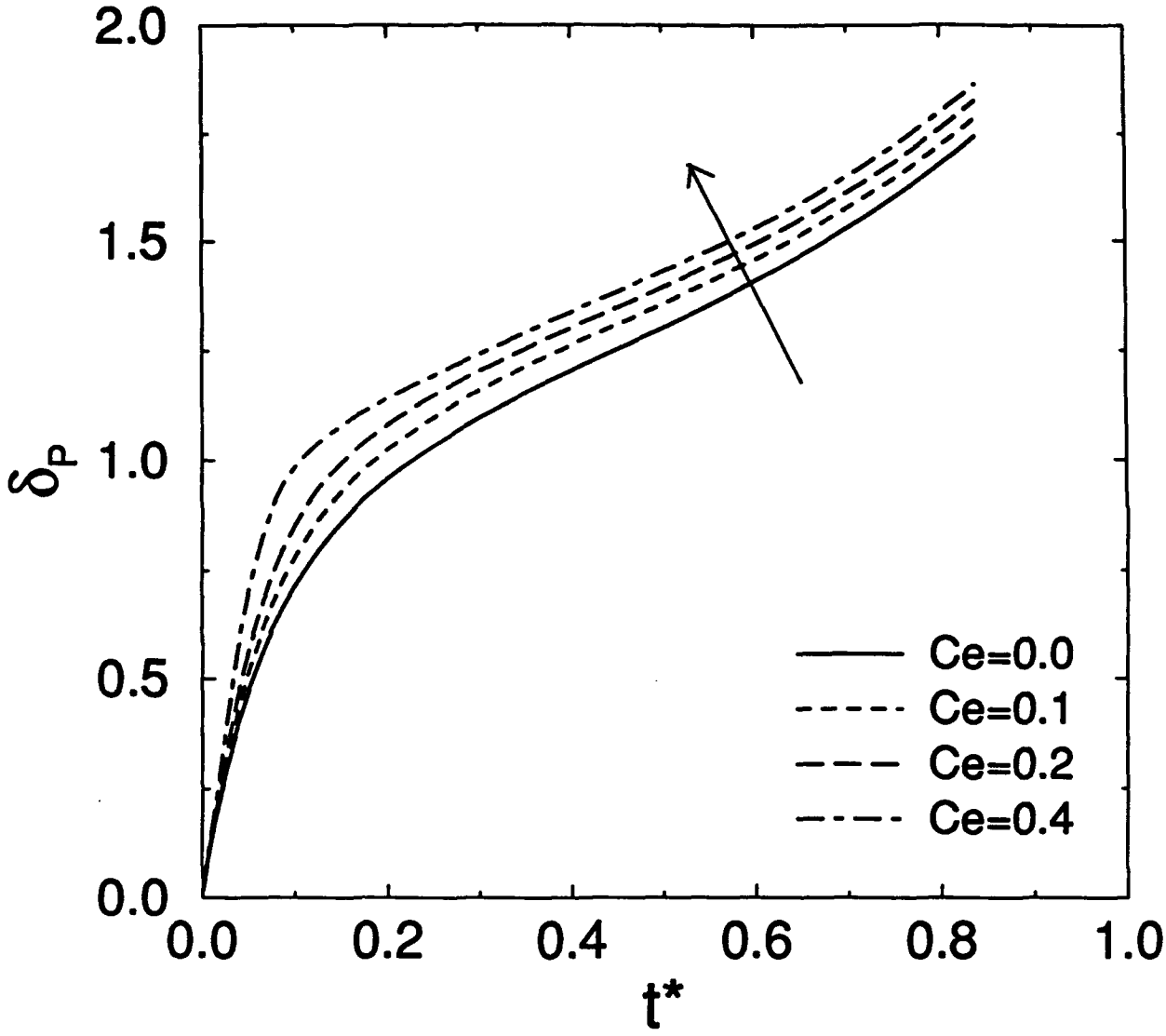

Figure 13(b)

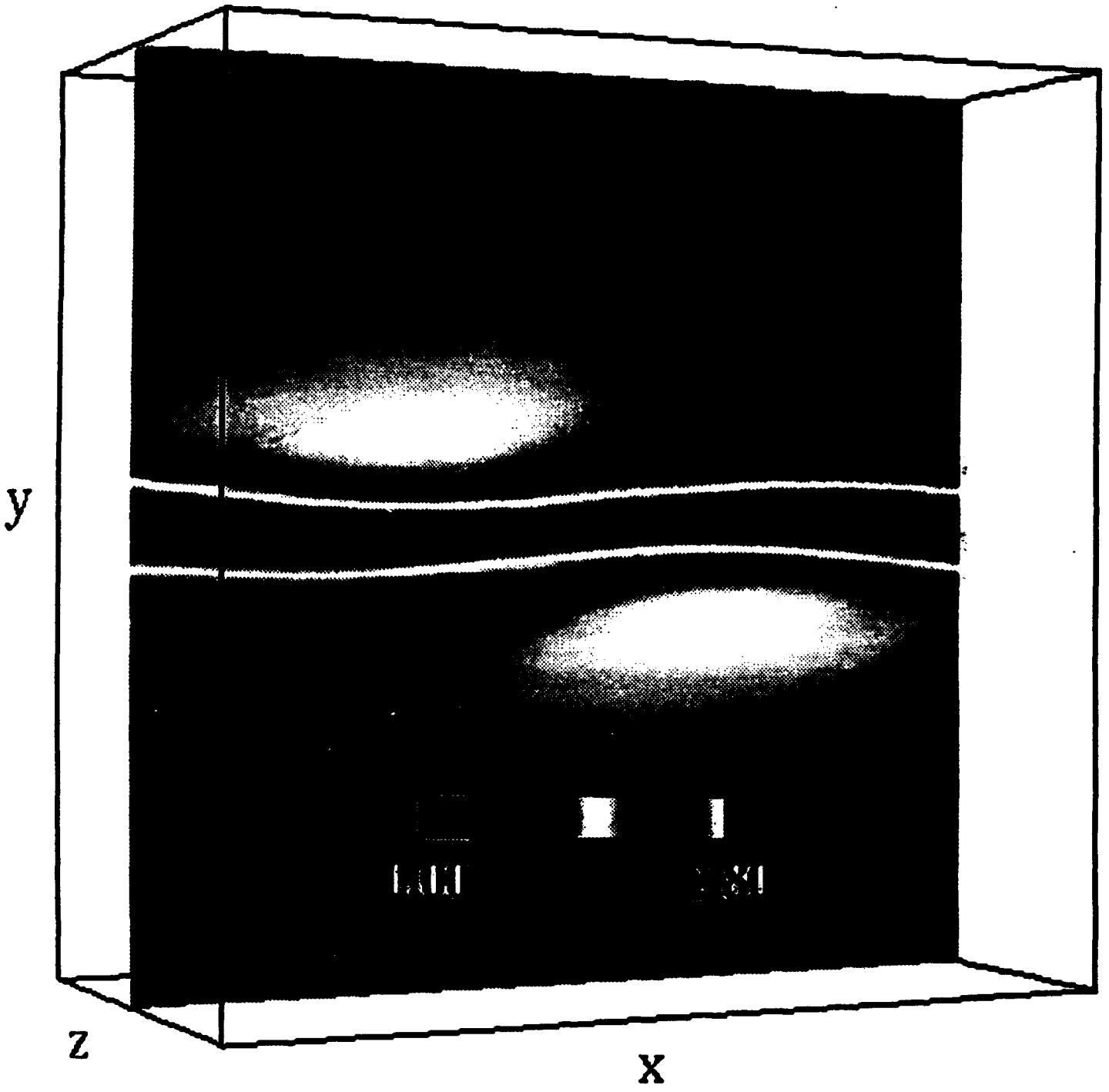

Figure 14

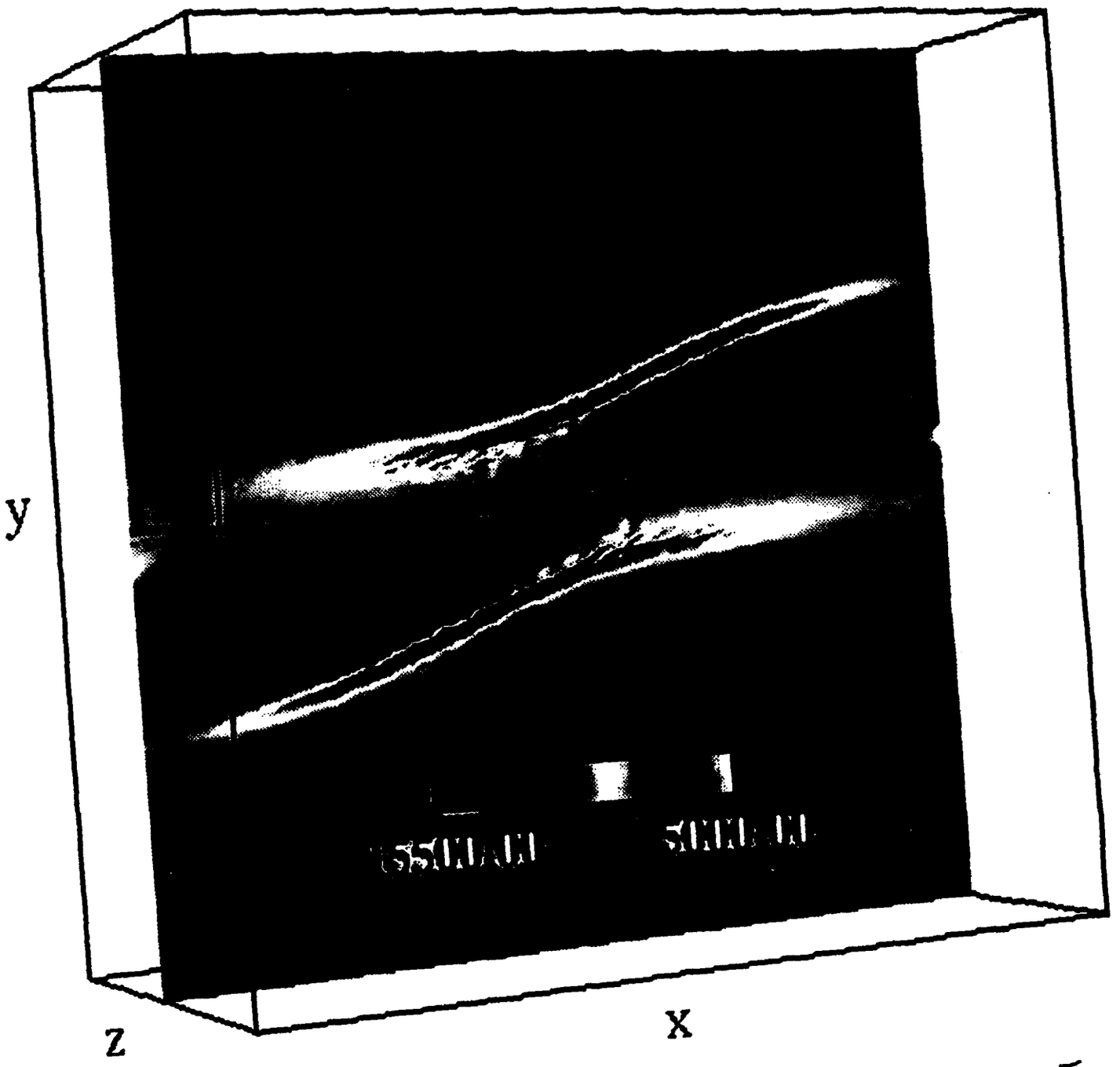

Figure 15

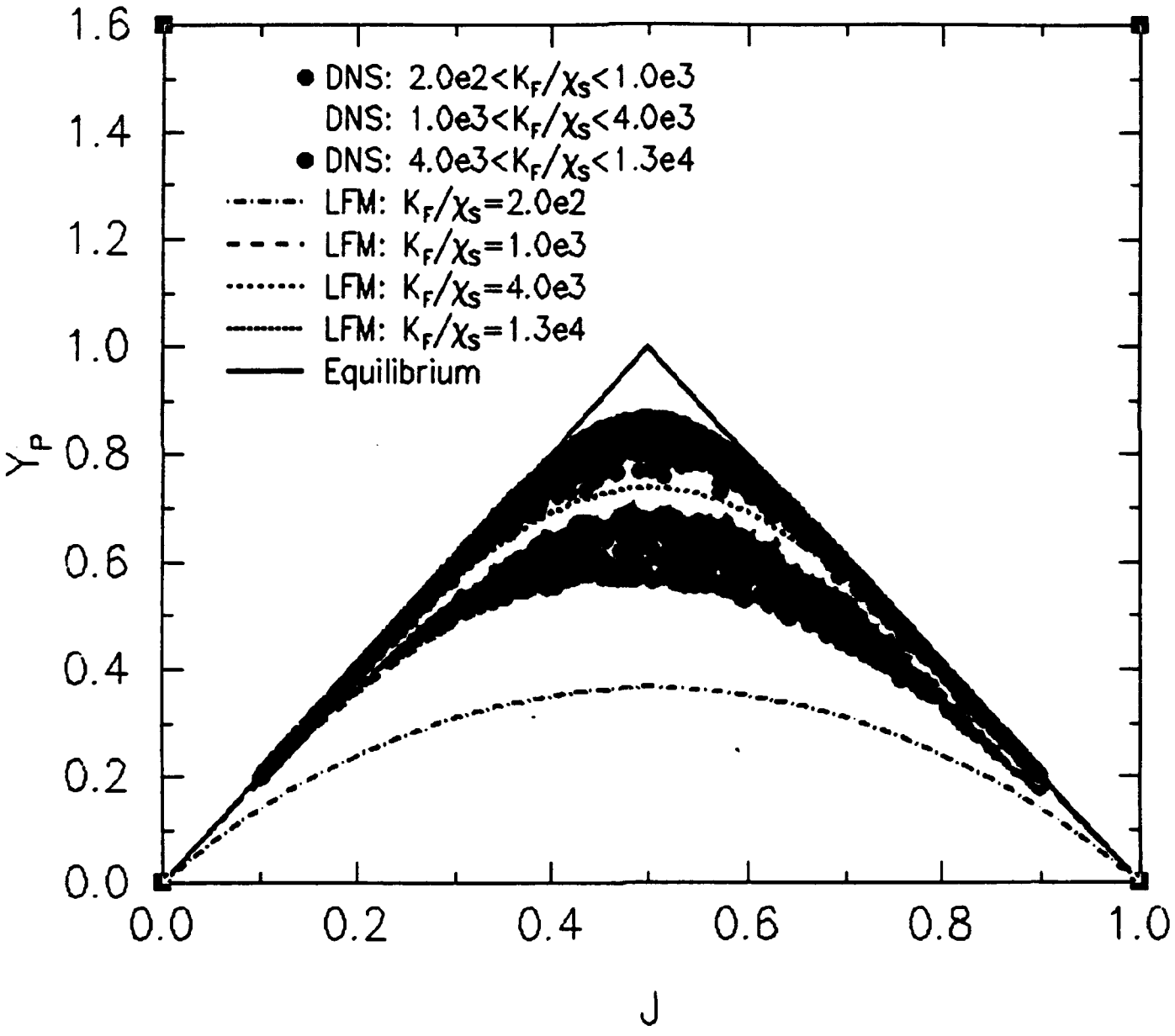
DNS: 2.0e2<K_F/χ_S<1.0e3
DNS: 1.0e3<K_F/χ_S<4.0e3
DNS: 4.0e3<K_F/χ_S<1.3e4
LFM: K_F/χ_S=2.0e2
LFM: K_F/χ_S=1.0e3
LFM: K_F/χ_S=4.0e3
LFM: K_F/χ_S=1.3e4
Equilibrium
Y_P
J
0.0
0.2
0.4
0.6
0.8
1.0
1.2
1.4
1.6

Figure 16

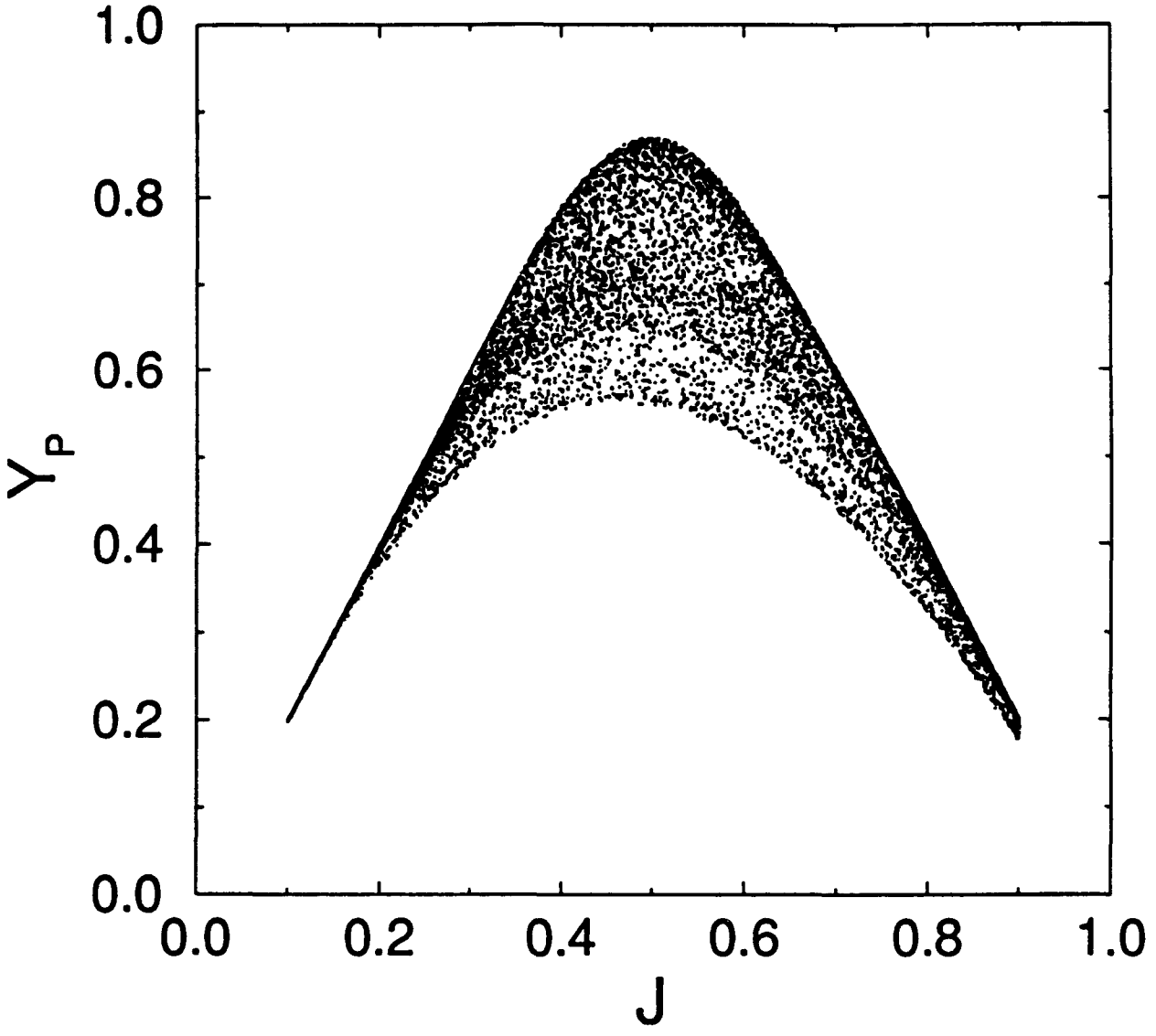

Figure 17(a)

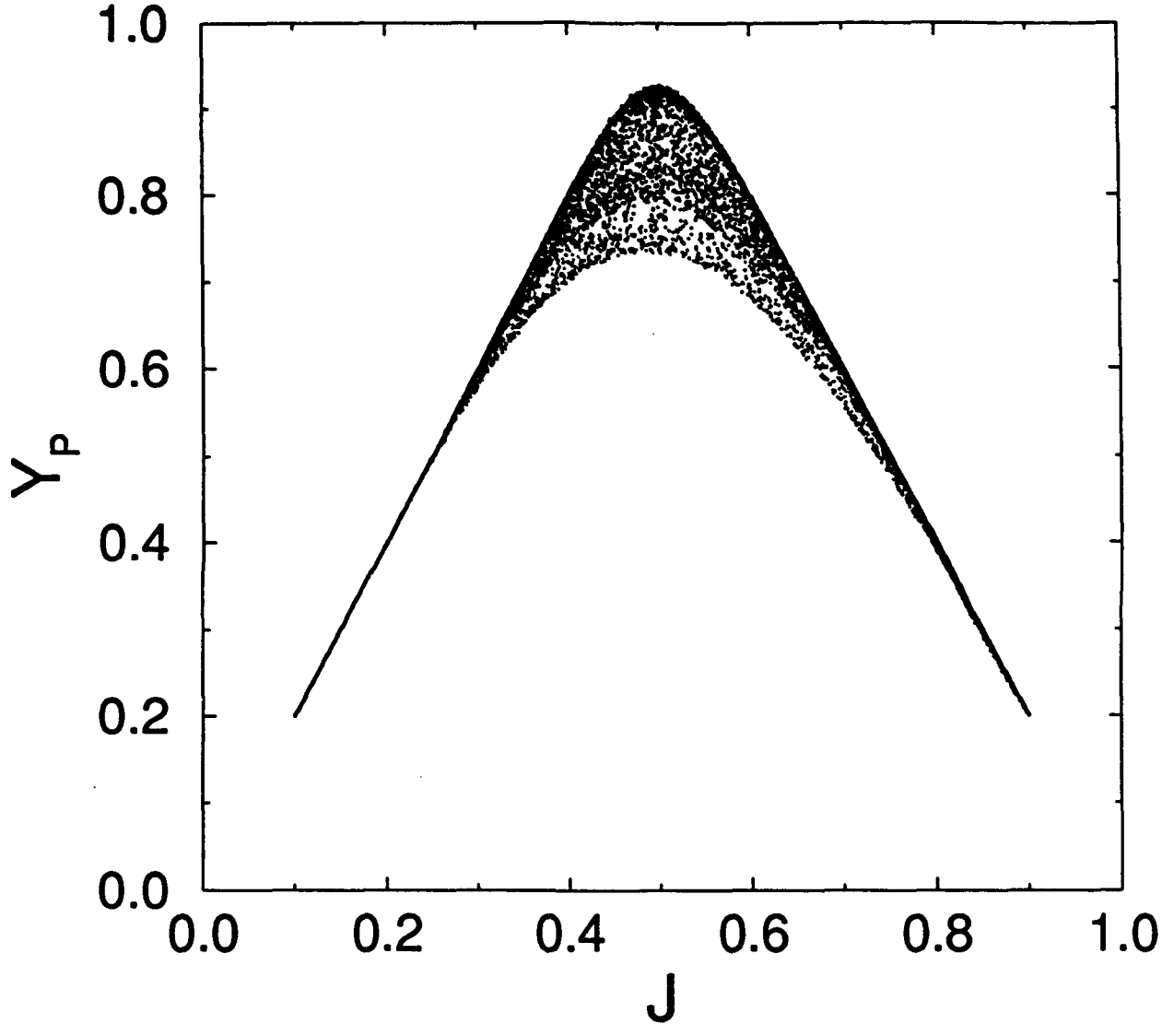

Figure 17(b)

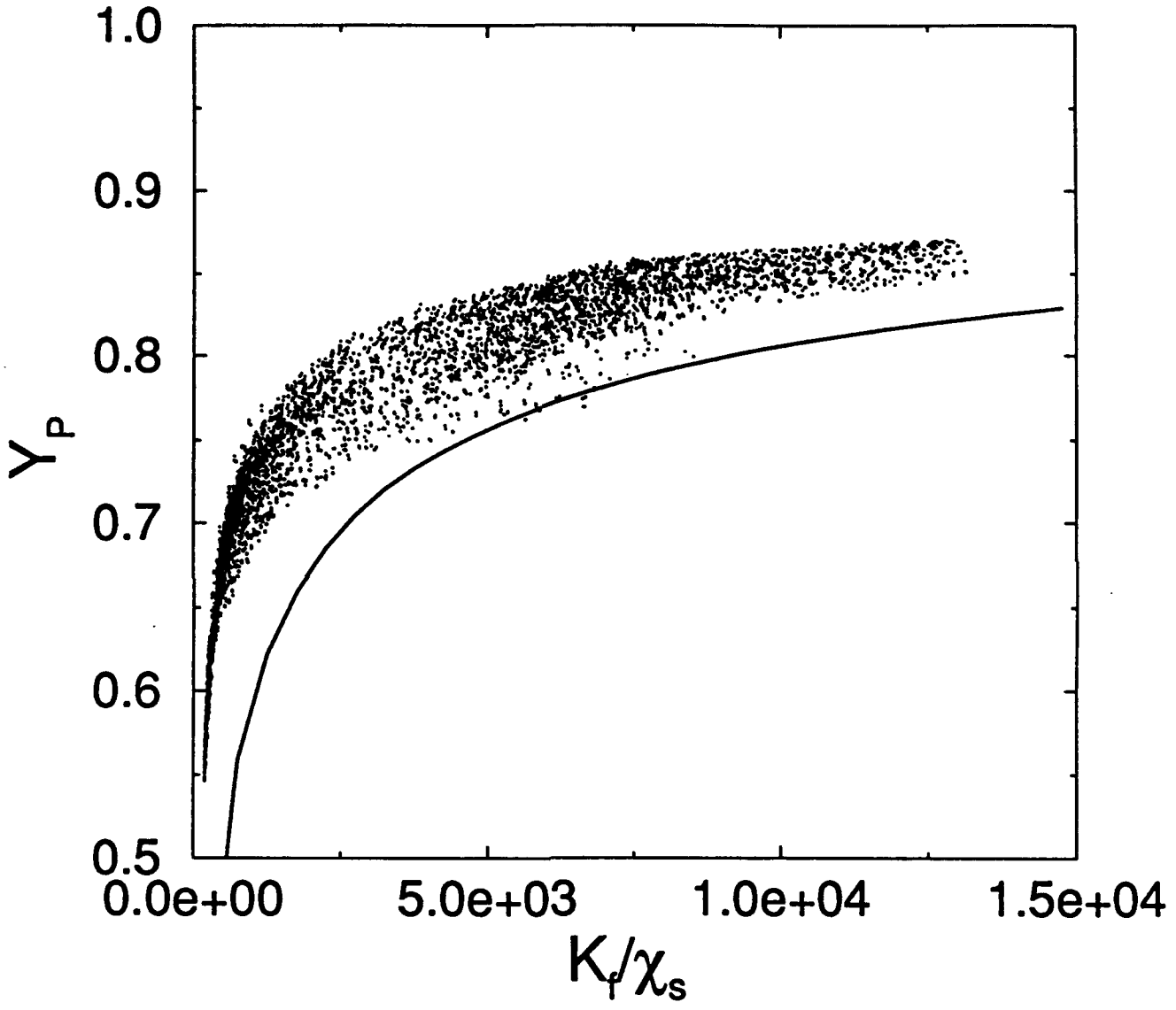

Figure 18(a)

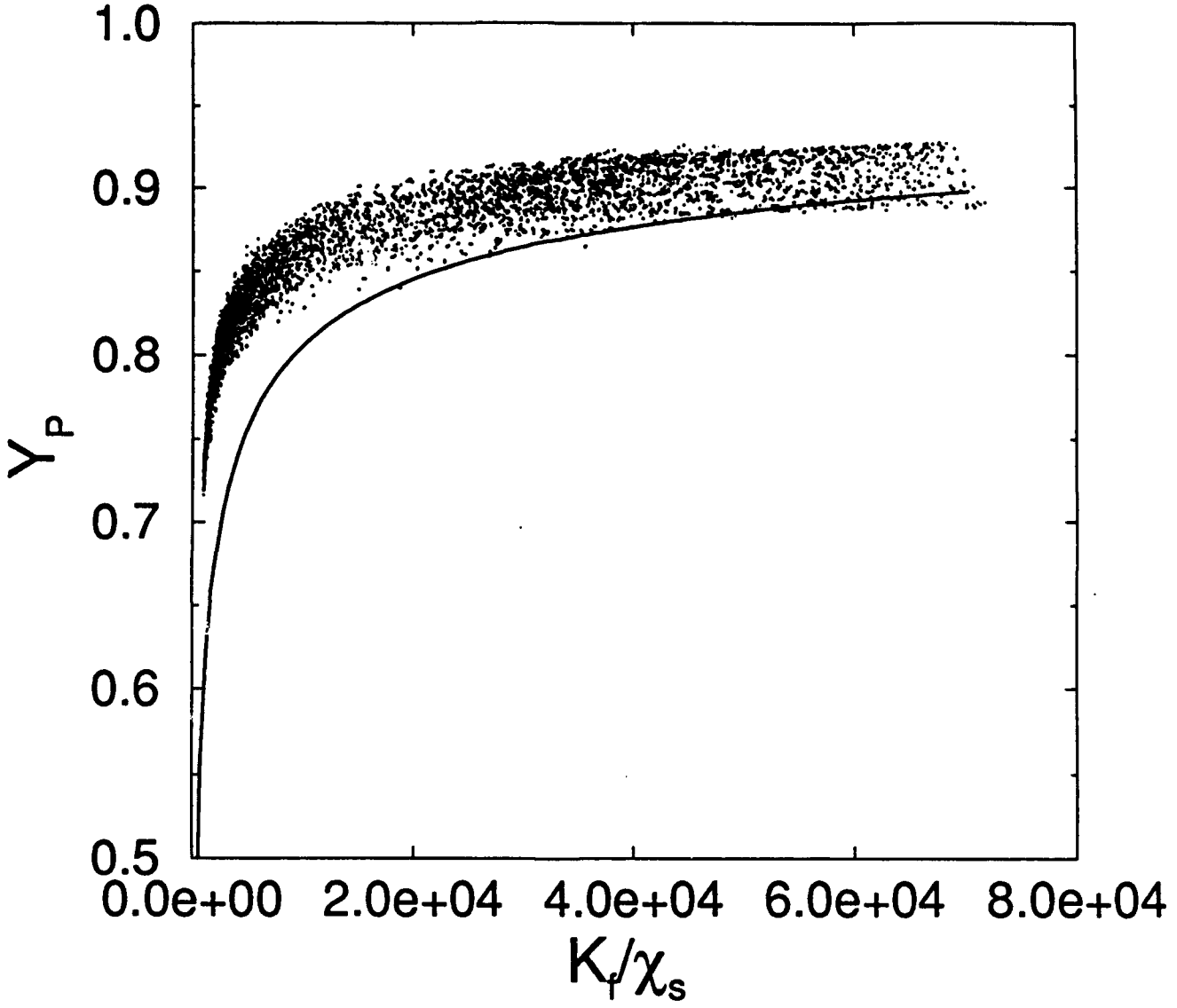

Figure 18(b)

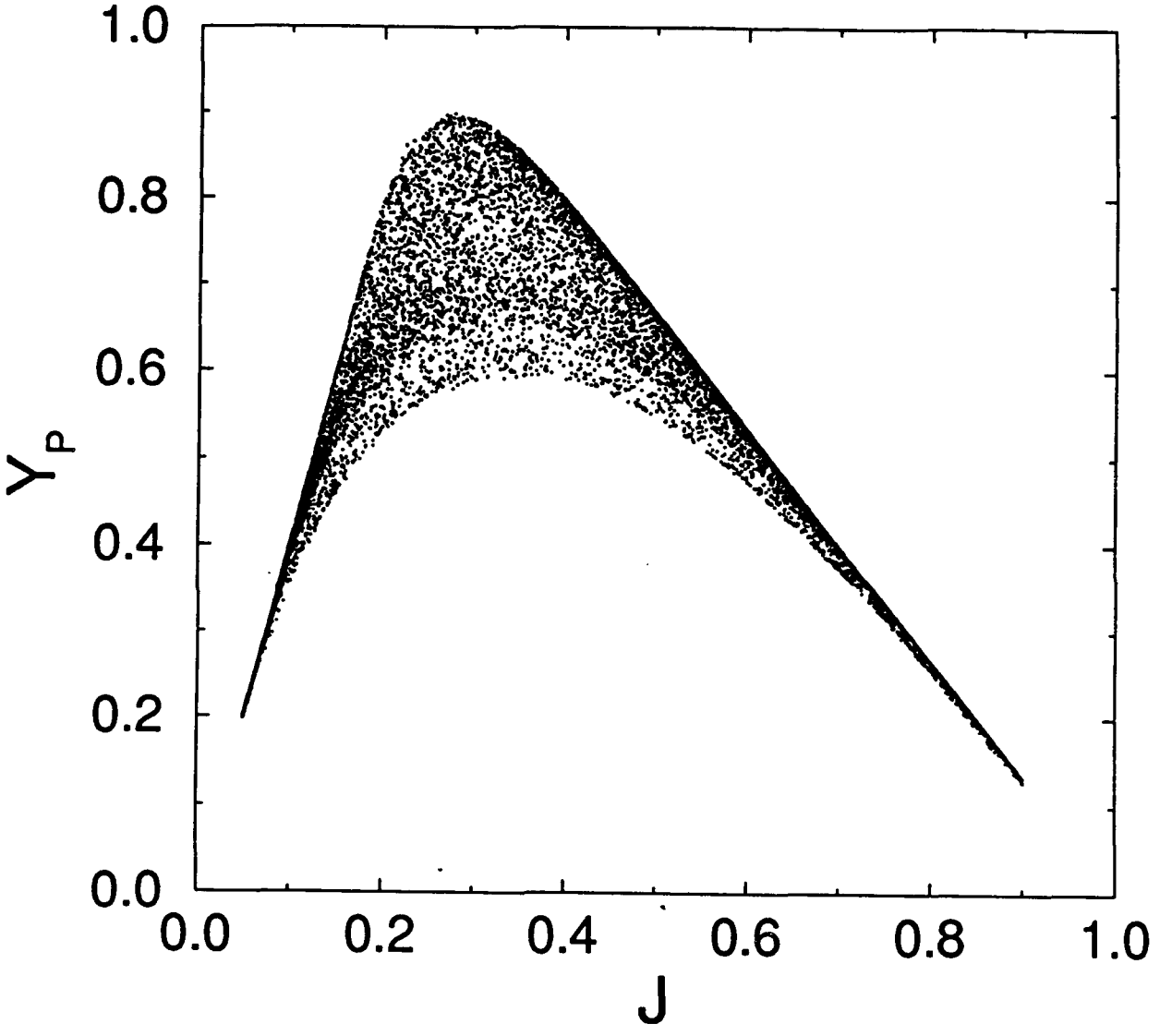

Figure 19

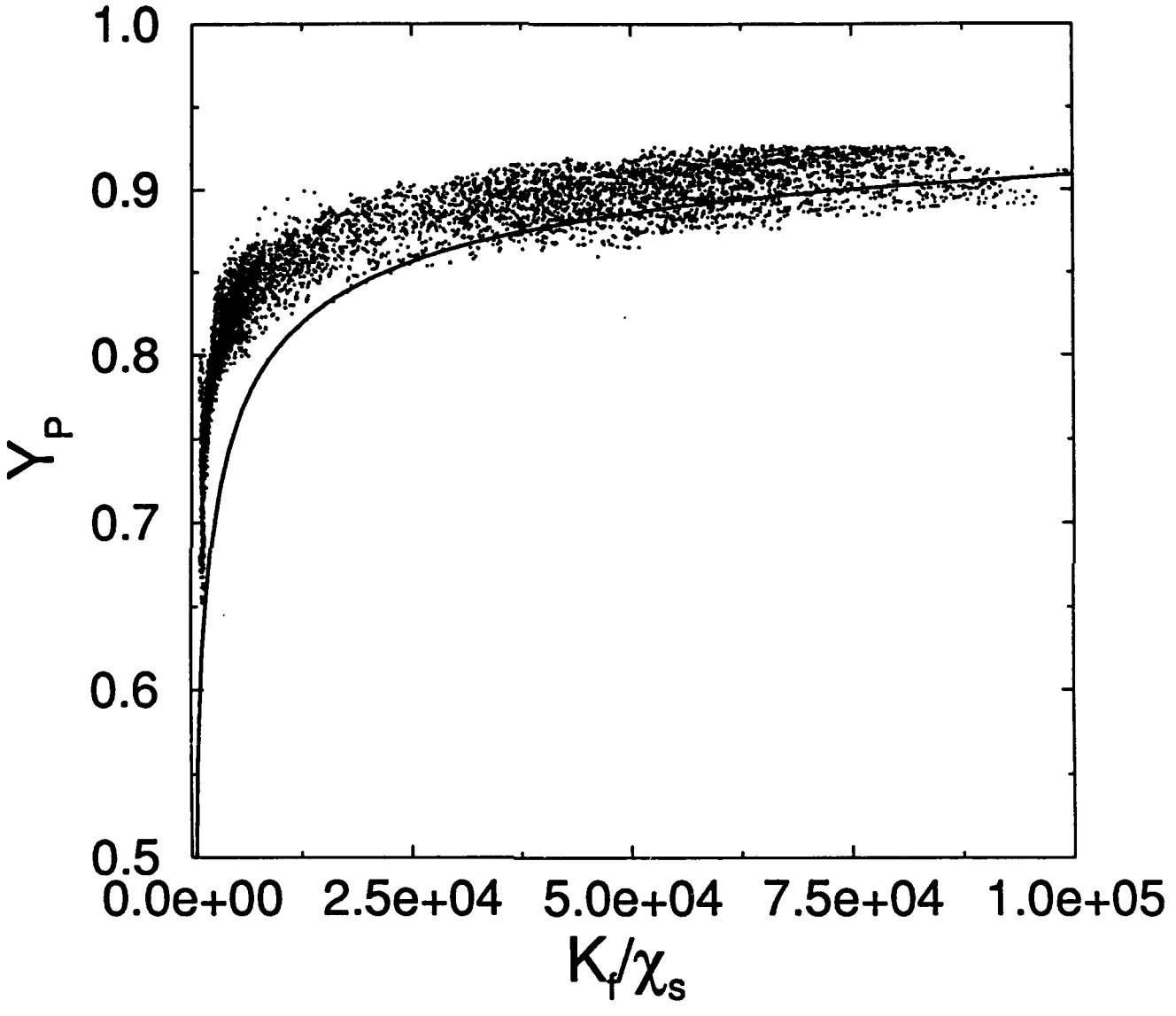

Figure 20

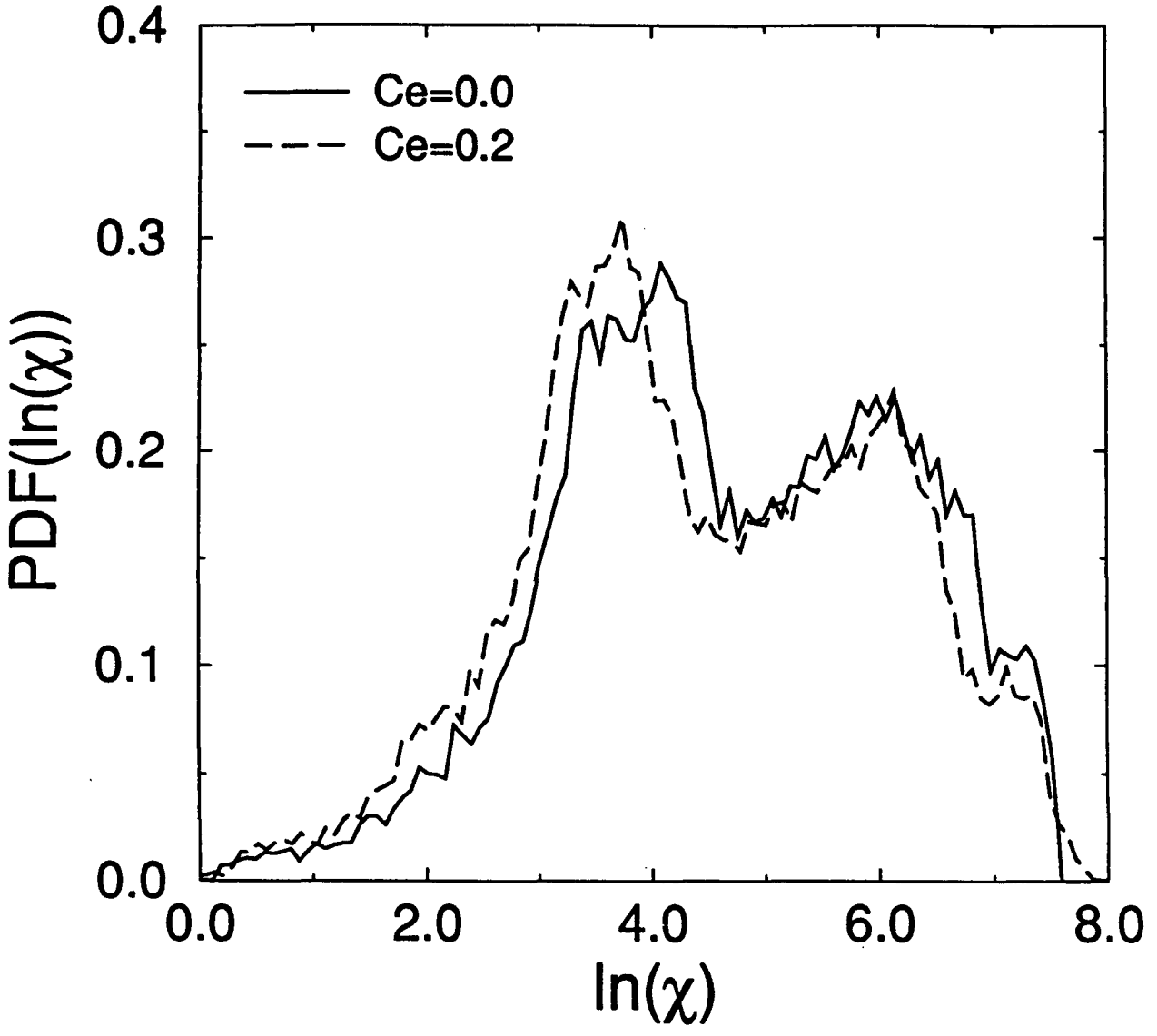

Figure 21

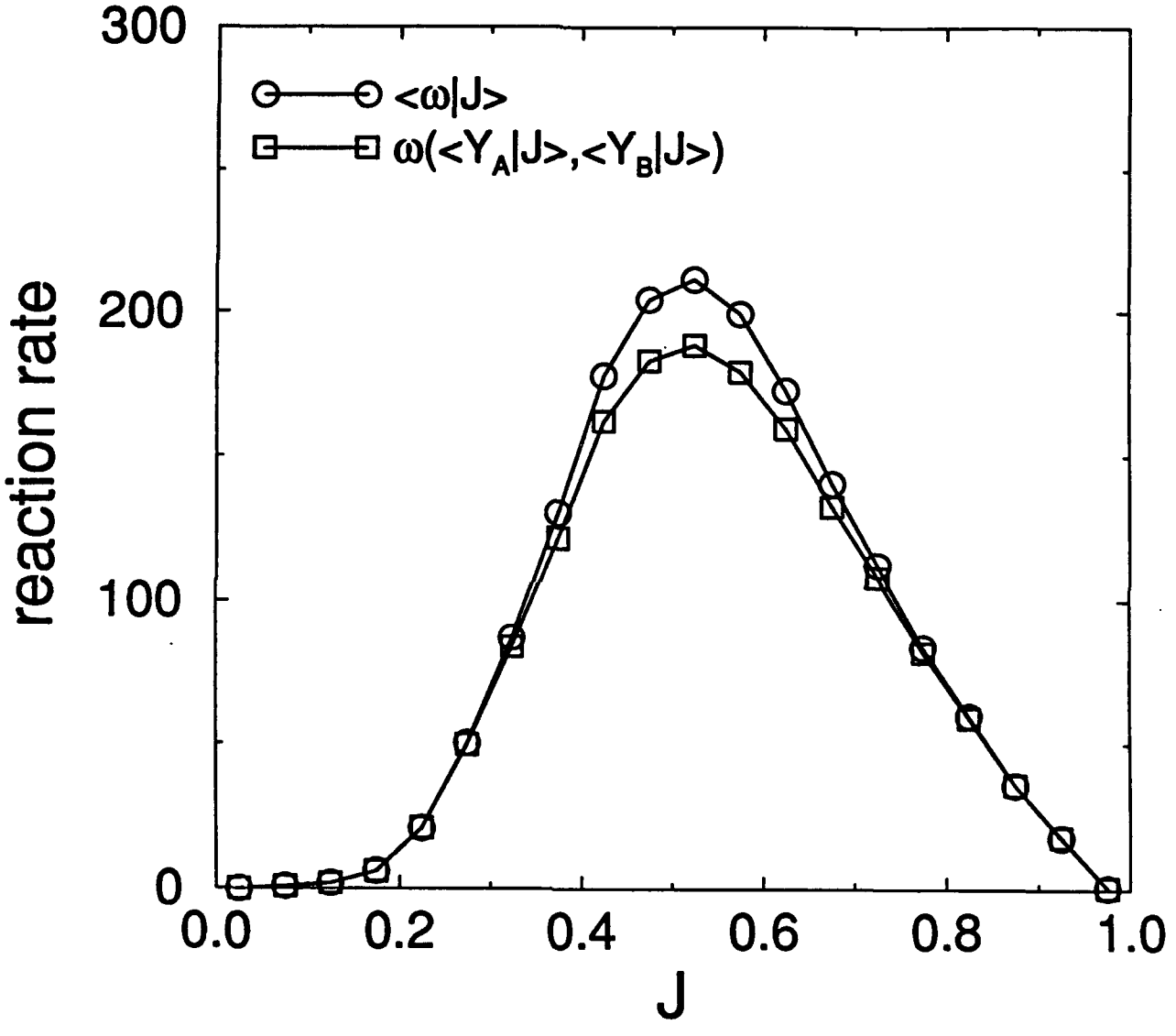

Figure 22(a)

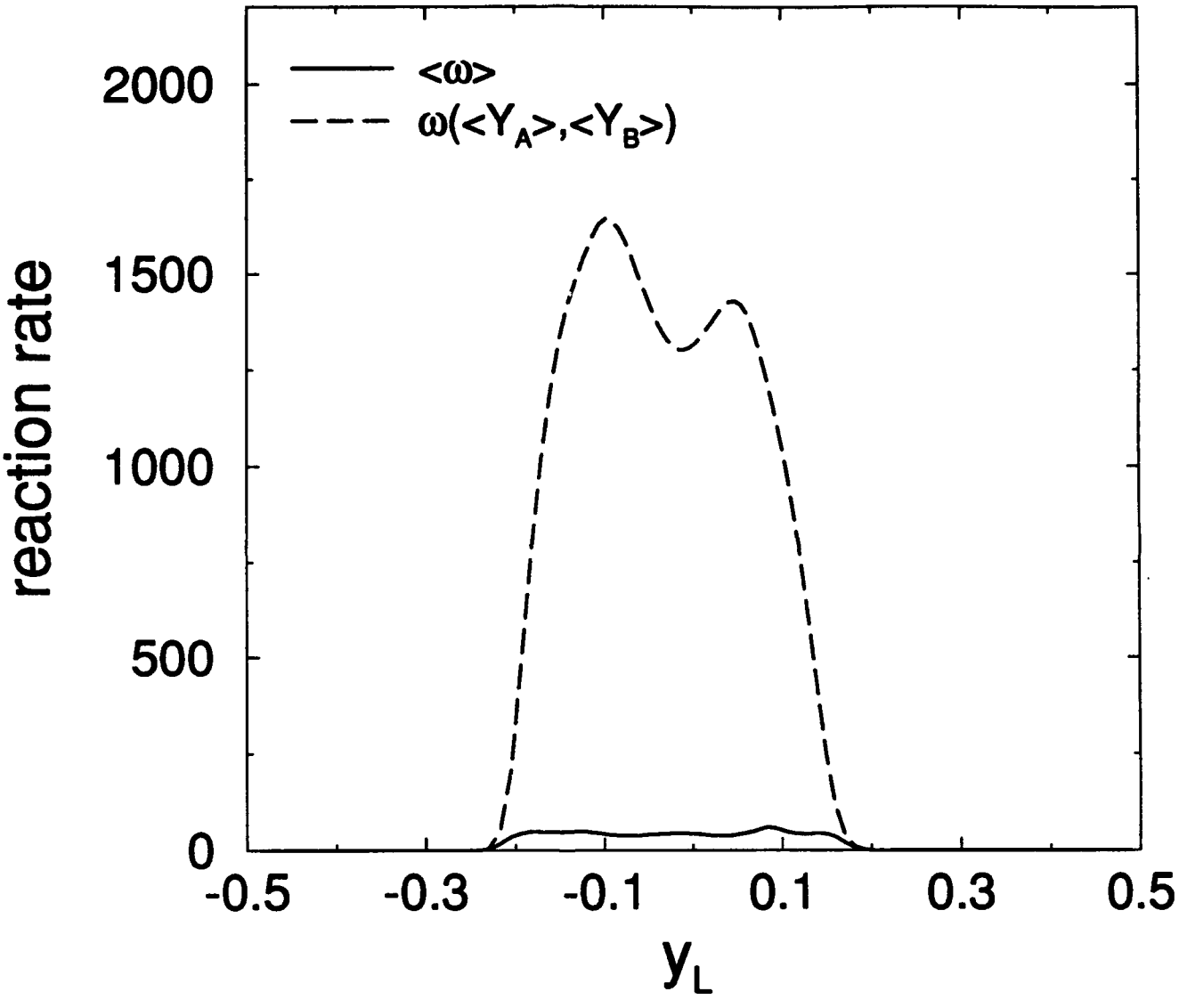

Figure 22(b)

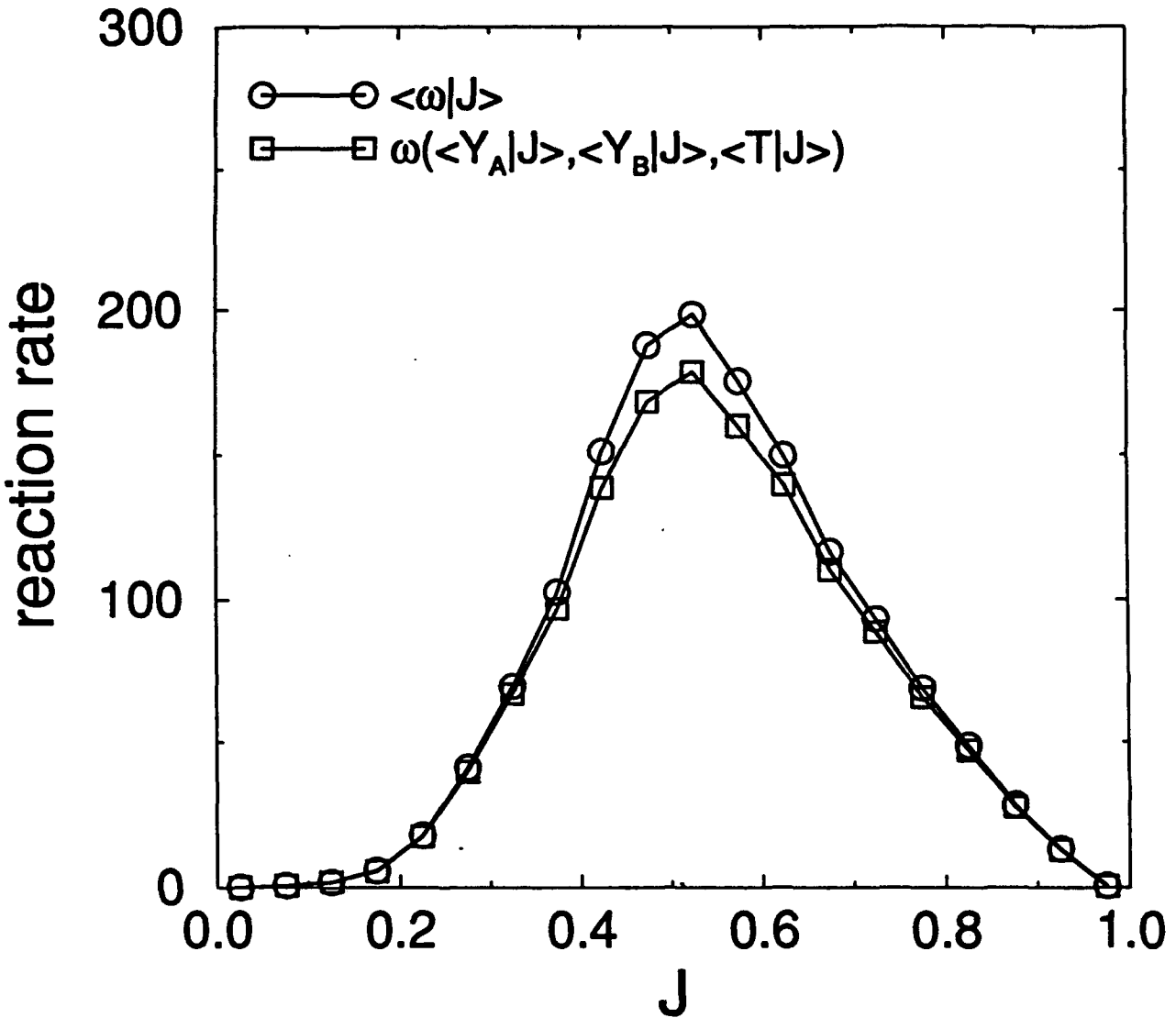

Figure 23

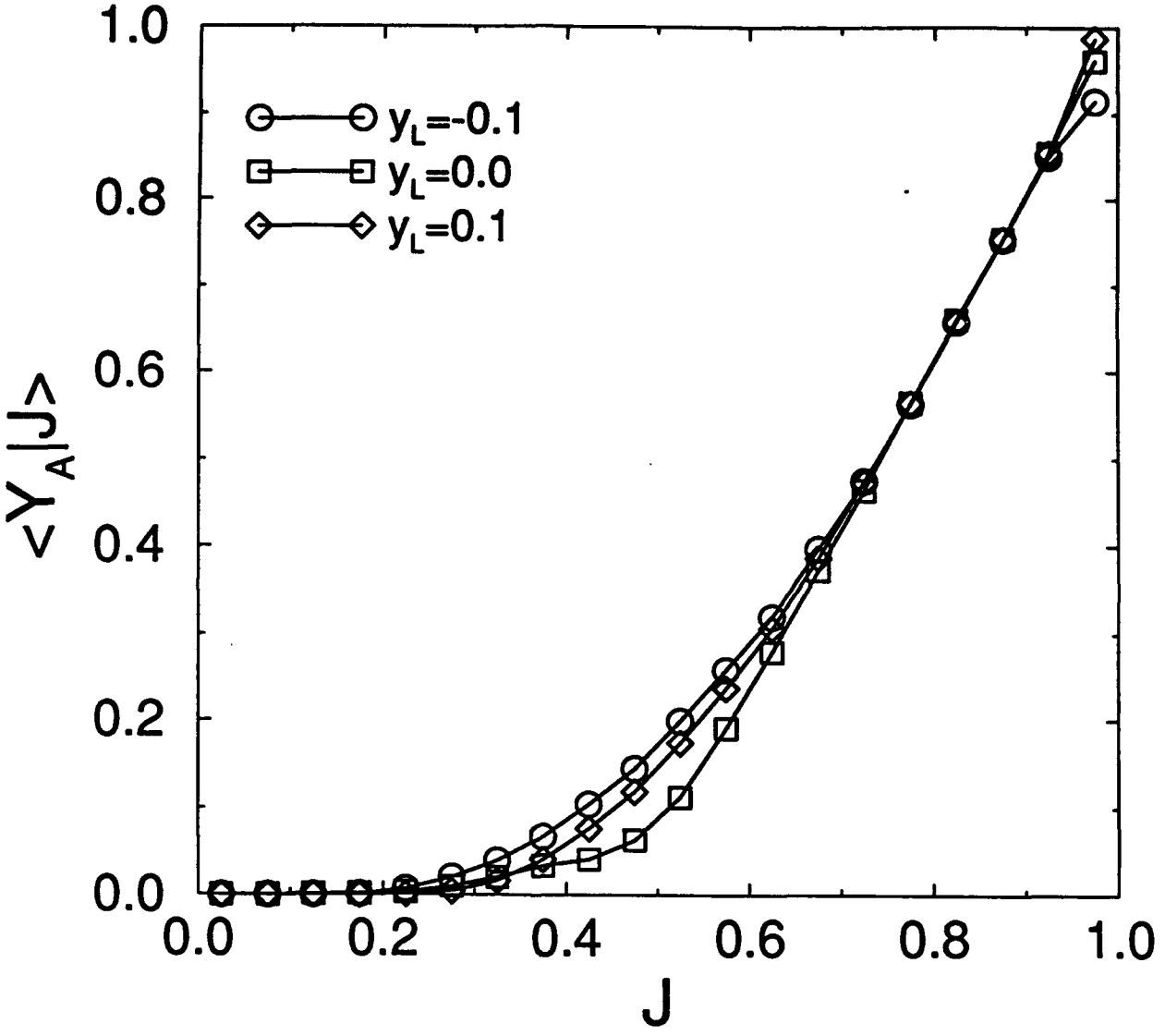

Figure 24(a)

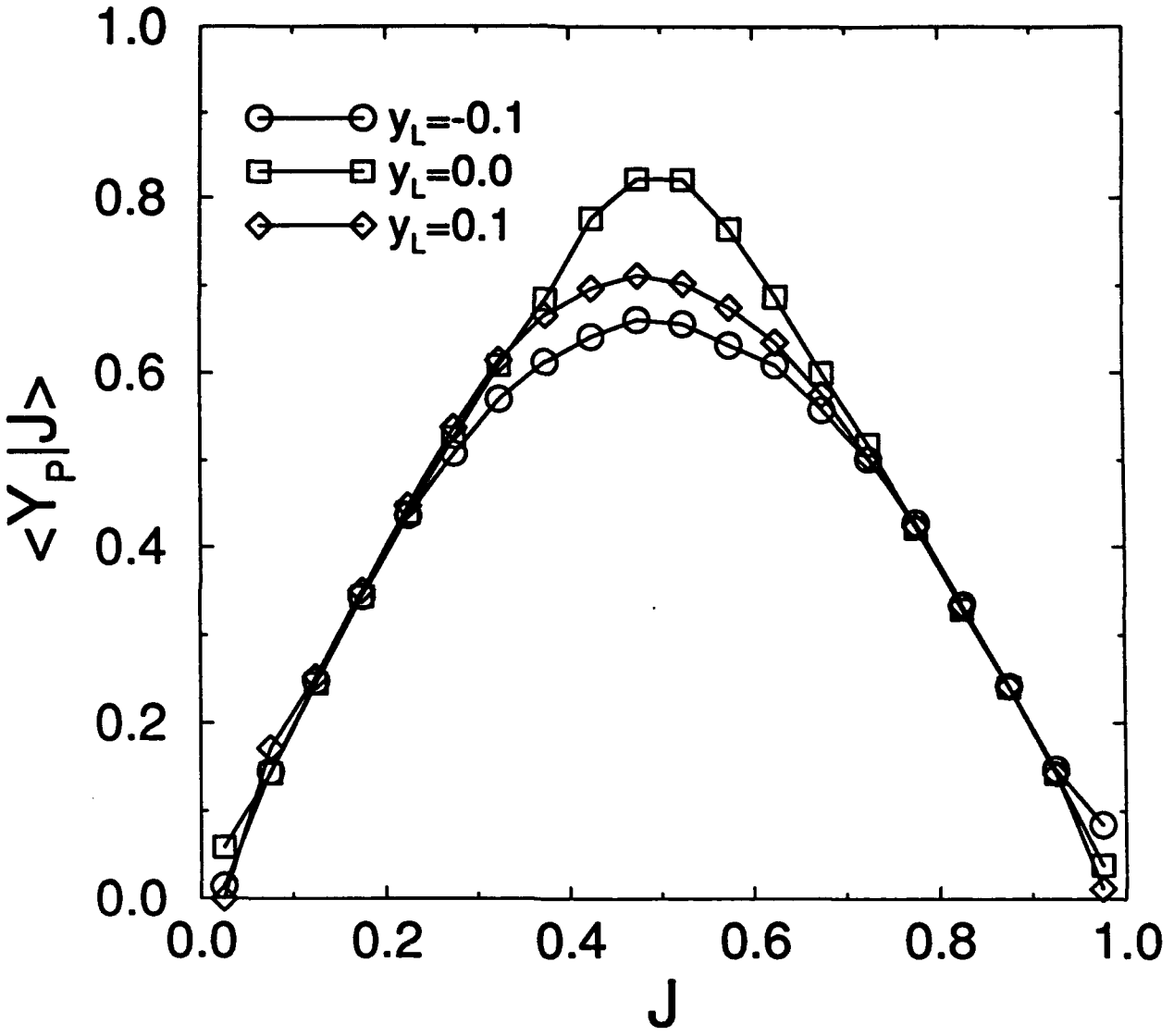

Figure 24(b)

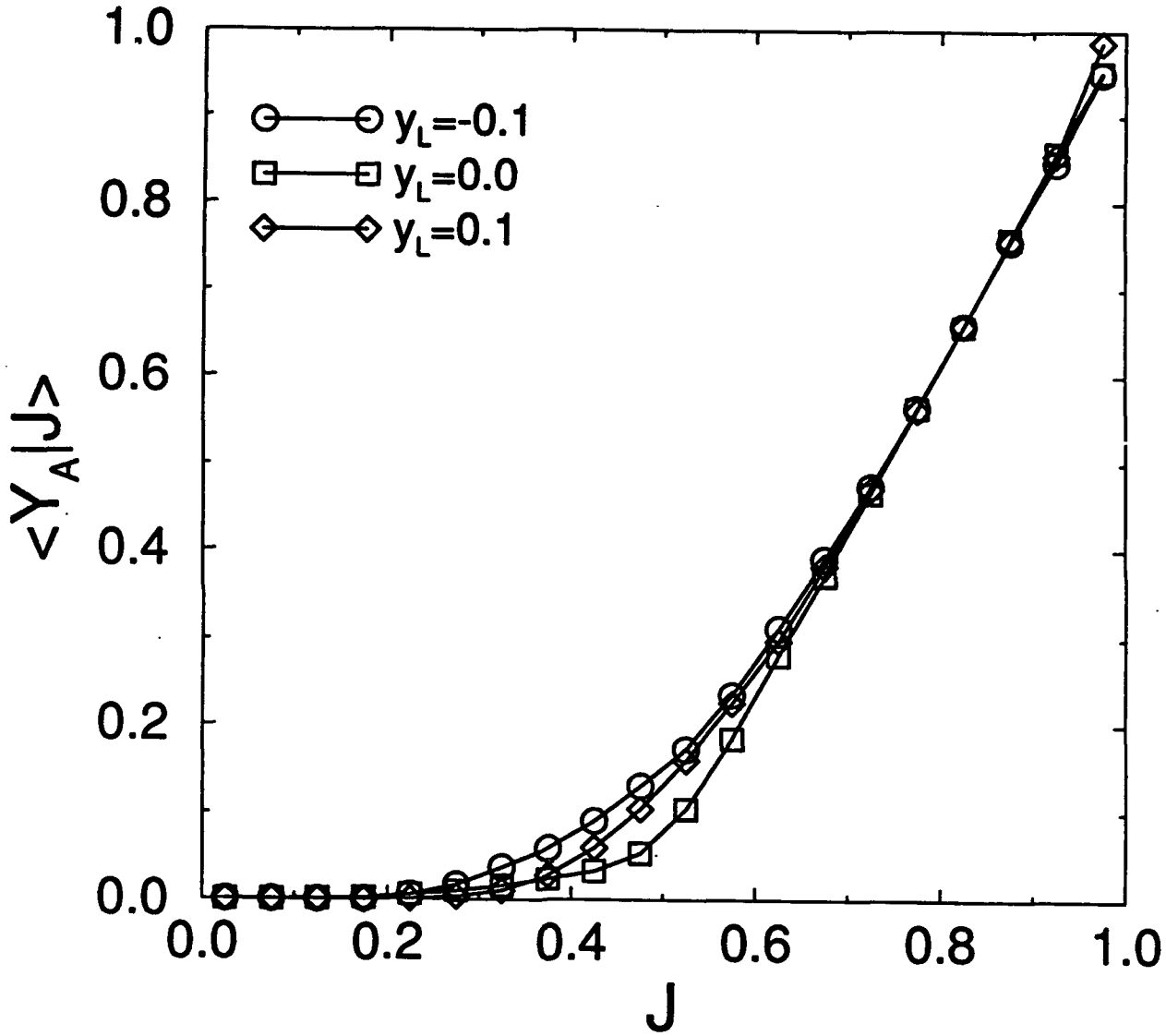

Figure 25(a)

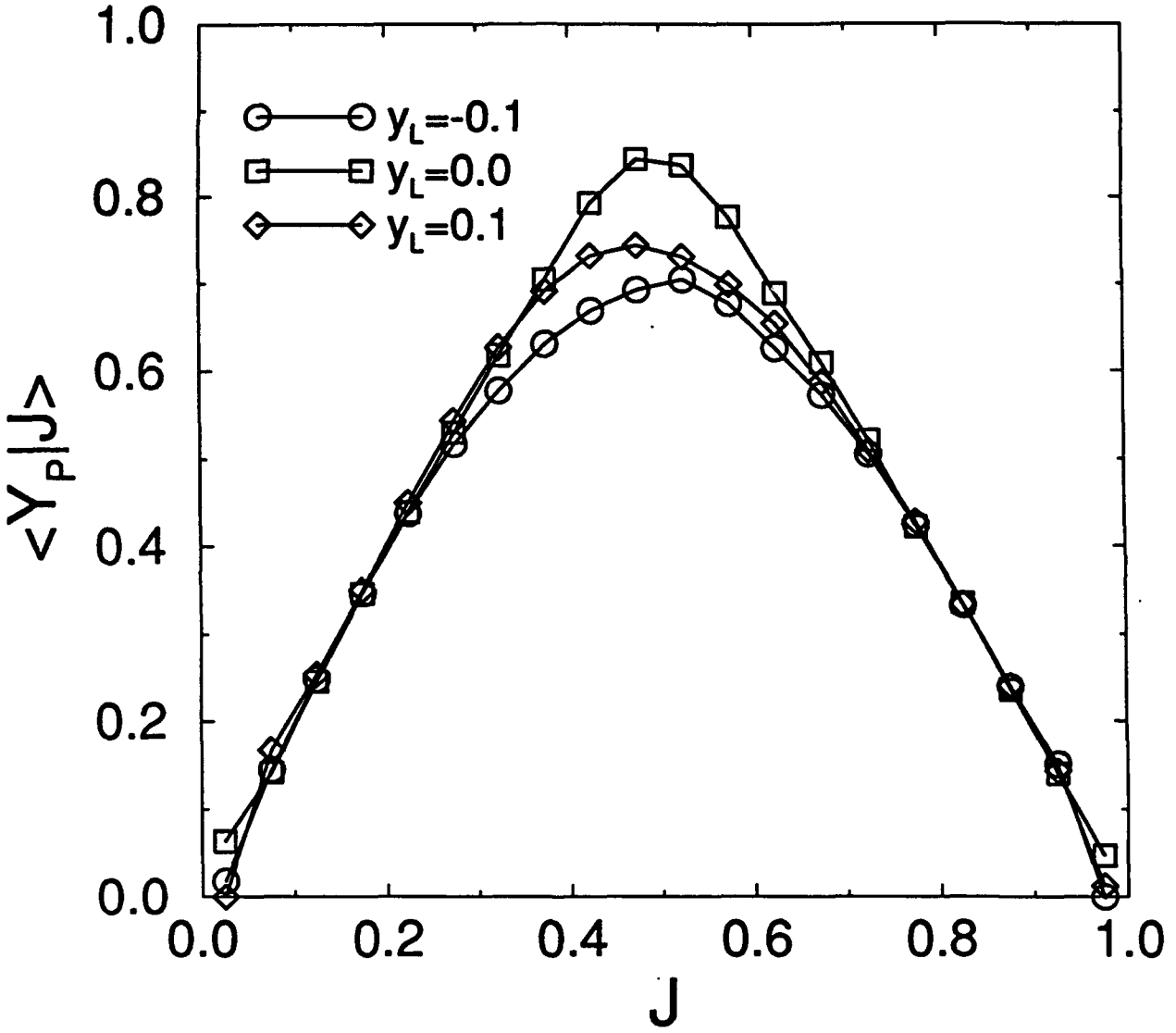

Figure 25(b)

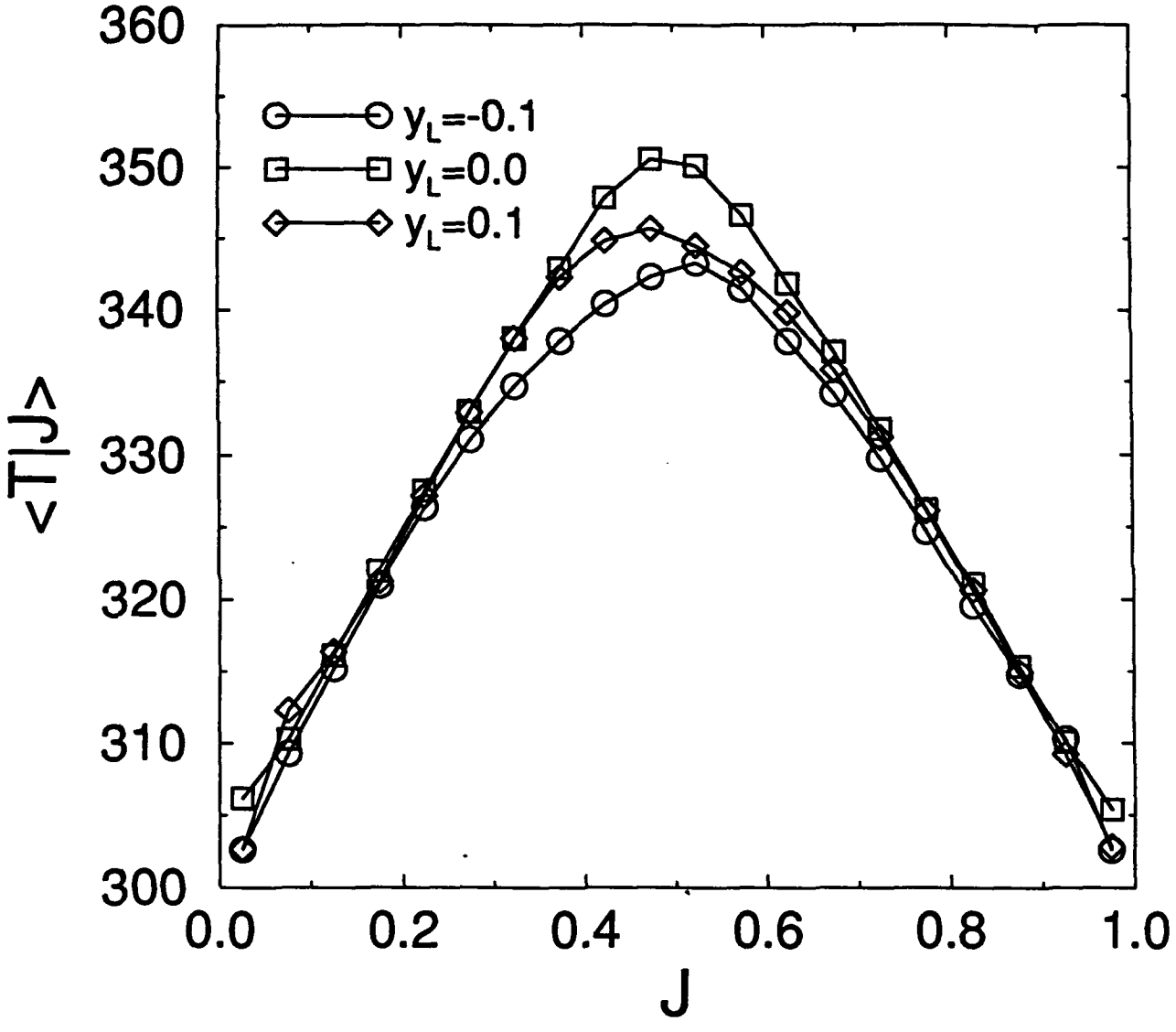

Figure 25(c)

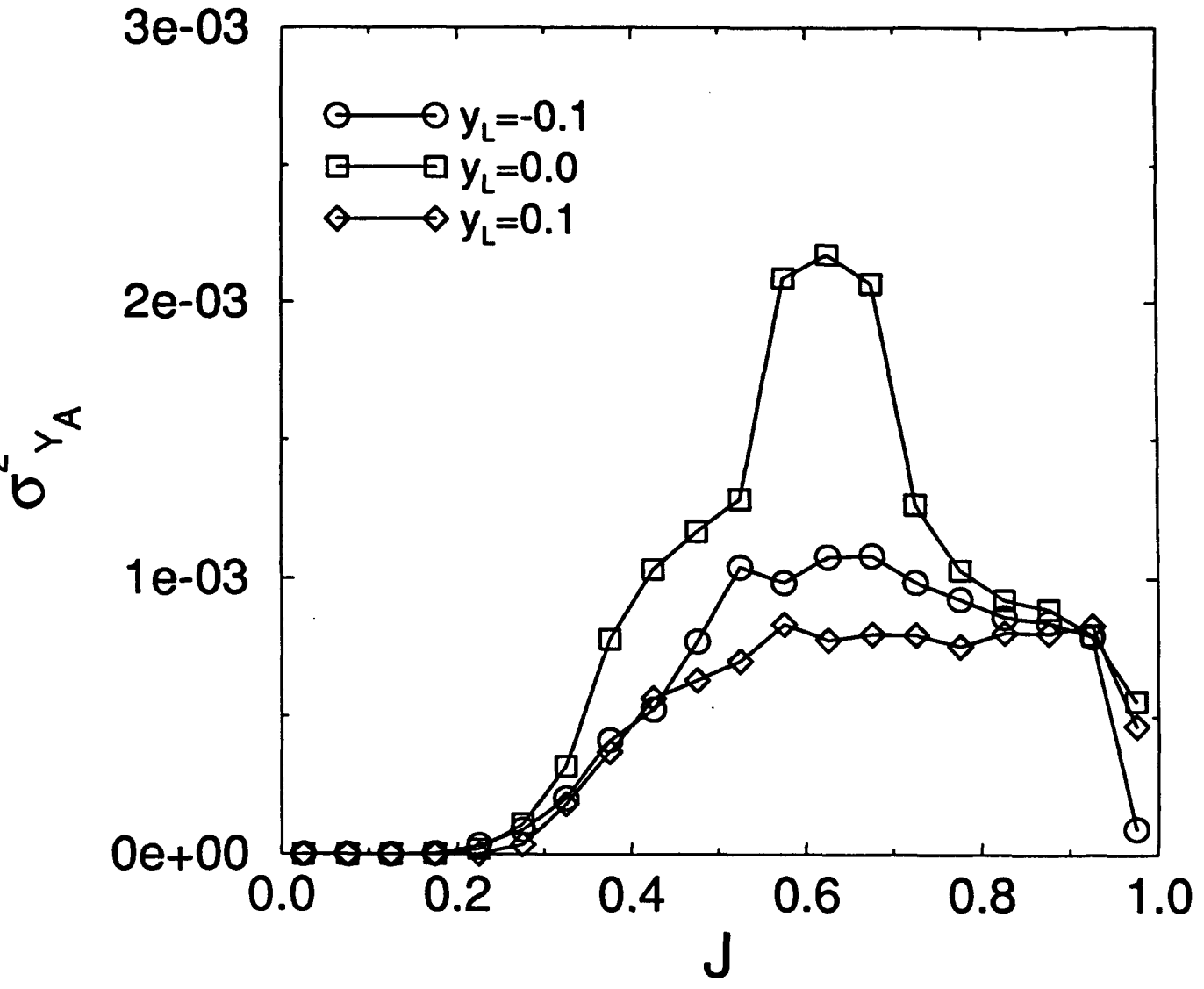

Figure 26(a)

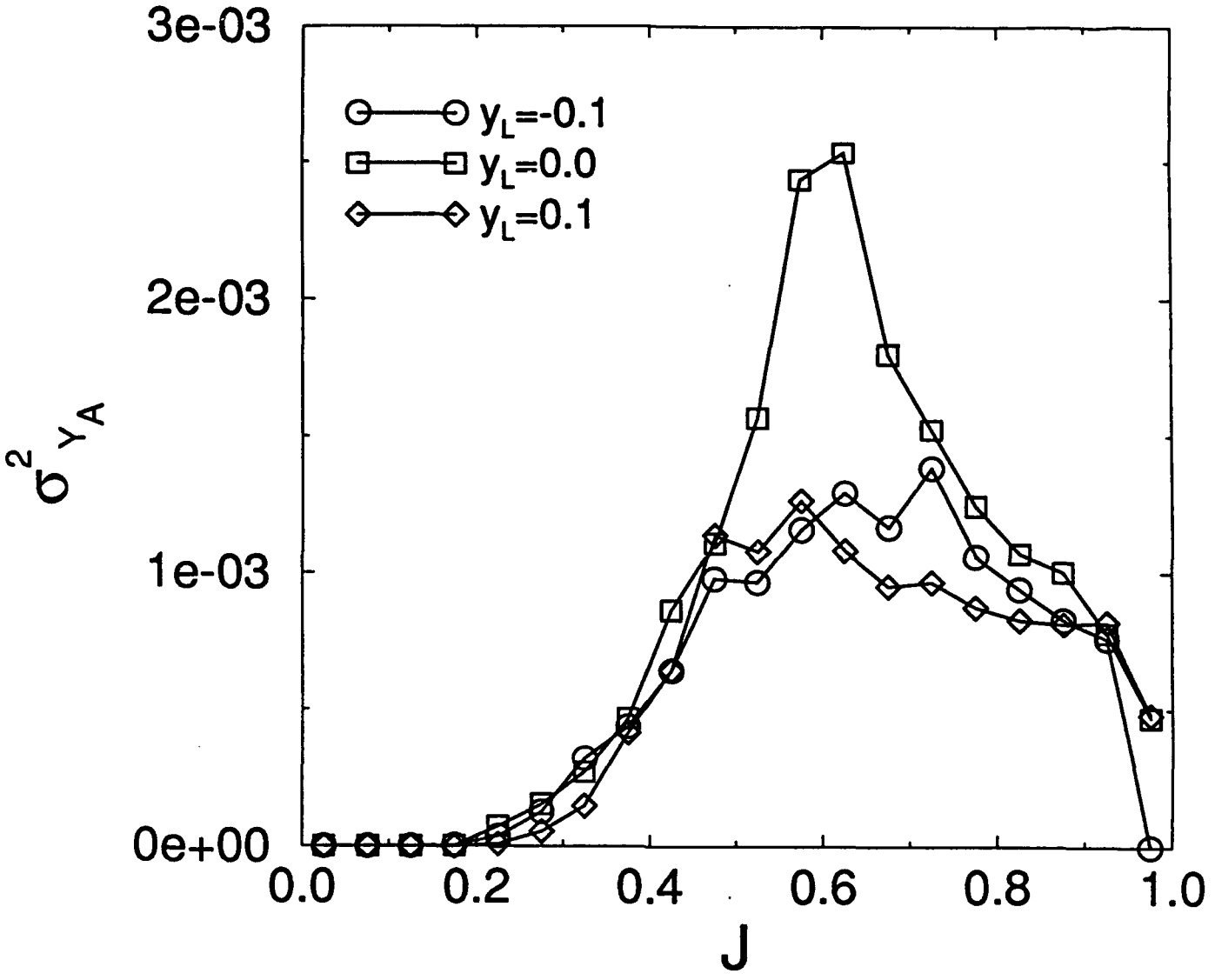

Figure 26(b)

APPENDIX 7

Suppression and Enhancement of Mixing in High-Speed Reacting Flows

SUPPRESSION AND ENHANCEMENT OF MIXING IN HIGH-SPEED REACTING FLOW FIELDS

J. Philip Drummond

NASA Langley Research Center
Hampton, Virginia 23681

Peyman Givi[1]

State University of New York
Buffalo, New York 14260

ABSTRACT

Work is underway at the NASA Langley Research Center to develop a hydrogen-fueled supersonic combustion ramjet, or scramjet, that is capable of propelling a vehicle at hypersonic speeds in the atmosphere. Recent research has been directed toward the optimization of the scramjet combustor and, in particular, the efficiency of fuel-air mixing and reaction taking place in the engine. With increasing Mach number, the degree of fuel-air mixing through natural convective and diffusive processes is significantly reduced leading to an overall decrease in combustion efficiency and thrust. Even though the combustor flow field is quite complex, it can be viewed as a collection of spatially developing and reacting supersonic mixing layers or jets from fuel injectors mixing with air, one of which serves as an excellent physical model for the overall flow field. This work is focused on understanding the mechanisms of mixing (or lack thereof) and on the development of techniques for its enhancement in compressible turbulent reacting flows. Results generated by direct numerical simulations (DNS) are first used to demonstrate the mechanisms for reduced mixing in shear layers. To counter the effects of suppressed mixing, several mixing enhancement techniques are then discussed. The most successful approaches involve longitudinal vorticity induced into the flow field. Several means for inducing vorticity are studied and assessed.

[1]The work at SUNY-Buffalo is sponsored by NASA Langley Research Center under Grant NAG-11122, and by the Office of Naval Research under Grant N00014-90-J-4013.

1. Introduction

Research has been underway for a number of years, both in the United States and abroad, to develop advanced aerospace propulsion systems for use late in this century and beyond. One program is now underway at the NASA Langley Research Center to develop a hydrogen-fueled supersonic combustion ramjet (scramjet) that is capable of propelling a vehicle at hypersonic speeds in the atmosphere. A part of that research has been directed toward the optimization of the scramjet combustor and, in particular, the efficiency of fuel-air mixing and reaction taking place in the engine. In the very high-speed vehicle configurations currently being considered, achieving a high combustor efficiency becomes particularly difficult. With increasing combustor Mach number, the degree of fuel-air mixing that can be achieved through natural convective and diffusive processes is reduced leading to an overall decrease in combustion efficiency and thrust.

Because of these difficulties, attention has now turned to the development of techniques for enhancing the rate of fuel-air mixing in the combustor. In an early study of high-speed mixing, Brown and Roshko (1974) show that the spreading rate of a supersonic mixing layer decreases with increasing Mach number, exhibiting a factor of three decrease in spread rate as compared with an incompressible mixing layer with the same density ratio. They conclude that the reduced spread rate is primarily due to compressibility. Papamoschou and Roshko (1986) and Papamoschou and Roshko (1988) also observe that the spreading rate of compressible mixing layers is significantly reduced over that of incompressible layers. To characterize the structure of the flow quantitatively, they define a convective Mach number (Bogdanoff, 1983). The reduction in mixing layer spreading rate (by approximately a factor of three or four) is shown in these experiments to correlate well with increasing convective Mach number. The results of linear stability analyses (Ragab and Wu, 1988; Ragab and Wu, 1989; Jackson and Grosch, 1989) also show that the decreased spreading rate of the mixing layer correlates well with the convective Mach number.

Faced with this challenge, several techniques have been developed for enhancing the mixing rates in supersonic mixing layers and jets. Guirguis *et al.* (1987) show that the spreading rate of a confined mixing layer can be improved if the pressure of the two streams

is different. Encouraged by this result, Guirguis (1988) employed a bluff body at the base of the splitter plate separating the two streams. It is shown that the body produces an instability further upstream in the layer and results in a more rapid rate of spread. Kumar *et al.* (1989) discuss a number of mixing problems that may exist in scramjet combustors. Several techniques for enhancing turbulence and mixing in combustor flow fields are suggested, and one enhancement technique that employs an oscillating shock is studied numerically. Drummond and Mukunda (1988) have studied fuel-air mixing and reaction in a supersonic mixing layer and have applied several techniques for enhancing mixing and combustion in the layer. They show that when the mixing layer, with its large gradients in velocity and species, is processed through a shock with strong curvature, vorticity is produced. The vorticity then interacts with the layer and results in a significant increase of the degree of mixing and reaction. Drummond *et al.* (1989) and Drummond *et al.* (1991) continued this investigation further by studying fuel-air mixing in a supersonic combustor. They describe a technique using swept-wedge fuel injectors (Northam *et al.*, 1989) to enhance the mixing processes and overall combustion efficiency in the flow. The swept-wedge injectors introduce streamwise vorticity in the inlet air passing over them, and that air then entrains fuel being injected from the base of the strut. Fuel-air mixing efficiency is shown to be significantly improved by the fuel-jet-air interaction. Marble *et al.* (1987) and Marble *et al.* (1990) employ a planar oblique shock to enhance the mixing between a co-flowing circular helium or hydrogen jet and air. They show that when the jet is processed by the oblique shock, a strong vorticity component is induced at the interface between the low density jet and the relatively high density airstream by the pressure gradient of the shock. Vorticity is generated when the density and pressure gradients are not aligned. The induced vorticity in the fuel jet provides a significant degree of mixing enhancement.

With the brief literature survey presented above, our hope in this article is to describe several numerical experiments on fuel-air mixing and reaction in mixing layers and jets. The initial studies involve simulations of mixing layers conducted to improve the understanding of mechanisms contributing to reduced mixing at high Mach numbers. The latter simulations involve studies of configurations designed to improve the degree of mixing and reaction in such flows.

2. Theory

The flow field considered in this study is described by the two-dimensional (2D) or three-dimensional (3D) Navier-Stokes, energy, and species continuity equations governing multiple species fluid undergoing chemical reaction (Drummond, 1988; Carpenter, 1989; Drummond, 1991). The finite-rate chemical reaction of gaseous hydrogen and air is modeled with either a three-species, one-reaction model or a seven-species, seven-reaction model. The coefficients governing the diffusion of momentum, energy, and mass are determined from models based on kinetic theory (Drummond, 1988). Sutherland's law is employed to compute the individual species viscosity; the mixture viscosity is evaluated by the Wilke's law. An alternate form of Sutherland's law is also used to compute the individual species thermal conductivity. The mixture thermal conductivity is then determined by the Wassilewa's formula. The Chapman and Cowling law is used to determine the binary diffusion coefficients which describe the diffusion of each species into the remaining species. Knowing the diffusion coefficients, the diffusion velocities of each species are determined by solving the multicomponent diffusion equation (Drummond, 1988). Alternately, in some simulations the calculation of diffusion velocities is simplified by assuming only binary diffusion and applying Fick's law.

Once the thermodynamic properties, chemical production rates, and diffusion coefficients have been computed, the governing equations are solved with the 2D or 3D SPARK computer code using Carpenter's convective fourth-order symmetric predictor-corrector compact algorithm (Carpenter, 1989). The algorithm is constructed on a compact three by three stencil which provides high-order accuracy while allowing boundary conditions to be specified to fourth-order accuracy in a straightforward manner. Details of the algorithm are given by Carpenter (1989).

3. Results

With the development of the theory and the solution procedure described above, several temporally developing mixing layer flows are studied to explore the phenomenon of reduced mixing with increasing Mach number. These results are summarized in the next subsection. Following these studies, two strategies for enhancing the mixing in high Mach number flow fields are examined to determine

their effectiveness for enhancing fuel-air mixing. These strategies are discussed in sections 3.2 and 3.3.

3.1. Temporally developing mixing layers

The results obtained by direct numerical simulations (DNS) have been very useful in portraying the problem of mixing in high-speed turbulent combustion. A reasonably updated review of the state of progress on DNS of shear flows is provided in the proceedings of the first ICASE Combustion Workshop (Givi and Riley, 1992). Since then, DNS have been widely utilized for the analysis of high-speed flows in both temporally developing and spatially developing mixing layers (Soetrisno *et al.*, 1988; Lele, 1989; Sandham and Reynolds, 1989; Sekar and Mukunda, 1990; Givi *et al.*, 1991; Grinstein and Kailasanath, 1991; Steinberger, 1992; Mukunda *et al.*, 1992; Planche and Reynolds, 1992; Steinberger *et al.*, 1993). To demonstrate the problems discussed above, it is useful to consider some of the results of these simulations. Here we discuss the results by Givi *et al.* (1991) and Steinberger (1992) of a temporally developing reacting mixing layer since these results contain all the information pertinent to this article.

The configuration of a temporally developing mixing layer is shown in Fig. 1. In this configuration the flow on the top stream is toward the right. The stream on the bottom side of the layer flows to the left with the same speed as that on the top stream. The justifications for temporal simulations are provided in several previous contributions (see Oran and Boris (1987) and Givi (1989) for reviews). The reacting species are introduced into the layer at the free streams. The chemical reaction occurring within the flow is idealized to a simple irreversible second-order form of $A + B \rightarrow Products + Heat$. Reactant A is introduced on the top stream and reactant B on the bottom stream. Calculations are performed with different values of the convective Mach number (M_c) and the heat release parameter (Ce) to assess the influence of these parameters on the structure of the layer (see Givi *et al.* (1991) for a definition of the non-dimensional parameters). In this assessment all of the other non-dimensional parameters are kept constant to isolate the effects of compressibility and exothermicity.

The influences of compressibility are captured by examining the effects of the convective Mach number on the rate of chemical product

formation. Figure 2 presents the plot of the product mass fraction contours for different values of the convective Mach numbers (keeping heat release rate at $Ce = 0$). This figure shows a reverse relation between the magnitude of the convective Mach number and the extent of large scale mixing and chemical product formation. As M_c increases it takes longer for background perturbations to grow, and the layer becomes more sluggish in responding to such perturbations. The trend is enhanced as the Mach number is increased; and at the largest Mach number considered, the rate of the layer's growth and the amount of products formed are the smallest.

The response of the shear layer to increased compressibility is further appraised by examining the statistical and the integral properties of the flow. In Figs. 3 and 4, the cross stream variations of the mean and the mean square of the streamwise velocity are shown. The most significant feature displayed in Fig. 3 is the steepness of the mean velocity profiles at high Mach numbers. In view of the contour plots of the product mass fraction, this is to be expected, and the increase in the velocity steepness (caused by the reduced growth rate) implies a reduced rate of mixing and, thus, decreased product formations. This trend can also be described by examining Fig. 4. Note the double hump characteristics of the mean square velocity profile at low Mach numbers. Also note that as the magnitude of the convective Mach number is increased, the amplitude of the fluctuations decreases, and this amplitude becomes very small at $M_c = 0.5$ and $M_c = 1.2$.

Another interesting characteristic of the increased compressibility is captured by examining the plots of pressure contours at high convective Mach numbers as shown in Fig. 5. The pressure response in Fig. 5 shows the regions of pressure maxima and minima at the braids and the cores of the vortices. At higher convective Mach numbers it is observed that the increased compressibility results in steepness of the gradients of instantaneous pressure and the formation of "eddy shocklets." These shocklets are initiated at the shear zone of the layer and extend to the outer region of the flow near the boundaries. A rationale for the formation of these shocklets is provided by noting the increased compressibility within the domain at high convective Mach numbers. In these cases, the layer is dominated by regions of supersonic and subsonic flows; and in order for the flow to adapt to high pressures at the braids, it must go through a shocklet to make the proper adjustment. Also, it is noted that the

currents do not necessarily have to be supersonic at the free streams, and compression occurs within the flow as a result of the formation of large scale structures. This point is demonstrated by examining the contour plots of the instantaneous Mach numbers in Fig. 6. It is shown in this figure that for the case of $M_c = 0.8$ the flow at the interior is characterized by localized regions of supersonic ($Ma > 1$) and subsonic ($Ma < 1$) flows. The adjustment from supersonic to subsonic conditions is provided by the formation of eddy shocklets. The strength of these shocklets becomes stronger as the convective Mach number is increased (*i.e.*, as the effects of compressibility become more pronounced).

The results of the simulations presented here are consistent with those of experimental measurements of Elliott and Samimy (1990) in that as the compressibility increases, the magnitudes of turbulence fluctuations decrease. The results are also in agreement with laboratory data of Hall (1991) in that mixing is reduced at higher compressibility. However, the conclusions drawn here are not in accord with those of Dutton *et al.* (1990), Clemens *et al.* (1991), and Clemens (1991) who suggest higher mixing at elevated compressibility levels. This issue is the subject of current investigations. Also, it has been suggested (Menon and Fernando, 1990; Sandham and Reynolds, 1989) that eddy shocklets form only in 2D simulations. However, the results of recent simulations by Lee *et al.* (1991) and Miller *et al.* (1993) indicate that such shocklets do indeed occur in 3D, both in isotropic and in shear flows.

The influence of the heat release on the structure of the reacting layer is assessed by examining the amount of normalized total product mass fraction shown in Fig. 7. In these simulations two chemistry models are considered; a constant rate kinetics model and an Arrhenius prototype. Figure 7 shows that at the initial stages of the layer development, the effect of heat release is a somewhat enhanced product formation, whereas at intermediate and final stages a reverse scenario holds. At early stages, the effect of heat release is to expand the fluid at the cores of the layers. Therefore, a mixing zone is expected and, thus, a higher amount of product is formed. However, as the extent of heat release increases and the layer thickens, the rate of growth of the instability modes becomes subdued, postponing the rate of formation of large scale vortices. After the initial stages, the non-heat releasing simulations predict a sharp increase in the product formation; and as the magnitude of the heat release is increased,

the time at which such structures are formed is delayed. The lowest rate of product formation is for $Ce = 6$ simulations in which the only mechanism of mixing is through diffusion. This reduction in product formation is also evidenced by a comparison between the contour plots of the product mass fraction with heat release (Fig. 8) and those without heat release (Fig. 2(a)). Further influences of heat release become evident by examining its effect on statistical quantities. In Fig. 9 the normalized profiles of mean streamwise velocity component are presented. This figure shows that heat liberation results in a steeper gradient of the velocity and, therefore, less mixing. This has a substantial influence on the two-dimensional turbulence transport, as indicated by the cross stream variations of the mean square velocity presented in Fig. 10. It is shown in this figure that as exothermicity becomes dominant, the amplitude of the fluctuation decreases. For the most significant heat release cases ($Ce = 6$ and the Arrhenius model), the amplitude of the mean square velocity is very close to zero, indicating virtually no turbulence fluctuations.

The conclusion drawn here in regard to mixing reduction caused by exothermicity is consistent with those of laboratory experiments (Hermanson and Dimotakis, 1989), inviscid linear stability analyses (Jackson and Grosch, 1990; Jackson, 1992) and previous DNS results based on low Mach number approximations (McMurtry *et al.*, 1989). However, it has recently been suggested by Steinberger *et al.* (1993) and Miller *et al.* (1993) that in flames where chemistry is described by an Arrhenius kinetics model, the effect of heat release is to increase the rate of product formation. This is due to the increase in the magnitude of the temperature due to heat release which is not considered in the experiments. Based on this observation, it is recommended to further assess the effects of exothermicity by means of laboratory measurements. These measurements must involve a reacting system whereby the rate of reaction conversion is temperature dependent and in which the large scale mixing intensity is not significantly affected by the heat release.

3.2. Mixing enhancement using swept wedges

A number of approaches have been suggested for enhancing the mixing of high-speed fuel-air flows. Several of these approaches are discussed in the Introduction. A particularly attractive option has been suggested by Northam *et al.* (1989) in their experimental study

of wall-mounted parallel injector ramps used to enhance the relatively slow mixing of fuel and air normally associated with parallel fuel injection. Parallel injection may be useful at high speeds to extract energy from hydrogen that has been used to cool the engine and the airframe of a hypersonic cruise vehicle. The ramp injector configurations are intended to induce vortical flow and local recirculation regions similar to the rearward-facing step that has been used for flame holding in reacting supersonic flow.

It is instructive to study some aspects of these experiments here. Two ramp configurations are considered in the experiment of Northam *et al.* (1989) as shown in Fig. 11. In both configurations, hydrogen gas is injected at Mach 1.7 from conical nozzles in the base of the two ramps which are inclined at 10.3 degrees to the combustor wall. The injector diameters are 0.762 cm. The sidewalls of the unswept ramps are aligned with Mach 2 streamwise airflow from a combustion facility, whereas the swept ramps are swept at an angle of 80 degrees. Each ramp is 7 cm long and ends in a nearly square base, 1.52 cm on a side. Both ramp designs are chosen to induce vorticity to enhance mixing and base flow recirculation to provide flame holding. The swept ramp injector, because of its delta shape, is intended to induce higher levels of vorticity and, therefore, higher levels of mixing. Hydrogen injection occurs at a streamwise velocity of 1,747 m/s, a transverse velocity of 308 m/s, and a static temperature and pressure of 187 K and 325,200 Pa, respectively. The facility air crosses the leading edge of the wedges at a streamwise velocity of 1,300 m/s, a static temperature of 1,023 K, and a static pressure of 102,000 Pa. The air is vitiated following heating by a burner with oxygen, nitrogen, and water mass fractions of 0.2551, 0.5533, and 0.1818, respectively. The overall fuel-air equivalence ratio is 0.6. Both the unswept and swept parallel injector ramps are studied computationally. Only fuel-air mixing is considered. The facility test section surrounding the ramps and considered in the computation is 13.97 cm long and 3.86 cm high. Symmetry planes are chosen to pass transversely through each fuel injector to define the spanwise computational boundaries.

Results from the computational study for both the unswept and swept injector ramps are shown in Figs. 12-17. Figures 12 and 13 show the cross-stream velocity vectors for the unswept and swept cases at two downstream planes (x = 6.6 and 13.2 cm) oriented perpendicular to the test section walls. Part (a) of the figures displays

the unswept ramp results and part (b) shows the swept ramp results. The planar cut extends from the lower to the upper wall of the test section, and it slices through the center of the right fuel jet. The left boundary is located halfway between the two ramps. At the $x = 6.6$ cm station, which lies just ahead of the end of the ramps, a streamwise vortex has formed at the edge of each ramp. The vortex formed by the swept ramp is considerably larger, however, and it persists well into the flow above the ramp and to the ramp centerline. At the $x = 13.2$ cm station, located 6.2 cm beyond the end of the ramps, the swept ramp vortex has significantly grown and has moved well toward the jet centerline. The swept ramp vortex has now interacted with the hydrogen fuel jet, enhancing its penetration into the airstream. There is pronounced fuel-air mixing enhancement as the vortex spreads across the test section, convecting hydrogen fuel into the airstream. Some enhancement is also provided by the unswept ramp, but it is not nearly as pronounced as that provided by the swept ramp.

The transport of hydrogen fuel into the airstream can be observed more clearly by studying the location of hydrogen mass fraction contours in several test section cross planes, plotted with increasing streamwise distance. Figures 14-17 show the hydrogen mass fraction contours at four successive downstream planes ($x = 7.3$, 9.6, 11.3, and 13.2 cm), again oriented perpendicular to the test section walls. As before, part (a) of the figures displays the unswept ramp results, and part (b) displays the swept ramp results. The results in Fig. 14 occur 0.3 cm downstream of the end of the ramp. With the swept ramp, the larger streamwise vortex has already begun to sweep the hydrogen fuel across into the airstream and away from the lower wall. The smaller streamwise vortex of the unswept ramp also begins to transport hydrogen away from the jet, but not nearly as much as does the swept ramp. As a result, more hydrogen is transported toward the lower wall boundary layer in the unswept case. The same trends continue at the $x = 9.6$ cm station as shown in Fig. 15. At $x = 11.3$ cm, as shown in Fig. 16, the swept ramp enhancer has lifted the fuel jet almost completely off the lower wall. Significant amounts of hydrogen have also been carried across the test section. On the other hand, the unswept ramp enhancer still allows a large amount of hydrogen to be transported along the lower wall, and the spanwise transport is not nearly as great. At $x = 13.2$ cm, the final streamwise station shown in Fig. 17, the spanwise spread of the

fuel jet enhanced by the swept ramp is 46 percent greater than the spanwise spread due to the unswept ramp. In addition, the swept enhancer has resulted in the fuel jet being transported completely off the lower wall. Finally, an eddy of hydrogen has broken completely away from the primary hydrogen jet, increasing the fuel-air interfacial area even further. Clearly then, the swept ramp enhancer significantly increases the overall spread and mixing of the hydrogen fuel jets.

3.3. Mixing enhancement using shocks

Following the analysis of swept wedge injectors, a study of the parallel fuel jet configuration described in the introduction is conducted. As noted before, fuel injected parallel to inlet air entering a combustor is normally assumed to mix relatively slowly with that air. Therefore, to employ parallel injection, it is quite important to enhance mixing of parallel fuel jets and air to the greatest extent possible.

The configuration used for the study of enhanced mixing of parallel fuel jets and air is shown in Fig. 18. It consists of a parallelepiped 6 cm long with a square cross-section 2 cm on a side. A circular hydrogen jet with a 2 mm diameter is injected into the domain from the left face. The hydrogen gas is introduced with a streamwise exponential velocity profile with a peak centerline value of 2,883 m/s, a temperature of 1,000 K, and a pressure of 101,325 Pa (1 atm.), resulting in a peak hydrogen Mach number of 1.2. Air, co-flowing with the hydrogen, is also introduced from the left face at a velocity of 1,270 m/s, a temperature of 1,000 K, and a pressure of 101,325 Pa, resulting in an air Mach number of 2. An oblique shock is introduced across the flow from the lower wall, by a 10 degree wedge also shown in Fig. 18. In the computations, the shock is produced by specifying the appropriate jump conditions for a 10 degree turning angle along the lower boundary where the shock enters the domain.

To establish a baseline for mixing and chemical reaction, calculations are first carried out without the shock. These calculations are conducted for 4 ms in time until a pseudo-steady state is reached following 85 computational sweeps of the flow field. Results for this computation are presented in Figs. 19-22. Figure 19 shows the streamwise development of the hydrogen jet along its centerline in the $x-z$ plane. Values of the hydrogen mass fraction, shown as contours

in the figure, are defined in the legend. The hydrogen jet develops very slowly with only a small degree of mixing. The cross- stream hydrogen mass fraction distribution at the 6 cm station is shown in Fig. 20. It is also clear from this figure that very little mixing of the hydrogen and air has occurred at the end of the domain, with peak values of hydrogen mass fraction as high as 0.56 still persisting in the flow. Figures 21 and 22 show the water mass fraction resulting from chemical reaction in the $x - z$ and $y - z$ planes, respectively. Due to poor fuel-air mixing, reaction occurs only on the edge of the hydrogen jet, and peak values of water mass fraction of only 0.008 are achieved in the outflow cross-plane at $x = 6$ cm. Combustion efficiency for this case rises to only 0.4 percent at the 6 cm station. Combustion efficiency is defined as the ratio of hydrogen in water to the total hydrogen, integrated over each cross-plane. Therefore, credit in efficiency is taken only for exothermically produced final product water, and not for the remaining product species.

To enhance the degree of mixing and combustion of the hydrogen jet and air, the flow is then processed through the 10 degree shock. It was earlier noted that the shock causes the hydrogen jet to split into a vortex pair and spread quickly downstream. The vortices convect hydrogen away from the jet centerline in a spanwise and transverse direction, entraining and mixing the hydrogen with the surrounding airstream. Reacting results for the shocked jet are given in Figs. 23-29. Figure 23 shows the streamwise development of the hydrogen jet along its centerline in the $x - z$ plane. The jet passes through the shock at $x = 1.1$ cm and flows downstream at an angle of 10 degrees to the original horizontal path. Due to jet mixing and initial chemical reaction, no hydrogen mass fraction contour greater than 0.09 exists beyond the 2 cm station. The water mass fraction distribution resulting from reaction is shown in Fig. 24. Water production begins a short distance downstream of the shock. Peak water production at each station occurs downstream along the stoichiometric line roughly located 75 percent across the water profile. This location is coincident with the lower hydrogen concentration lying between and above the stable hydrogen vortex pair. However, water production is still significant above and below this line as indicated in Fig. 24. The streamwise temperature distribution in the $x - z$ plane is given in Fig. 25. Consistent with the previous results, maximum temperatures occur along the stoichiometric line, with a peak temperature of 2,105 K at and beyond 4.8 cm.

The vorticity field with chemical reaction in the $y-z$ cross-plane at the $x = 6$ cm station is shown in Fig. 26. Two streamwise vortices have formed in the hydrogen jet, with the left vortex containing positive and the right vortex containing negative components of vorticity when viewed from the outflow of the domain. This vortex structure distorts the initial circular cross-section of the hydrogen jet, entraining fuel and air and enhancing mixing. The jet distortion can be seen in Fig. 27 which shows the hydrogen species mass fractions at the same station displayed in the previous figure. Hydrogen is concentrated toward the interior of each vortex with peak values of around 0.012. Hydrogen is stretched away from the upper portion of the jet, however, and the mass fraction is most greatly reduced in that region. This region of reduced concentration favors the highest initial degree of combustion since the fuel-air ratio is nearest to stoichiometric conditions.

Figure 28 shows the resulting water mass fraction distribution in the $y-z$ plane at the $x = 6$ cm station. Combustion begins in the stoichiometric region at the top of the vortices and along the outer edge of the remainder of the vortices. At $x = 6$ cm, the flame has propagated into the interior of the vortex structure such that significant reaction is occurring near the center of each vortex. The peak water mass fraction of 0.2 occurs at this location. As shown in Fig. 29, there is also a significant temperature rise near the top and near the center of the vortices due to reaction. A peak temperature of $2,158$ K occurs at this location. It is quite interesting to compare the resulting combustion efficiency for the shocked reacting case with the unshocked reacting jet case. Recall that in the unshocked case, the combustion efficiency at $x = 6$ cm is only 0.4 percent whereas in the shocked case, a combustion efficiency of 72 percent is achieved.

4. Concluding Remarks

In high-speed airbreathing propulsion systems, the extent of fuel-air mixing is significantly reduced with increasing Mach number. Direct numerical simulations of reacting mixing layer flows indicate that there is a reduction in turbulence levels with both increased compressibility due to an increase in either Mach number or heat release. To counter the effects of suppressed mixing and reaction, two mixing enhancement techniques have been developed. The first one involves the use of swept wedges placed in the airstream to introduce lon-

gitudinal vorticity leading to large scale mixing enhancement. The second technique utilizes the interaction of a shock with the large density gradient existing between a hydrogen fuel jet and the surrounding airstream to introduce streamwise vorticity and mixing. Both of these approaches have proven effective in providing mixing enhancement mechanisms in nonpremixed high-speed reacting flows.

References

Bogdanoff, D. W., 1983, Compressibility effects in turbulent shear layers, *AIAA J.* **21**, 926–927.

Brown, G. L. and Roshko, A., 1974, On density effects and large structure in turbulent mixing layers, *J. Fluid Mech.* **64**, 775–816.

Carpenter, M. H., 1989, Three-dimensional computations of cross-flow injection and combustion in a supersonic flow, AIAA Paper 89-1870.

Clemens, N. T., Paul, P. H., Mungal, M. G., and Hanson, R. K., 1991, Scalar mixing in the supersonic shear layer, AIAA Paper 91-1720.

Clemens, N. T., 1991, An experimental investigation of scalar mixing in supersonic turbulent shear layers, Stanford University Report HTGL T-274, Department of Mechanical Engineering, Stanford University, Stanford, CA.

Drummond, J. P. and Mukunda, H. S., 1988, A numerical study of mixing enhancement in supersonic reacting flow fields, AIAA Paper 88-3260.

Drummond, J. P., Carpenter, M. H., Riggins, D. W., and Adams, M. S., 1989, Mixing enhancement in a supersonic combustor, AIAA Paper 89-2794.

Drummond, J. P., Carpenter, M. H., and Riggins, D. W., 1991, Mixing and mixing enhancement in supersonic reacting flow fields, in Murthy, S. N. B. and Curran, E. T., editors, *High Speed Propulsion Systems*, volume 137 of *AIAA Progress Series*, chapter 7, pages 383–455, American Institute of Aeronautics and Astronautics.

Drummond, J. P., 1988, Two-dimensional numerical simulation of a supersonic, chemically reacting mixing layer, NASA TM 4055.

Drummond, J. P., 1991, Supersonic reacting internal flow fields, in Oran, E. S. and Boris, J. P., editors, *Numerical Approaches to Combustion Modeling*, volume 135 of *Progress in Astronautics and Aeronautics*, chapter 12, pages 365–420, AIAA Publishing Co., Washington, D.C.

Dutton, J. C., Burr, R. F., Goebel, S. G., and Messersmith, N. L., 1990, Compressibility and mixing in turbulent free shear layers, in *12th Symposium on Turbulence*, Rolla, MO.

Elliott, G. S. and Samimy, M., 1990, Compressibility effects in free shear layers, AIAA Paper 90-0705.

Givi, P. and Riley, J. J., 1992, Some current issues in the analysis of reacting shear layers: Computational challenges, in Hussaini, M. Y., Kumar, A., and Voigt, R. G., editors, *Major Research Topics in Combustion*, pages 588–650, Springer-Verlag.

Givi, P., Madnia, C. K., Steinberger, C. J., Carpenter, M. H., and Drummond, J. P., 1991, Effects of compressibility and heat release in a high speed reacting mixing layer, *Combust. Sci. and Tech.* **78**, 33–68.

Givi, P., 1989, Model free simulations of turbulent reactive flows, *Prog. Energy Combust. Sci.* **15**, 1–107.

Grinstein, F. F. and Kailasanath, K., 1991, Chemical energy release, spanwise excitation, and dynamics of transitional, reactive, free shear flows, AIAA Paper 91-0247.

Guirguis, R. H., Grinstein, F. F., Young, T. R., Oran, E. S., Kailasanath, K., and Boris, J. P., 1987, Mixing enhancement in supersonic shear layers, AIAA Paper 87-0373.

Guirguis, R. H., 1988, Mixing enhancement in supersonic shear layers: III. effect of convective Mach number, AIAA Paper 88-0701.

Hall, J. L., 1991, *An Experimental Investigation of Structure, Mixing and Combustion in Compressible Turbulent Shear Layers*, Ph.D. Thesis, California Institute of Technology, Pasadena, CA.

Hermanson, J. C. and Dimotakis, P. E., 1989, Effects of heat release in a turbulent, reacting shear layer, *J. Fluid. Mech.* **199**, 333–375.

Jackson, T. L. and Grosch, C. E., 1989, Inviscid spatial stability of a compressible mixing layer, *J. Fluid Mech.* **208**, 609–637.

Jackson, T. L. and Grosch, C. E., 1990, Inviscid spatial stability of a compressible mixing layer. Part 2. The flame sheet model, *J. Fluid Mech.* **217**, 391–420.

Jackson, T. L., 1992, A review of spatial stability analysis of compressible reacting mixing layers, in Hussaini, M. Y., Kumar, A., and Voigt, R. G., editors, *Major Research Topics in Combustion*, pages 131–161, Springer-Verlag.

Kumar, A., Bushnell, D. M., and Hussaini, M. Y., 1989, A mixing augmentation technique for hypervelocity scramjets, *J. Propulsion and Power* **5**, 514–522.

Lee, S., Lele, S. K., and Moin, P., 1991, Eddy shocklets in decaying compressible turbulence, *Phys. Fluids A* **3**, 657–664.

Lele, S. K., 1989, Direct numerical simulation of compressible free shear flows, AIAA Paper 89-0374.

Marble, F. E., Hendricks, G. J., and Zukoski, E. E., 1987, Progress toward shock enhancement of supersonic combustion processes, AIAA Paper 87-1880.

Marble, F. E., Zukoski, E. E., Jacobs, J. W., Hendricks, G. J., and Waitz, I. A., 1990, Shock enhancement of and control of hypersonic mixing and combustion, AIAA Paper 90-1981.

McMurtry, P. A., Riley, J. J., and Metcalfe, R. W., 1989, Effects of heat release on the large scale structures in a turbulent reacting mixing layer, *J. Fluid Mech.* **199**, 297–332.

Menon, S. and Fernando, E., 1990, A numerical study of mixing and chemical heat release in supersonic mixing layers, AIAA Paper 90-0152.

Miller, R. S., Madnia, C. K., and Givi, P., 1993, The structure of a reacting turbulent mixing layer, Submitted for publication.

Mukunda, H. S., Sekar, B., Carpenter, M. H., Drummond, J. P., and Kumar, A., 1992, Direct simulation of high-speed mixing layers, NASA TP 3186.

Northam, G. B., Greenberg, I., and Byington, C. S., 1989, Evaluation of parallel injector configurations for supersonic combustion, AIAA Paper 89-2525.

Oran, E. S. and Boris, J. P., 1987, *Numerical Simulations of Reactive Flows*, Elsevier Publishing Company, Washington, D.C.

Papamoschou, D. and Roshko, A., 1986, Observations of supersonic free shear layers, AIAA Paper 86-0162.

Papamoschou, D. and Roshko, A., 1988, The compressible turbulent shear layer: An experimental study, *J. Fluid Mech.* **197**, 453–477.

Planche, O. H. and Reynolds, W. C., 1992, A numerical investigation of the compressible reacting mixing layers, Report No. TF-56, Stanford University, Department of Mechanical Engineering, Thermosciences Division, Stanford, CA.

Ragab, S. A. and Wu, J. L., 1988, Instabilities in the free shear layer formed by two supersonic streams, AIAA Paper 88-0038.

Ragab, S. A. and Wu, J. L., 1989, Linear instabilities in two dimensional compressible mixing layers, *Phys. Fluids A* **1**, 957–966.

Sandham, N. D. and Reynolds, W. C., 1989, A numerical investigation of the compressible mixing layer, Report No. TF-45, Stanford University, Department of Mechanical Engineering, Thermosciences Division, Stanford, CA.

Sekar, B. and Mukunda, H. S., 1990, A computational study of direct numerical simulation of high speed mixing layers without and with chemical heat release, in *Proceedings of 23rd Symp. (Int.) on Combustion*, pages 707–713, The Combustion Institute, Pittsburgh, PA.

Soetrisno, M., Eberhardt, D. S., Riley, J. J., and McMurtry, P. A., 1988, A study of inviscid. supersonic mixing layers using a second-order TVD scheme, AIAA Paper 88-3676-CP.

Steinberger, C. J., Vidoni, T. J., and Givi, P., 1993, The compositional structure and the effects of exothermicity in a non-premixed planar jet flame, *Combust. Flame*, in press.

Steinberger, C. J., 1992, Model free simulations of a high speed reacting mixing layer, AIAA Paper 92-0257.

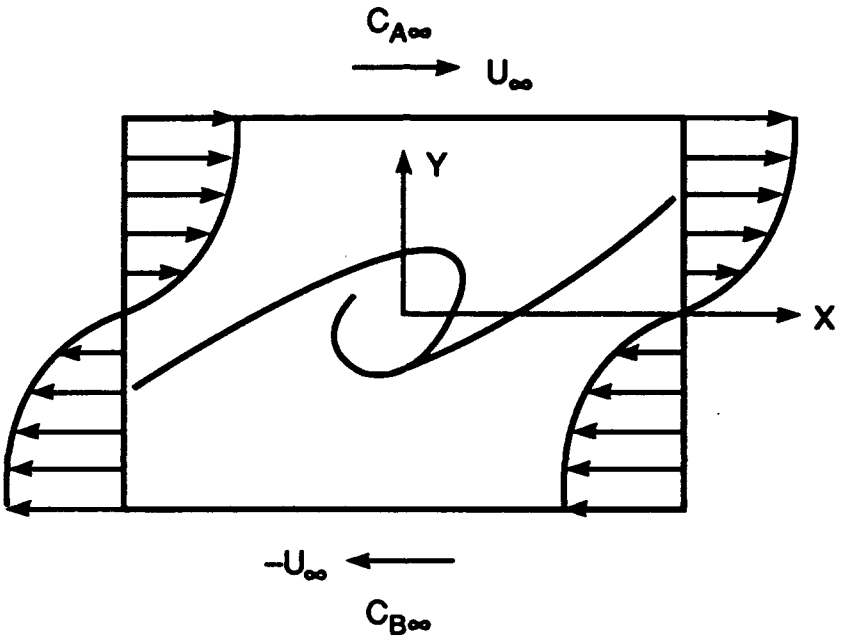

Figure 1. Schematic diagram of a temporally evolving mixing layer.

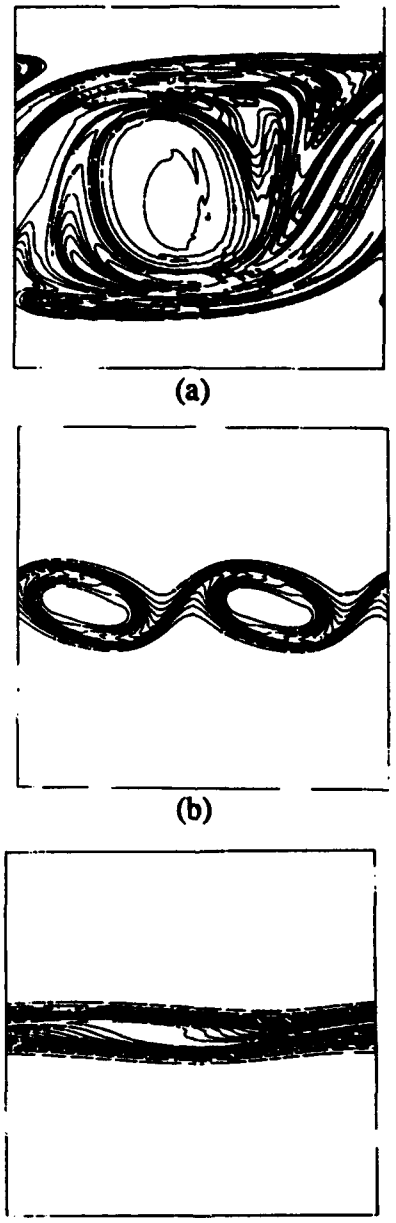

Figure 2. Plots of product mass fraction contours at three convective Mach numbers (M_c). (a) $M_c = 0.2$, (b) $M_c = 0.8$, (c) $M_c = 1.2$.

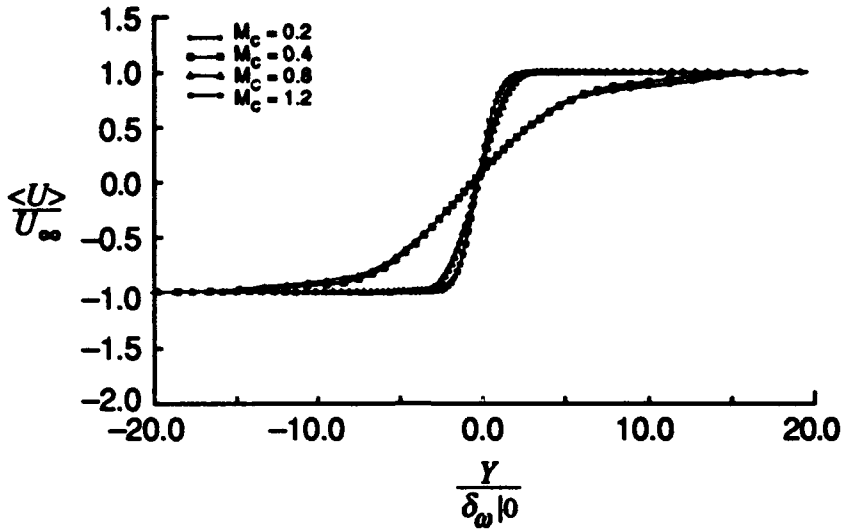

Figure 3. Profiles of normalized mean velocity $\frac{\langle U \rangle}{U_\infty}$ versus the normalized cross-stream direction $\frac{Y}{\delta_\omega|0}$ for different values of the convective Mach number. U_∞ represents the free-stream velocity and $\delta_\omega|0$ denotes the vorticity thickness at the initial time.

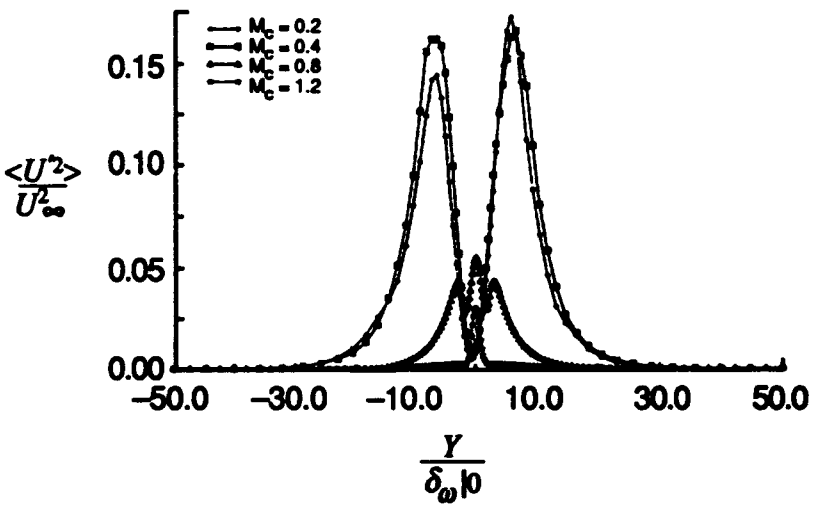

Figure 4. Profiles of normalized mean square velocity $\frac{\langle U^2 \rangle}{U^2_\infty}$ versus $\frac{Y}{\delta_\omega|0}$ for different values of the convective Mach number.

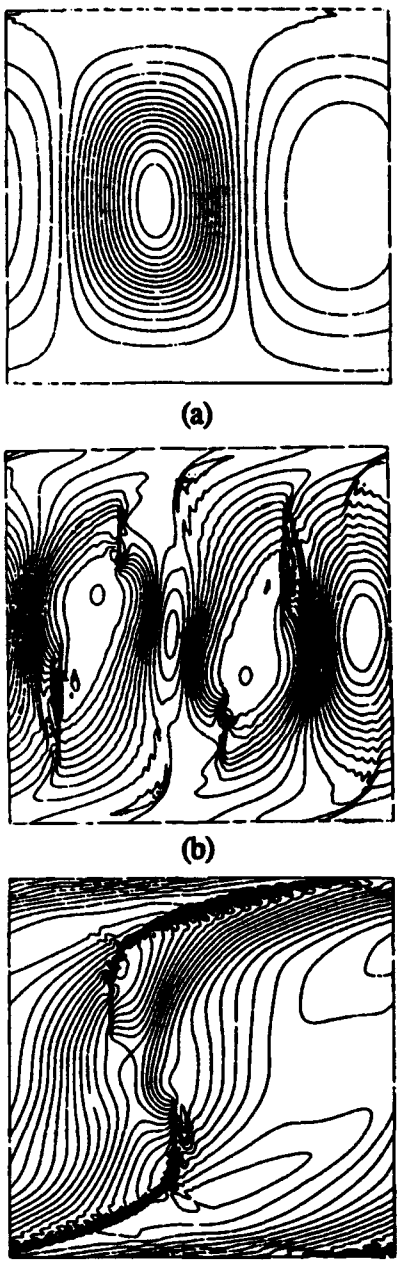

Figure 5. Plots of pressure contours. (a) $M_c = 0.4$, (b) $M_c = 0.8$, (c) $M_c = 1.2$.

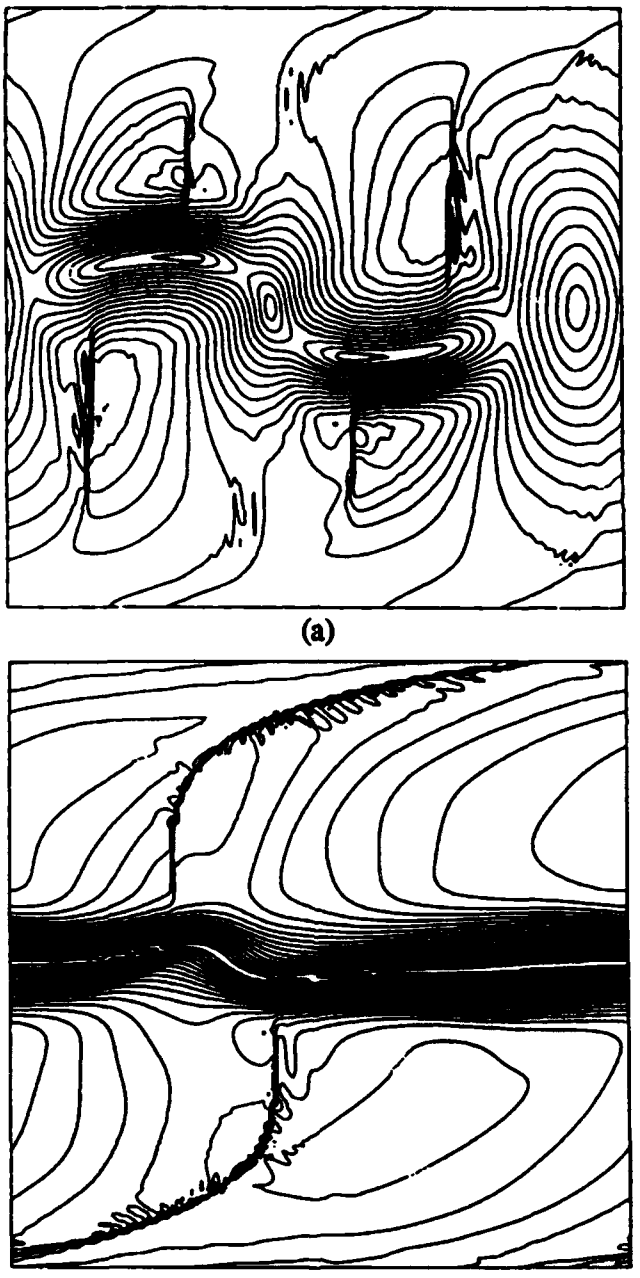

Figure 6. Plots of Mach number contours. (a) $M_c = 0.8$, (b) $M_c = 1.2$.

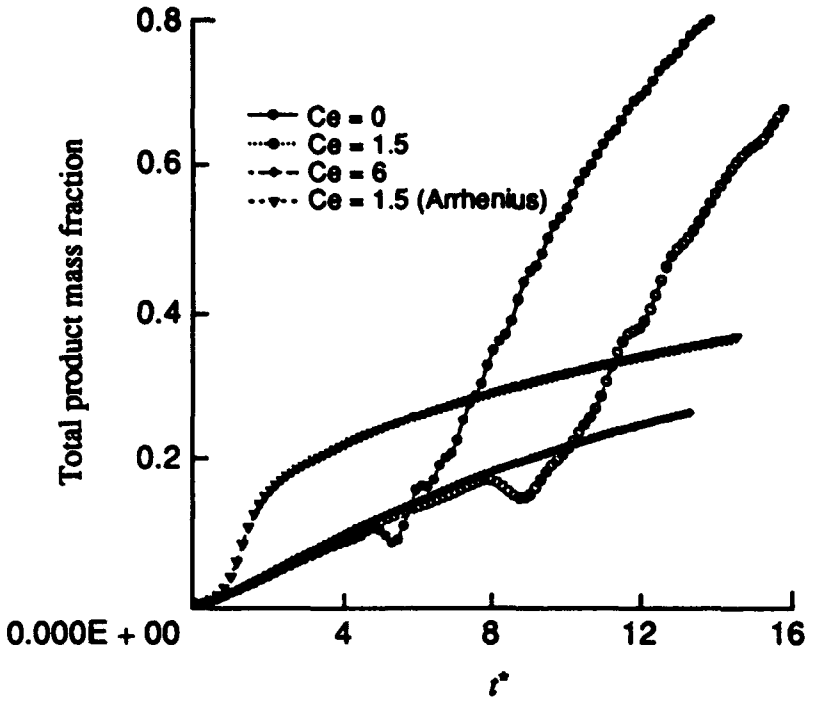

Figure 7. Normalized total product mass fraction versus normalized time (t^*) for different values of the heat release parameter. $t^* = tU_\infty/L$, where L is the size of the computational box.

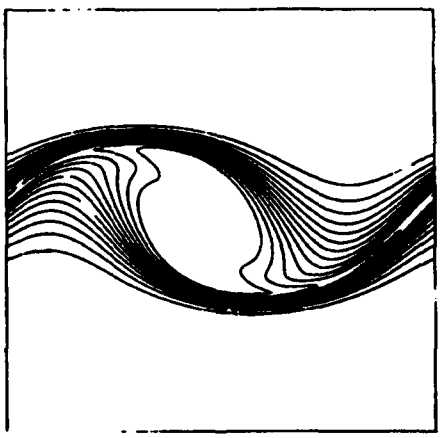

Figure 8. Plots of product mass fraction contours for $M_c = 0.2$, and $Ce = 1.5$.

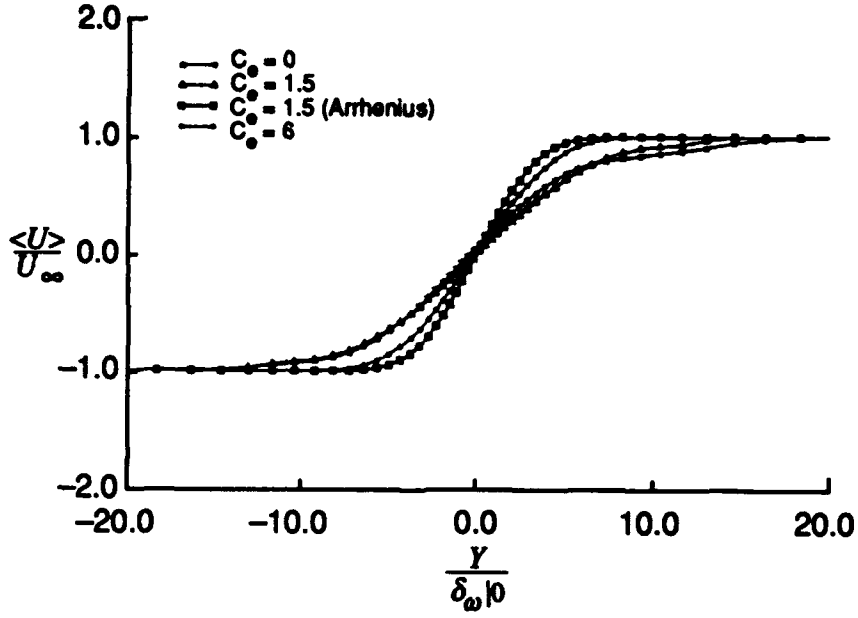

Figure 9. Profiles of normalized mean velocity $\frac{<U>}{U_\infty}$ versus $\frac{Y}{\delta_\omega|0}$ for different values of the heat release parameter.

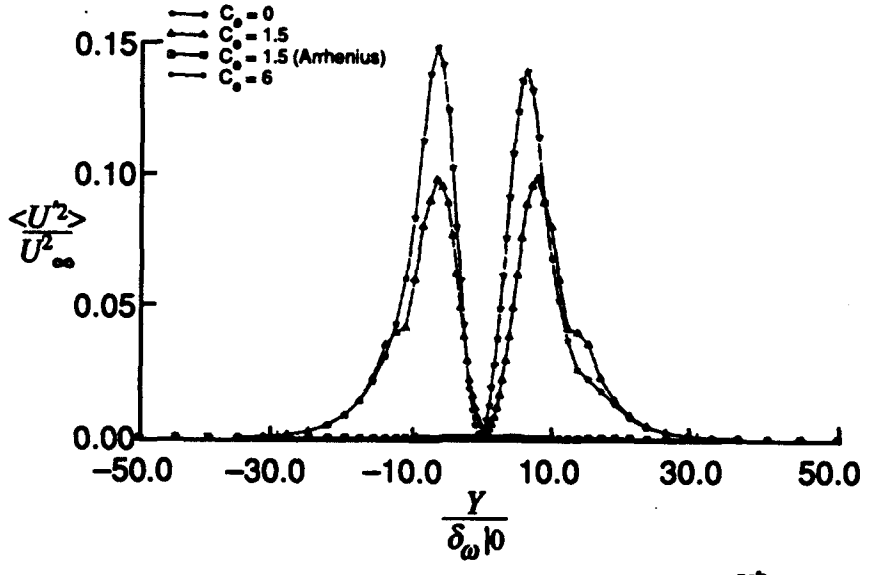

Figure 10. Profiles of normalized mean square velocity $\frac{<U'^2>}{U^2_\infty}$ versus $\frac{Y}{\delta_\omega|0}$ for different values of the heat release parameter.

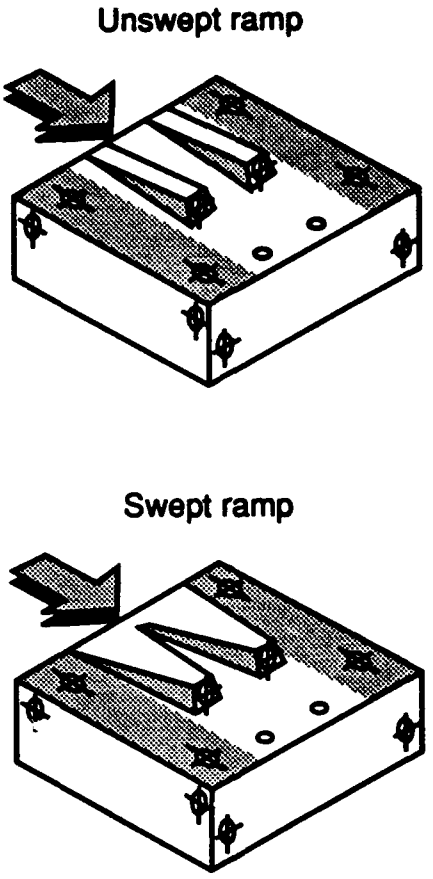

Figure 11. Swept and unswept ramp fuel-injector configurations.

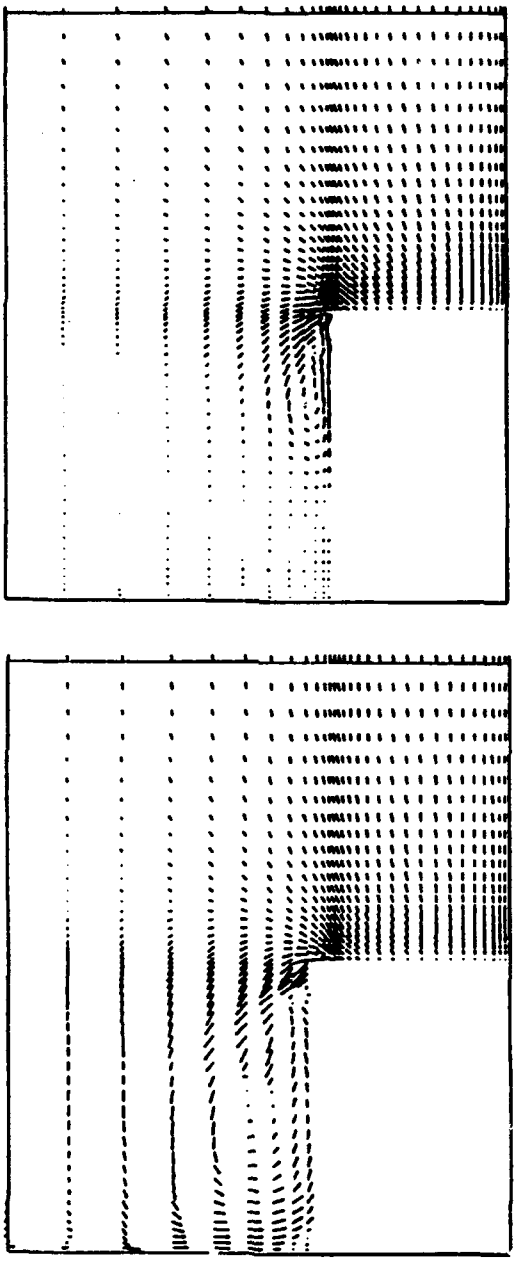

Figure 12. Cross-stream velocity vectors for (a) unswept, and (b) swept, ramp at $x = 6.60$ cm.

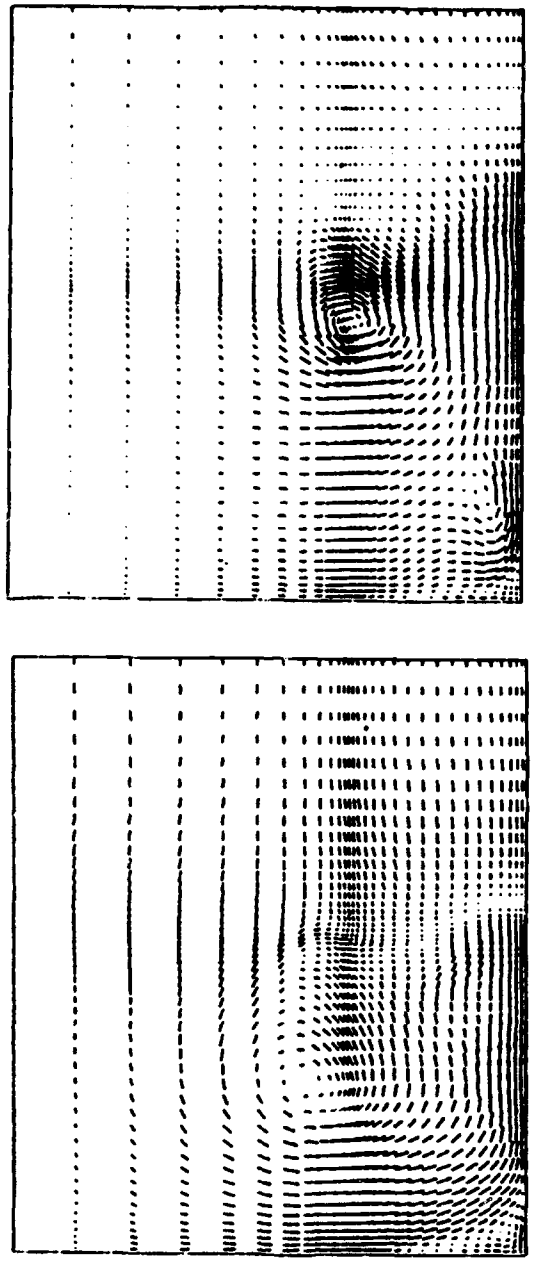

Figure 13. Cross-stream velocity vectors for (a) unswept, and (b) swept, ramp at $x = 13.2$ cm.

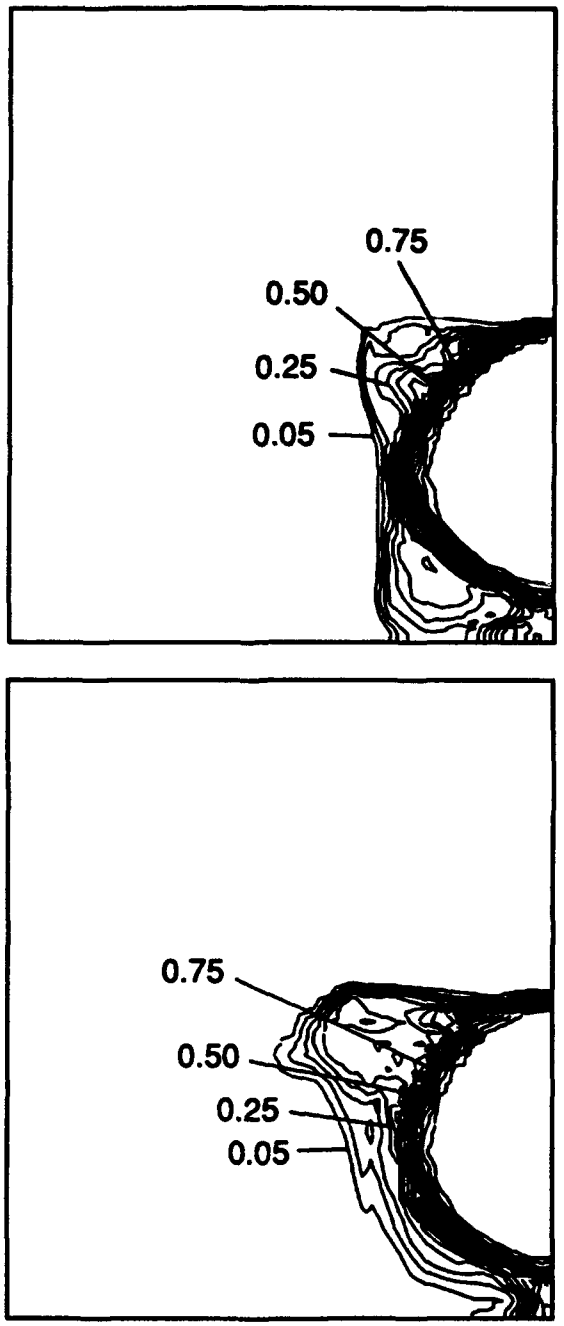

Figure 14. Cross-stream hydrogen mass fraction contours for (a) unswept, and (b) swept, ramp at $x = 7.30$ cm.

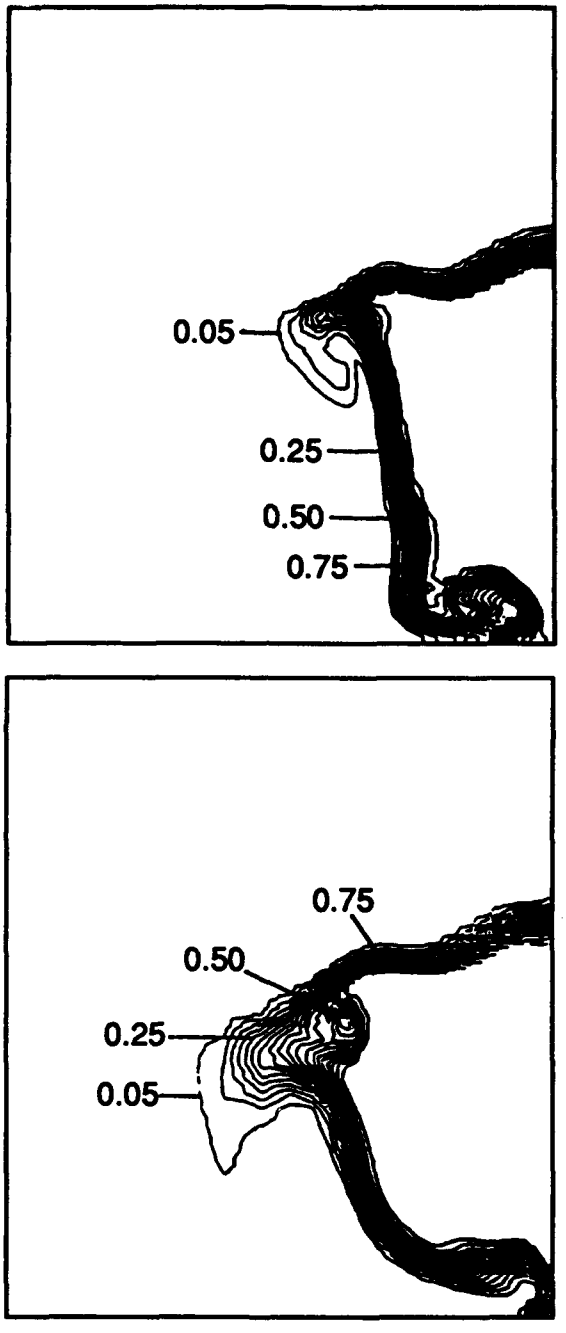

Figure 15. Cross-stream hydrogen mass fraction contours for (a) unswept, and (b) swept, ramp at $x = 9.60$ cm.

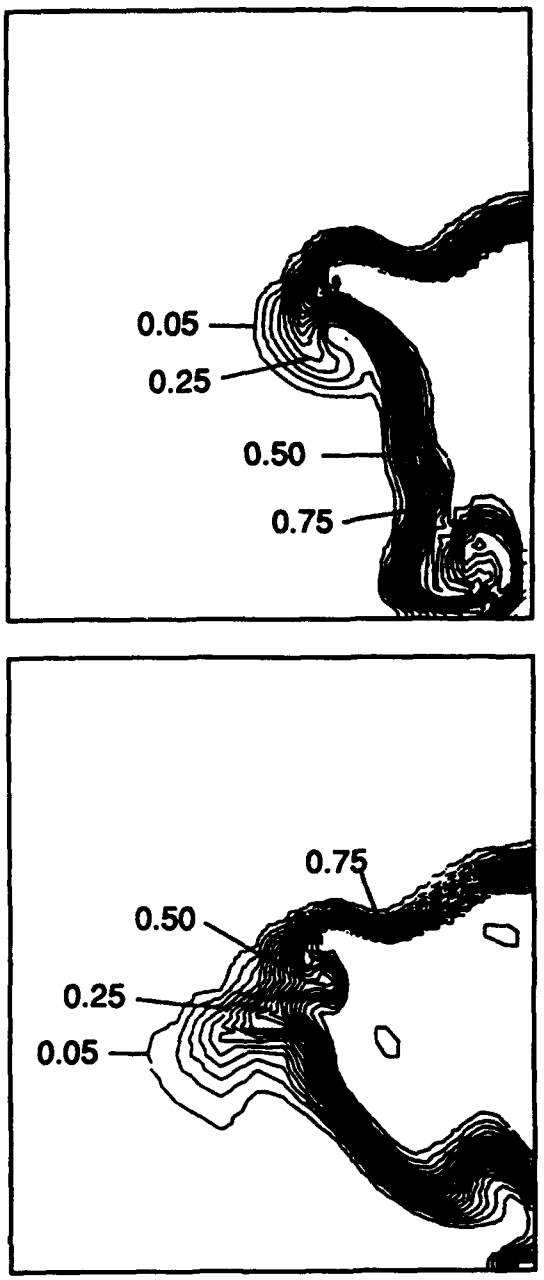

Figure 16. Cross-stream hydrogen mass fraction contours for (a) unswept, and (b) swept, ramp at $x = 11.3$ cm.

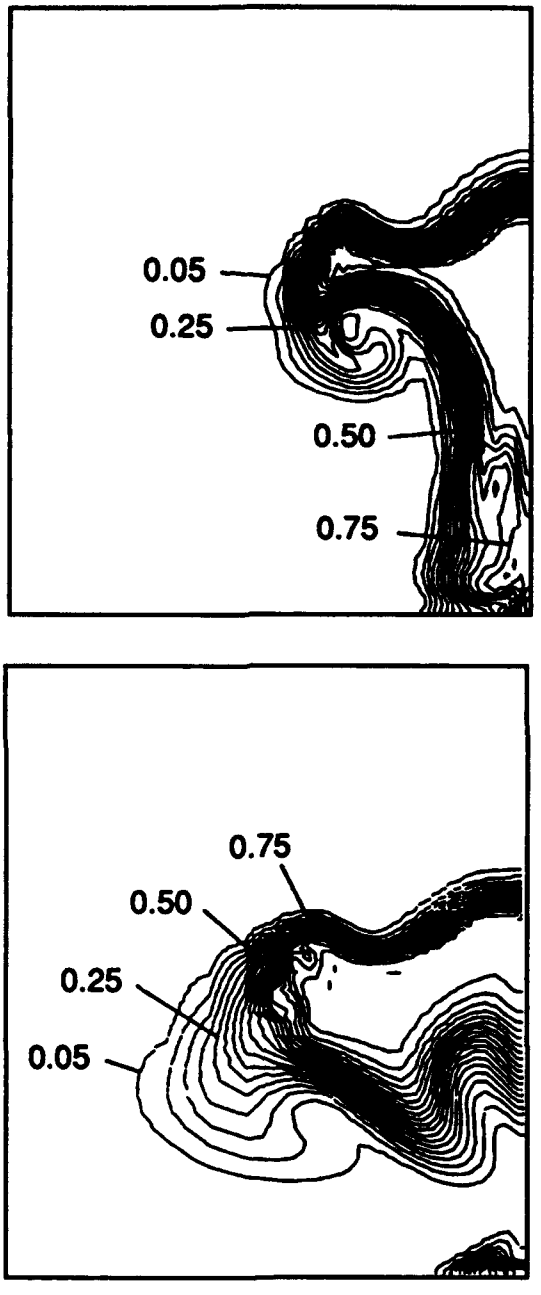

Figure 17. Cross-stream hydrogen mass fraction contours for (a) unswept, and (b) swept, ramp at $x = 13.2$ cm.

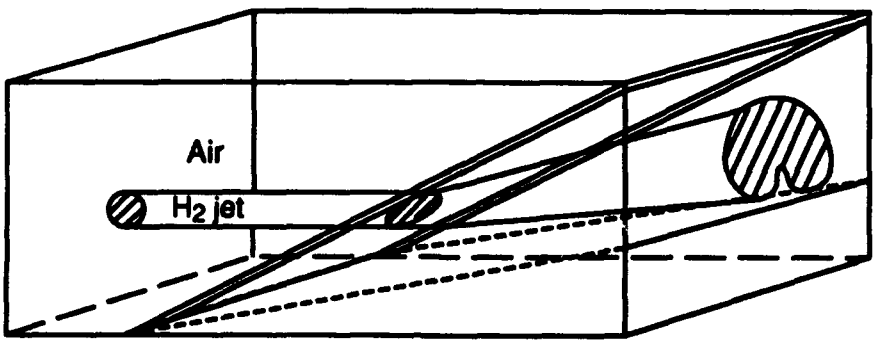

Figure 18. Schematic of shocked, parallel hydrogen fuel jet in air.

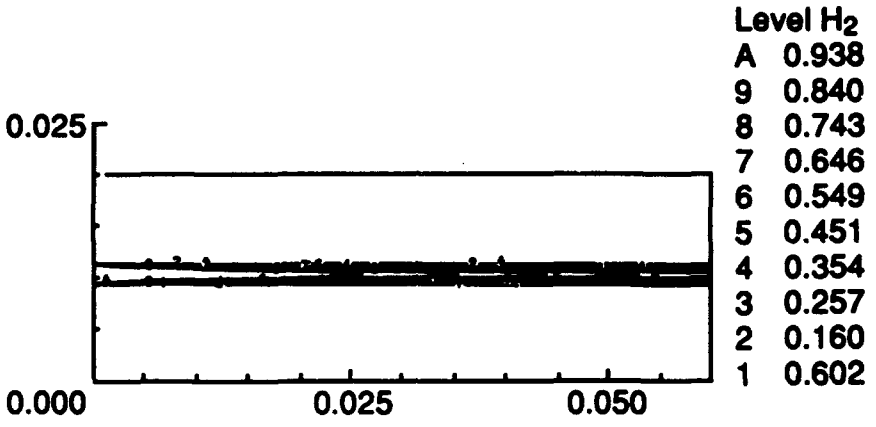

Figure 19. Hydrogen mass fraction of reacting, unshocked jet in $x - z$ plane at $y = 1$ cm.

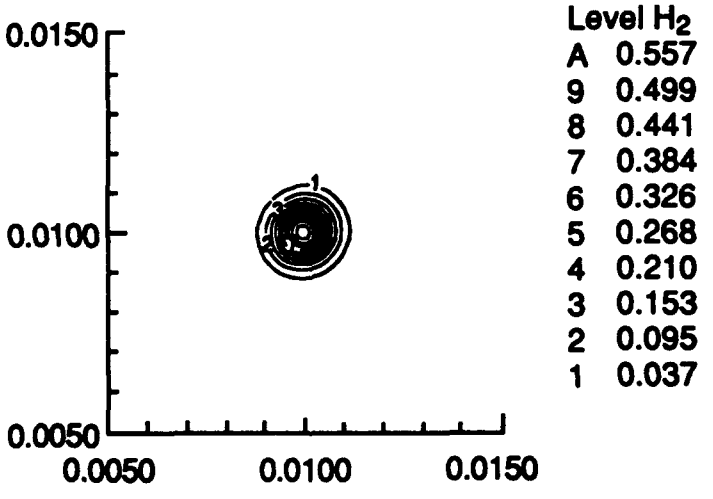

Figure 20. Hydrogen mass fraction of reacting, unshocked jet in $y - z$ plane at $x = 6$ cm.

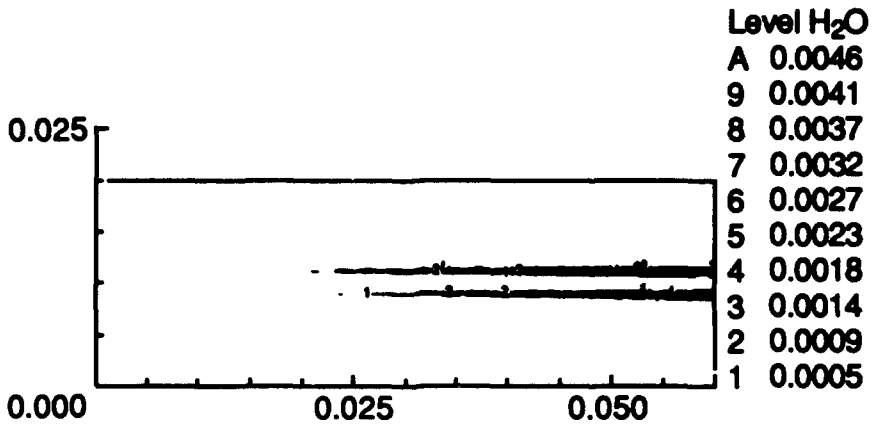

Figure 21. Water mass fraction of reacting, unshocked jet in $x - z$ plane at $y = 1$ cm.

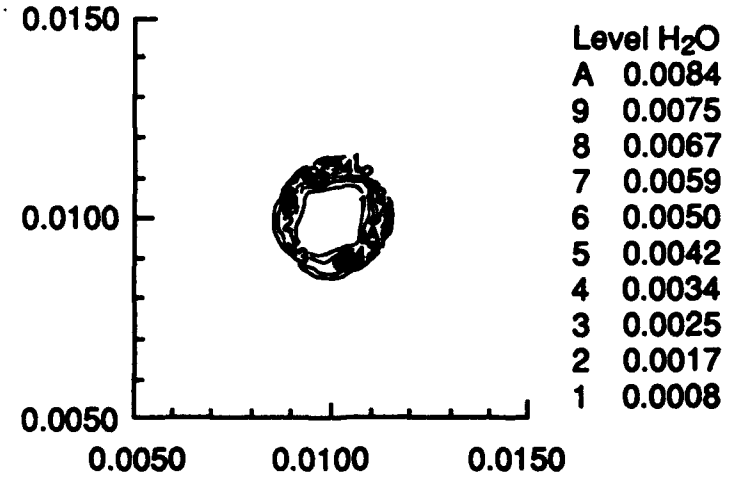

Figure 22. Water mass fraction of reacting, unshocked jet in $y - z$ plane at $x = 6$ cm.

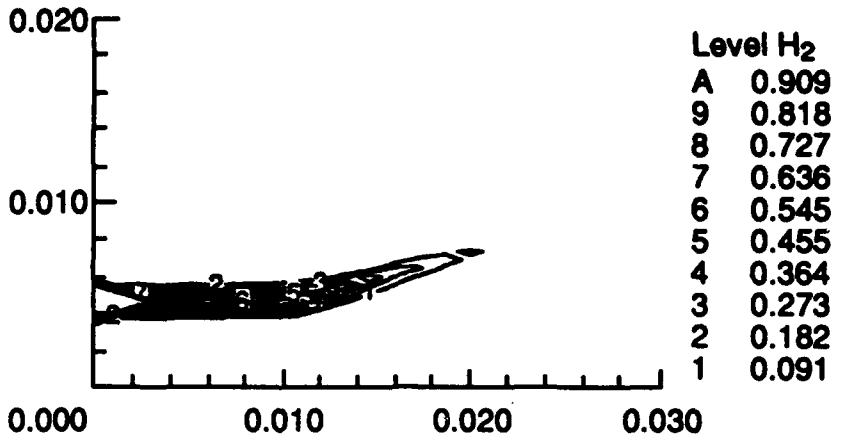

Figure 23. Hydrogen mass fraction of reacting, shocked jet in $x-z$ plane at $y = 1$ cm.

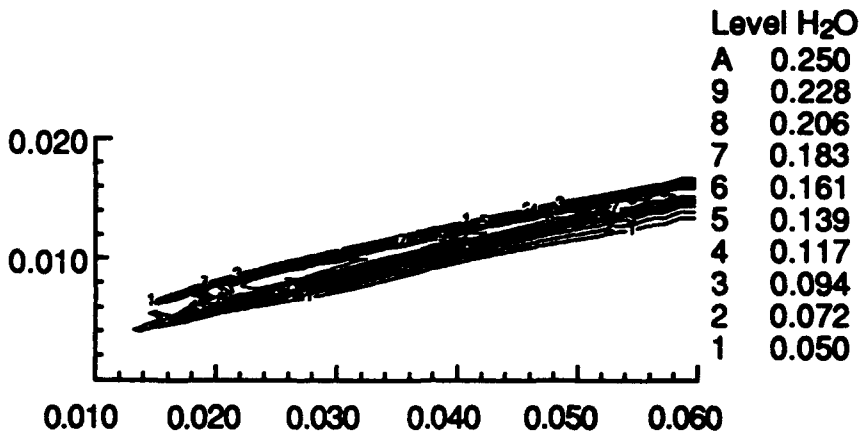

Figure 24. Water mass fraction of reacting, shocked jet in $x-z$ plane at $y = 1$ cm.

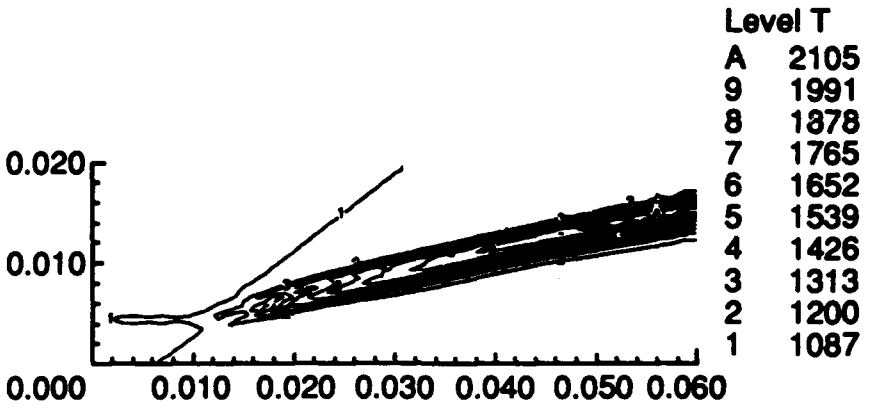

Figure 25. Temperature of reacting, shocked jet in $x - z$ plane at $y = 1$ cm.

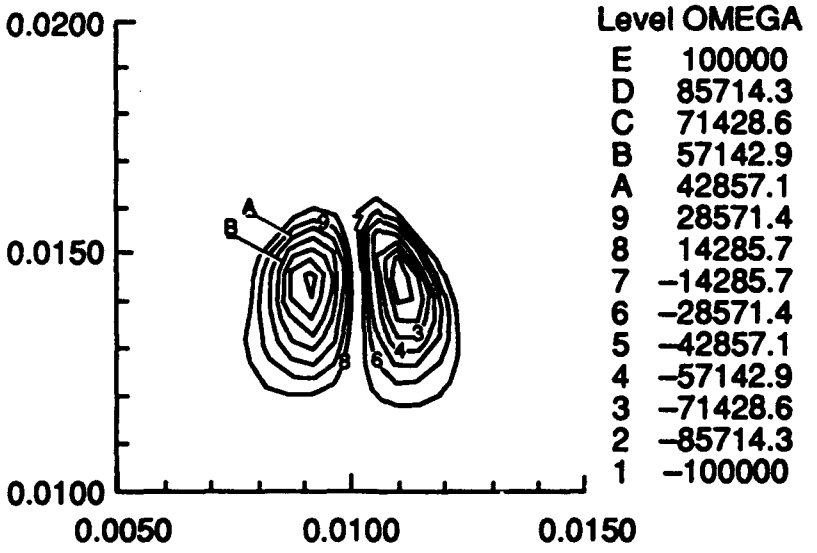

Figure 26. Streamwise vorticity of reacting, shocked jet in $y - z$ plane at $x = 6$ cm.

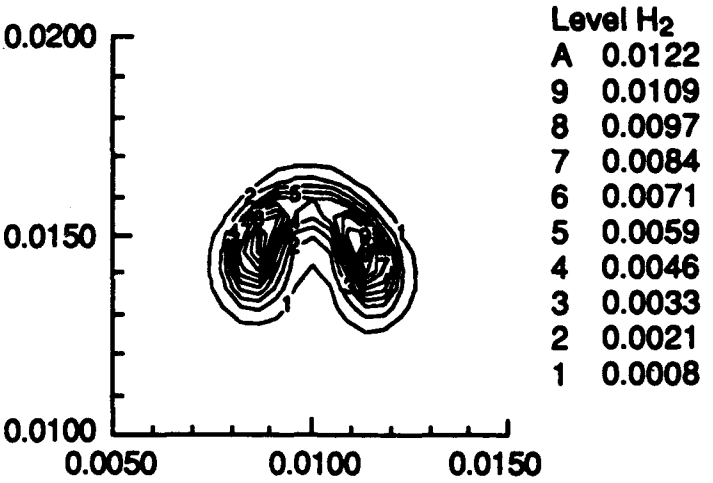

Figure 27. Hydrogen mass fraction of reacting, shocked jet in $y-z$ plane at $x = 6$ cm.

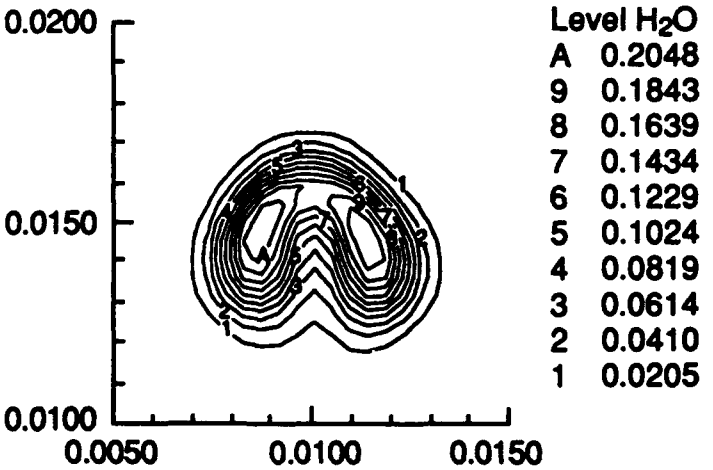

Figure 28. Water mass fraction of reacting, shocked jet in $y-z$ plane at $x = 6$ cm.

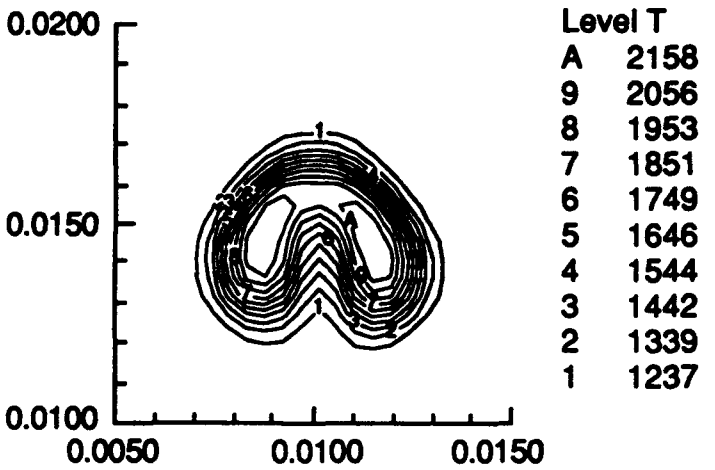

Figure 29. Temperature of reacting, shocked jet in $y - z$ plane at $x = 6$ cm.

APPENDIX 8

DNS of Non-Circular Jets

94-102

NUMERICAL SIMULATION OF NON-CIRCULAR JETS

R.S. Miller, C.K. Madnia and P. Givi
Department of Mechanical and Aerospace Engineering
State University of New York at Buffalo
Buffalo, NY 14260-4400

REVISED MAY 1994

Submitted to Computers and Fluids

Numerical Simulation of Non-Circular Jets

R.S. Miller, C.K. Madnia and P. Givi*
Department of Mechanical and Aerospace Engineering
State University of New York at Buffalo
Buffalo, NY 14260-4400

Abstract

Results are presented of numerical simulations of spatially developing, three dimensional jets issued from circular and non-circular nozzles of identical equivalent diameters. Elliptic, rectangular and triangular jets are considered with aspect-ratios of 1:1 and 2:1. Flow visualization results show that large scale coherent structures are formed in both cornered and non-cornered jets. The axis-switching phenomenon is captured in all non-unity aspect-ratio jets and also in the equilateral triangular jet. The square jet does not show axis-switching; however, the rotation of its axes by 45° is shown to play a significant role in its entrainment characteristics. All the non-circular configurations are shown to provide more efficient mixers than does the circular jet; the isosceles triangular jet is the most efficient one. It is demonstrated that the near field entrainment and mixing is characterized by the mean secondary flow induced by the stream-wise vortices. The transport of a passive Shvab-Zeldovich scalar variable is used to determine the limiting rate of mean reactant conversion in a chemical reaction of the type Fuel + Air → Products. The results show that the largest product formation occurs in the isosceles triangular jet and the lowest occurs in the circular jet. It is also shown that the 2:1 triangular jet has the shortest scalar core whereas the rectangular jet has the longest core.

1 Introduction

The phenomenon of mixing (or lack thereof) is a subject of crucial importance in devices involving chemically reacting turbulent flows [1]. In these devices, the flow field produced by

*To whom all the correspondence should be addressed. Tel: 716-645-2433, Fax: 716-645-3875, E-mail: givi@eng.buffalo.edu.

a "jet" discharging into a stagnant or moving (either in the parallel- or the cross-direction) fluid is the most common configuration in current use. In the majority of previous investigations on turbulent jets, circular and planar configurations have been considered [2–7]; with relatively little effort on the analyses of jets with other cross-sectional shapes [8]. Results of early investigations of three-dimensional (3D) rectangular jets have been reported in Refs. [9–11], and of elliptic jets in Refs. [12–15]. In studies pertaining to elliptic jets, it is now well recognized that the deformation of large scale vortical structures is somewhat similar to that of an isolated elliptic ring [16, 17]. This ring is inherently unstable due to the azimuthal variation of the "nozzle" curvature which causes a non-uniform self-induction mechanism. As a result, the ring deforms in such a way that its two axes are interchanged. This axis-switching mechanism plays an important role in promoting mixing by causing an increase of the entrainment as compared to that in circular and planar jets. While the extent of recent literature on elliptic jets is growing, relatively few experimental investigations of 3D jets with "corners" have been conducted. Gutmark *et al.* [8] use a one-component hot-wire anemometry system to measure the mean and turbulent characteristics and the effect of upstream forcing on the flow evolution of several non-circular jets. Their main conclusion is that the spatial growth rates and the amplification of velocity fluctuations vary around the circumference of the jet and are dependent on the initial local curvature. More recently, Gutmark *et al.* [18] have studied reactive non-circular jets by means of the Planar Laser Induced Fluorescence (PLIF) technique. They studied the effects of sharp corners on the dynamics of vortical structures as applied to enhancement of mixing and combustion. These results suggest that a combination of small- and large-scale mixing in a flow is advantageous in enhancing the product formation in combustion systems.

Most efforts in analytical treatment of non-circular jets have been based on linear stability analyses [19–23]. The extent of literature on detailed numerical simulations of 3D jet flows is very limited. This is understandable in view of the severe computational resources required for such simulations. With recent advances in supercomputer technology, however, this situation is gradually changing [24]. Owing to this technology, it is now possible to perform "model-free" simulations [25] of jet flows without resorting to "turbulence model-

ing". Givi [25] subdivides model-free simulations into Direct Numerical Simulation (DNS) and Large Eddy Simulation (LES). Currently the range of physical parameters, such as the Reynolds number, that can be treated by model free methods is significantly less than that in laboratory experiments. Such simulations, nevertheless, have proven very effective in elucidating many important features of turbulent flows; in some cases not easily amenable by other means.

In this work, we make use of model-free simulations to broaden our understanding of some of the underlying mechanisms involved in the near field of jet flows originating from non-circular nozzles. Our primary objective is to assess the influence of the nozzle on the subsequent evolution of the jet flows and their mixing characteristics. This is facilitated by analyzing the processes involved in entrainment. Six nozzle geometries are considered: circular, elliptic, square, rectangular, and triangular (equilateral and isosceles). Simulations are of a duration sufficient to determine statistics up to second moments. The flow fields produced by these jets are analyzed to determine the advantages and/or the drawbacks of non-circular nozzles for mixing enhancement, as compared with a circular nozzle. Consideration of these nozzles is motivated, at least partly, by recent experimental findings alluding to their capabilities in facilitating efficient turbulent combustion systems (*e.g.* Ref. [18]). The emphasis here is on extracting detailed information from the numerical simulations to complement the results obtained in laboratory experiments. Details of the geometrical configurations considered are given in Section 2. Results pertaining to hydrodynamic transport and those for the analysis of mixing-controlled reacting flows are presented in Section 3. A summary and conclusions are furnished in Section 4.

2 Description of the Problem

The flow configurations are produced by unsteady, 3D, spatially-developing jets in the presence of a co-flowing free-stream. The evolution of the flow is considered for several different inflow conditions. These conditions are produced via six different nozzle configurations:

circular, elliptic, square, rectangular, triangular (equilateral and isosceles); see table 1 and figure 1. The aspect-ratio for the elliptical, rectangular, and isosceles triangular jets is 2:1 (for the isosceles triangle the ratio refers to that of the height to the base). The dimensions in each jet are set in such a way as to yield the same equivalent diameter, D_e. This diameter corresponds to that of a circle with an equivalent area. The flow field is considered within the domain identified by Cartesian coordinates x (stream-wise), and y, z (cross-stream); see figure 1 for the orientation of the coordinates with respect to the cross sections of the jets.

The analysis is based on the numerical simulations of the compressible Navier-Stokes equations, the energy conservation, and a passive scalar conservation equation with Fourier heat conduction and Fickian diffusion assumptions. These equations are solved numerically without resorting to any turbulence or imposed subgrid models. The fluid is assumed calorically perfect and the magnitudes of the kinematic viscosity, thermal conductivity, and scalar diffusion coefficients are assumed constant. The values of the Prandtl number and the Schmidt number are set to unity and the ratio of the specific heats is set equal to 1.4. The fluid density and the temperature at the inflow are uniform and are set to $\rho = 1.0 kg/m^3$ and $T = 300K$, respectively. The jet exit velocity is $U_e = 86.8m/s$, and the co-flowing free-stream is $U_\infty = 17.4m/s$. In all the cases, the flows are initialized with identical Reynolds number, $Re = \Delta U D_e/\nu$, where $\Delta U = U_e - U_\infty$ and ν denotes the kinematic viscosity. This implies $Re = 800$ for the jets with $D_e = 0.02m$. The Mach numbers at the two streams are $M = 0.25$ and $M = 0.05$, respectively. This yields a convective Mach number [26] of $M_c = 0.15$ which is sufficiently low to not cause significant compressibility effects.

In order to provide a measure of the extent of mixing, the transport of a conserved scalar variable J is considered. This scalar is initialized in such a way as to yield the limiting values of 0 and 1 in the jet and in the free stream, respectively. The transport of this scalar determines the limiting rate of reactant conversion in a binary chemical reaction of the type "Fuel + Oxidizer $\rightarrow$ Products." With the usual definition of the Shvab-Zeldovich variable [27], the limiting values $J = 0, 1$ correspond to pure fuel and to pure oxidizer, respectively. In this way, effectively, the maximum rate of product formation of a fuel jet issuing into a co-flowing oxidizer is being simulated. With the assumption of unity mass

fractions at the feeds of each of the two respective reactants, $J_s = 1/2$ corresponds to the stoichiometric surface where, by definition, the rate of chemical reaction is infinitely fast and the product mass fraction is unity.

Several other parameters are calibrated in order to facilitate a direct comparison of the flow field produced by the jets. The flow is initialized by a "smooth" top-hat stream-wise velocity profile at the jet exit. The normalized cross-stream gradient of the Shvab-Zeldovich scalar is the same as that of the stream-wise mean velocity distribution. The velocity and the scalar gradients at the inlet are adjusted such that all inflows have identical momentum inflow and product thickness ($\delta_P(x) = \int\int_{jet} < \rho Y_P > dydz$; where $< >$ indicates the time average). The ratio of the maximum to minimum value of momentum thickness (denoted by θ_e) at the exit of the jets is listed in table 1. These values are in good agreement with those in the experiments [13, 12]. In addition to the base flow, low frequency perturbations are added at the inflow. The forcing is with the same Strouhal number, $St_{D_e} = \frac{\beta D_e}{U_e} = 0.4$ in all the jets. The integrated perturbed momentum is held constant for all jets. The amplitude of the velocity perturbation is set at approximately 15% of the jet exit velocity to expedite the formation of large scale structures within the domain considered.

The computational scheme is based on an explicit time marching procedure by means of a monotone Flux Corrected Transport (FCT) finite difference algorithm [28]. The algorithm used here is second order accurate in time, fourth order phase accurate in space and has been successfully employed in transitional shear layer studies [24, 29]. At the outflow, the first derivatives of the variables are assumed zero. Free slip conditions are employed at the boundaries in the cross-stream directions. The grid configuration consists of $120 \times 95 \times 95$ nodes for the unity aspect-ratio jets and varies slightly for the remaining cases. In all cases, the grid is compressed at the location of maximum mean gradients to provide a finer resolution. The computational requirements associated with each simulation vary slightly from one simulation to the other. In total, approximately 500 hours of CPU time on a Cray-YMP supercomputer were required to complete this study. The resolution employed here is to a large extent dictated by the available computational resources. With the magnitudes of the physical parameters considered, this resolution is less than that required to resolve

the Kolmogorov length scale. No explicit models are employed for the closure of subgrid fluctuations; the numerical dissipation inherent in the FCT algorithm provides the only means of modeling such fluctuations [30]. For "debates" on the usage of an appropriate label (DNS or LES) for these simulations we refer to Boris [31] and Givi [32].

3 Results

Simulations are performed within a domain large enough to accommodate for the growth of the jets and to minimize the effects of boundaries in the cross-stream direction. With available computational resources, it is possible to consider a domain with $L_x = 9D_e$, and $L_y \approx L_z \approx 4D_e$, where L_i denotes the length in the i-th direction. The simulated results are analyzed both instantaneously and statistically. The instantaneous results provide an effective means of flow visualization whereas the statistical data are useful for comparative assessments with laboratory data. Of course with the low value of the Reynolds number considered, it is not possible to make quantitative comparisons with such data. Qualitative comparisons, nevertheless, are possible and are made.

3.1 Flow Visualization

A qualitative assessment of the formation and dynamics of large scale flow vortical structures formed at the near field of the jets is possible by examining the instantaneous surfaces of constant vorticity magnitude. Figure 2 represents an iso-surface of vorticity magnitude for the non-cornered jets of Run 1 and Run 2. Part (a) of this figure shows that for the circular jet the growth of perturbations introduced at the inflow results in circular vortex-ring-like structures [33]. The shape and the dynamics of the structures formed in the elliptic jet are markedly different as shown in figure 2(b). The structures observed in this figure show the azimuthal variation of the vorticity magnitude. This variation is due to the initial shape of the ellipse which causes a non-uniform self-induction velocity leading to a three-dimensional

deformation. The iso-surfaces of vorticity magnitude for Runs 3 and 4 are shown in figure 3. This figure suggests that as the aspect ratio is increased, the initial structure of the jet is less preserved. The triangular jets (Run 5 and Run 6) exhibit different characteristics as observed in figure 4. In these jets, larger scale structures are produced near the flat surfaces and are masked by small scale structures produced near the corners. As a result, the flows appear to be characterized by a much more "turbulent" vorticity distribution than those produced by the other jets.

3.2 Statistical Consideration

The statistical analysis of the generated data is based on an ensemble of 1200 realizations. This is conducted within a time period equal to 2.5 times the residence time of the flow within the domain considered. The downstream evolution of the mean stream-wise velocity profiles in both cross-stream directions is shown in figure 5. All distances are normalized by the equivalent diameter (*e.g.* $x^* = x/D_e$). In the circular jet (figure 5(a)), it is apparent that the velocity profiles in the vertical and the horizontal center-planes are very similar. This suggests the radial symmetry of the flow and indicates adequacy of the numerical resolution. This is not the case for the elliptic jet (figure 5(b)). In this case, the width of the profile in the major plane is observed to contract for the first four equivalent diameters, and then to expand slowly. In contrast, the width in the minor plane spreads rapidly throughout the evolution. This trend is in good agreement with that observed in previous investigations (*e.g.* Ref. [12]). An interesting feature observed in this figure is the formation of shoulders on the minor plane velocity profiles downstream of $x^* = 6$. This is associated with the cross-stream mean secondary flow, as will be discussed in section 3.3. The results for the square jet (figure 5(c)) show that the profiles in both planes are very similar and grow uniformly in the stream-wise direction. Downstream of $x^* = 5$, two additional peaks appear on the mean velocity profiles. They are formed as a result of the induced flow field of the stream-wise vortices (section 3.3). No contraction of the width of the profiles is observed in either axes of the rectangular jet (figure 5(d)). For $x^* > 5$ the width along the minor axis becomes larger

than that along the major axis. This behavior is different from that observed in the elliptic jet. The peaks in the velocity profiles are also observed in the rectangular jet and are more pronounced in the major axis plane. The spread of the two triangular jets, shown in figures 5(e) and 5(f) is the most complex. The contraction and the subsequent expansion of the profiles in the transverse direction y is observed in both jets. The initial non-symmetry with respect to the minor axis prevails throughout the entire stream-wise evolution in both jets.

The downstream evolution of the normalized mean centerline velocity (U_{CL}/U_e) is shown in figure 6. This figure shows that the magnitude of this velocity initially rises slightly above unity due to forcing and then decays. The rate of decay is highest for the isosceles triangular jet. The variation of the longitudinal fluctuating velocity along the jet centerline is presented in figure 7. Except for the two triangular jets, a peak intensity occurs at $x^* \approx 4.5$ for all cases. As discussed in Ref. [13] the amplitude and location of this peak are dependent on the value of the Strouhal number.

The stream-wise evolution of the mean jet half velocity $< U_h >=< \frac{(U_{CL}+U_\infty)}{2} >$ contours is presented in figure 8 for Runs 2 through Run 6. Each contour represents conditions within the range $0 \leq x^* \leq 5$, with an increment of $x^* = 1$. Figure 8(a) indicates that at the first two stream-wise locations, the jet maintains its initial elliptic shape with the major axis in the y direction. Further downstream, there is a continuous reduction of the local aspect-ratio due to a larger spreading of the jet in the minor-axis plane. By $x^* = 5$, the mean profile is rotated by 90° and the axes are switched. In contrast, the results in figure 8(b) indicate that the flow field of the square jet does not experience an axis-switching; however, a 45° rotation is observed. Figure 8(c) portrays the axis-switching of the rectangular jet. A 90° rotation of the major axis is observed. The evolved shape is nearly elliptical except for small stretching along the $y-$axis. In triangular configurations, a very different behavior is experienced (figures 8(d) and 8(e)). In both jets, a 180° "flip-flop" of the original profile is observed, climaxed with a triangular shaped profile which is nearly equilateral.

The location of axis-switching is determined by monitoring the stream-wise variations of the major and the minor axis half velocity widths for all the jet configurations. These widths

are non-dimensionalized by D_e and are denoted by B_y^* and B_x^* for the major- and the minor-axis, respectively. The stream-wise variations of these widths are shown in figure 9 and the axis-switching location for each run is listed in table 2. Figure 9(a) indicates that the elliptic jet switches its axes at $x^* \approx 3$. The experimental data of the switch-over location for a 2:1 elliptic jet is $x^* \approx 2.4$ as reported in Ref. [13], and $x^* \approx 2.8$ as suggested in Ref. [12]. In the experiments of Ref. [13], the jet is forced at $St_{D_e} = 0.4$ and the momentum thickness at the jet exit is uniform. In the experiments of Ref. [12], an unforced jet is considered with a non-uniform momentum thickness. The square jet does not switch its axes and both widths grow monotonically in x^* as shown in figure 9(b). The switching location for the rectangular jet is further downstream than that for the elliptic jet (figure 9(c)). This can be attributed to the influence of corners. As indicated in figure 8(c), the rectangular jet evolves into a rotated elliptic configuration. It must, therefore, smooth its corners while simultaneously switching axes. Thus, its spreading rate in the minor plane is slower than that in the elliptic jet. Figures 9(d) and 9(e) show two axis-switchings for the two triangular jets. In both jets, B_y^* initially decreases to a minimum corresponding to the maximum of B_x^*, and then increases. The first axis-switching in the isosceles triangular jet occurs approximately twice as far downstream as that in the equilateral triangular jet (table 2). This can be attributed to the larger aspect-ratio of the isosceles triangular nozzle which results in an initial gap between the major and the minor axis half widths.

3.3 Entrainment of Free-Stream Fluid

A measure of entrainment of the free-stream fluid provides an effective means of estimating the mixing efficiency of the jets. Here, the entrainment is quantified by measuring the difference between the average mass flow rate (conditioned on $< J > \leq 0.99$) at a downstream location $Q(x^*)$ and that at the nozzle exit, $Q_o = Q(x^* = 0)$. Figure 10 shows the normalized value of this parameter as a function of the stream-wise coordinate. This figure shows that the isosceles triangular jet entrains nearly 125% of its initial mass flow rate as compared to 50% obtained for the circular jet. The mass entrained by the other jets fall somewhere

in between these two extremes. Conceptual understanding of the entrainment process is aided by examining the time-averaged cross-stream velocity vectors. Figures 11-15 show these vectors for Runs 2 through 6, at stream-wise locations $x^* = 2$, 4, and 6 (except for Run 3 in which vectors at $x^* = 1$, 4, and 6 are shown). The solid line in these figures denote the $< U_h >$ iso-line. Stream-wise vortical structures are observed for all the non-circular jets. The elliptic jet (figure 11) is shown to entrain fluid into the mixing zone along the $y-$axis and to eject it along the $z-$axis. The effect is to contract the major axis of the jet while simultaneously stretching the minor axis, resulting in axis-switching. Notice the recirculation pattern caused by the four vortices. The flow field associated with this recirculation pattern is responsible for the formation of the shoulders observed on the minor plane velocity profiles presented in figure 5(b). A more complex flow pattern is observed for the square jet (figure 12). The velocity field induced by the four counter-rotating pairs of vortices (figure 12(a)) causes an outflow of the fluid on the flat sides and an inflow at the corners. By $x^* = 4$ the original configuration is rotated by 45° about the $y-$axis (figure 12(b)). At this location, four additional pairs of vortices are formed inside the original ones. Farther downstream, the flow pattern induced by these vortices results in further stretching of the new corners (figure 12(c)). Also, the inner set of vortex pairs are no longer distinct and tend to lose their identity. As the flow evolves downstream, the induced velocity field due to the outer set of stream-wise vortex pairs results in the formation of two additional peaks on the velocity profiles in both the major plane and the minor plane as shown in figure 5(c). The rectangular jet displays characteristics similar to those of the square and the elliptic jets (figure 13). Initially, two vortex pairs are formed with their axes coincident with the $z-$axis. This enables the jet to adopt an elliptic configuration and to display a recirculation pattern similar to that in figure 11(a). However, the influence of the jet origin (nozzle geometry) is not completely lost and the subsequent evolution is considerably different from that of the elliptic jet. At $x^* = 4$, the cross-section becomes diamond shaped, similar to that in the square jet at the same location. By $x^* = 6$, four vortex pairs are formed and the shape of the jet is elliptic with major axis on the $z-$axis and with a slightly stretched minor axis. Due to the delay in its axis-switching, the rectangular jet is a relatively inefficient mixer in the near field. The evolution of the cross-section of the equilateral triangular jet is depicted

in figure 14. At $x^* = 2$ the profile for this jet adopts an approximate square shape. However, the flow pattern and the subsequent evolution are clearly different from that in the square jet. By $x^* = 4$ (figure 14(b)) the profile is heart-shaped with a strong outflow induced by two vortex pairs located at the corners. The interaction of these vortices continues to distort the profile downstream (figure 14(c)). For the isosceles triangular jet, figure 15(a) shows the entrainment from the top corner and the base, and ejection of the fluid from the two long flat sides. Further downstream, this causes a "flip-flop" of the profile. The fluid is entrained from the bottom corner and is ejected through the top corners.

The results presented here indicate the influence of large scale structures on the global mixing process in both circular and non-circular jets. These results also show that near-field mixing and entrainment is characterized by the induced secondary flow field of the stream-wise vortices.

3.4 Influence on Reactant Conversion

The consequences of the flow evolution on the rate of reactant conversion in reacting jets are portrayed by considering the transport of the Shvab-Zeldovich scalar variable, J. Figure 16 depicts the instantaneous stoichiometric surface $J = J_s$, corresponding to the flame sheet, for each jet. This figure shows a severe distortion of the flame surface in the non-circular jets. In particular, the two triangular jets show a highly stretched and convoluted topology with the formation of small scale structures. The extent of distortion of the stoichiometric surface provides a measure of the combustion efficiency as measured by the magnitude of the product formation. The downstream evolution of the mean product mass fraction in the $y - x$ and $z - x$ planes is shown in figure 17. Examination of figure 17(a) indicates that for the circular jet, the initial reaction occurs along the jet boundaries and proceeds to spread both outward and inward. The two spikes at $x^* = 0$ are due to finite gradients of the Shvab-Zeldovich profile at the inflow. For the circular jet it is about eight diameters downstream before the product reaches the centerline. The profile for the elliptic jet is initially similar to that of the circular jet. The difference is in the widths of the profiles in the major and the

minor planes. As the jet evolves downstream, the profiles in the two planes start to differ and some of the profiles in the minor axis plane develop blunt topped humps (figure 17 (b)). Similar flat-topped peaks are observed in the profiles in the square and the rectangular jets (figures 17(c) and 17(d)). The stream-wise vortex pairs (shown in figures 12(c) and 13(c)) are responsible for increasing mixing in these regions and the reaction takes place over a larger volume. The square jet profiles portray approximately the same shape in the $y-x$ and $z-x$ planes. The rectangular jet for which the initial axis-switching occurs at the stream-wise location of $x^* = 6.3$ maintains its maximum value of the mean product mass fraction at its outer edges. Both the equilateral and the isosceles triangular jets (figures 17(e) and 17(f)) are characterized by a large increase in the product formation in the center of the jet as compared to those in the other jets.

The stream-wise variations of the integrated product thickness are shown in figure 18. This figure shows that for $x^* < 3$ the extent of products formed in the circular jet is lower than those in the square and the triangular jets, but is higher than those in the elliptic and the rectangular jets. In the region $3 < x^* < 5$ the products formed in all the jets are lower than that in the circular jet with the exception of the isosceles triangular jet. Further downstream ($x^* > 6$) all the non-circular jets yield higher values of product thickness as compared to the circular jet. The results presented in this figure are consistent with those in figure 10 which indicate that the product formation is directly related to the entrainment. Therefore, the ratio of the integrated product thickness to the physical area of the jet is considered. This area refers to regions in the stream-wise planes where $< J > \lesssim 0.99$. This ratio is denoted as γ and is referred to as the cross-stream product density [34, 29]. The stream-wise variation of this ratio is shown in figure 19 for all jets. This figure suggests that after a period of rapid growth, a plateau at the value of $\gamma \approx 0.55$ is reached in all cases. This provides an explanation for the correlation between the growth rate of the area and that of the product thickness. Experimental confirmation of the existence of a plateau value of γ for higher Reynolds number turbulent jets is desirable.

The traditional definition of the jet potential core is not very applicable to the quasi-transitional jets studied here. Pertaining to mixing, a scalar core is defined as the stream-wise

length of the jet containing pure, unmixed fuel within the non-reacting jets. This corresponds to $J = C$. Figure 20 presents the normalized integrated mass of fuel as a function of stream-wise location. A near linear decrease of fuel mass fraction is observed in all the cases. The lengths of the scalar cores in all the jets are listed in table 3. The square and the rectangular jets, with no axis-switching and axis-switching far downstream respectively, have the longest cores. The shortest core occurs for the isosceles triangular jet.

4 Summary and Concluding Remarks

Detailed numerical experiments are conducted to study the entrainment and mixing characteristics of the flow fields generated by non-circular turbulent jets. Simulations are conducted of jet flows originating from elliptic, rectangular, and triangular nozzles with aspect-ratios of 1:1 and 2:1. The results are compared with those of a circular jet of the same equivalent diameter to determine the relative efficiency of non-circular nozzles in mixing enhancement. Flow visualization results show that for both cornered and non-cornered jets, large scale coherent structures are formed. The shape and dynamics of these structures depend on the azimuthal variation of the curvature of the profiles at the jet exit. The triangular jets exhibit characteristics markedly different from the other jets. Coherent large scale structures in these jets are quickly masked by the small scale structures formed at the corners. In the elliptic and the rectangular jets, the orientations of the cross-sections are modified by axis-switching. The rectangular jet switches its axes at a stream-wise distance approximately twice that of the elliptic jet. This can be attributed to the effects of the corners. Although the square jet does not show axis-switching, it is shown that a 45° rotation of its initial profile results in entrainment of the free-stream fluid. The triangular jets switch their axes twice. In the isosceles triangular jet, the first axis cross-over occurs approximately twice as far downstream as that in the equilateral triangle. This is attributed to the larger aspect-ratio of the isosceles triangular jet.

The entrainment and mixing in the near field of these jets are shown to be characterized by

the induced mean secondary flow field of the stream-wise vortices. Non-unity aspect-ratios, sharp corners, and long flat surfaces are important factors in facilitating an efficient mixing configuration. In the case of the rectangular jet, although it contains many of these features, its axes switch too far downstream to cause significant near-field mixing. Although a non-unity aspect-ratio is important for mixing enhancement, it is not sufficient for large entrainment in the near-field. The isosceles triangular jet is shown to be the most efficient mixer. This jet produces the most intricate network of stream-wise vortices which are responsible for enhanced mixing. The square jet ranks as the second most efficient mixer, and the circular jet is the least efficient one. A comparison of the flow fields produced by the two triangular jets reveals that the formation of small scale structures at the corners does not have a significant influence in entraining the free-stream fluid. The aspect-ratio is the primary difference between these two jets. The effect of the larger aspect-ratio of the isosceles triangular jet is to alter the vorticity dynamics in this jet as compared to the equilateral triangular jet. This results in a different stream-wise vorticity pattern which enhances entrainment.

The limiting rate of the mean reactant conversion in reacting jets in which the fuel is discharged to ambient oxidizer is evaluated by considering the transport of a Shvab-Zeldovich scalar variable. It is shown that the isosceles triangular jet yields the highest amount of chemical products, whereas the circular jet yields the lowest. However, the magnitudes of the cross-stream product density approaches a plateau in all the jets. The magnitudes at this plateau are approximately the same for all the cases. With the transport of the Shvab-Zeldovich variable, a scalar core is also defined. It is shown that the 2:1 aspect-ratio triangular jet has the shortest, and the rectangular jet has the longest core.

The examination of the effects of harmonic forcing and the role of the initial momentum thickness on the subsequent development of jet flows under the influence of non-equilibrium chemical reactions are the subject of our current investigations.

Acknowledgments

This work is part of an effort sponsored by the Office of Naval Research under Grant N00014-90-J-4013 and by the National Science Foundation under Grant CTS-9253488. Computational resources are provided by the NSF through the National Center for Supercomputing Applications at the University of Illinois.

References

[1] Drummond, J. P. and Givi, P., Suppression and Enhancement of Mixing in High-Speed Reacting Flow Fields, in Hussaini, M. Y., Buckmaster, J. D., Jackson, T. L., and Kumar, A., editors, *Combustion in High-Speed Flows*, Kluwer Academic Publishers, The Netherlands, 1994, in press.

[2] Wygnanski, I. and Fiedler, H., Some Measurements in the Self-Preserving Jet, *J. Fluid Mech.*, **38**:577–612 (1969).

[3] Crow, S. C. and Champagne, F. H., Orderly Structure in Jet Turbulence, *J. Fluid Mech.*, **48**:547–591 (1971).

[4] Yule, A. J., Large-Scale Structure in the Mixing Layer of a Round Jet, *J. Fluid Mech.*, **89**:413–432 (1978).

[5] Dimotakis, P. E., Maike-Lye, R. C., and Papantoniou, D. A., Structure and Dynamics of Round Turbulent Jets, *Phys. Fluids*, **26**(11):3185–3192 (1983).

[6] Gutmark, E. and Wygnanski, I., The Planar Turbulent Jet, *J. Fluid Mech.*, **73**:465–495 (1976).

[7] Everett, W. K. and Robins, G. A., The Development and Structure of Plane Jets, *J. Fluid Mech.*, **88**:563–584 (1978).

[8] Gutmark, E., Schadow, K. C., Parr, D. M., Harris, C. K., and Wilson, K. J., The Mean and Turbulent Structure of Non-Circular Jets, AIAA Paper 85-0543, 1985.

[9] Sforza, P. M., Steiger, M. H., and Trentacoste, N., Studies on Three Dimensional Viscous Jets, *AIAA J.*, **4**:800–806 (1966).

[10] Trentacoste, N. and Sforza, M. P., Further Experimental Results for Three-Dimensional Free Jets, *AIAA J.*, **5**:885–891 (1967).

[11] Krothapalli, A., Baganoff, D., and Karamcheti, K., On the Mixing of a Rectangular Jet, *J. Fluid Mech.*, **107**:201–220 (1981).

[12] Ho, C.-M. and Gutmark, E., Vortex Induction and Mass Entrainment in a Small-Aspect-Ratio Elliptic Jet, *J. Fluid Mech.*, **179**:383 (1987).

[13] Husain, H. S. and Hussain, F., Elliptic Jets. Part 1. Characteristics of Unexcited and Excited Jets, *J. Fluid Mech.*, **208**:257–320 (1989).

[14] Husain, H. S. and Hussain, F., Elliptic Jets. Part 2. Dynamics of Coherent Structures: Pairing, *J. Fluid Mech.*, **233**:439–482 (1991).

[15] Husain, H. S. and Hussain, F., Elliptic Jets. Part 3. Dynamics of Preferred Mode Coherent Structure, *J. Fluid Mech.*, **248**:315–361 (1993).

[16] Dhanak, M. R. and B., D. B., The Evolution of an Elliptic Vortex Ring, *J. Fluid Mech.*, **109**:189–216 (1981).

[17] Viets, H. and Sforza, P. M., Dynamics of Bilaterally Symmetric Vortex Rings, *Phys. Fluids*, **15**:230–240 (1972).

[18] Gutmark, E., Schadow, K. C., Parr, T. P., Hanson-Parr, M., D., and Wilson, K. J., Noncircular Jets in Combustion Systems, *Experiments in Fluids*, **7**:248–258 (1989).

[19] Koshigoe, S. and Tubis, A., Wave Structures in Jets of Arbitrary Shape: I. Linear Inviscid Spatial Stability Analysis, *Phys. Fluids*, **29**(12):3982–3992 (1986).

[20] Koshigoe, S. and Tubis, A., Wave Structures in Jets of Arbitrary Shape: II. Applications of a Generalized Shooting Method to Linear Stability Analysis, *Phys. Fluids*, **30**(6):1715–1723 (1987).

[21] Koshigoe, S., Ho, C. M., and Tubis, A., Application of a generalized Shooting Method to the Linear Stability Analysis of Elliptic Core Jets, AIAA Paper 87-2722, 1987.

[22] Koshigoe, S., Gutmark, E., Schadow, K. C., and Tubis, A., Instability Analysis on Non-Circular Free Jets, AIAA Paper 88-0037, 1988.

[23] Tam, C. K. W. and Thies, A. T., Instability of Rectangular Jets, *J. Fluid Mech.*, **248**:425–448 (1993).

[24] Grinstein, F. F. and DeVore, C. R., Coherent Structure Dynamics in Spatially-Developing Square Jets, AIAA Paper 92-3441, 1992.

[25] Givi, P., Model Free Simulations of Turbulent Reactive Flows, *Prog. Energy Combust. Sci.*, **15**:1–107 (1989).

[26] Papamoschou, D. and Roshko, A., The Compressible Turbulent Shear Layer: An Experimental Study, *J. Fluid Mech.*, **197**:453–477 (1988).

[27] Williams, F. A., *Combustion Theory*, The Benjamin/Cummings Publishing Company, Menlo Park, CA, 2nd edition, 1985.

[28] Boris, J. P. and Book, D. L., Solution of the Continuity Equations by the Method of Flux Corrected Transport, in *Methods in Computational Physics*, pp. 85–129, Academic Press, New York, NY, 1976.

[29] Miller, R. S., Madnia, C. K., and Givi, P., Structure of a Turbulent Reacting Mixing Layer, *Combust. Sci. and Tech.*, (1994), In press.

[30] Boris, J. P., Grinstein, F. F., Oran, E. S., and Kolbe, R. L., New Insights into Large Eddy Simulations, NRL Report NRL/MR/4400-92-6979, Naval Research Laboratory, Washington, D.C., 1992.

[31] Boris, J. P., On Large Eddy Simulation Using Subgrid Turbulence Models, in Lumley, J. L., editor, *Whither Turbulence? Turbulence at the Crossroads, Lecture Notes in Physics*, Vol. 357, pp. 344–353, Springer-Verlag, New York, NY, 1990.

[32] Givi, P., Spectral and Random Vortex Methods in Turbulent Reacting Flows, in Libby, P. A. and Williams, F. A., editors, *Turbulent Reacting Flows*, chapter 8, Academic Press, London, UK, 1994, in press.

[33] James, S., Direct Numerical Simulation of Laminar Vortex Rings, M.S. Thesis, Department of Mechanical and Aerospace Engineering, State University of New York at Buffalo, Buffalo, NY, 1994.

[34] Koochesfahani, M. M. and Dimotakis, P. E., Mixing and Chemical Reactions in a Turbulent Liquid Mixing Layer, *J. Fluid. Mech.*, **170**:83–112 (1986).

Figure Captions

Figure 1. Jet profiles as represented by U_h contours.

Figure 2. Surfaces of constant vorticity magnitude ($|\omega|/|\omega|_{max} = 0.55$). (a) Run 1, (b) Run 2.

Figure 3. Surfaces of constant vorticity magnitude ($|\omega|/|\omega|_{max} = 0.55$). (a) Run 3, (b) Run 4.

Figure 4. Surfaces of constant vorticity magnitude ($|\omega|/|\omega|_{max} = 0.60$). (a) Run 5, (b) Run 6.

Figure 5. Stream-wise evolution of $< U >$ in both $y - x$ and $z - x$ planes. Scale: One stream-wise equivalent diameter corresponds to 100 m/s. (a) Circular jet, (b) Elliptic jet, (c) Square jet, (d) Rectangular jet, (e) Equilateral triangular jet, (f) Isosceles triangular jet.

Figure 6. Downstream evolution of the normalized mean centerline velocity for Runs 1-6.

Figure 7. Downstream evolution of fluctuating centerline velocity for Runs 1-6. Legends are the same as those in figure 6.

Figure 8. Axis switching as depicted by $< U_h >$ contours. Contours are in increments of $x^* = 1$. (a) Run 2, (b) Run 3, (c) Run 4, (d) Run 5, (e) Run 6.

Figure 9. Evolution of the jet half width *vs.* stream-wise direction. (a) Run 2, (b) Run 3, (c) Run 4, (d) Run 5, (e) Run 6.

Figure 10. Downstream variation of the entrainment ratio. Legends are the same as those in figure 6.

Figure 11. Time averaged cross-stream velocity vectors for Run 2. (a) $x^* = 2$, (b) $x^* = 4$, (c) $x^* = 6$.

Figure 12. Time averaged cross-stream velocity vectors for Run 3. (a) $x^* = 1$, (b) $x^* = 4$, (c) $x^* = 5$.

Figure 13. Time averaged cross-stream velocity vectors for Run 4. (a) $x^* = 2$, (b) $x^* = 4$, (c) $x^* = 6$.

Figure 14. Time averaged cross-stream velocity vectors for Run 5. (a) $x^* = 2$, (b) $x^* = 4$, (c) $x^* = 6$.

Figure 15. Time averaged cross-stream velocity vectors for Run 6. (a) $x^* = 2$, (b) $x^* = 4$, (c) $x^* = 6$.

Figure 16. Instantaneous surface of the flame sheet. (a) Run 1, (b) Run 2, (c) Run 3, (d) Run 4, (e) Run 5, (f) Run 6.

Figure 17. Profiles of the mean product mass fraction in the $y-x$ and $z-x$ planes. (a) Run 1, (b) Run 2, (c) Run 3, (d) Run 4, (e) Run 5, (f) Run 6. Scale: 0.9 stream-wise equivalent diameter corresponds to unity mass fraction.

Figure 18. Equilibrium product thickness *vs.* stream-wise direction. Legends are the same as those in figure 6.

Figure 19. Cross-stream product density *vs.* stream-wise direction. Legends are the same as those in figure 6.

Figure 20. Normalized mass of unmixed fuel *vs.* stream-wise direction. Legends are the same as those in figure 6.

Tables

Table 1. Flow configurations.

Table 2. Streamwise location(s) of axis switching.

Table 3. Streamwise location of the scalar core.

TABLE 1

Run	Configuration	Aspect ratio	$(\theta_e)_{max}/(\theta_e)_{min}$
1	Circle	1 : 1	1.00
2	Ellipse	2 : 1	1.51
3	Square	1 : 1	1.23
4	Rectangle	2 : 1	1.59
5	Triangle	1 : 1	1.28
6	Triangle	2 : 1	2.00

TABLE 2

Run	Axis Switch (x^*)
1	no switch
2	3.1
3	no switch
4	6.3
5	1.5, 4.6
6	2.9, 6.5

TABLE 3

Run	Scalar Core (x^*)
1	7.5
2	7.0
3	8.0
4	8.5
5	6.5
6	6.0

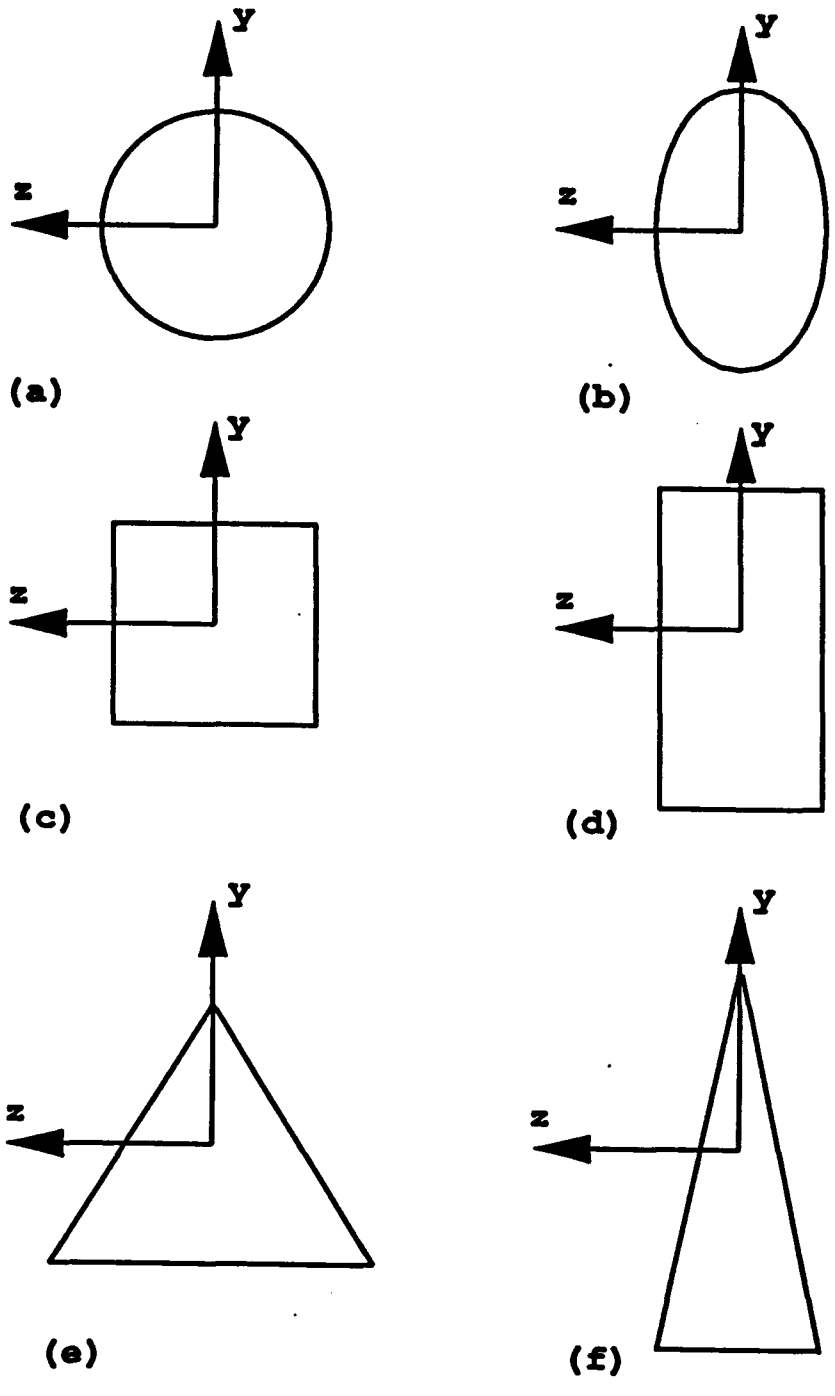

FIG. 1

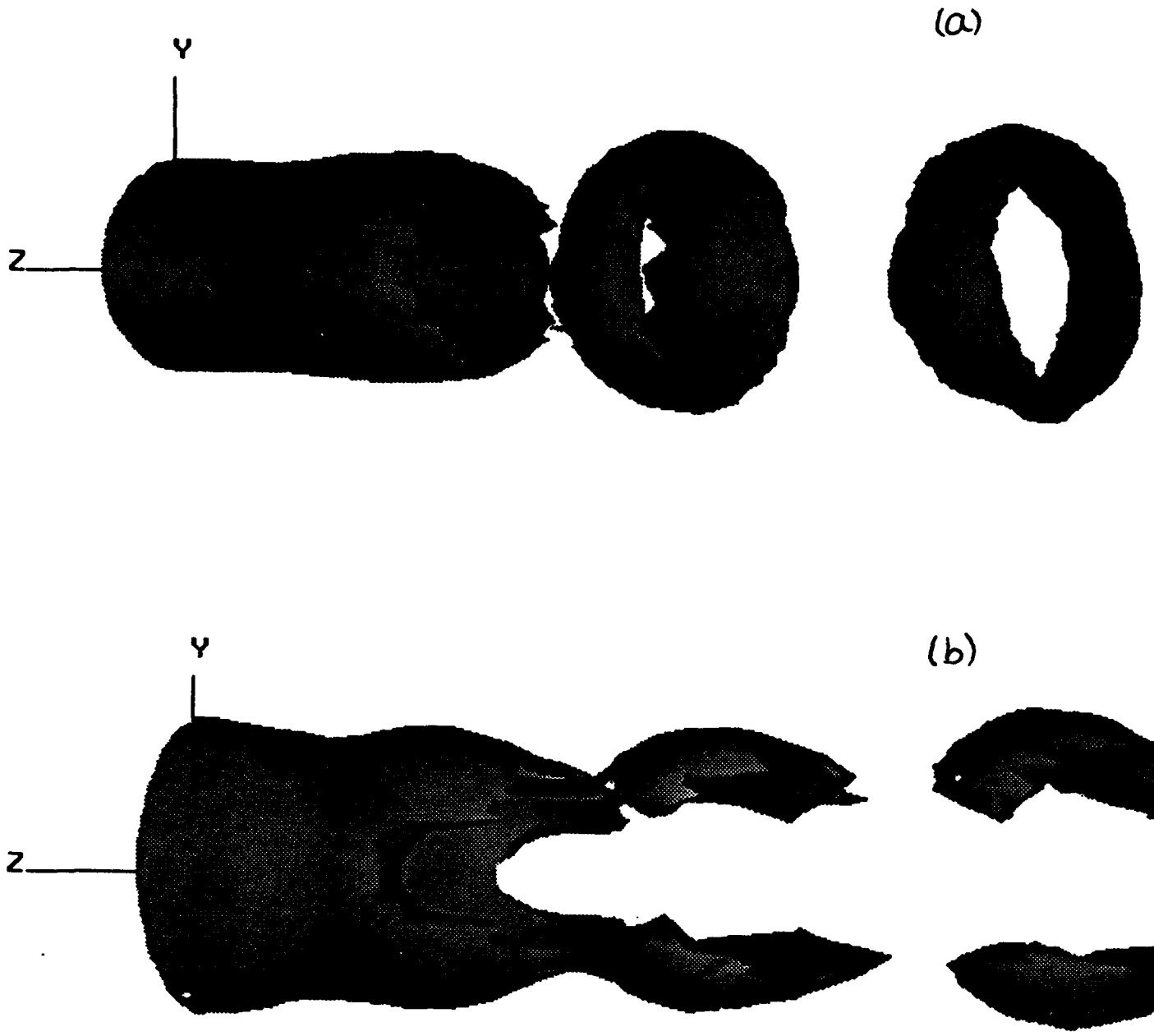

FIG. 2

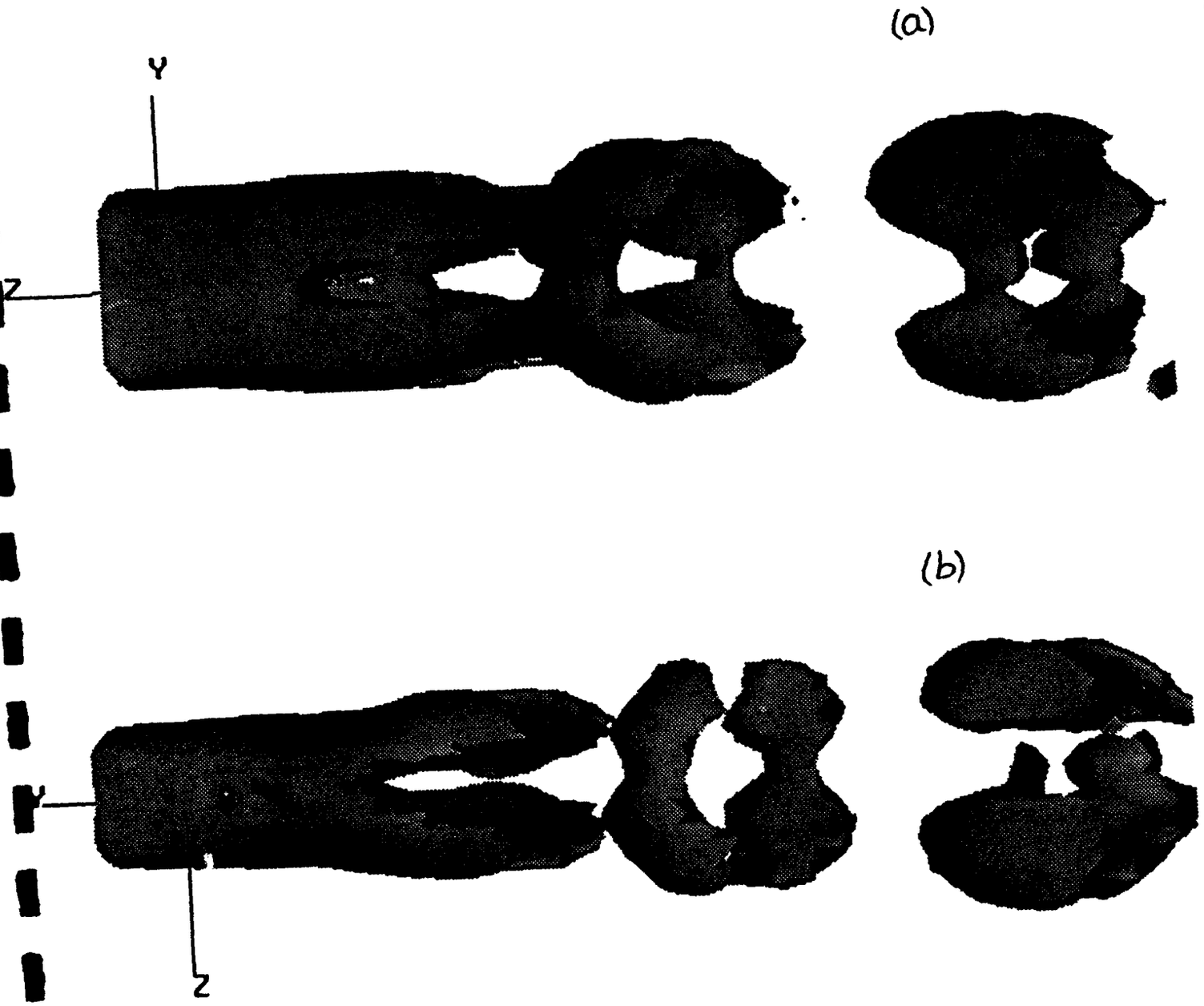

FIG. 3

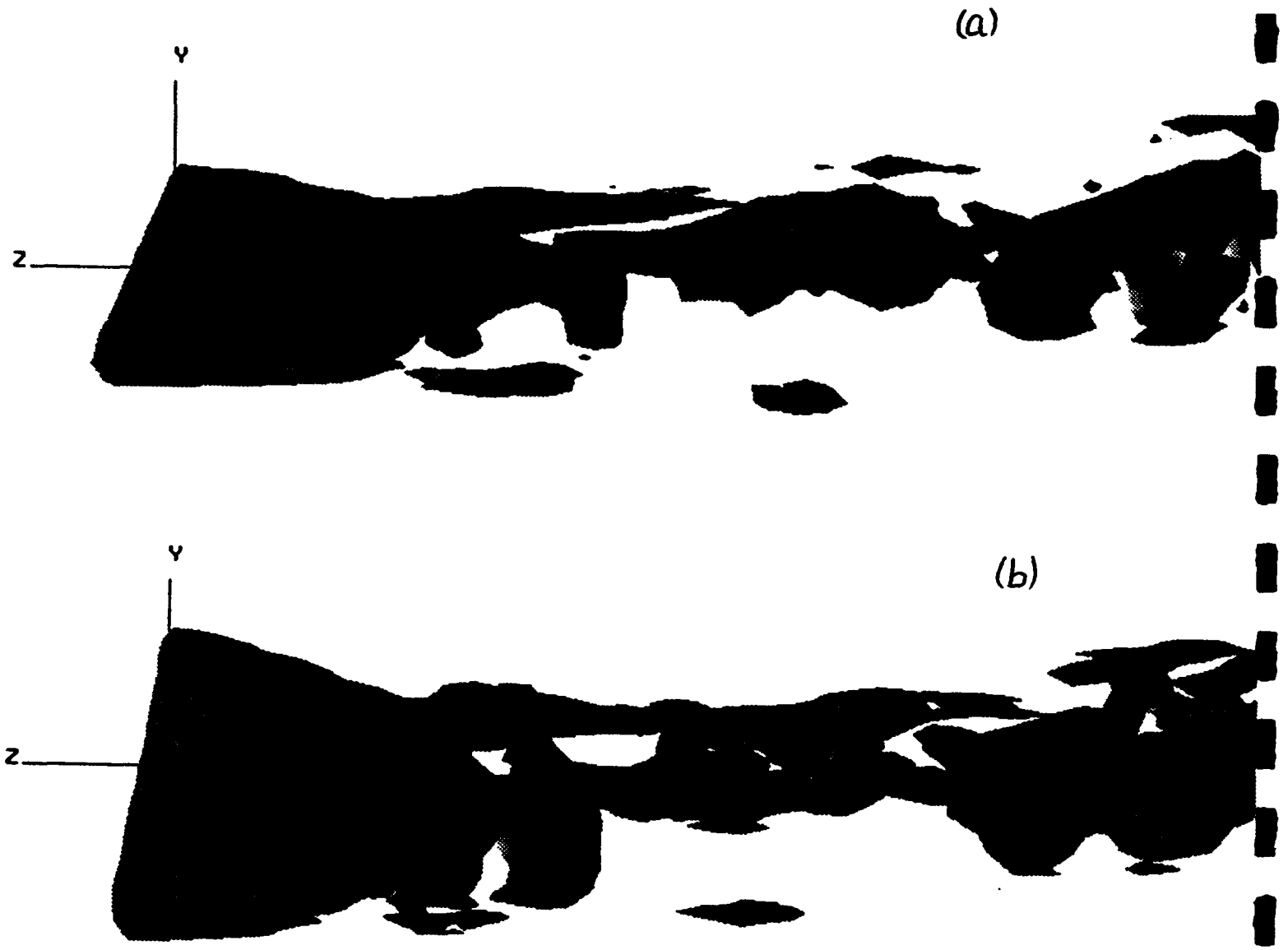

FIG. 4

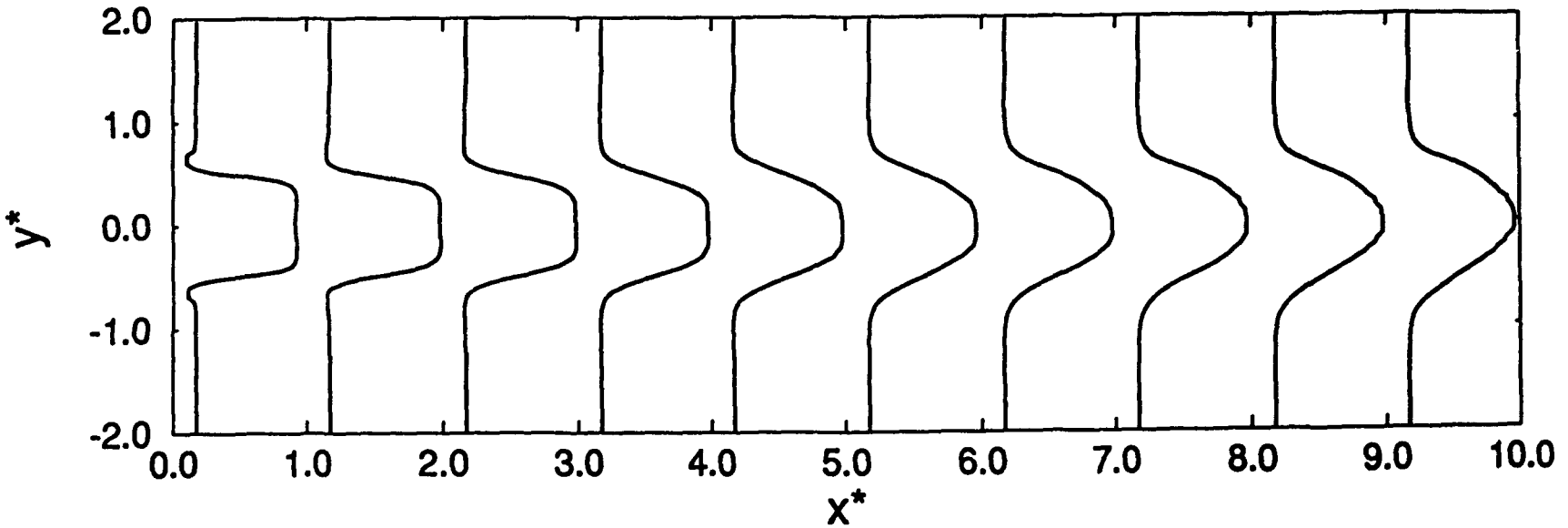
2.0
1.0
0.0
-1.0
-2.0
y*
0.0
1.0
2.0
3.0
4.0
5.0
6.0
7.0
8.0
9.0
10.0
x*

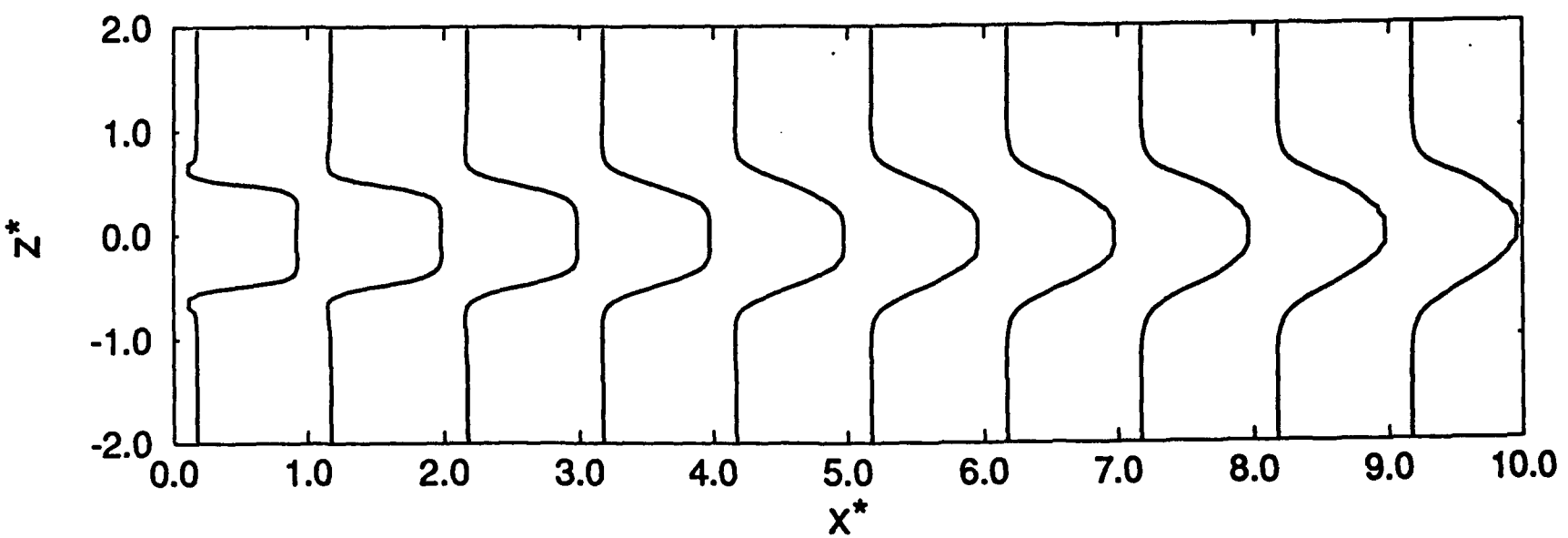
2.0
1.0
0.0
-1.0
-2.0
z*
0.0
1.0
2.0
3.0
4.0
5.0
6.0
7.0
8.0
9.0
10.0
x*

FIG. 5(a)

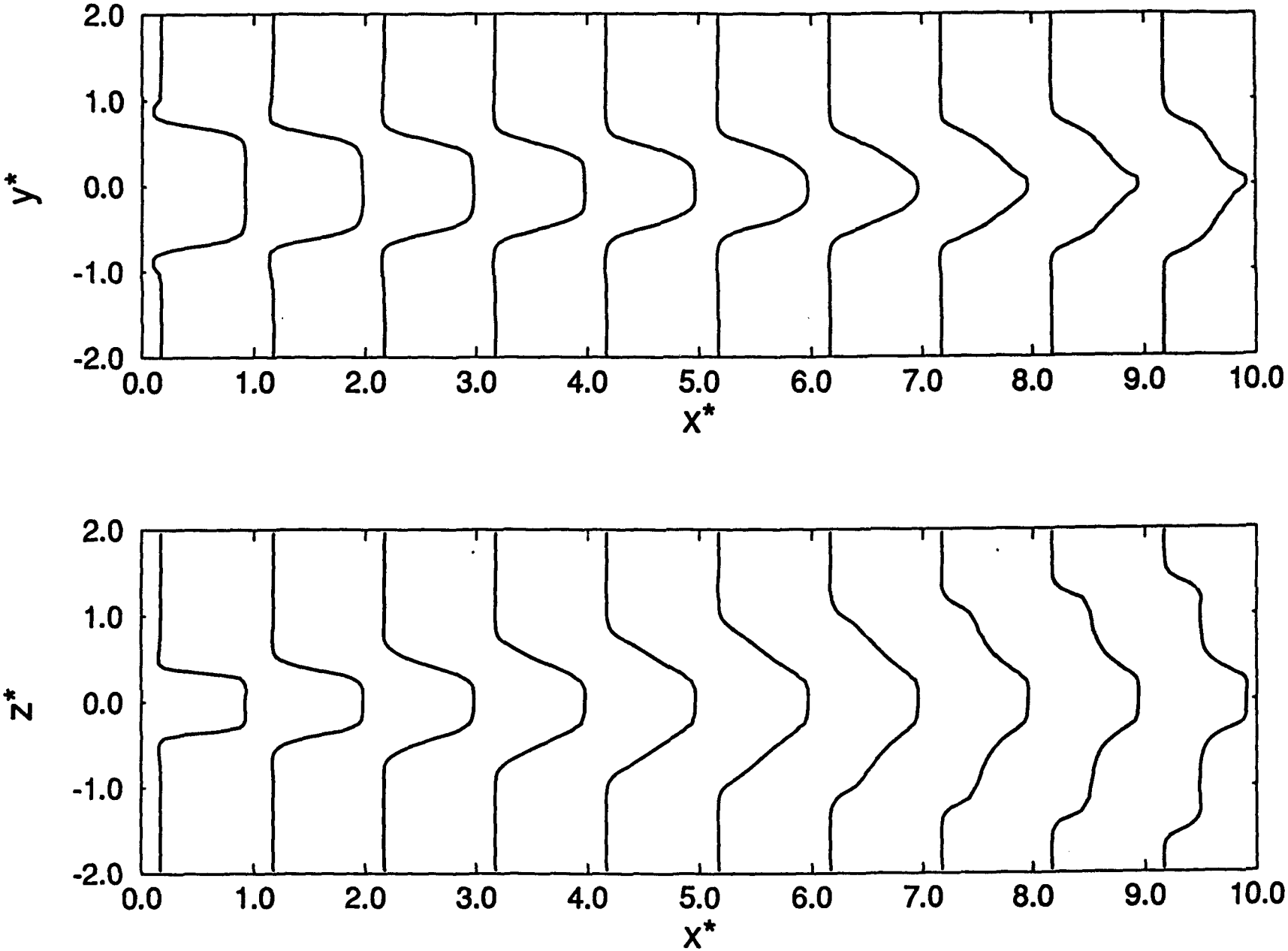
2.0
1.0
0.0
-1.0
-2.0
y*
0.0
1.0
2.0
3.0
4.0
5.0
6.0
7.0
8.0
9.0
10.0
X*
2.0
1.0
0.0
-1.0
-2.0
z*
0.0
1.0
2.0
3.0
4.0
5.0
6.0
7.0
8.0
9.0
10.0
X*

FIG. 5(b)

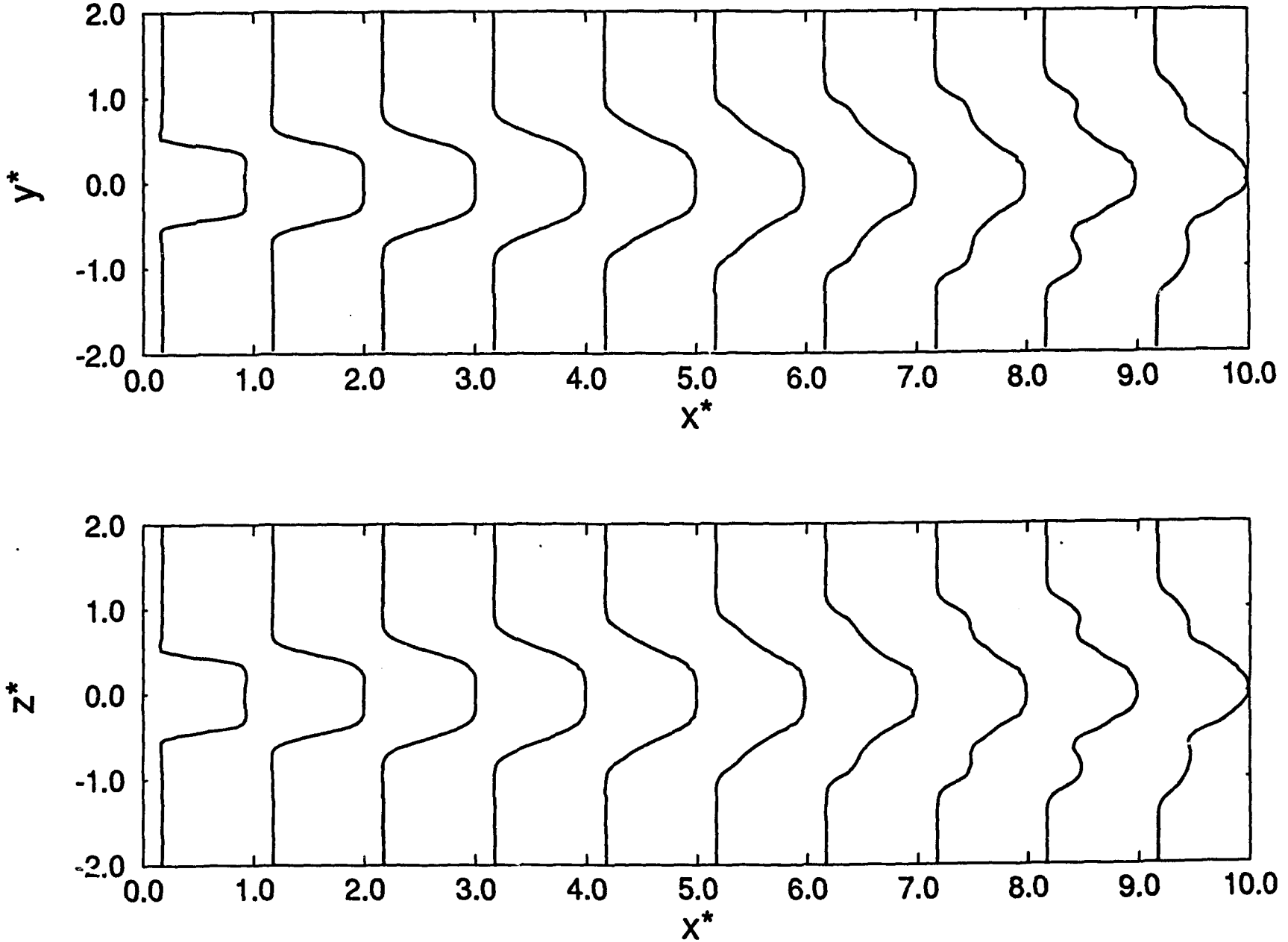
2.0
1.0
0.0
-1.0
-2.0
y*
0.0
1.0
2.0
3.0
4.0
5.0
6.0
7.0
8.0
9.0
10.0
x*
2.0
1.0
0.0
-1.0
-2.0
z*
0.0
1.0
2.0
3.0
4.0
5.0
6.0
7.0
8.0
9.0
10.0
x*

FIG. 5(c)

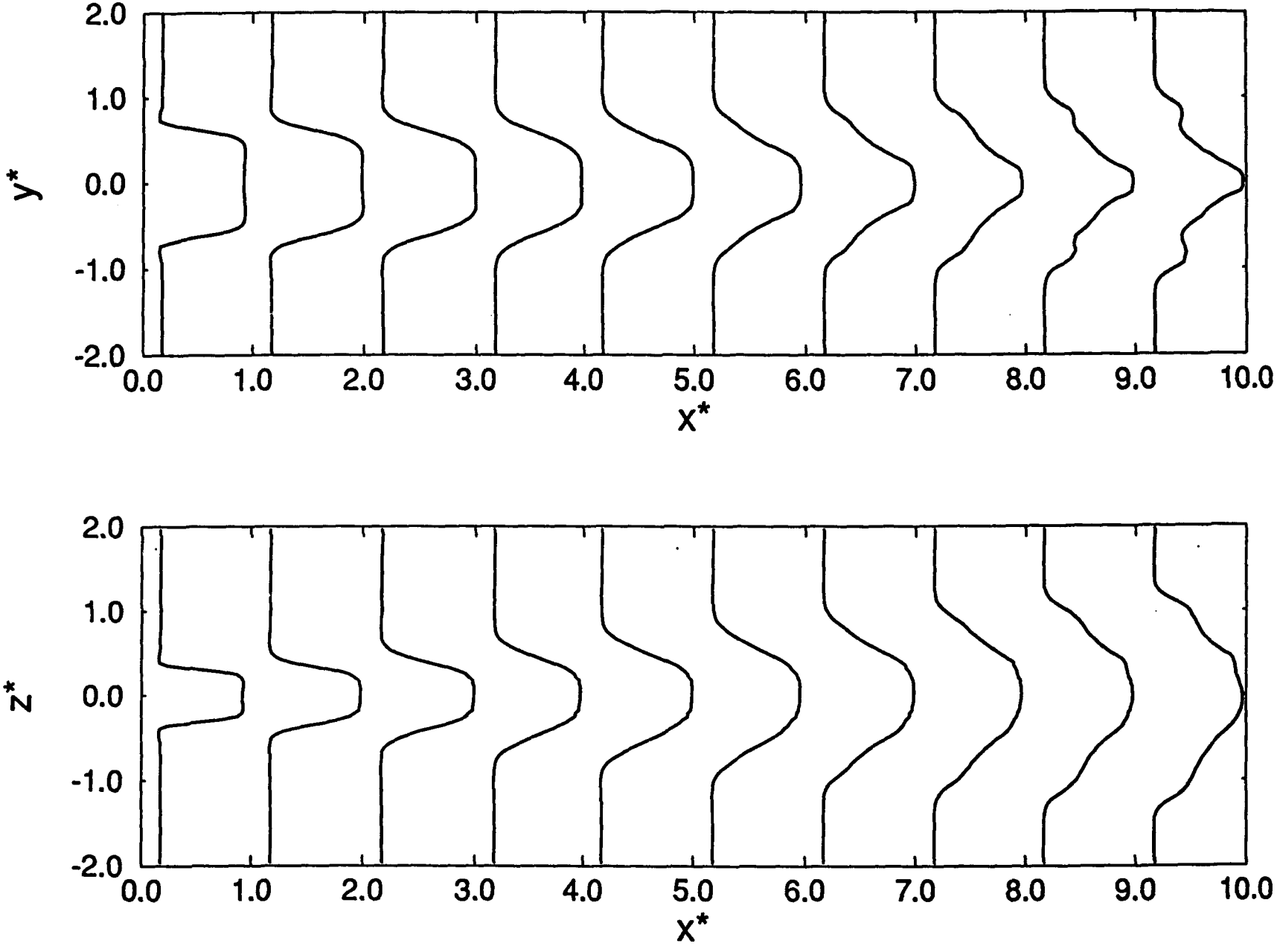
2.0
1.0
0.0
-1.0
-2.0
y*
0.0
1.0
2.0
3.0
4.0
5.0
6.0
7.0
8.0
9.0
10.0
X*
2.0
1.0
0.0
-1.0
-2.0
z*
0.0
1.0
2.0
3.0
4.0
5.0
6.0
7.0
8.0
9.0
10.0
X*

FIG. 5(d)

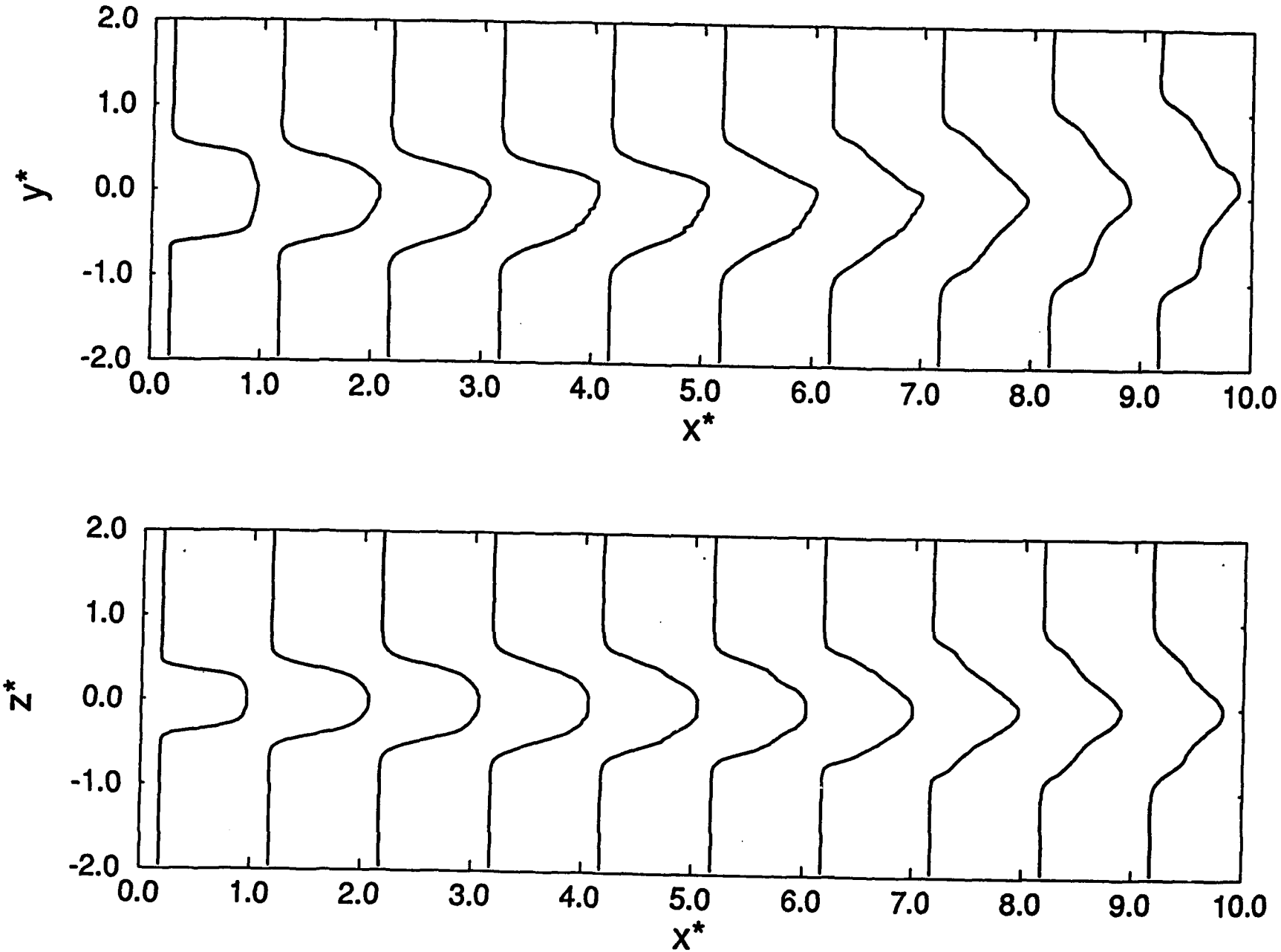
2.0
1.0
0.0
-1.0
-2.0
y*
0.0
1.0
2.0
3.0
4.0
5.0
6.0
7.0
8.0
9.0
10.0
X*
2.0
1.0
0.0
-1.0
-2.0
z*
0.0
1.0
2.0
3.0
4.0
5.0
6.0
7.0
8.0
9.0
10.0
X*

FIG. 5(e)

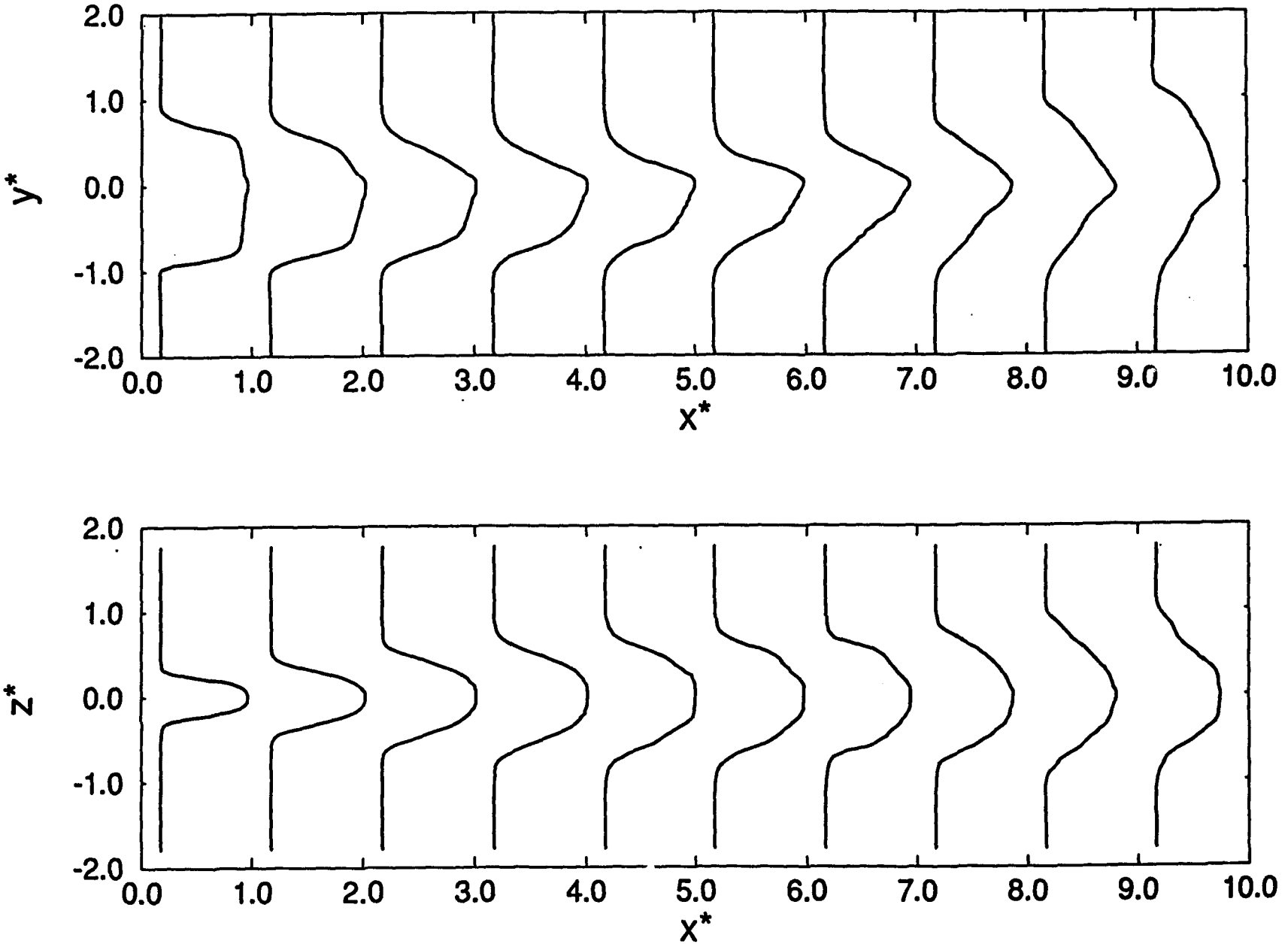
2.0
1.0
0.0
-1.0
-2.0
y*
0.0
1.0
2.0
3.0
4.0
5.0
6.0
7.0
8.0
9.0
10.0
x*
2.0
1.0
0.0
-1.0
-2.0
z*
0.0
1.0
2.0
3.0
4.0
5.0
6.0
7.0
8.0
9.0
10.0
x*

FIG. 5 (f)

FIG. 6

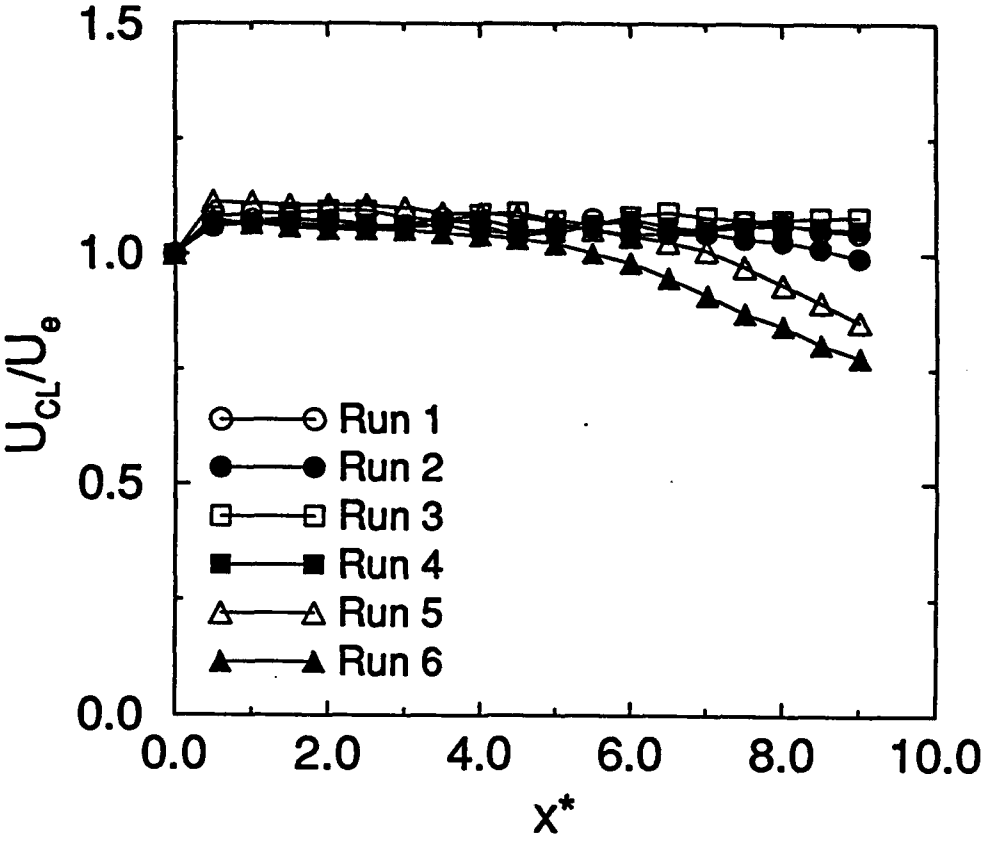
1.5
1.0
0.5
0.0
U_{CL}/U_e
Run 1
Run 2
Run 3
Run 4
Run 5
Run 6
0.0
2.0
4.0
6.0
8.0
10.0
x*

FIG. 7

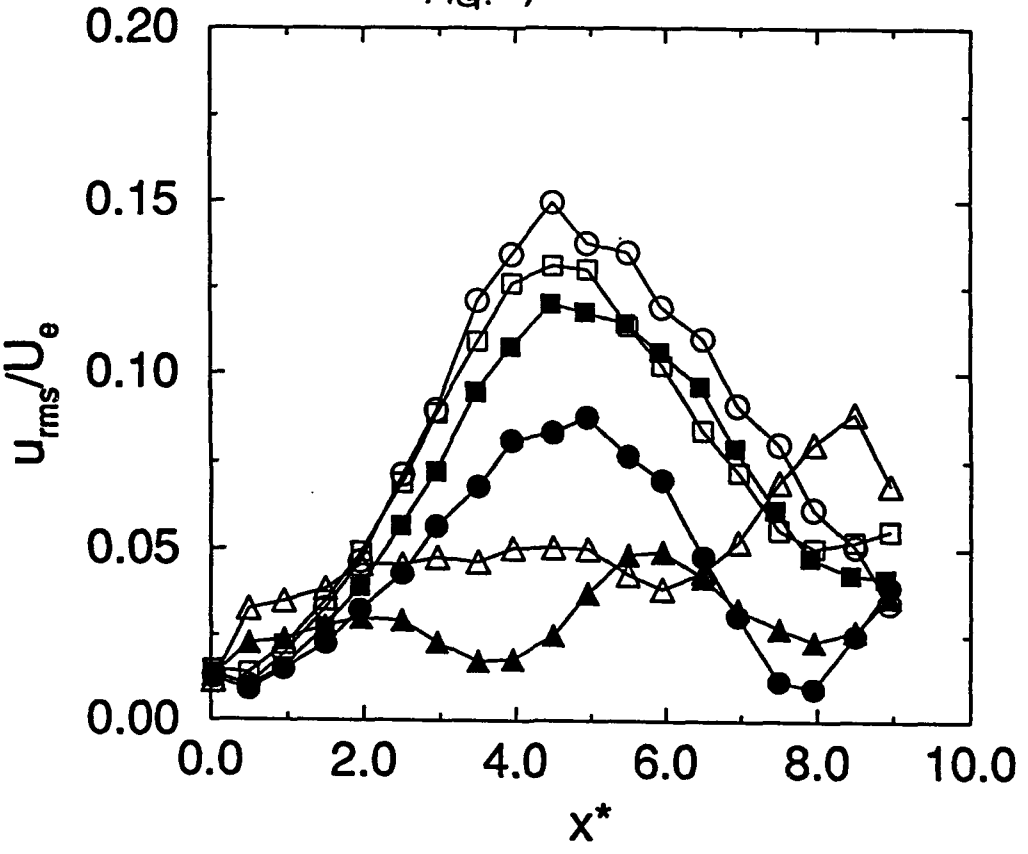
0.20
0.15
0.10
0.05
0.00
u_{rms}/U_e
0.0
2.0
4.0
6.0
8.0
10.0
x*

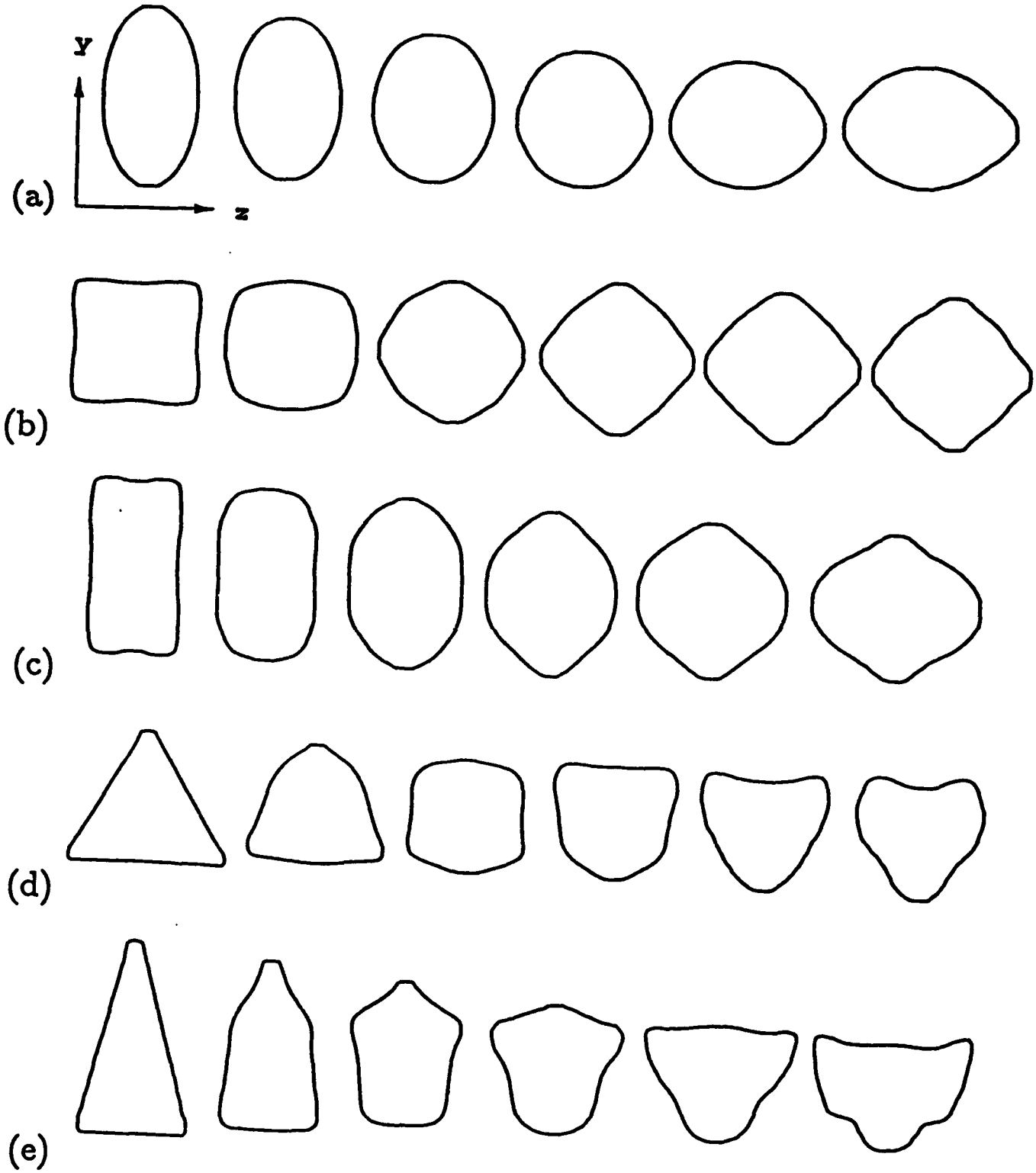

FIG. 8

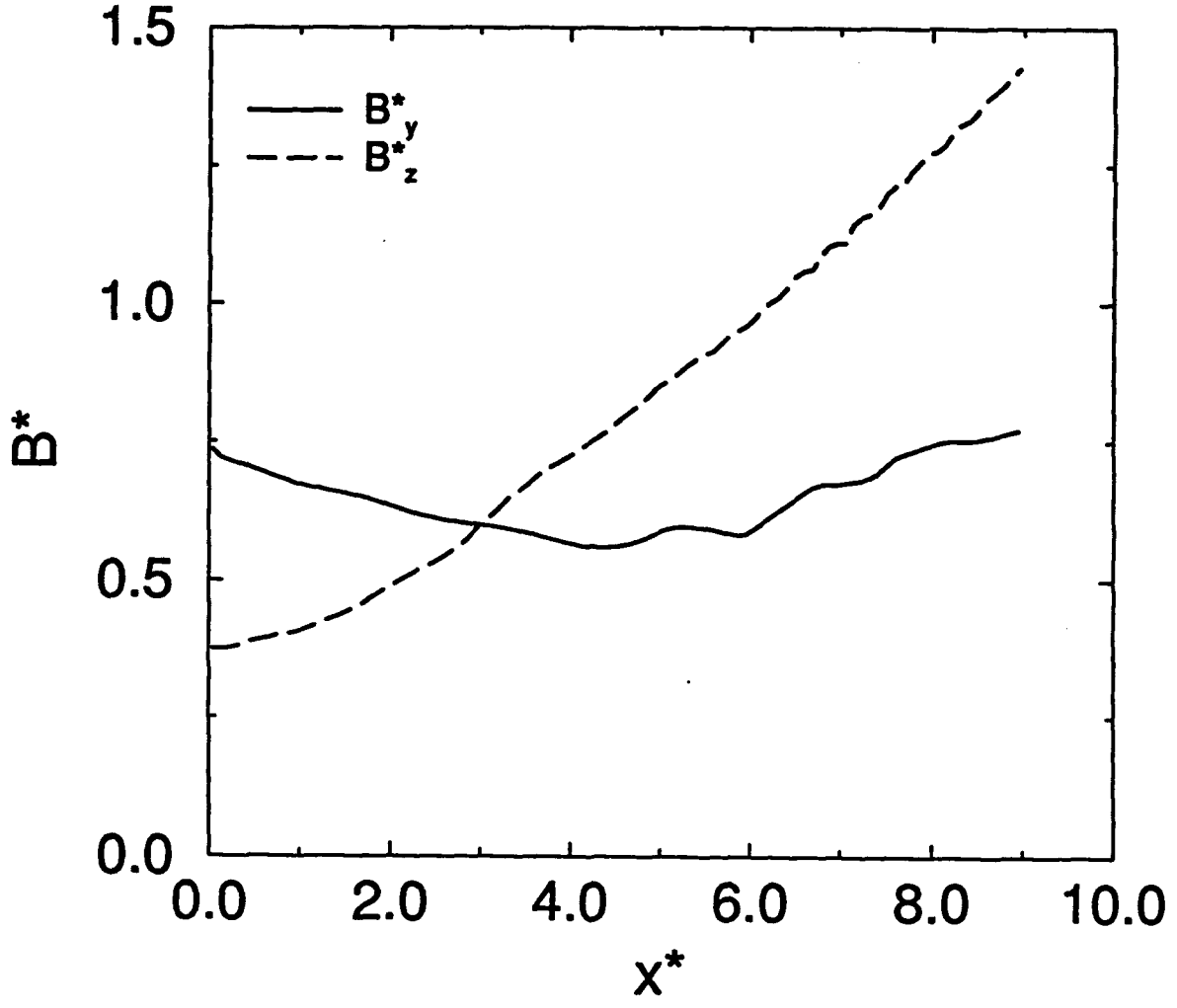

FIG. 9(a)

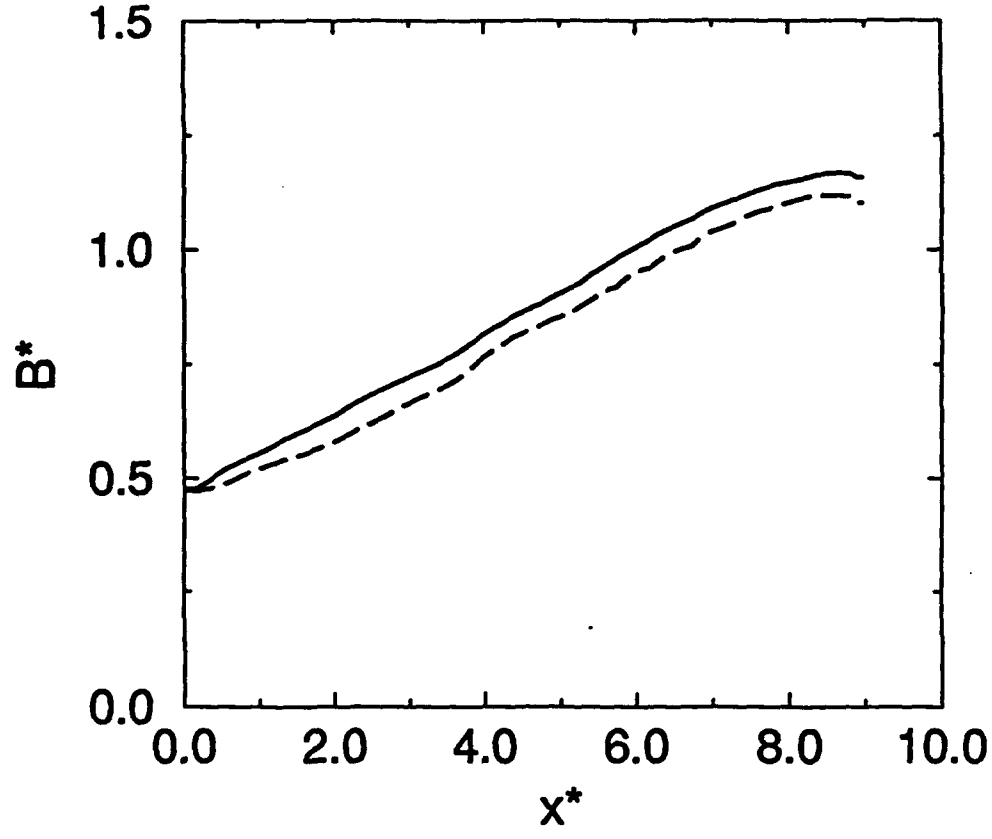

(b)

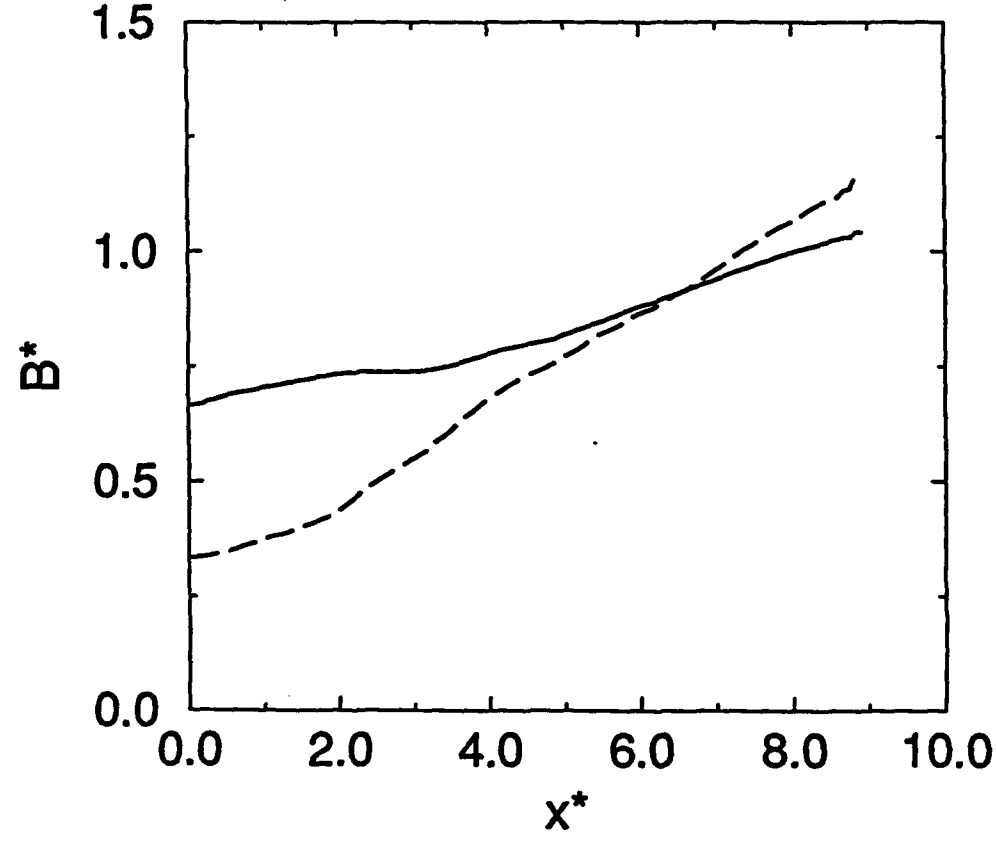

(c)

FIG. 9(B)

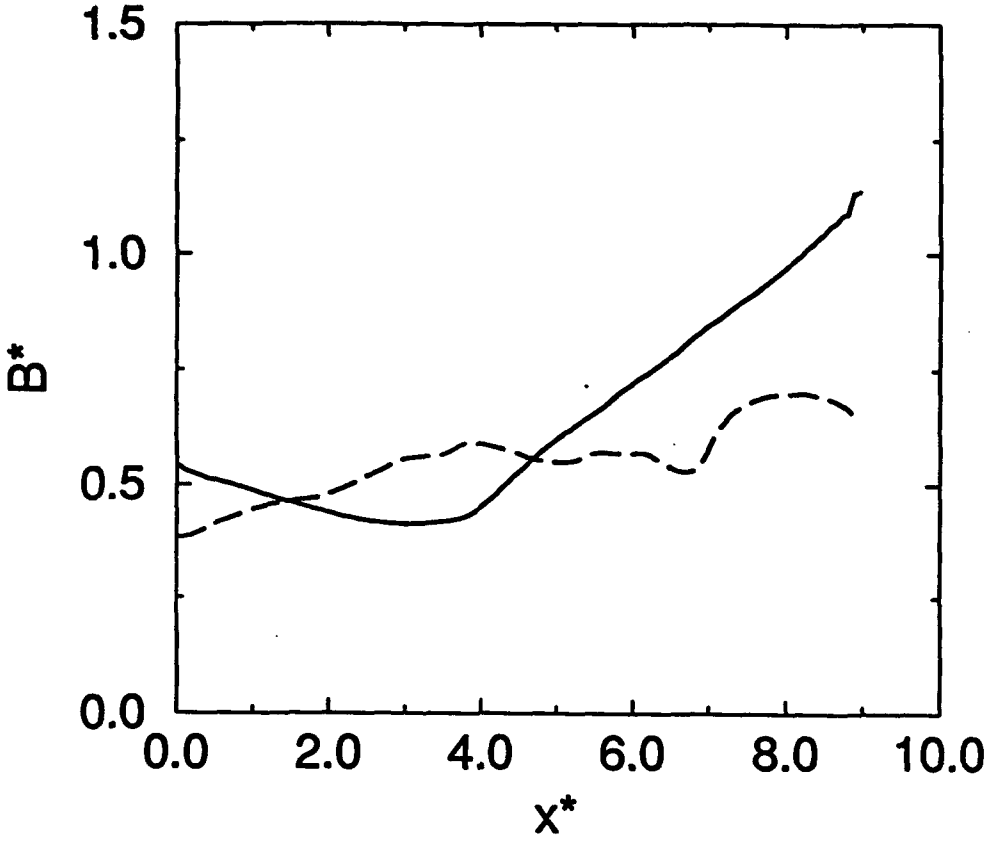

(d)

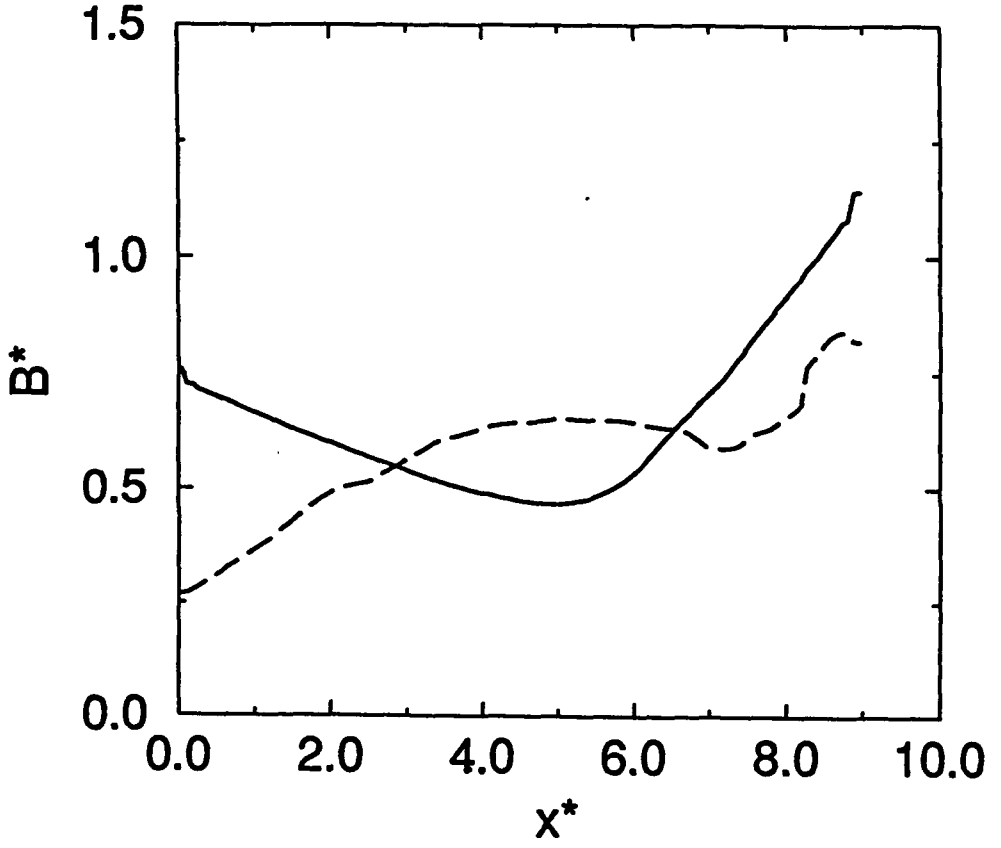

(e)

FIG. 9(c)

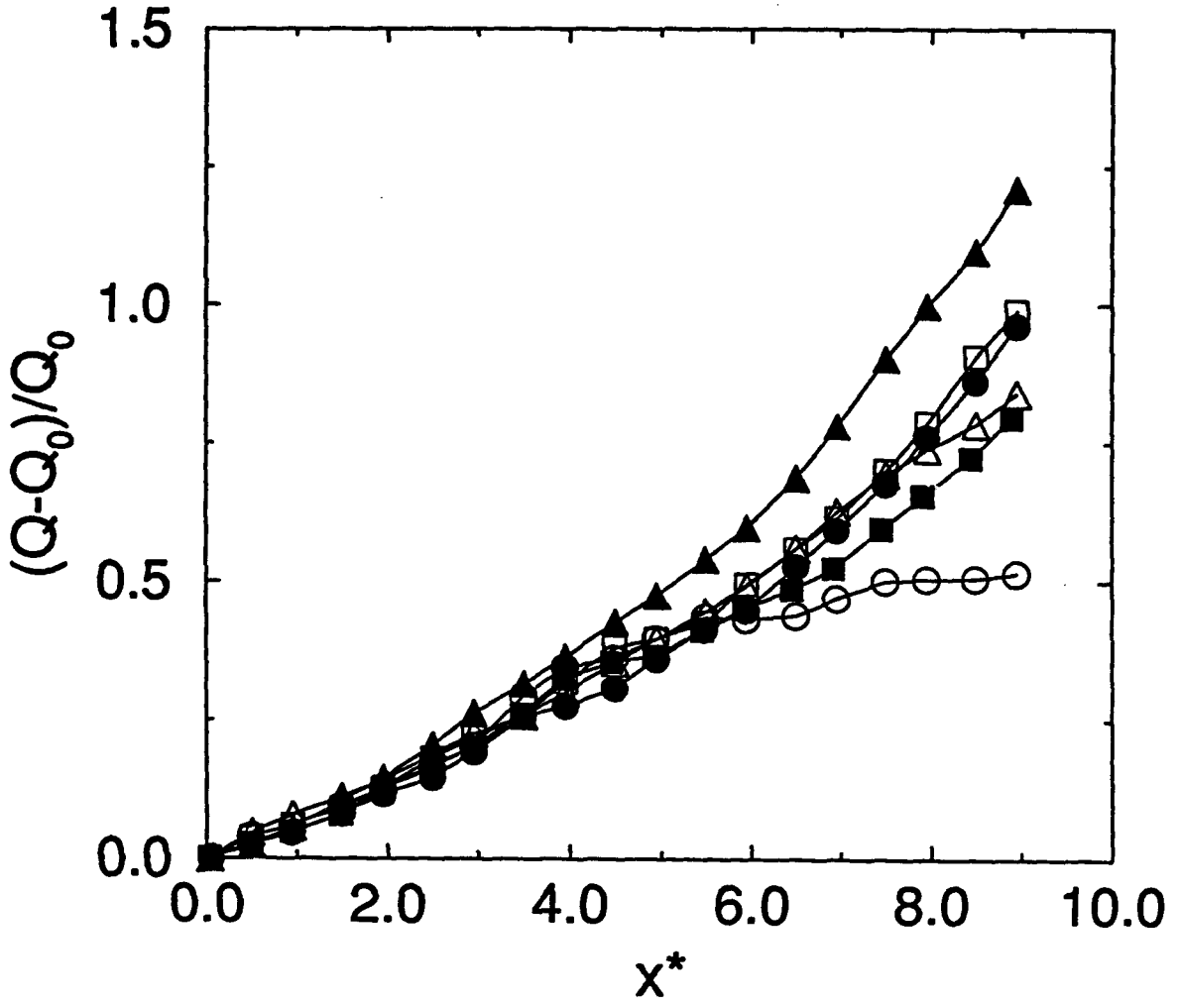

FIG. 10

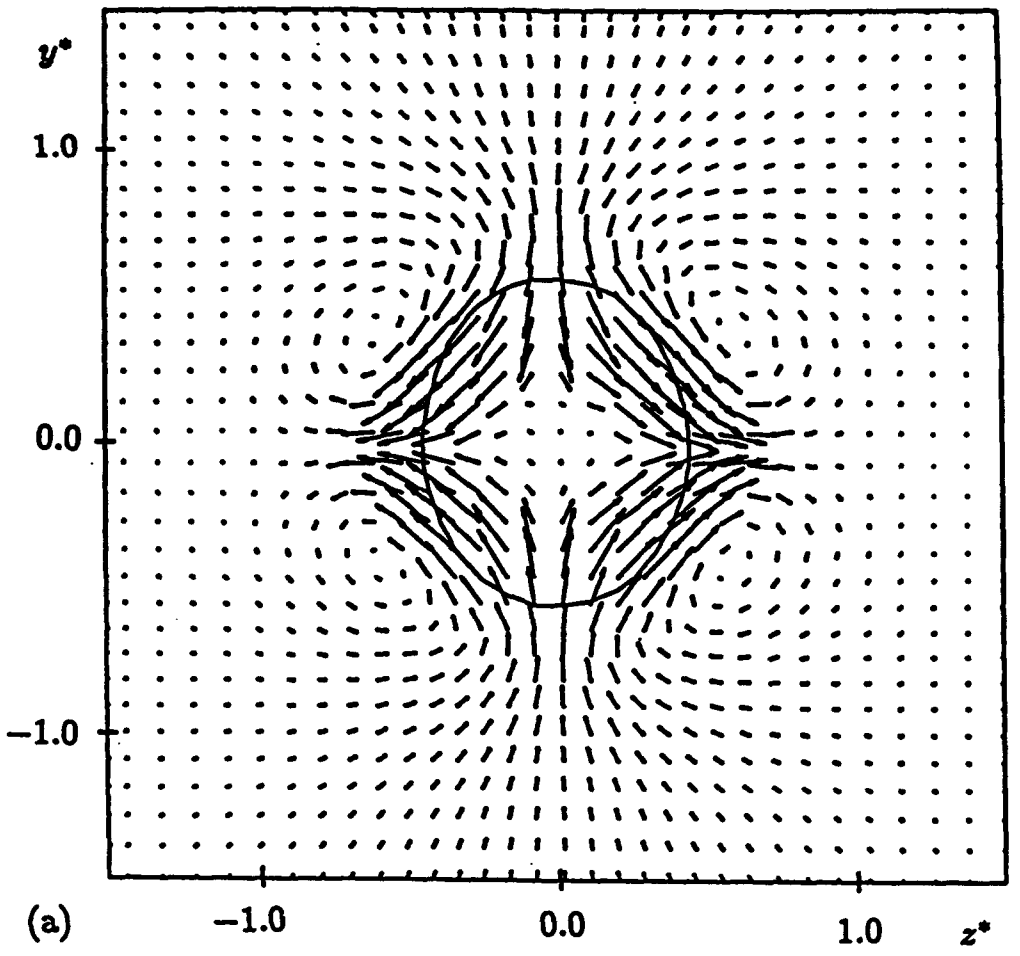

FIG. 11 (a)

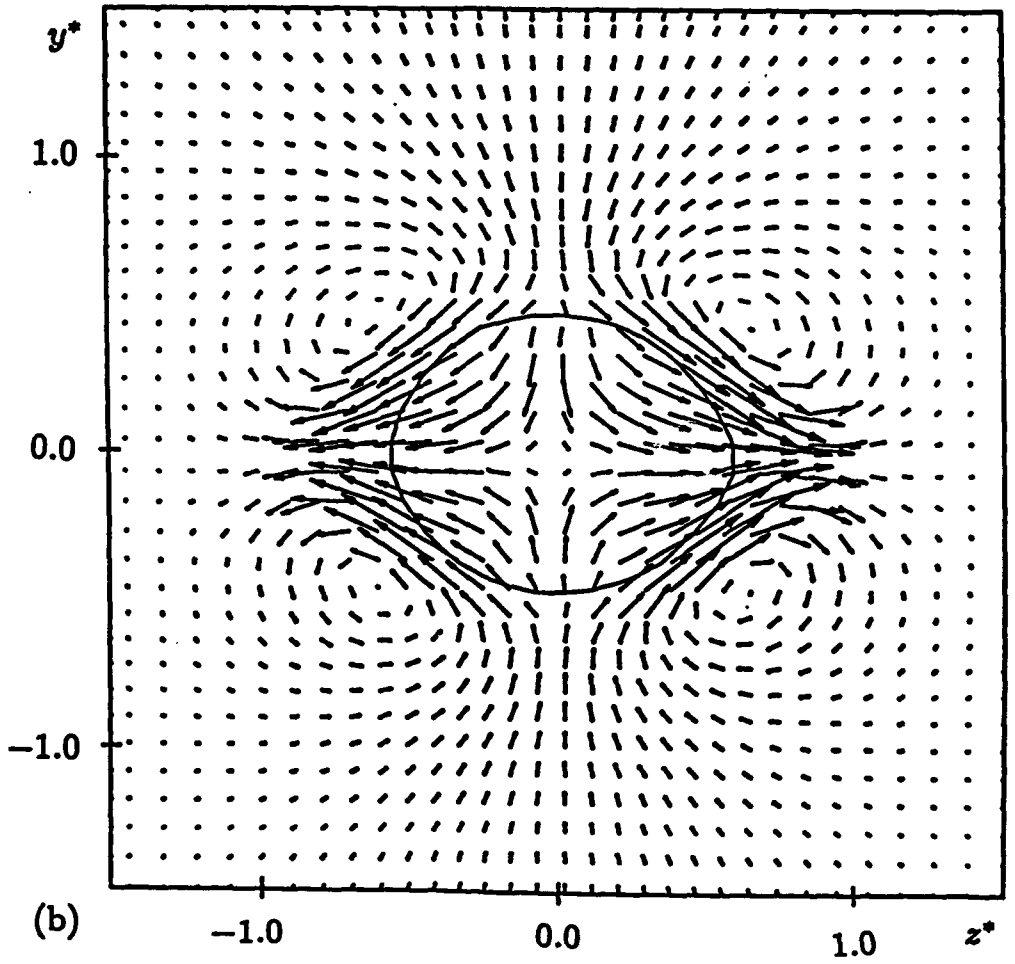

FIG. 11 (b)

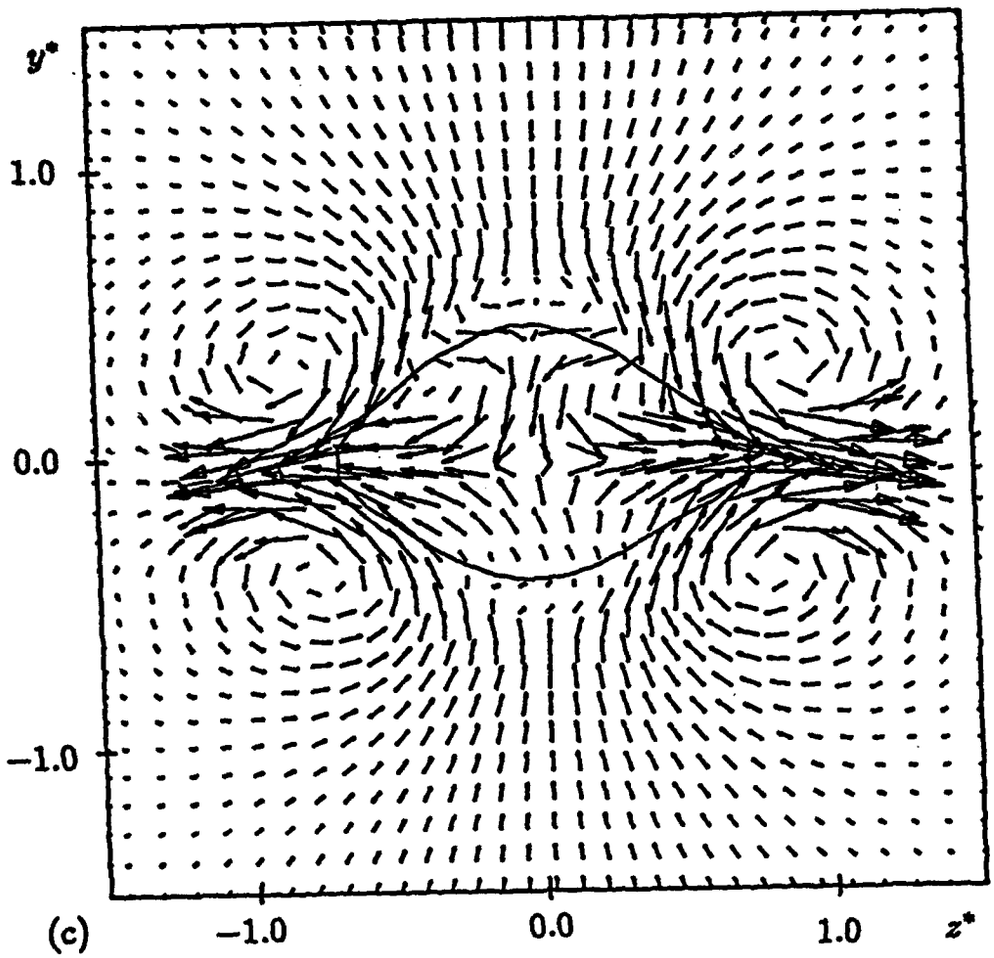

FIG. 11 (C)

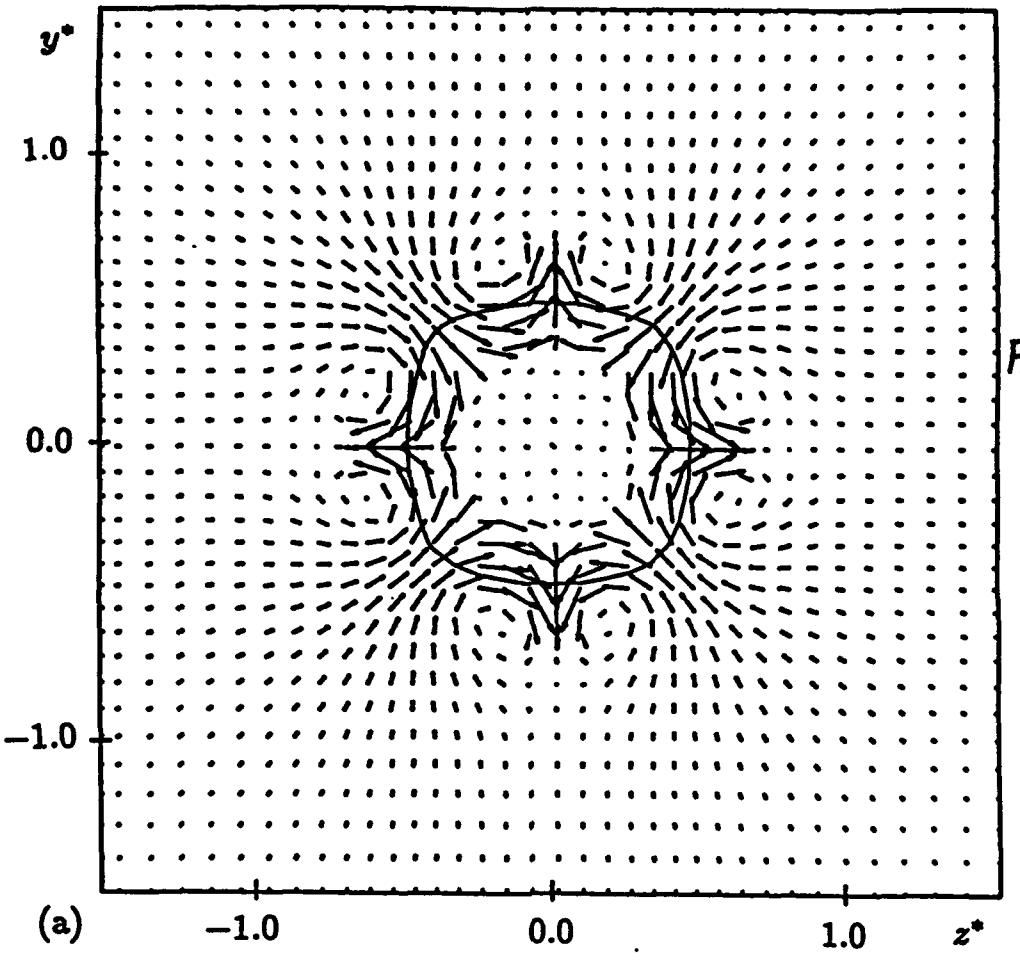

FIG. 12(a)

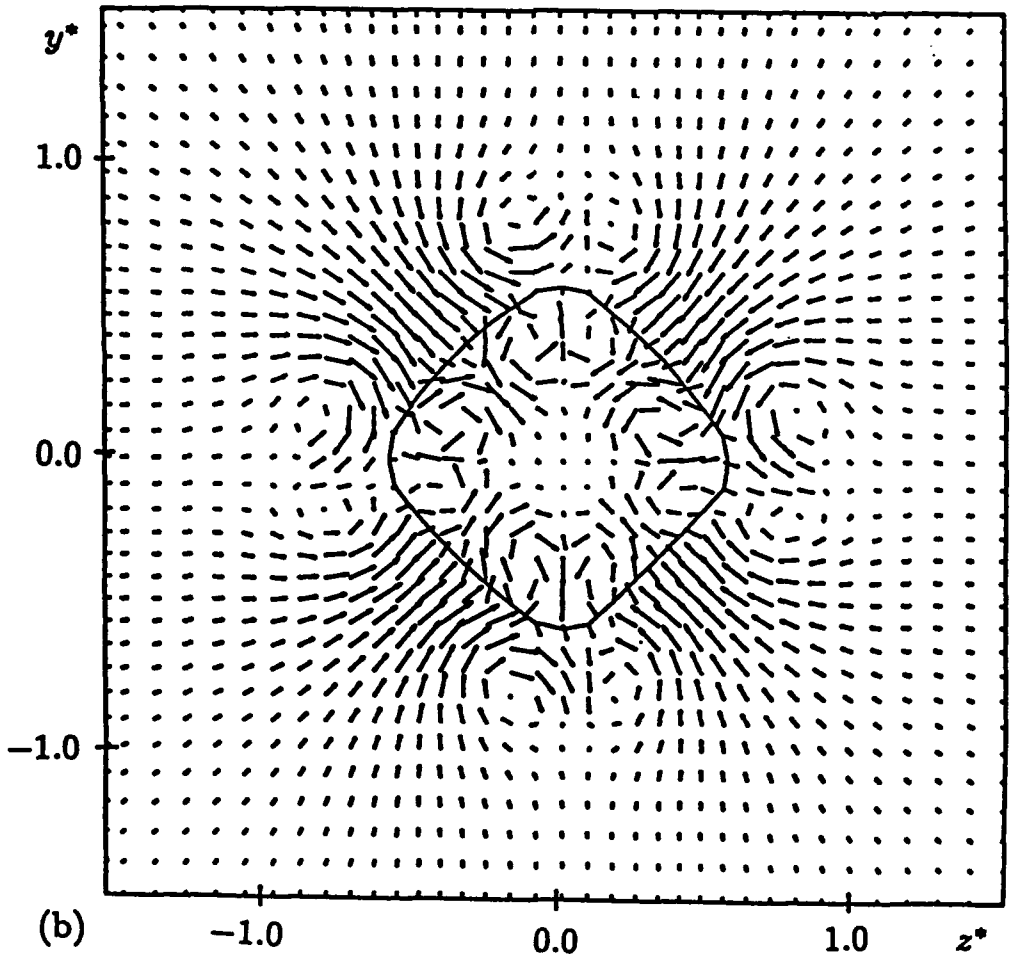

FIG. 12(b)

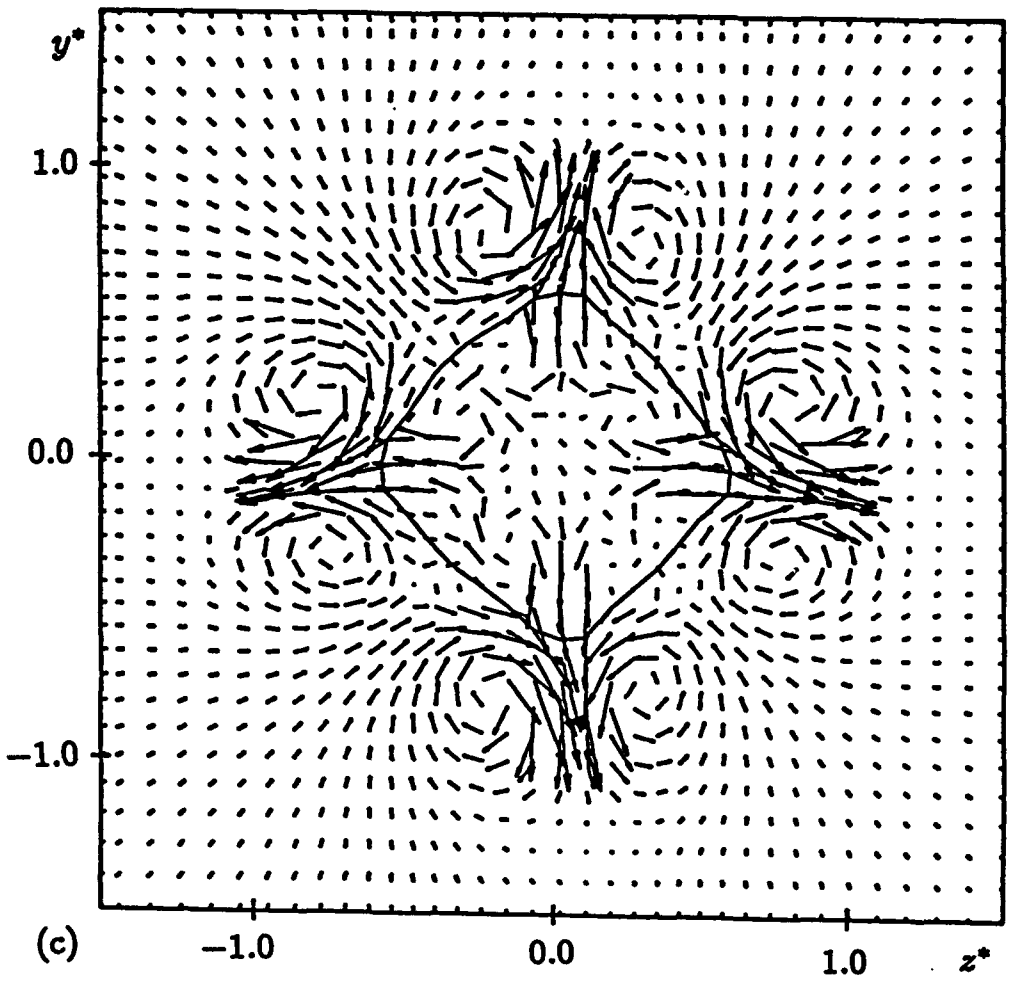

FIG. 12(c)

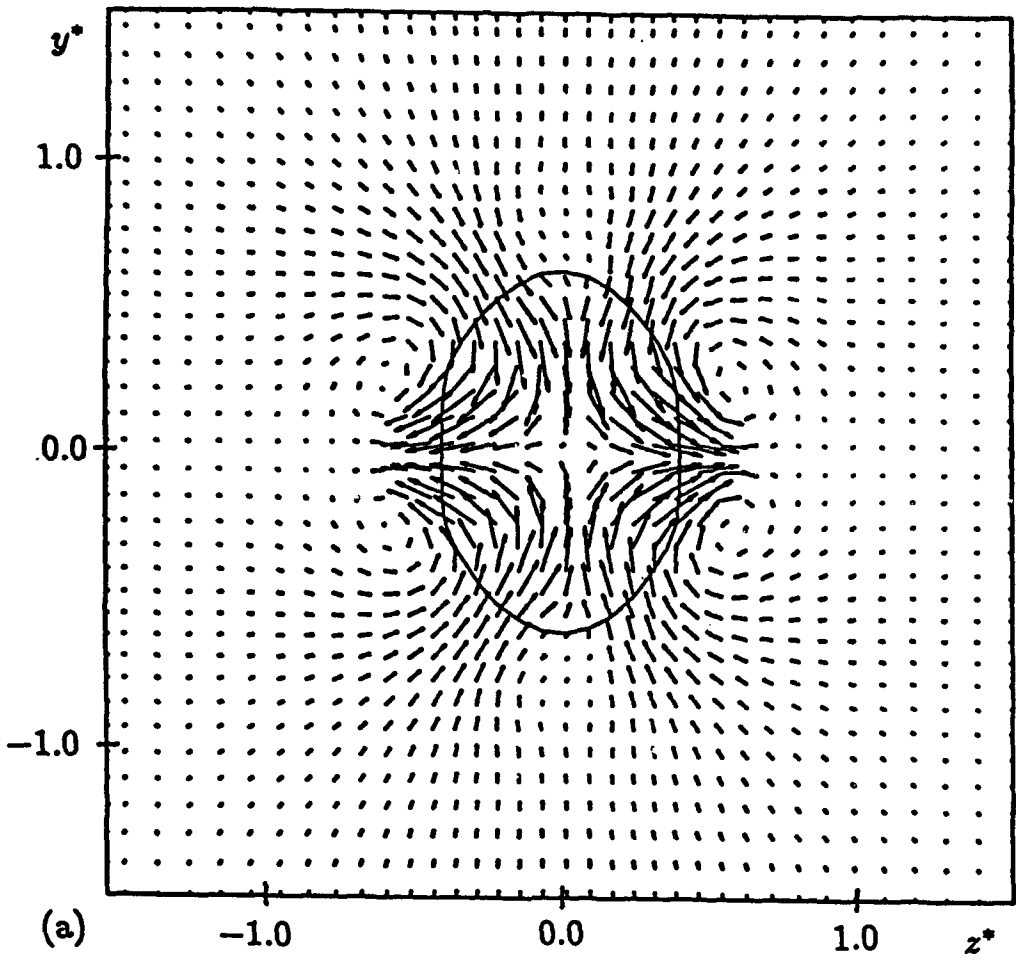

FIG. 13(a)

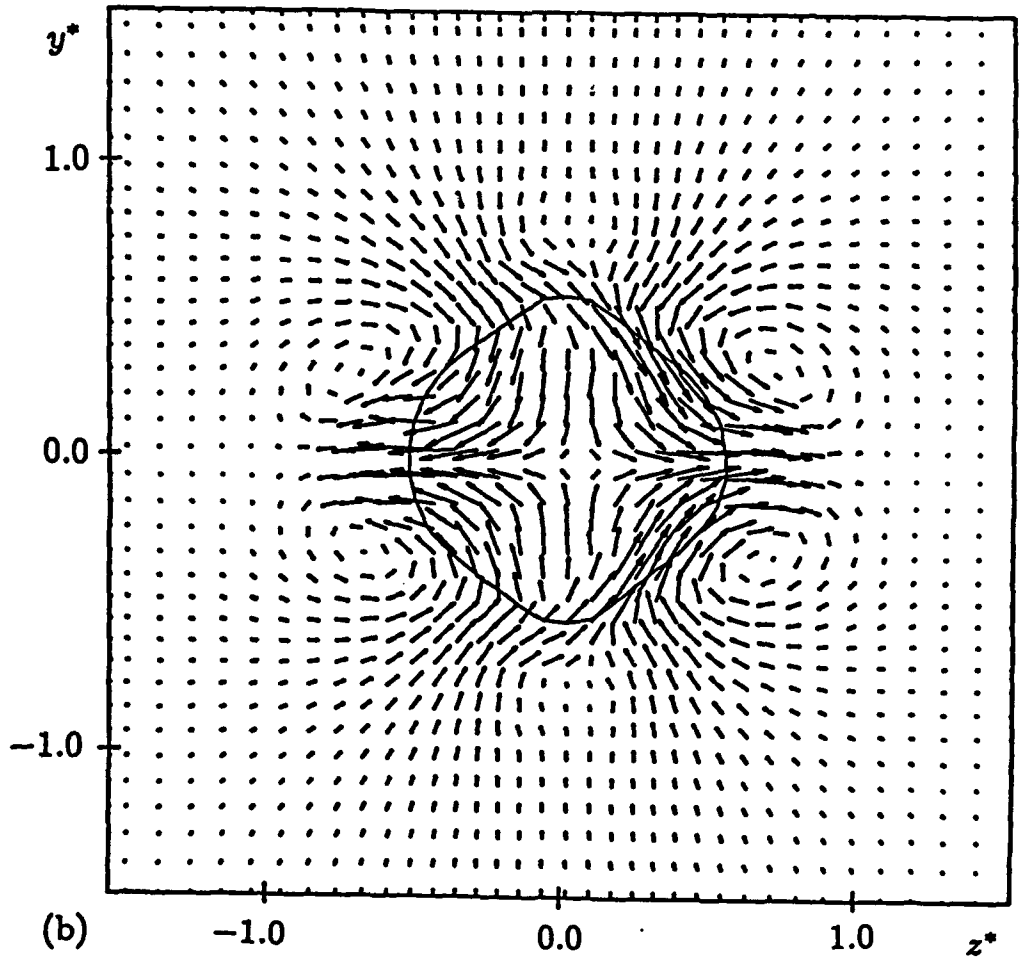

FIG. 13(b)

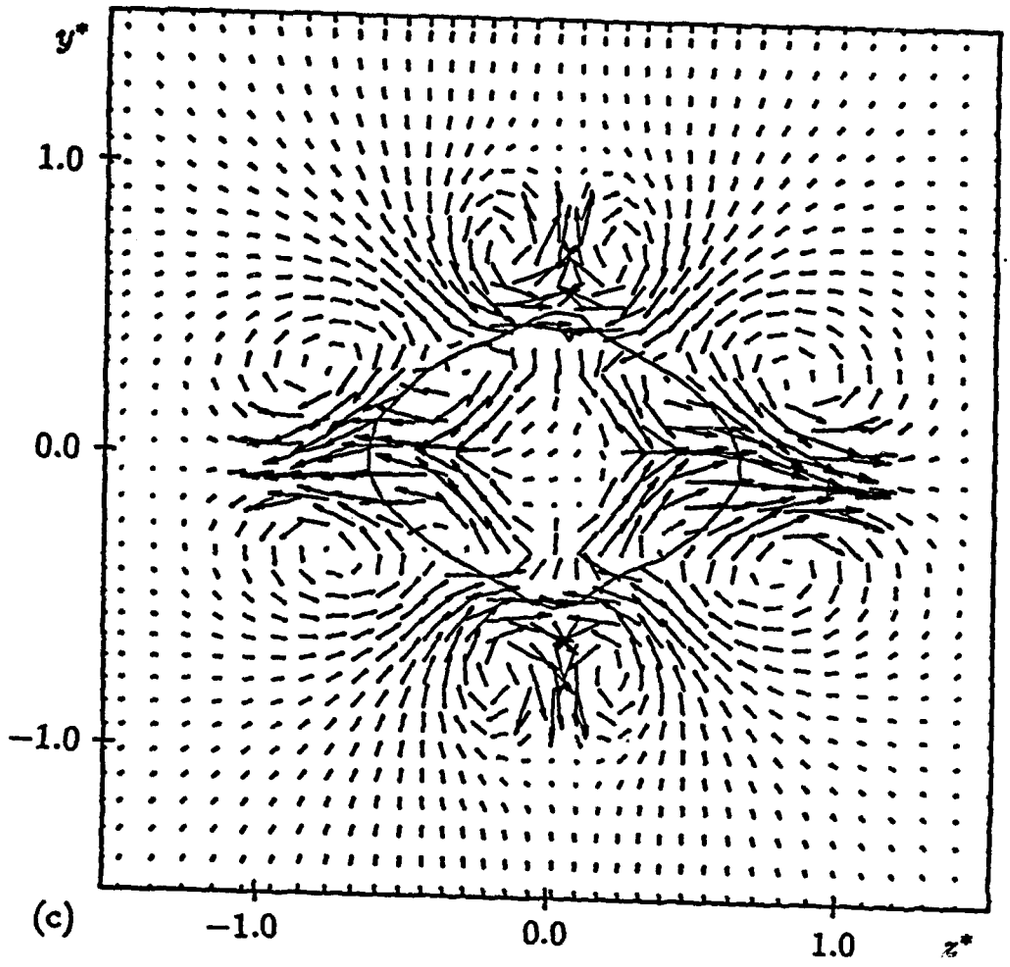

FIG. 13(c)

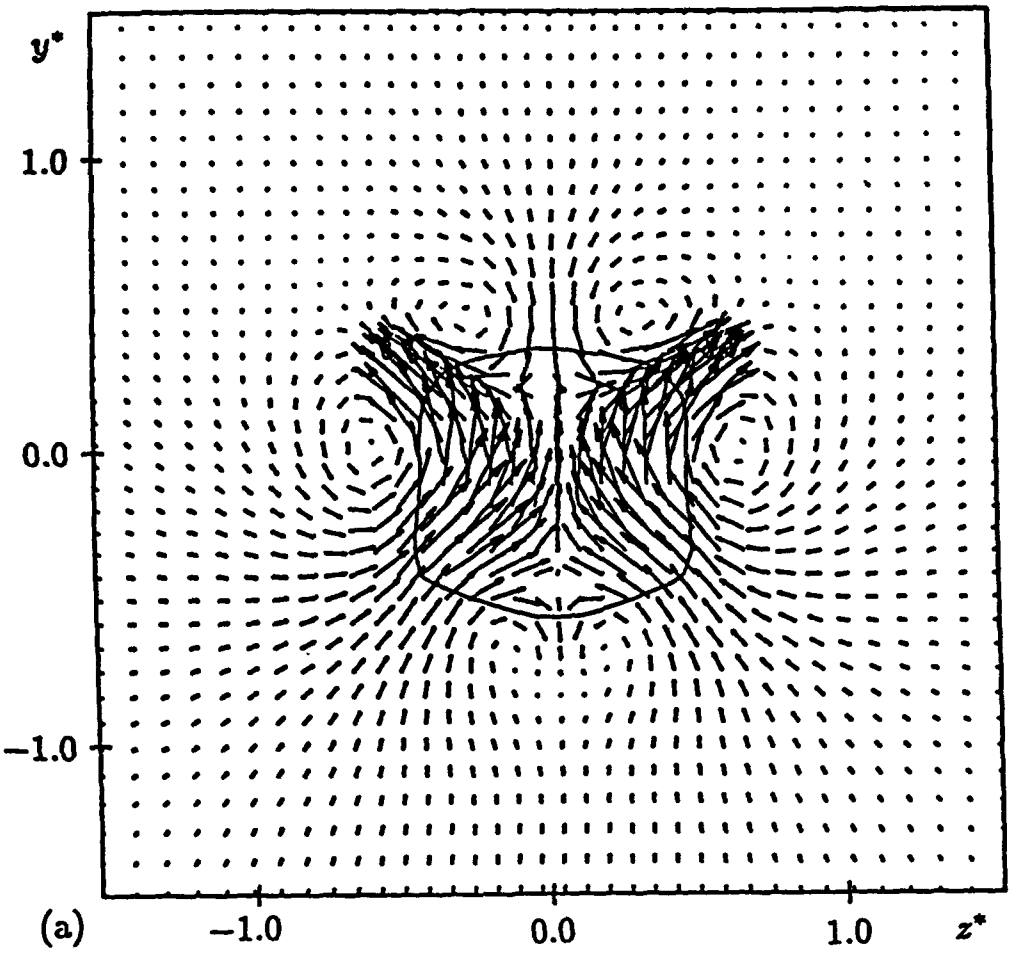

FIG. 14(a)

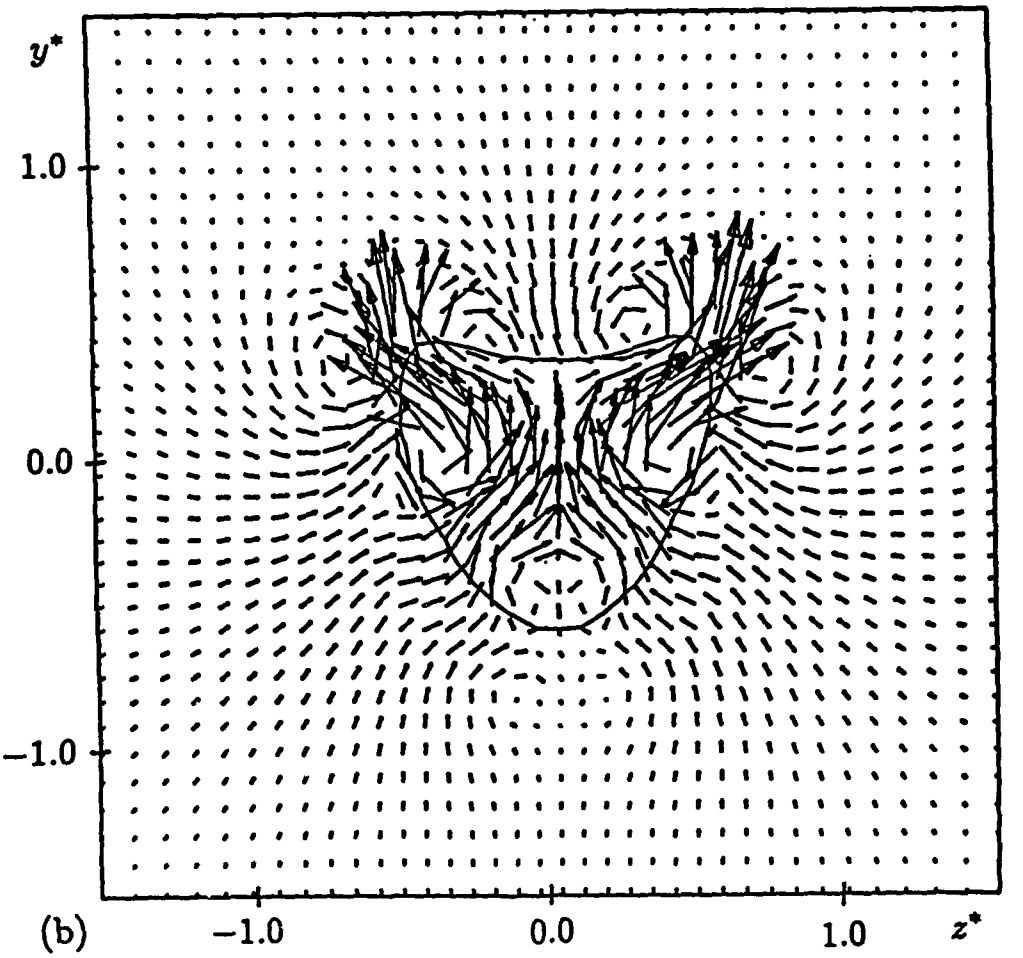

FIG. 14(b)

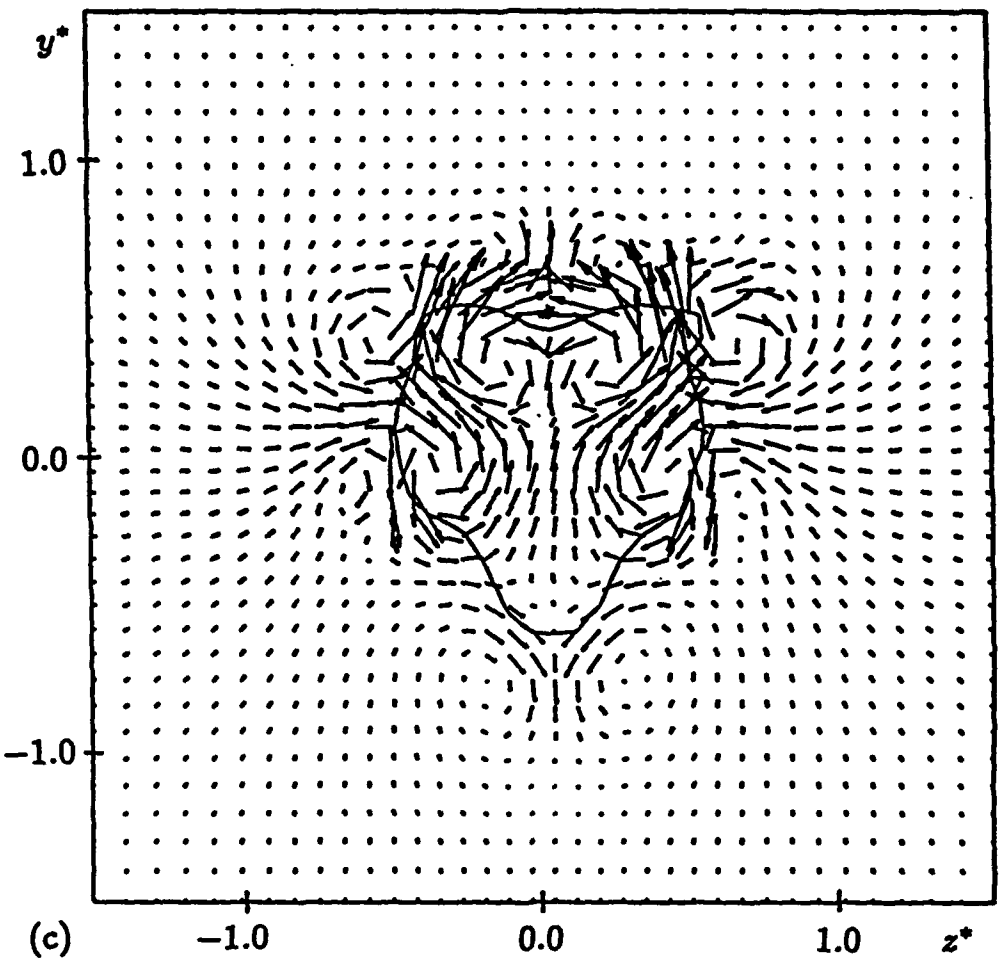

FIG. 14 (c)

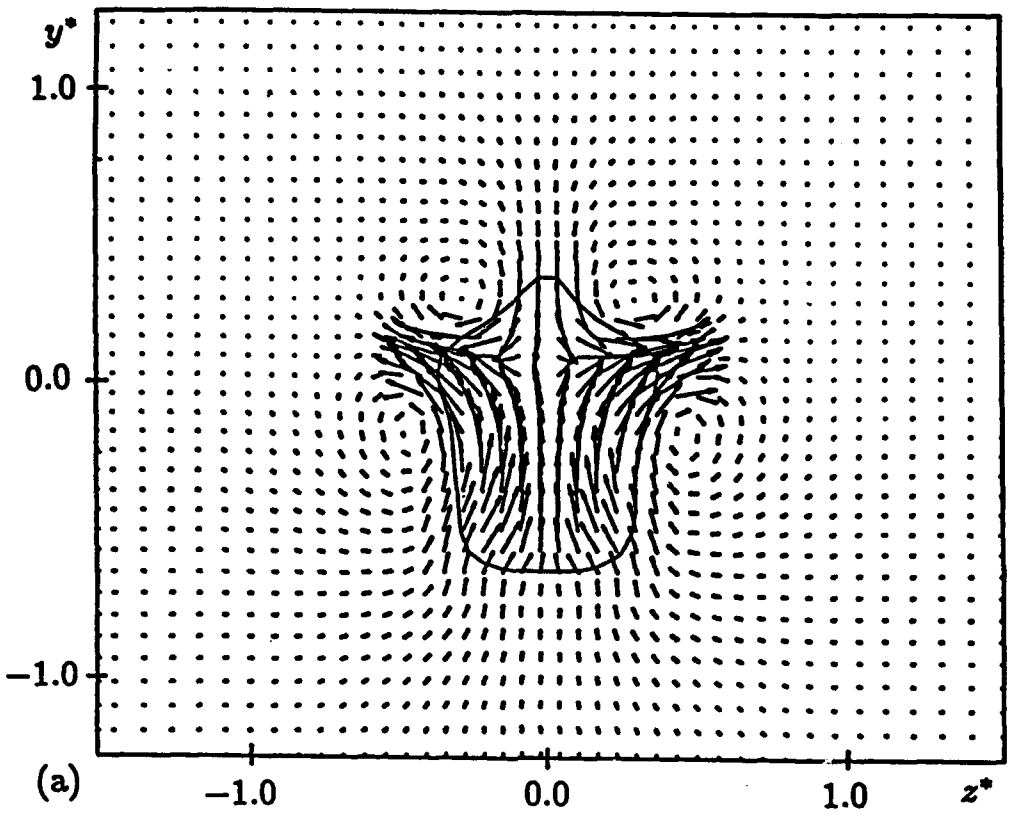

FIG. 15(a)

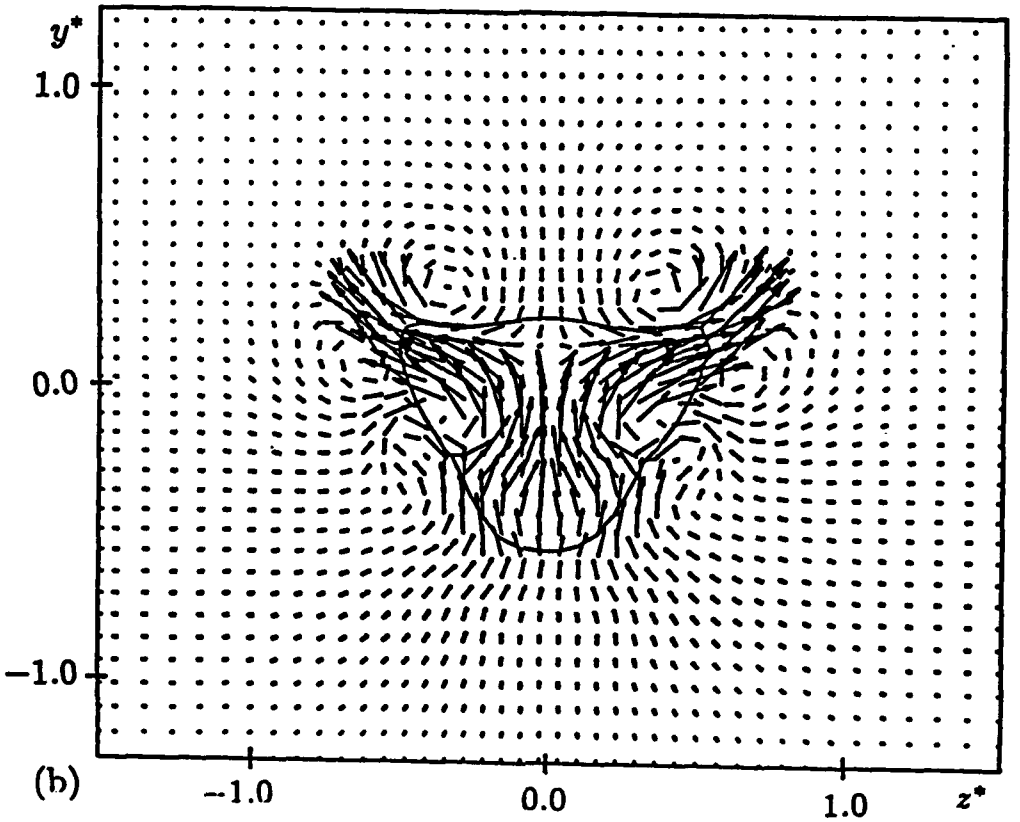

FIG. 15(b)

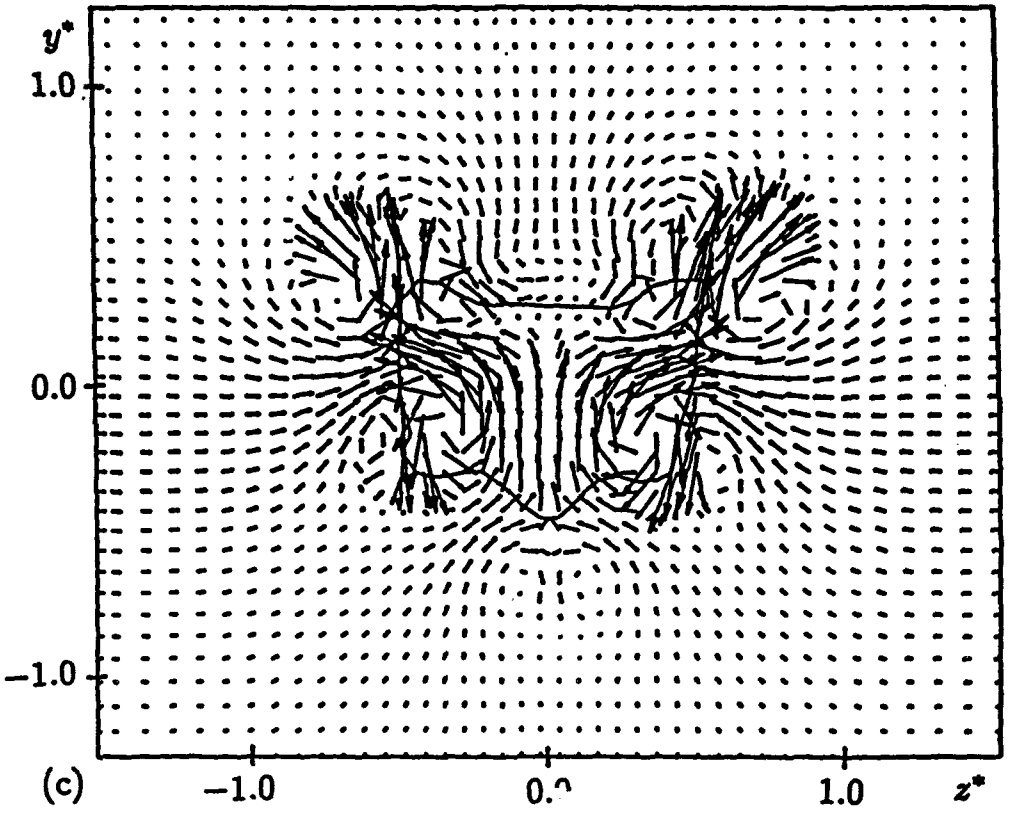

FIG. 15(c)

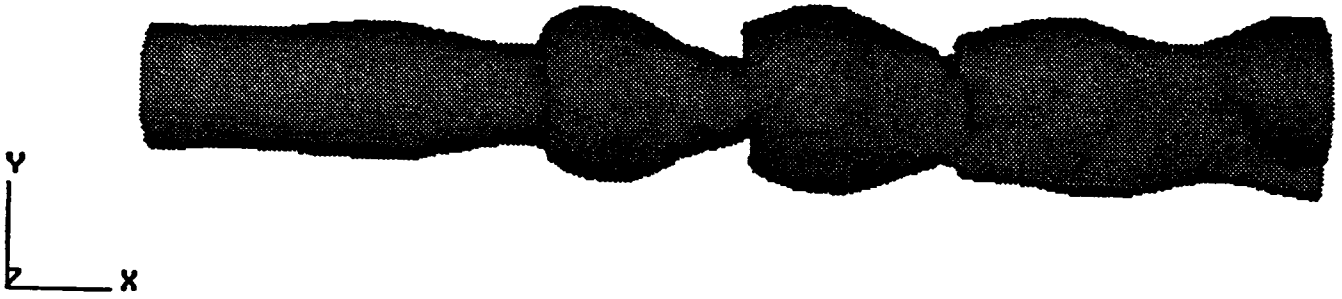

FIG. 16 (a)

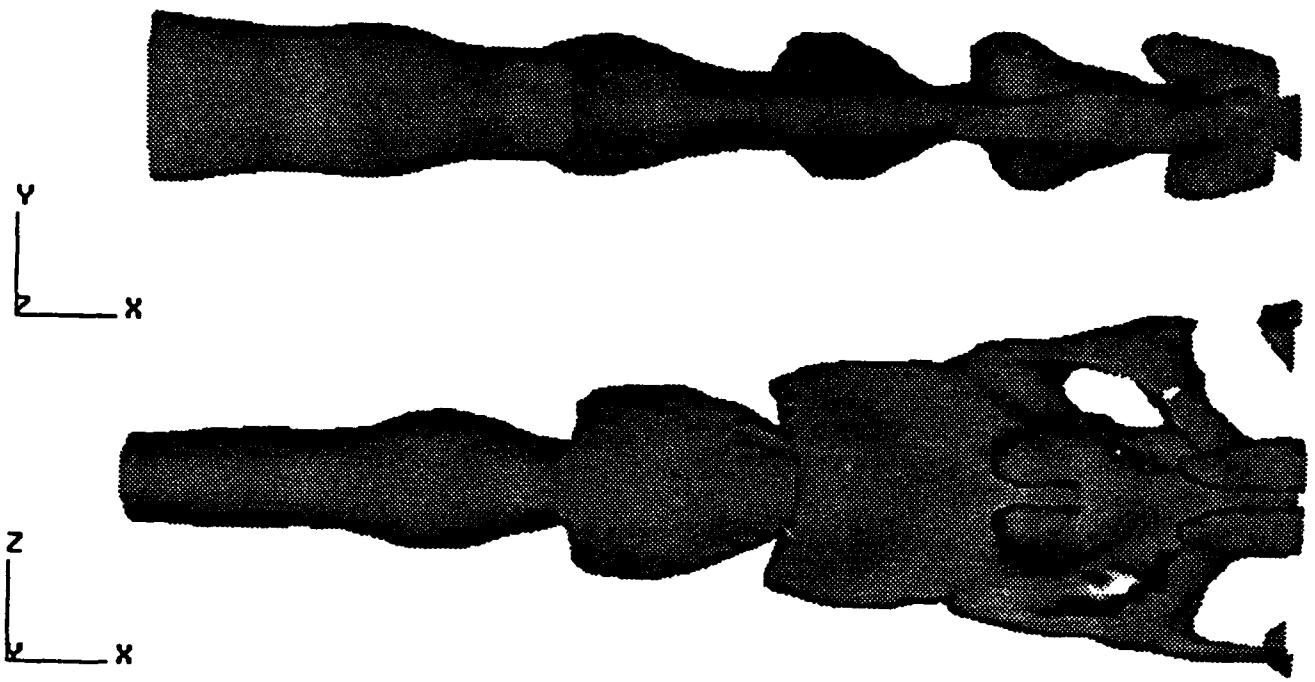

FIG. 16 (b)

FIG. 16 (C)

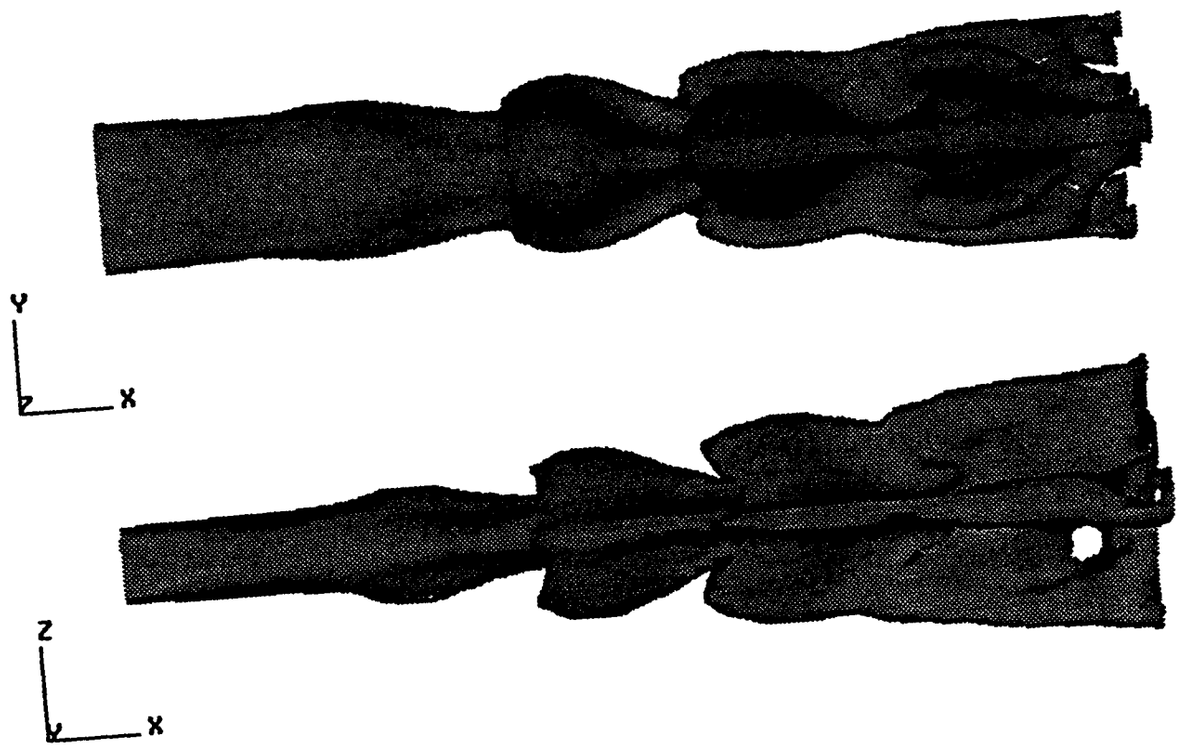

FIG. 16(d)

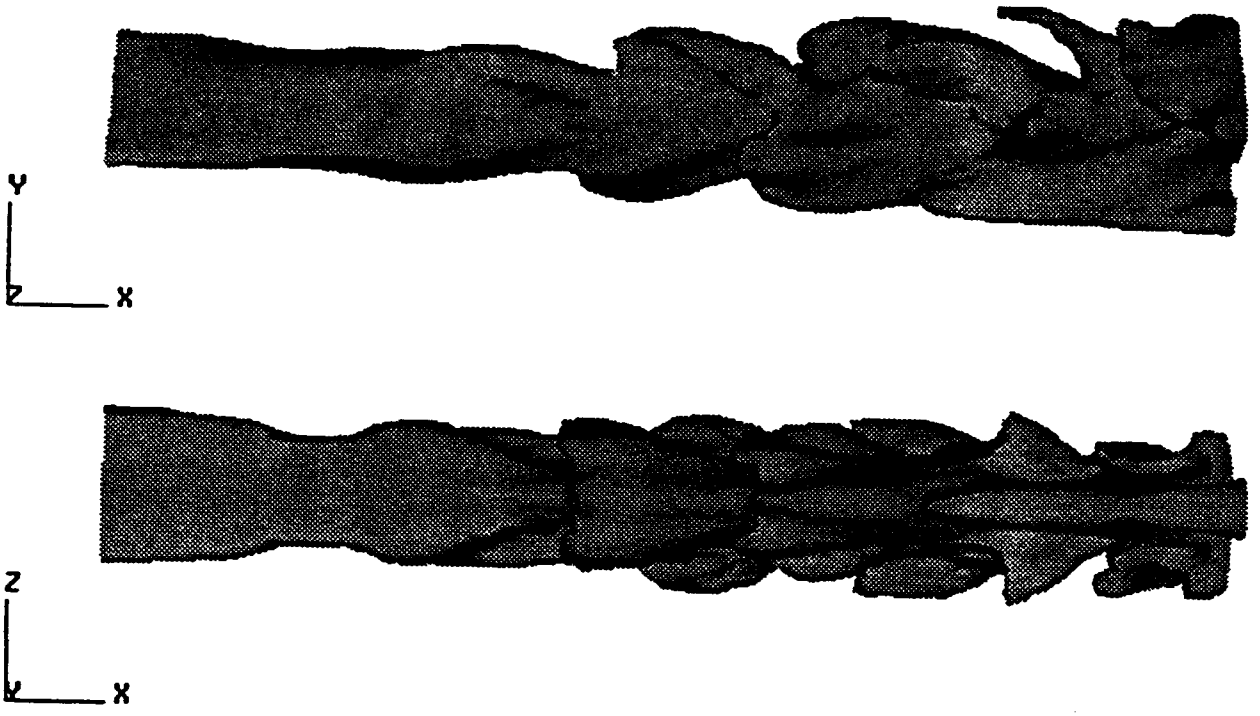

FIG. 16 (e)

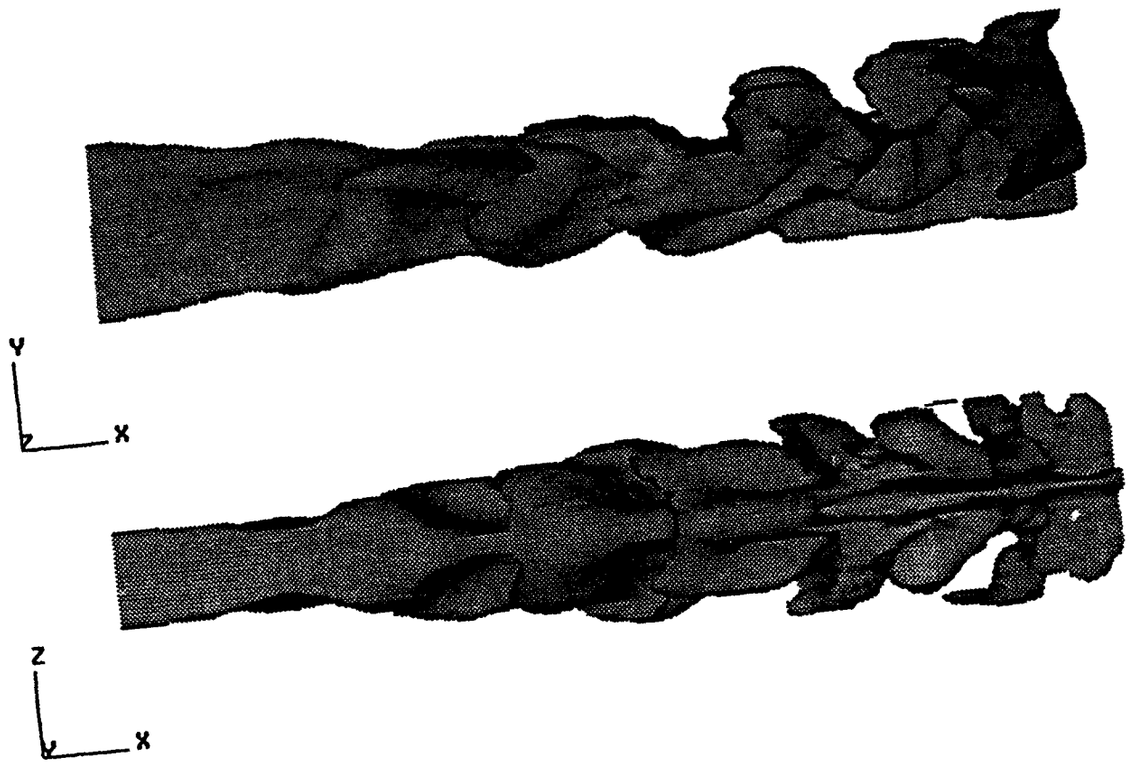

FIG. 16 (f)

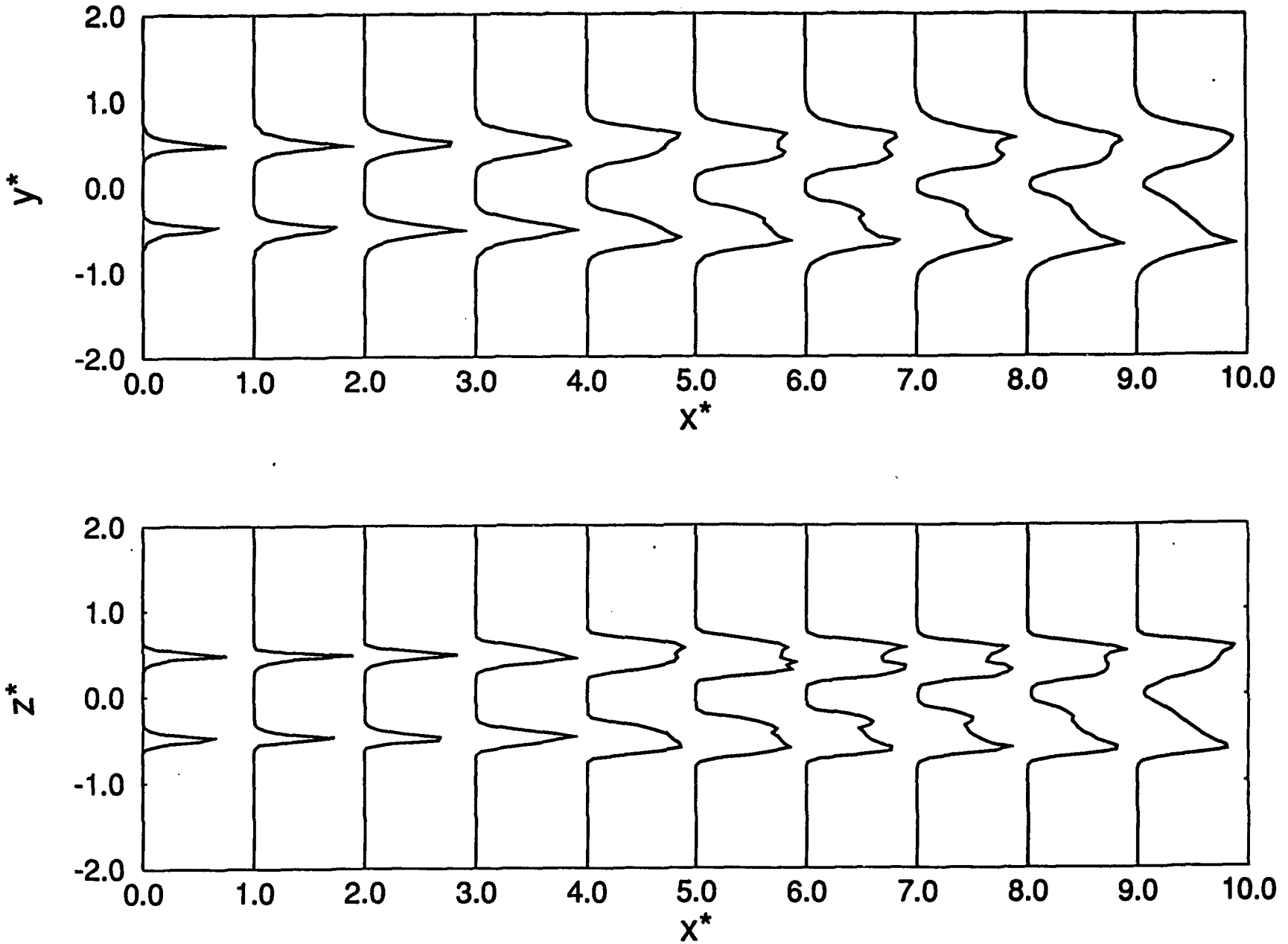
2.0
1.0
0.0
-1.0
-2.0
y*
0.0
1.0
2.0
3.0
4.0
5.0
6.0
7.0
8.0
9.0
10.0
X*
2.0
1.0
0.0
-1.0
-2.0
z*
0.0
1.0
2.0
3.0
4.0
5.0
6.0
7.0
8.0
9.0
10.0
X*

FIG. 17 (a)

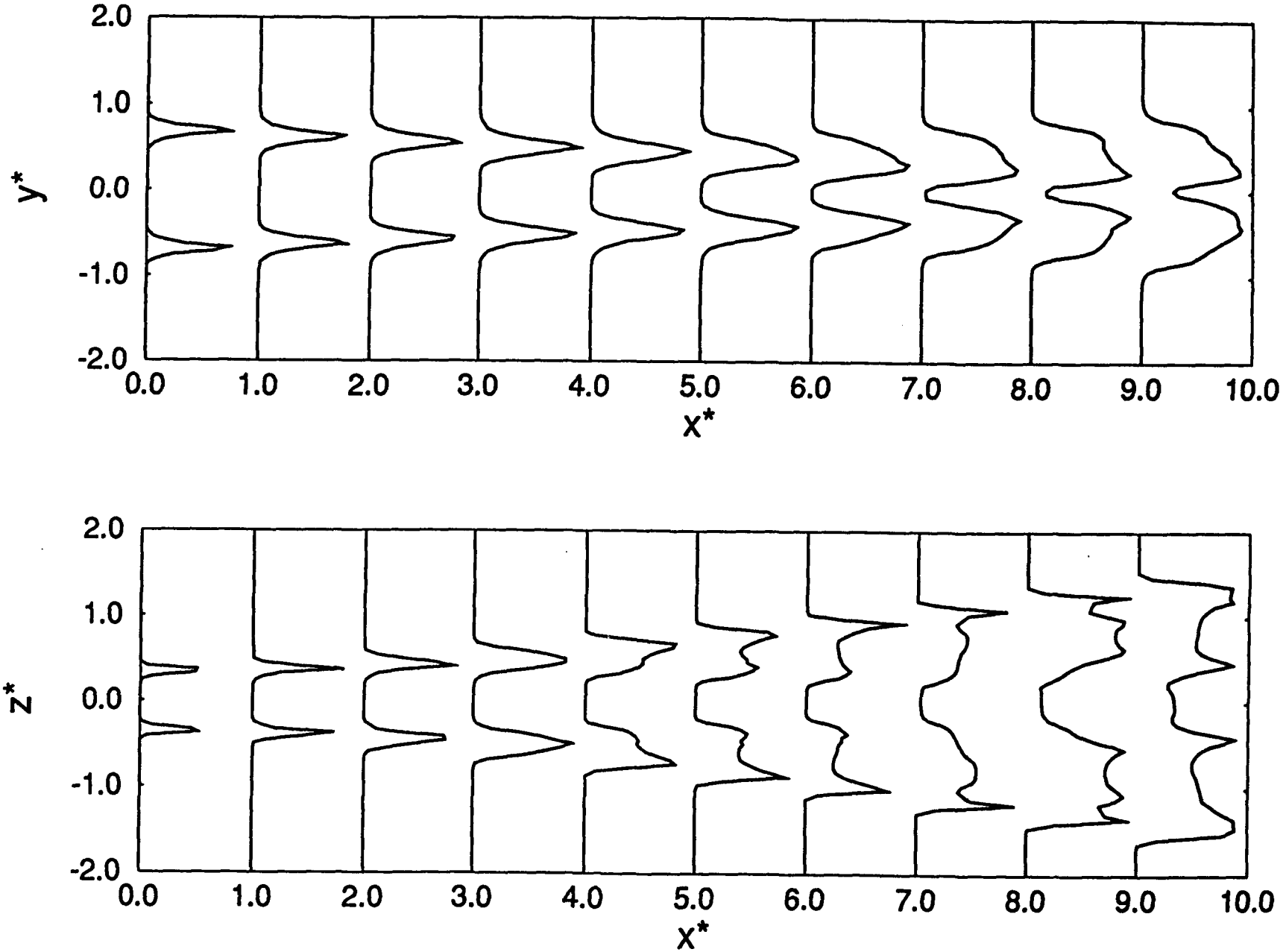
2.0
1.0
0.0
-1.0
-2.0
y*
0.0
1.0
2.0
3.0
4.0
5.0
6.0
7.0
8.0
9.0
10.0
X*
2.0
1.0
0.0
-1.0
-2.0
z*
0.0
1.0
2.0
3.0
4.0
5.0
6.0
7.0
8.0
9.0
10.0
X*

FIG. 17(b)

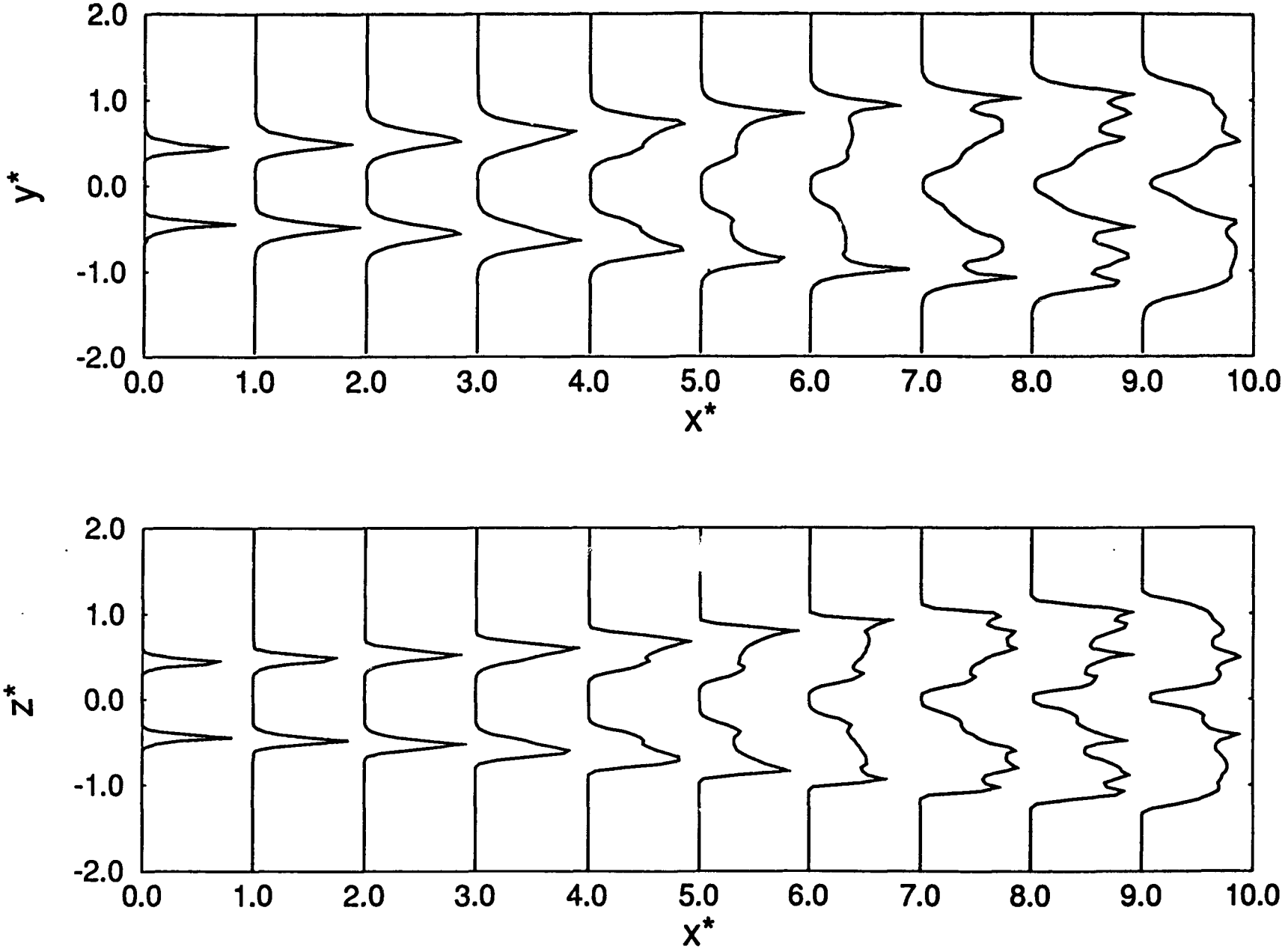
2.0
1.0
0.0
-1.0
-2.0
y*
0.0
1.0
2.0
3.0
4.0
5.0
6.0
7.0
8.0
9.0
10.0
x*
2.0
1.0
0.0
-1.0
-2.0
z*
0.0
1.0
2.0
3.0
4.0
5.0
6.0
7.0
8.0
9.0
10.0
x*

FIG. 17(c)

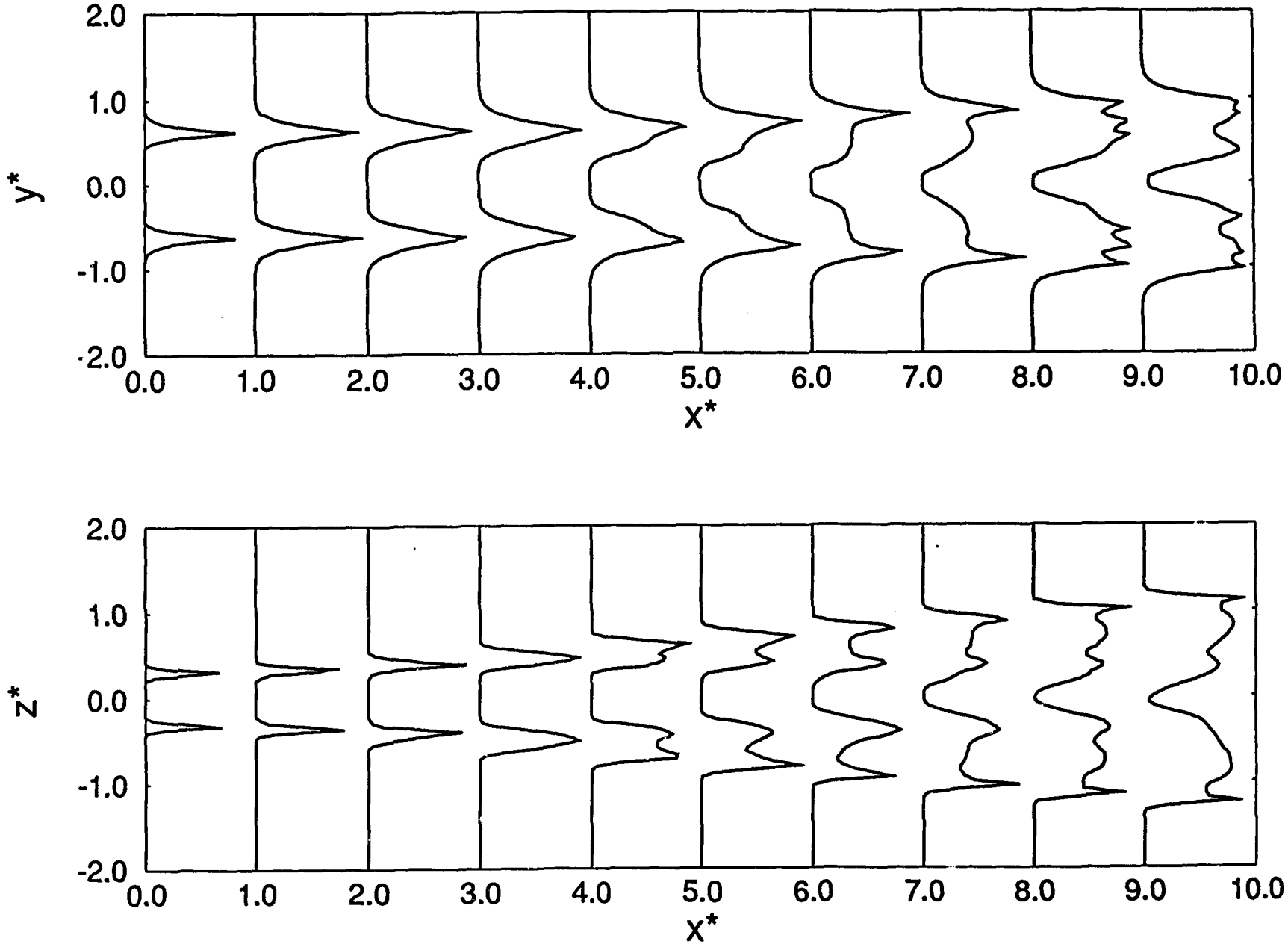
2.0
1.0
0.0
-1.0
-2.0
y*
0.0
1.0
2.0
3.0
4.0
5.0
6.0
7.0
8.0
9.0
10.0
X*
2.0
1.0
0.0
-1.0
-2.0
z*
0.0
1.0
2.0
3.0
4.0
5.0
6.0
7.0
8.0
9.0
10.0
X*

FIG. 17 (d)

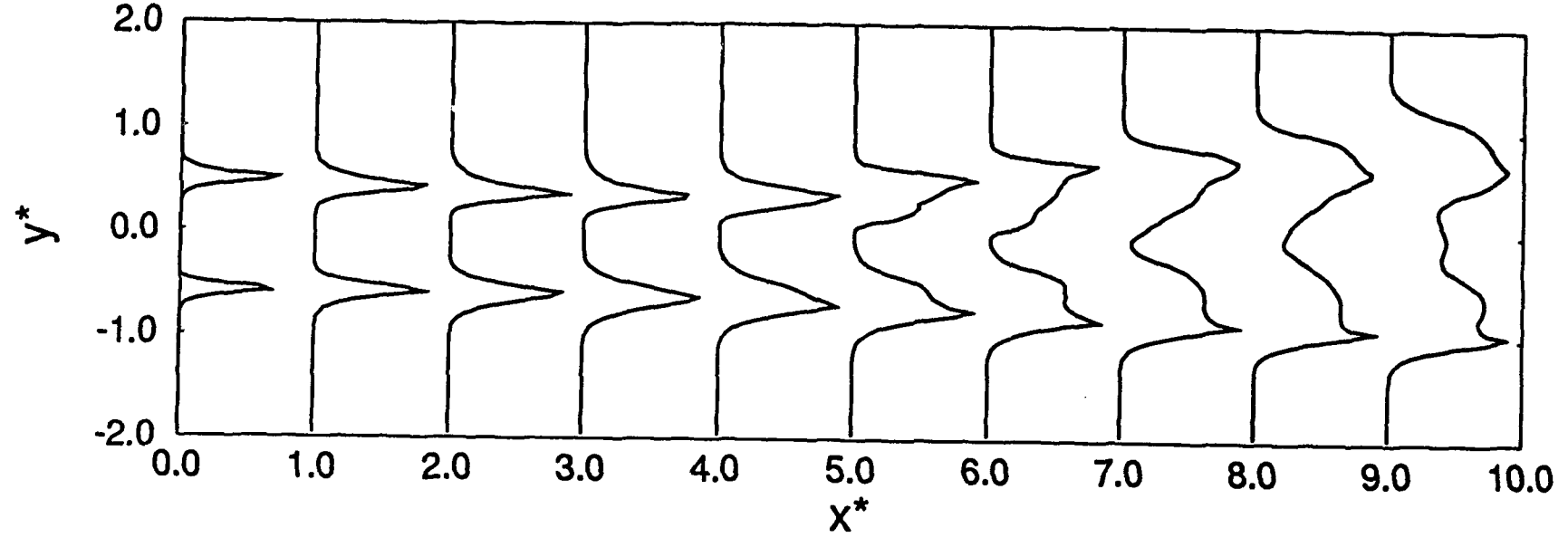
2.0
1.0
0.0
-1.0
-2.0
y*
0.0
1.0
2.0
3.0
4.0
5.0
6.0
7.0
8.0
9.0
10.0
X*

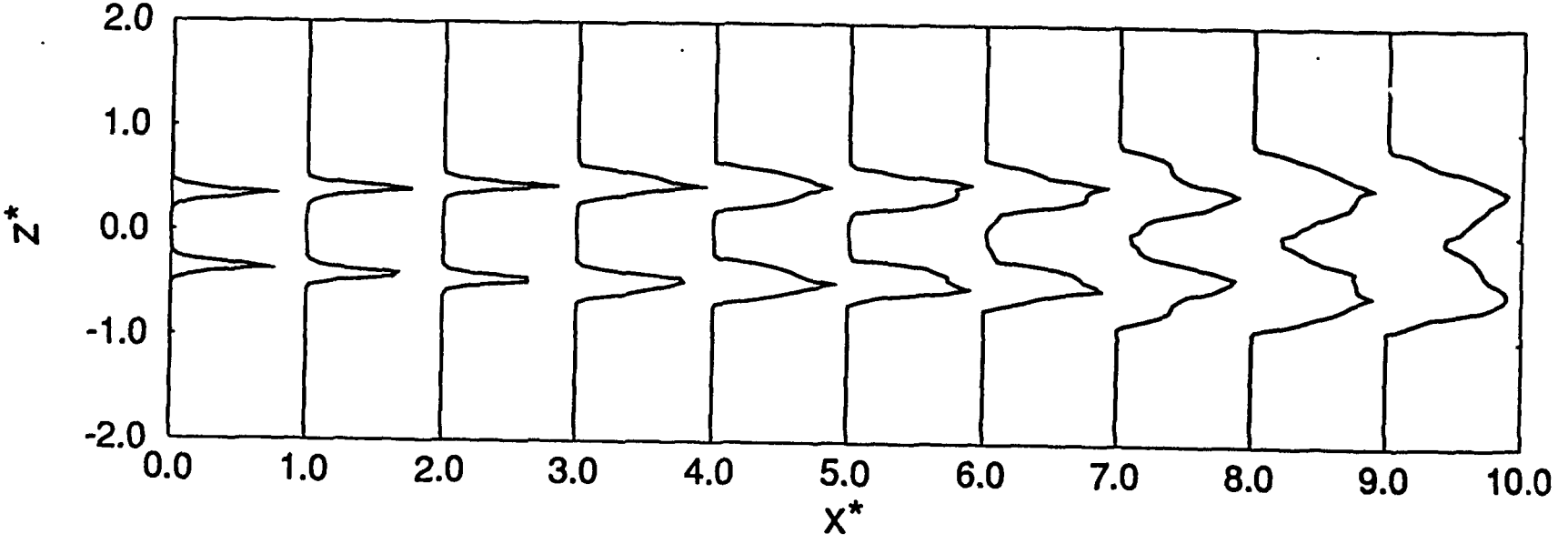
2.0
1.0
0.0
-1.0
-2.0
z*
0.0
1.0
2.0
3.0
4.0
5.0
6.0
7.0
8.0
9.0
10.0
X*

FIG. 17(e)

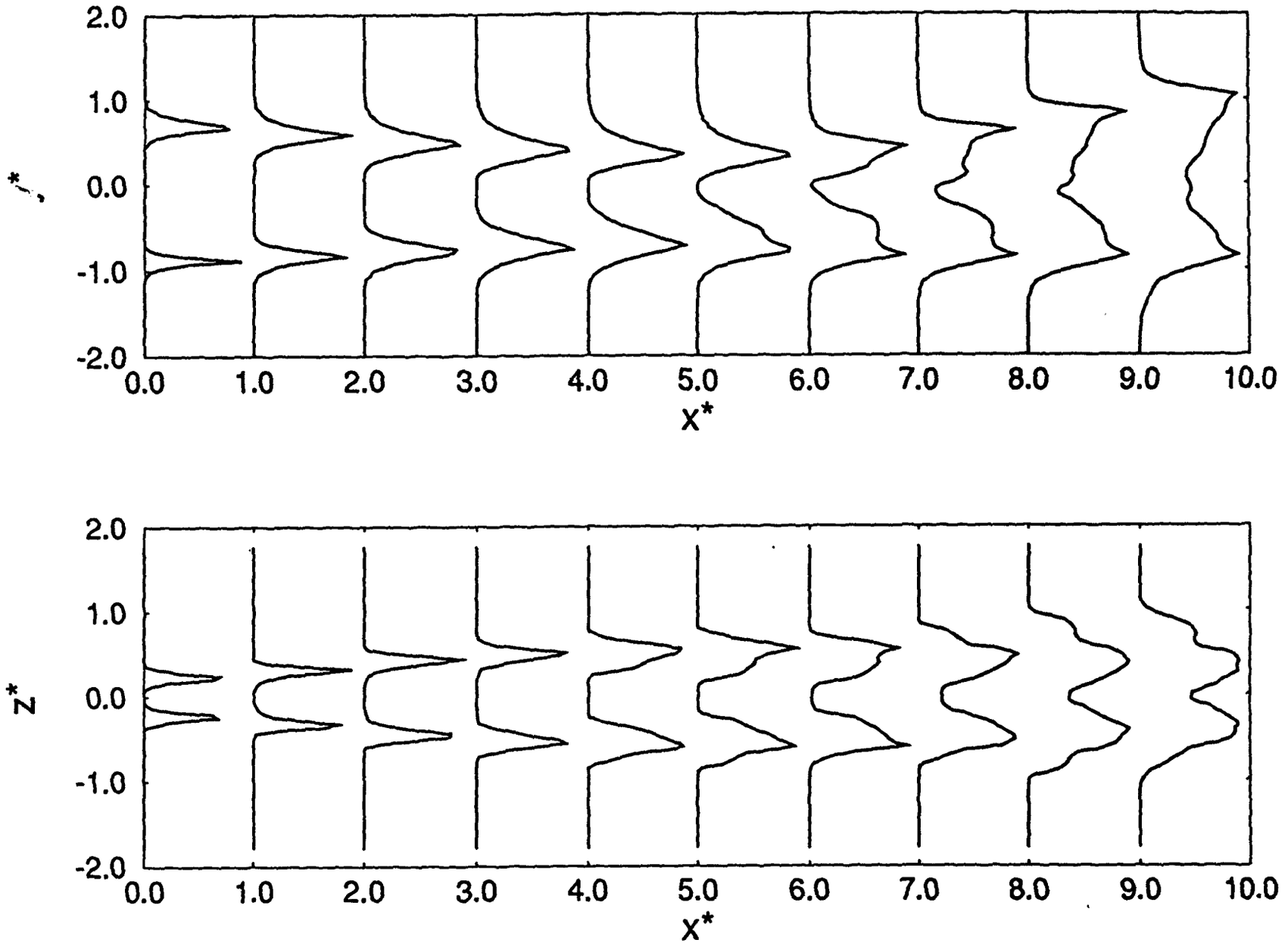

FIG. 17(f)

FIG. 18

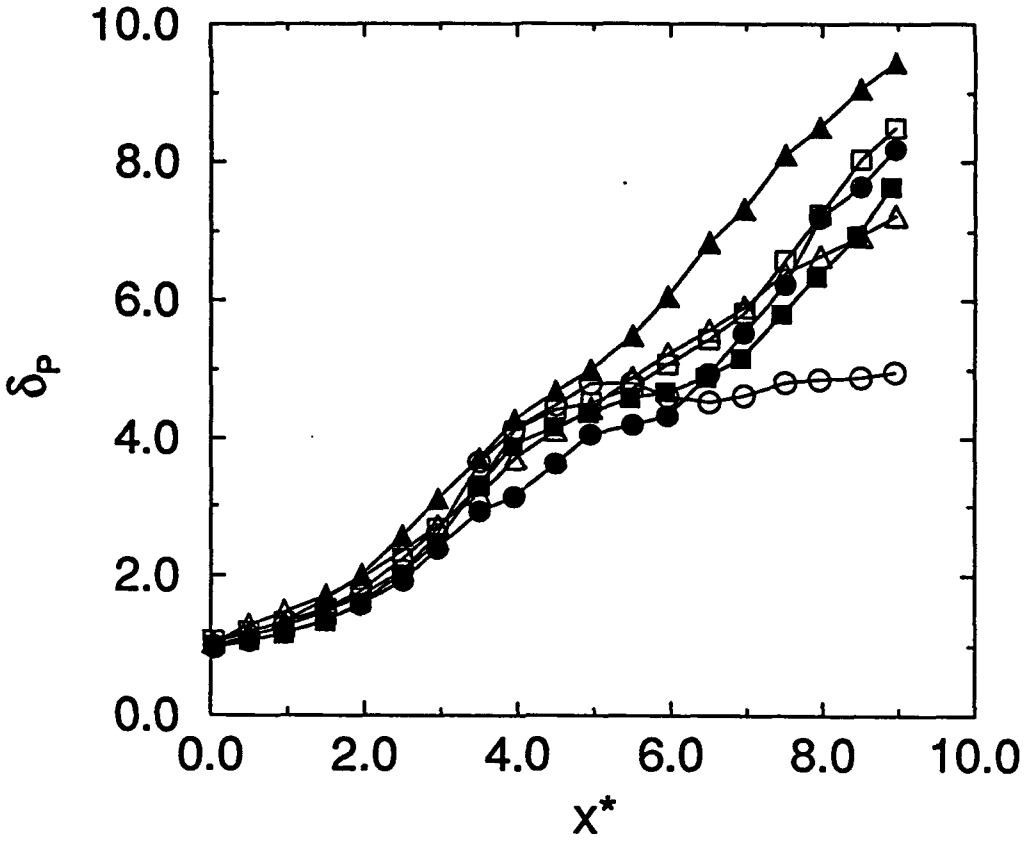
10.0
8.0
6.0
4.0
2.0
0.0
δ_p
0.0
2.0
4.0
6.0
8.0
10.0
x*

FIG. 19

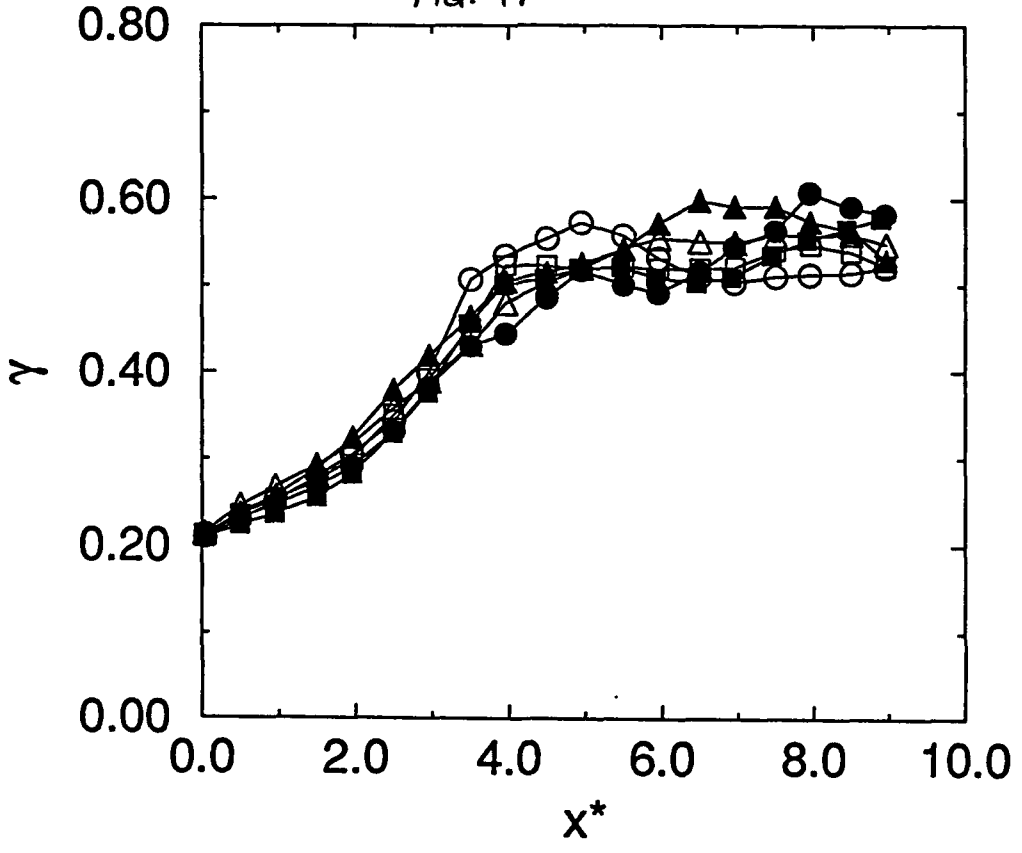
0.80
0.60
0.40
0.20
0.00
γ
0.0
2.0
4.0
6.0
8.0
10.0
x*

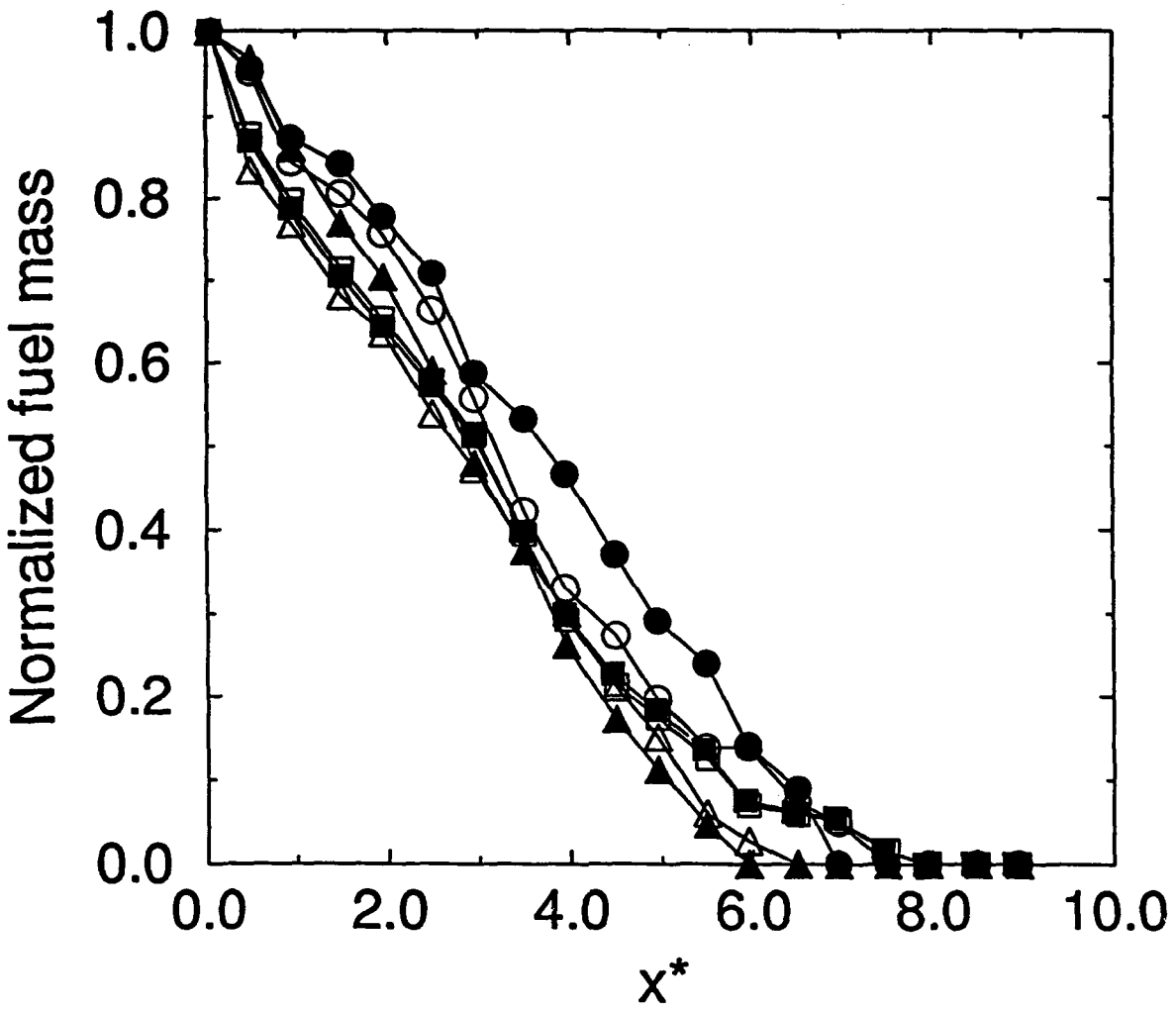

FIG. 20

APPENDIX 9

LES of Turbulent Reacting Flows

LARGE EDDY SIMULATION OF TURBULENT REACTING FLOWS BY ASSUMED PDF METHODS

S.H. Frankel, V. Adumitroaie, C.K. Madnia, and P. Givi
Department of Mechanical and Aerospace Engineering
State University of New York at Buffalo
Buffalo, New York

ABSTRACT

A priori and *a posteriori* analyses are conducted for validity assessments of assumed Probability Density Function (PDF) methods as potential subgrid scale (SGS) closures for Large Eddy Simulation (LES) of turbulent reacting flows. Simple non-premixed reacting systems involving an isothermal reaction of the type $A + B \rightarrow$ *Products* under both chemical equilibrium and non-equilibrium conditions are considered. *A priori* analyses are conducted of a homogeneous box flow, and a spatially developing planar mixing layer to investigate the performance of the *Pearson Family* of PDF's as SGS models. *A posteriori* analyses are conducted of the mixing layer using a hybrid one-equation Smagorinsky/PDF SGS closure. The Smagorinsky closure au[illegible]ted by the solution of the subgrid turbulent kinetic [illegible] TKE) equation is employed to account for hydrodyn[illegible]uctuations, and the PDF is employed for modeling the effects of scalar fluctuations. The implementation of the model requires the knowledge of the local values of the first two SGS moments. These are provided by additional modeled transport equations. In both *a priori* and *a posteriori* analyses, the predicted results are appraised by comparison with subgrid averaged results generated by Direct Numerical Simulations (DNS).

INTRODUCTION

Large Eddy Simulation (LES) is considered somewhere between Direct Numerical Simulation (DNS) and Reynolds Averaged Navier-Stokes (RANS) computation (Ferziger, 1981; Ferziger, 1983; Rogallo and Moin, 1984; Ferziger, 1987; Love, 1979; Ferziger and Leslie, 1979; Voke and Collins, 1983; Schumann and Friedrich, 1986; Schumman and Friedrich, 1987; Givi, 1989; Jou and Riley, 1989; Reynolds, 1990; Moin, 1991; Galperin and Orszag, 1993). Over the past thirty years, since the early work of Smagorinsky (1963) there has been relatively little effort, compared to that in RANS calculations, to make full use of LES for engineering applications. The most prominent model has been the Smagorinsky based eddy viscosity closure which relates the unknown subgrid scale (SGS) Reynolds stresses to the local large scale rate of strain. This viscosity is aimed to provide the role of mimicking the dissipative behavior of the unresolved small scales. The extensions to one-equation models, typically based on the SGS turbulent kinetic energy (Lilly, 1967; Schumman, 1975), have shown some improvements (Horuiti, 1985; Claus *et al.*, 1989). This is particularly the case in simulating transitional flows where the assumption of a balance between production and dissipation of turbulent kinetic energy may not always be valid. Thus, the higher degree of freedom provided by one-equation closures allow more flexibility for the subgrid scale eddies to adjust to local flow conditions.

A survey of combustion literature reveals relatively little work in LES of chemically reacting turbulent flows (Givi, 1989; Pope, 1990). It appears that Schumann (1989) was one of the first to conduct LES of a reacting flow. However, the assumption made in this work to simply neglect the contribution of SGS scalar fluctuations to the filtered reaction rate is debatable. The importance of such fluctuations is well recognized in RANS of reacting flows in both combustion (Libby and Williams, 1980; Kollmann, 1980; Jones and Whitelaw, 1982) and chemical engineering (Brodkey, 1975; Toor, 1975; Hill, 1976; Brodkey, 1981) problems. Therefore, it is natural to expect that these fluctuations will also have a significant influence in LES.

Modeling of scalar fluctuations in RANS has been the subject of intense investigations since the pioneering work

of Toor (1962). One approach which has proven particularly useful is based on the Probability Density Function (PDF) or joint PDF of scalar quantities (Dopazo, 1973; Pope, 1979; O'Brien, 1980; Pope, 1985; Givi, 1989; Kollmann, 1990; Pope, 1990). This approach offers the advantage that all the statistical information pertaining to the scalar field is embedded within the PDF. Therefore, once the PDF is known, the effects of scalar fluctuations are easily determined. Because of their capabilities, PDF methods have been widely used in RANS for a variety of reacting systems (see Pope (1990); Libby and Williams (1993) for recent reviews). A systematic approach for determining the PDF is by means of solving the transport equation governing its evolution (Lundgren, 1967; Lundgren, 1969). In this equation the effects of chemical reactions appear in a closed form. However, modeling is needed to account for transport of the PDF in the domain of the random variables. This transport describes the role of molecular action on the evolution of PDF. In addition, there is an extra dimensionality associated with the composition domain which must be treated. These two problems have constituted a stumbling block in utilizing PDF methods in practical applications, and developments of turbulence closures and numerical schemes which can effectively deal with these predicaments have been the subject of numerous investigations within the past two decades.

An alternative approach in PDF modeling is based on *assumed* methods. In these methods the PDF is not determined by solving a transport equation. Rather, its shape is assumed *a priori*, usually in terms of the low order moments of the random variable(s). Obviously, this method is *ad hoc* but it offers more flexibility than the first approach. Presently, the use of assumed methods in RANS is justified in cases where there is strong evidence that the PDF assumes a particular distribution.

Among these two approaches, obviously the first one is preferable if an appropriate closure is available to account for the effects of molecular action. In its application in RANS, traditionally, the family of models based on the coalescence/dispersion (C/D) closures (Curl, 1963; Janicka *et al.*, 1979; Norris and Pope, 1991), or least mean square methods (Dopazo and O'Brien, 1976) have been employed. These closures are plausible from a computational standpoint and can be effectively simulated via Monte Carlo numerical methods (Pope, 1981). However, there are several drawbacks associated with these closures that restrict their use for accurate and reliable predictions (Pope, 1982; Kosaly and Givi, 1987). Some of these drawbacks are overcome in the newly developed *Amplitude Mapping* Closure (AMC) (Kraichnan, 1989; Chen *et al.*, 1989). This has been established in a number of recent validation assessments of the AMC by means of comparison of its predicted results with those of DNS (Pope, 1991; Madnia *et al.*, 1992; Jiang *et al.*, 1992; Frankel *et al.*, 1993), and experimental (Frankel *et al.*, 1992a) data.

Despite its demonstrated properties, there are some deficiencies associated with the AMC which require further investigations. These are discussed in detail by Miller *et al.* (1993a); the most serious of these are: (1) the "single-point" nature of the closure, (2) the difficulties associated with its numerical implementation, and (3) its inability to account for the migration of scalar bounds as mixing proceeds. The first problem is shared with C/D models and indicates the deficiency of the approach in accounting for the variation of turbulent length (or time) scales. The other problems are exclusive to AMC and can cause difficulties in its applications.

Considering the current state of affairs in PDF modeling, it can be cautiously concluded that assumed PDF methods are somewhat more "feasible" than the transport equation approach for simulating practical problems. This is not to advocate the superiority of assumed methods. Rather, it is to encourage further research on the first approach before it can be implemented routinely. In this regard, in several recent studies Miller *et al.* (1993a) and Frankel *et al.* (1993) have conducted detailed investigations pertaining to both these approaches. The general conclusion drawn from these studies is that in cases where the AMC has proven useful, other approaches based on assumed probability distributions are also effective. In the cases considered by Miller *et al.* (1993a), it is shown that in simple flows where the AMC can be employed, the class of PDF's based on *Johnson Edgeworth Translation* (JET) (Johnson, 1949a; Edgeworth, 1907) can also be used. In fact, for the simple problem of binary mixing in isotropic turbulence - a standard test case - the solution generated by AMC (Pope, 1991; Gao, 1991) can be viewed as a member of the JET family. Furthermore, due to established similarities of JET with the simpler distributions belonging to the *Pearson Family* (PF) of PDF's (Pearson, 1895), it can be argued that the PF can also be considered as a viable alternative.

In turbulent combustion there has been widespread use of PF assumed PDF's (*e.g.* Rhodes (1975); Jones and Priddin (1978); Lockwood and Moneib (1980); Peters (1984); Janicka and Peters (1982); Frankel *et al.* (1990); for recent reviews see Williams (1985); Givi (1989); Priddin (1991)). In most applications to date, this family has been used in the form of the Beta density of the first kind (Pearson Type I and Type II distributions). This is due to the flexibility of this density in portraying bimodal distributions. The capabilities of this density for the purpose of RANS have been studied by Madnia *et al.* (1992); Miller *et al.* (1993a); Frankel *et al.* (1993). According to these studies there are some similarities between the PF and the AMC, as well as some distinct differences. As indicated before, both these methods are utilized in the context of a single-point closure. Therefore, in both cases the magnitudes of the moments up to second order must be provided externally. Also, both methods suffer from an inability to account for the shrinking bounds of the scalar domain as mixing proceeds. This is manifested by the failure of both closures in producing a correct evo-

lution for the conditional statistics of the scalar; namely, the conditional expected dissipation and the conditional expected diffusion. This behavior could be troublesome and may produce significant errors especially in predicting the rate of reactant conversion in non-equilibrium flames. In their application for modeling of reacting homogeneous flows, both closures are satisfactory for equilibrium flames, regardless of the equivalence ratio (Madnia *et al.*, 1992; Frankel *et al.*, 1993). However, the use of AMC is very difficult, if not impossible, for modeling of non-homogeneous flows regardless of the chemistry model. In such systems the mapping transfer function must be evaluated numerically and in the non-equilibrium case the multivariate form of the PDF must be considered. These require further investigations before they can be implemented routinely (Pope, 1991). In these cases the application of the PF is much more straightforward but obviously cannot be justified rigorously for all applications. The corresponding multivariate form of the Beta density is the *Dirichlet* distribution (Johnson, 1987; Johnson and Kotz, 1972; Wilks, 1962; Narumi, 1923) and its mathematical implementation is straightforward.

In this work, we report the results of our investigations pertaining the use of the Pearson family of PDF's in LES of turbulent reacting flows. This investigation is based on *a priori* and *a posteriori* analyses of simple homogeneous and shear flows under reacting, non-premixed conditions. Both equilibrium and non-equilibrium chemical reactions are considered. *A priori* analyses are performed of equilibrium flames in both flow configurations. *A posteriori* analyses are performed only for the shear flow with non-equilibrium chemistry. In all cases, the LES generated results are appraised by comparison with data provided via DNS.

FLOW CONFIGURATIONS

Two flow configurations are considered: (1) two- and three-dimensional homogeneous box flows, and (2) a two-dimensional spatially developing planar mixing layer. In both configurations, a constant rate, non heat releasing chemical reaction of the type $A + B \rightarrow P$ is considered. The procedure in homogeneous DNS is similar to that of previous simulations of this type. For a detailed description we refer to Madnia and Givi (1993). The computational package is based on a modification of the computer code developed by Erlebacher *et al.* (1987); Erlebacher *et al.* (1990); Erlebacher *et al.* (1992). This code is based on a spectral-collocation procedure for the spatial discretization of the transport variables and a third order Runge-Kutta method for temporal discretization. The hydrodynamic field is assumed isotropic and is initialized in a manner similar to that of Erlebacher *et al.* (1990); Passot and Pouquet (1987). The turbulent field is of decaying nature and the initial species field is composed of out of phase square waves for the two reactants A and B. The code is capable of simulating flows with different levels of compressibility (Hussaini *et al.*, 1990). Here, only the results obtained for a low compressible case are analyzed. In 2D, the resolution consists of 256 collocation points in each direction. In $3D$ simulations 96^3 collocation points are utilized. With this resolution, reliable calculations with a Reynolds number (based on the Taylor microscale) of $Re_\lambda \approx 41$ are attainable. Only the 3D results are used for *a priori* analyses.

The mixing layer configuration consists of two co-flowing streams traveling at different velocities and merging at the trailing edge of a partition plate. Two reactants, A and B, are introduced into the high- and the low-speed streams, respectively. To expedite the formation of large scale vortices, low amplitude perturbations are imposed at the inflow plane of the layer. The flow field which develops in this setting is dominated by large scale coherent structures. The numerical procedure employed for simulating this flow is based on a hybrid finite-difference/pseudospectral scheme. A third order upwinding method is used in the streamwise direction and a spectral collocation method employing Fourier expansions is used for cross stream discretization. Time discretization is done by the Adams-Bashforth technique. The computational domain is bounded by $0 < x < 32\delta, -8\delta < y < 8\delta$, where δ is the vorticity thickness at the inflow. The highest resolution consists of 512 finite difference nodes and 256 collocation nodes. With this resolution, reliable DNS with a Reynolds number $Re = 1000$ and a Damköhler number $Da = 10$ (based on the velocity difference and the vorticity thickness at the inlet) are possible.

In both flows, all the species (A, B, P) are assumed thermodynamically identical and the fluid is assumed to be calorically perfect. The value of the molecular Schmidt number is set equal to unity in all simulations. It is also assumed that there is no trace of one of these species at the feed of the other one, *i.e.* complete initial segregation. With unity normalized mass fractions of the two species at their respective streams, a mixture fraction denoted by $\mathcal{J}$ can be defined (Williams, 1985):

$$\mathcal{J}(x_i, t) = \frac{Y_A(x_i, t) - Y_B(x_i, t) + 1}{2}, \quad \mathcal{J} \in [0, 1]. \qquad (1)$$

where Y_i denotes the mass fraction of species i. With total initial segregation the magnitude of the mixture fraction is unity in the stream containing A, and zero in the stream containing B. In non-reacting flows, the transport of this mixture fraction portrays the mixing process. In reacting flows, the variable $\mathcal{J}$ denotes a conserved "Shvab-Zeldovich" scalar variable (Williams, 1985). In the limit of an infinitely fast chemical reaction all the statistics of the two reactants are directly related to those of the Shvab-Zeldovich variable (Toor, 1962; O'Brien, 1971; Bilger, 1980; Williams, 1985; Kosaly and Givi, 1987):

The assessment of the models is facilitated by direct comparison with DNS data. The resolution in DNS is dictated by the magnitudes of the physical parameters, with sufficient testing on the independency of the results to the number of

grid points. All the subgrid statistics are constructed directly from the filtered DNS data bank. In *a priori* analyses the statistical properties of subgrid data are considered. In *a posteriori* analyses, the results predicted by LES on coarse grids are compared with those of filtered DNS. These analyses, correspond effectively to simulations with a homogeneous box filter in which the values of the filtered means are constant within the box. The ratio between the coarse grid and the fine grid is, therefore, a measure of the filter width. That is, it determines the scale at which the subgrid fluctuations are not accounted for deterministically. Consequently, the statistical behavior of the variable within the subgrid is dependent on the magnitude of the sample size there. If this size is too small, statistical analyses are meaningless. If it is too large, the essential features of large scale transport are masked. In *a priori* analysis of the box flow, a corse grid consisting of 12^3 grid points are considered. In the shear flow, LES is performed on the domain with 64 finite difference grid points and 32 Fourier collocation points.

PROBLEM FORMULATION AND LES METHODOLOGY

Fluid Dynamics

With the assumptions made above, transport of the aerothermochemical variables is described by a decoupled system of conservation equations, together with the continuity equation. Denoting the velocity field by a Cartesian vector u_i, the pressure by p, the kinematic viscosity by ν, the space vector by x_i and time by t, we have:

$$\frac{\partial u_i}{\partial x_i} = 0 \tag{2}$$

$$\frac{\partial u_i}{\partial t} + \frac{\partial (u_i u_j)}{\partial x_j} = -\frac{1}{\rho}\frac{\partial p}{\partial x_i} + \nu \frac{\partial^2 u_i}{\partial x_j \partial x_j} \tag{3}$$

In LES, these equations are filtered to distinguish the resolved or large scale field from the subgrid scale field. This is facilitated by employing a convolution integral of the type (Aldama, 1990):

$$\overline{u}(\mathbf{x}) = \int_{\Delta} G(\mathbf{x}-\mathbf{x}')u(\mathbf{x}')\,d\mathbf{x}' \tag{4}$$

where the overbar indicates the filtered variable and G is a filter function with characteristic length Δ. There are two ways of performing this filtering process. These are the prefiltering approach and the grid averaging approach. Here we employ the latter for its ease of implementation. With this, the SGS fluctuations are given by:

$$u_i' = u_i - \overline{u_i} \tag{5}$$

Applying the filtering process to the governing equations yields:

$$\frac{\partial \overline{u_i}}{\partial x_i} = 0 \tag{6}$$

$$\frac{\partial \overline{u_i}}{\partial t} + \frac{\partial (\overline{u_i u_j})}{\partial x_j} = -\frac{1}{\rho}\frac{\partial \overline{p}}{\partial x_i} + \nu \frac{\partial^2 \overline{u_i}}{\partial x_j \partial x_j} \tag{7}$$

The nonlinear term, $\overline{u_i u_j}$, can be written as:

$$\overline{u_i u_j} = (\overline{u_i'} + \overline{u_i})(\overline{u_j'} + \overline{u_j}) = \overline{u_i' u_j'} + \overline{u_i' \overline{u_j}} + \overline{\overline{u_i} u_j'} + \overline{\overline{u_i}\,\overline{u_j}} \tag{8}$$

The last term depends on large scale components and is computable in LES. The SGS Reynolds' stresses are defined as

$$R_{ij} = \overline{u_i' u_j'} + \overline{u_i' \overline{u_j}} + \overline{\overline{u_i} u_j'} \tag{9}$$

In the context of the grid averaged approach pursued here, the cross terms are zero and the only term requiring modeling is $\overline{u_i' u_j'}$. This forms the focus of hydrodynamic SGS modeling. Typically one decomposes the SGS stress into the sum of a trace-free tensor and a diagonal tensor,

$$R_{ij} = (R_{ij} - \frac{1}{3}\delta_{ij}R_{kk}) + \frac{1}{3}\delta_{ij}R_{kk} = \tau_{ij} + \frac{1}{3}\delta_{ij}R_{kk} \tag{10}$$

Substituting this into the averaged equations yields;

$$\frac{\partial \overline{u_i}}{\partial t} + \frac{\partial (\overline{u_i}\,\overline{u_j})}{\partial x_j} = -\frac{1}{\rho}\frac{\partial \overline{p}}{\partial x_i} - \frac{\partial \tau_{ij}}{\partial x_j} - \frac{\partial (\frac{1}{3}\delta_{ij}R_{kk})}{\partial x_j} + \nu \frac{\partial^2 \overline{u_i}}{\partial x_j \partial x_j} \tag{11}$$

or defining,

$$\overline{P} = \frac{\overline{p}}{\rho} + \frac{1}{3}R_{kk} \tag{12}$$

and employing the Smagorinsky eddy viscosity model for closure of the Reynolds' stress, we have:

$$\tau_{ij} = -\nu_T \left(\frac{\partial \overline{u_i}}{\partial x_j} + \frac{\partial \overline{u_j}}{\partial x_i} \right) = -2\nu_T S_{ij} \tag{13}$$

In the Smagorinsky model the eddy viscosity, ν_T, is related to the large scale strain rate, S_{ij}. A suggestion made by Kwak *et al.* (1975) and discussed by Mansour *et al.* (1978) is to model the eddy viscosity in terms of the trace of the resolved vorticity field. Here, since the SGS moments up to second order are required for the species field, an extension is made to utilize a one-equation hydrodynamics closure. Specifically, the transport equation for the SGS turbulent kinetic energy, $k = \frac{1}{2}(\overline{u_i' u_i'})$, is considered. With this, the eddy viscosity is of the form:

$$\nu_T = C_k \Delta \sqrt{k} \tag{14}$$

where C_k is a model constant and Δ is the filter width. With this, the momentum equation becomes:

$$\frac{\partial \overline{u_i}}{\partial t} + \frac{\partial (\overline{u_i}\,\overline{u_j})}{\partial x_j} = -\frac{\partial \overline{P}}{\partial x_i} + \frac{\partial}{\partial x_j}\left((\nu + \nu_T)\frac{\partial \overline{u_i}}{\partial x_j} \right) + \frac{\partial \nu_T}{\partial x_j}\frac{\partial \overline{u_j}}{\partial x_i} \tag{15}$$

and the modeled TKE equation is:

$$\frac{Dk}{Dt} = \frac{\partial}{\partial x_i}\left((\nu + \frac{\nu_T}{\sigma_k})\frac{\partial k}{\partial x_i} \right) + P_k - C_D \frac{k^{\frac{3}{2}}}{\Delta} \tag{16}$$

with C_D, σ_k as empirical constants. In Eq. (16), P_k is the

production term given by,

$$P_k = \nu_T \left(\frac{\partial \overline{u_j}}{\partial x_i} + \frac{\partial \overline{u_i}}{\partial x_j} \right) \frac{\partial \overline{u_j}}{\partial x_i} \tag{17}$$

Thermochemistry

Following the same procedure, the filtered conservation equation for the mass fraction of species A, denoted by Y_A, is given by:

$$\frac{\partial \overline{Y_A}}{\partial t} + \frac{\partial \overline{u_i}\,\overline{Y_A}}{\partial x_i} = \frac{\partial}{\partial x_i} \left((\mathcal{D} + \mathcal{D}_T) \frac{\partial \overline{Y_A}}{\partial x_i} \right) + \overline{\dot{\omega}_A} \tag{18}$$

where $\mathcal{D}$ is the molecular diffusion coefficient and $\dot{\omega}$ indicates the chemical source term. The unresolved SGS velocity-scalar fluctuations are modeled by Smagorinsky type model with $\mathcal{D}_T = \nu_T / \sigma_T$ where σ_T is the turbulent Schmidt number. Similar equations hold for Y_B and Y_P. For the reaction considered here, the chemical source term is of the form:

$$\dot{\omega}_A = -Da Y_A Y_B \tag{19}$$

where Da denotes the Damköhler number and represents a non-dimensional measure of the speed of reaction. With this, the filtered non-dimensionalized source term can be defined in terms of the probability average,

$$\overline{\dot{\omega}} = \int \dot{\omega}(\psi', \psi'') \mathcal{P}_{AB}(\psi', \psi'')\, d\psi'\, d\psi'' \tag{20}$$

where (ψ', ψ'') denotes the probability sample space for the random variables (Y_A, Y_B), and $\mathcal{P}_{AB}$ denotes their SGS joint PDF.

Pearson Family of PDF's

The formulation presented above is in a closed form with the specification of the PDF within the subgrid. In general, the knowledge of the joint PDF of the reactants, *i.e.* $\mathcal{P}_{AB}$, is required. However, in flows under chemical equilibrium the procedure is simplified. In this case, the PDF of the Shvab-Zeldovich variable, $\mathcal{P}_{\mathcal{J}}$, provides all the necessary information. As discussed above, the Pearson family of PDF's are assumed to represent the statistical behavior within the subgrid. Therefore, for equilibrium chemistry, the Beta density of the first kind is employed. In non-equilibrium simulations the multivariate form of this PDF, in the form of the Dirichlet density, is assumed.

For a non-symmetric distribution the Beta density corresponds to the Pearson Type I, and for the symmetric case to Pearson Type II. In both cases, the PDF of the Shvab-Zeldovich variable is represented by (Abramowitz and Stegun, 1972):

$$\mathcal{P}_{\mathcal{J}}(\xi) = \frac{1}{B(\beta_1, \beta_2)} \xi^{\beta_1 - 1} (1 - \xi)^{\beta_2 - 1}, \quad 0 \le \xi \le 1. \tag{21}$$

where $B(\beta_1, \beta_2)$ denotes the Beta function and the parameters β_1 and β_2 depend on the mean and the variance of the random variable $\mathcal{J}$. In applications to equilibrium chemistry all the statistics of the reacting scalar are easily determined from this PDF. For example, the filtered values of the species mass fractions are given by (Madnia *et al.*, 1992):

$$\begin{aligned} \overline{Y_A} &= \frac{\mathcal{J}_{st}^{\beta_1} (1 - \mathcal{J}_{st})^{\beta_2 - 1}}{(\beta_1 + \beta_2) B(\beta_1, \beta_2)} \\ &\quad + \frac{1}{1 - \mathcal{J}_{st}} \left(\frac{\beta_1}{\beta_1 + \beta_2} - \mathcal{J}_{st} \right) (1 - \mathcal{I}_{\mathcal{J}_{st}}(\beta_1, \beta_2)) \end{aligned} \tag{22}$$

$$\overline{Y_B} = \frac{\mathcal{J}_{st}^{\beta_1 - 1} (1 - \mathcal{J}_{st})^{\beta_2}}{(\beta_1 + \beta_2) B(\beta_1, \beta_2)} + \left(1 - \frac{\beta_1}{(\beta_1 + \beta_2) \mathcal{J}_{st}} \right) \mathcal{I}_{\mathcal{J}_{st}}(\beta_1, \beta_2) \tag{23}$$

Here $\mathcal{I}$ denotes the Incomplete Beta Function (Abramowitz and Stegun, 1972), and the subscript "st" denotes the stoichiometric value of the Shvab-Zeldovich variable; here obviously $\mathcal{J}_{st} = 0.5$. It is noted that these relations are significantly simplified when the mixture within the subgrid is in stoichiometric proportion, *i.e.* when $\beta_1 = \beta_2$.

For the non-equilibrium case, the Dirichlet or joint Beta distribution for the two species A and B is given by (Wilks, 1962):

$$\begin{aligned} &\mathcal{P}_{AB}(\psi', \psi'') = \\ &\quad \frac{\Gamma(p_1 + p_2 + p_3)}{\Gamma(p_1)\Gamma(p_2)\Gamma(p_3)} (\psi')^{p_1 - 1} (\psi'')^{p_2 - 1} (1 - \psi' - \psi'')^{p_3 - 1} \end{aligned} \tag{24}$$

where,

$$\psi' \ge 0\,, \ \psi'' \ge 0\,, \ \psi' + \psi'' \le 1\,, \ p_1, p_2, p_3 > 0 \tag{25}$$

The parameters p_1, p_2, p_3 are determined from the knowledge of any three of the following five quantities: the average (filtered) values $\overline{Y_A}$, $\overline{Y_B}$, the SGS variances $\overline{Y_A''^2}$, $\overline{Y_B''^2}$, and/or the SGS covariance $\overline{Y_A' Y_B'}$. The chemical source term should depend on all of the above turbochemical quantities. However, the degree of freedom of the Dirichlet distribution allows only three of these variables to be used. If the two mean values and the covariance are used, the parameters of the density are related by:

$$p_1 = -\overline{Y_A} S \tag{26}$$

$$p_2 = -\overline{Y_B} S \tag{27}$$

$$p_3 = (\overline{Y_A} + \overline{Y_B} - 1) S \tag{28}$$

where,

$$S = 1 + \overline{Y_A}\,\overline{Y_B} / \overline{Y_A' Y_B'} \tag{29}$$

The normalized chemical source term can be analytically integrated to yield:

$$\overline{\dot{\omega}_A} = -Da \frac{p_1 p_2}{(a + 1) a} \tag{30}$$

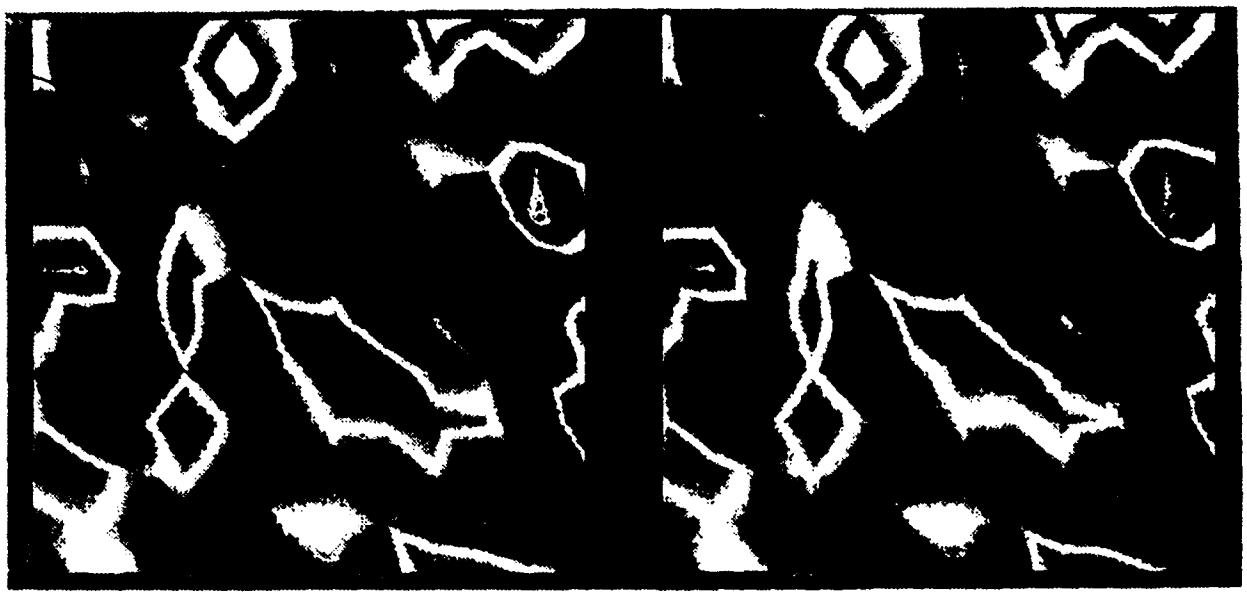

(a) (b)

Figure 1: Contour plots of filtered product mass fraction in homogeneous simulations: (a) DNS, (b) PDF.

where $a = p_1 + p_2 + p_3$.

With this formulation, the filtered mean values and SGS covariance are determined by transport equations. These equations are coupled with the joint PDF to determine the effects of chemistry. The modeled equations for the mean values are similar to Eq. (18). The modeled SGS species covariance equation is of the form (Pope, 1979):

$$\frac{D\overline{Y_A'Y_B'}}{Dt} = \frac{\partial}{\partial x_i}\left((\mathcal{D}+\mathcal{D}_T)\frac{\partial \overline{Y_A'Y_B'}}{\partial x_i}\right) + C_1\mathcal{D}_T\left(\frac{\partial \overline{Y_A}}{\partial x_i}\frac{\partial \overline{Y_B}}{\partial x_i}\right) - C_2\overline{Y_A'Y_B'}\frac{k^{\frac{1}{2}}}{\Delta} + \overline{\dot{\omega}_A Y_B'} + \overline{\dot{\omega}_B Y_A'} \quad (31)$$

where C_1 and C_2 are adjustable constants. The chemical source/sink terms in this equation are given by:

$$\overline{\dot{\omega}_B Y_A'} = -Da\left(\frac{(p_1+1)p_1p_2}{(a+2)(a+1)a} - \overline{Y_A}\frac{p_1p_2}{(a+1)a}\right) \quad (32)$$

$$\overline{\dot{\omega}_A Y_B'} = -Da\left(\frac{(p_2+1)p_1p_2}{(a+2)(a+1)a} - \overline{Y_B}\frac{p_1p_2}{(a+1)a}\right) \quad (33)$$

Equations (26)-(33) provide all the essential information pertaining to the effects of chemistry for the Dirichlet density. It is noted that other moments (or joint moments) of the species field can be used for parameterizing this PDF (Johnson and Kotz, 1972). In fact, Girimaji (1991a); Girimaji (1991b); Narayan and Girimaji (1992) suggest the use of the scalar energy (summation of the scalar variances) instead of the covariance for this parameterization (also see Baurle *et al.* (1992)). This issue is addressed further in the next section.

The formulation above is in a closed form with the specification of the model constants appearing in the LES transport equations. A nominal parametric study was done to estimate the values of these constants. From this study, the magnitudes of some of these constants were found different from those typically used in RANS (Launder and Spalding, 1972). The results presented in the next section are based on $C_1 = 2.97, C_2 = 0.15, \sigma_T = \sigma_k = 1.0, C_k = 0.01$, and $C_D = 0.5$. No attempt was made to determine the optimized values of these constants.

RESULTS

The validity assessments of the Beta density in Reynolds averaging of reacting flows under chemical equilibrium have been reported by Madnia *et al.* (1991) for a homogeneous box flow and by Frankel *et al.* (1992b) for a non-

homogeneous shear flow. According to these studies, the Beta density provides a reasonable approximation of the probabilistic behavior of the Shvab-Zeldovich variable in these flows. The agreement is somewhat better for the box flow since the model cannot predict the trimodal behavior of the PDF (Koochesfahani and Dimotakis, 1986; Masutani and Bowman, 1986; Givi and McMurtry, 1988; Lowery *et al.*, 1987) in shear flows. Since, the flow within the subgrid can be assumed homogeneous (and also isotropic), it is therefore speculated that the model may also perform well in the context of LES. In order to examine this, some analyses are made of the *a priori* performance of the closure with the 3D DNS data. In Fig. 1 plots are presented of the contours of averaged product mass fraction in one subgrid plane for the box flow with equilibrium chemistry. Part (a) of this figure corresponds to data obtained by directly filtering the DNS data, and part (b) represents the solution predicted by the Beta density model. In the implementation of this model, the first two SGS moments of the Shvab-Zeldovich variable are inputs from DNS. The comparisons shown in these figures reveal good agreement between the model predictions and the DNS data.

A similar agreement is observed in the analysis of the non-homogeneous flow. This is shown in Fig. 2 by means of the instantaneous product thickness of the layer. Here also the first two SGS moments of the Shvab-Zeldovich variable are extracted from DNS. From an engineering standpoint, the agreements noted in these figures advocate the use of the Beta density, at least in absence of better alternatives, for describing the probabilistic behavior of the conserved scalar variables within the subgrid. However, since the first two moments of the Shvab-Zeldovich variable are taken from DNS, the procedure followed here is not useful for a predictive analysis, *i.e.* it is not an actual LES. Furthermore, the agreement can be guaranteed only at this statistical level. This is due to lack of sufficient data for the assessment of higher order moments.

For the non-equilibrium chemistry case, the joint PDF of the two species must be considered. First, the performance of the Dirichlet density for the purpose of RANS should be examined. For the case of zero Damköhler number, this implies that the marginal density of each reactant is a Beta PDF. Therefore, the higher order statistics predicted by this density should match with those generated by DNS. This comparison is made in Fig. 3, and as expected the agreement is very good up to the sixth order moment. For finite values of the Damköhler number, the agreement is less satisfactory. This is shown in Figs. 4-5, where the temporal evolutions of the third order cross moments are considered. The difference between these two figures is due to the procedure by which the Dirichlet density is parameterized. In the calculation resulting in Fig. 4, the PDF is based on the means of the two species and the covariance. In those of Fig. 5, the two means and the scalar energy are used to construct the PDF. The results portrayed in these figures indicate that in both cases, the general trends are captured well but an exact agreement

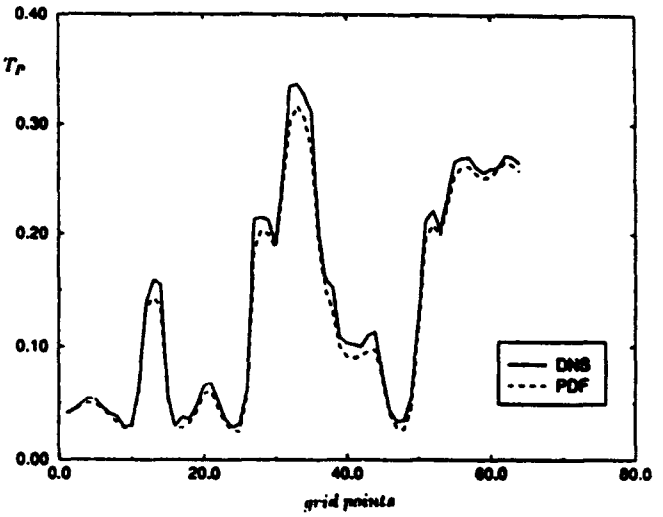

Figure 2: Streamwise variation of instantaneous product mass fraction thickness for the mixing layer under chemical equilibrium

with DNS data cannot be established. Also, the differences in the statistical predictions between the two closures do not clearly favor one approach over the other. However, since the SGS covariance appears directly in the source term in the filtered species equation, this version is employed in *a posteriori* analyses.

In employing assumed PDF methods in an actual LES, the filtered mean values and SGS moments of the scalar variable must be provided without resorting to DNS. Here, LES results obtained by the full Smagorinsky/PDF closure are presented to examine the overall performance of the hybrid model. This examination is conducted for the mixing layer flow since it provides a more stringent test for model assessments. In Fig. 6, cross-stream profiles of the instantaneous streamwise velocity component are shown at several downstream locations. This figure shows that the large scale velocity field is predicted well in LES as the results compare reasonably well with those of filtered DNS. The comparison of the subgrid scale TKE as predicted by the model, with the TKE obtained from the filtered DNS are shown in Figs. 7-8. These figures also indicate a relatively good agreement between the LES predictions and the DNS filtered results. The exception is at far distances from the inlet, where it is shown that the TKE equation severely underpredicts the subgrid turbulence level. This trend has also been observed in the simulations of Claus *et al.* (1989) and may be due to deficiencies in modeling of the Reynolds stresses in terms of the strain tensor alone. Inclusion of other terms such as the rotation tensor and/or products of the strain rate and rotation tensors may be necessary to improve the predictions of TKE (Taulbee, 1992; Lund and Novikov, 1991).

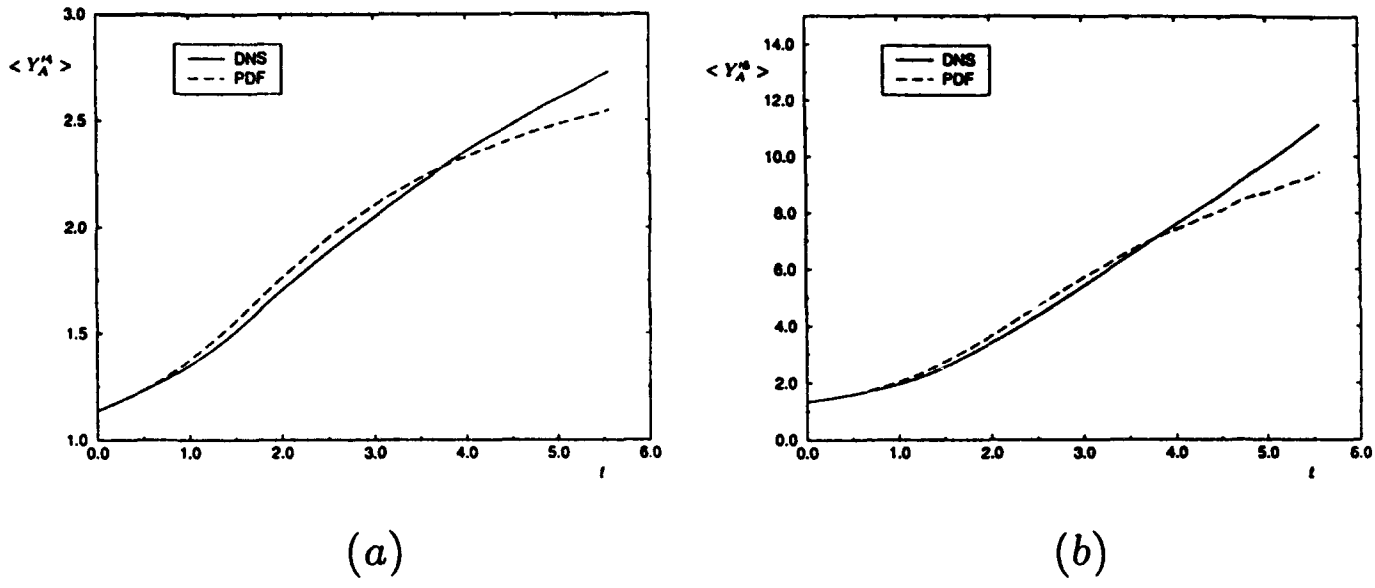

Figure 3: Temporal variations of Reynolds moments of the mass fraction of species A in homogeneous simulations ($Da = 0$), (a) fourth and (b) sixth moments.

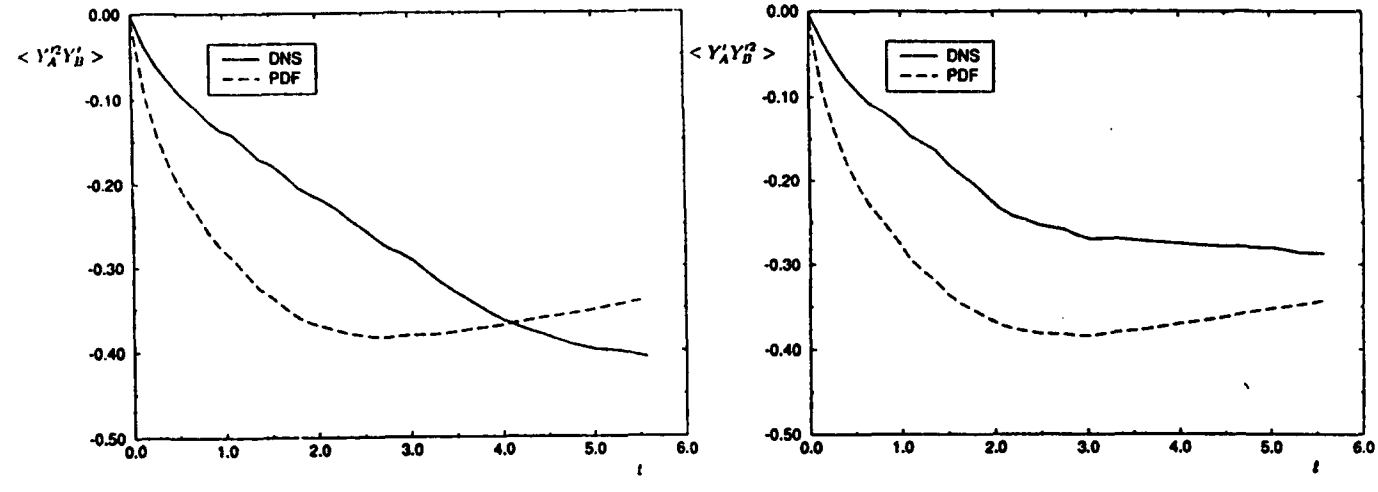

Figure 4: Temporal variations of third order cross moments of the mass fraction of species A in homogeneous simulations ($Da = 5$). The PDF is parameterized by the values of the Reynolds mean values of the reactants mass fraction and the scalar covariance.

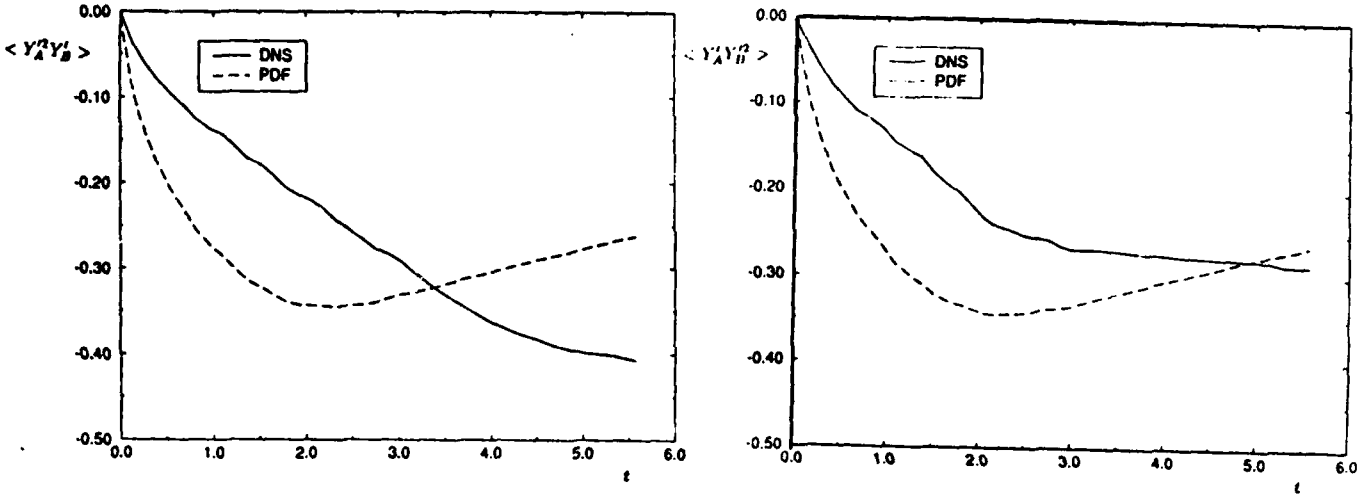

Figure 5: Temporal variations of third order cross moments of the mass fraction of species A in homogeneous simulations ($Da = 5$). The PDF is parameterized by the values of the Reynolds mean values of the reactants mass fraction and the scalar energy.

Figure 9 portrays the LES and DNS contours of the filtered mass fraction of species A in the non-reacting case. The agreement is generally good and the two results are relatively close. The difference is due to the effects of the gradient diffusion closure in Eq. (18) which results in smearing of the small scale features within the large scale coherent structures. The lack of agreement becomes more pronounced for the covariance. This is shown in Fig. 10 where contour plots of the SGS species covariance are presented. Despite this difference, it is useful to examine the model's performance in the reacting shear flow LES. In Fig. 11, contour plots of the filtered product species mass fraction obtained from LES and DNS are presented. Figure 12 shows an instantaneous product thickness distribution obtained from the filtered DNS and LES data, including also some LES results without the PDF model. These figures suggest that LES captures the large scale feature in accord with DNS. The figures also suggest that the inclusion of SGS fluctuations gives results which are closer to DNS data than those predicted by the mean chemistry model. However, the PDF method still needs to be improved further in order to exhibit a better predictive capability.

The primary reasons for the discrepancies above are attributed to errors associated with: (1) the estimation the covariance, and (2) the shape of the PDF. We feel that with the simplified reaction mechanism considered in this flow, the first factor is more important. This is indicated in Fig. 13, where contour plots of SGS covariance are presented. Again, while the LES and filtered DNS results show similar trends, the agreement is not very good (see Fig. 14 for a quantitative comparison of the covariance thickness). These two figures, along with Fig. 10, highlight the modeling deficiencies associated with the covariance transport equation for LES applications. Therefore, while this equation has been met with some success in RANS, its use here does not provide acceptable predictions. The same is true for the SGS kinetic energy as shown in Figs. 7-8. In this regard, it must be noted that these problems do not vanish in PDF approaches based on a transport equation for the single-point PDF (AMC, C/D, LMSE, *etc*). That is, the first two SGS moments must be determined by a reliable subgrid closure. The problem may be somewhat alleviated by considering the transport equations for SGS correlations (Taulbee, 1989). This is very challenging and computationally demanding. Some savings in computations can be made by approximating the transport terms in the scalar flux equation in a way analogous to what is done in algebraic Reynolds stress closures (see Gibson and Launder (1976); Rodi (1980); Schmidt and Schumann (1989); Taulbee (1992)). The performance of these more elaborate models are presently being assessed for the modeling of SGS covariance and TKE.

SOME FINAL REMARKS

During the past century, dating back to the early pioneering contributions of Pearson (1895); Edgeworth (1907); Johnson (1949a), and Johnson (1949b), the construction of "appropriate" PDF shapes has been a subject of broad interest within the statistics and (old) biometrics research communities. The outgrowth of these contributions has been useful to investigators in other branches of physical science. In fact, in classical turbulence research, statistical methods (Taylor, 1935) of one form or another had been the primary means of dealing with turbulence and its "random" causes and effects (Panchev, 1970; Lumley, 1970; Lesieur, 1990). In statistical modeling of turbulent reacting flows, the use of PDF methods has proven particularly useful. This is especially true if the PDF (or joint PDF) of

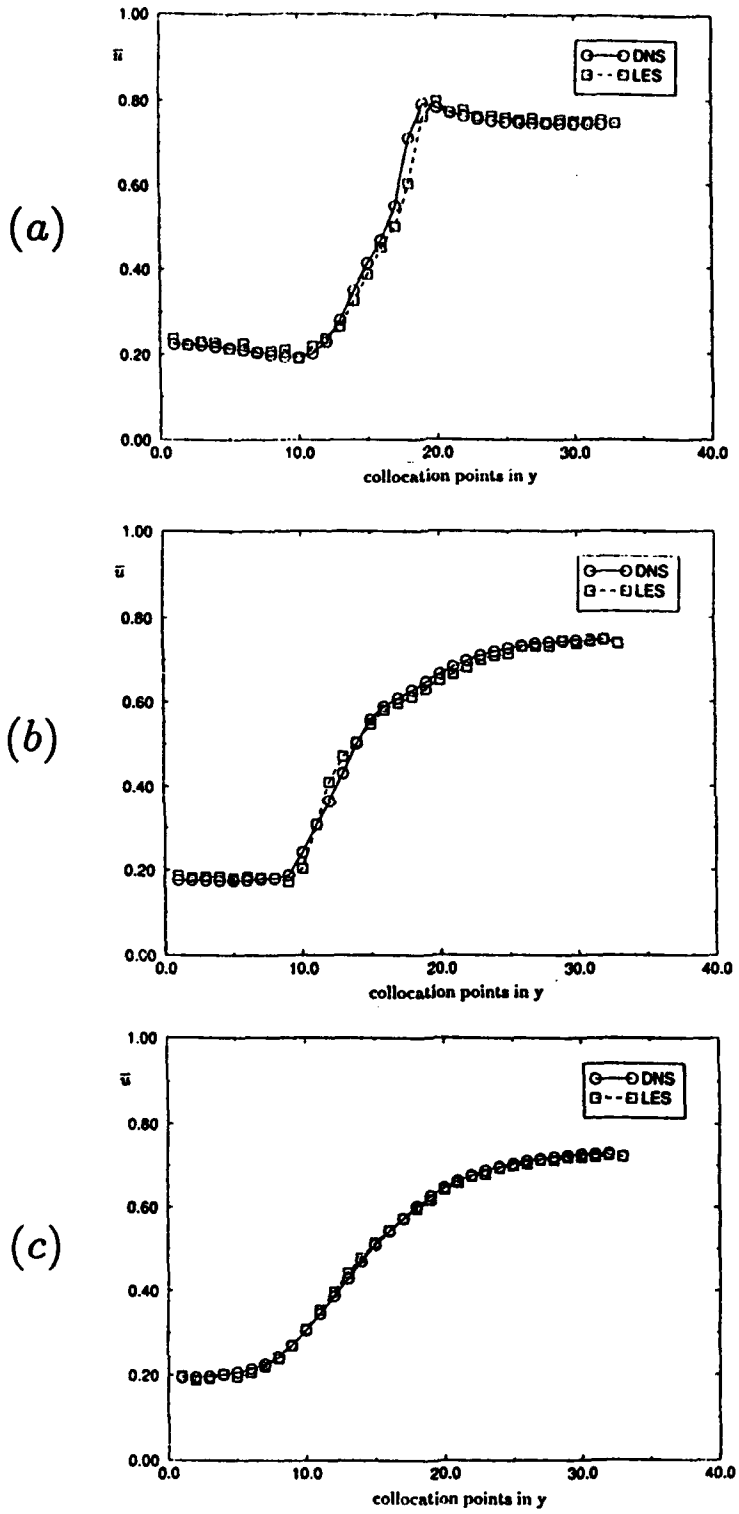

Figure 6: Cross-stream variations of the streamwise filtered velocity at several streamwise locations of the mixing layer: (a) $x = 5\delta$, (b) $x = 20\delta$, (c) $x = 25\delta$.

(a)

(b)

Figure 7: Contour plots of SGS turbulent kinetic energy: (a) LES, (b) DNS

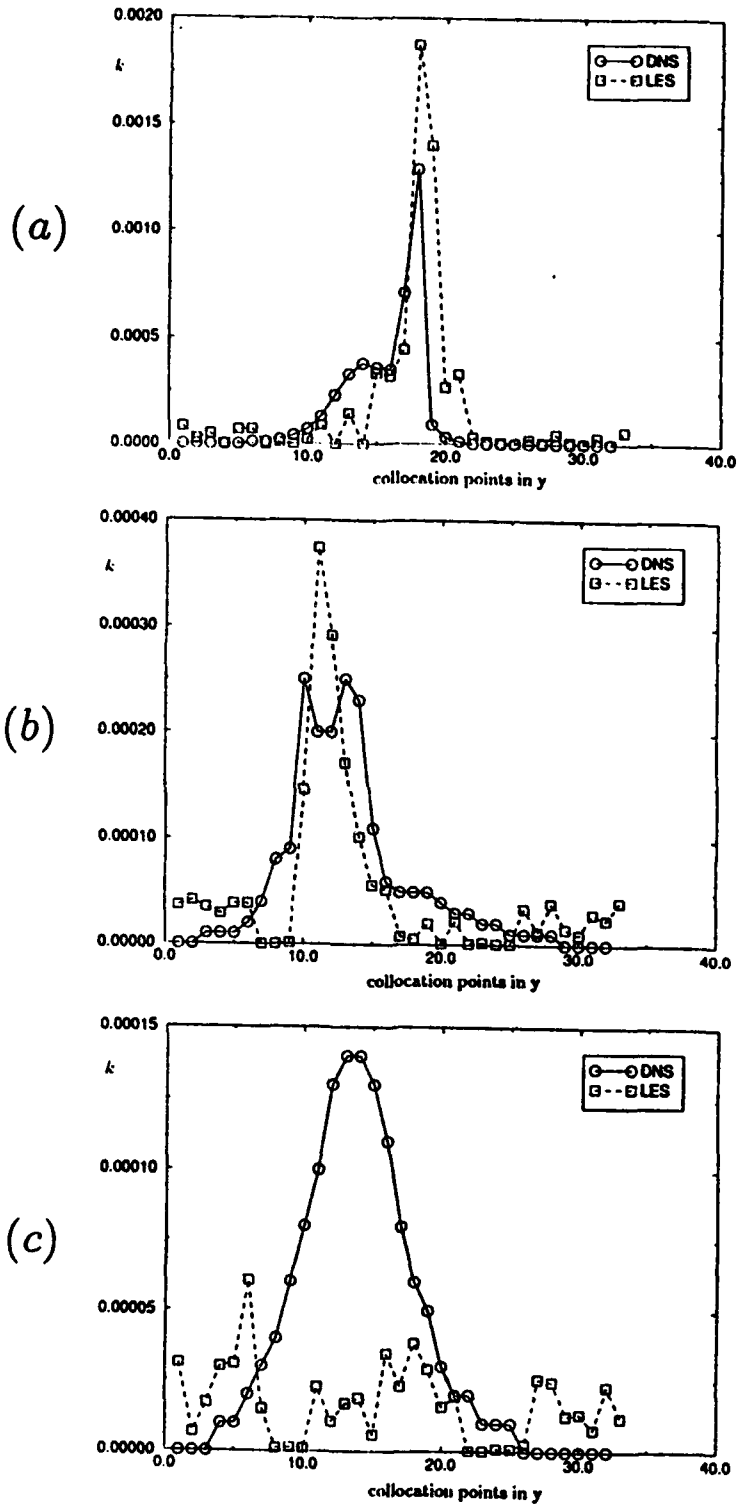

Figure 8: Cross-stream variations of the SGS turbulent kinetic energy at several streamwise locations of the mixing layer: (a) $x = 5\delta$, (b) $x = 20\delta$, (c) $x = 25\delta$.

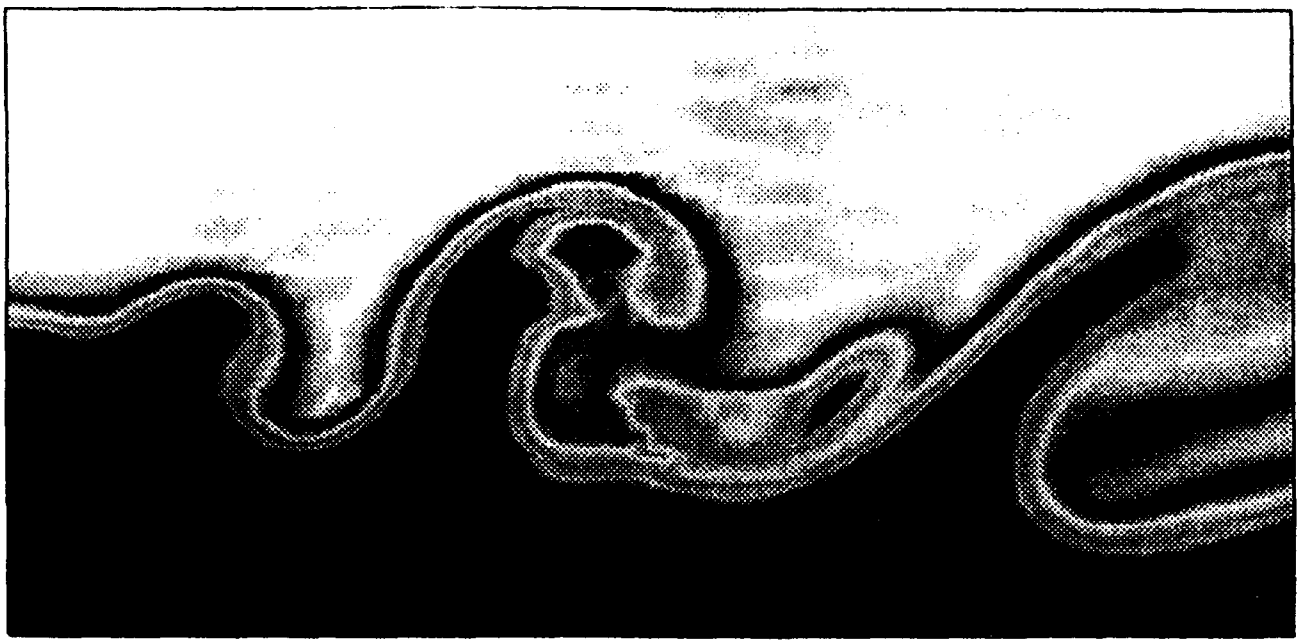

(a)

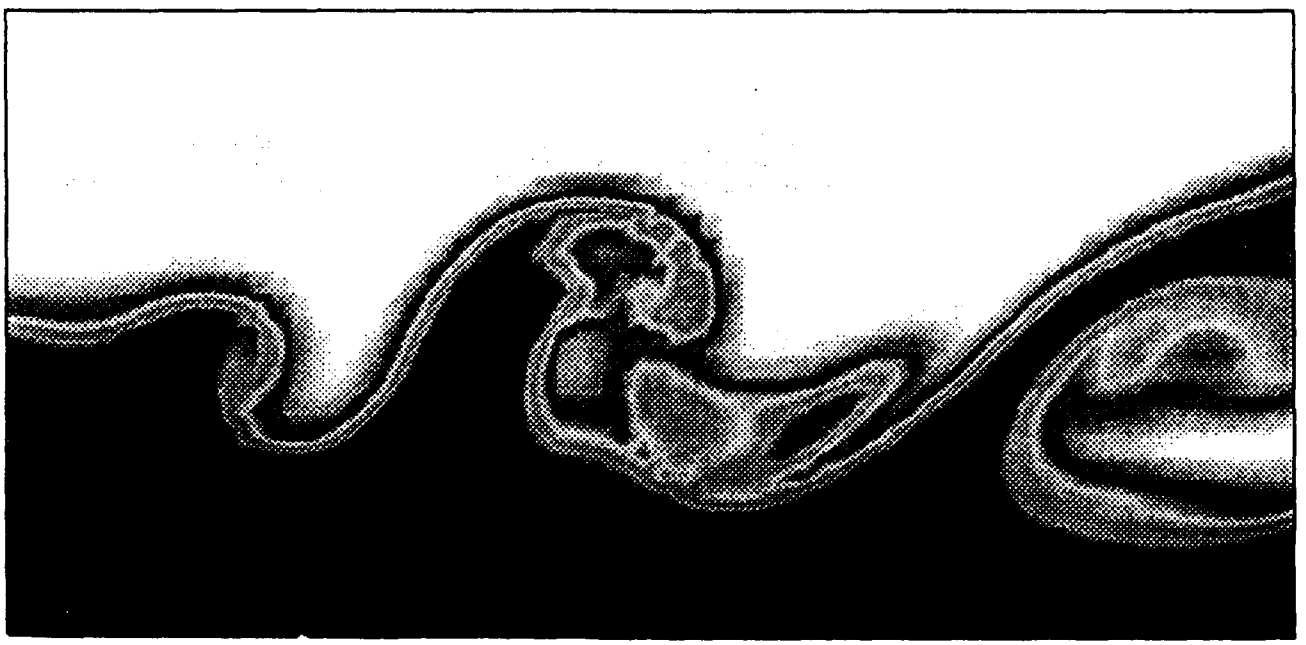

(b)

Figure 9: Contour plots of SGS species A mass fraction (Da=0): (a) LES, (b) DNS

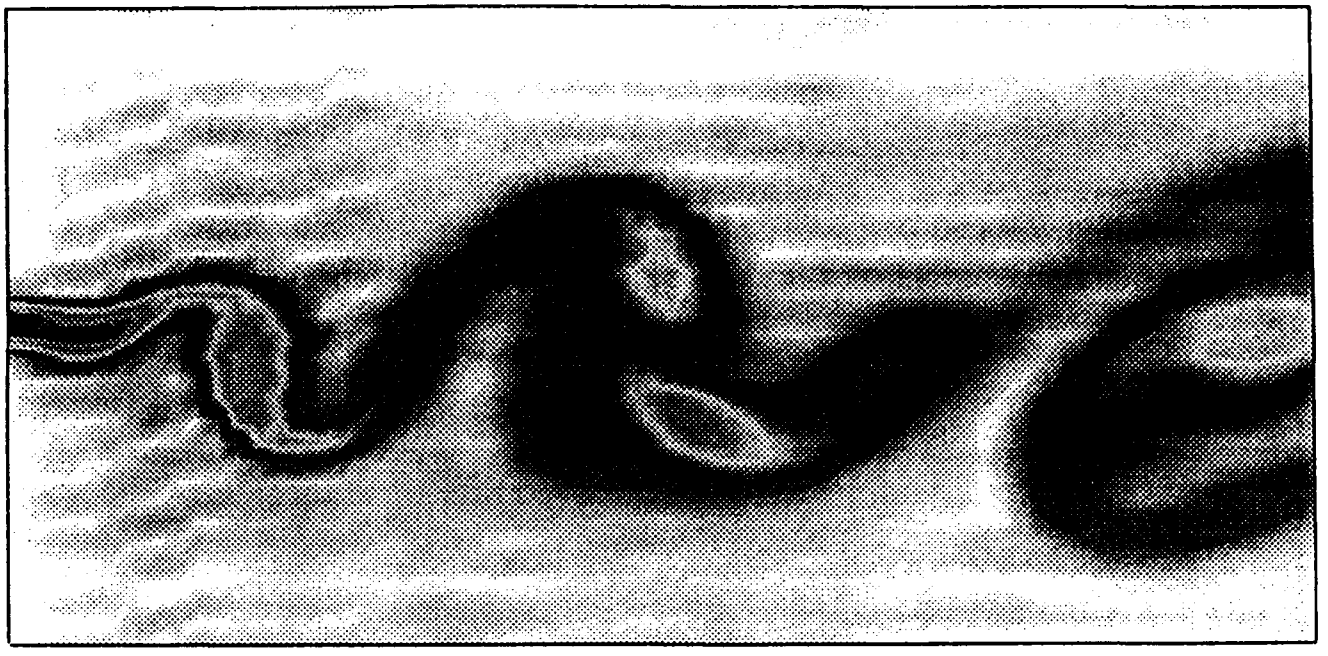

(a)

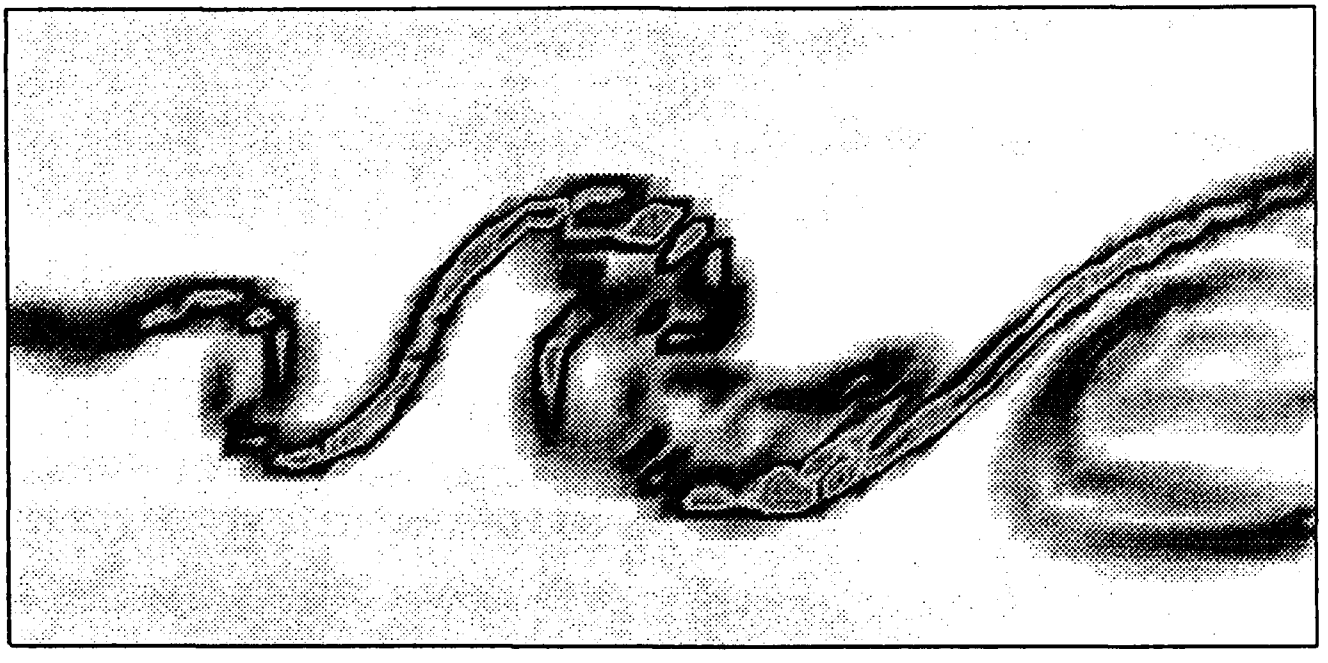

(b)

Figure 10: Contour plots of SGS species covariance (Da=0): (a) LES, (b) DNS

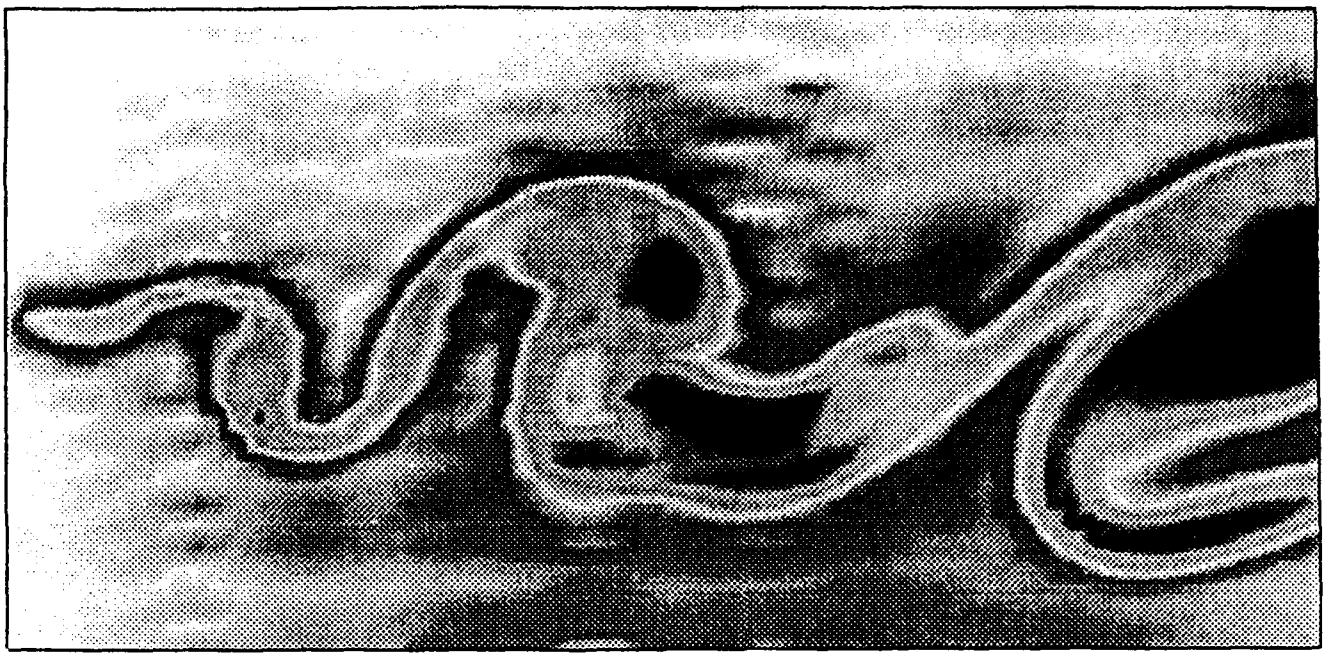

(a)

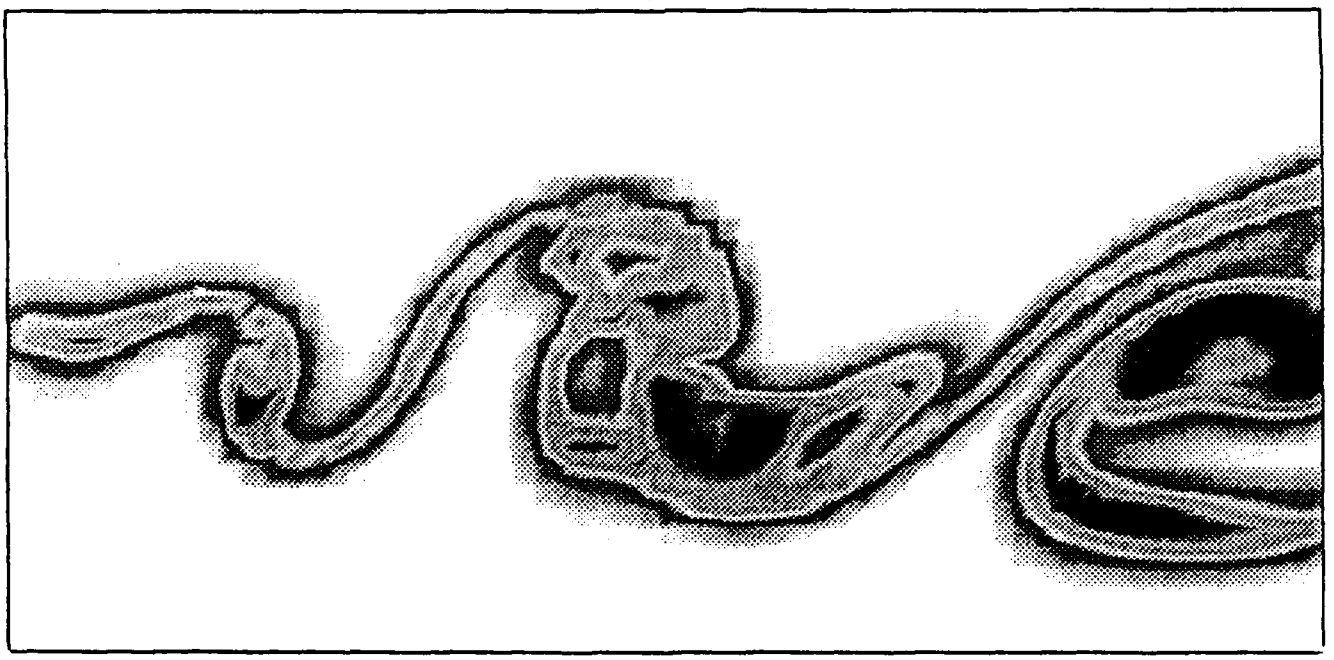

(b)

Figure 11: Contour plots of SGS product P mass fraction (Da=10): (a) LES, (b) DNS

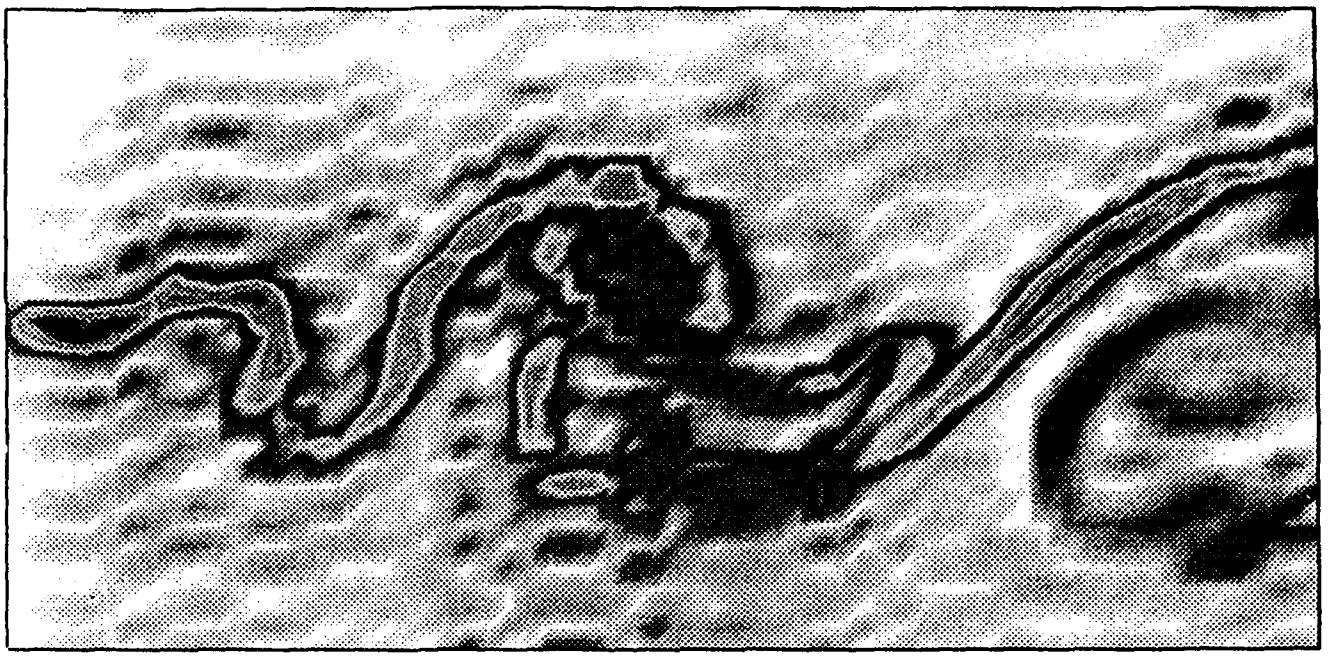

(a)

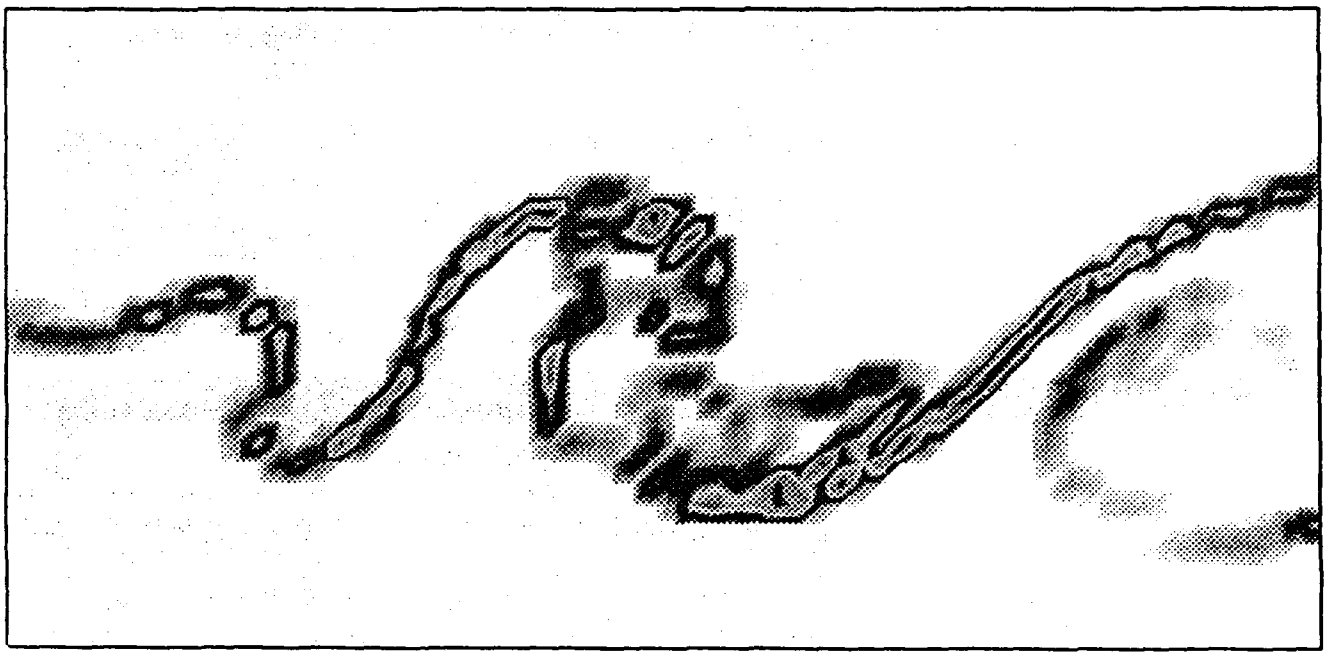

(b)

Figure 13: Contour plots of SGS species covariance (Da=10): (a) LES, (b) DNS

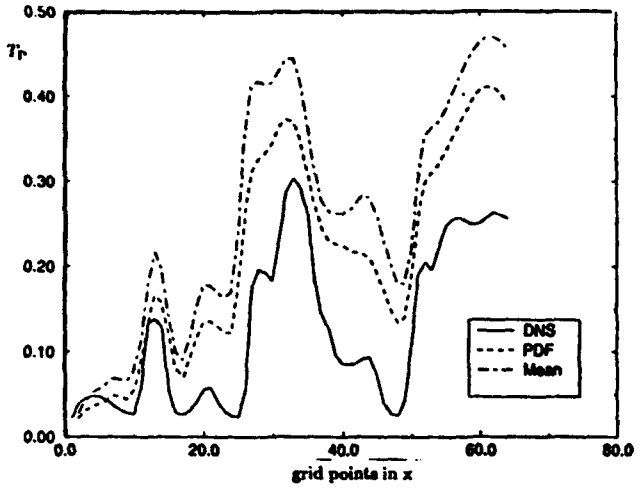

Figure 12: Streamwise variation of instantaneous product mass fraction thickness for the mixing layer under chemical non-equilibrium

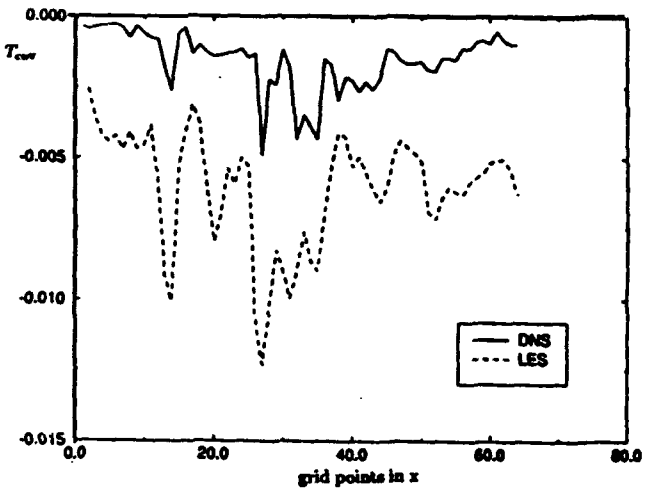

Figure 14: Streamwise variation of instantaneous covariance thickness for the mixing layer under chemical non-equilibrium

scalar quantities is considered. The preferred method is to obtain the PDF by means of its transport equation. This method is a subject of ongoing research (Pope, 1990) and there are still a number of questions in regard to its suitability for practical applications. LES can be viewed as an example of such an application, since it is viewed as more of a potential engineering tool than a robust scientific tool. With this view, assumed PDF methods are advocated as the present method of choice, at least in the context of the simple flows considered here.

In this work, an attempt has been made to borrow knowledge from the statistics literature in order to "presume" an appropriate PDF which performs reasonably well in LES. In simple flows of research interest such as a homogeneous box flow or a parallel shear flow this is a viable approach in light of the richness of literature on their behavior (see Givi and Riley (1992) for a recent review). Consistent with the current state of affairs in RANS, these PDF's are all considered in the context of a single point. This implies that all the moments up to the second order (either Reynolds moments or SGS moments) have to be provided externally. Based on our earlier investigations along these lines (Madnia *et al.*, 1992; Frankel *et al.*, 1993; Miller *et al.*, 1993a), the use of the Pearson family of PDF's appears to be most practical. This suggests a Beta density of the first kind for equilibrium (and frozen) chemistry, and the Dirichlet density for non-equilibrium chemistry. In the specific cases considered, the use of the Beta density provides a reasonable model for SGS probability description of a conserved scalar variable. However, its actual use in LES requires the knowledge of the filtered mean and the SGS variance. This is currently troublesome in that conventional turbulence closures do not seem to work well for predicting second order SGS moments. The same problem exists in LES of non-equilibrium flows and manifests itself in the inability to accurately predict SGS scalar covariance (and/or SGS scalar energy). Moreover, it is not clear which of the sets of low order moments are to be used to parameterize the multivariate PDF. This drawback is, however, deemed less troublesome in that the Dirichlet density can be replaced with other members of the joint Beta family which are constructed with a higher degree of freedom. Again, the statistics and biometrics literature can be helpful for this purpose, and this issue is currently under investigation.

At this point, it is useful to make some remarks in regard to some situations where assumed PDF methods are not very successful. These correspond to cases where an obvious choice for the PDF can not be made. For example, in highly non-equilibrium flames with complex multi-step multi-scalar chemistry with strong temperature dependent reactions rates. In LES of such flows, the application of the PDF transport equation may also be difficult. However, other less computational intensive closures may prove useful. For example, the "laminar diffusion flamelet model" (Williams, 1975; Peters, 1984; Peters, 1986), or the "conditional moment method" (Bilger, 1993; Smith *et al.*, 1992; Klimenko, 1990) may provide some alternatives. An appraisal study of the performance of these models in RANS of turbulent mixing layers has been reported by Miller *et al.* (1993b). The first model is applicable to cases where chemical reactions occur in a narrow region near the flame surface. For sufficiently fast chemistry, but with finite values of the Damköhler number, the flame is located somewhere within the (unresolved) subgrid. The actual LES with this model requires the construction of a flamelet library within the subgrid by which the reacting scalar values can be approximated. The approximation requires the knowledge of

the filtered mean values of the mixture fraction (*e.g.* the Shvab-Zeldovich variable), and its SGS rate of dissipation. Therefore, modeled transport equations are needed to approximate these quantities. How effectively the dissipation field can be modeled and how accurate the whole procedure would be, needs to be determined. The second approach can be considered somewhere between the PDF approach and traditional moment methods. In its implementation for LES, the averages of the reacting scalar field are defined "conditionally" on the values of the mixture fraction. The argument in support of this closure is that such conditional statistics portray less scatter than their unconditional counterparts. Therefore, their treatment may be easier. However, an extra dimensionality (associated with the domain of the mixture fraction) is involved. Also, the actual application of the model requires the input of the SGS conditional expected dissipation. This could be very difficult since the behavior of this dissipation is less understood (Jiang *et al.*, 1992). Furthermore, as discussed by Miller *et al.* (1993b), the use of the model can be recommended only for determining the first order moments in flames near equilibrium. This is acceptable if the mean compositional structure in near-equilibrium flames is desired. Otherwise, the usage of the method is complicated in RANS and even more complex in LES.

References

Abramowitz, M. and Stegun, I. A. (1972). *Handbook of Mathematical Functions and Formulas, Graphs, and Mathematical Tables.* Government Printing Office, Washington, D.C.

Aldama, A. A. (1990). *Filtering Techniques for Turbulent Flow Simulations*, volume 49 of *Lecture Notes in Engineering.* Springer-Verlag, New York, NY.

Baurle, R. A., Alexopoulos, G. A., Hassan, H. A., and Drummond, J. P. (1992). An assumed joint-beta pdf approach for supersonic turbulent combustion. AIAA paper AIAA-92-3844.

Bilger, R. W. (1980). Turbulent flows with nonpremixed reactants. In Libby, P. A. and Williams, F. A., editors, *Turbulent Reacting Flows*, chapter 3, pages 65–113. Springer-Verlag, Heidelberg.

Bilger, R. W. (1993). Conditional moment closure for turbulent reacting flow. *Phys. Fluids A.* **5**, 436–444.

Brodkey, R. S., editor. (1975). *Turbulence in Mixing Operation.* Academic Press, New York, NY.

Brodkey, R. S. (1981). Fundamental of turbulent motion. *Chem. Eng. Comm.* **8**, 1–23.

Chen, H., Chen, S., and Kraichnan, R. H. (1989). Probability distribution of a stochastically advected scalar field. *Phys. Rev. Lett.* **63**, 2657–2660.

Claus, R. W., Huang, P. G., and MacInnes, J. M. (1989). Mesh refinement in a two-dimensional large eddy simulation of a forced shear layer. NASA TM 102129.

Curl, R. L. (1963). Dispersed phase mixing: I. Theory and effects in simple reactors. *AIChE J.* **9**, 175–181.

Dopazo, D. and O'Brien, E. E. (1976). Statistical treatment of non-isothermal chemical reactions in turbulence. *Combust. Sci. and Tech.* **13**, 99–112.

Dopazo, C. (1973), *Non-Isothermal Turbulent Reactive Flows: Stochastic Approaches.* Ph.D. Thesis, Department of Mechanical Engineering, State University of New York at Stony Brook, Stony Brook, NY.

Edgeworth, F. Y. (1907). On the representation of statistical frequency by a series. *Journal of the Royal Statistical Society, Series A.* **70**, 102–106.

Erlebacher, G., Hussaini, M. Y., Speziale, C. G., and Zang, T. A. (1987). Toward the large eddy simulation of compressible turbulent flows. ICASE Report 87-20, NASA Langley Research Center, Hampton, VA. Also available as *NASA CR 178273.*

Erlebacher, G., Hussaini, M. Y., Speziale, C. G., and Zang, T. A. (1990). Toward the large eddy simulation of compressible turbulent flows. ICASE Report 90-76, NASA Langley Research Center, Hampton, VA. Also available as *NASA CR 187460.*

Erlebacher, G., Hussaini, M. Y., Speziale, C. G., and Zang, T. A. (1992). Toward the large eddy simulation of compressible turbulent flows. *J. Fluid Mech.* **238**, 155–185.

Ferziger, J. H. and Leslie, D. C. (1979). Large eddy simulation: A predictive approach to turbulent flow computation. AIAA Paper AIAA-79-1471.

Ferziger, J. H. (1981). Higher level simulations of turbulent flows. Stanford University Report TF-16, Department of Mechanical Engineering, Stanford University, Stanford, CA.

Ferziger, J. H. (1983). Higher-level simulations of turbulent flows. In Essers, J. H., editor, *Computational Methods for Turbulent, Transonic and Viscous Flows*, pages 93–182. Hemisphere Publishing Co.

Ferziger, J. H. (1987). Large eddy simulations: Its role in turbulence research. In Dwoyer, D. L., Hussaini, M. Y., and Voigt, R. G., editors, *Theoretical Approaches in Turbulence*, pages 51–72. Springer-Verlag, New York, NY.

Frankel, S. H., Drummond, J. P., and Hassan, H. A. (1990). A hybrid reynolds averaged/pdf closure model for supersonic turbulent combustion. AIAA paper AIAA-90-1573.

Frankel, S. H., Jiang, T.-L., and Givi, P. (1992). Modeling of isotropic reacting turbulence by a hybrid mapping-EDQNM closure. *AIChE J.* **38**, 535–543.

Frankel, S. H., Madnia, C. K., and Givi, P. (1992). Modeling of the reactant conversion rate in a turbulent shear flow. *Chem. Eng. Comm.* **113**, 197–209.

Frankel, S. H., Madnia, C. K., and Givi, P. (1993). Comparative assessment of closures in turbulent reacting flows. *AIChE J.* . In press.

Galperin, B. and Orszag, S. A., editors. (1993). *Large Eddy Simulations of Complex Engineering and Geophysical Flows*. Cambridge University Press, Cambridge, U.K. In press.

Gao, F. (1991). An analytical solution for the scalar probability density function in homogeneous turbulence. *Phys. Fluids A* **3**, 511–513.

Gibson, M. M. and Launder, B. E. (1976). On the calculation of horizontal, turbulent, free shear flows under gravitational influence. *ASME Journal of Heat Transfer* **98C**, 81–87.

Girimaji, S. S. (1991a). Assumed β-pdf model for turbulent mixing: Validation and extension to multiple scalar mixing. *Combust. Sci. and Tech.* **78**, 177–196.

Girimaji, S. S. (1991b). A simple recipe for modeling reaction-rates in flows with turbulent-combustion. AIAA paper AIAA-91-1792.

Givi, P. and McMurtry, P. A. (1988). Direct numerical simulation of the PDFs of a passive scalar in forced mixing layer. *Combust. Sci. and Tech.* **57**, 141–147.

Givi, P. and Riley, J. J. (1992). Some current issues in the analysis of reacting shear layers: Computational challenges. In Hussaini, M. Y., Kumar, A., and Voigt, R. G., editors, *Major Research Topics in Combustion*, pages 588–650. Springer-Verlag.

Givi, P. (1989). Model free simulations of turbulent reactive flows. *Prog. Energy Combust. Sci.* **15**, 1–107.

Hill, J. C. (1976). Homogeneous turbulent mixing with chemical reaction. *Ann. Rev. Fluid Mech.* **8**, 135–161.

Horuiti, K. (1985). Large eddy simulation of turbulent channel flow by one-equation modeling. *J. Phys. Soc. Japan* **54**, 2855–2865.

Hussaini, M. Y., Speziale, C. G., and Zang, T. A. (1990). The potential and limitations of direct and large eddy simulations. In Lumley (1990), pages 354–368.

Janicka, J. and Peters, N. (1982). Prediction of turbulent jet diffusion flame lift-off using a pdf transport equation. In *Proceedings of 19th Symp. (Int.) on Combustion*, pages 367–374. The Combustion Institute, Pittsburgh, PA.

Janicka, J., Kolbe, W., and Kollmann, W. (1979). Closure of the transport equation for the probability density function of turbulent scalar field. *J. Nonequil. Thermodyn.* **4**, 47–66.

Jiang, T.-L., Gao, F., and Givi, P. (1992). Binary and trinary scalar mixing by Fickian diffusion-Some mapping closure results. *Phys. Fluids A* **4**, 1028–1035.

Johnson, N. L. and Kotz, S. (1972). *Distributions in Statistics: Continious Multivariate Distributions*. John Wiley and Sons, New York, NY.

Johnson, N. L. (1949a). Systems of frequency curves generated by methods of translation. *Biometrika* **36**, 149–176.

Johnson, N. L. (1949b). Bivariate distributions based on simple translation systems. *Biometrika* **36**, 297–304.

Johnson, M. E. (1987). *Multivariate Statistical Simulation*. John Wiley and Sons, New York, NY.

Jones, W. P. and Priddin, C. H. (1978). Predictions of the flowfield and local gas composition in gas turbine combustors. In *17th Symp. (Int.) on Combustion*, pages 399–409. The Combustion Institute, Pittsburgh, PA.

Jones, W. P. and Whitelaw, J. H. (1982). Calculation methods for reacting turbulent flows: A review. *Combust. Flame* **48**, 1–26.

Jou, W.-H. and Riley, J. J. (1989). Progress in direct numerical simulations of turbulent reacting flows. *AIAA J.* **27**, 1543–1556.

Klimenko, A. Y. (1990). Multicomponent diffusion of various mixtures in turbulent flow. *Fluid Dynamics* **25**, 327–334.

Kollmann, W. (1980). *Prediction Methods for Turbulent Flows*. Hemisphere Publishing Co., New York, NY.

Kollmann, W. (1990). The pdf approach to turbulent flow. *Theoret. Comput. Fluid Dynamics* **1**, 249–285.

Koochesfahani, M. M. and Dimotakis, P. E. (1986). Mixing and chemical reactions in a turbulent liquid mixing layer. *J. Fluid. Mech.* **170**, 83–112.

Kosaly, G. and Givi, P. (1987). Modeling of turbulent molecular mixing. *Combust. Flame* **70**, 101–118.

Kraichnan, R. H. (1989). Closures for probability distributions. *Bull. Amer. Phys. Soc.* **34**, 2298.

Kwak, D., Reynolds, W. C., and Ferziger, J. H. (1975). Three dimensional time dependent computation of turbulent flows. Stanford University Report TF-5, Department of Mechanical Engineering, Stanford University, Stanford, CA.

Launder, B. E. and Spalding, D. B. (1972). *Lectures in Mathematical Modeling of Turbulence.* Academic Press.

Lesieur, M. (1990). *Turbulence in Fluids.* Kluwer Academic Publishers, Boston, MA. Second Revised Edition.

Libby, P. A. and Williams, F. A., editors. (1980). *Turbulent Reacting Flows*, volume 44 of *Topics in Applied Physics.* Springer-Verlag, Heidelberg.

Libby, P. A. and Williams, F. A., editors. (1993). *Turbulent Reacting Flows.* Academic Press, New York, NY. In Progress.

Lilly, D. K. (1967). The representation of small-scale turbulence in numerical simulation experiments. In *Proceedings of IBM Scientific Computing Symposium Environmental Sciences*, pages 195–210. IBM Form No. 320-1951.

Lockwood, F. C. and Moneib, H. A. (1980). Fluctuating temperature measurement in a heated round free jet. *Combust. Sci. and Tech.* **22**, 63–81.

Love, M. D. (1979). An introduction to the large eddy simulation technique. *J. Inst. Nuc. Eng.* **20**, 35–42.

Lowery, P. S., Reynolds, W. C., and Mansour, N. N. (1987). Passive scalar entrainment and mixing in a forced, spatially-developing mixing layer. AIAA paper AIAA-87-0132.

Lumley, J. L. (1970). *Stochastic Tools in Turbulence.* Academic Press, New York, NY.

Lumley, J. L., editor. (1990). *Whither Turbulence? Turbulence at the Crossroads*, volume 357 of *Lecture Notes in Physics.* Springer-Verlag.

Lund, T. S. and Novikov, E. A. (1991). Parameterization of subgrid-scale stress by the velocity gradient tensor. Ctr manuscript, Center for Turbulence Research Annual Brief, Stanford, CA.

Lundgren, T. S. (1967). Distribution functions in the statistical theory of turbulence. *Phys. Fluids* **10**, 969–975.

Lundgren, T. S. (1969). Model equation for nonhomogeneous turbulence. *Phys. Fluids* **12**, 485–497.

Madnia, C. K. and Givi, P. (1993). On DNS and LES of homogeneous reacting turbulence. In Galperin and Orszag (1993). In press.

Madnia, C. K., Frankel, S. H., and Givi, P. (1991). Direct numerical simulations of the unmixedness in homogeneous reacting turbulence. *Chem. Eng. Comm.* **109**, 19–29.

Madnia, C. K., Frankel, S. H., and Givi, P. (1992). Reactant conversion in homogeneous turbulence: Mathematical modeling, computational validations and practical applications. *Theoret. Comput. Fluid Dynamics* **4**, 79–93.

Mansour, N. N., Ferziger, J. H., and Reynolds, W. C. (1978). Large eddy simulations of a turbulent mixing layer. Report TF-11, Department of Mechanical Engineering, Stanford University, Stanford, CA.

Masutani, S. M. and Bowman, C. T. (1986). The structure of a chemically reacting plane mixing layer. *J. Fluid Mech.* **72**, 93–126.

Miller, R. S., Frankel, S. H., Madnia, C. K., and Givi, P. (1993). Johnson-Edgeworth translation for probability modeling of binary mixing in turbulent flows. *Combust. Sci. and Tech.* . In press.

Miller, R. S., Madnia, C. K., and Givi, P. (1993). The structure of a reacting turbulent mixing layer. Submitted for publication.

Moin, P. (1991). Towards large eddy and direct numerical simulations of complex turbulent flows. *Computer Methods in Applied Mechanics and Engineering* **87**, 329–334.

Narayan, J. R. and Girimaji, S. S. (1992). Turbulent reacting flow computations including turbulent-chemistry interactions. AIAA paper AIAA-92-0342.

Narumi, S. (1923). On the general form of bivariate frequency distributions which are mathematically possible when regression and variation are subjected to limiting conditions, I. *Biometrika* **15**, 77–88.

Norris, A. T. and Pope, S. B. (1991). Turbulent mixing model based on ordered pairing. *Combust. Flame* **83**, 27.

O'Brien, E. E. (1971). T nt mixing of two rapidly reacting chemical species. . *Fluids* **14**, 1326–1331.

O'Brien, E. E. (1980). The probability density function (PDF) approach to reacting turbulent flows. In Libby, P. A. and Williams, F. A., editors, *Turbulent Reacting Flows*, chapter 5, pages 185–218. Springer-Verlag, Heidelberg.

Panchev, S. (1970). *Random Functions and Turbulence.* Pergamon Press, Oxford, U.K.

Passot, T. and Pouquet, A. (1987). Numerical simulation of compressible homogeneous flows in the turbulent regime. *J. Fluid Mech.* **181**, 441–466.

Pearson, K. (1895). Contributions to the mathematical theory of evolution: II. skew variations in homogeneous material. *Philos. Trans. of the Royal Soc. of London, Series A.* **186**, 343–414.

Peters, N. (1984). Laminar diffusion flamelet models in non-premixed turbulent combustion. *Prog. Energy Combust. Sci.* **10**, 319–339.

Peters, N. (1986). Laminar flamelet concepts in turbulent combustion. In *Proceedings of 21st Symp. (Int.) on Combustion*, pages 1231–1250. The Combustion Institute, Pittsburgh, PA.

Pope, S. B. (1979). The statistical theory of turbulent flames. *Phil. Trans. Royal Soc. London* **291**, 529–568.

Pope, S. B. (1981). A Monte Carlo method for the pdf equations of turbulent reactive flow. *Combust. Sci. and Tech.* **25**, 159–174.

Pope, S. B. (1982). An improved turbulent mixing model. *Combust. Sci. and Tech.* **28**, 131–145.

Pope, S. B. (1985). PDF methods for turbulent reacting flows. *Prog. Energy Combust. Sci.* **11**, 119–192.

Pope, S. B. (1990). Computations of turbulent combustion: Progress and challenges. In *Proceedings of 23rd Symp. (Int.) on Combustion*, pages 591–612. The Combustion Institute, Pittsburgh, PA.

Pope, S. B. (1991). Mapping closures for turbulent mixing and reaction. *Theoret. Comput. Fluid Dynamics* **2**, 255–270.

Priddin, C. H. (1991). Turbulent combustion modeling-A review. In Johansson, A. V. and Alfredsson, P. H., editors, *Advances in Turbulence 3*, pages 279–299. Springer-Verlag, Berlin.

Reynolds, W. C. (1990). The potential and limitations of direct and large eddy simulations. In Lumley (1990), pages 313–343.

Rhodes, P. R. (1975). A probability distribution function for turbulent flows. In Murthy, S. N. B., editor, *Turbulent Mixing in Non-Reactive and Reactive Mixing*, pages 235–241. Plenum Press, New York, NY.

Rodi, W. (1980). Turbulence models for environmental problems. In Kollmann (1980), pages 260–349.

Rogallo, R. S. and Moin, P. (1984). Numerical simulation of turbulent flow. *Ann. Rev. Fluid Mech.* **16**, 99–137.

Schmidt, H. and Schumann, U. (1989). Coherent structure of the convective boundary layer derived from large-eddy simulations. *J. Fluid Mech.* **200**, 511–562.

Schumann, U. and Friedrich, R., eds., editors. (1986). *Direct and Large Eddy Simulations of Turbulence*. Proc. EUROMECH Coll. No. 199. Vieweg-Verlag, Braunschweig.

Schumann, U. (1989). Large eddy simulation of turbulent diffusion with chemical reactions in the convective boundary layer. *Atmospheric Environment* **23**, 1713–1726.

Schumman, U. and Friedrich, R. (1987). On direct and large eddy simulation of turbulence. In Comte-Bellot, G. and Mathieu, J., editors, *Advances in Turbulence*, pages 88–104. Springer-Verlag.

Schumman, U. (1975). Subgrid scale model for finite difference simulations of turbulent flows in plane channels and annuli. *J. Comp. Phys.* **18**, 376–404.

Smagorinsky, J. (1963). General circulation experiments with the primitive equations. I. The basic experiment. *Monthly Weather Review* **91**, 99–164.

Smith, N. S., Bilger, R. W., and Chen, J.-Y. (1992). Modeling of non-premixed hydrogen jet flames using a conditional moment closure method. In *Proceedings of 24th Symp. (Int.) on Combustion*. The Combustion Institute, Pittsburgh, PA. In press.

Taulbee, D. B. (1989). Engineering turbulence models. In George, W. K. and Arndt, R., editors, *Advances in Turbulence*, pages 75–125. Hemisphere Publishing Corp., New York, N.Y.

Taulbee, D. B. (1992). An improved algebraic reynolds stress model and corresponding nonlinear stress model. *Phys. Fluids A* **4**, 2555–2561.

Taylor, G. I. (1935). Statistical theory of turbulence. *Proc. Roy. Soc. (A).* **151**, 421–478.

Toor, H. L. (1962). Mass transfer in dilute turbulent and nonturbulent systems with rapid irreversible reactions and equal diffusivities. *AIChE J.* **8**, 70–78.

Toor, H. L. (1975). The non-premixed reaction: $A + B \rightarrow$ *Products*. In Brodkey, R. S., editor, *Turbulence in Mixing Operations*, pages 123–166. Academic Press, New York, NY.

Voke, P. R. and Collins, M. W. (1983). Large eddy simulation: Petrospect and prospect. *PhysicoChemical Hydrodynamics* **4**, 119–161.

Wilks, S. S. (1962). *Mathematical Statistics*. Wiley, New York, NY, 2nd edition.

Williams, F. A. (1975). Recent advances in theoretical description of turbulent diffusion flames. In Brodkey, R. S., editor, *Turbulence in Mixing Operations*, pages 189–209. Academic Press, New York, NY.

Williams, F. A. (1985). *Combustion Theory*. The Benjamin/Cummings Publishing Company, Menlo Park, CA, 2nd edition.

APPENDIX 10

Inter-Layer Diffusion Model of Turbulent Scalar Mixing

Inter-Layer Diffusion Model of Scalar Mixing in Homogeneous Turbulence

F.A. Jaberi and P. Givi*
Department of Mechanical and Aerospace Engineering
State University of New York at Buffalo
Buffalo, NY 14260-4400

PACS Number: 47.25.Jn, 47.25.Cg, 47.25.-c

Abstract

A mechanistic model termed the *Inter-Layer Diffusion Model* (ILDM) is developed and is implemented for the probabilistic description of scalar mixing in homogeneous turbulent flows. The essential element of the model is based on the lamellar theory of mixing in the context developed by Kerstein,[1] and proposes that there are two distinct but coupled mechanisms by which the mixing process is described. These mechanisms are due to: (1) local events and (2) integrated global events. The mathematical formalities by which the closure is invoked are described and it is shown that the conditional expected diffusion of the scalar field depicted by the model depends more directly on local events. With the manipulation of each of these two mechanisms, several families of scalar probability density functions (PDF's) are generated. These families include some of the distributions generated by other mixing closures. The ILDM provides a physical format by which these other closures can be viewed. The similarity of local events imply the similarity of the conditional expected diffusion as generated via these models. The global events manifest themselves by the evolution of the conditional expected dissipation, and also the boundedness of the composition domain. While the PDF's generated in this way are very different, their applications for modeling of mixing limited reactions do not yield significantly different results.

*Please address all the correspondence to P. Givi. Tel: 716-645-2433, Fax: 716-645-3875, E-Mail: givi@eng.buffalo.edu.

I Introduction

Description of scalar mixing continues to be a challenging task in mathematical modeling of turbulent flows.[2–4] Within this past decade alone, several strategies have been devised and implemented for a variety of applications. Examples are the approaches based on scalar probability density function (PDF) via modeled transport equations,[5–11] assumed PDF methods,[10,12,13] and other procedures such as the Linear Eddy Model (LEM),[3,14,15] the Fokker-Plank equation,[16] spectral closures[17,18] and lamellar structures,[4,1] amongst others. Due to the complexity of the subject, the extent of success of these closures has been appraised only in a limited context. In some cases, the performance of the models has been assessed by comparison with data generated by direct numerical simulations (DNS).[19,20] However, because of the limitations of DNS the generality of the conclusions drawn by such comparisons cannot be guaranteed without caution. Also, the extent of data obtained by laboratory experiments is not significant; it has been only recently that substantiated data, useful for modeling purposes, have been generated.[21,22] However, the challenges associated with the problem are well-recognized, warranting continued work on the subject.

A standard test case that has proven very useful in the contributions cited above, is the problem of passive scalar mixing from an initial binary state in homogeneous-isotropic turbulence.[8–12,18,23–28] In this setting, the problem of mixing is isolated from other competing physical mechanisms. It also provides a relatively simple condition to configure in both laboratory and numerical experiments. In this context, turbulent mixing involves two physical mechanisms: turbulent convection and molecular diffusion. The first is a mechanical "stirring" process which results in the stretching of intermaterial area of the scalar. Mixing induced by such stirring is completed at small scales by the molecular action through diffusion of substances across intermaterial surface areas. The results of recent laboratory experiments[29] and numerical simulations[30] suggest that a major part of scalar diffusion oc-

curs in a system of *layer-like striation*, or *lamellae*. Each of these lamellae have a thickness ($2w$) which in general is a function of space and time, *i.e.* $w = w(\vec{x}, t)$. The rate of stretching and folding of the lamellar structures is governed by turbulent eddies. Development of a physical model which can accurately portray the mechanisms of lamellar stretching as well as the distribution of these lamellae are the subject of current research.[4,31-34]

The lamellar description has proven useful in depicting the kinematics of turbulent mixing and also to reproduce the results obtained by other closures. For example, Kerstein[1] shows that with particular specifications of the scalar profile within each lamellae and the PDF of lamellae thickness, the family of PDF's generated by the Amplitude Mapping Closure (AMC)[35,6,8] are obtained. Fox[16] employs the lamellar theory and provides an evolution equation for the joint PDF of the scalar and its gradient based on the stochastic Fokker-Planck equation. The unknown coefficients of this equation are pre-specified to provide the evolution of the PDF. With this method, the statistical behavior at the asymptotic stage must be known *a priori*, since the parameters of the model are adjusted to yield this behavior.

Our purpose in this work is to further examine the lamellar theory and to investigate some of its salient features for statistical modeling of mixing in turbulent flows. The formalities on which the model is based are discussed in a mathematical context with an explicit description of the assumptions made in its simplifications for general applications. In the format presented, the model is capable of characterizing the effects of various competing events on the mixing process. An attractive feature of the model is its capability in explaining the reasoning for the success (or lack thereof) of other closures in describing turbulent mixing phenomena. However, as will be shown, a wide variety of solutions emerge. In the context considered, a specific selection cannot be made. Neither is such a selection recommended without further knowledge of the turbulent field, as many of these solutions are justifiable on physical grounds. In fact, in a complicated turbulent mixing problem, a combination of

these cases may exist.

II Probability Modeling and the Lamellar Description

With the assumption of Fickian diffusion, the transport equation for a passive scalar variable, $\phi(\vec{x},t) \in [\phi_l, \phi_u]$, in a homogeneous incompressible turbulent flow is expressed by:

$$\frac{\partial \phi}{\partial t} + \vec{U} \cdot \nabla \phi = \mathcal{D}_M \nabla^2 \phi, \tag{1}$$

where $\vec{U}(\vec{x},t)$ and $\mathcal{D}_M$ denote the velocity vector and the molecular diffusion coefficient, respectively. Using standard methods[5] the evolution equation for the single-point PDF, $P(\phi(\vec{x},t))$ of the scalar is expressed by:

$$\frac{\partial P}{\partial t} + \frac{\partial (DP)}{\partial \phi} = 0, \quad \phi_l \leq \phi \leq \phi_u, \tag{2}$$

or alternatively by:

$$\frac{\partial P}{\partial t} + \frac{\partial^2 (EP)}{\partial \phi^2} = 0. \tag{3}$$

In these equations, ϕ_l, ϕ_u denote the scalar bounds, D represents the expected value of the scalar diffusion conditioned on the scalar value, ϕ, and E denotes the expected value of scalar dissipation conditioned on ϕ. E and D are related to the total scalar dissipation ε by:

$$\epsilon(t) = \int_{\phi_l}^{\phi_u} E(\phi,t)P(\phi,t)d\phi = -\int_{\phi_l}^{\phi_u} \phi D(\phi,t)P(\phi,t)d\phi. \tag{4}$$

At the single-point level, D, E and ϵ are unknown and must be provided externally. This describes the closure problem inherent in a statistical description at the single-point PDF level.

Equation (1) indicates that mixing evolution is governed by two mechanisms: molecular diffusion and turbulent advection. The former occurs primarily at small scales, whereas the latter is a multi-scale phenomenon. For thin diffusion zones and sufficiently steep scalar gradients across the scalar interfaces, the diffusion process takes place in a direction approximately normal to the interface and can be treated as unidirectional. We represent this direction by y which is bounded by *striation thickness*, w, that is $-w \leq y \leq w$. This thickness is defined as a positive random variable which has a frequency defined by the *Striation Thickness Distribution* (STD)[31,4] $h(w)$. The PDF of the scalar, conditioned on the lamellae thickness is denoted by $g(\phi|w)$ and is given by its definition:

$$g(\phi|w) = \begin{cases} \frac{1}{2w}|\frac{dy}{d\phi}| & \text{if } -w \leq y \leq w \\ 0 & \text{elsewhere} \end{cases}. \tag{5}$$

The unconditional PDF of the scalar is determined by the Bayes' theorem:

$$P(\phi,t) = \int_{|y|}^{\infty} f(w)g(\phi|w)dw. \tag{6}$$

where $f(w)dw$ is the probability of the event that the scalar falls within the domain $[w, w + dw]$. The corresponding PDF of this event is:

$$f(w) = \frac{wh(w)}{\int_0^\infty wh(w)dw}, \tag{7}$$

Therefore, with the use of Eq. (5), we have:[1]

$$P(\phi(y,t),t) = |\frac{dy}{d\phi}|G(|y|), \tag{8}$$

where | | indicates the absolute value, and

$$G(y) = \frac{1 - C(y)}{2 < w >}, \tag{9}$$

with $C(w)$ denoting the cumulative distribution function (CDF) of w. Embedded in Eq. (5) is the assumption that $\frac{dy}{d\phi}$ is independent of the lamellae thickness. This relation which was first obtained by Kerstein[1] yields a variety of PDF families depending on the STD and the scalar profile within the lamellae. In general, both of these are time and space dependent. The first term on RHS of Eq. (8) is governed primarily by molecular diffusion which is dispersed by turbulent eddies. The second term on the RHS represents the role of the STD and manifest the influences of stirring. It is useful to think of the first term as a representation of local events, and consider the second term as the influence of global events. Of course these two are not independent and each of them is influenced by the other.

III Conditional Statistics

Given the scalar PDF, Eqs. (2)-(3) can be used to determine the conditional expected diffusion and the conditional expected dissipation of the scalar field. With the PDF specified,

the conditional expected diffusion is given by;

$$D(\phi,t) = -\frac{1}{P(\phi,t)}\frac{\partial F}{\partial t}, \tag{10}$$

where F denotes the CDF of the scalar. From Eq. (8), we have:

$$F(\phi(y)) = \int_{y_l}^{y} P(y)|\frac{\partial \phi}{\partial y}|dy = \int_{y_l}^{y} G(|y|)dy, \tag{11}$$

where $y = y(\phi,t)$, and y_l denotes the value of y corresponding to ϕ_l. Using Eqs. (8), (10) and (11), D can be expressed as:

$$D(\phi(y,t),t) = -\frac{1}{|\frac{\partial y}{\partial \phi}|G(|y|)}\frac{\partial\left(\int_{y_l}^{y} G(|y|)dy\right)}{\partial y}\frac{\partial y}{\partial t}. \tag{12}$$

Now with the assumption that the scalar distribution is monotonic within the lamella and also assuming that y_l is fixed, the conditional expected diffusion simplifies to the form:

$$D(\phi(y,t),t) = -(\frac{\partial y}{\partial \phi})^{-1}(\frac{\partial y}{\partial t}). \tag{13}$$

This relation exhibits an important feature. It indicates that D is not "directly" dependent on the STD and is chiefly governed by the transient scalar evolution within the lamellae. Therefore, if the scalar distribution within the lamellar structures is the same - even approximately - the conditional expected diffusion portrays the same behavior. With this view, it is not surprising that the majority of PDF closures and data obtained by DNS and laboratory experiments yield similar conditional diffusion fields.[10,36,37] This issue will become clear by a comparative assessment of the closures.

The conditional expected dissipation is determined by using Eqs. (3), (8) and (11):

$$E(\phi(y,t),t) = -\frac{1}{|\frac{\partial y}{\partial \phi}|G(|y|)}\int_{y_l}^{y} G(|y|)|\frac{\partial \phi}{\partial y}|\frac{\partial y}{\partial t}dy. \tag{14}$$

If $y = y(\phi,t)$ and $G = G(|y|)$ are known, Eqs. (8), (11), (13) and (14) determine the PDF, the CDF, D, and E.

IV ILDM

The specification of a self-similar scalar distribution within the inter-material domain alleviates the formulation of the mixing problem in that the "exact" spatial variation of the scalar field is not considered. Instead, this variation is governed by the STD. Thus, two closure problems are involved: (1) specification of the time-variant domains and accounting for their stretching, and (2) determination of the scalar transport in each of these domains. Clearly, the first closure is to determine $h(w)$, and the second one deals with the specification of scalar distribution within the lamellae.

In the absence of a velocity field, one expects that the STD retains its initial form and the scalar profile evolves according to a pure diffusion equation. In a turbulent flow, however, the STD is influenced by turbulent stirring, and the scalar distribution is governed by a convection-diffusion transport equation expressed in a frame of reference attached to the moving material element. This transport is governed by Eq. (1) with the velocity vector replaced by a relative velocity vector ($\vec{U} = \vec{U}_{rel}$). In the context of the lamellar theory, as indicated before, it is assumed that the transport occurs in one principal direction. By expressing Eq. (1) along the direction aligned with the local gradient of scalar, we have:

$$\frac{\partial \phi}{\partial t} + V_{rel}\frac{\partial \phi}{\partial y} = \mathcal{D}_{\mathcal{M}}\frac{\partial^2 \phi}{\partial y^2}. \tag{15}$$

Here, V_{rel} is a time and space dependent function and denotes the effects of the relative velocity field $\vec{U}_{rel}$ in the direction of principal scalar transport. Ottino[4] argues that in a small size material region, the relative velocity can be approximated by a linear profile and for an incompressible flow, Eq. (15) can be expressed as:

$$\frac{\partial \phi}{\partial t} + \alpha(Y,t)y\frac{\partial \phi}{\partial y} = \mathcal{D}_{\mathcal{M}}\frac{\partial^2 \phi}{\partial y^2} \tag{16}$$

where $-\alpha(Y,t)$ is the surface area stretch function and is governed by hydrodynamics. Ottino[4] also suggests that in chaotic flows, α on average is approximately constant. Therefore, by a change of variable, $\mathcal{D}_{\mathcal{M}}$ can be set equal to unity. Equation (15), together with a striation thickness PDF constitutes the basis of what we term the *Inter-Layer Diffusion Model* (ILDM). With this model, turbulent mixing is modeled in terms of two distinct but coupled mechanisms: (1) those associated with local events, and (2) those of the summation of these events. The local events are described by the modeled form of the transport equation within the inter-layer material (Eq. (15)), and the global influences are exhibited through the specification of $h(w)$. In the ILDM, the effect of large eddies is implicitly subtracted from that of all the other eddies. That is, in a frame of reference moving with large eddies (those much larger than the scalar size), the remaining eddies determine the evolution of the STD and the dispersion of the scalar within the lamellae. The (indirect) dependency of the conditional expected diffusion on the striation thickness is governed by transport within the normalized fixed region. This transport is described by the normalizing Eq. (15) with the use of $x = \delta(y/w + 1)$, where δ is an arbitrary constant;

$$\frac{\partial \phi}{\partial t} + \frac{\delta V_{rel}}{w}\frac{\partial \phi}{\partial x} = \frac{\delta^2 \mathcal{D}_{\mathcal{M}}}{w^2}\frac{\partial^2 \phi}{\partial x^2}. \tag{17}$$

This equation indicates that the striation thickness affects both the convection and the diffusion of the scalar within the lamellae. For a linear velocity distribution, the influence of hydrodynamic is exhibited only through the diffusion term. Therefore, in this case the effects of the STD can be effectively manipulated by adjusting its parameters. This is well understood since the molecular diffusion is a fluid property with a fixed length scale, and turbulent diffusion is a flow phenomenon involving a spectrum of length scales. Therefore, by normalizing the length with its thickness, each lamellae can be effectively treated with a fixed size and a modified diffusion coefficient. In the form presented, a "specific" striation thickness distribution cannot be suggested. However, it is argued that different physical scenarios observed in either DNS, or laboratory measurements, or obtained by means of other mixing closures can be expressed in terms of the model.

V Other Closures

For clarity of the discussions below, a brief summary of some of the other recently proposed closures of turbulent mixing phenomena are presented. In these discussions, only the Amplitude Mapping Closure (AMC) and the Linear Eddy Model (LEM) are considered, since these two models are the subject of broad current investigations.

The AMC provides an implicit manner by which the conditional expected dissipation and/or the conditional expected diffusion are modeled. The basic element of the AMC involves the mapping of the scalar field (ϕ) into a stationary Gaussian field ϕ_0, $-\infty < \phi_0 < \infty$ by the mapping $\phi = \chi(\phi_0, t)$. The transport equation for this mapping is of the form:[6,8]

$$\frac{\partial \chi}{\partial t} + \phi_0 \frac{\partial \chi}{\partial \phi_0} = \frac{\partial^2 \chi}{\partial \phi_0^2}. \tag{18}$$

In this equation, t denotes a "normalized time" whose relation with the physical time cannot be determined in the context of a single-point description.[8] For an initial binary state, $\phi \in [-1, 1]$, composed of two delta functions at $\phi = \pm 1$, the solution of Eq. (18) is of the form:[8]

$$\phi = \chi(\phi_0, 0) = \mathrm{erf}(d\phi_0 + c), \tag{19}$$

where $d = \frac{1}{\sqrt{2}\tau}$, $c = \frac{-\phi^* \sqrt{1+\tau^2}}{\sqrt{2}\tau}$, and $\tau(t) = \sqrt{\exp(2t) - 1}$, and $\phi^* = -\sqrt{2}\mathrm{erf}^{-1}(< \phi >)$ is a measure of the initial asymmetry of the PDF. This mapping results in an explicit equation for the PDF.

$$P(\phi, t) = \frac{\tau}{2} \exp\left(\left[\mathrm{erf}^{-1}(\phi)\right]^2 - \tau^2 \left[\mathrm{erf}^{-1}(\phi) + \frac{\phi^* \sqrt{1+\tau^2}}{\sqrt{2}\tau} \right]^2 \right). \tag{20}$$

By a combination of Eqs. (20), (2) and (3), all the important statistical features of the closure are determined. The final results for the conditional statistics, after significant manipulations, yield:

$$D(\phi, t) = \frac{2}{\tau\sqrt{\pi}} \frac{\partial \tau}{\partial t} \left(\frac{\tau}{\sqrt{1+\tau^2}} \mathrm{erf}^{-1}(< \phi >) - \mathrm{erf}^{-1}(\phi) \right) \exp\left[-(\mathrm{erf}^{-1}(\phi))^2 \right] \tag{21}$$

and

$$E(\phi, t) = \frac{2}{\pi\tau(1+\tau^2)} \frac{\partial \tau}{\partial t} \exp\left(-2\left[\mathrm{erf}^{-1}(\phi)\right]^2 \right) \tag{22}$$

In the LEM, the primary feature of the closure is its treatment of the mixing phenomenon in one direction. This one-dimensional description allows the resolution of *all* length scales even for flows with relatively large Reynolds and Peclet numbers. This is facilitated by differentiating between turbulent stirring (convection) and molecular diffusion (and chemical reaction). The physical interpretation of the one-dimensional domain is dependent on the particular case under consideration[3,15,38-41] (see Ref.[42] for a recent review). Along the one-dimensional domain, the diffusion (and the chemical reaction) process is implemented deterministically by the solution of the appropriate molecular transport equation(s). The manner by which turbulent convection is treated constitutes the primary feature of the LEM. This is modeled by random rearrangement (stirring) events of the scalar field along the domain. The rules by which these rearrangement processes occur are established in such a way that the random displacements of fluid elements mimic the effects of a turbulent diffusivity. The application of this model in interpreting the results obtained by DNS data and those based on the lamellar theory has been useful.[43,44] This warrants further investigation of the model and its capabilities.

Both of these models can be described in the context of the ILDM. In the AMC, the evolution equation for mapping, Eq. (18) is analogous to Eq. (16) with $\phi \equiv \chi(\phi_0, t)$, and $\phi_0 \equiv y$. Also, for an initial binary state, the initial condition for Eq. (16) is similar to that of the AMC. Therefore the solutions of these two equations are similar (of error-function type as given by Eq. (19)). For a linear velocity field, the effect of the STD can be absorbed into the diffusion coefficient. In the AMC this coefficient is embedded within the normalized time scale. Therefore, with the utilization of the error function distribution within the lamella, the results based on the ILDM are expected to be similar to that of the AMC. Kerstein[1] shows that with the further assumption of a Rayleigh density for $h(w)$, the two models become identical. This assumption implies a Gaussian PDF for $G(|y|)$ which yields an asymptotic Gaussian-like density for the scalar PDF. Note that this asymptotic behavior is independent

of the distributions within the lamellae and can be obtained for other members of the family of the PDF's generated by the Johnson Edgeworth Translation (JET).[10]

The ILDM also portrays some similarities with the LEM. It can be argued that the LEM provides a means of solving Eq. (17) with a random stirring mechanism to simulate the influence of turbulence. Kerstein[3] argues that this simulation is to be conducted by means of a random *triplet* stirring. In this way, the effects of all eddies are taken into account by equating the implied "effective diffusivity" to the "turbulent diffusivity". This is enacted in a one-dimensional representation of the system, regardless of the configuration. In the ILDM, the linear effects of the largest eddies are implicitly subtracted from those of the remaining ones. These remaining effects are modeled into two parts: (1) the dispersion effects are captured by solving the scalar transport equation (Eq. (17)) between two interfaces, and (2) the distribution of these interfaces due to stirring are modeled. In other words, the LEM considers the whole scalar field in a fixed size domain and simulates its evolution in a probabilistic manner. In a homogeneous flow, the whole domain is considered for statistical analysis. It is obvious that this sampling is not the same as that in the ILDM, since the integration over all lamellae is dependent on the configuration of intermaterial structures (Eq. (7)).

VI PDF Generation

In the context of the ILDM, several families of scalar PDF's are generated. In the format presented here, it is not possible to prescribe $h(w)$ *a priori*; its *exact* specification depends on the evolution of the length scales of the hydrodynamic and the scalar fields. Therefore, the contribution of this term is modeled. The other modeling assumption, in the form presented, involves the behavior of the advection term in Eq. (15). In this section, the family of PDF's

generated by the manipulations of these two terms is presented, together with a discussion of their relations with other closures. Both symmetric and non-symmetric PDF's are considered and all the results are compared with data obtained by DNS. These data are taken from homogeneous turbulence simulations in Refs.[9,10,12] With this comparison, it is not implied that these DNS data provide an absolute standard for model validation, as various other mixing conditions have been generated by DNS (*e.g.* see Refs.[27,28]). Rather, the results here are intended to promote more future DNS (or laboratory experiments) with the aim of capturing some of the trends predicted here.

VI.1 Error-Function Distribution within the Lamella

For an initial binary state, one solution of Eq. (15) is of the form:

$$\phi = \mathrm{erf}\left(\frac{y}{\sqrt{2}\tau} + c'\right) \tag{23}$$

where similar to those in AMC (Eq. (19)), τ and c' are functions of time. Substituting this equation into Eqs. (8), (9), (13) and (14) yields the scalar PDF,

$$P(\phi(y)) = \sqrt{\frac{\pi}{2}}\,\tau \exp\left[\left(\frac{y}{\sqrt{2}\tau} + c'\right)^2\right] G(|y|), \tag{24}$$

the conditional expected diffusion,

$$D(\phi(y)) = \frac{-2}{\sqrt{\pi}\tau}\left(\frac{y}{\sqrt{2}\tau}\,\frac{d\tau}{dt} - \tau\frac{dc'}{dt}\right)\exp\left[-\left(\frac{y}{\sqrt{2}\tau} + c'\right)^2\right], \tag{25}$$

and the conditional expected dissipation,

$$E(\phi(y)) = \frac{-2\sqrt{2}}{\pi\tau^2}\frac{\exp\left[-\left(\frac{y}{\sqrt{2}\tau}+c'\right)^2\right]}{G(|y|)}\left(\frac{1}{\sqrt{2}\tau}\frac{d\tau}{dt}\int_{y_l}^{y} yG(|y|)\exp\left[-\left(\frac{y}{\sqrt{2}\tau}+c'\right)^2\right]dy\right.$$
$$\left.-\tau\frac{dc'}{dt}\int_{y_l}^{y} G(|y|)\exp\left[-(\frac{y}{\sqrt{2}\tau}+c)^2\right]dy\right). \quad (26)$$

In these equations, the variable c' is determined implicitly by knowing the average value of the scalar $< \phi >$ which is time invariant and is given by

$$< \phi >= \int_{y_l}^{y_u} \phi(y)G(|y|)dy = \text{constant}. \quad (27)$$

An important feature of Eq. (25) is that regardless of the choice of a STD, the conditional expected diffusion obtained here is similar to that generated by the AMC (Eq. (21)).

Exponential STD:

The exponential STD represent the general case of a Rayleigh distribution and has been proposed by Kerstein.[1] It has the form:

$$h(w) = \beta(n+1)w^n\exp(-\beta w^{n+1}), \quad (28)$$

where $\beta = \left[\sqrt{\frac{2}{\pi}}\Gamma(\frac{n+2}{n+1})\right]^{n+1}$ and Γ denotes the gamma function. Using this STD, the scalar PDF adopts the form:

$$P((\phi(y)) = \frac{\tau}{2}\exp\left[(\frac{y}{\sqrt{2}\tau}+c')^2-\beta|y|^{n+1}\right]. \quad (29)$$

It is noted that for the special case of the Rayleigh distribution ($n = 1$), the generated PDF is the same as that obtained by the AMC (Eq. 20), and the conditional expected diffusion is expressed by Eq. (25). In general, the conditional expected dissipation cannot be presented by an analytical expression. The exception is the Rayleigh distribution by which Eq. (26) which can be analytically integrated:

$$E(\phi(y)) = \frac{\frac{d\tau}{dt}}{\pi\tau^3 A}\exp(-\left[(A+D)y^2 + 2By + 2c'^2\right]) + \sqrt{\frac{1}{\pi A}}\frac{1}{\tau^3}$$
$$\left[\frac{d\tau}{dt}(\frac{B}{2A} + \frac{dc'}{dt})\right]\left[1 - \mathrm{erf}\frac{(2Ay+B)}{2\sqrt{A}}\right]\exp\left[\frac{B^2}{4A} - (Dy^2 + By + c'^2)\right]. \qquad (30)$$

Here, $A = \frac{1}{2}(\frac{1}{\tau^2} + 1)$, $B = \frac{\sqrt{2}c'}{\tau}$, and $D = \frac{1}{2}(\frac{1}{\tau^2} - 1)$. As expected, Eq. (30) is exactly the same as Eq. (22).

The family of PDF's generated (Eq. 29) is characterized by the counter-b[illegible]ce of the two terms in the exponential term. The positive term exhibits the influence of scalar gradient and is minimum around $\phi = 0$. The negative term denotes the STD effect and is maximum near the mean scalar value. In both terms, y is determined through Eq. (23). With fixed scalar bounds, the positive term does not change but depending on the magnitudes of n and τ, the negative term varies. The influence of the STD on scalar PDF becomes more dominant as n decreases and/or τ increases. The statistical results generated for $n = 0, 1, 3$ are presented in Figs. 1-2. These results are for a symmetric PDF within $[-1, 1]$, *i.e.* $< \phi >= 0$. As anticipated, the parameter n has a strong influence of PDF and on the conditional expected dissipation, as Fig. 1(b) is markedly different from the self-similar bell shape observed for $n = 1$.[26] The influence of the parameter on the conditional expected diffusion is not significant and all the results resemble that shown in Fig. 1(c). For a system composed of randomly distributed lamellae thickness, Sokolov and Blumen[33,34] suggest that in the absence of stretching the STD is close to a gamma function. This corresponds to

$n = 0$. In this case, the PDF's have non-negligible values at the scalar bounds and exhibit the characteristics of an exponential-tail PDF (Fig. 1(a)). This figure indicates that even for an error-function scalar distribution within the lamellae, it is possible to have long-tail PDF's. From a physical standpoint this scenario corresponds to a case where there are noticeable slabs of materials with long intermaterial distances. In these slabs, the molecular diffusion process with large characteristic time scales is unable to mix the scalar sufficiently, thus unmixed regions prevail. This results in a concave up, basin-shaped profile for the conditional expected dissipation near the mean scalar value. The existence of two maximum and one minimum in these curves is a logical consequence of tendency of the conditional expected dissipation to be zero at its bounds.[10] Also, it is noted that the scalar is always bounded within the same domain. That is the conditional expected dissipation is anchored at $\phi = \pm 1$. This is due to the unboundedness of the STD. With the exponential distribution, there are always slabs with infinite thickness which do not mix completely; therefore, the limits of the scalar field remain unchanged. The results for $n = 3$ suggest that the PDF is somewhat uniform near the mean scalar value, but has sharp gradients in the composition domain. This is understandable since as the magnitude of n increases, the STD approaches a delta function and the PDF portrays a double-delta like distribution. This behavior is similar to the PDF evolution corresponding to a uniform STD which is presented below. In this presentation, the results for different STD are compared with those corresponding to a Rayleigh STD ($n = 1$) and also with DNS data extracted form the simulations in Ref.[9] This comparison is made at the same magnitude of the normalized scalar variance.

Uniform Striation Thickness:

Here, w is assumed constant ($= w^*$) for all lamellae. This implies that a uniform field of equal inter-material distances is considered. In this case, the PDF of the striation thickness is composed of a delta function, *i.e.* $h(w) = \delta(w - w^*)$. With this STD,

$$G(|y|) = \begin{cases} \frac{1}{2w^*} & \text{if } -w^* \leq y \leq w^* \ ; \\ 0 & \text{elsewhere} \end{cases}.$$

which yields the PDF:

$$P(\phi(y)) = \begin{cases} \sqrt{\frac{\pi}{2}} \frac{\tau}{2w^*} \exp\left((\frac{y}{\sqrt{2\tau}} + c')^2 \right) & \text{if } -w^* \leq y \leq w^* \ ; \\ 0 & \text{elsewhere,} \end{cases} \tag{31}$$

and the conditional expected dissipation:

$$E(\phi(y)) = \frac{2}{\pi} \exp(-\frac{3}{2}s^2) \left(\frac{1}{\tau} \frac{d\tau}{dt} D_{-2}(\sqrt{2}s) - (\frac{1}{\tau^2} \frac{d\tau}{dt} y - \sqrt{2} \frac{dc'}{dt}) D_{-1}(\sqrt{2}s) \right) \tag{32}$$

Here, D_ν denote the parabolic cylinder function of order ν,[45] and $s = (\frac{y}{\sqrt{2\tau}} + c') = \text{erf}^{-1}(\phi)$.

For $|y| \leq w^*$, the conditional expected diffusion is determined by Eq. (25). With this bounded STD, the bounds of the composition domain are not fixed as shown in Figs. 3-4. The PDF's generated by the model are composed of two marching peaks and asymptotically form a single peak at the mean scalar value. This evolution is similar to that of the Linear Mean Square Estimation[46] and is similar to that obtained from the solution of for the case of pure diffusion with an initial double delta distribution.[16] This type of PDF evolution characterizes mixing problems with small velocity effects and corresponds to the scalar evolution in a flow dominated by small scales. The physical reasoning for this behavior is that small velocity length scales do not produce a substantial large scale mixing and their influence is exhibited only through enhanced diffusion. These results are also consistent with those generated by the LEM in Ref.[44]

Constant STD:

For a constant STD, $h(w)$ is given by:

$$h(w) = \begin{cases} \frac{1}{w_u} & \text{if } 0 \leq w \leq w_u \ ; \\ 0 & \text{otherwise.} \end{cases}$$

where, w_u is a constant. With this distribution, Eq. (9) indicates that $G(|y|)$ is a linear function of y,

$$G(|y|) = \begin{cases} \frac{w_u - |y|}{w_u^2} & \text{if } |y| \leq w_u \\ 0 & \text{elsewhere.} \end{cases}$$

This results in the scalar PDF,

$$P(\phi(y)) = \begin{cases} \sqrt{\frac{\pi}{2}}\tau \exp\left[\left(\frac{y}{\sqrt{2}\tau} + c'\right)^2\right] \frac{w_u - |y|}{w_u^2} & \text{if } |y| \leq w_u \\ 0 & \text{elsewhere.} \end{cases} \tag{33}$$

In the range $|y| \leq w_u$, D is given by Eq. (25), and E is given by Eq. (26) in which Eq. (27) determines the magnitude of c'. After significant mathematical manipulations, the final results yield the form:

$$\begin{aligned} E(\phi(y)) \;=\; & \frac{2}{\pi} \frac{\exp(-\frac{3}{2}s^2)}{w_u - |y|} \left(\left[y(\pm y - w_u) \frac{1}{\tau^2} \frac{d\tau}{dt} + \sqrt{2} w_u \frac{dc'}{dt} \right] D_{-1}(\sqrt{2}s) \right. \\ & \left. + \left[w_u \frac{1}{\tau} \frac{d\tau}{dt} \mp \sqrt{2}\tau \frac{dc'}{dt} \right] D_{-2}(\sqrt{2}s) \mp 2 \frac{d\tau}{dt} D_{-3}(\sqrt{2}s) \right). \end{aligned} \tag{34}$$

Here again, D_ν denotes a parabolic cylinder function of order ν, and $\pm$ signs correspond to those of y. The results for the PDF and the conditional statistics (Figs. 3-5) indicate that with mixing progression, the PDF migrates towards the mean value of the scalar. The

boundedness of the striation thickness also yields the migration of the scalar bounds as evident by the profiles of the conditional expected dissipation and the conditional expected diffusion. The trimodal nature of the PDF at early times has not been observed in available DNS but has been captured by LEM.[43]

Linear STD:

The linear STD is defined by:

$$h(w) = \begin{cases} \frac{2w}{w_u{}^2} & \text{if } 0 \leq w \leq w_u; \\ 0 & \text{otherwise.} \end{cases}$$

With this STD, we have:

$$G(|y|) = \begin{cases} \frac{3}{4}\frac{w_u{}^2 - y^2}{w_u{}^3} & \text{if } |y| \leq w_u; \\ 0 & \text{elsewhere} \end{cases}$$

and,

$$P(\phi(y)) = \begin{cases} \frac{3}{4}\sqrt{\frac{\pi}{2}}\tau \exp\left[\left(\frac{y}{\sqrt{2\tau}} + c'\right)^2\right]\frac{w_u{}^2 - y^2}{w_u{}^3} & \text{if } |y| \leq w_u; \\ 0 & \text{elsewhere} \end{cases} \tag{35}$$

For $|y| \leq w_u$, D is determined by Eq. (25) and E is expressed in terms of parabolic cylinder functions through the relation:

$$\begin{aligned} E(\phi(y)) \;=\; & \frac{2}{\pi}\frac{\exp(-\frac{3}{2}s^2)}{w_u^2 - y^2}\left(\left[y(y^2 - w_u^2)\frac{1}{\tau^2}\frac{d\tau}{dt} + \sqrt{2}(w_u^2 - y^2)\frac{dc}{dt}\right] D_{-1}(\sqrt{2}s)\right. \\ & \left. + \left[(w_u^2 - 3y^2)\frac{1}{\tau}\frac{d\tau}{dt} + 2\sqrt{2}\tau\frac{dc'}{dt}y\right] D_{-2}(\sqrt{2}s)\right. \end{aligned}$$

$$+\left[6\frac{d\tau}{dt}y - 2\sqrt{2}\tau^2\frac{dc'}{dt}\right] D_{-3}(\sqrt{2}s) - \left[6\tau\frac{d\tau}{dt}\right] D_{-4}(\sqrt{2}s)\Big). \qquad (36)$$

The results for PDF, E and D in this case also show the influence of migration of scalar bounds as mixing proceeds.

The comparative assessment in Figs. 3-5 shows the properties of each of the closures. It is noted that the profiles of the PDF and the conditional expected dissipation are different, each case indicating a possible mixing condition. None of the PDF's generated in this way yield an asymptotic Gaussian state as exhibited by the profiles of the conditional expected dissipation. Despite these differences, the profiles of the conditional expected diffusion are very similar in all the models. The primary difference is near the bounds. For the cases with finite striation thickness, the models allow for the migration of scalar bounds. For the case with infinite bounds, the conditional statistics are anchored at scalar bounds. For the cases with linear and constant STD's the PDF's resemble those produced by the JET.[10] However, the conditional statistics as depicted by the models here are closer to DNS results.

The difference between the closures is better exhibited by the results for the non-symmetric case. A comparison of all the closures is made in Figs. 6-8 for $< \phi >= 0.25$. The procedure for producing these results is identical to that for the symmetric PDF. However, the numerical means of evaluating the constant c' is somewhat more involved. For non-symmetric PDF's, this evaluation is made by an iterative procedure based on Eq. (27). In this case, the PDF's as produced by all the closure are very close and asymptotically tend to be concentrated near the mean scalar value. However, the difference between the closures is most obvious in the profiles of the conditional statistics. It is noted that the conditional expected dissipation for $n = 1$ (AMC) always yields a symmetric profile regardless of the extent of asymmetry in the PDF. The rigorous mathematical reasoning for this behavior is given in Ref.[47] The distributions produced by other models (Fig. 7) and also with other values of n (not shown)

do not portray this behavior. As indicated in Fig. 7, the results for all cases with a finite STD bounds are close to DNS data. The conditional diffusion for $n = 1$ does portray the non-symmetric nature of mixing, but is still always anchored at the bounds of the composition domain. The same trend is observed for all the cases with unbounded STD's.

VI.2 Effects of Scalar Distribution within the Lamellae

There are other scalar profiles which satisfy Eq. (17). The solution of this equation depends primarily on the velocity field. Here, several simple velocity fields are considered along with a Rayleigh and a linear STD. These two distributions are selected to show the influence of the striation boundedness. The scalar profiles are obtained by the spectral-collocation solution of Eq. (17) within a fixed physical domain ($0 \leq x \leq 2\pi$).

Rayleigh STD:

With the specification of this STD, the results are dependent on the velocity distribution. For a pure diffusion transport within the lamellae, *i.e.* $V_{rel} = 0$ in Eq. (17), the generated PDF is Gaussian-like as expected. This is shown in Fig. 9(a) and indicates that the integrated influence of local diffusion effects results in a global diffusion behavior. For a linear velocity profile ($V_{rel} = \alpha y$), the results exhibit similar trends as those governed by the AMC; for $\alpha = 1$ the results are identical to those of the AMC. By varying the magnitude of α, the counter-balance between the convection term and the diffusion term in Eq. (17) changes but the general behavior of the scalar PDF remains the same. Therefore, the primary difference is displayed through the time scale of the PDF evolution. For a constant velocity profile, the results in Fig. 9(b) show a significant departure from those of AMC and those shown in Fig. 9(a). Figure 9(b) indicates a significant magnitude of the PDF at the bounds of the composition domain, yielding an exponential type PDF. The results for this case are

also compared with those based on AMC and LEM in Fig. 10. The exponential nature of the PDF, which cannot be generated by AMC, is captured by LEM. This is shown both in PDF plots and in the profiles of the conditional expected dissipation. Note the basin shape structure of the conditional dissipation profile. This structure, similar to that in Fig. 1(b) imply tails close to a Laplace (double exponential) distribution for the PDF. As before, there are no significant changes in the conditional diffusion profiles. An increase in the amplitude of the velocity results in a faster evolution of the PDF towards the mean value. An asymptotic exponential scalar distribution has not been observed in most previous numerical simulations,[24,37,23,25,10] the exceptions are those in LES results of Ref.[27] and in DNS results of Ref.[28]

Linear STD:

For this bounded STD, the results with different velocity profiles are presented in Figs. 11-13. For the pure diffusion case, the scalar PDF adopts an approximate rectangular form. This implies the same probability at all the scalar ranges with an accommodation of the boundary encroachment. Again, the results are very similar to those produced by the LMSE characterized by linear profiles of the conditional expected diffusion (Fig. 11(c)). For a linear velocity profile, the migration of scalar bounds (Fig. 12) results in an approximate Gaussian-like asymptotic PDF. However, the conditional expected dissipation is not uniform. A constant velocity profile results, as before, in the formation of exponential-like PDF's (Fig. 13). Therefore, the conditional expected dissipation portrays a basin like profile at the mean scalar value. This profile becomes steeper as time increases. The profiles for the conditional diffusion are similar to those presented in Fig. 11(c) and are not shown.

The results presented in Figs. 9-13 reveal the dominant influence of the velocity field on the evolution of the PDF. These "simple" profiles are selected here only for the purpose of demonstration. Obviously, in a turbulent flow field with a wide spectrum of eddy sizes, the

influence of the velocity field is more complex. Motivated by the results here, the assessment of the role of velocity field by DNS is strongly recommended. However, due to the small range of the Reynolds numbers that can be considered by DNS, such an assessment could be very difficult- but is currently under way. In the meantime, other approaches by which the effects of convection in Eq. (17) can be examined, should be followed. For example, the LEM provides one means of doing exactly so.

VII Applications for Modeling of Reacting Flows

Perhaps one of the most important applications of mixing closures is due their use for modeling of turbulent combustion.[5,19,2] The results generated here can be used directly for modeling of *mixing controlled* homogeneous chemically reacting systems. Namely, in determining the limiting rate of reactant conversion in a simple chemistry of the type $\mathcal{F}+\mathcal{O} \rightarrow Products$. It is now well-established that in a binary irreversible reaction of this type, the statistics of the reacting field can be related to those of an appropriately defined mixture fraction.[48] This mixture fraction is a conserved scalar variable, similar to the variable ϕ considered above. Therefore, all the PDF's produced by the ILDM can be utilized for estimating the statistics of the reacting field in a homogeneous flow with an initially segregated (nonpremixed) reactants.

The ensemble-mean values of the mass fractions of the reacting species are the most important physical variables from a practical standpoint. Therefore, it is useful to examine the differences between the PDF's in predicting the rate of mean reactants' decay. For unity mass fractions for the free stream fuel and oxidizer, the conserved scalar variable ϕ can be defined as $\phi = F - O$, where F and O denote the mass fractions of the fuel and the oxidizer, respectively. Nonpremixed reactants imply an initial binary state for the variable ϕ. There-

fore, the initial PDF of ϕ is composed of two delta functions at $\phi = \pm 1$. If the reactants are introduced in stoichiometric proportions, $< \phi >= 0$ and non unity equivalence ratios imply non-zero values for the mean mixture fraction. In fuel-rich mixtures, $< \phi > > 0$. With the AMC, Madnia *et al.*[9] have analytically integrated the PDF for the evaluation of the mean reactants mass fractions. In non-stoichiometric mixture, *i.e.*, the final results are in the form of definite integrals of the parabolic cylinder functions. In stoichiometric mixtures, the results simplify considerably and are directly related to the mixture fraction through:

$$\frac{< F > (t)}{< F > (0)} = \frac{< O > (t)}{< O > (0)} = \frac{2}{\pi} \arcsin \left(\sqrt{\sin \left[\frac{\pi I_s}{2} \right]} \right). \tag{37}$$

I_s denotes the "intensity of segregation" and represents the normalized variance of the mixture fraction:

$$I_s = \frac{< \phi'^2 > (t)}{< \phi'^2 > (0)} \tag{38}$$

For non-stoichiometric mixtures and for other probability distributions generated here, analytical solutions are not possible and the results can be obtained only by integrating the PDF numerically. The final results for all cases are presented in Figs. 14-16. These figures represent the rate of mean mass fraction decay in terms of I_s for both stoichiometric and non-stoichiometric mixtures. For the stoichiometric case, obviously both reactants decay at the same rate (Fig. 14-15). For the fuel-rich mixture, the oxidizer is depleted faster and there is a surplus of fuel left at the final stages of mixing ($I_s \approx 0$). In all the cases considered, the results indicate that there is not a substantial difference between the closure predictions. Based on these observations, the analytical relations of Madnia *et al.*[9] are recommended for predicting the limiting rate of mean reactant conversion in both homogeneous and non-homogeneous mixtures, at least until the development of more accurate closures.

VIII Summary

It is shown that the lamella theory provides a simple means of "mimicking" several scalar mixing scenarios in homogeneous turbulent flows. The model described here is an extension of that first proposed by Kerstein[1] and suggests that there are two mechanisms by which the mixing process is described. These mechanisms are due to: (1) local events and (2) global events. The local effects are described by the distribution of the scalar within the lamellae, and the global effects are exhibited by the statistical distribution of the striation thickness. The properties of the model are described with a detailed examinations of the statistical features of the scalar field. It is shown that the difference between all the closures are exhibited in the profiles of the Probability Density Function (PDF) of the scalar and the conditional expected value of the scalar dissipation. However, all the cases yield similar profiles for the conditional expected diffusion of the scalar. This behavior is mathematically described in the framework of the model and explains the similarity of the conditional diffusion as observed in previous contributions.[10,36,37] In all the cases, the *primary* influence of the conditional diffusion is shown to be through its behavior at the bounds in the composition domain. It is also shown that with the manipulations of each of the two primary mechanisms, many different PDF's can be generated. Some of these PDF's have been observed in previous DNS studies and some have been captured by other mixing closures. However, some of the cases considered here are yet to be observed (in DNS, experiments, other closures *etc.*). It is claimed that this does not necessarily imply the non-physical character of the mixing scenario in these cases. Rather, it indicates the need for further test cases to be considered in future simulations and experiments. In these efforts, one must be careful in identifying the roles of the velocity and scalar length scales as these scales may lead to different asymptotic behaviors. In this regard an assessment of the model by means of DNS in the form recently reported in Ref.[28] and by LEM in the context proposed in Ref.[44] is

useful. Also, the flexibility of the model may offer an assistance to other closures which are based on *a priori* knowledge of the statistical evolution (such as Ref.[16]). Some work in these regards is currently underway. Finally, it is shown that while the PDF's generated by the model are very different, their application for determining the limiting rate of mean reactant conversion in mixing limited nonpremixed turbulent flows do not yield significantly different results. Thus, the closed form expression obtained for one of the models is approximately valid and is recommended for all the other cases.

References

[1] Kerstein, A. R., Flapping Model of Scalar Mixing in Turbulence, *Phys. Fluids A*, **27**(12):2819–2827 (1991).

[2] Pope, S. B., Computations of Turbulent Combustion: Progress and Challenges, in *Proceedings of 23rd Symp. (Int.) on Combustion*, pp. 591–612, The Combustion Institute, Pittsburgh, PA, 1990.

[3] Kerstein, A. R., Linear-Eddy Modeling of Turbulent Transport. Part 6. Microstructure of Diffusive Scalar Mixing Fields, *J. Fluid Mech.*, **231**:361–394 (1991).

[4] Ottino, J. M., *The Kinematics of Mixing: Stretching, Chaos, and Transport*, Cambridge University Press, Cambridge, U.K., 1989.

[5] Pope, S. B., PDF Methods for Turbulent Reacting Flows, *Prog. Energy Combust. Sci.*, **11**:119–192 (1985).

[6] Chen, H., Chen, S., and Kraichnan, R. H., Probability Distribution of a Stochastically Advected Scalar Field, *Phys. Rev. Lett.*, **63**(24):2657–2660 (1989).

[7] Sinai, Y. G. and Yakhot, V., Limiting Probability Distributions of a Passive Scalar in a Random Velocity Field, *Phys. Rev. Lett.*, **63**(18):1962–1964 (1989).

[8] Pope, S. B., Mapping Closures for Turbulent Mixing and Reaction, *Theoret. Comput. Fluid Dynamics*, **2**:255–270 (1991).

[9] Madnia, C. K., Frankel, S. H., and Givi, P., Reactant Conversion in Homogeneous Turbulence: Mathematical Modeling, Computational Validations and Practical Applications, *Theoret. Comput. Fluid Dynamics*, **4**:79–93 (1992).

[10] Miller, R. S., Frankel, S. H., Madnia, C. K., and Givi, P., Johnson-Edgeworth Translation for Probability Modeling of Binary Mixing in Turbulent Flows, *Combust. Sci. and Tech.*, **91**(1-3):21–52 (1993).

[11] Girimaji, S. S., A Mapping Closure for Turbulent Scalar Mixing Using a Time-Evolving Reference Field, *Phys. Fluids A.*, **4**(12):2875–2886 (1992).

[12] Frankel, S. H., Madnia, C. K., and Givi, P., Comparative Assessment of Closures for Turbulent Reacting Flows, *AIChE J.*, **39**(5):899–903 (1993).

[13] Girimaji, S. S., On the Modeling of Scalar Diffusion in Isotropic Turbulence, *Phys. Fluids A.*, **4**(11):2529–2537 (1992).

[14] Kerstein, A. R., A Linear Eddy Model of Turbulent Scalar Transport and Mixing, *Combust. Sci. and Tech.*, **60**:391-421 (1988).

[15] Kerstein, A. R., Linear-Eddy Modeling of Turbulent Transport. Part V. Geometry of Scalar Interfaces, *Phys. Fluids A*, **3**(5):1110–1114 (1991).

[16] Fox, R. O., The Fokker-Planck Closure for Turbulent Molecular Mixing: Passive Scalars, *Phys. Fluids A.*, **4**(6):1230–1244 (1992).

[17] Larcheveque, M. and Lesieur, M., The Applications of Eddy-Damped Markovian Closures to the Problem of Dispersion of Particle Pairs, *J. Mech.*, **20**:113 (1981).

[18] Frankel, S. H., Jiang, T.-L., and Givi, P., Modeling of Isotropic Reacting Turbulence by a Hybrid Mapping-EDQNM Closure, *AIChE J.*, **38**(4):535–543 (1992).

[19] Givi, P., Model Free Simulations of Turbulent Reactive Flows, *Prog. Energy Combust. Sci.*, **15**:1–107 (1989).

[20] Rogallo, R. S. and Moin, P., Numerical Simulation of Turbulent Flow, *Ann. Rev. Fluid Mech.*, **16**:99–137 (1984).

[21] Jayesh and Warhaft, Z., Probability Distribution of a Passive Scalar in Grid-Generated Turbulence, *Phys. Rev. Lett.*, **67**(25):3503–3506 (1991).

[22] Jayesh and Warhaft, Z., Probability Distribution, Conditional Dissipation, and Transport of Passive Temperature Fluctuations in Grid-Generated Turbulence, *Phys. Fluids A*, **4**(10):2292–2307 (1992).

[23] Givi, P. and McMurtry, P. A., Non-Premixed Reaction in Homogeneous Turbulence: Direct Numerical Simulations, *AIChE J.*, **34**(6):1039–1042 (1988).

[24] Eswaran, V. and Pope, S. B., Direct Numerical Simulations of the Turbulent Mixing of a Passive Scalar, *Phys. Fluids*, **31**(3):506–520 (1988).

[25] McMurtry, P. A. and Givi, P., Direct Numerical Simulations of Mixing and Reaction in a Nonpremixed Homogeneous Turbulent Flow, *Combust. Flame*, **77**:171–185 (1989).

[26] Jiang, T.-L., Gao, F., and Givi, P., Binary and Trinary Scalar Mixing by Fickian Diffusion-Some Mapping Closure Results, *Phys. Fluids A*, **4**(5):1028–1035 (1992).

[27] Metais, O. and Lesieur, M., Spectral Large-Eddy Simulation of Isotropic and Stably Stratified Turbulence, *J. Fluid Mech.*, **239**:157–194 (1992).

[28] Kimura, Y. and Kraichnan, R. A., Statistics of an Advected Passive Scalar, *Phys. Fluids A.*, **5**(9):2264–2277 (1993).

[29] Dahm, W. J. A., Southerland, K. B., and Buch, K. A., Direct, High Resolution, Four-Dimensional Measurements of Fine Scale Structure of $Sc \gg 1$ Molecular Mixing in Turbulent Flows, Technical Report AFOSR-89-0541-1, Department of Aerospace Engineering, University of Michigan, Ann Arbor, MI, 1990.

[30] Ruetsch, G. R. and Maxey, M. R., The Evolution of Small-Scale Structures in Homogeneous-Isotropic Turbulence, *Phys. Fluids A*, **4**(12):2747–2760 (1992).

[31] Muzzio, F. J. and Ottino, J. M., Evolution of a Lamellar System with Diffusion and Reaction: A Scaling Approach, *Phys. Rev. Lett.*, **63**(1):47–50 (1989).

[32] Muzzio, F. J. and Ottino, J. M., Dynamics of a Lamellar System with Diffusion and Reaction: Scaling Analysis and Global Kinetics, *Phys. Rev. A*, **40**(12):7182–7192 (1989).

[33] Sokolov, I. M. and Blumen, A., Diffusion-Controlled Reactions in Lamellar Systems, *Phys. Rev. A*, **43**(6):2714–2719 (1991).

[34] Sokolov, I. M. and Blumen, A., Distribution of Striation Thicknesses in Reacting Lamellar Systems, *Phys. Rev. A*, **43**(12):6546–6549 (1991)

[35] Kraichnan, R. H., Closures for Probability Distributions, *Bull. Amer. Phys. Soc.*, **34**:2298 (1989).

[36] Pope, S. B. and Ching, E. S. C., Stationary Probability Density Functions: An Exact Result, *Phys. Fluids A*, **5**(7):1529–1531 (1993).

[37] Leonard, A. D. and Hill, J. C., Scalar Dissipation and Mixing in Turbulent Reacting Flows, *Phys. Fluids A.*, **3**(5):1286–1299 (1991).

[38] Kerstein, A. R., Linear Eddy Modeling of Turbulent Transport. II: Applications to Shear Layer Mixing, *Combust. Flame*, **75**:397–413 (1989).

[39] Kerstein, A. R., Linear Eddy Modeling of Turbulent Transport. Part 3. Mixing and Differential Molecular Diffusion in Round Jets, *J. Fluid. Mech.*, **216**:411–435 (1990).

[40] Kerstein, A. R., Linear-Eddy Modeling of Turbulent Transport. Part 4. Structure of Diffusion Flames, *Combust. Sci. Tech.*, **81**:75–96 (1992).

[41] Kerstein, A. R., Linear-Eddy Modeling of Turbulent Transport. Part 7. Finite -Rate Chemistry and Multi-Stream Mixing, *J. Fluid Mech.*, **240**:289–313 (1992).

[42] McMurtry, P. A., Menon, S., and Kerstein, A. R., Linear Eddy Modeling of Turbulent Mixing and Reactions: A Review, *Energy and Fuels*, (1993), in press.

[43] McMurtry, P. A., Gansauge, T. C., Kerstein, A. R., and Krueger, S. K., Linear Eddy Simulations of Mixing in a Homogeneous Turbulent Flow, *Phys. Fluids A.*, **5**(4):1023–1034 (1993).

[44] Cremer, M. A., McMurtry, P. A., and Kerstein, A. R., Effects of Turbulence length-Scale Distribution on Scalar Mixing in Homogeneous Turbulent Flow, *Phys. Fluids A.*, (1993), Submitted.

[45] Abramowitz, M. and Stegun, I. A., *Handbook of Mathematical Functions and Formulas, Graphs, and Mathematical Tables*, Government Printing Office, Washington, D.C., 1972.

[46] Dopazo, C. and O'Brien, E. E., Statistical Treatment of Non-Isothermal Chemical Reactions in Turbulence, *Combust. Sci. and Tech.*, **13**:99–112 (1976).

[47] Frankel, S. H., Probabilistic and Deterministic Description of Turbulent Flows with Nonpremixed Reactants, Ph.D. Thesis, Department of Mechanical and Aerospace Engineering, State University of New York at Buffalo, Buffalo, NY, 1993.

[48] Williams, F. A., *Combustion Theory*, The Benjamin/Cummings Publishing Company, Menlo Park, CA, 2nd edition, 1985.

Figure Captions

Figure 1. Statistical results based on an exponential STD. $n = 0$, $< \phi >= 0$. (a) PDF, (b) Normalized conditional expected dissipation. (c) Normalized conditional expected diffusion.

Figure 2. PDF results based on an exponential STD. $< \phi >= 0$. (a) $n = 1$, (b) $n = 3$.

Figure 3. Comparison amongst the PDF's generated via various closures and with DNS. $< \phi >= 0$. (a) $\sigma^2 = 0.3175$, (b) $\sigma^2 = 0.0526$, (c) $\sigma^2 = 0.01346$.

Figure 4. Comparison amongst the conditional expected dissipation generated via various closures and with DNS. $< \phi >= 0$. (a) $\sigma^2 = 0.3175$, (b) $\sigma^2 = 0.0526$, (c) $\sigma^2 = 0.01346$.

Figure 5. Comparison amongst the conditional expected diffusion generated via various closures and with DNS. $< \phi >= 0$. (a) $\sigma^2 = 0.3175$, (b) $\sigma^2 = 0.0526$, (c) $\sigma^2 = 0.01346$.

Figure 6. Comparison amongst the PDF's generated via various closures and with DNS. $< \phi >= 0.25$. (a) $\sigma^2 = 0.39$, (b) $\sigma^2 = 0.13$.

Figure 7. Comparison amongst the conditional expected dissipation generated via various closures and with DNS. $< \phi >= 0.25$. (a) $\sigma^2 = 0.39$, (b) $\sigma^2 = 0.13$.

Figure 8. Comparison amongst the conditional expected diffusion generated via various closures and with DNS. $< \phi >= 0.25$. (a) $\sigma^2 = 0.39$, (b) $\sigma^2 = 0.13$.

Figure 9. ILDM prediction of the scalar PDF with a Rayleigh STD, $< \phi >= 0$, and (a) $V_{rel} = 0$, (b) a constant inter-layer velocity profile.

Figure 10. Comparison of ILDM prediction based on a Rayleigh STD and a constant inter-layer velocity profile with the results based on the AMC and the LEM. $< \phi >= 0$. (a) PDF, (b) Normalized conditional expected dissipation. (c) Normalized conditional expected diffusion.

Figure 11. ILDM prediction with a linear STD and $V_{rel} = 0, < \phi >= 0$. (a) PDF, (b) Normalized conditional expected dissipation. (c) Normalized conditional expected diffusion.

Figure 12. ILDM prediction with a linear STD and a linear inter-layer velocity profile. $< \phi >= 0$. (a) PDF, (b) Normalized conditional expected dissipation.

Figure 13. ILDM prediction with a linear STD and a constant inter-layer velocity. $< \phi >= 0$. (a) PDF, (b) Normalized conditional expected dissipation.

Figure 14. Decay of mean reactants' concentration in a stoichiometric mixture as predicted by the ILDM with an exponential STD.

Figure 15. Decay of mean reactants' concentration in a stoichiometric mixture as predicted

by the ILDM with several different STD's.

Figure 16. Decay of mean reactants' concentration in a fuel-rich mixture as predicted by the ILDM with an exponential STD.

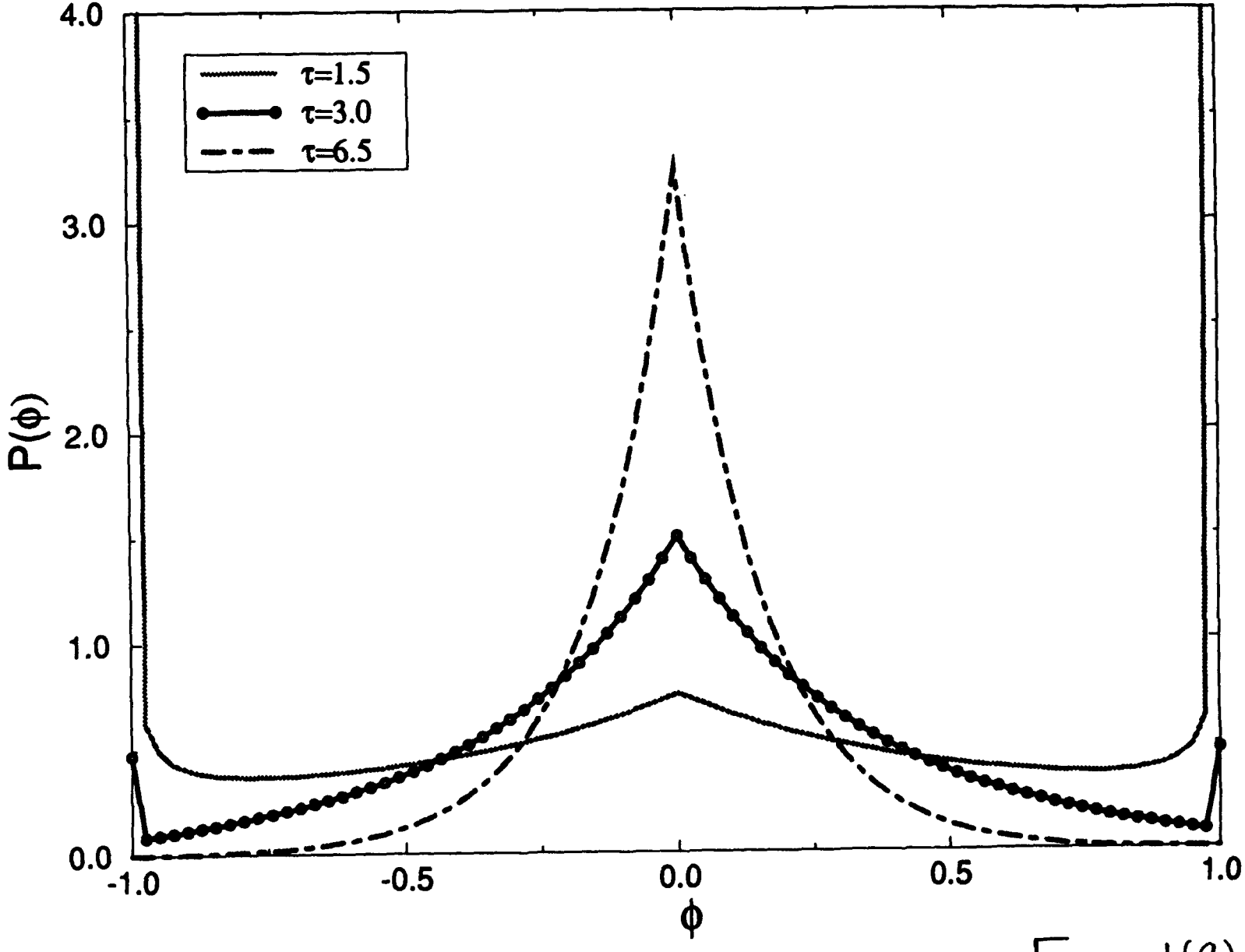

Fig. 1(a)

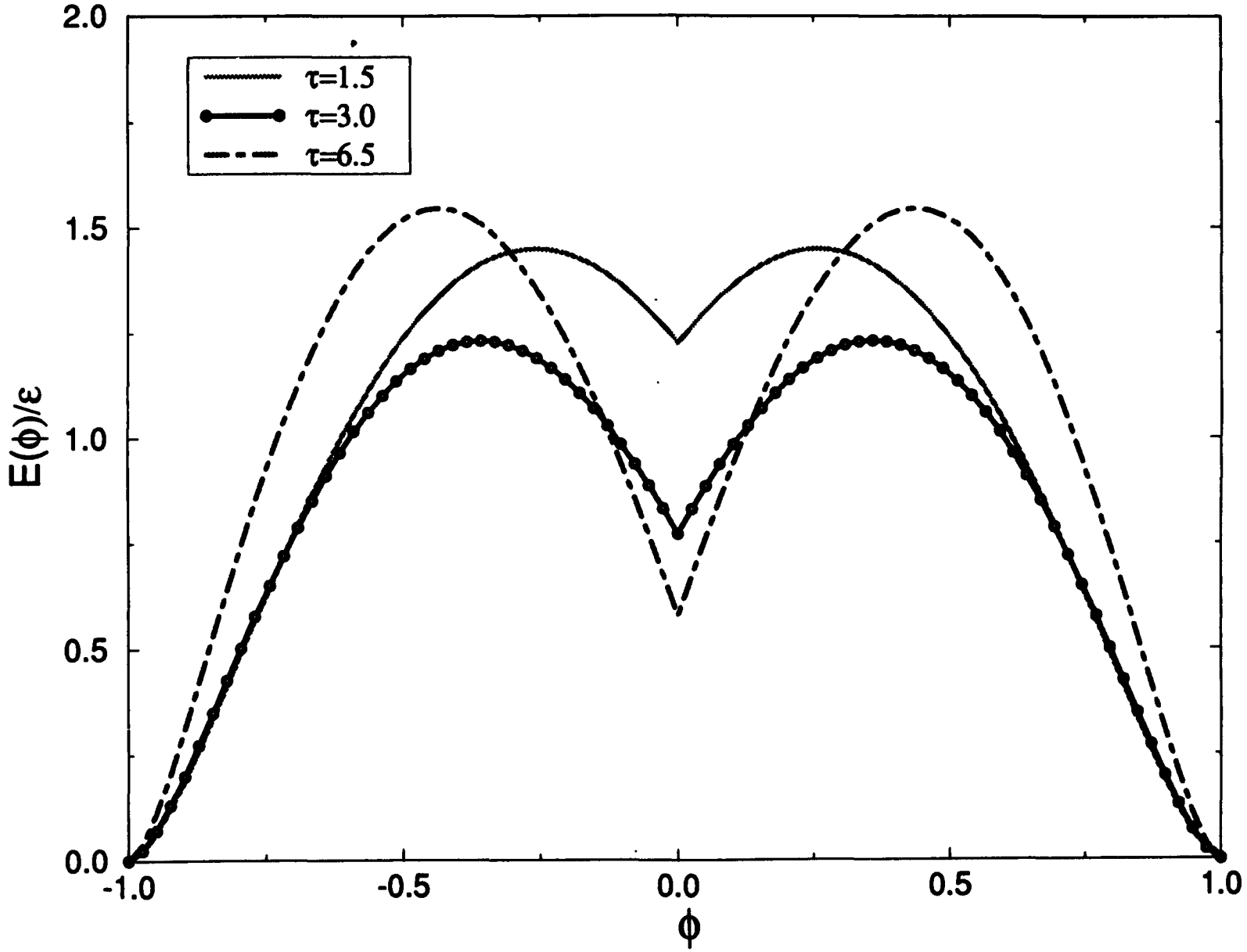

Fig. 1(b)

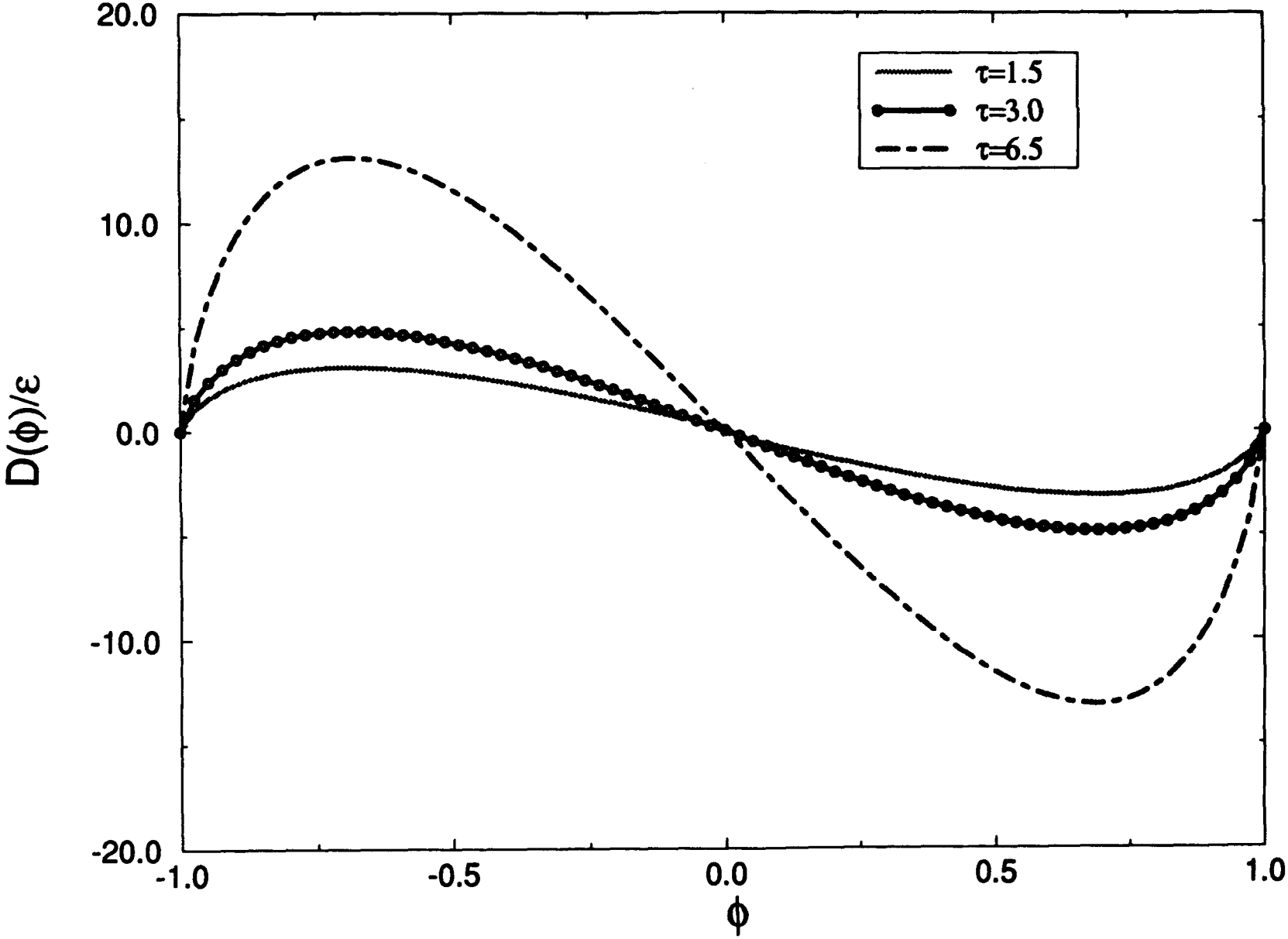

Fig. 1(c)

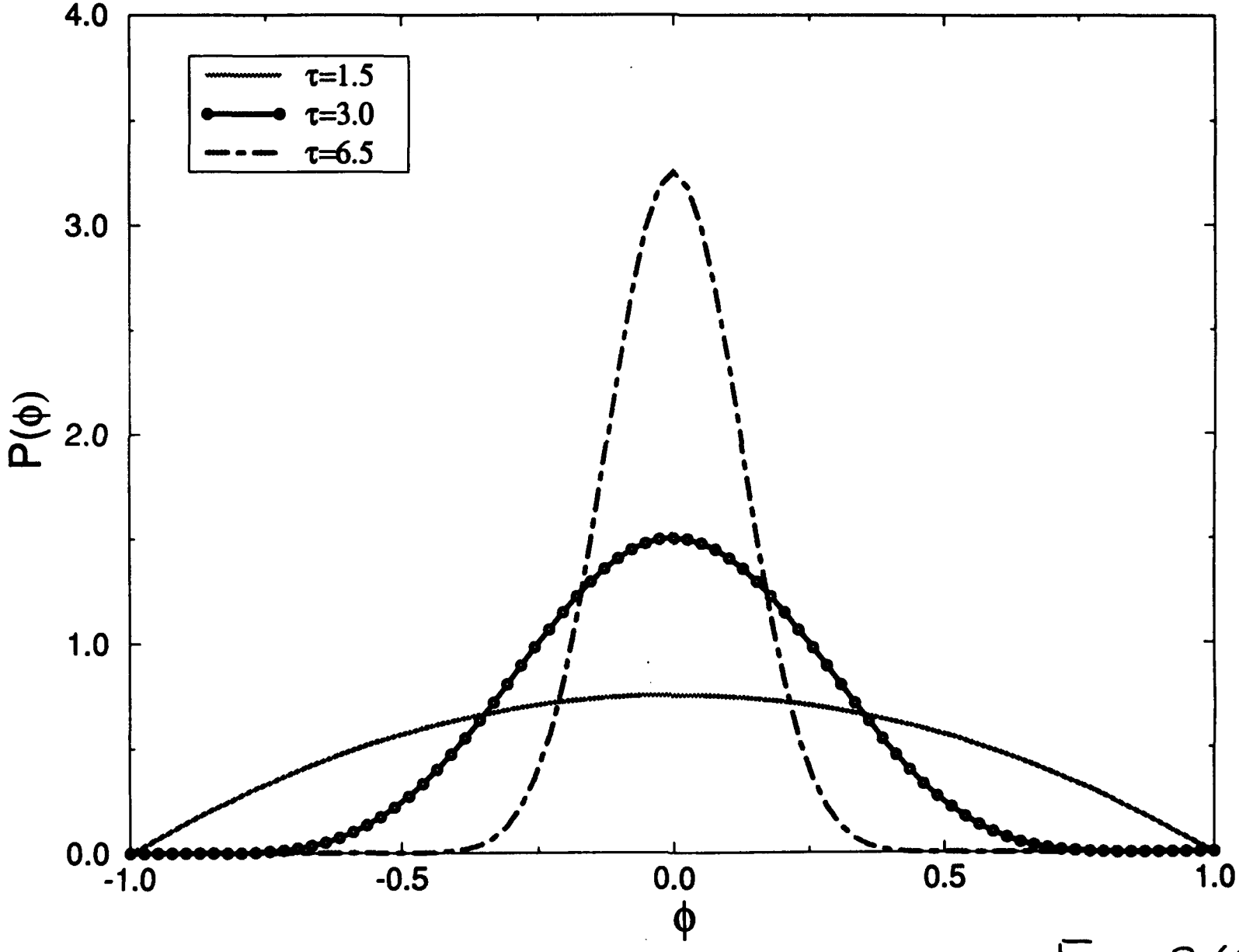

Fig. 2(a)

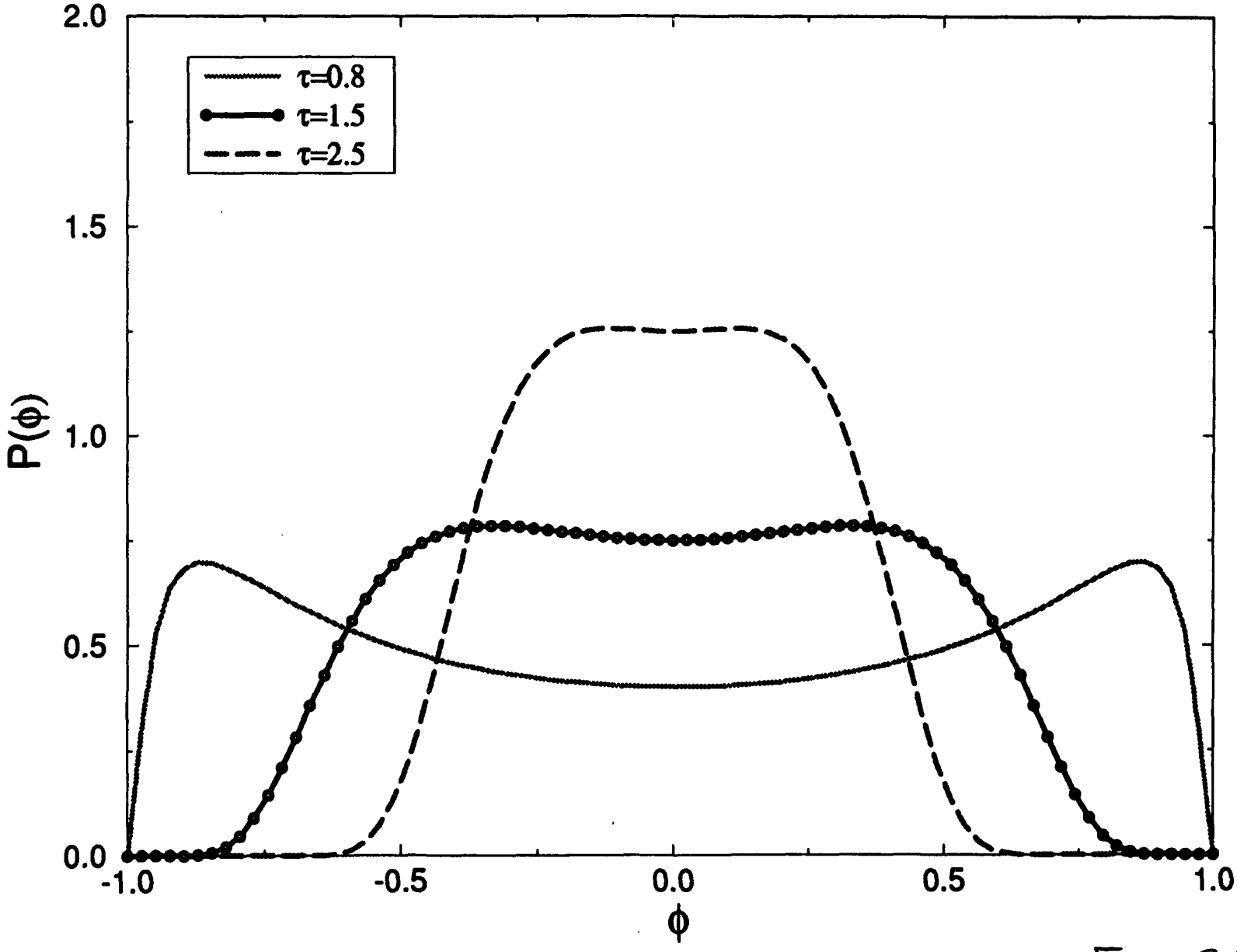

Fig. 2(b)

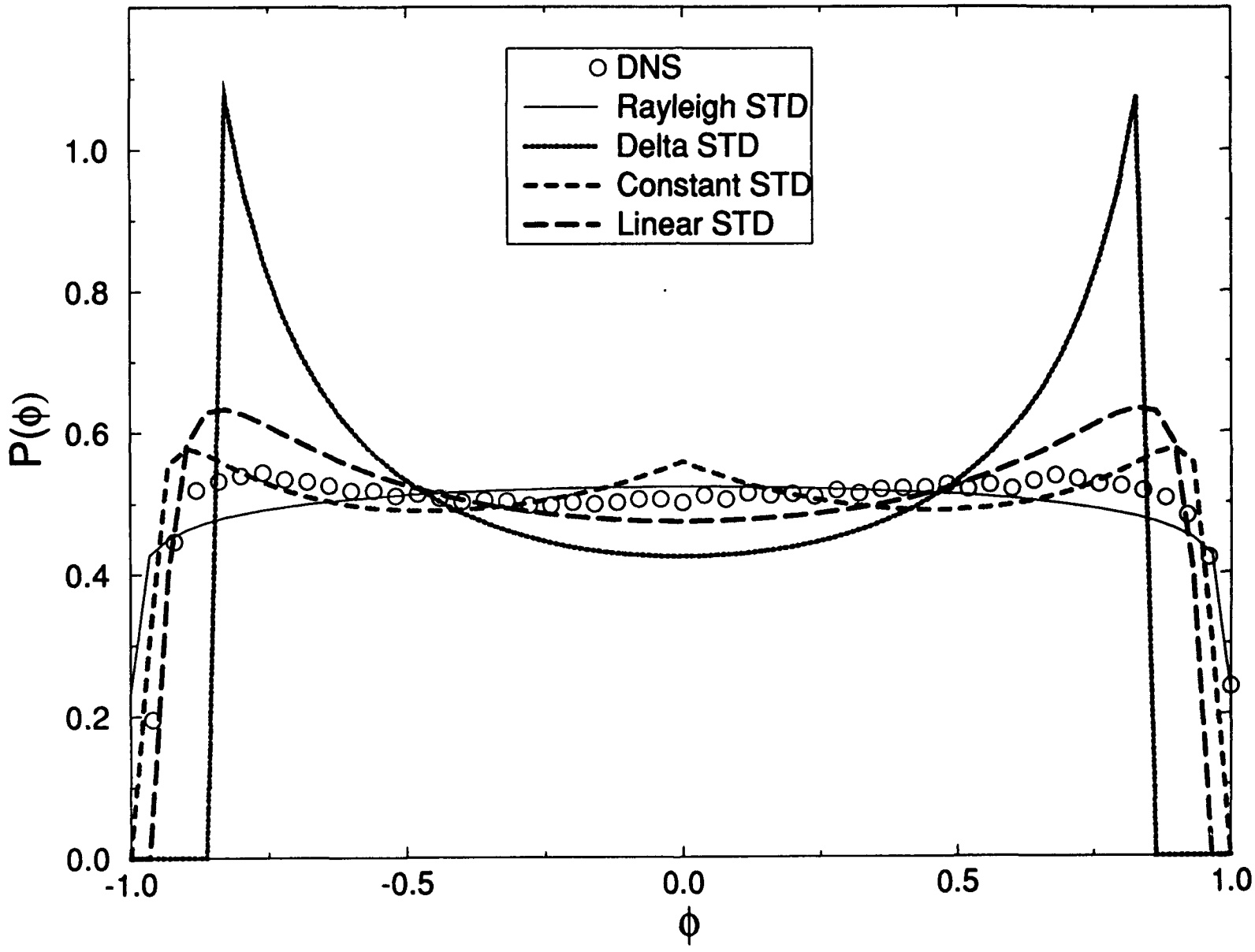
DNS
Rayleigh STD
Delta STD
Constant STD
Linear STD
P(ϕ)
ϕ
0.0
0.2
0.4
0.6
0.8
1.0
-1.0
-0.5
0.0
0.5
1.0

Fig. 3(a)

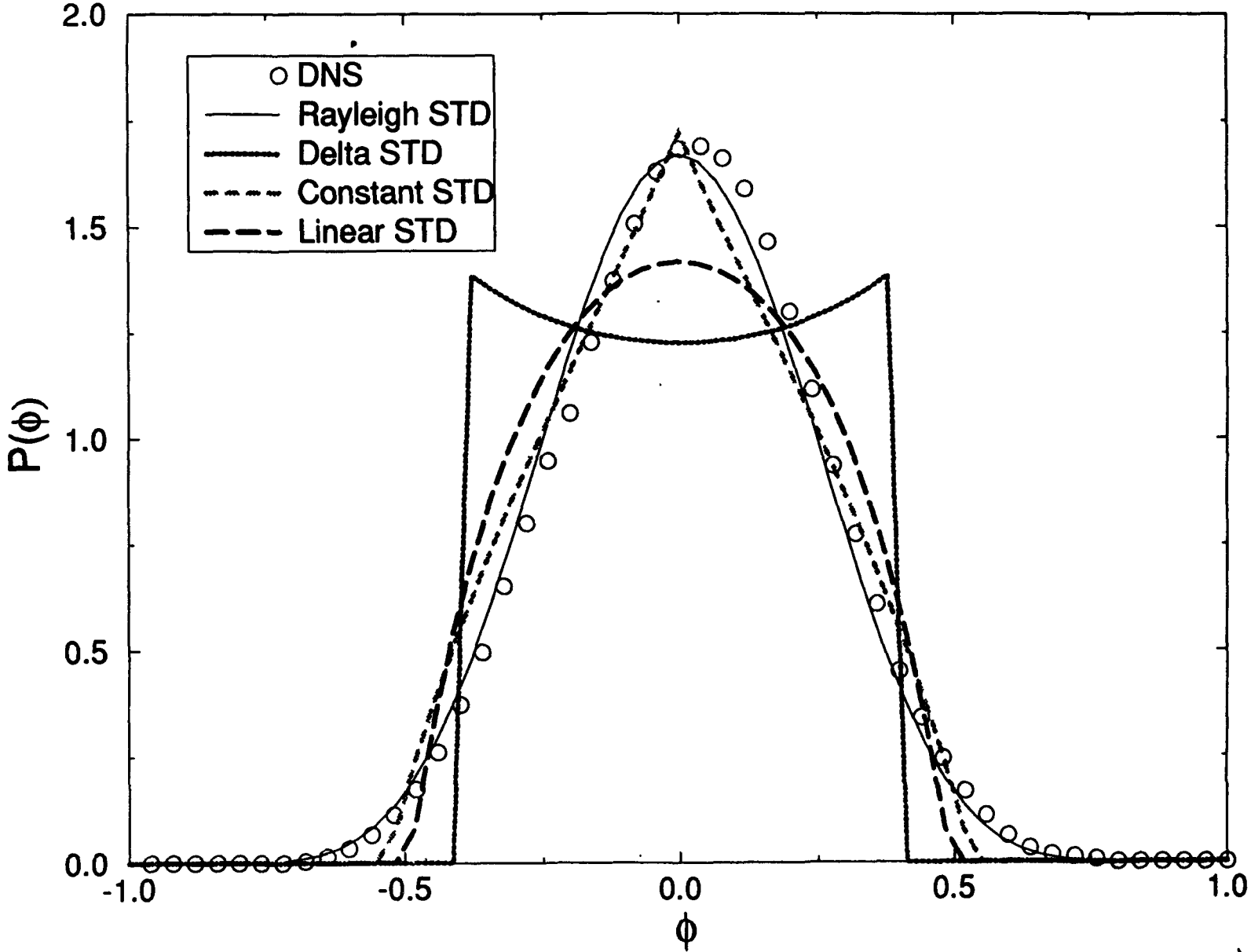
DNS
Rayleigh STD
Delta STD
Constant STD
Linear STD
P(ϕ)
ϕ
2.0
1.5
1.0
0.5
0.0
-1.0
-0.5
0.0
0.5
1.0

Fig. 3(b)

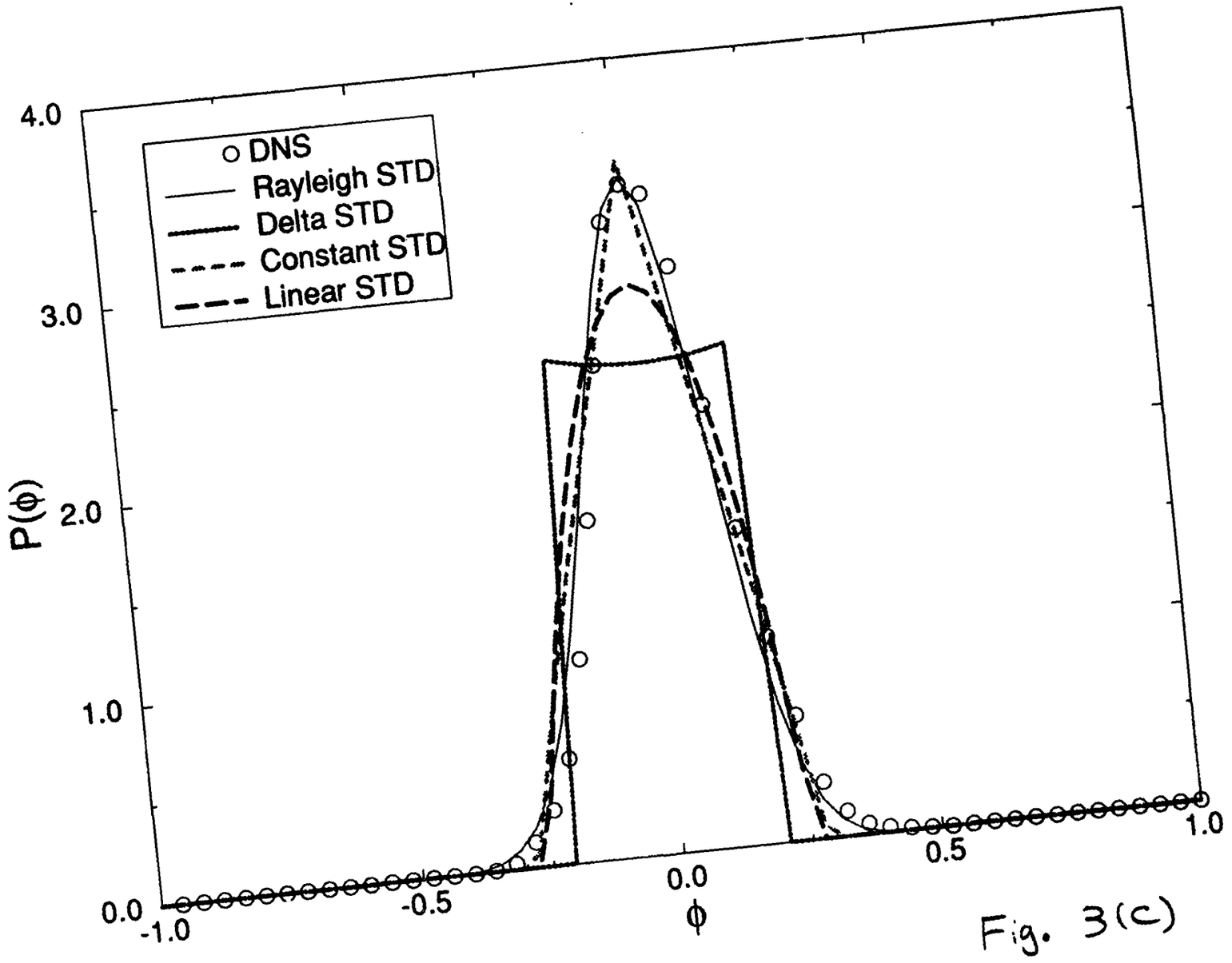
DNS
Rayleigh STD
Delta STD
Constant STD
Linear STD
4.0
3.0
2.0
1.0
0.0
P(ϕ)
-1.0
-0.5
0.0
0.5
1.0
ϕ

Fig. 3(c)

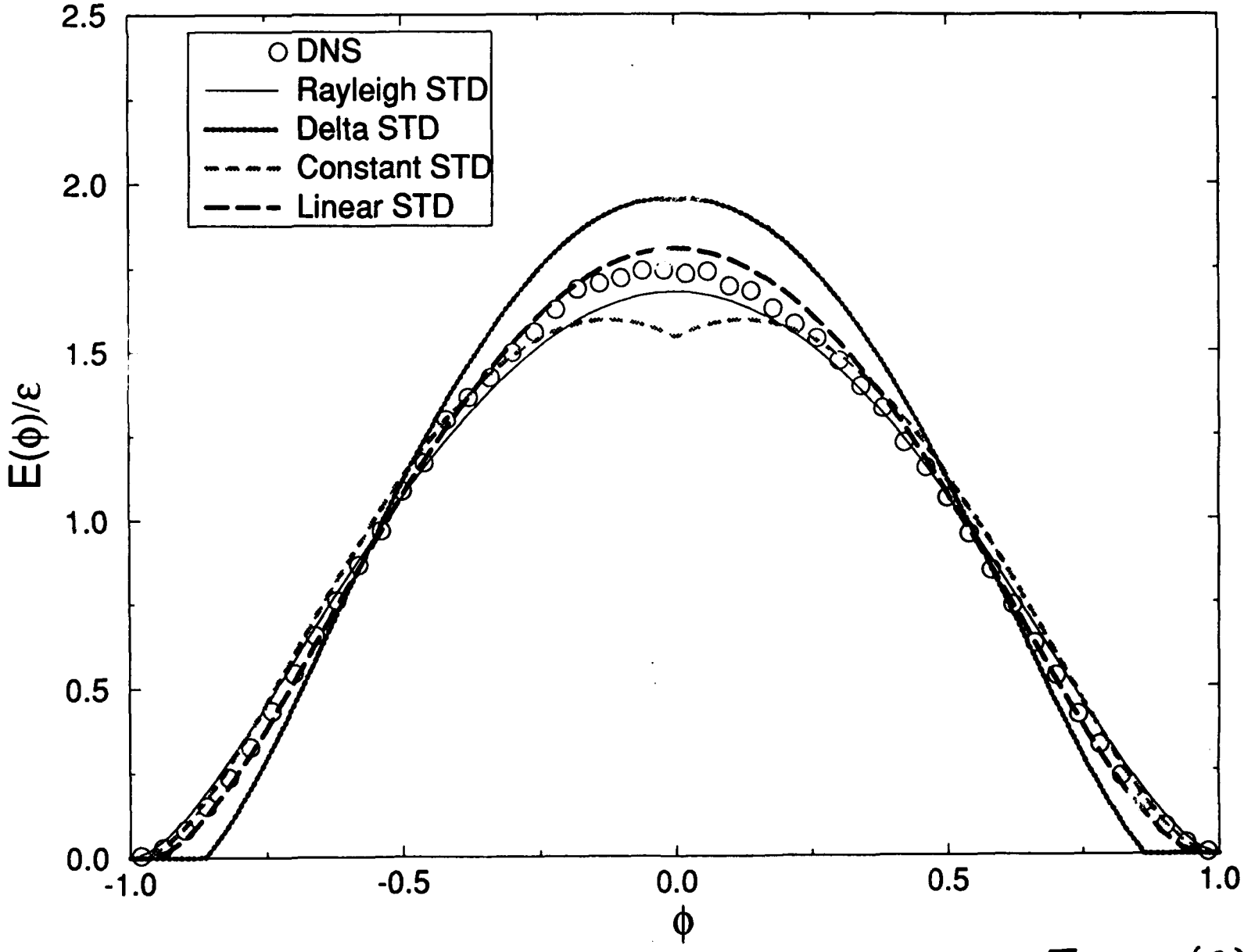
DNS
Rayleigh STD
Delta STD
Constant STD
Linear STD
2.5
2.0
1.5
1.0
0.5
0.0
E(ϕ)/ε
-1.0
-0.5
0.0
0.5
1.0
ϕ

Fig. 4(a)

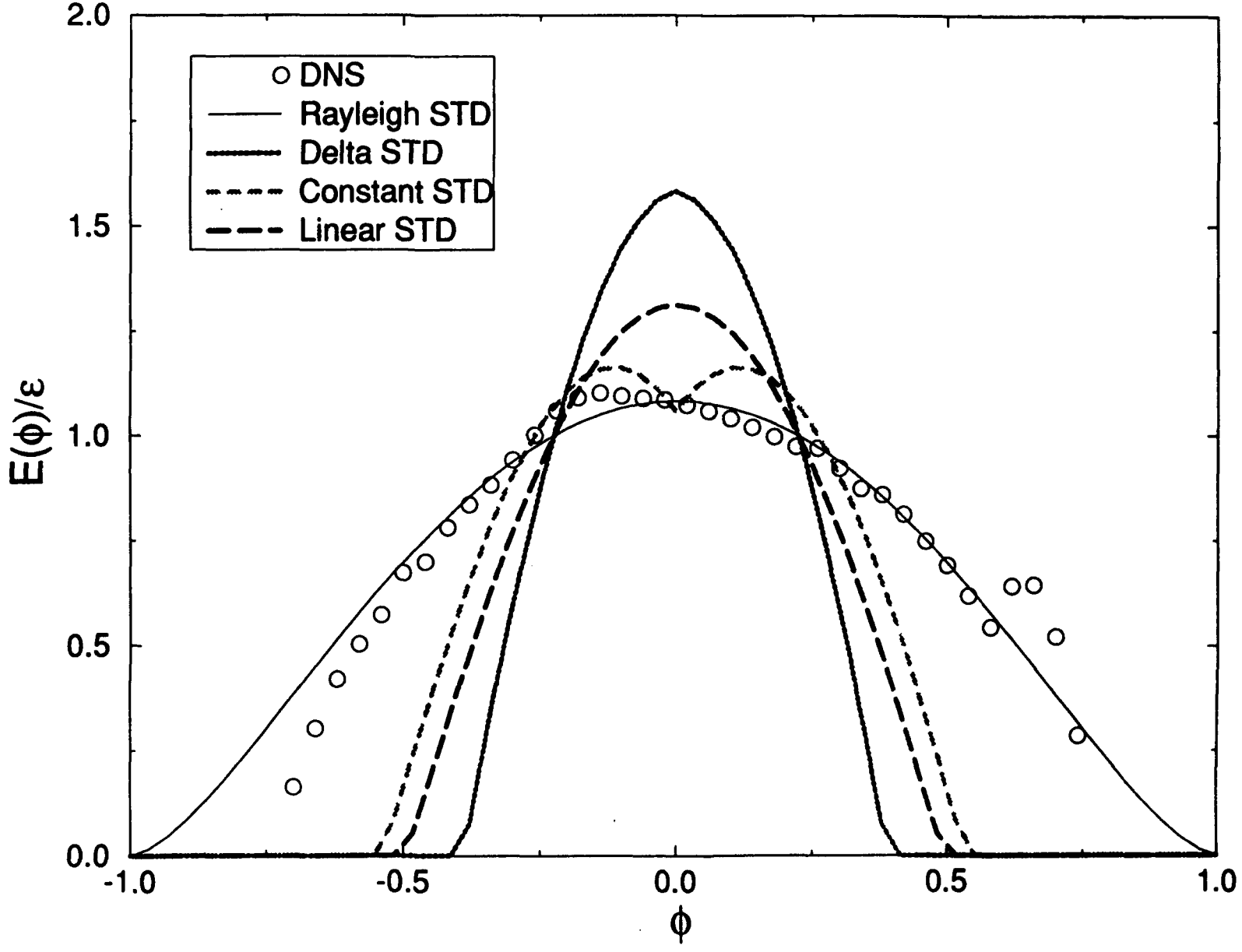
DNS
Rayleigh STD
Delta STD
Constant STD
Linear STD
E(ϕ)/ε
ϕ
2.0
1.5
1.0
0.5
0.0
-1.0
-0.5
0.0
0.5
1.0

Fig. 4(b)

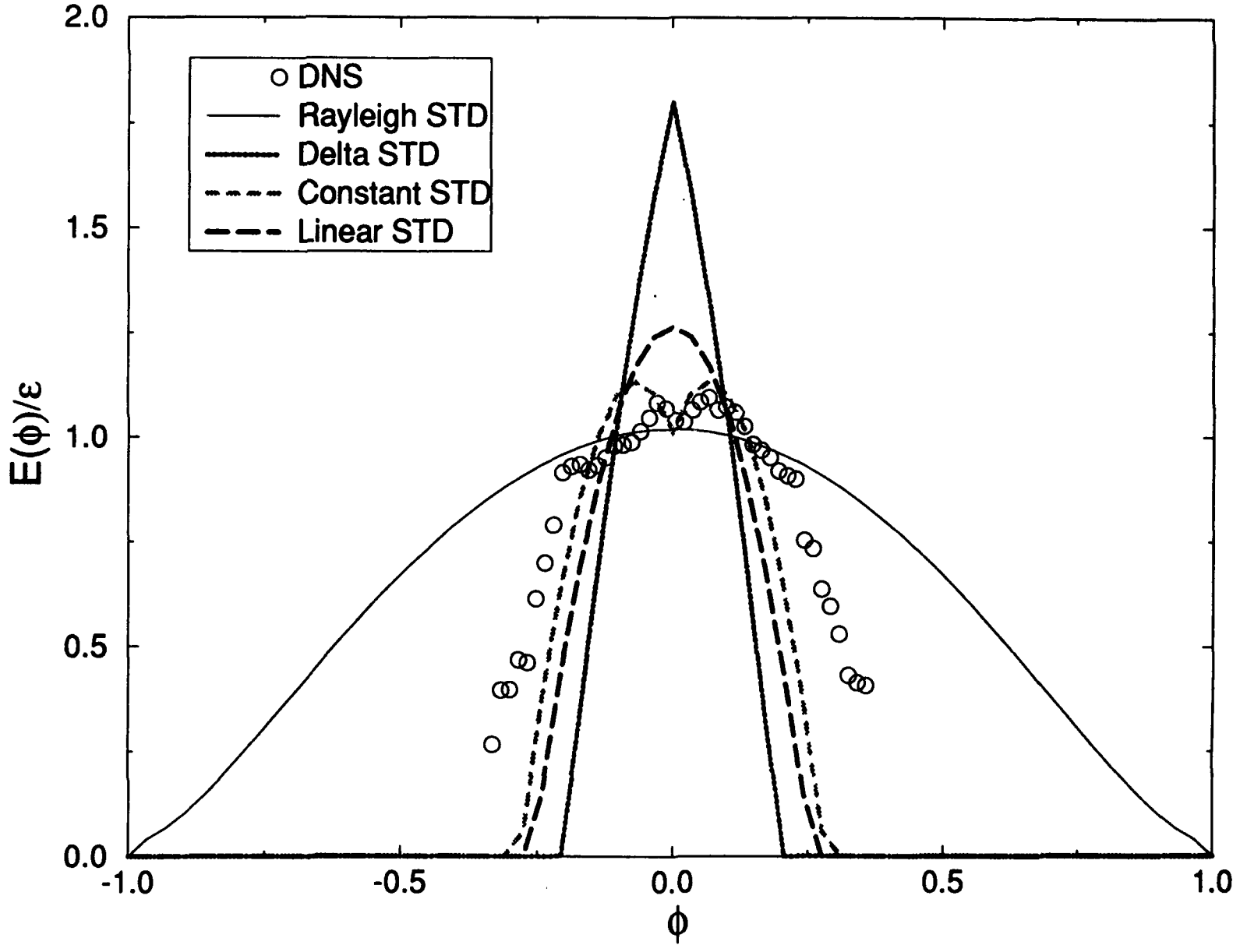
DNS
Rayleigh STD
Delta STD
Constant STD
Linear STD
E(ϕ)/ε
ϕ
2.0
1.5
1.0
0.5
0.0
-1.0
-0.5
0.0
0.5
1.0

Fig. 4(c)

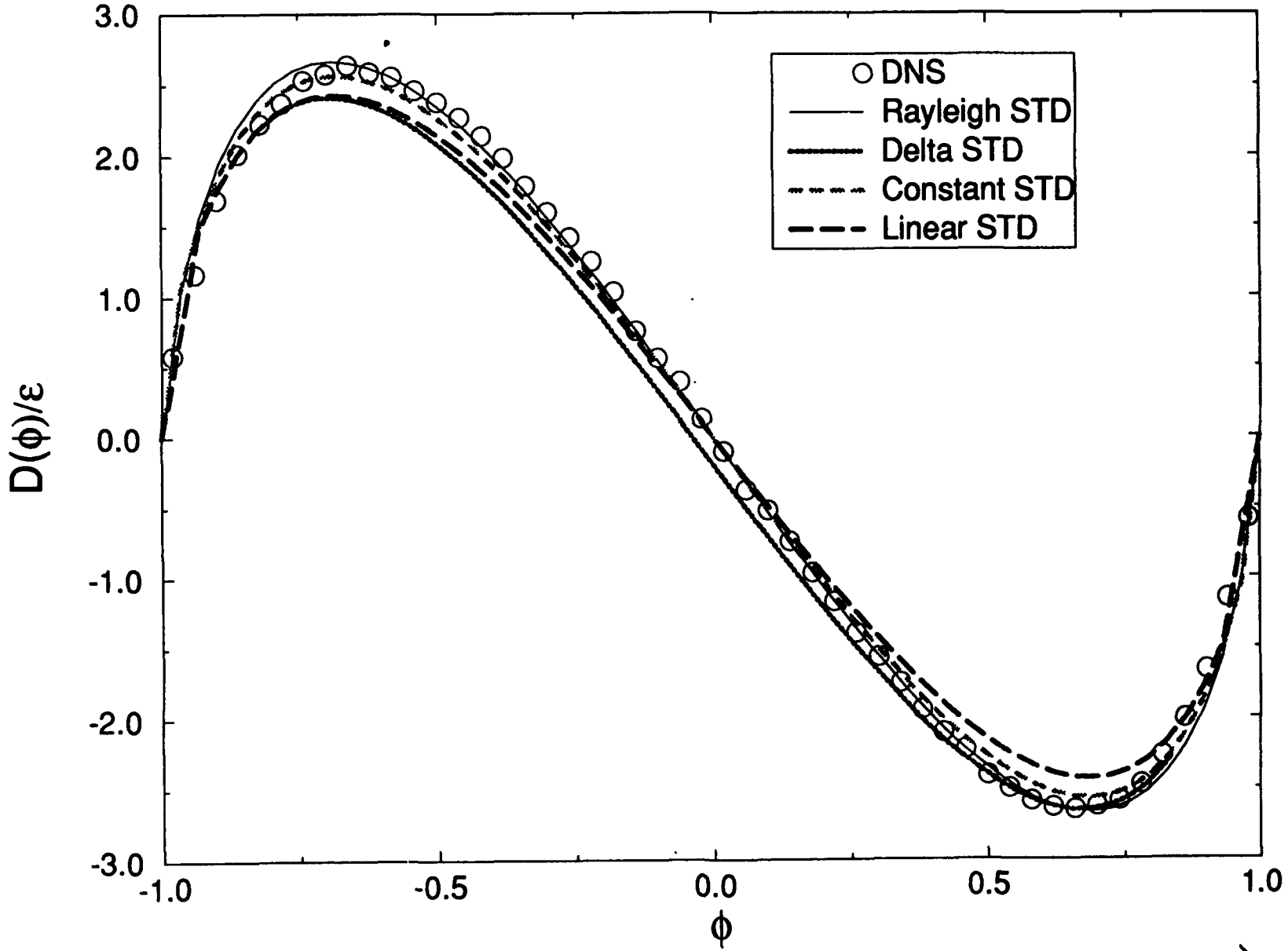
DNS
Rayleigh STD
Delta STD
Constant STD
Linear STD
D(ϕ)/ε
ϕ
3.0
2.0
1.0
0.0
-1.0
-2.0
-3.0
-1.0
-0.5
0.0
0.5
1.0

Fig. 5(a)

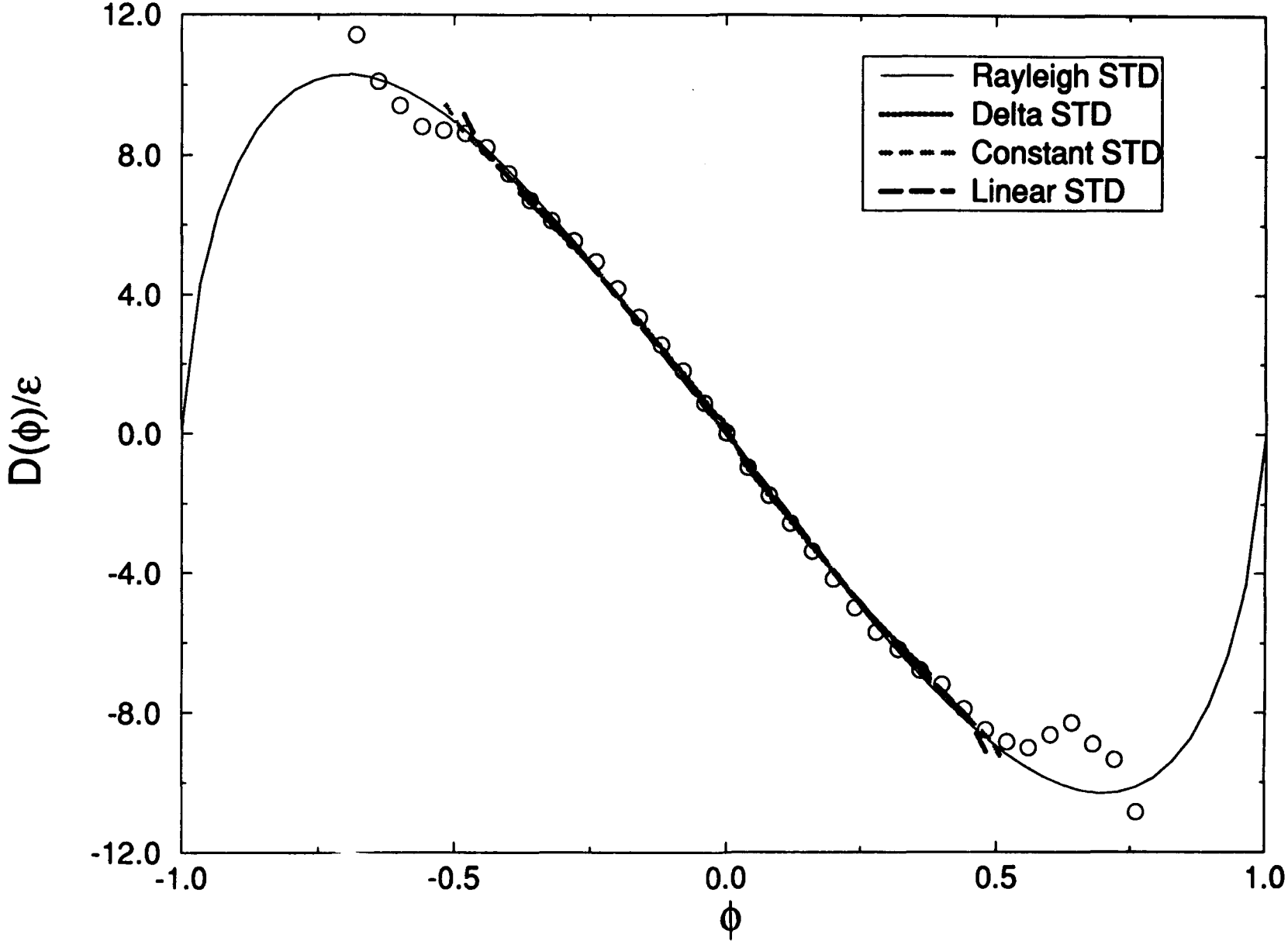
12.0
8.0
4.0
0.0
-4.0
-8.0
-12.0
-1.0
-0.5
0.0
0.5
1.0
D(ϕ)/ε
ϕ
Rayleigh STD
Delta STD
Constant STD
Linear STD

Fig 5(b)

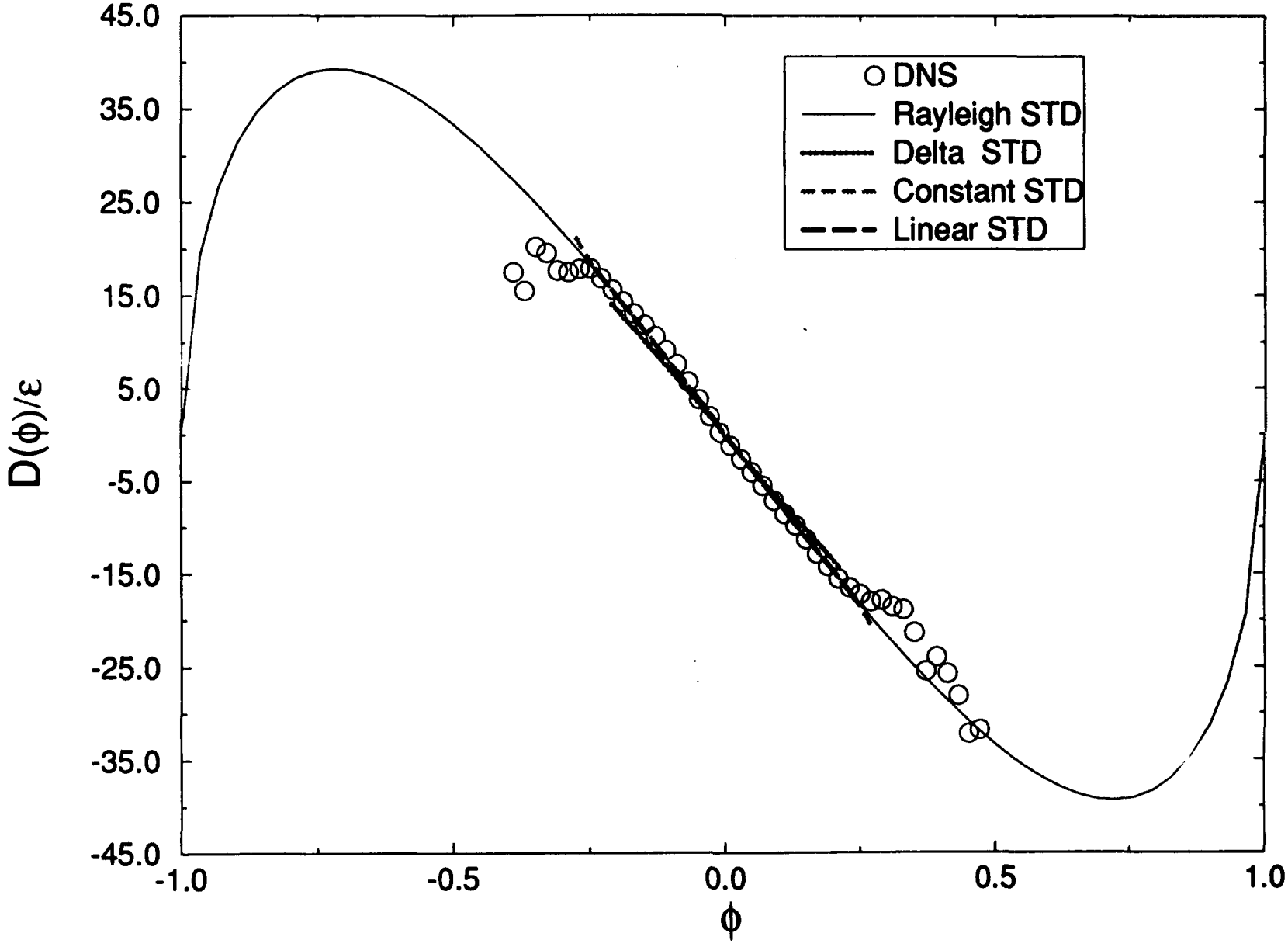
45.0
35.0
25.0
15.0
5.0
-5.0
-15.0
-25.0
-35.0
-45.0
-1.0
-0.5
0.0
0.5
1.0
D(ϕ)/ε
ϕ
DNS
Rayleigh STD
Delta STD
Constant STD
Linear STD

Fig. 5(c)

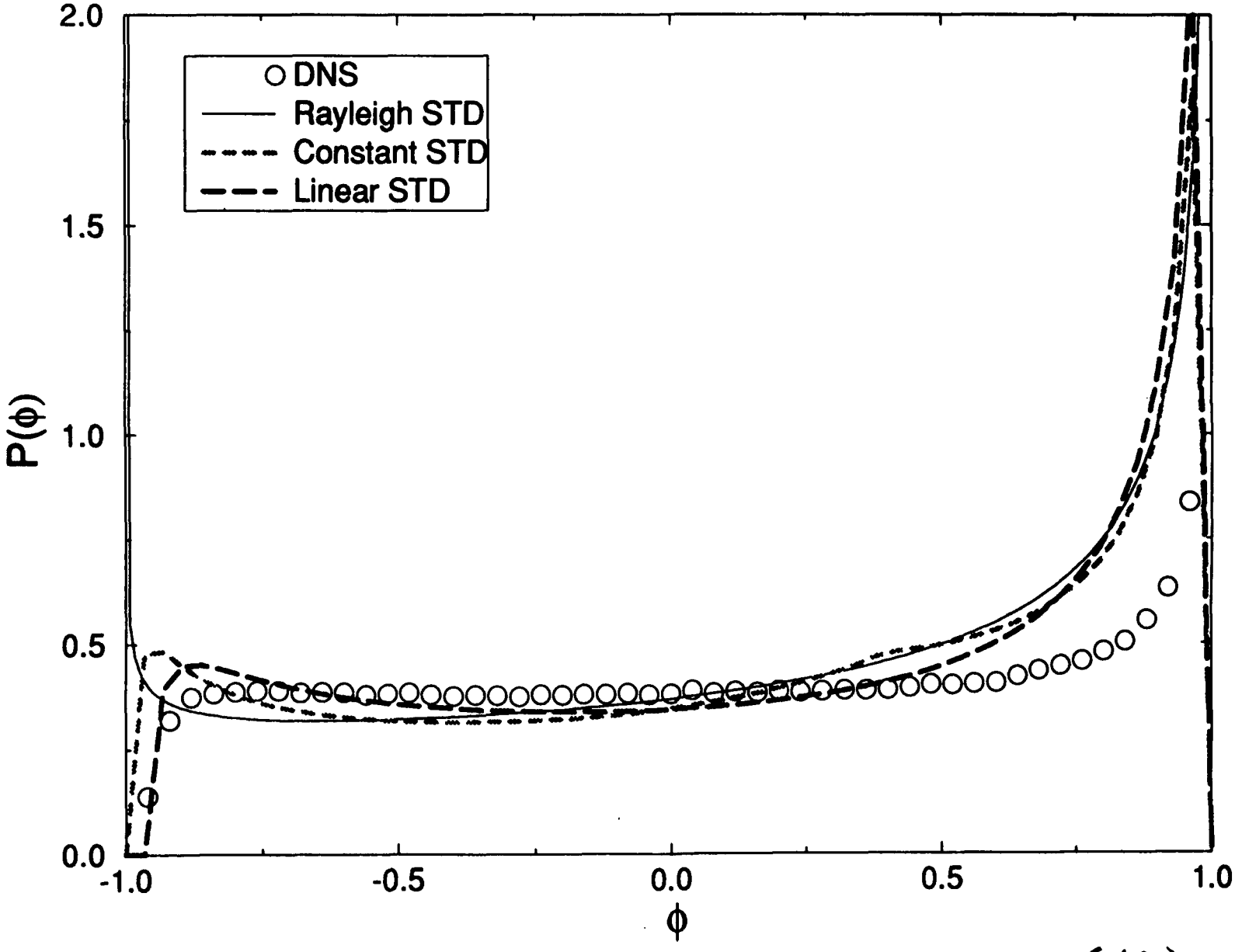
DNS
Rayleigh STD
Constant STD
Linear STD
P(ϕ)
ϕ
2.0
1.5
1.0
0.5
0.0
-1.0
-0.5
0.0
0.5
1.0

Fig. 6(a)

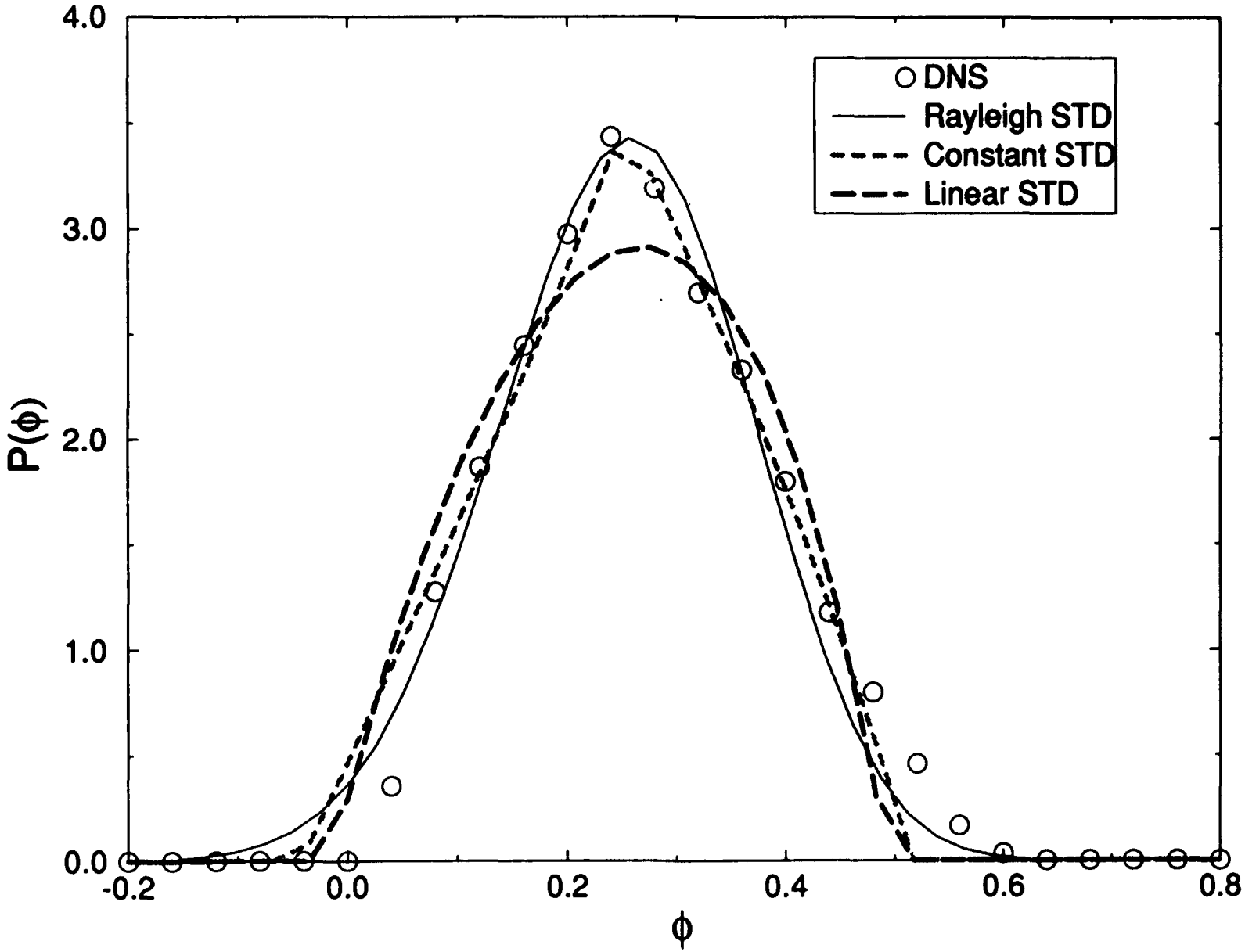
4.0
3.0
2.0
1.0
0.0
P(ϕ)
-0.2
0.0
0.2
0.4
0.6
0.8
ϕ
DNS
Rayleigh STD
Constant STD
Linear STD

Fig. 6(b)

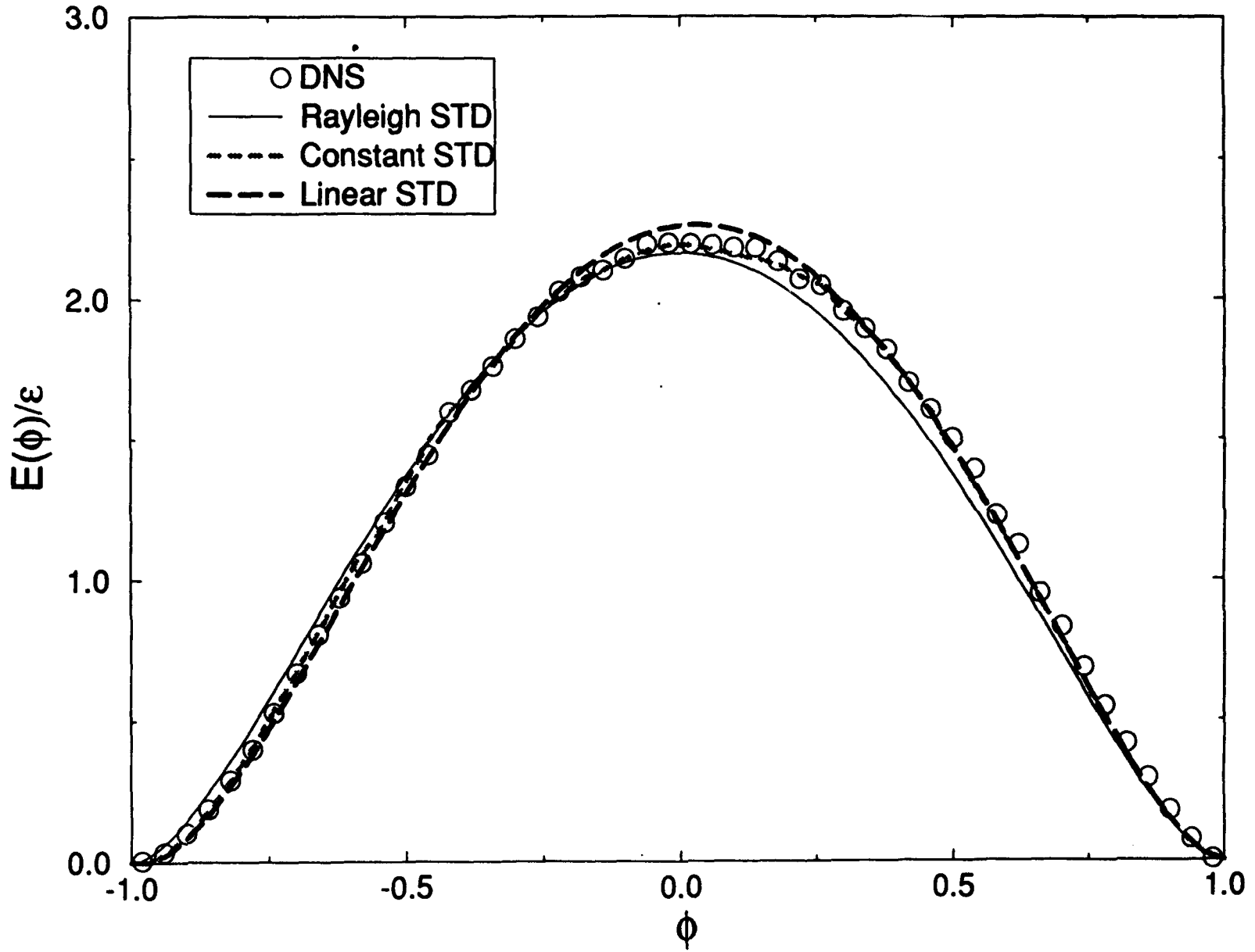
3.0
2.0
1.0
0.0
E(ϕ)/ε
DNS
Rayleigh STD
Constant STD
Linear STD
-1.0
-0.5
0.0
0.5
1.0
ϕ

Fig. 7(a)

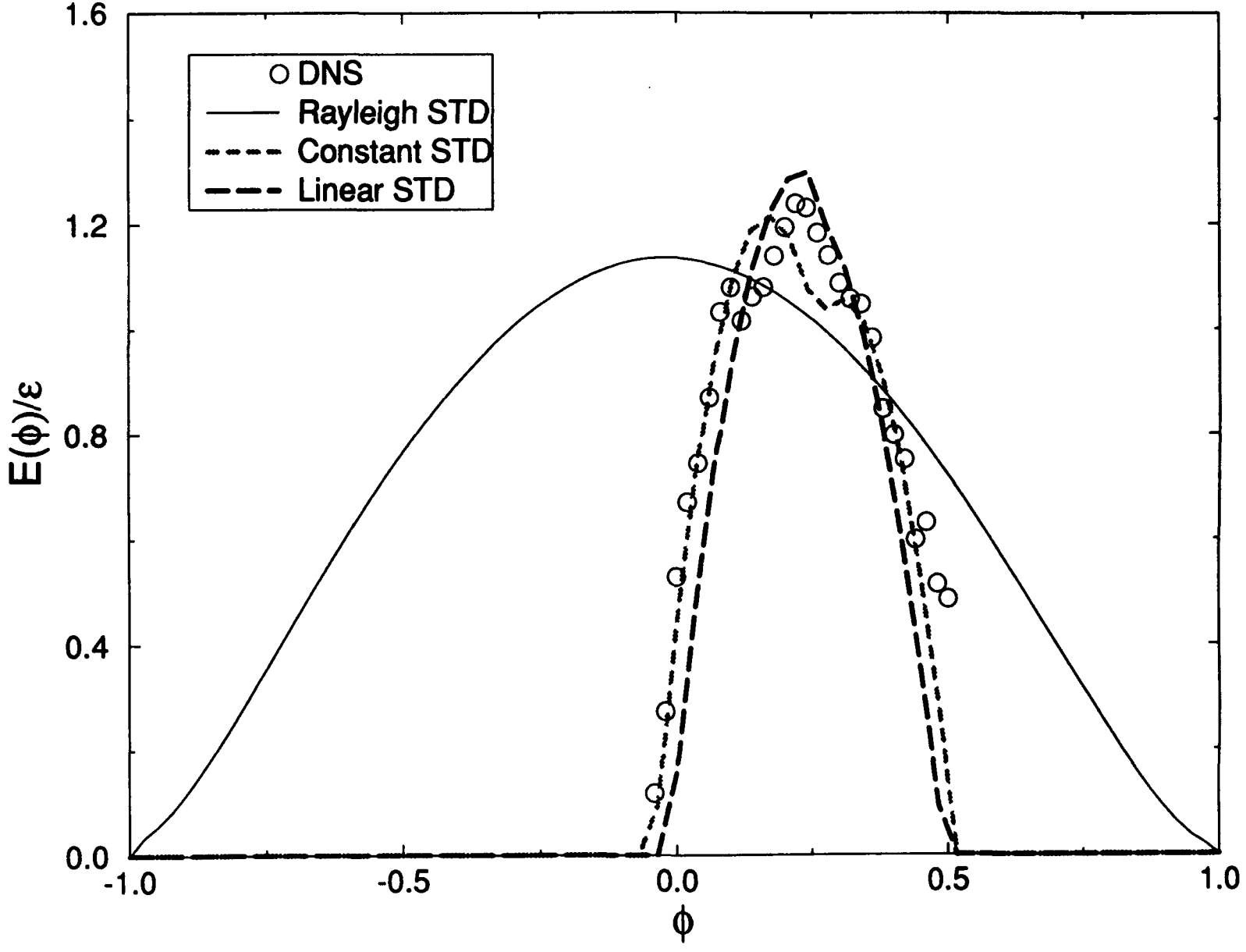
DNS
Rayleigh STD
Constant STD
Linear STD
E(ϕ)/ε
ϕ
1.6
1.2
0.8
0.4
0.0
-1.0
-0.5
0.0
0.5
1.0

Fg. 7(b)

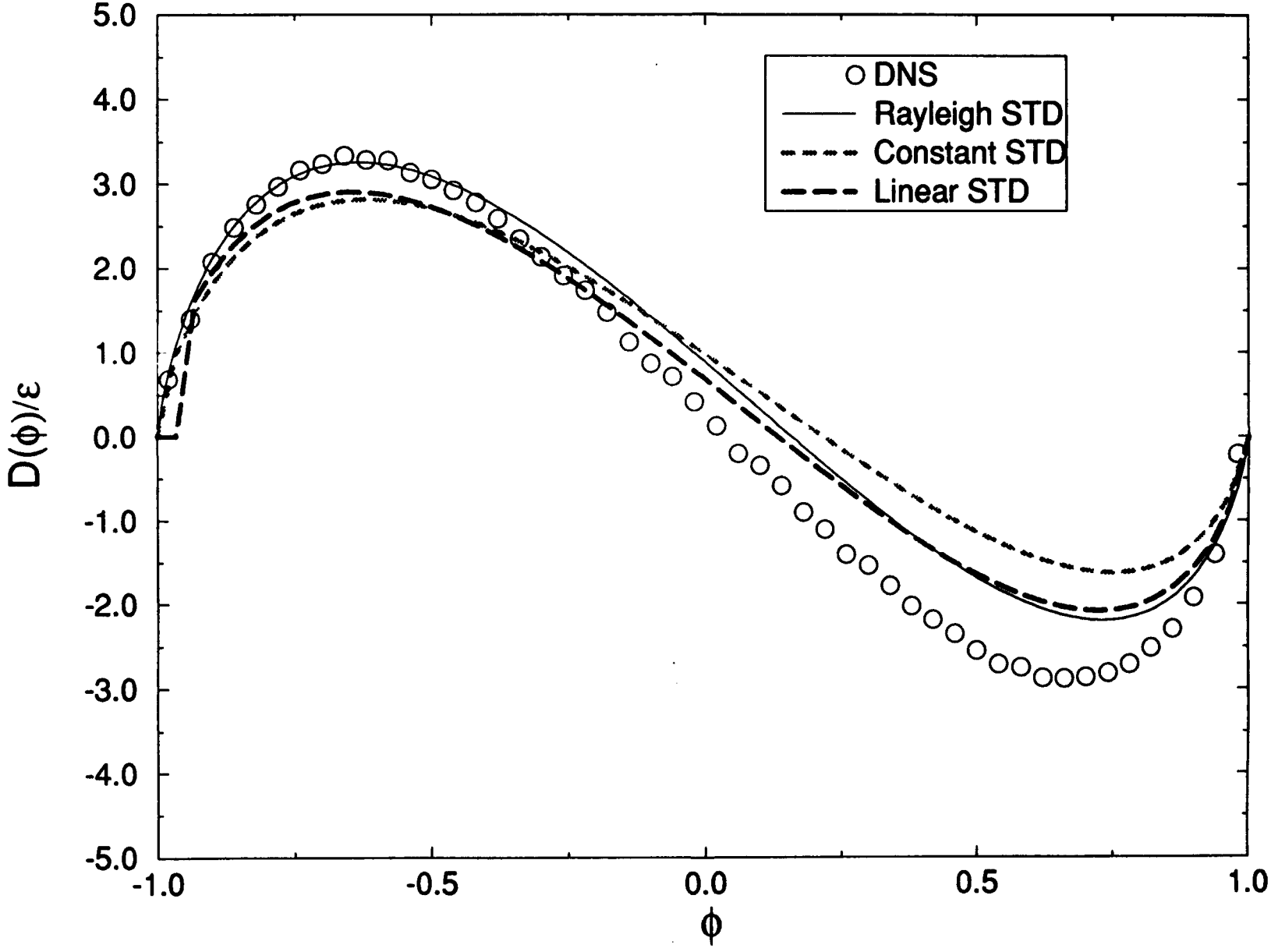
DNS
Rayleigh STD
Constant STD
Linear STD
D(ϕ)/ε
ϕ
5.0
4.0
3.0
2.0
1.0
0.0
-1.0
-2.0
-3.0
-4.0
-5.0
-1.0
-0.5
0.0
0.5
1.0

Fig. 8(a)

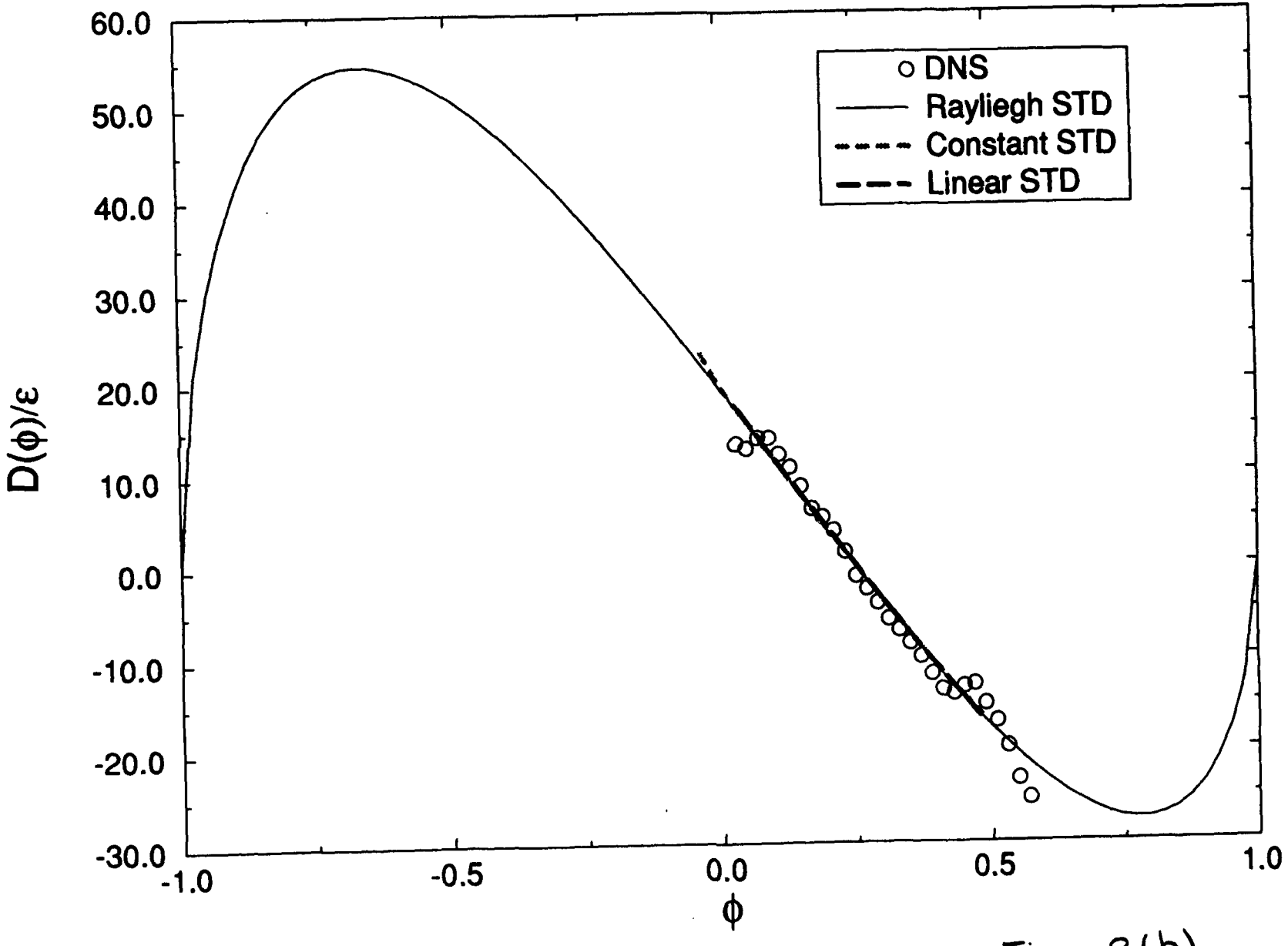
DNS
Rayliegh STD
Constant STD
Linear STD
D(φ)/ε
φ
60.0
50.0
40.0
30.0
20.0
10.0
0.0
-10.0
-20.0
-30.0
-1.0
-0.5
0.0
0.5
1.0

Fig. 8(b)

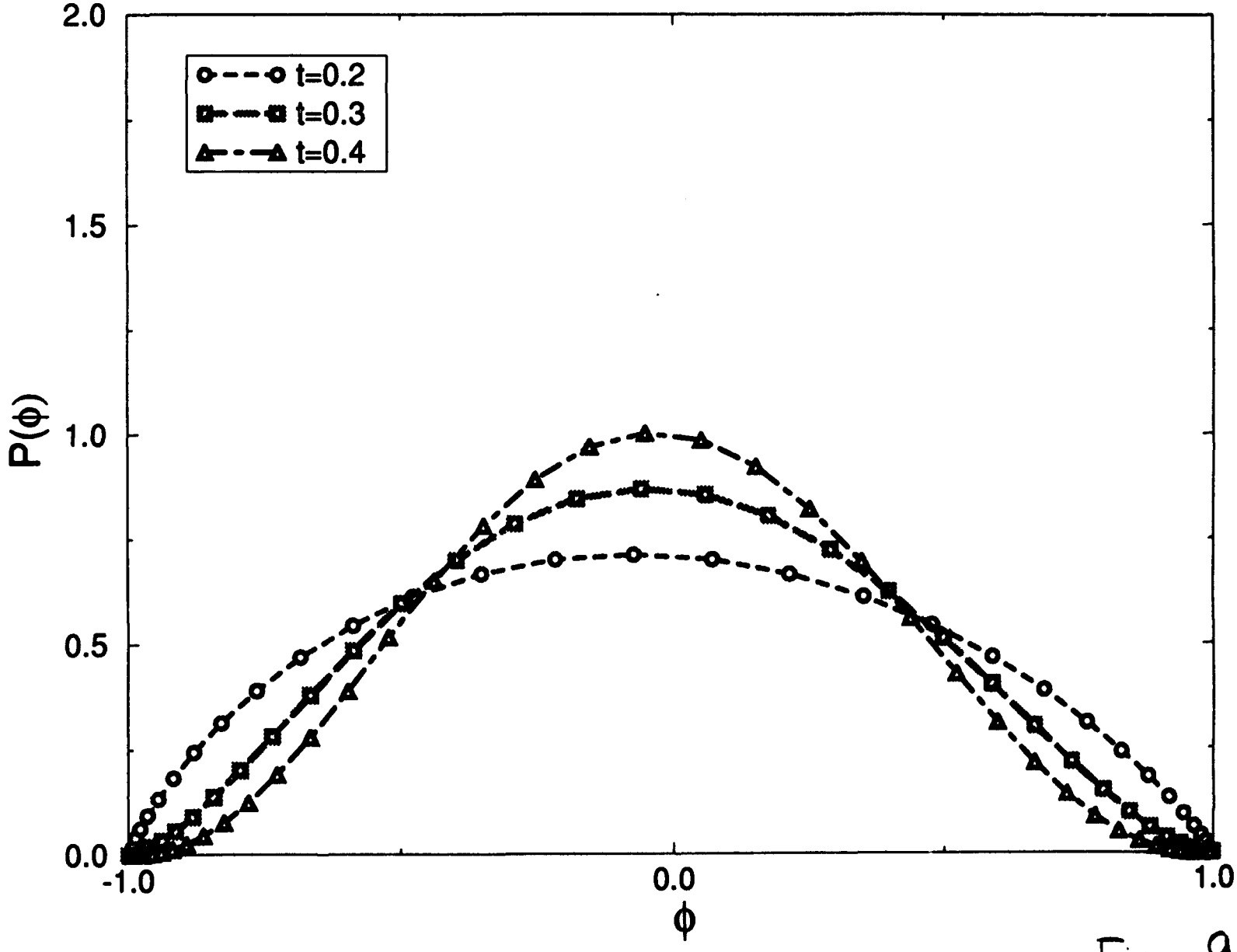

Fig. 9(a)

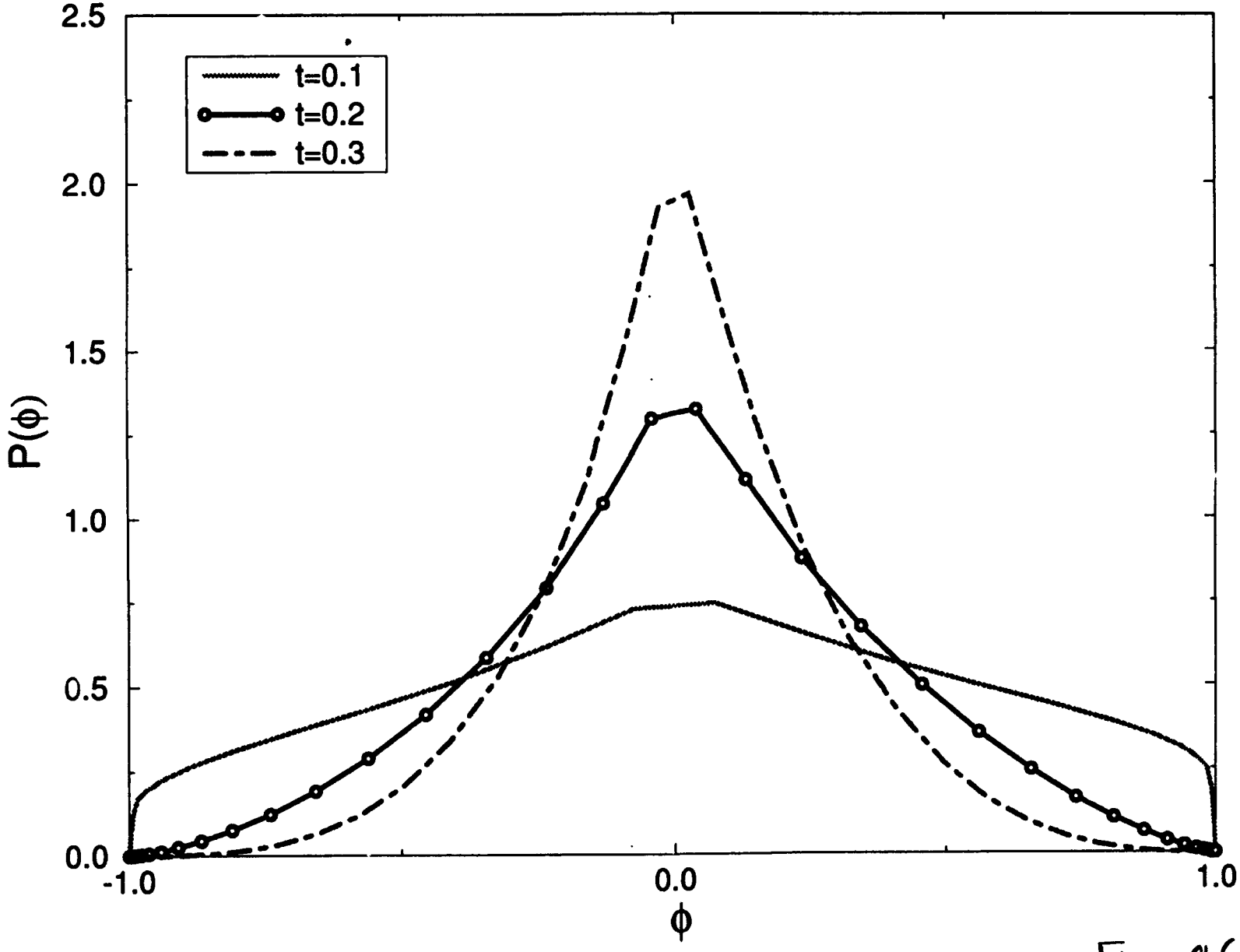

Fig. 9(b)

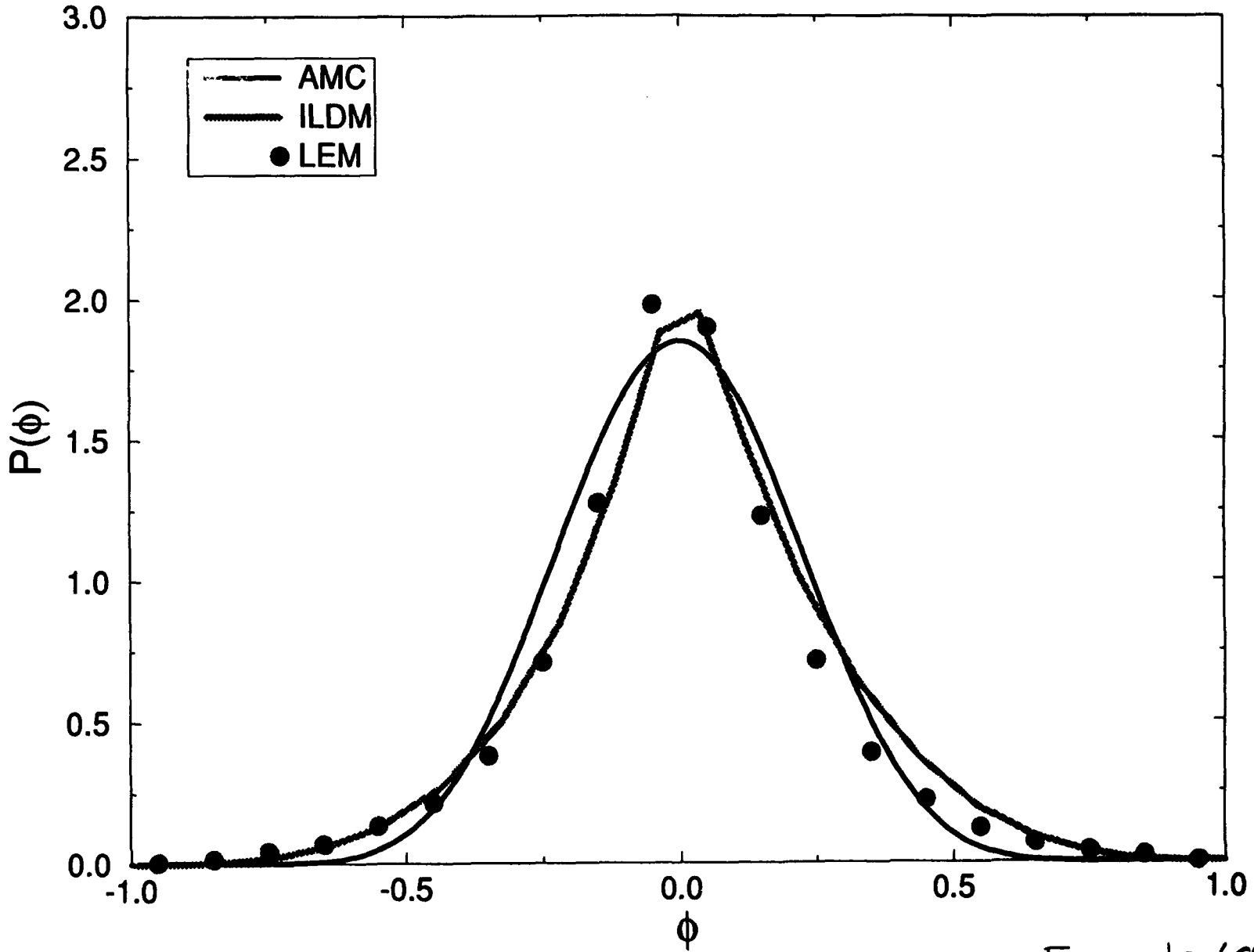

Fig. 10(a)

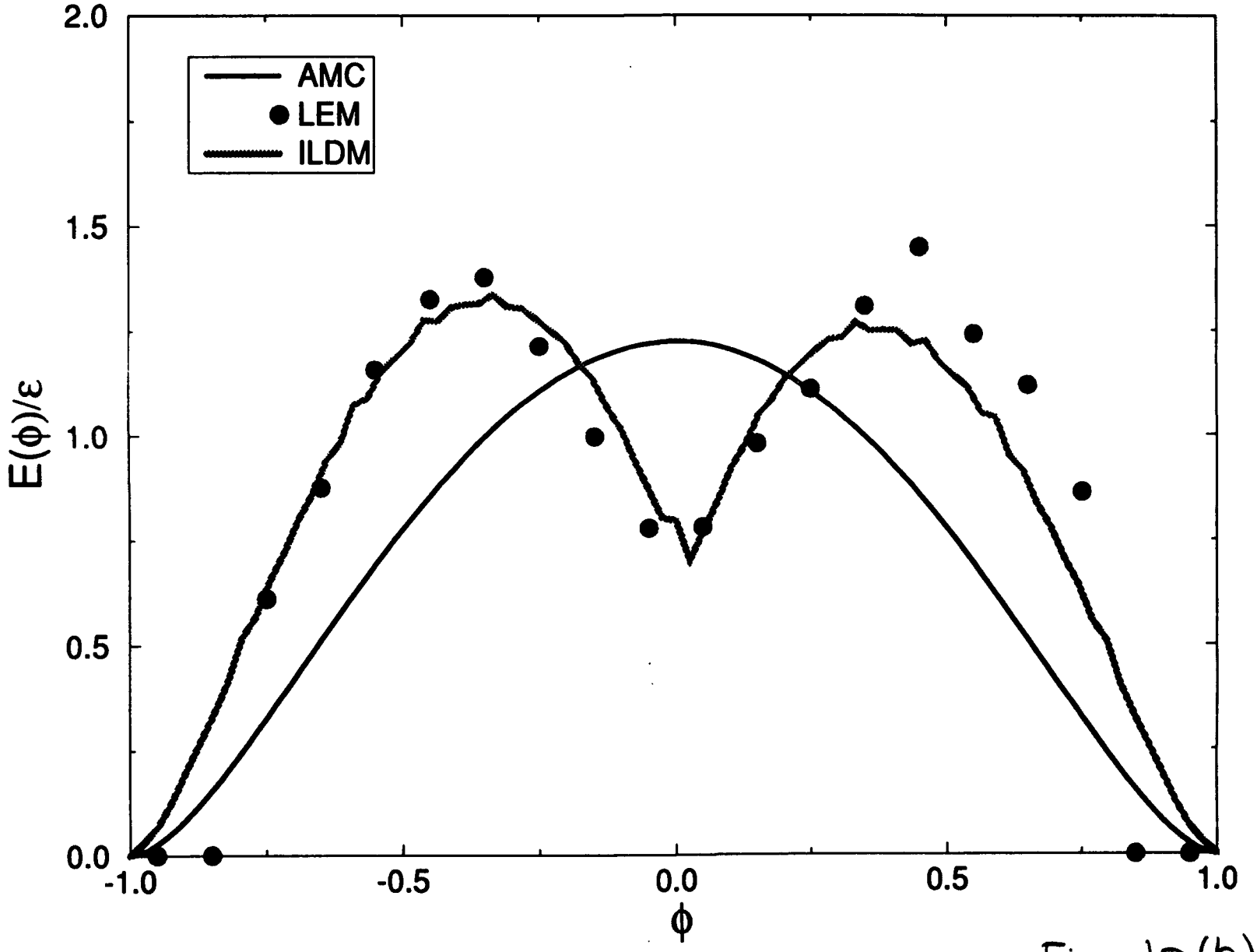

Fig. 10(b)

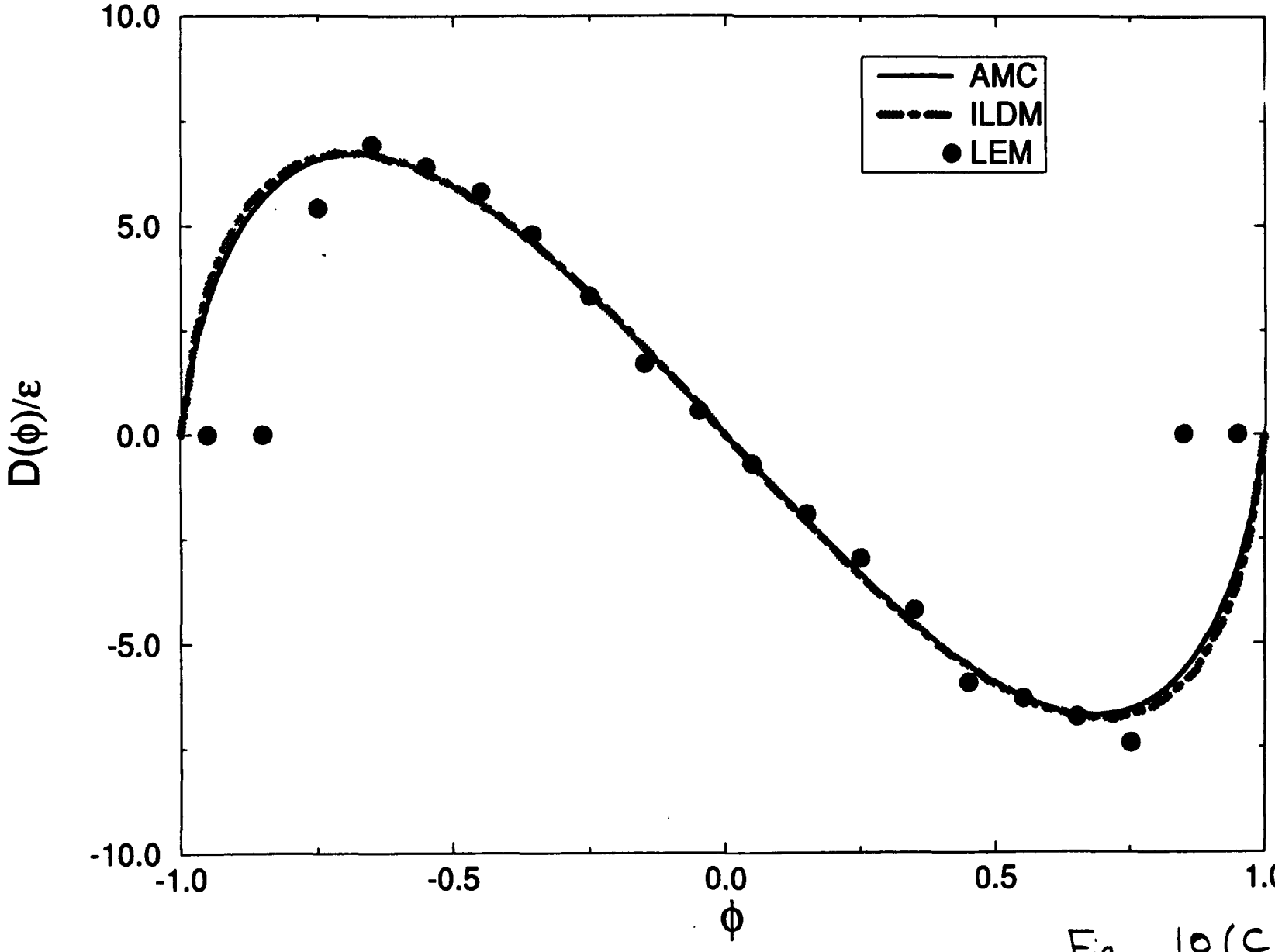

Fig. 10(c)

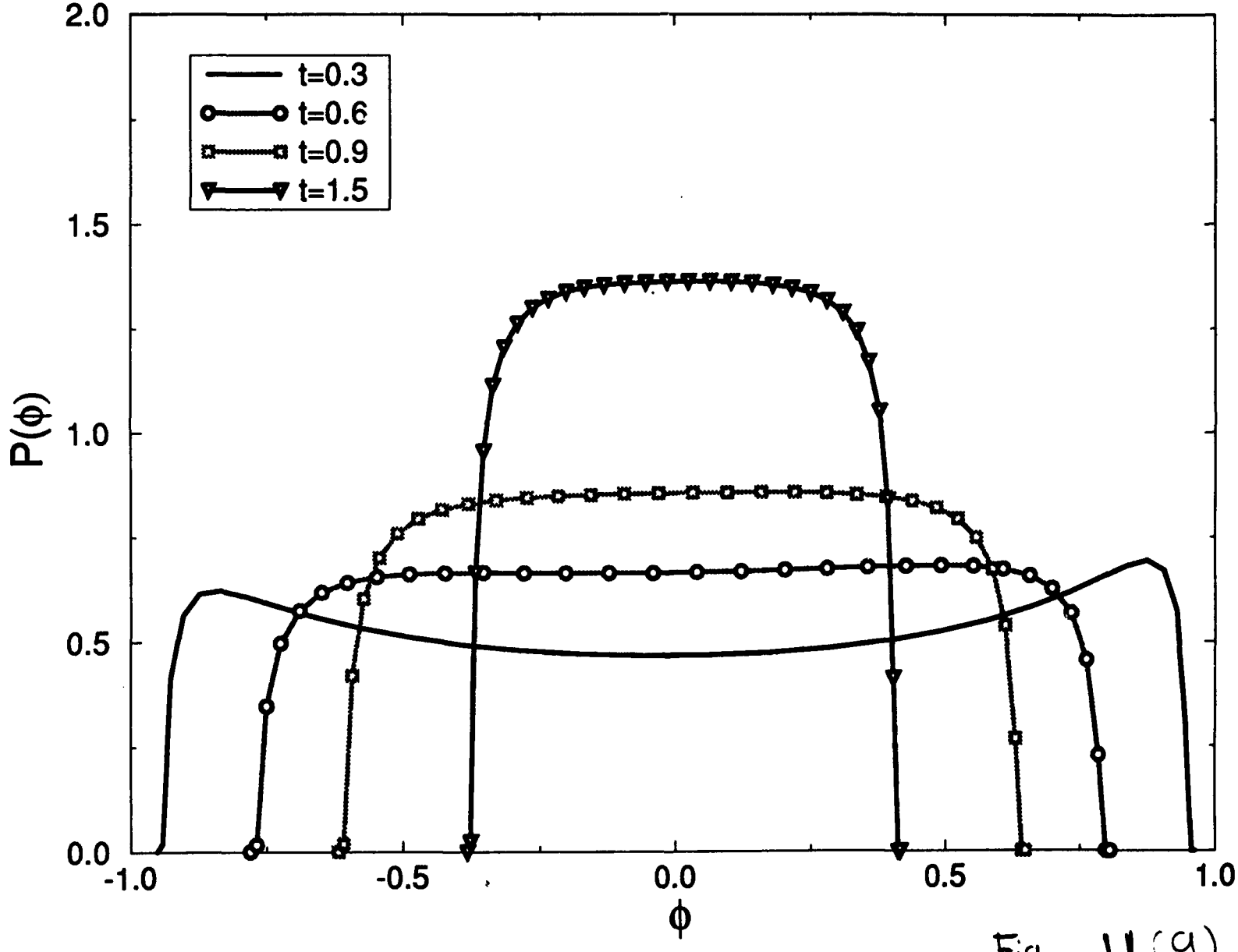

Fig. 11 (a)

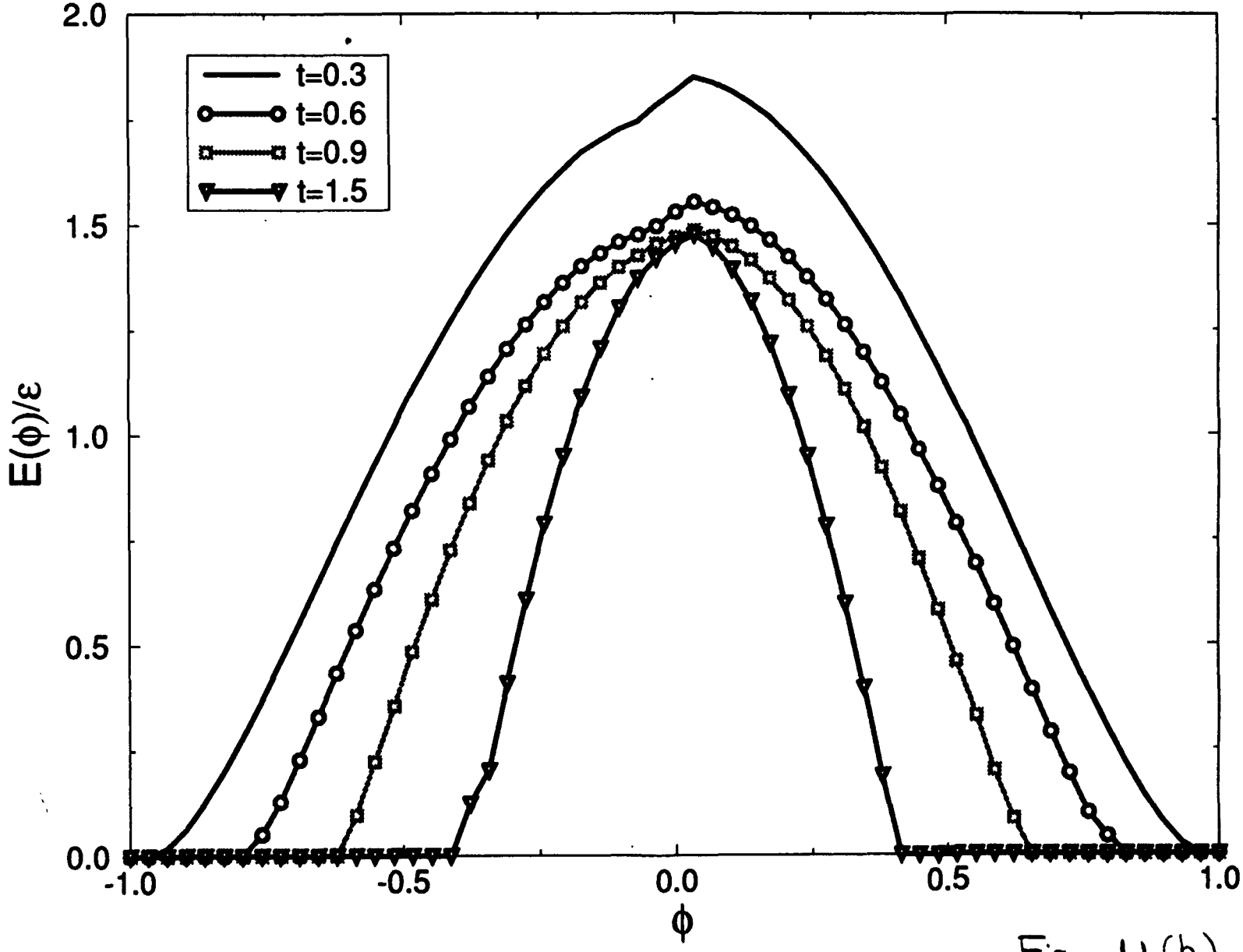

Fig. 11(b)

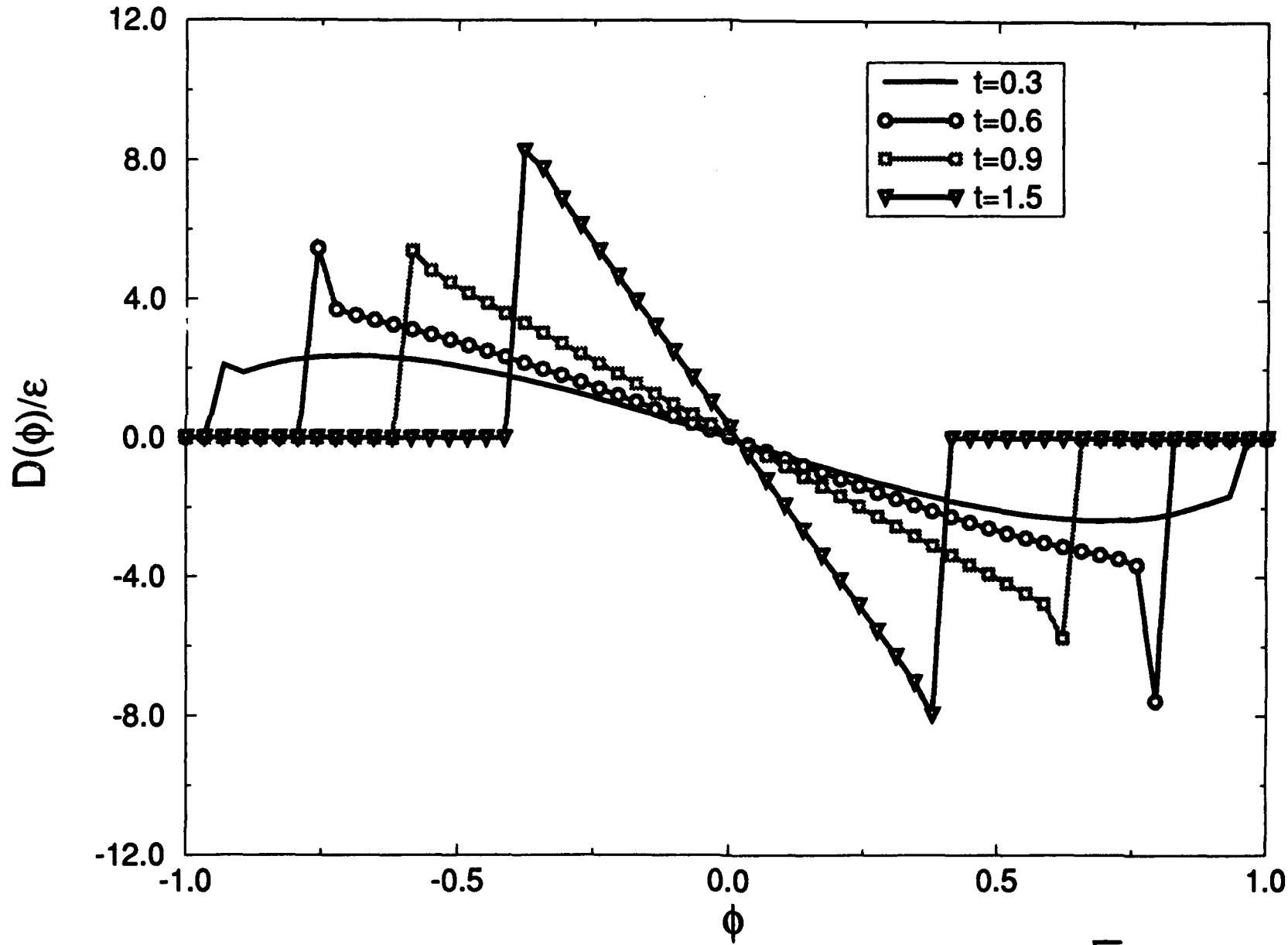

Fig. 11.c)

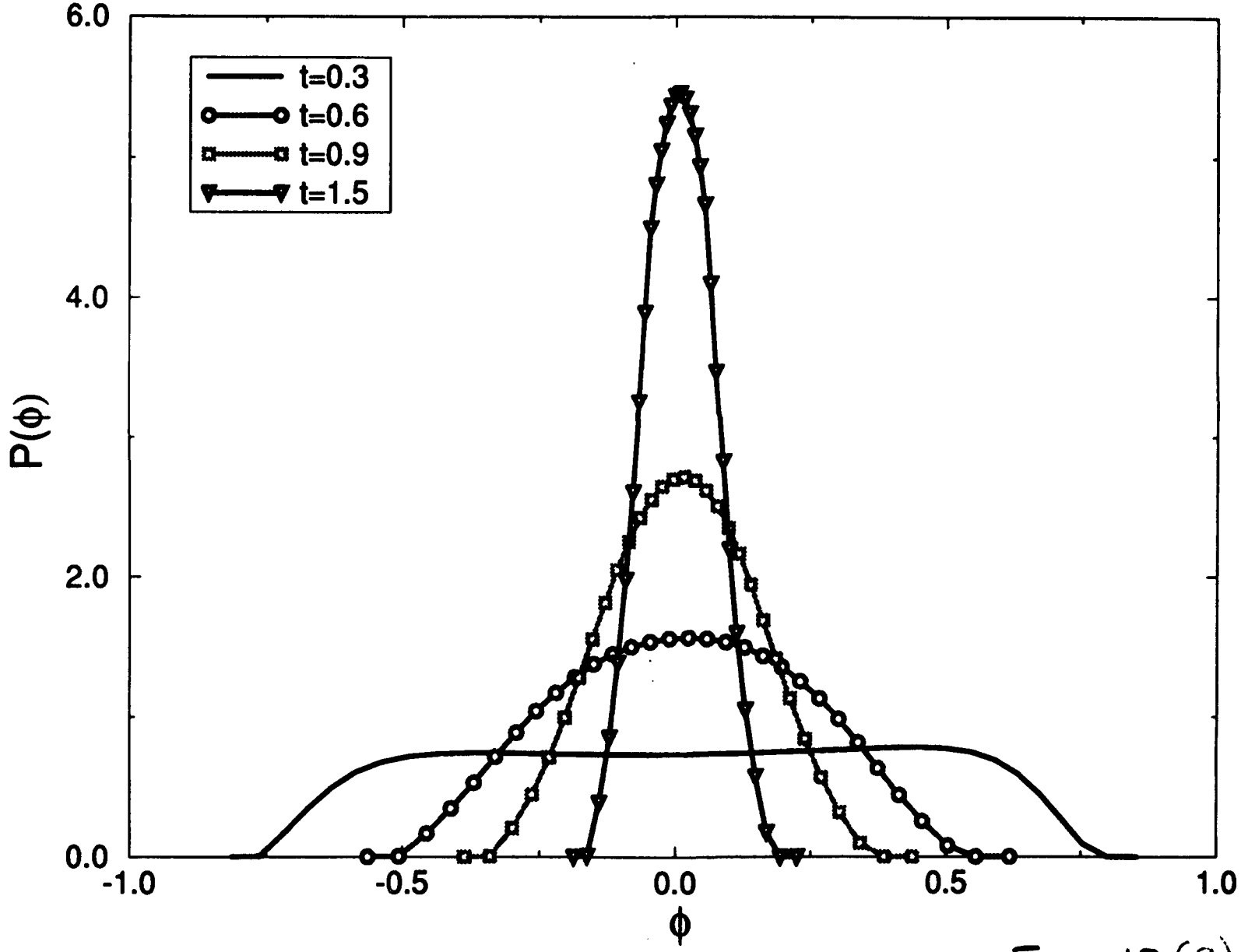

Fig. 12.(a)

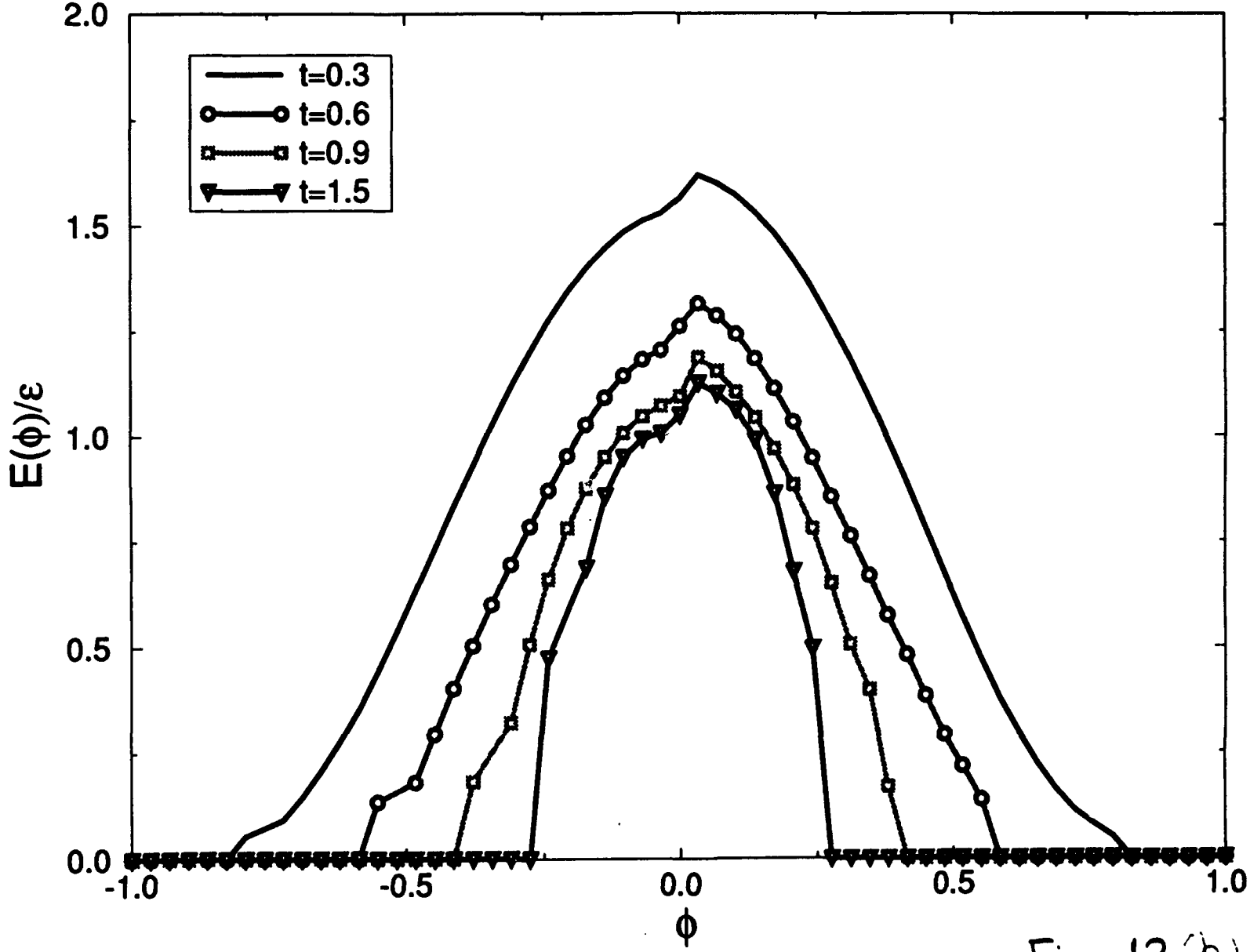

Fig. 12(b)

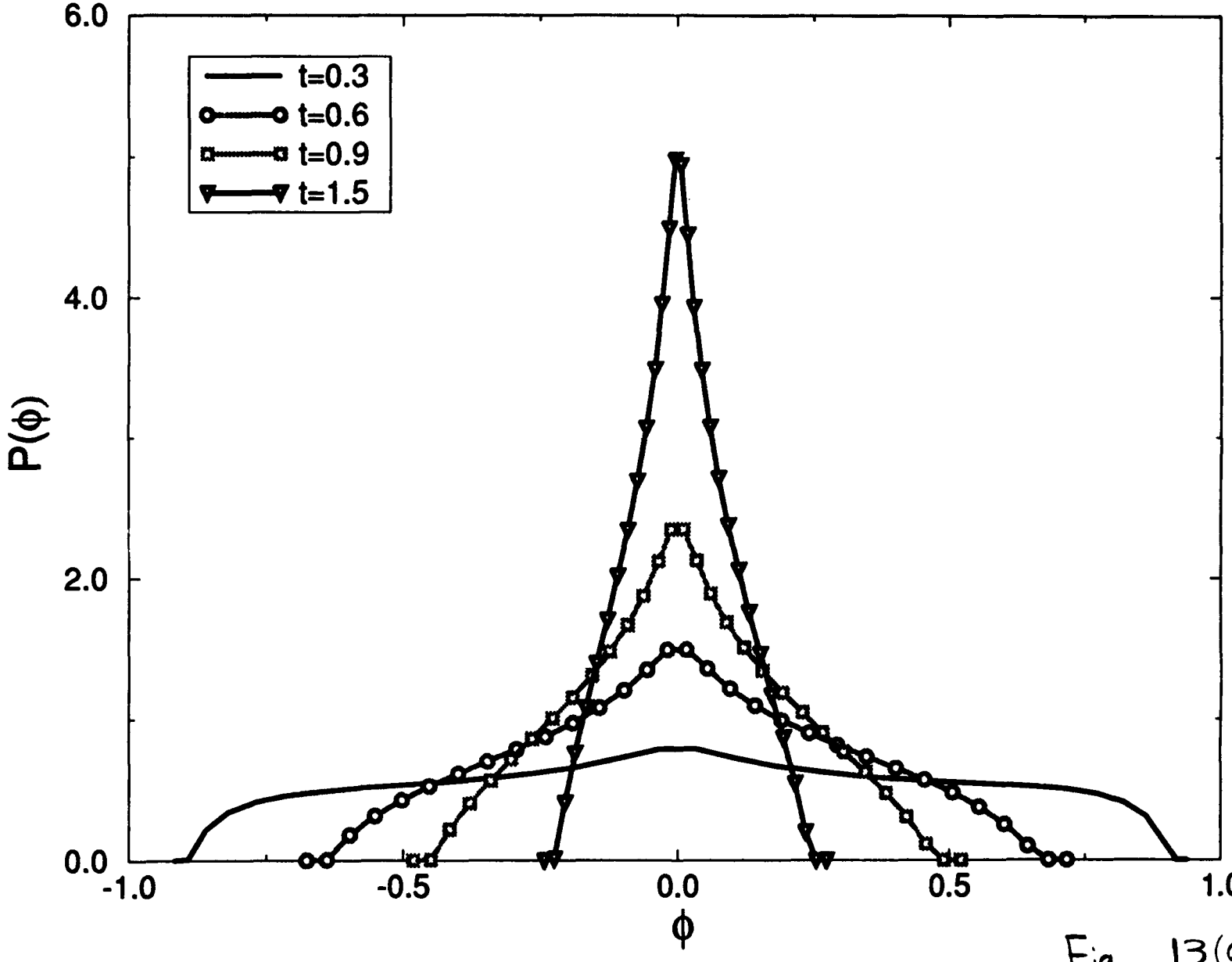

Fig. 13(a)

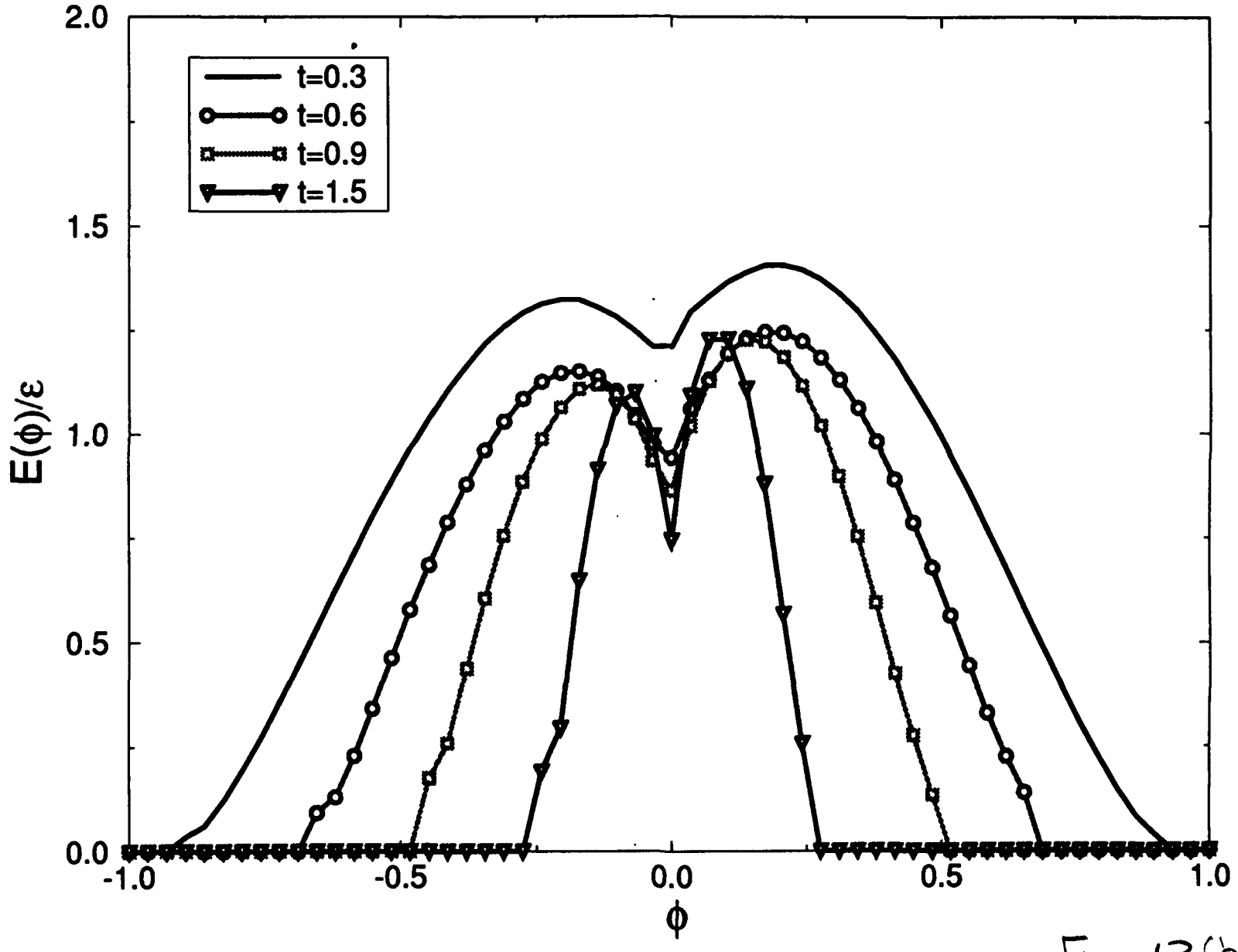

Fig. 13(b)

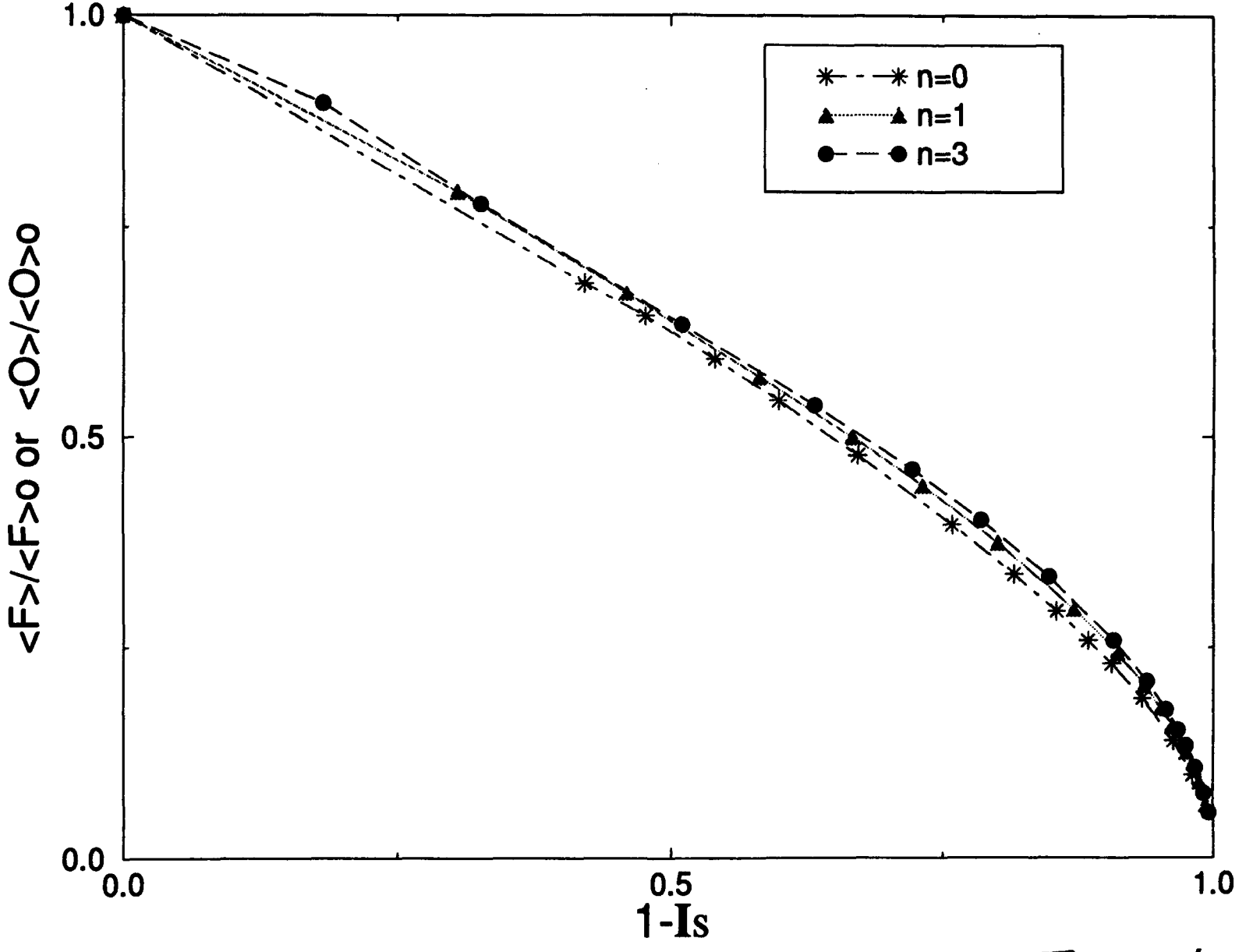

Fig. 14

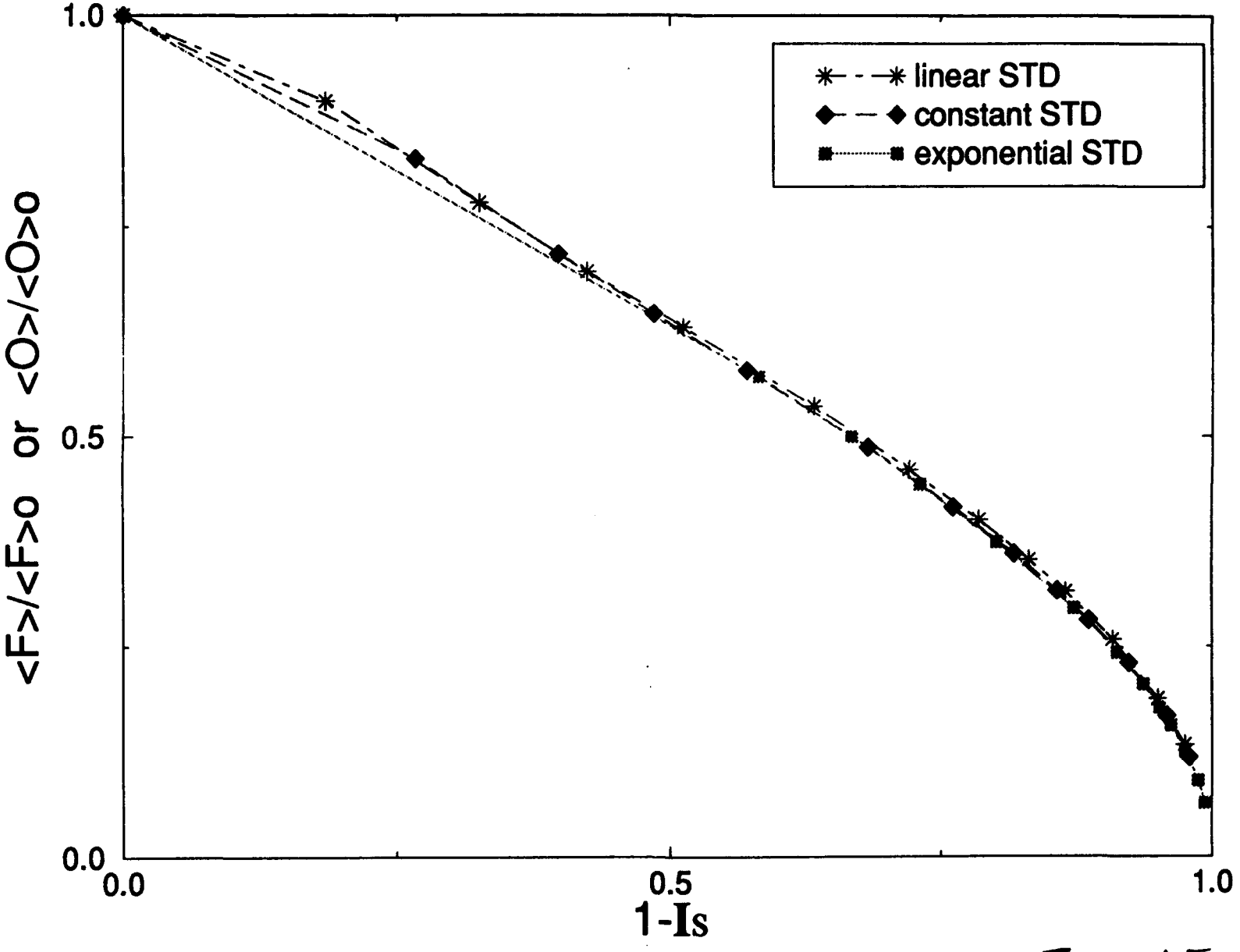
linear STD
constant STD
exponential STD
1.0
0.5
0.0
0.0
0.5
1.0
<F>/<F>o or <O>/<O>o
1-Is

Fig. 15

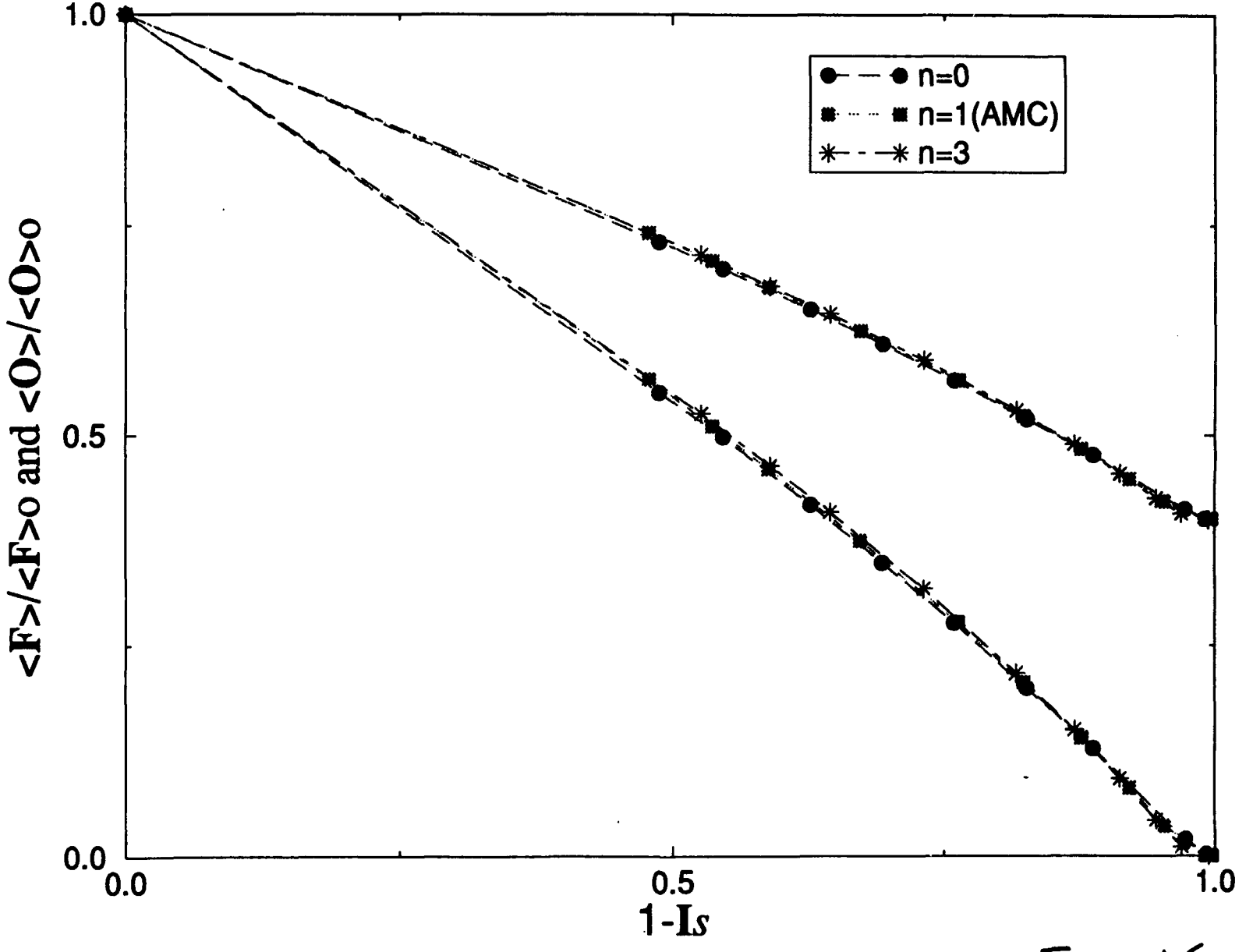

Fig. 16